frontiers | Research Topics

Enhancement of nutritional profile/ biological activity of plant-based foods by fermentation

Edited by
Yu Xiao, Xiaolong Ji and Xiudong Xia

Published in
Frontiers in Nutrition

ISSN 1664-8714
ISBN 978-2-83251-293-7
DOI 10.3389/978-2-83251-293-7

About Frontiers

Frontiers is more than just an open access publisher of scholarly articles: it is a pioneering approach to the world of academia, radically improving the way scholarly research is managed. The grand vision of Frontiers is a world where all people have an equal opportunity to seek, share and generate knowledge. Frontiers provides immediate and permanent online open access to all its publications, but this alone is not enough to realize our grand goals.

Frontiers journal series

The Frontiers journal series is a multi-tier and interdisciplinary set of open-access, online journals, promising a paradigm shift from the current review, selection and dissemination processes in academic publishing. All Frontiers journals are driven by researchers for researchers; therefore, they constitute a service to the scholarly community. At the same time, the *Frontiers journal series* operates on a revolutionary invention, the tiered publishing system, initially addressing specific communities of scholars, and gradually climbing up to broader public understanding, thus serving the interests of the lay society, too.

Dedication to quality

Each Frontiers article is a landmark of the highest quality, thanks to genuinely collaborative interactions between authors and review editors, who include some of the world's best academicians. Research must be certified by peers before entering a stream of knowledge that may eventually reach the public - and shape society; therefore, Frontiers only applies the most rigorous and unbiased reviews. Frontiers revolutionizes research publishing by freely delivering the most outstanding research, evaluated with no bias from both the academic and social point of view. By applying the most advanced information technologies, Frontiers is catapulting scholarly publishing into a new generation.

What are Frontiers Research Topics?

Frontiers Research Topics are very popular trademarks of the *Frontiers journals series*: they are collections of at least ten articles, all centered on a particular subject. With their unique mix of varied contributions from Original Research to Review Articles, Frontiers Research Topics unify the most influential researchers, the latest key findings and historical advances in a hot research area.

Find out more on how to host your own Frontiers Research Topic or contribute to one as an author by contacting the Frontiers editorial office: frontiersin.org/about/contact

Enhancement of nutritional profile/biological activity of plant-based foods by fermentation

Topic editors

Yu Xiao — Hunan Agricultural University, China

Xiaolong Ji — Zhengzhou University of Light Industry, China

Xiudong Xia — Jiangsu Academy of Agricultural Sciences (JAAS), China

Citation

Xiao, Y., Ji, X., Xia, X., eds. (2023). *Enhancement of nutritional profile/biological activity of plant-based foods by fermentation*. Lausanne: Frontiers Media SA. doi: 10.3389/978-2-83251-293-7

Table of contents

frontiers in Nutrition

ORIGINAL RESEARCH
published: 06 December 2021
doi: 10.3389/fnut.2021.786571

Effects of *Lactobacillus plantarum* FZU3013-Fermented *Laminaria japonica* on Lipid Metabolism and Gut Microbiota in Hyperlipidaemic Rats

Jin-Peng Hu, Ting-Ting Zheng, Bin-Fen Zeng, Man-Ling Wu, Rui Shi, Ye Zhang, Li-Jiao Chen, Wen-Jian Cheng and Peng Liang**

College of Food Science, Fujian Agriculture and Forestry University, Fuzhou, China

In this study, we explored the effect of *Lactobacillus plantarum* FZU3013-fermented *Laminaria japonica* (LPLJ) supplementation to prevent hyperlipidaemia in rats fed with a high-fat diet (HFD). The results indicate that LPLJ supplementation improved serum and hepatic biochemical indicators ($p < 0.05$), elevated short-chain fatty acid levels, reduced HFD-induced accumulation of lipid droplets in the liver, modulated the relative abundance of some microbial phylotypes, and reduced hyperlipidaemia in HFD-fed rats by adjusting the aminoacyl-tRNA, phenylalanine, tyrosine, and tryptophan biosynthetic pathways, as well as the phenylalanine, D-glutamine and D-glutamate, and glutathione metabolic pathways. Additionally, hepatic mRNA levels of the genes involved in lipid metabolism and bile acid homeostasis were significantly reduced by LPLJ intervention ($p < 0.05$). These results suggest that LPLJ has a positive effect on modulating lipid metabolism and has the potential to be a functional food that can help prevent hyperlipidaemia.

Keywords: ***Laminaria japonica*, *Lactobacillus plantarum* FZU3013, hyperlipidaemia, lipid metabolism, gut microbiota**

OPEN ACCESS

Edited by:
Yu Xiao,
Hunan Agricultural University, China

Reviewed by:
Choong Hwan Lee,
Konkuk University, South Korea
Guijie Chen,
Nanjing Agricultural University, China

****Correspondence:***
Wen-Jian Cheng
chengwj@fafu.edu.cn
Peng Liang
liangpeng137@sina.com

Specialty section:
This article was submitted to Food Chemistry, a section of the journal Frontiers in Nutrition

Received: *30 September 2021*
Accepted: *12 November 2021*
Published: *06 December 2021*

Citation:
Hu J-P, Zheng T-T, Zeng B-F, Wu M-L, Shi R, Zhang Y, Chen L-J, Cheng W-J and Liang P (2021) Effects of Lactobacillus plantarum FZU3013-Fermented Laminaria japonica on Lipid Metabolism and Gut Microbiota in Hyperlipidaemic Rats. Front. Nutr. 8:786571. doi: 10.3389/fnut.2021.786571

INTRODUCTION

The incidence of hyperlipidaemia is rapidly increasing owing to improved socio-economic status and consumption of unhealthy diets. Hyperlipidaemia is linked to the development of cardiovascular diseases, resulting in non-alcoholic fatty liver (NAFL) to a certain extent, and this has received considerable critical attention (1–4). The main treatment for hyperlipidaemia is drug therapy, which often leads to various adverse reactions (5). Currently, researchers are focusing their attention on food therapy to prevent hyperlipidaemia because of its high efficacy complemented with few or no side effects.

Laminaria japonica (LJ) has diverse bioactive compounds, such as proteins, polysaccharides, and vitamins (6, 7). Polysaccharides are an important active constituent of LJ and have a variety of physiological functions, including hypolipidemic capacity, bile acid (BA)-binding, anti-atherosclerosis, and anti-bacterial activities (8–10). With the development of microbial fermentation technology, many researchers have applied this technology to the processing and development of LJ-containing foods. The fermentation of lactic acid bacteria (LAB) can promote the transformation of nutrients and hydrolysis of biological macromolecules, as well as increase

the content of bioactive substances. As the most commonly used probiotics in food fermentation, LAB have been shown to relieve hyperlipidaemia. For example, *Lactobacillus plantarum* regulates dyslipidaemia, the intestinal microbiome, and hepatic metabolism in high-fat diet (HFD)-induced hyperlipidaemic rats (11). However, the regulatory mechanism of *L. plantarum*-fermented LJ (LPLJ) on hyperlipidaemia is not yet known.

Previous studies have shown that lipid metabolism in the liver is one of the most critical factors in maintaining lipid metabolism and homeostasis (12, 13). The synergistic changes in the transport of lipoprotein and the absorption, biosynthesis, and catabolism of cholesterol in the liver are closely correlated with the modulation of lipid metabolism (14). In addition, as a significant pathway of liver lipid metabolism, enterohepatic circulation is pivotal to human health. The major factors influencing the composition of gut microbiota are diet (15), lifestyle (16), mood (17), and antibiotic treatment (18). Clinical research has shown that the consumption of high-fat food for a long period results in the reduction of gut microbial diversity (19). Emerging evidence indicates that intestinal flora dysbiosis might result in obesity (20), hyperlipidaemia (21), and NAFL (22). To date, the impact of LPLJ on lipid metabolism in the liver and its relationship with intestinal flora regulation have not been reported.

Metabolomic analysis can detect changes in metabolism under different stimuli by analyzing the changes in endogenous small molecule metabolites (23). A previous study applied ultra-high performance liquid chromatography-quadrupole time-of-flight mass spectrometry (UPLC-QTOF/MS) for serum metabolomics and showed that the levels of amino acids and BAs are closely related to the occurrence and development of hyperlipidaemia (24, 25). However, there have been no reports on the mechanism of action of LPLJ supplementation in liver metabolomics based on UHPLC-QTOF/MS in patients with hyperlipidaemia.

Therefore, liver metabolomics and high-throughput sequencing of the gut microflora were used in this study to investigate the effect of LPLJ on lipid metabolism and determine its lipid-lowering mechanism in hyperlipidaemic rats. The findings of this study will provide useful information to identify functional foods that can prevent hyperlipidaemia.

MATERIALS AND METHODS

Preparation of *L. plantarum* FZU3013-Fermented LJ

L. plantarum FZU3013, isolated from the fermentation of *Hongqu* rice wine, was obtained from the Institute of Food Science and Technology, Fuzhou University (6, 26). This strain was cultured in the MRS medium for 36 h under static conditions, and then sub-cultured three times. Fermentation of LJ was conducted according to a previously described method (27). LJ was purchased from the Yonghui supermarket (Fuzhou, China). Briefly, LJ was washed, dried, and crushed (80 mesh). The powder (3 g) was dissolved in 100 mL of deionised water, autoclaved at 110 °C for 15 min, and, after cooling, inoculated with 1 mL of a cell suspension (1.0×10^9 CFU/mL) of *L. plantarum* FZU3013. Then, the mixture was fermented at 37 °C for 24 h.

Measurement of Chemical Characteristics

The total sugar content in LJ before and after fermentation was determined by the phenol-sulfuric method. The sample was centrifuged (8,000 × g, 15 min), and 1 mL of the supernatant was mixed with 1 mL of 5% phenol solution, and then 6 mL of concentrated sulfuric acid was added. The reaction mixture was left standing at room temperature for 30 min. The absorbance was measured at 490 nm with D-glucose as a standard. The reducing sugar content was determined by the dinitrosalicylic acid (DNS) method. Briefly, 1 mL of sample supernatant was mixed with 2 mL DNS (3, 5-dinitrosalicylic acid, 2M NaOH, and potassium sodium tartrate) in boiling water for 15 min, and the absorbance was measured at 540 nm. The total polyphenol content was measured using a total phenol content detection kit (Beijing Solaibao Science & Technology Co., Ltd). In short, 3 mL of the sample was mixed with 2.5 mL of 60% ethanol and extracted using ultrasound (300 W, 60°C, 30 min). After centrifugation (8,000 × g, 25 °C, 10 min), the supernatant was collected, and the absorbance was measured at 760 nm with gallic acid as the standard compound.

Animal Experiments

Forty male specific pathogen-free rats (6 weeks of age) were purchased from Sipeifu Biotechnology Co., Ltd. (Beijing, China) and maintained under a specific environment (temperature 22 ± 4 °C, humidity 60% ± 10%, 12-h light/dark cycle). After a week of acclimation, the rats were randomly split into five groups (n = 8): (1) a normal-fat diet (NFD), (2) an HFD, (3) an HFD with 10 mg/kg simvastatin (Simv) per day, (4) an HFD with 2.0 g/kg LJ powder suspension per day, and (5) an HFD with 2.0 g/kg LPLJ per day.

Biochemical Analysis of Serum and Liver

At the 8th week of these experiments, rats were euthanized after overnight fasting. Blood samples were collected from the heart into 2-mL centrifuge tubes and incubated at 25 °C for 1 h. Serum was obtained by centrifugation (3,000 × *g*, 8 min). Serum total cholesterol (TC), triglyceride (TG), and non-esterified fatty acid (NEFA) levels were measured using rapid detection kits (Kilton Biotechnology Co., Ltd., Shanghai, China). The liver samples were dispersed in a saline solution (1: 9) and then homogenized. The sediment was removed by centrifugation at 3,000 × *g* for 10 min. TC, TG, NEFA, and total BA (TBA) levels in the livers were also determined using commercial kits (Kilton Biotechnology Co., Ltd., Shanghai, China). Fecal TBA, TC, and TG levels were measured using kits from Kilton Biotechnology Co., Ltd.

Histopathologic Evaluation

Fresh liver or adipose tissue samples were fixed in formalin solution (4%) overnight. Tissue sections (5 μm) were prepared, stained with haematoxylin and eosin (5), and examined under light microscopy (Bresser, Borken, Germany).

Determination of Fecal Short-Chain Fatty Acids (SCFAs)

SCFAs were analyzed by the method described by Guo et al. (28). In brief, feces (50 mg) were diluted with 500 μL of saturated NaCl solution and incubated at 25 °C for 30 min. The mixture was then homogenized for 3 min, followed by the addition of 20 μL of 10% sulphuric acid solution and shaking for 30 s. Subsequently, 800 μL of diethyl ether and 20 μL of 10% sulphuric acid solution were added. Total SCFAs were extracted by centrifugation (4 °C, 8,000 × *g*, 15 min). To remove trace water, 0.25 g of Na_2SO_4 (anhydrous) was added to the supernatant. After sequential centrifugation (3,000 × *g*, 4 °C, 1 min) and filtration through a 0.22-μm filter, the extracted fecal SCFAs were evaluated using capillary gas chromatography.

High-Throughput Sequencing of Gut Microbiota

Genomic DNA was extracted from cecum samples using a fecal DNA isolation kit (MoBio, USA). Bacterial full-length 16S rDNA was amplified by PCR with primers 338F/806R. The purified PCR products were used to construct DNA libraries with the Pacific Biosciences Template Prep Kit 2.0 (Pacific Biosciences). The high-throughput sequencing was performed on the PacBio RS II platform at Shanghai Personal Biotechnology Co., Ltd. (Shanghai, China). Sequences were classified as operational taxonomic units with a similarity threshold of 97%. Significant differences in gut microbial phylotypes between different groups were demonstrated by STAMP (Ver. 2.1.3). The R software (Ver. 3.3.3) was used to draw a heat map of the correlation between lipid metabolism and key intestinal microbial phylotypes. The correlation network was visualized by Cytoscape (Ver. 3.6.0).

UPLC-QTOF/MS-Based Liver Metabolomics

Fifty milligrams of specimen (liver lobe) was added to an Eppendorf tube, and 1,000 μL of extracting solvent was added. After 30 s of vortexing, the mixture was homogenized in an ice water bath with an ultrasonic instrument for 4 min at a frequency of 35 Hz. The specimens were incubated at−40 °C for 1 h and centrifuged (8,000 × g, 4 °C, 15 min). The detailed operating parameters of UPLC-QTOF/MS were performed as described in a previous study (29). The mobile phase consisted of 25 mmol/L ammonium acetate and 25 mmol/L ammonia hydroxide in water (pH = 9.75) (A) and acetonitrile (B). The analysis was carried out with an elution gradient as follows: 0–1.0 min, 95 % B; 1.0–8.0 min, 95–65% B; 8.0–9.0 min, 65–40% B; 9.0–10.0 min, 40% B; 10.0–10.2 min, 40–95% B; and 10.3–12.0 min, 95% B.

Real-Time Quantitative PCR

The liver total RNA was extracted according to the kit instructions and reverse-transcribed into cDNA by the PrimeScript™RT reagent kit (Takara, Japan). The sequences of primers are listed in **Table 1**. qRT-PCR was performed in StrataGene Mx3005P (Agilent, Colorado, USA) in combination with SYBR Premix Ex Taq II (Takara, Dalian, China). The mRNA expression level was normalized to that of β-Actin as a reference. The combination of experimental data was expressed as the mean ± standard deviation (SD).

Statistical Analysis

All data are expressed as the mean ± SD. Statistical differences were analyzed using GraphPad Prism 7.0 for one-way ANOVA with Tukey's comparisons test ($p < 0.05$). The significance levels of test were set at $p < 0.05$.

RESULTS

Changes in Chemical Characteristics

Changes by fermentation are shown in **Table 2**. The log CFU of LJ after fermentation was 8.89 ± 0.02, and the pH decreased significantly compared with before fermentation ($p < 0.05$). After 24 h of fermentation, the total sugar was obviously decreased ($p < 0.05$). Reducing sugar and polyphenols were not significantly decreased.

Effects of LPLJ on Physiological Indices

After 8 weeks of feeding, the body weight of the HFD-fed rat group was markedly higher than that of the NFD group (**Figures 1A,B**). The increasing trend caused by the HFD was reduced by dietary supplementation with LPLJ. In addition, HFD-fed rats showed an evident increase in the levels of physiological indices of the liver, perirenal adipocytes, and epididymal adipocytes compared with NFD-fed rats (**Figures 1C–E**). However, these increased levels were significantly alleviated by dietary supplementation with LPLJ ($p < 0.05$). Perirenal and epididymal adipocytes were with smaller size and volume in the other three groups than in the HFD group (**Figures 1F,G**) ($p < 0.05$).

Effects of LPLJ on Biochemical Indicators of Blood Serum

After 8 weeks of treatment, serum TG, TC, and NEFA levels were effectively increased in rats in the HFD group compared with those in the NFD group (**Figure 2**). Dietary supplementation with LPLJ effectively reduced the serum TC, TG, and NEFA levels that were increased by the HFD ($p < 0.05$).

Effects of LPLJ on Liver Biochemical Indices and Histopathology

To determine the potential regulatory effects of LPLJ on lipid accumulation, the hepatic TG, TC, TBA, and NEFA levels of HFD-fed rats were determined. HFD-fed rats showed higher hepatic TG, TC, TBA, NEFA, and FAT levels (**Figures 3A–D**). Similar to the effect of Simv, the oral administration of LPLJ significantly prevented these adverse changes caused by the HFD ($p < 0.05$). Dietary supplementation with LPLJ was observed to reduce the hepatic TG, TC, TBA, and NEFA levels. Moreover, liver fat levels in the HFD group were markedly decreased by the oral administration of LPLJ (**Figure 3E**) (*p*

TABLE 1 | Primer sequences for quantitative real-time PCR.

Gene	Forward primer (5'-3')	Reverse primer (5'-3')
HMGCR	AGTGGTGCGTCTTCCTCG	CGAATCTGCTGGTGCTAT
SREBP-1C	GCTGTTGGCATCCTGCTATC	TAGCTGGAAGTGACGGTGGT
CYP7A1	CTGCGAAGGCATTTGGACACAGA	GCATCTCCCTGGAGGGTTTTGGT
ACOX1	TTACATGCCTTTGTTGTCCCTATC	CGGTAATTGTCCATCTTCAGGTA
ACAT2	GAACGTGGTGGTCCATGACT	TTCAGCAGACCTCCAACCAC
BSEP	CGTGCTTGTGGAAGAAGTTG	GGGAGTAGATGGGTGTGACTG
CD36	GACAATCAAAAGGGAAGTTG	CCTCTCTGTTTAACCTTGAT
LDLR	ATGCTGGAGATAGAGTGGAGTT	CCGCCAAGATCAAGAAAG

TABLE 2 | Changes of pH, CFU, total sugars, reducing sugars, and total phenolic compounds by fermentation.

Sample	pH	Log CFU/mL	Total sugars (mg/mL)	Reducing sugars (mg/mL)	Total phenolic compounds (μg gallic acid/ML)
Before (LJ)	6.42 ± 0.12	\	0.39 ± 0.02	0.12 ± 0.01	1.11 ± 0.02
After (LPLJ)	4.03 ± 0.09[a]	8.32 ± 0.02	0.26 ± 0.03 [a]	0.14 ± 0.01	0.97 ± 0.04

Values are mean ± standard deviation (n = 3; [a]$p < 0.05$, significantly different from the LJ group).

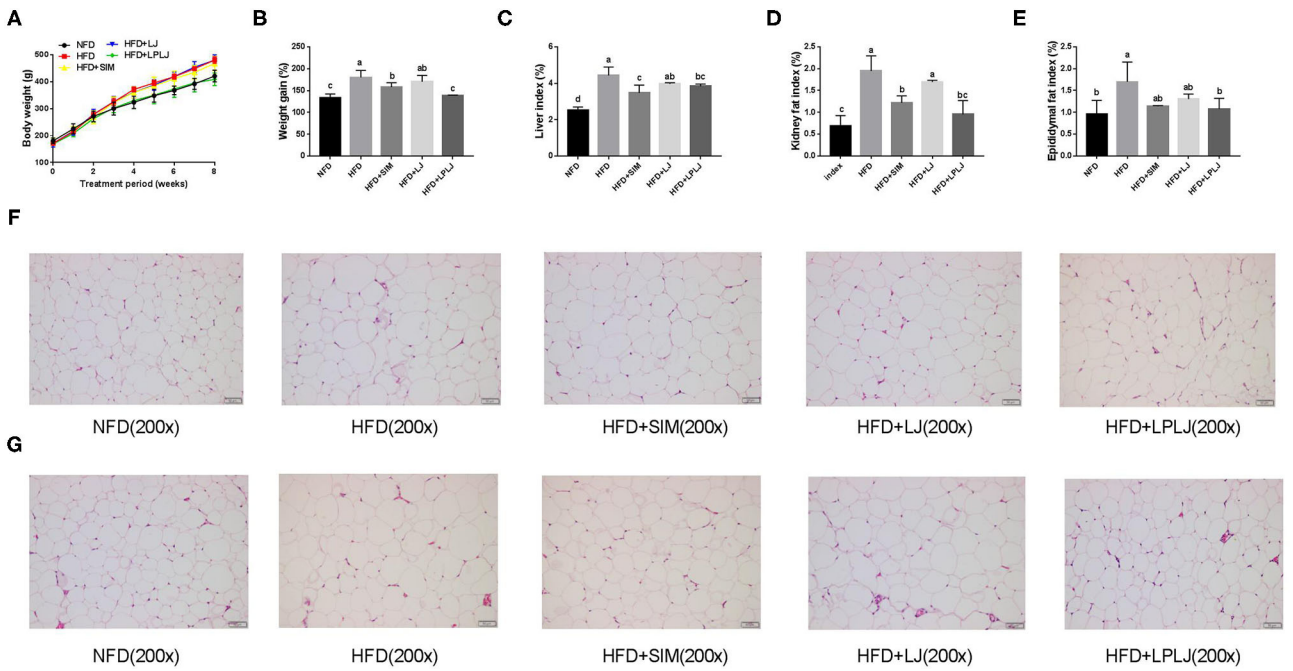

FIGURE 1 | Effects of LPLJ consumption on **(A)** body weight, **(B)** weight gain, **(C)** liver index, **(D)** kidney fat index, **(E)** epididymal fat index, **(F)** the size of perirenal adipocytes and **(G)** the size of epididymal adipocytes in rats fed a high fat diet. a-c, Mean values with different letters in the same column differ significantly ($p < 0.05$).

< 0.05). Furthermore, histological analysis demonstrated that lipid droplet accumulation was markedly increased in HFD-fed rats. Notably, the size and quantity of fat vacuoles in the LPLJ group were much lower than those in the HFD group (**Figures 3F–J**). The results suggest that supplementation with Simv, LJ, and LPLJ effectively reduces hepatic lipid accumulation in hyperlipidaemic rats.

Effects of LPLJ on the Level of Fecal Lipid and SCFAs in HFD-Fed Rats

Fecal levels of TBA, TG, and TC were increased by LPLJ diet intervention compared with those in the HFD group (**Figures 4A–C**) ($p < 0.05$). The results suggest that daily supplementation with LPLJ effectively increases the fecal excretion of lipids. In addition, compared with the NFD group,

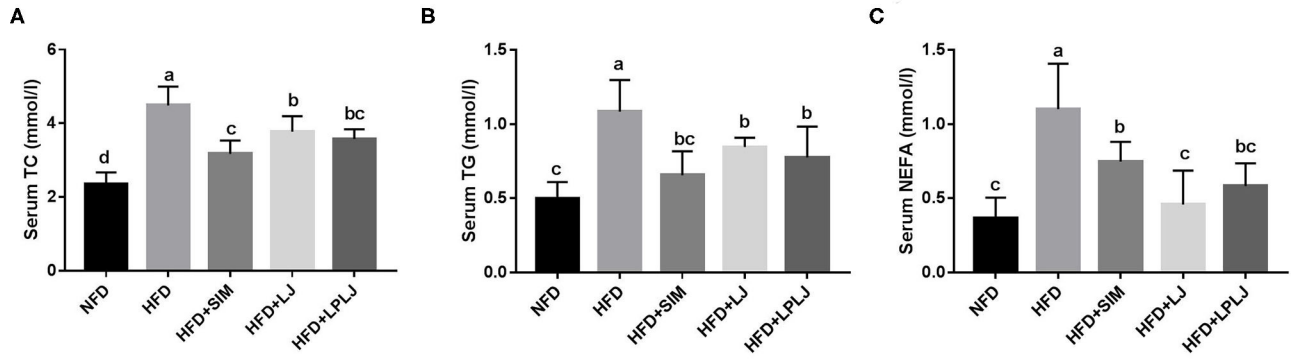

FIGURE 2 | Effects of LPLJ consumption on the serum biochemical parameters in rats fed a high-fat diet for consecutive 8 weeks. **(A)** serum TC, **(B)** serum TG, and **(C)** serum NEFA. a-d, Mean values with different letters in the same column differ significantly ($p < 0.05$).

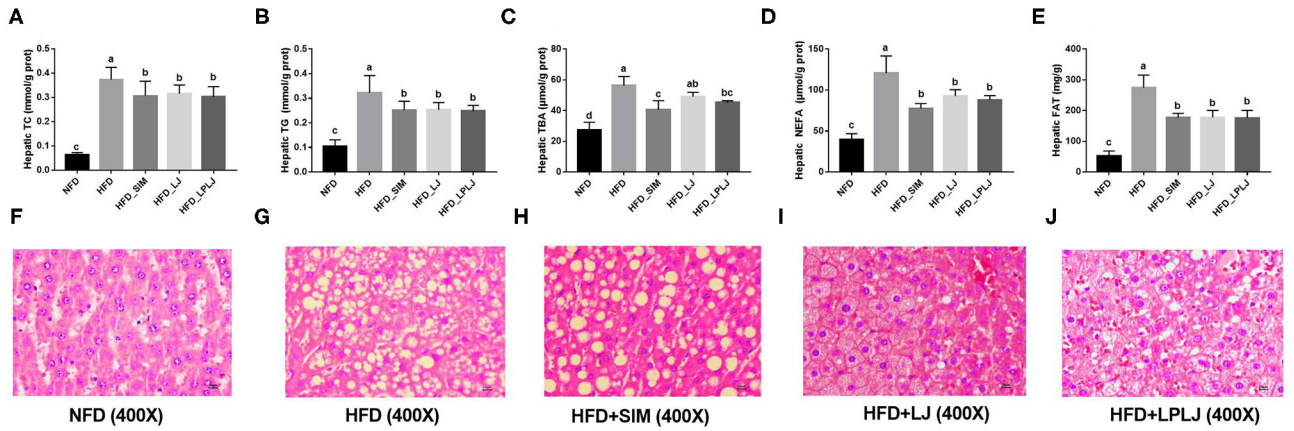

FIGURE 3 | Effects of LPLJ consumption on the liver biochemical parameters and histopathology in rats fed a high-fat diet for consecutive 8 weeks. **(A)** hepatic TC, **(B)** hepatic TG, **(C)** hepatic TBA, **(D)** hepatic NEFA, **(E)** hepatic FAT, and **(F–J)** liver morphology (magnification × 400) in rats fed a high fat diet. a-d, Mean values with different letters in the same column differ significantly ($p < 0.05$).

the fecal acetate, butyrate, isobutyrate, valerate, and isovalerate levels were reduced by high-fat feeding (**Figures 4D–G**) ($p < 0.05$). However, supplementation with LPLJ remarkably increased the acid acetate, butyrate, propionate, and isobutyrate levels (**Figures 4H,I**) ($p < 0.05$).

LPLJ Supplementation Regulated the Intestinal Microbiota

To evaluate the influence of LPLJ on intestinal microbial composition, the V3–V4 region of the HFD+LPLJ group was sequenced using high-throughput sequencing. Key microbial system types with significant differences between the NFD (cyan) and HFD (red), and HFD (red) and HFD+LPLJ (blue), were revealed using the STAMP software (**Figure 5**). Compared with that in the NFD group, the relative richness of 15 key microbial system types was markedly different in the HFD group; that of eight system types was significantly increased and that of seven system types was significantly decreased (**Figure 5**), indicating that changes in intestinal microflora occurred in HFD-induced hyperlipidaemic rats. However, supplementation with LPLJ effectively modified the intestinal microbiota induced by the HFD. Supplementation with LPLJ increased the relative abundance of *Akkermansia*, *Eubacteriumcoprostanoligenes_group*, *Erysipelotrichaceae_UCG-003*, *unclassified_f_Ruminooccaceae*, *Negativibaillus*, *Dubosiella*, and *unclassifed_f_Erysipelotrichaceae*, but decreased that of *Corynebacterium_1*, *Lachnoclostridium*, *Collinsella*, *Jeotgalcoccus*, *Atopostipes*, *Pseudograllibacllus*, *Pygmaiobacter*, *Vagooccus*, *Sporosarcina*, and *Lacticigenium.*

Correlations Between Key Intestinal Microflora Phylotypes and Lipid Metabolic Parameters

Correlations between lipid metabolic parameters and key intestinal microflora phylotypes were investigated using a network and heat map (**Figure 6**). Specifically, *Corynebacterum_1*, *Jeotgalicoccus*, *Atopostipes*, *Pygmaiobacter*, *Pscudgraililuls*, *Sporosarcina*, *Lacticigenium*, and *Vagococcus* were directly proportional to body weight gain, the liver index, epididymal fat, serum TC, TG, and NEFA levels,

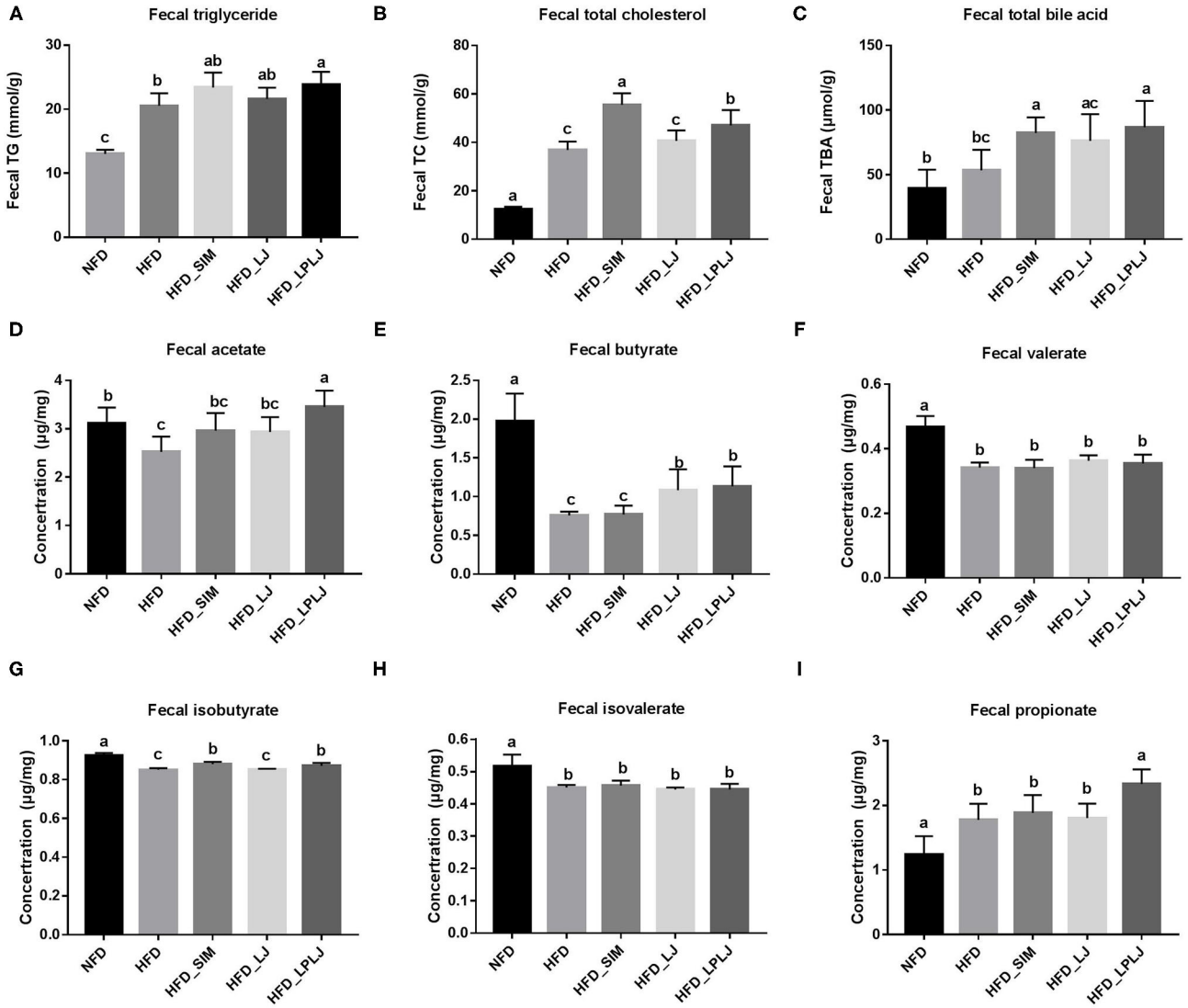

FIGURE 4 | Effect of LPLJ consumption on the fecal lipid levels and short-chain fatty acids (SCFAs) in rats fed a high fat diet. **(A)** TG, **(B)** TC, **(C)** TBA, **(D)** fecal acetate, **(E)** fecal butyrate, **(F)** fecal valerate, **(G)** fecal isobutyrate, **(H)** fecal isovalerate, and **(I)** fecal propionate levels. a-c, Mean values with different letters in the same column differ significantly ($p < 0.05$).

and hepatic TC, FAT, TG, TBA, and NEFA levels, but inversely related to fecal TC, TG, TBA, acetate, and butyrate levels. In addition, *unclassified_f_Ruminococcaceae*, *Eubacterium_coprostanoligenes_group*, and *Dubosiella* had a negative correlation with the liver index, serum NEFA, TG, and TC levels, and hepatic TBA, TC, TG, NEFA, and FAT levels, but a positive relationship with fecal TC, TG, TBA, acetate, and butyrate levels.

Effects of LPLJ Supplementation on the Liver Metabolites in HFD-Fed Rats

Principal component analysis (PCA) and orthogonal partial least-squares discrimination analysis (OPLS-DA) were used to observe the distinct changes in metabolite patterns in the liver. The results indicated that supplementation with LPLJ caused remarkable hepatic biochemical changes (**Figures 7A,B**, **8A,B**). In the negative-ion mode, 42 potential biomarkers were identified. In the LPLJ group, 8 metabolites were upregulated, and 34 metabolites were downregulated compared with those in the HFD group. One hundred and thirty potential biomarkers were successfully identified between HFD and LPLJ groups in the positive ion mode (**Figures 7C,D**). The levels of six metabolites were increased and those of 124 metabolites were decreased in the LPLJ group compared with those in the HFD group (**Figures 8C,D**). To increase our understanding of metabolic changes after LPLJ supplementation in hyperlipidaemic rats, MetaboAnalyst 4.0 was used for the metabolic pathway

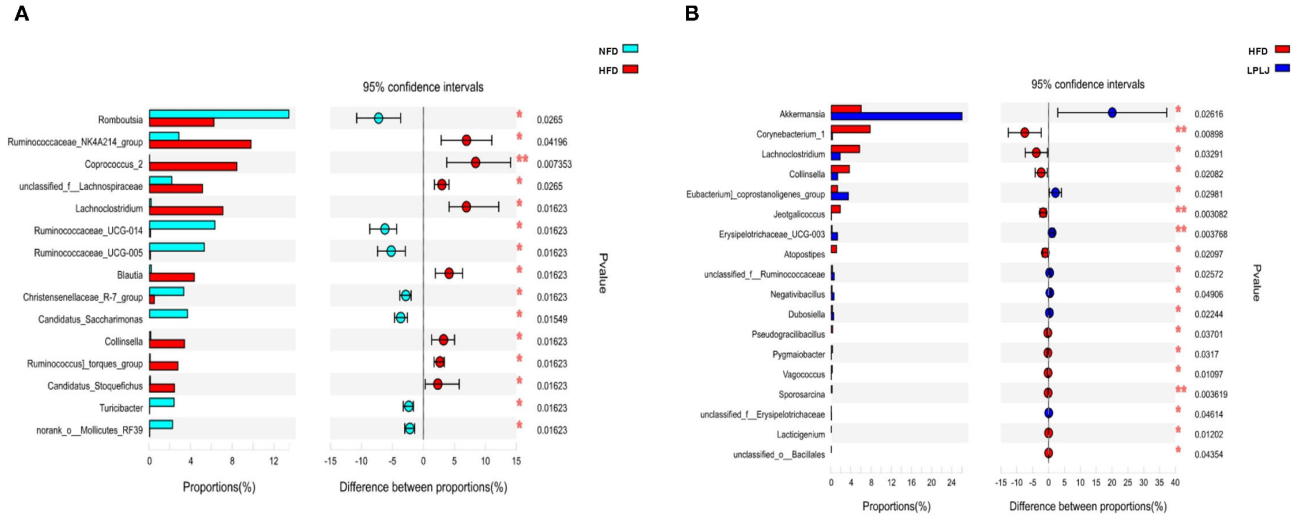

FIGURE 5 | Extended error bar plot comparing the differences in the mean proportions of the significantly altered intestinal microbial phylotypes. The differences between groups were determined using a Welsh's *t*-test, and the Benjamini-Hochberg procedure was used to control the false-discovery rate due to multiple testing. Corrected *P* values are shown at right. **(A)** NFD group vs. HFD group, **(B)** HFD+LPLJ group vs. HFD group. Values were expressed as mean ± SEM in each group ($n = 8$). $^{*}p < 0.05$, $^{**}p < 0.01$.

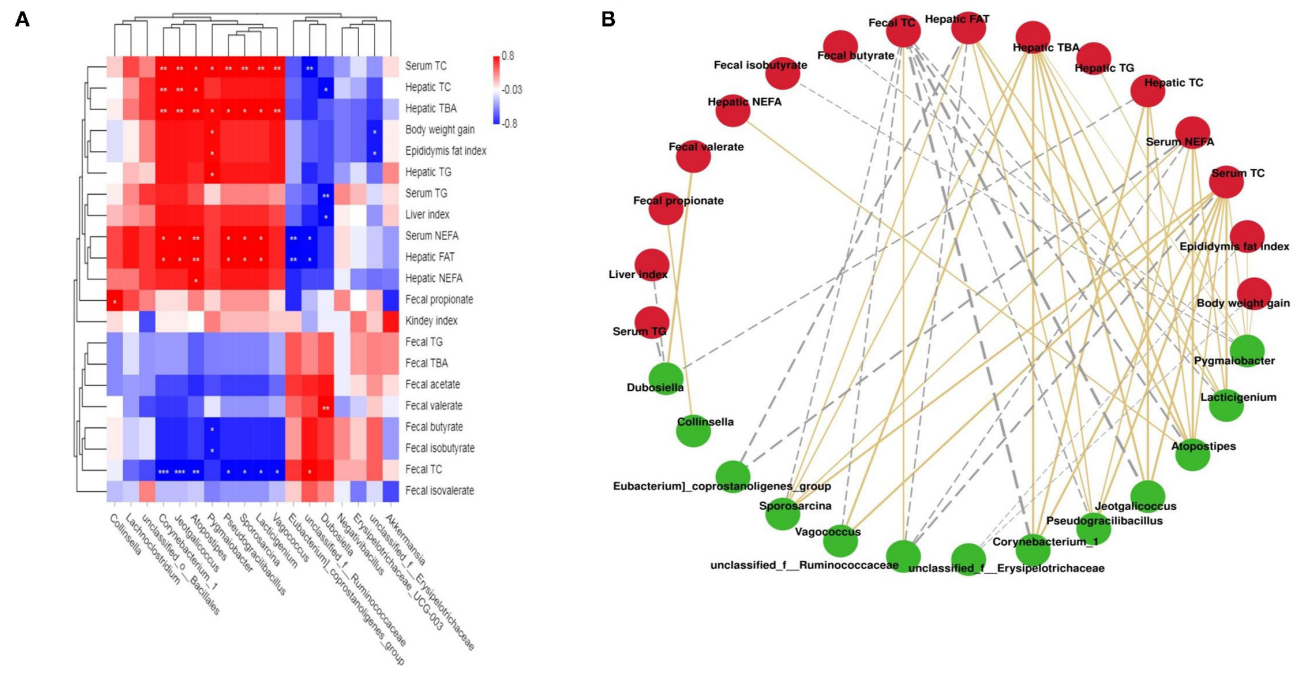

FIGURE 6 | Statistical Spearman's correlations between the fecal microbiota of significant differences and lipid metabolic parameters. **(A)** Heatmap of Spearman's correlation. The intensity of the color represents the degree of association; **(B)** Correlation network constructed between bacterial species and microbial metabolic pathways. The edge width and color (gold: positive and gray: negative) are proportional to the correlation strength.

enrichment analysis of differential liver metabolites (**Figures 7E**, **8E**). The metabolic pathways in the negative-ion mode that were changed by LPLJ supplementation mainly included aminoacyl-tRNA biosynthesis, phenylalanine, tyrosine, and tryptophan biosynthesis, phenylalanine metabolism, glutathione metabolism, methane metabolism, D-glutamine and D-glutamate metabolism, and ascorbate and aldarate metabolism. In the positive ion mode, aminoacyl-tRNA biosynthesis, nitrogen metabolism, phenylalanine metabolism, glutathione metabolism, thiamine metabolism, cyanoamino acid

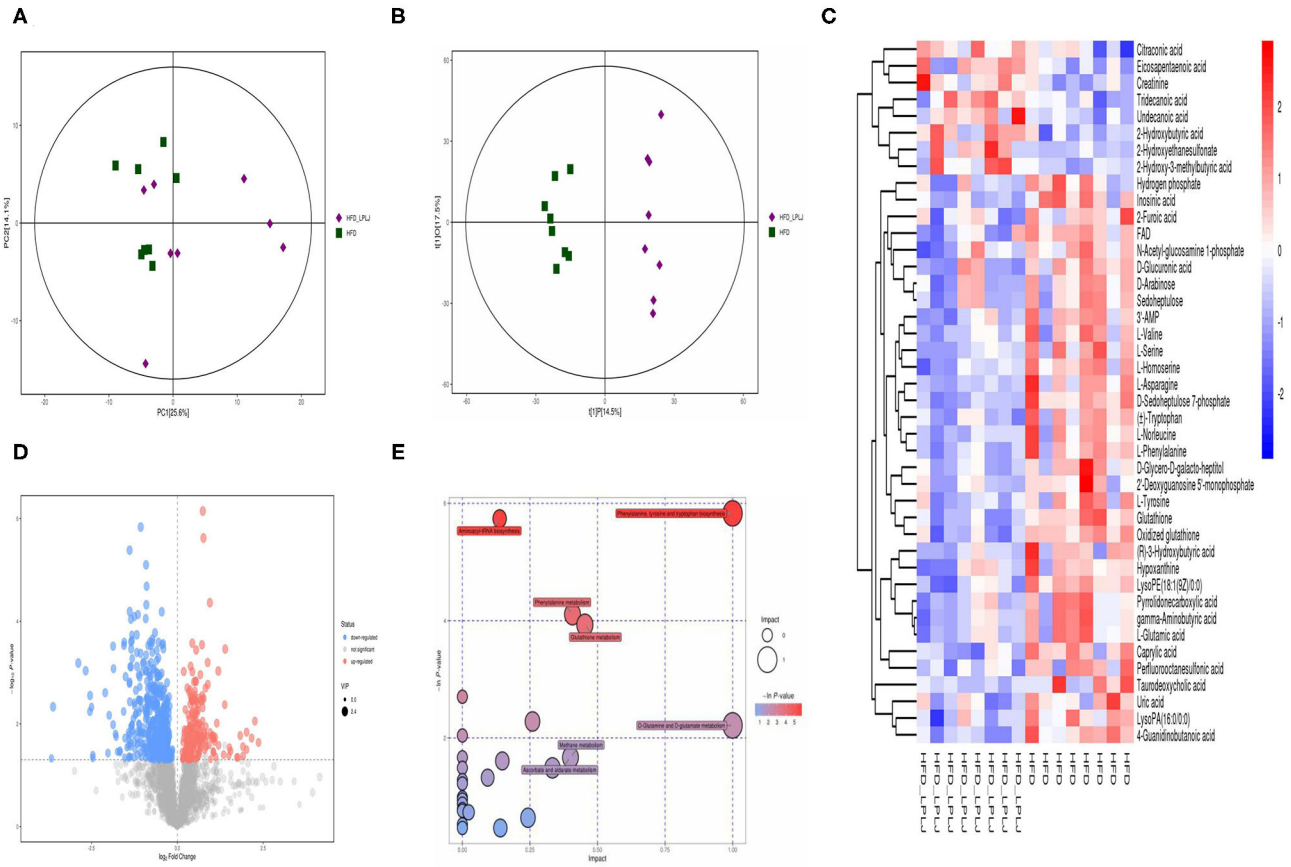

FIGURE 7 | Liver metabolomic profiling by UPLC-QTOF/MS in negative model (ESI-) ($n = 8$ for each group). **(A)** PCA score plot for the HFD and LPLJ groups; **(B)** OPLS-DA score plot for the HFD and LPLJ groups; **(C)** Heatmap of relative abundance of significantly different metabolites (VIP > 1.0, and $p < 0.05$) between the HFD and LPLJ groups; **(D)** Permutation test from PLS-DA models, **(E)** The metabolic pathway impact prediction between the HFD and LPLJ groups in liver based on KEGG online database. The -ln(p) values from the pathway enrichment analysis are indicated on the horizontal axis, and the impact values are indicated on the vertical axis.

metabolism, glycine, serine, and threonine metabolism, and methane, nicotinate, and nicotinamide metabolism were the primary metabolic pathways altered by LPLJ supplementation.

Effects of LPLJ Supplementation on Hepatic MRNA Expression

To identify the mechanisms underlying the moderating effect of LPLJ supplementation in rats fed an HFD, the liver mRNA expression levels of genes related to lipid metabolism were measured using qRT-PCR (**Figure 9**). HFD feeding increased the expression levels of cluster of differentiation 36 (CD36), recombinant acetyl coenzyme A acetyltransferase 2 (*ACAT2*), sterol regulatory element-binding protein-1c (SREBP-1c), and hydroxymethylglutaryl-CoA reductase (*HMGCR*) compared with those in the NFD group, and supplementation with LPLJ markedly reduced these abnormal expression levels ($p < 0.05$). On the contrary, the levels of bile salt export pump (*BSEP*), low-density lipoprotein receptor (*LDLR*), cholesterol 7α-hydroxylase (*CYP7A1*), and acyl-Coenzyme A oxidase 1 (*ACOX1*) in rats of the HFD group were reduced. Supplementation with LPLJ remarkably increased the mRNA levels of *LDLR*, *BESP*, *CYP7A1*, and *ACOX1* ($p < 0.05$).

DISCUSSION

Hyperlipidaemia has become an important public health problem worldwide (30). There is increasing evidence of diet interventions that have considered nutritional strategies for preventing or treating hyperlipidaemia (31–34). LJ is rich in nutrients and other diverse bioactive compounds, which have a variety of physiological functions, including reducing hyperlipidaemia (31, 32). Previous studies have shown that *Lactobacillus* can also regulate dyslipidaemia, the intestinal microbiome, and liver metabolism (33, 34). The results showed that dietary supplementation with LPLJ significantly prevent obesity, hyperlipidaemia, and NAFL disease (NAFLD) in HFD-fed rats. However, the exact regulatory mechanism of LPLJ that may reduce hyperlipidaemia and NAFLD requires further exploration.

In this study, HFD-fed rats showed increased weight gain, increased blood lipid levels, and liver lipid accumulation

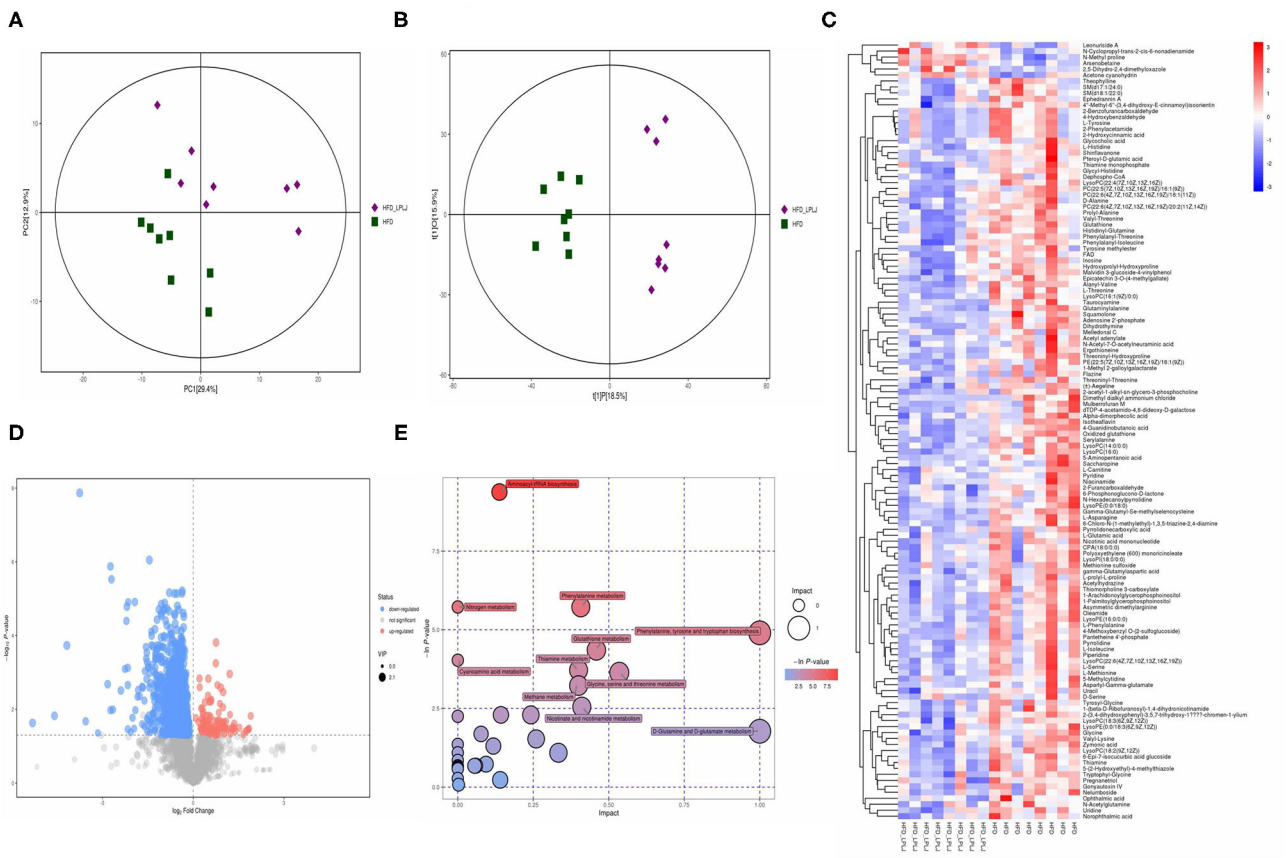

FIGURE 8 | Liver metabolomic profiling by UPLC-QTOF/MS in positive model (ESI+) ($n = 8$ for each group). **(A)** PCA score plot for the HFD and LPLJ groups; **(B)** OPLS-DA score plot for the HFD and LPLJ groups; **(C)** Heatmap of relative abundance of significantly different metabolites (VIP > 1.0, and $p < 0.05$) between the HFD and LPLJ groups; **(D)** Permutation test from PLS-DA models, **(E)** The metabolic pathway impact prediction between the HFD and LPLJ groups in liver based on KEGG online database. The -ln(p) values from the pathway enrichment analysis are indicated on the horizontal axis, and the impact values are indicated on the vertical axis.

compared with those in the NFD group. Changes in serum biochemical indices can directly explain the metabolic status of the organism. Supplementation with LPLJ effectively reverses the increase in serum TC, TG, and NEFA levels in HFD-induced hyperlipidaemic rats, indicating that LPLJ may lower the risk of cardiovascular and atherosclerosis diseases (35). Moreover, oral supplementation with LPLJ reduces the fat indices of the liver, kidney, and epididymus, as well as reduces the adipocyte size in HFD-induced hyperlipidaemia. HFD promotes the abnormal accumulation of intrahepatic fat droplets, thereby leading to fatty liver. Using histopathological analysis, we also found a difference in liver lipid accumulation between the NFD and HFD group. The levels of lipid droplets in liver tissue were markedly decreased by dietary supplementation with LPLJ, indicating that it significantly improves liver lipid metabolism.

Hepatic lipid metabolism is one of the most critical factors in maintaining normal lipid metabolism *in vivo*. Cholesterol is usually absorbed from the small intestine after food intake, and then enters the enterohepatic circulation. It is transferred to the liver with BAs, and a small amount of BAs is excreted through the stool (36). BAs are commonly considered significant factors in the regulation of lipid and cholesterol metabolism. We found that dietary supplementation with LPLJ markedly increased the levels of hepatic BAs and excretion of fecal BAs. Moreover, the levels of TC and TG in the liver were similar to the serum biochemical parameters, which are consistent with the current study (37). We speculated that LPLJ supplementation may promote the excretion of BAs and lower the lipid level in serum and accumulation in the liver.

To further investigate the regulatory mechanism of LPLJ dietary supplementation for hyperlipidaemia related to NAFLD, liver metabolomics was used in this study. The results showed that supplementation with LPLJ mainly relieved hyperlipidaemia by regulating the pathways involved in aminoacyl-tRNA biosynthesis, phenylalanine, tyrosine, and tryptophan biosynthesis, as well as those involved in phenylalanine, glutathione, and D-glutamine, and D-glutamate metabolism. It is worth noting that phenylalanine, tyrosine, and tryptophan are essential amino acids in the human body. Tyrosine, which is inversely associated with the risk of obesity, is synthesized from phenylalanine in a reaction catalyzed by phenylalanine hydroxylase, and affects the metabolism of glucose

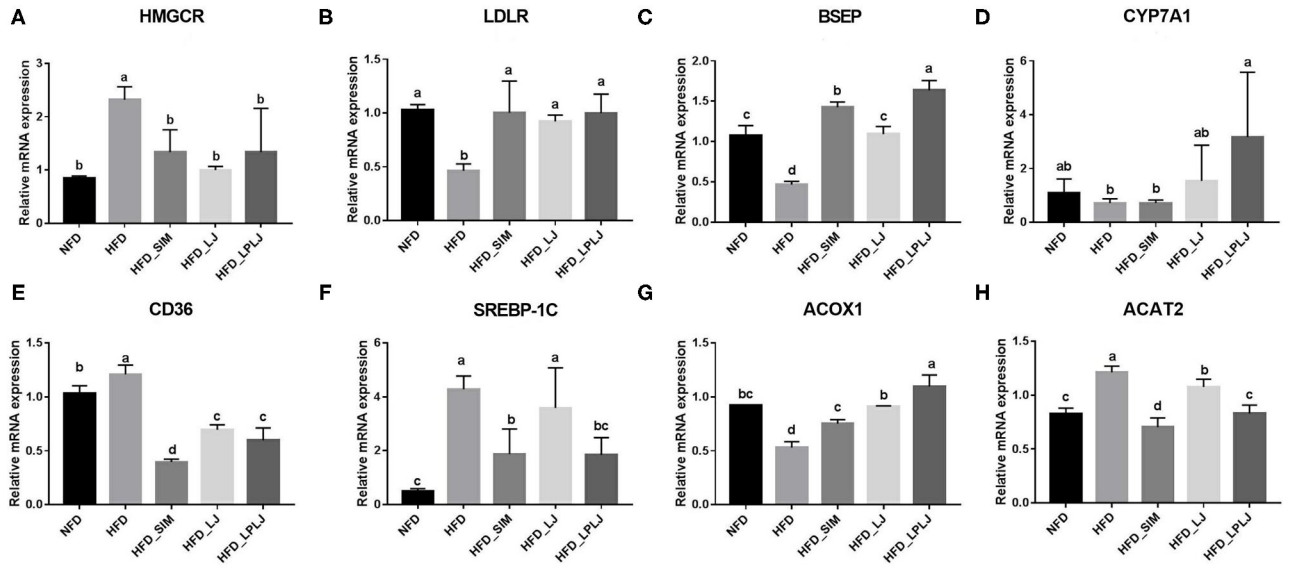

FIGURE 9 | Effects of LPLJ consumption on the expression of hepatic related genes in HFD-fed rats. The bar graphs showed mRNA levels of **(A)** HMGCR, **(B)** LDLR, **(C)** BSEP, **(D)** CYP7A1, **(E)** CD36, **(F)** SREBP-1C, **(G)** ACOX1 and **(H)** ACAT2, which were determined by RT-qPCR. a-d, Mean values with different letters in the same column differ significantly ($p < 0.05$).

and lipids in the body (38). Glutamate metabolism is important in the regulation of protein and nucleic acid biosynthesis. Glutamine is a non-essential amino acid that participates in central metabolic processes as a substrate for the tricarboxylic acid cycle (39). Petrus et al. found that glutamine reduces inflammation in adipose tissue in rats and is inversely associated with fat mass (40). Our results show that dietary supplementation with LPLJ ameliorates dyslipidaemia in hyperlipidaemic rats by affecting these metabolic pathways.

The intestinal flora has a significant influence on the treatment of hyperlipidaemia (41, 42). Previous research has shown that a variety of bioactive components in seaweeds can regulate the microecology of gut microbiota (43). High-throughput sequencing showed that compared with that in the NFD group, the relative abundance of 15 key microbial phylotypes were altered in HFD-fed rats, indicating that a gut microbial disorder occurred in HFD-induced hyperlipidaemic rats. However, supplementation with LPLJ distinctly regulated the gut microbiota in HFD-fed rats, including modulating the relative abundance of functionally related microbial system types. Compared with that in the NFD group, the relative abundances of *Collinsella* and *Lachnoclostridium* in the HFD group significantly increased. *Collinsella* is associated with obesity and atherosclerosis in human studies (44–46). Another study has shown that the relative abundance of *Collinsella* is significantly elevated in patients with non-alcoholic steatohepatitis (47). In addition, it has been reported that *Lachnoclostridium* is significantly positively associated with TGs and TC (48). However, dietary supplementation with LPLJ reversed the abnormal elevation of the relative abundance of *Collinsella* and *Lachnoclostridium*. In the current study, we speculated that compared with that in the HFD group, the abundance of *Collinsella* and *Lachnoclostridium* increased in the LPLJ group to exert lipid-lowering effects. Notably, the relative abundance of *Akkermansia* and *unclassified _f_Erysipelotrichaceae* was dramatically increased by dietary supplementation with LPLJ. As the most abundant probiotic member of the human gut, the abundance of *Akkermansia* is negatively correlated with obesity (49). Growing evidence shows that *Akkermansia* can ameliorate intestinal dysbiosis caused by HFD (50). A previous study has shown that the relative abundance of *unclassified _f_Erysipelotrichaceae* could also be increased to reduce abnormal lipid metabolism (51). These results suggest that this is one of the mechanisms by which LPLJ regulates hyperlipidaemia. Correlation analysis results using heat map and network showed that the types of intestinal microbial systems are closely correlated with lipid metabolism parameters. Supplementation with LPLJ decreased the relative abundance of *Corynebacterium_1*, *Jeotgalcoccus*, and *Atopostipes*, and exhibited negative relationships with fecal TG, TC, and TBA levels and the metabolism of SCFAs, but was positively associated with serum TC, TG, TBA, and NEFA levels, hepatic TG, TC, TBA, and FAT levels, body weight gain, and epididymal fat index. This association is thought to be related to effects on the lipid metabolism and the diet of the host. These results showed that dietary supplementation with LPLJ can improve the intestinal microbiota disturbance caused by the HFD, thereby alleviating obesity and lipid abnormalities in the liver.

Moreover, the expression of mRNA genes related to adipogenesis, fatty acid oxidation, and BA production was analyzed to evaluate the effect of LPLJ intervention on cholesterol and lipid metabolism. Compared with the NFD group, HFD feeding markedly increased mRNA levels of liver genes encoding HMGCR, CD36, SREBP-1c, and ACAT2,

whereas LPLJ intervention significantly lowered these abnormal transcription levels. Among them, SREBP-1c plays a significant role in adjusting the expression of adipogenic genes involved in liver fatty acid synthesis (52). CD36 plays an important role in transmembrane transport and energy metabolism of long-chain fatty acids (53). Previous experiments have indicated that ACAT2 inhibits TG synthesis by decreasing the transition of esterified cholesterol to cholesterol ester, which is consistent with the results of the current study that dietary supplementation with LPLJ notably reduced the level of ACAT2 in the liver (54). The present study also found that HFD increased the level of TC in the liver by increasing HMGCR expression, and these findings were consistent with those of a previous study (55). However, HMGCR expression was significantly reduced after dietary supplementation with LPLJ. Conversely, the mRNA levels of LDLR, BSEP, CYP7A1, and ACOX1 in rats of the HFD group were lower than those in rats in the NFD group. Supplementation with LPLJ remarkably increased the expression of LDLR, BSEP, CYP7A1, and ACOX1. Notably, the expression of BA synthetic genes, such as CYP7A1, was significantly increased, and that of BSEP, a transporter of BAs, was also increased, which was consistent with Kwon's findings (56). In addition, ACOX1 is involved in the β-oxidative activation of fatty acids (57). BA, an endogenous signaling molecule synthesized by liver cholesterol, affects insulin secretion and the regulation of glucose and lipid metabolism. The results of this study show that dietary supplementation with LPLJ significantly upregulated the mRNA levels of genes related to BA homeostasis and decreased hepatic BA levels that were increased by HFD.

In conclusion, we found that dietary supplementation with LPLJ has the potential to modulate hyperlipidaemia in HFD-fed rats, by reducing serum and liver lipid levels, as well as higher fecal lipid and SCFA levels. In addition, the regulatory effect of LPLJ intervention on hyperlipidaemia may be related to the significant changes in liver metabolites, genes related to liver lipid metabolism, and intestinal microbiota. However, this study was limited by the lack of a group with HFD and *L. plantarum FZU3013* supplementation. Thus, further research is required to identify the functional components of LPLJ that are essential for regulating lipid metabolism.

DATA AVAILABILITY STATEMENT

The original contributions presented in the study are included in the article/supplementary material, further inquiries can be directed to the corresponding authors.

ETHICS STATEMENT

The animal study was reviewed and approved by Institutional Animal Care and Use Committee of College of Food Science, Fujian Agriculture and Forestry University.

AUTHOR CONTRIBUTIONS

J-PH, W-JC, and PL contributed to conception and design of the study. T-TZ, B-FZ, and M-LW performed the statistical analysis. J-PH wrote the first draft of the manuscript. T-TZ, B-FZ, RS, YZ, and L-JC wrote sections of the manuscript. All authors contributed to manuscript revision, read, and approved the submitted version.

FUNDING

This study was supported by the Innovative Scientific Research Program of Fujian Agriculture and Forestry University (Grant nos. CXZX2018066 and CXZX2017017).

REFERENCES

1. Teng Y, Wang Y, Tian Y, Chen Y-y, Guan W-y, Piao C-h, et al. Lactobacillus plantarum LP104 ameliorates hyperlipidemia induced by AMPK pathways in C57BL/6N mice fed high-fat diet. *J Funct Foods.* (2020) 64:103665. doi: 10.1016/j.jff.2019.103665
2. Ascha MS, Hanouneh IA, Lopez R, Tamimi TA-R, Feldstein AF, Zein NN. The incidence and risk factors of hepatocellular carcinoma in patients with Nonalcoholic steatohepatitis. *Hepatology.* (2010) 51:1972–8. doi: 10.1002/hep.23527
3. Coilly A, Desterke C, Guettier C, Samuel D, Chiappini F. FABP4 and MMP9 levels identified as predictive factors for poor prognosis in patients with nonalcoholic fatty liver using data mining approaches and gene expression analysis. *Sci Rep.* (2019) 9:19785. doi: 10.1038/s41598-019-56235-y
4. Davidson MH. Cardiovascular risk factors in a patient with diabetes mellitus and coronary artery disease: therapeutic approaches to improve outcomes: perspectives of a preventive cardiologist. *Am J Cardiol.* (2012) 110:43B—9B. doi: 10.1016/j.amjcard.2012.08.033
5. Zhang Q, Fan X, Ye R, Hu Y, Zheng T, Shi R, et al. The effect of simvastatin on gut microbiota and lipid metabolism in hyperlipidemic rats induced by a high-fat diet. *Front Pharmacol.* (2020) 11:522. doi: 10.3389/fphar.2020.00522
6. Zhang Q, Fan X-Y, Cao Y-J, Zheng T-T, Cheng W-J, Chen L-J, et al. The beneficial effects of Lactobacillus brevis FZU0713-fermented Laminaria japonica on lipid metabolism and intestinal microbiota in hyperlipidemic rats fed with a high-fat diet. *Food Funct.* (2021) 12:7145–60. doi: 10.1039/d1fo00218j
7. Catarino MD, Silva AMS, Cardoso SM. Phycochemical Constituents and Biological Activities of Fucus spp. *Mar Drugs.* (2018) 16:249. doi: 10.3390/md16080249
8. Peng F-H, Zha X-Q, Cui S-H, Asghar M-N, Pan L-H, Wang J-H, et al. Purification, structure features and anti-atherosclerosis activity of a Laminaria japonica polysaccharide. *Int J Biol Macromol.* (2015) 81:926–35. doi: 10.1016/j.ijbiomac.2015.09.027
9. Lopez-Santamarina A, Miranda JM, del Carmen Mondragon A, Lamas A, Cardelle-Cobas A, Manuel Franco C, et al. Potential Use of Marine Seaweeds as Prebiotics: A Review. *Molecules.* (2020) 25:1004. doi: 10.3390/molecules25041004
10. Gao J, Lin L, Chen Z, Cai Y, Xiao C, Zhou F, et al. In vitro digestion and fermentation of three polysaccharide fractions from laminaria japonica and their impact on lipid metabolism-associated human gut microbiota. *J Agric Food Chem.* (2019) 67:7496–505. doi: 10.1021/acs.jafc.9b00970
11. Chen M, Guo W-L, Li Q-Y, Xu J-X, Cao Y-J, Liu B, et al. The protective mechanism ofLactobacillus plantarumFZU3013 against non-alcoholic fatty liver associated with hyperlipidemia in mice fed a high-fat diet. *Food Funct.* (2020) 11:3316–31. doi: 10.1039/c9fo03003d
12. Huang Q, Yin P, Wang J, Chen J, Kong H, Lu X, et al. Method for liver tissue metabolic profiling study and its application in type 2 diabetic rats based on ultra performance liquid chromatography-mass

spectrometry. *J Chromatogr B Analyt Technol Biomed Life Sci.* (2011) 879:961–7. doi: 10.1016/j.jchromb.2011.03.009
13. Zhao H, Luo Ye, Wu Z, Zhou Y, Guo D, Wang H, et al. Hepatic lipid metabolism and oxidative stress responses of grass carp (Ctenopharyngodon idella) fed diets of two different lipid levels against Aeromonas hydrophila infection. *Aquaculture.* (2019) 509:149–58. doi: 10.1016/j.aquaculture.2019.05.029
14. Schaefer A, von Toerne C, Becker S, Sarioglu H, Neschen S, Kahle M, et al. Two-dimensional peptide separation improving sensitivity of selected reaction monitoring-based quantitative proteomics in mouse liver tissue: comparing off-gel electrophoresis and strong cation exchange chromatography. *Anal Chem.* (2012) 84:8853–62. doi: 10.1021/ac3023026
15. Nagano T, Katase M, Tsumura K. Inhibitory effects of dietary soy isoflavone and gut microbiota on contact hypersensitivity in mice. *Food Chem.* (2019) 272:33–8. doi: 10.1016/j.foodchem.2018.08.043
16. Castro-Penalonga M, Roca-Saavedra P, Manuel Miranda J, Julio Porto-Arias J, Nebot C, Cardelle-Cobas A, et al. Influence of food consumption patterns and Galician lifestyle on human gut microbiota. *J Physiol Biochem.* (2018) 74:85–92. doi: 10.1007/s13105-017-0570-4
17. Slykerman RF, Kang J, Van Zyl N, Barthow C, Wickens K, Stanley T, et al. Effect of early probiotic supplementation on childhood cognition, behaviour and mood a randomised, placebo-controlled trial. *Acta Paediatr.* (2018) 107:2172–8. doi: 10.1111/apa.14590
18. Stark CM, Susi A, Nylund C. Antibiotic and acid suppression medications during infancy are associated with early childhood obesity. *Pediatrics.* (2018) 141. doi: 10.1542/peds.141.1_MeetingAbstract.742
19. Gao R, Zhu C, Li H, Yin M, Pan C, Huang L, et al. Dysbiosis signatures of gut microbiota along the sequence from healthy, young patients to those with overweight and obesity. *Obesity.* (2018) 26:351–61. doi: 10.1002/oby.22088
20. Shen S, Liao Q, Huang L, Li D, Zhang Q, Wang Y, et al. Water soluble fraction from ethanolic extract of Clausena lansium seeds alleviates obesity and insulin resistance, and changes the composition of gut microbiota in high-fat diet-fed mice. *J Funct Foods.* (2018) 47:192–9. doi: 10.1016/j.jff.2018.05.057
21. Lv X-C, Guo W-L, Li L, Yu X-D, Liu B. Polysaccharide peptides from Ganoderma lucidum ameliorate lipid metabolic disorders and gut microbiota dysbiosis in high-fat diet-fed rats. *J Funct Foods.* (2019) 57:48–58. doi: 10.1016/j.jff.2019.03.043
22. Moreira GV, Azevedo FF, Ribeiro LM, Santos A, Guadagnini D, Gama P, et al. Liraglutide modulates gut microbiota and reduces NAFLD in obese mice. *J Nutr Biochem.* (2018) 62:143–54. doi: 10.1016/j.jnutbio.2018.07.009
23. Noorbakhsh H, Yavarmanesh M, Mortazavi SA, Adibi P, Moazzami AA. Metabolomics analysis revealed metabolic changes in patients with diarrhea-predominant irritable bowel syndrome and metabolic responses to a synbiotic yogurt intervention. *Eur J Nutr.* (2019) 58:3109–19. doi: 10.1007/s00394-018-1855-2
24. Lei F, Gao D, Zhang X, Xu J, Xu M-J. *In Vivo* Metabolism Study of Xiamenmycin A in Mouse Plasma by UPLC-QTOF-MS and LC-MS/MS. *Mar Drugs.* (2015) 13:727–40. doi: 10.3390/md13020727
25. Liu Y-C, Zhu H, Shakya S, Wu J-W. Metabolic profile and pharmacokinetics of polyphyllin I, an anticancer candidate, in rats by UPLC-QTOF-MS/MS and LC-TQ-MS/MS. *Biomed Chromatograp.* (2017) 31:e3817. doi: 10.1002/bmc.3817
26. Lv X-C, Huang R-L, Chen F, Zhang W, Rao P-F, Ni L. Bacterial community dynamics during the traditional brewing of Wuyi Hong Qu glutinous rice wine as determined by culture-independent methods. *Food Control.* (2013) 34:300–6. doi: 10.1016/j.foodcont.2013.05.003
27. Gupta S, Abu-Ghannam N, Scannell AGM. Growth and kinetics of Lactobacillus plantarum in the fermentation of edible Irish brown seaweeds. *Food And Bioproducts Processing.* (2011) 89:346–55. doi: 10.1016/j.fbp.2010.10.001
28. Guo W-L, Pan Y-Y, Li L, Li T-T, Liu B, Lv X-C. Ethanol extract of Ganoderma lucidum ameliorates lipid metabolic disorders and modulates the gut microbiota composition in high-fat diet fed rats. *Food Funct.* (2018) 9:3419–31. doi: 10.1039/c8fo00836a
29. Zhang LH, Xiu X, Wang ZR, Jiang YN, Fan H, Su J, et al. Increasing Long-Chain Dicarboxylic Acid Production in Candida tropicalis by Engineering Fatty Transporters. *Mol Biotechnol.* (2021) 63:544–55. doi: 10.1007/s12033-021-00319-6
30. Porez G, Prawitt J, Gross B, Staels B. Bile acid receptors as targets for the treatment of dyslipidemia and cardiovascular disease. *J Lipid Res.* (2012) 53:1723–37. doi: 10.1194/jlr.R024794
31. Zhang YP, Zhao NN, Yang LH, Hong Z, Cai B, Le QQ, et al. Insoluble dietary fiber derived from brown seaweed Laminaria japonica ameliorate obesity-related features via modulating gut microbiota dysbiosis in high-fat diet-fed mice. *Food Funct.* (2021) 12:587–601. doi: 10.1039/d0fo02380a
32. Shirosaki M, Koyama T. Laminaria japonica as a food for the prevention of obesity and diabetes. *Adv Food Nutr Res.* (2011) 64:199–212. doi: 10.1016/B978-0-12-387669-0.00015-6
33. Ji Y, Park S, Park H, Hwang E, Shin H, Pot B, et al. Modulation of active gut microbiota by Lactobacillus rhamnosus gg in a diet induced obesity murine model. *Front Microbiol.* (2018) 9:710. doi: 10.3389/fmicb.2018.00710
34. Yadav R, Khan SH, Mada SB, Meena S, Kapila R, Kapila S. Consumption of probiotic lactobacillus fermentum mtcc: 5898-fermented milk attenuates dyslipidemia, oxidative stress, and inflammation in male rats fed on cholesterol-enriched diet. *Probiotics Antimicrob Proteins.* (2019) 11:509–18. doi: 10.1007/s12602-018-9429-4
35. Li T-T, Tong A-J, Liu Y-Y, Huang Z-R, Wan X-Z, Pan Y-Y, et al. Polyunsaturated fatty acids from microalgae Spirulina platensis modulates lipid metabolism disorders and gut microbiota in high-fat diet rats. *Food and Chemical Toxicology.* (2019) 131:110558. doi: 10.1016/j.fct.2019.06.005
36. Hosomi R, Fukunaga K, Arai H, Kanda S, Nishiyama T, Yoshida M. Fish protein decreases serum cholesterol in rats by inhibition of cholesterol and bile acid absorption. *J Food Sci.* (2011) 76:H116–H21. doi: 10.1111/j.1750-3841.2011.02130.x
37. Lin H, An Y, Tang H, Wang Y. Alterations of bile acids and gut microbiota in obesity induced by high fat diet in rat model. *J Agric Food Chem.* (2019) 67:3624–32. doi: 10.1021/acs.jafc.9b00249
38. Okekunle AP, Wu X, Feng R, Li Y, Sun C. Higher intakes of energy-adjusted dietary amino acids are inversely associated with obesity risk. *Amino Acids.* (2019) 51:373–82. doi: 10.1007/s00726-018-2672-x
39. Yelamanchi SD, Jayaram S, Thomas JK, Gundimeda S, Khan AA, Singhal A, et al. A pathway map of glutamate metabolism. *J Cell Commun Signal.* (2016) 10:69–75. doi: 10.1007/s12079-015-0315-5
40. Petrus P, Lecoutre S, Dollet L, Wiel C, Sulen A, Gao H, et al. Glutamine Links Obesity to Inflammation in Human White Adipose Tissue. *Cell Metabolism.* (2020) 31:375. doi: 10.1016/j.cmet.2019.11.019
41. Singh V, Yeoh BS, Chassaing B, Xiao X, Saha P, Olvera RA, et al. Dysregulated microbial fermentation of soluble fiber induces cholestatic liver cancer. *Cell.* (2018) 175:679. doi: 10.1016/j.cell.2018.09.004
42. Rath S, Rud T, Karch A, Pieper DH, Vital M. Pathogenic functions of host microbiota. *Microbiome.* (2018) 6:174. doi: 10.1186/s40168-018-0542-0
43. Penalver R, Lorenzo JM, Ros G, Amarowicz R, Pateiro M, Nieto G. Seaweeds as a functional ingredient for a healthy diet. *Mar Drugs.* (2020) 18:301. doi: 10.3390/md18060301
44. Gomez-Arango LF, Barrett HL, Wilkinson SA, Callaway LK, McIntyre HD, Morrison M, et al. Low dietary fiber intake increases Collinsella abundance in the gut microbiota of overweight and obese pregnant women. *Gut Microbes.* (2018) 9:189–201. doi: 10.1080/19490976.2017.1406584
45. Karlsson FH, Fak F, Nookaew I, Tremaroli V, Fagerberg B, Petranovic D, et al. Symptomatic atherosclerosis is associated with an altered gut metagenome. *Nat Commun.* (2012) 3:1245. doi: 10.1038/ncomms2266
46. Kourosh A, Luna RA, Balderas M, Nance C, Anagnostou A, Devaraj S, et al. Fecal microbiome signatures are different in food-allergic children compared to siblings and healthy children. *Pediatric Allergy and Immunology.* (2018) 29:545–54. doi: 10.1111/pai.12904
47. Astbury S, Atallah E, Vijay A, Aithal GP, Grove JI, Valdes AM. Lower gut microbiome diversity and higher abundance of proinflammatory genus Collinsella are associated with biopsy-proven nonalcoholic steatohepatitis. *Gut Microbes.* (2020) 11:569–80. doi: 10.1080/19490976.2019.1681861
48. Tang W, Yao X, Xia F, Yang M, Chen Z, Zhou B, et al. Modulation of the Gut Microbiota in Rats by Hugan Qingzhi Tablets during the Treatment of High-Fat-Diet-Induced Nonalcoholic Fatty Liver Disease. *Oxid Med Cell Longev.* (2018) 2018:7261619. doi: 10.1155/2018/7261619
49. He K, Hu Y, Ma H, Zou Z, Xiao Y, Yang Y, et al. Rhizoma Coptidis alkaloids alleviate hyperlipidemia in B6 mice by modulating gut

microbiota and bile acid pathways. *Biochim Biophys Acta.* (2016) 1862:1696–709. doi: 10.1016/j.bbadis.2016.06.006
50. Delzenne NM, Neyrinck AM, Cani PD. Modulation of the gut microbiota by nutrients with prebiotic properties: consequences for host health in the context of obesity and metabolic syndrome. *Microb Cell Fact.* (2011) 10:S10. doi: 10.1186/1475-2859-10-s1-s10
51. Chen G, Xie M, Wan P, Chen D, Dai Z, Ye H, et al. Fuzhuan brick tea polysaccharides attenuate metabolic syndrome in high-fat diet induced mice in association with modulation in the gut microbiota. *J Agric Food Chem.* (2018) 66:2783–95. doi: 10.1021/acs.jafc.8b00296
52. Coburn CT, Hajri T, Ibrahimi A, Abumrad NA. Role of CD36 in membrane transport and utilization of long-chain fatty acids by different tissues. *J Molecular Neurosci.* (2001) 16:117–21. doi: 10.1385/jmn:16:2-3:117
53. Howell GE. III, Kondakala S, Holdridge J, Lee JH, Ross MK. Inhibition of cholinergic and non-cholinergic targets following subacute exposure to chlorpyrifos in normal and high fat fed male C57BL/6J mice. *Food and Chemical Toxicology.* (2018) 118:821–9. doi: 10.1016/j.fct.2018.06.051
54. Vergara-Jimenez M, Conde K, Erickson SK, Fernandez ML. Hypolipidemic mechanisms of pectin and psyllium in guinea pigs fed high fat-sucrose diets: alterations on hepatic cholesterol metabolism. *J Lipid Res.* (1998) 39:1455–65. doi: 10.1016/S0022-2275(20)32527-X
55. Chiu C-Y, Chang T-C, Liu S-H, Chiang M-T. The regulatory effects of fish oil and chitosan on hepatic lipogenic signals in high-fat diet-induced obese rats. *Journal of Food and Drug Analysis.* (2017) 25:919–30. doi: 10.1016/j.jfda.2016.11.015
56. Kwon J, Kim B, Lee C, Joung H, Kim B-K, Choi IS, et al. Comprehensive amelioration of high-fat diet-induced metabolic dysfunctions through activation of the PGC-1 alpha pathway by probiotics treatment in mice. *PLoS One.* (2020) 15:e0228932. doi: 10.1371/journal.pone.0228932
57. Guo W-L, Chen M, Pan W-L, Zhang Q, Xu J-X, Lin Y-C, et al. Hypoglycemic and hypolipidemic mechanism of organic chromium derived from chelation of Grifola frondosa polysaccharide-chromium (III) and its modulation of intestinal microflora in high fat-diet and STZ-induced diabetic mice. *Int J Biol Macromol.* (2020) 145:1208–18. doi: 10.1016/j.ijbiomac.2019.09.206

Conflict of Interest: The authors declare that the research was conducted in the absence of any commercial or financial relationships that could be construed as a potential conflict of interest.

Publisher's Note: All claims expressed in this article are solely those of the authors and do not necessarily represent those of their affiliated organizations, or those of the publisher, the editors and the reviewers. Any product that may be evaluated in this article, or claim that may be made by its manufacturer, is not guaranteed or endorsed by the publisher.

frontiers in Nutrition

ORIGINAL RESEARCH
published: 24 December 2021
doi: 10.3389/fnut.2021.798273

Hepatoprotective Effect of Cereal Vinegar Sediment in Acute Liver Injury Mice and Its Influence on Gut Microbiota

*Qijie Guan[1,2], Tingting Gong[3], Zhen-Ming Lu[2,4], Yan Geng[3], Wenhui Duan[3], Yi-Lin Ren[3,5], Xiao-Juan Zhang[2,4], Li-Juan Chai[2,4], Jin-Song Shi[3] and Zheng-Hong Xu[1,2,4]**

[1] Key Laboratory of Industrial Biotechnology, Ministry of Education, Jiangnan University, Wuxi, China, [2] National Engineering Laboratory for Cereal Fermentation Technology, Jiangnan University, Wuxi, China, [3] School of Pharmaceutical Science, Jiangnan University, Wuxi, China, [4] Jiangsu Engineering Research Center for Bioactive Products Processing Technology, Jiangnan University, Wuxi, China, [5] Department of Gastroenterology, Affiliated Hospital of Jiangnan University, Wuxi, China

OPEN ACCESS

Edited by:
Xiudong Xia, Jiangsu Academy of Agricultural Sciences (JAAS), China

Reviewed by:
Ling Lu, Nanjing Normal University, China
Sui Kiat Chang, South China Botanical Garden, Chinese Academy of Sciences (CAS), China

***Correspondence:**
Zheng-Hong Xu
zhenghxu@jiangnan.edu.cn

Specialty section:
This article was submitted to Food Chemistry, a section of the journal Frontiers in Nutrition

Received: *19 October 2021*
Accepted: *29 November 2021*
Published: *24 December 2021*

Citation:
Guan Q, Gong T, Lu Z-M, Geng Y, Duan W, Ren Y-L, Zhang X-J, Chai L-J, Shi J-S and Xu Z-H (2021) Hepatoprotective Effect of Cereal Vinegar Sediment in Acute Liver Injury Mice and Its Influence on Gut Microbiota. Front. Nutr. 8:798273. doi: 10.3389/fnut.2021.798273

Cereal vinegar sediment (CVS) is a natural precipitate formed during the aging process of traditional grain vinegar. It has been used as Chinese traditional medicine, while its composition and function are reported minimally. In this study, we measured CVS in terms of saccharide, protein, fat and water content, and polyphenol and flavonoid content. Furthermore, we determined the amino acids, organic acids, and other soluble metabolites in CVS using reverse-phase high-performance liquid chromatography (RP-HPLC), HPLC, and liquid chromatography with tandem mass spectrometry (LC-MS/MS) platforms. The hepatoprotective effect of CVS was evaluated in acute CCl_4-induced liver injury mice. Administration of CVS for 7 days prior to the CCl_4 treatment can significantly decrease liver alanine aminotransferase (ALT) and aspartate aminotransferase (AST) levels and reactive oxygen species (ROS) levels, compared with those in the hepatic injury model group. The gut microbiota was changed by CCl_4 administration and was partly shifted by the pretreatment of CVS, particularly the Muribaculaceae family, which was increased in CVS-treated groups compared with that in the CCl_4 administration group. Moreover, the abundances of *Alistipes* genus and Muribaculaceae family were correlated with the liver ALT, AST, and malondialdehyde (MDA) levels. Our results illustrated the composition of CVS and its hepatoprotective effect in mice, suggested that CVS could be developed as functional food to prevent acute liver injury.

Keywords: cereal vinegar sediment, composition analysis, liver injury prevention, gut microbiota, CCl_4 induced liver injury

INTRODUCTION

Cereal vinegar sediment (CVS) is a natural precipitate during the aging process of traditional solid-state fermented vinegar with grain as raw material. Vinegar sediment has reported pharmacological activities in several human diseases, including hyperlipidemia (1), hyperglycemia (2), allergic diseases (3), dermatitis (4), senile dementia (5), and osteoporosis (6). Vinegar sediment also has

several effects on the intestinal tract. Fukuyama et al. (7) found that Japanese black vinegar *Kurozu Moromi* paste inhibited the development of colon cancer in mice, but vinegar itself could not inhibit the growth of colon cancer. Shizuma et al. (8) found that vinegar had anti-colitis and anti-oxidation effects in dextran sulfate sodium-induced mice models and speculated that its amino acids and oligopeptides, and other organic substances, might be biologically active. It was also found that *Kurozu Moromi* could inhibit the growth of hepatoma cells and prolong the survival time of hepatoma mice (9). However, the research on its material basis and mechanism of liver protection is still insufficient.

Gut–liver communications play important role in liver diseases (10). The growing evidence indicates that the pathogenetic role of microbe-derived metabolites, such as trimethylamine, secondary bile acids, short-chain fatty acids, and ethanol, in the pathogenesis of the non-alcoholic fatty liver disease (NAFLD) (11), modulation of the gut microbiota may represent a new way to treat or prevent NAFLD (12). Two kinds of traditional vinegar in China, Shanxi aged vinegar and Hengshun aromatic vinegar, have hepatoprotective effects through antioxidants and regulating the blood lipid levels and inflammatory response levels (13, 14). Shanxi aged vinegar extract could modulate gut microbiota, improve intestinal homeostasis, and can be used as a novel gut microbiota manipulator against alcohol-induced liver damage (15). Moreover, monascus vinegar could reduce lipids, intestinal *Lactobacillus*, *Roseburia*, and *Lachnoclostridium*, which had a positive correlation with antioxidative parameters and a negative correlation with lipid metabolism (16). Waste vinegar residue, which was similar to CVS, was able to help modify intestinal pH value and affect the lower gut microflora (17).

However, studies aiming to illustrate the bioactive functions of vinegar and vinegar by-products are still limited. In the present study, we measured the chemical compositions in CVS and explored the hepatoprotective effect of CVS on acute liver injury in mice induced by CCl_4. These findings may illuminate the potential mechanism of CVS on intestinal microbiota and acute liver injury.

MATERIALS AND METHODS

Preparation of CVS and Chemical Analysis

The vinegar was made with a traditional solid-state fermentation method, based on Shanxi aged vinegar fermentation method (18), using sorghum as raw material in Zhangjiajie, Hunan Province, China. The total acidity of vinegar products is 6% (w/v), including 2.1% (w/v) non-volatile acid. The vinegar was naturally aged in pottery jars for 5 years. After aging, aged vinegar and its natural sediment were mixed and centrifuged with 7,500 × *g* for 20 min. The sediment was collected as CVS after the centrifugation.

Because of the lack of chemical composition in CVS, the authors applied multiple analyses to illustrate the construction of CVS. The measurements include the water content (19), the crude protein and fat content (20), total saccharide and polysaccharide content (21), total polyphenol content (22), and total flavonoid content (23).

Reverse-Phase High-Performance Liquid Chromatography Analysis

Amino acids were determined by using reverse-phase high-performance liquid chromatography (RP-HPLC) via pre-column derivatization with O-phthalaldehyde (OPA) and 9-fluorenylmethyl chloroformate (FMOC-Cl). The 17 amino acid standards for quantification included glutamic acid, proline, aspartic acid, glycine, alanine, arginine, histidine, serine, tyrosine, cysteine, valine, leucine, isoleucine, phenylalanine, threonine, lysine, and methionine.

An Agilent 1100 HPLC (NYSE: A; Agilent Technologies Inc., Palo Alto, CA, USA) and an Agilent Hypersil ODS column (5 μm, 4.0 × 250 mm) were applied for RP-HPLC analysis. A 27.6 mM sodium acetate–triethylamine–tetrahydrofuran (500:0.11:2.5, v/v/v, pH = 7.2) was used as solvent A, and an 80.9 mM sodium acetate–ethanol–acetonitrile (1:2:2, v/v/v, pH = 7.2) was used as solvent B for mobile phases at a flow rate of 1 ml/min. The elution gradient employed was as follows: 0–17 min, 8–50% B; 17–20 min, 50–100% B; 20–24 min, 100–0% B. Amino acids were detected by ultraviolet (UV) detector at 338 nm, whereas proline was detected at 262 nm.

HPLC Analysis

Ten milliliter distilled water was added to 1 g CVS, shaken fully, and centrifuged. About 5 ml supernatant, 2 ml 0.25 M potassium ferrocyanide, and 2 ml 30% (w/v) zinc sulfate were mixed and then centrifuged. The organic acids in the supernatant were analyzed by using HPLC with Waters Atlantis T3 column (5 μm, 4.6 × 250 mm; Waters Corp., Milford, MA, USA) and quantified by external standard methods. The mobile phase was 20 mM NaH_2PO_4 (pH = 2.7), flowing at a speed of 0.7 ml/min. Injection volume was 10 μl. It was detected by a UV detector at 210 nm. Seven kinds of organic acid standards were used for quantification included oxalic acid, tartaric acid, pyruvic acid, lactic acid, acetic acid, citric acid, and succinic acid.

LC-MS/MS Analysis

For each CVS replicate, 600 μl 2-chlorophenylalanine in 80% methanol was added to 100 mg CVS sample, vortexed for 30 s. After the vortex, 100 mg glass beads were added into the sample tube, the sample was ground in a tissue grinder for 90 s at 60 Hz. After ultrasonication, the sample was centrifuged at 8,000 g at 4°C for 10 min. About 300 μl supernatant was filtered through a 0.22-μm membrane, and the filtrate was collected for further analysis.

A Vanquish liquid chromatography system connected to a Q Exactive HF-X mass spectrometer (Thermo Fisher Scientific, Bremem, Germany) was used for untargeted metabolomics analysis. The metabolites were resuspended in a loading solvent and loaded onto an ACQUITY UPLC® HSS T3 (150 × 2.1 mm, 1.8 μm, Waters Corp., Milford, MA, USA) column. Gradient elution of analytes was carried out with 0.1% formic acid in water (A1) and 0.1% formic acid in acetonitrile (B1) or 5 mM ammonium formate in water (A2) and acetonitrile (B2) at a flow

rate of 0.25 ml/min. Injection of 2 μl of each sample was done after equilibration. An increasing linear gradient of solvent B (v/v) was used as follows: 0–1 min, 2% B2/B1; 1–9 min, 2–50% B2/B1; 9–12 min, 50–98% B2/B1; 12–13.5 min, 98% B2/B1; 13.5–14 min, 98–2% B2/B1; and 14–20 min, 2% B1-positive model (14–17 min, 2% B2-negative model). The analyzer was scanned over a mass range of *m/z* 81–1,000 for the full scan at a mass resolution of 60,000. Data-dependent acquisition (DDA) MS/MS experiments were performed with higher-energy collisional dissociation (HCD) scan. The MS/MS data were then searched with Human Metabolome Database (HMDB) (http://www.hmdb.ca), METLIN (http://metlin.scripps.edu), Massbank (http://www.massbank.jp), LipidMaps (http://www.lipidmaps.org), and mzClound (https://www.mzcloud.org) for metabolites identification.

Animals and Treatments

Male Balb/c mice (6–8 weeks old) were purchased from Shanghai SLAC Laboratory Animal Co. Ltd., Shanghai, China. The animals were kept under specific-pathogen-free (SPF) conditions at 20–26°C and 40–70% relative humidity and acclimated for 1 week prior to use. Feed pellets and sterile water were provided for cafeteria feeding. All mice procedures and protocols were approved by the Institutional Animal Care and Use Committee of Jiangnan University, Wuxi, China [Approval No. JN. No 20170329-20170515 (24)]. Sixty mice were divided randomly into seven groups: normal control group (CTL), low-dose CVS treated group (CVSL), hepatic injury model group (CTC), high-dose CVS-treated hepatic injury group (CTC.CVSH), low-dose CVS-treated hepatic injury group (CTC.CVSL), vinegar-treated hepatic injury group (CTC.CV), and silymarin-treated hepatic injury group (CTC.SIL). Feeding was continued for 14 days. For each group, mice were equally divided into two cages at the beginning of the experiment, the concrete treatment was shown in **Figure 1**. About 1.4 g/kg dose of CVS was determined as high-dose CVS and 0.7 g/kg dose of CVS was determined as low-dose CVS according to the Kurozu dose (25) combined with our preliminary results (26). The CCl_4-induced hepatic injury model was based on Taniguchi et al. (27); in our experiment, each hepatic injury model mouse was injected with 0.4 g/kg 40% CCl_4 olive oil solution once (**Figure 1**). All solutions for intragastric administration used 0.5% CMC as solvent.

At the end of a week, feces in the cecum were collected after a 12-h fast. Mice were weighed and anesthetized via intraperitoneal injection of 1% sodium pentobarbital. Serum samples were collected from the eyeball to determine activities of serum aspartate aminotransferase (AST) and alanine aminotransferase (ALT), and the AST and ALT were measured using the corresponding kits (Nanjing Jiancheng Bioengineering Institute, Nanjing, China). All measurements were carried out with a microplate reader (Spectra max M5; Molecular Devices, San Jose, CA, USA).

The liver tissue and spleen were immediately excised, washed in normal saline, and weighed. The liver was cut into slices, some of which were kept in buffered formalin for histopathological observation, and the remaining were used to analyze hepatic malondialdehyde (MDA), superoxide dismutase (SOD), and catalase (CAT) levels.

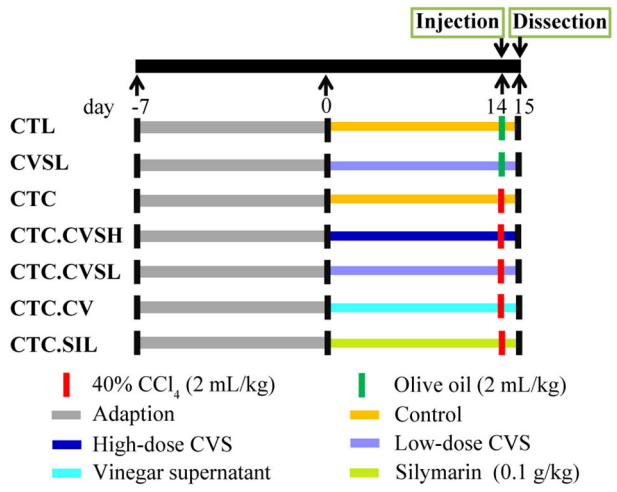

FIGURE 1 | Animal experiences design of the study on cereal vinegar sediment (CVS) hepatoprotective effect.

Determination of Liver Index and Spleen Index

The liver index of mice was calculated according to the following equation: tissue index = tissue weight (mg)/body weight (mg) × 100%.

The spleen index of mice was calculated according to the following formula: spleen index (mg/g) = spleen weight (mg)/animal body weight (mg) × 100%.

Histological Examination

For the microscopic evaluation, the parts of the liver were fixed in 10% buffered formalin, embedded in paraffin, sectioned at 4 μm, and subsequently stained with hematoxylin-eosin (H&E). The magnifications were 100 times and 200 times with at least three areas of each tissue slice observed.

Determination of Hepatic Antioxidant Index

Liver tissue was ground with a cross-paddle homogenizer, and 10% liver homogenate was prepared by adding normal saline. MDA levels along with SOD and CAT activities in the liver were measured using the corresponding kits (A001, A002, and A003; Nanjing Jiancheng Bioengineering Institute, Nanjing, China).

16S rRNA Sequencing and Analysis

Four fecal samples from each group were used for the DNA extraction using QIAamp DNA Stool Mini Kit (QIAGEN, Hilden, Germany) as directed in manual instructions. The V3 to V4 region of the bacterial 16S rRNA gene was amplified using the primers 338F (5′-barcode-ACTCCTACGGGAGGCAGCAG-3′) and 806R (5′-GGACTACHVGGGTWTCTAAT-3′). Barcodes were synthesized at the 5′ end of primer 338F to assign sequences for different samples. The PCR products were then checked by

running a 2% agarose gel, purified using the GeneJET DNA Gel Extraction Kit (Thermo Fisher Scientific, Waltham, MA, USA), and quantified using Qubit (Thermo Fisher Scientific, Waltham, MA, USA). The purified amplifications were pooled and sequenced on Ion S5^{TM}XL (Thermo Fisher Scientific, Waltham, MA, USA).

Cutadapt (28) was used for quality control and cutting of reads. The chimera sequences were detected by comparing them with a species annotation database (https://github.com/torognes/vsearch/) (29) and then removed. Uparse (30) was used for operational taxonomic unit (OTU) selection (at 97% similarity). A representative sequence was selected for each OTU and annotated with the taxonomic information in the SILVA132 SSUrRNA database (31) using Mothur. The confidence score threshold was set at 0.8, and sequences with a bootstrap value below 0.8 were assigned to an unclassified category. The resulting OTU table was further subsampled and followed by linear discriminant analysis effect size (LEfSe) analysis (32) and co-expression analysis based on the Pearson correlation coefficient (33).

Statistical Analysis

Results are expressed as means ± SD. Statistical comparisons were calculated by python 3.7 (https://www.python.org/) using the Kruskal–Wallis test. Significance presents as: $p < 0.001^{***}$, $p < 0.01^{**}$, and $p < 0.05^{*}$. There are also significant differences ($p < 0.05$) between data marked with different letters.

RESULTS

Chemical Composition of CVS

The chemical analysis of CVS was summarized in **Figure 2**. The CVS contained 65% (w/w) water and 35% (w/w) dry matter. The contents of carbohydrates, crude protein, crude fat, and others in dry matter were 66.37% (w/w), 22.28% (w/w), 0.65% (w/w), and 10.70% (w/w). The CVS dry matter mainly consisted of carbohydrates and proteins. Compared with *Kurozu Moromi* (34), the CVS we used in this study had relatively a higher protein content.

The hydrolyzed amino acid (HAA) and free amino acid (FAA) contents inside CVS were measured and listed in **Supplementary Table 1**. About 100 g of CVS contained 4.68 g HAA and 0.43 g FAA. Glutamic acid, proline, glycine, aspartic acid, and alanine were the major non-essential amino acids. Valine content was highest in essential amino acids, followed by leucine, isoleucine, phenylalanine, threonine, lysine, and methionine. Total saccharide content (12.08% w/w) and polysaccharide content (0.39% w/w) in CVS was measured separately. The composition of saccharides was determined with hydrolyzation. Saccharides in CVS mainly consisted of glucosamine, xylose, arabinose, galactose, mannose, and glucose. Seven organic acids were determined and quantified in this study, including acetic acid (5.29% w/w), citric acid (1.35% w/w), succinic acid (0.35% w/w), lactic acid (0.14% w/w), tartaric acid (0.09% w/w), pyruvic acid (0.01% w/w), and oxalic acid (0.00% w/w). In addition, total polyphenol and total flavonoid content in CVS were derived from the calibration curve. The contents of polyphenols and flavonoids in CVS were 0.40 g GAE/100 g and 0.26 g RE/100 g, respectively.

From the liquid chromatography with tandem mass spectrometry (LC-MS/MS) analysis, we detected 3,175 metabolites from CVS (**Supplementary Table 2**), in which 379 metabolites had MS_2 matching. As shown in **Table 1**, ten metabolites are having the largest peak areas in CVS including 5 acids, indicating the complexity of CVS.

Effects of CVS on CCl_4-Induced Liver Injury Mice

As shown in **Supplementary Figure 1**, after 7 days of high- and low-dose CVS, vinegar supernatant, and silymarin administrations, mice in the different groups grow similarly on body weights. After CCl_4 and fasting treatment, the body weight decreased significantly as expected.

Free radicals generated during the CCl_4 metabolism could cause liver damage. Thus, the CCl_4 administration was expected to have a profound effect on the liver index, which is the ratio of liver weight to body weight. The liver and spleen indices of the CTC group were increased significantly by 39.30 and 34.84% compared with the CTL group and by 35.71 and 11.76% compared with the CVSL group, the observation of hepatomegaly in CTC mice indicating that the CCl_4 injection could successfully cause liver injury and spleen enlargement in mice. Compared with the CTC group, the liver index in the silymarin and CVS-treated hepatic injury groups decreased by 14.11% (CTC.CVSH), 13.27% (CTC.CVSL), and 13.13% (CTC.SIL) (**Figure 3A**), indicating that the preventive feeding of CVS (both high- and low-dose) and silymarin could significantly reduce the impact of CCl_4 on the liver index. Compared with the CTC group, the spleen indexes in the CTC.CVSL, CTC.CV, and CTC.SIL groups decreased by 28.95, 15.79, and 23.68%, respectively (**Figure 3B**), indicating that the preventive feeding of low-dose CVS, vinegar supernatant, and silymarin could significantly raise the abnormal spleen index reduction caused by CCl_4 in mice. Meanwhile, the preventive feeding of high-dose CVS could only improve the abnormal spleen index to a certain extent.

Liver tissue in the CTL group appeared reddish-brown and shiny with normal lobular architecture, central veins, and radiating hepatic cords (**Figure 3C**). Meanwhile, in the CTC group, most of the normal hepatic lobules were destroyed or had disappeared. Additionally, the nucleus in the CTC group was squeezed away from the center. The CTC.CSVL and CTC.SIL groups demonstrated a preventive effect in the arrangement of hepatic lobules and nucleus location (**Figure 3C**).

CVS Pre-treatment Lowered Mice Serum ALT and AST Levels After CCl_4 Administration

Serum ALT and AST contents in the CTC group were 10.68 times and 8.96 times higher than that in the CTL group, respectively (**Figures 3D,E**), proving that CCl_4 injection could cause liver injury in mice and reduce serum transaminase levels. Compared with the CTC group, the serum ALT and AST levels

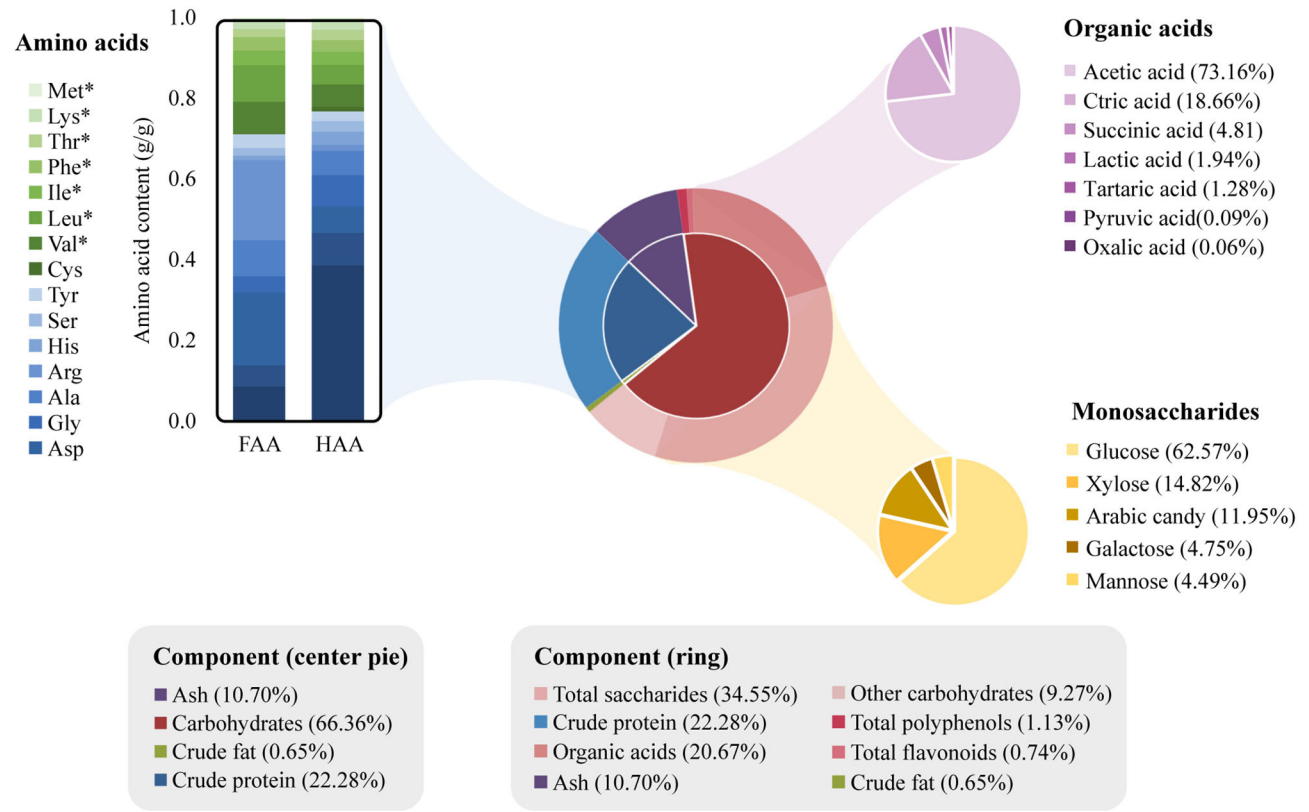

FIGURE 2 | Chemical composition of cereal vinegar sediment (CVS). The four major components of CVS are shown in the center pie chart. The outer ring shows the specific components of crude protein and carbohydrates. The amino acids, organic acids, and monosaccharide composition of total saccharides are further shown in the bar, purple pie, and golden pie charts, respectively. The amino acids marked with asterisks (*) are essential amino acids.

TABLE 1 | Top ten metabolites identified in CVS based on peak areas.

Metabolite name	Formula	Retention Time	KEGG ID	Peak area ($\times 10^9$)
2-Hydroxypyridine	C_5H_5NO	102.5745	C02502	26.17 ± 4.38
6-Hydroxyhexanoic acid	$C_6H_{12}O_3$	305.2525	C06103	20.95 ± 1.19
Succinic acid	$C_4H_6O_4$	162.4425	C00042	12.21 ± 0.95
Erucic acid	$C_{22}H_{42}O_2$	837.8375	C08316	8.32 ± 1.41
p-Coumaroylagmatine	$C_{14}H_{20}N_4O_2$	246.035	C04498	8.25 ± 2.96
Acetylcholine	$C_7H_{16}NO_2$	102.1025	C01996	6.87 ± 0.69
Linatine	$C_{10}H_{17}N_3O_5$	234.234	C05939	6.81 ± 2.33
Pyridoxal	$C_8H_9NO_3$	124.159	C00250	6.19 ± 1.67
Homocitrulline	$C_7H_{15}N_3O_3$	149.3205	C02427	6.18 ± 0.34
N-Acetyl-L-aspartic acid	$C_6H_9NO_5$	145.8805	C01042	5.47 ± 0.33

in the CTC.CVSH, CTC.CVSL, and CTC.SIL groups decreased significantly. This result indicated that the preventive feeding of CVS (both high- and low-dose) or silymarin could significantly restrain the severe increase of serum ALT and AST levels caused by the CCl_4 injection in mice.

CVS Pre-treatment Minimized Hepatic MDA, SOD, and CAT Levels Changing in CCl_4-Induced Liver Injury Mice

As shown in **Figure 3F**, compared with the CTL group, the MDA content in liver tissue of the CTC group increased by 73.02%. The change of MDA content indicated that the CCl_4 injection promoted the lipid peroxidation process leading to the accumulation of MDA in the liver. Compared with the CTC group, the hepatic MDA content in the CTC.CVSH, CTC.CVSL, and CTC.SIL groups decreased by 31.19, 28.44, and 41.28%, respectively. It could be possible that the oxidative damage of hepatocytes could be significantly prevented by feeding CVS (both high- and low-dose) and silymarin in advance.

Superoxide dismutase is one of the important antioxidant enzymes that can scavenge free radicals in the body. The CTC group has a significantly lower level of SOD compared with the CTL, CTC.CVSL, CTC.CV, and CTC.SIL groups, whereas there was no statistical difference between the CTL group and the CVSL, CTC.CVSH, CTC.CVSL, CTC.CV, and CTC.SIL groups.

As shown in **Figure 3G**, compared with CTL, the hepatic SOD activity of CTC mice decreased by 48.74%, indicating that CCl_4 significantly reduced the activity of SOD, thereby reducing the ability to eliminate free radicals in liver tissue.

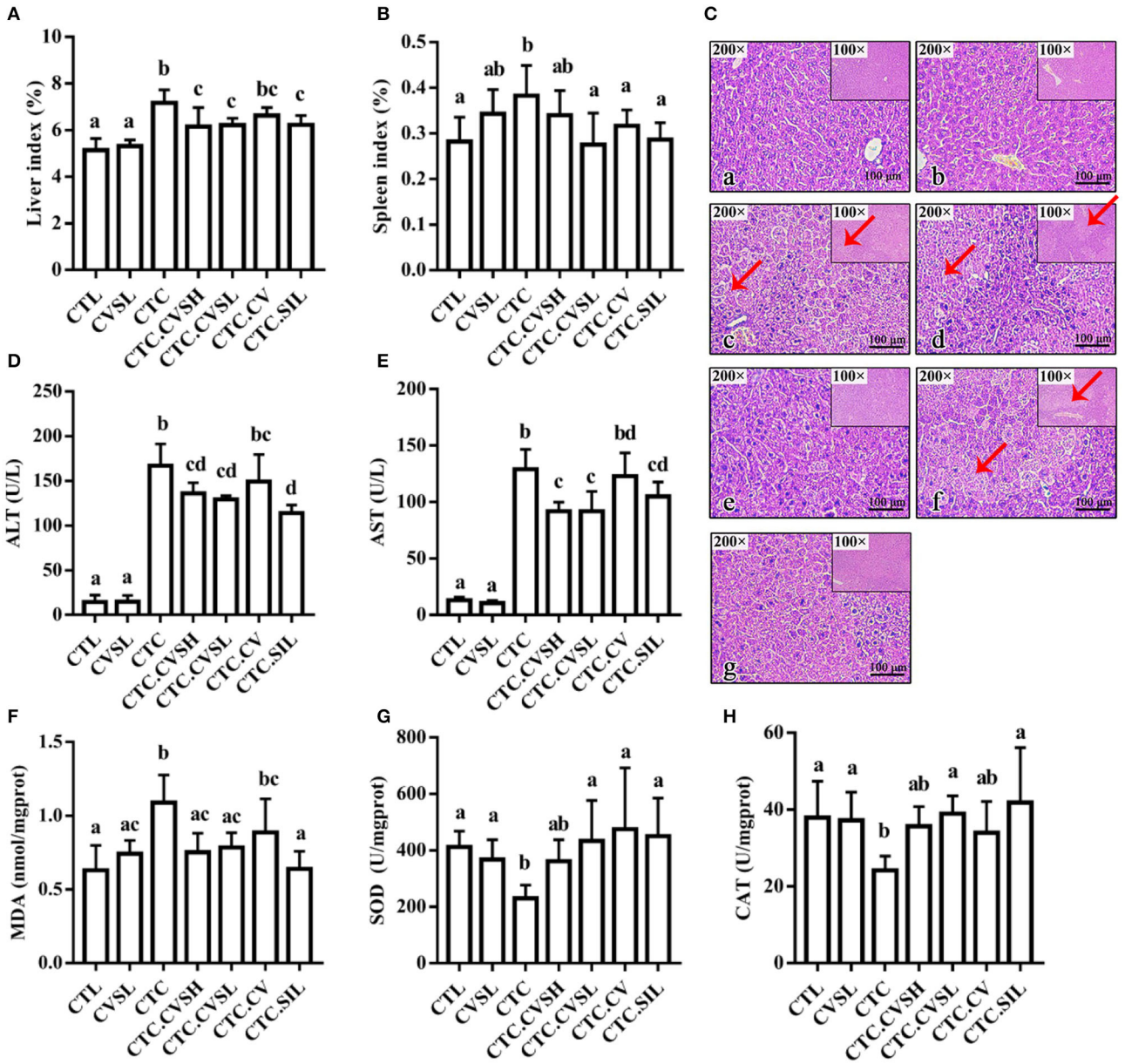

FIGURE 3 | Liver-related indicators and the histology of the H&E stained liver under different treatments. **(A)** Liver index calculated in groups; **(B)** spleen index calculated in groups; **(C)** the histology of the H&E stained liver slices in the (a) CTL, (b) CVSL, (c) CTC, (d) CTC.CVSH, (e) CTC.CVSL, (f) CTC.CV, and (g) CTC.SIL groups. Scale bar is given in the figures. Red arrow points to hepatocyte without nuclei structure; **(D)** serum ALT levels measured in the groups; **(E)** serum AST levels measured in the groups; **(F)** hepatic MDA content levels measured in the groups; **(G)** SOD activity measured in the groups; **(H)** CAT activity measured in the groups. Different letters represent a significant difference between groups calculated with the Kruskal–Wallis one-way ANOVA, and error bars represent SD. AST, aspartate aminotransferase; CTL, normal control group; CVSL, low-dose CVS treated group; CTC, hepatic injury model group; CTC.CVSH, high-dose CVS-treated hepatic injury group; CTC.CVSL, low-dose CVS-treated hepatic injury group; CTC.CV, vinegar-treated hepatic injury group; CTC.SIL, silymarin-treated hepatic injury group; MDA, malondialdehyde; SOD, superoxide dismutase.

Compared with CTC, the hepatic SOD activity of CTC.CVSL, CTC.CV, and CTC.SIL mice increased by 104.97, 124.37, and 112.88%, respectively. This result indicated that the feeding of low-dose CVS, vinegar supernatant and silymarin could significantly restrain the hepatic SOD inactivation caused by the CCl_4 injection.

Compared with CTL, the hepatic CAT activity of CTC mice decreased by 36.25% (**Figure 3H**), which indicates that the CCl_4 injection reduces the CAT activity and, thus, reduces the ability of the liver to decompose hydroxyl radicals. Compared with CTC, the hepatic CAT activity of CTC.CVSL and CTC.SIL mice increased by 58.77 and 72.95%, respectively, indicating that

feeding low-dose CVS and silymarin in advance could restrain the hepatic CAT inactivation resulting from CCl_4 and protect the stable internal environment of cells.

CVS Influenced Gut Microbiota in Mice

An average of 75,536 valid reads for 28 samples were obtained, and the effective rate of quality control was 94.76%. A total of 606 OTUs were obtained from 16s rRNA sequencing, in which 250 OTUs were annotated to genus level and 60 OTUs were annotated to species level.

The rarefaction curve of the 16s rRNA sequencing result was smooth and flat (**Supplementary Figure 2A**), and the Good's coverage index was >99.8% (**Supplementary Figure 2B**). Therefore, the sequencing depth of this study is sufficient to study the majority of bacteria in the intestinal tract with high reliability. Compared with the CTL group, Chao 1, and ACE in CTC decreased significantly. On the contrary, CVS (both high- and low-dose) and vinegar supernatant could decrease the Chao1 index and ACE index in mice with liver injury (**Supplementary Figures 2C,D**). Although only low-dose CVS could significantly decrease the Chao1 index, it is certain that vinegar sediment and vinegar supernatant could reverse the richness of intestinal microorganisms in mice with liver injury. In addition, there was no clear difference between the Shannon and Simpson indices of gut microorganisms among different groups (**Supplementary Figures 2E,F**).

Constrained principal coordinate analysis (CPCoA, **Figure 4A**) based on the Bray–Curtis distance matrix revealed that samples in the same treatment group could be well-clustered. The CVSL and CTL groups could separate from other groups in the CPCoA1 axis with 33.16% representative, whereas the CTC group could separate from the CTC.CVSH, CTC.CVSL, and CTC.CV groups in CPCoA2 axis with 19.43% representative. The CTC.CVSH, CTC.CVSL, and CTC.CV groups showed some overlap among individuals and were clustered together. This result indicated that the CCl_4 intervention changed the gut microbiota structure of mice.

At the phylum level (**Figure 4B**), *Bacteroidetes*, *Firmicutes*, and *Proteobacteria* were the dominant phyla in the gut microbial communities in all samples. At the genus level (**Supplementary Table 3**), *Helicobacter*, *unidentified_Muribaculaceae*, *Bacteroides*, *Alistipes*, *unidentified_Ruminococcaceae*, *Ruminiclostridium*, *Alloprevotella*, *unidentified_Desulfovibrionaceae*, and *unidentified_ Rhodospirillales* were detected in all samples; *unidentified_Muribaculaceae*, *Helicobacter*, *Alloprevotella,* and *Bacteroides* were the dominant genera in the gut microbial communities in all samples. According to the LEfSe analyses (**Figure 4C**, **Supplementary Figure 3**), we observed that the gut microbial community selected by the latent Dirichlet allocation (LDA) algorithm of three comparisons, CTC.CVSL vs. CTC, CTC.CVSH vs. CTC, and CTC.SIL vs. CTC had *Alphaproteobacteria* phylum in common.

Compared with the CTL group, the relative abundance of three genera (*unidentified_Clostridiales*, *Lactobacillus*, and *Anaerovorax*) in CTC mice increased significantly, whereas the relative abundance of ten genera (*Ruminiclostridium*, *Anaerotruncus*, *unidentified_Ruminococcaceae*, *Desulfovibrio, Atopostipes*, *Peptococcus*, *Sporosarcina*, *Blautia*, *Catabacter*, and *Jeotgalicoccus*) decreased significantly (**Supplementary Figure 4**). High-dose CVS could reverse the relative abundance of *Peptococcus, Lactobacillus*, and *Catabacter* of mice with liver injury. The relative abundance of *Peptococcus* is positively correlated with butyric acid (35). The relative abundance of *Parabacteroides*, *Sporosarcina*, *Staphylococcus*, *Paraprevotella*, and *Erysipelatoclostridium* in healthy mice treated with low-dose CVS was significantly decreased, and the relative abundance of *Stenotrophomonas*, *Candidatus*, and *Soleaferrea* was significantly increased (**Supplementary Figure 5**).

CVS Pre-treatment Reversed Part of Gut Microbiota Changed by CCl_4 Treatment

Compared with the CTL group, 69 OTUs (27 increased, 42 decreased) were significantly altered in the CTC group. Compared with the CTC group, 31 OTUs were significantly altered in total in the CTC.CVSH, CTC.CVSL, CTC.CV, and CTC.SIL groups. These 31 OTUs were then further analyzed (**Figure 5**) as interesting OTUs.

Among the 31 OTUs altered by CCl_4, 28 OTUs were reversed by high-dose CVS or low-dose CVS, and 10 OTUs were reversed by both high-dose CVS and low-dose CVS. Among these, only OTU153 was annotated at the genus level, namely *Alistipes*. Sulfobacin B, a lipid consisting of 18 different fatty acid chains, was found to increase in mice that were fed with a high-fat diet, only produced by *Alistipes* and *Odoribacter* (36). In addition to these 10 OTUs, only 4 OTUs reversed by high-dose CVS were identified at the species level, namely OTU96 (*Faecalibacterium prausnitzii*), OTU473 (*Mucispirillum* sp. 69), OTU187 (*Christensenella timonensis*), and OTU102 (*Blautia coccoides*), and only 3 OTUs were identified at the genus level, including OTU170 (*Mucispirillum*), OTU433 (*Staphylococcus*), and OTU21 (*Lactobacillus*).

Predicted Metabolic Functions of Gut Microbiota

Function prediction analysis of Tax4Fun (37) was implemented. Compared with the CTL group, the relative abundance of genes predicted in 36 metabolic pathways were significantly altered in the CTC group, among which glycerophospholipid metabolism, methane metabolism, tropane, piperidine and pyridine alkaloid biosynthesis, valine, leucine and isoleucine biosynthesis, and pyruvate metabolism were reversed by high-dose CVS (**Figure 6**).

The relative abundance of pentose and glucuronate interconversions was significantly reduced in normal mice fed with low-dose CVS, which were increased by CCl_4 and decreased by prevention of CVS (both low-dose and high-dose) in advance, but there was no statistical difference between CVSL and CTC.CVSL groups (**Supplementary Figure 6**).

Correlations Between Mice Microbiota Structures and Physicochemical Indexes

The degree of liver injury is positively correlated with liver and spleen indices, and ALT, AST, and MDA levels. However,

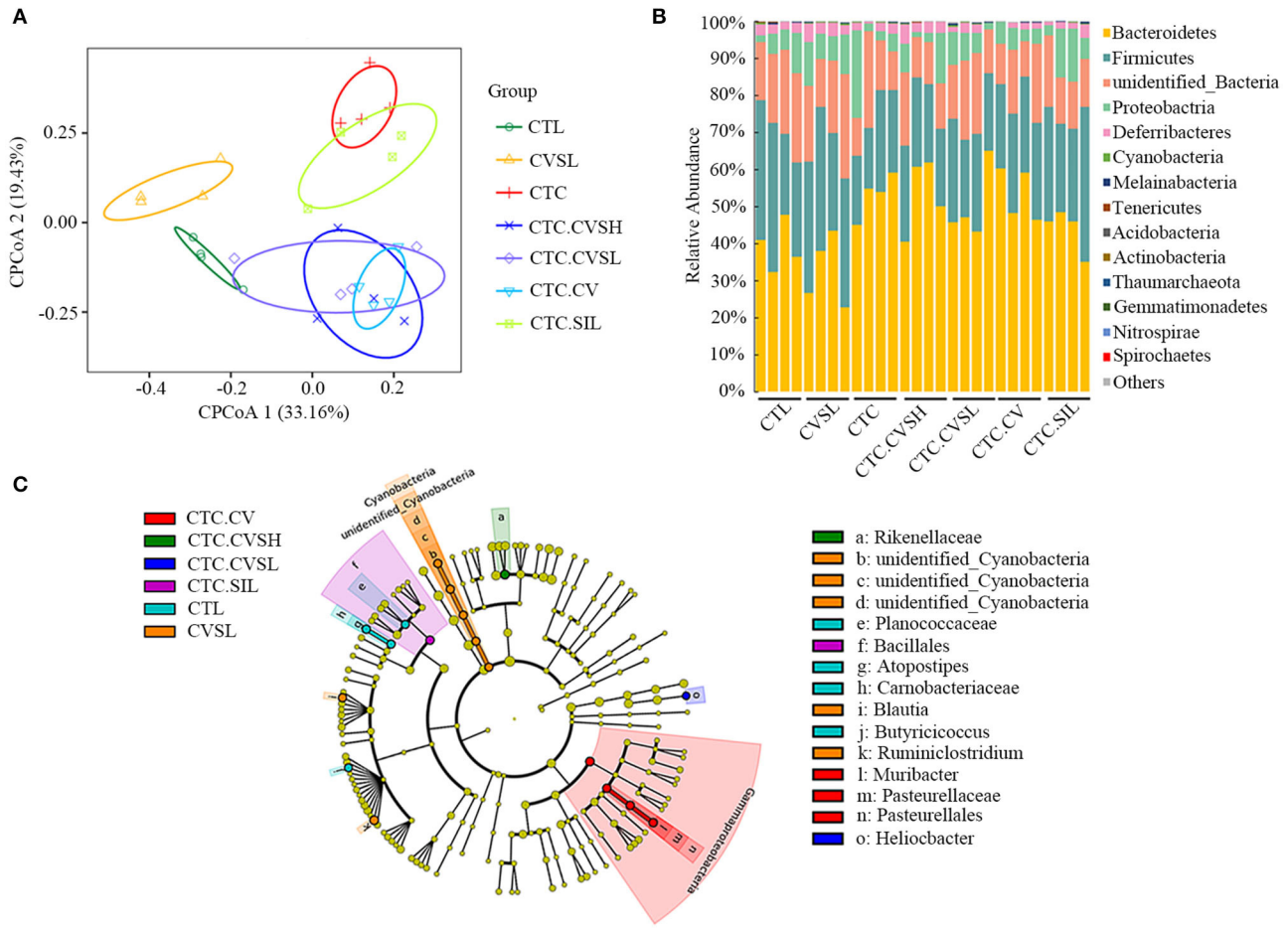

FIGURE 4 | 16s rRNA sequencing result of mice gut microbiota in different groups. **(A)** Constrained principal coordinate analysis (CPCoA) according to Bray–Curtis distance matrix was carried out to access beta diversity among the CTL group (green hollow circle), the CVSL group (yellow hollow triangle), CTC group (red line), the CTC.CVSH group (blue cross), the CTC.CVSL group (purple hollow diamond), the CTC.CV group (sky blue hollow inverted triangle), and the CTC.SIL group (light green hollow square); **(B)** bar plots showing the relative abundance and distribution of the phyla in different groups; **(C)** differential bacterial composition of the different groups based on linear discriminant analysis effect size (LEfSe) analysis. Cladogram showing different abundant taxa between samples from different groups (LDA scores > 1.5, $p < 0.1$), p, phylum; c, class; o, order; f, family; g, genus.

it is negatively correlated with CAT and SOD activities. Four OTUs, namely OTU5 (*Bacteroides*), OTU34 (*Alistipes*), OTU31 (Muribaculaceae), and OTU19 (*Bacteroides sartorii*), were positively correlated with liver and spleen indices and ALT, AST, and MDA levels. The same OTUs were also negatively correlated with CAT and SOD activities (**Figure 7**). It has been reported that the severity of NAFLD is positively correlated with Bacteroides abundance (38). OTU1 (*Helicobacter ganmani*), OTU7 (*Rhodospirillales*), and OTU289 (*Helicobacter ganmani*) were negatively correlated with liver and spleen indices and ALT, AST, and MDA levels, whereas the same OTUs were positively correlated with CAT and SOD activities.

As shown in **Supplementary Figure 7**, low-dose CVS could significantly reduce the relative abundance of OTU34 (*Alistipes*), and CVS (both high- and low-dose), vinegar supernatant, and silymarin could significantly reduce the relative abundance of OTU31 (Muribaculaceae). It was speculated that the preventive effect of low-dose CVS on liver injury might be related to OTU34 (*Alistipes*) and OTU31 (Muribaculaceae), and the preventive effects of high-dose CVS, vinegar supernatant, and silymarin on liver injury may be related to OTU31 (Muribaculaceae). So, the degree of liver injury might be positively correlated with the relative abundance of OTU34 (*Alistipes*) and OTU31 (Muribaculaceae).

DISCUSSION

Traditionally, CSV was made during the cereal vinegar aging process for years. As an insoluble mixture, a typical understanding of the formation of vinegar sediment is because of polymerizations, gravity, (bio-)chemistry reactions and evaporation of undegraded starch, protein, pectin, and cellulose (39). Our untargeted metabolomics analysis of CVS proved this understanding, *p*-coumaroylagmatine was likely carried from

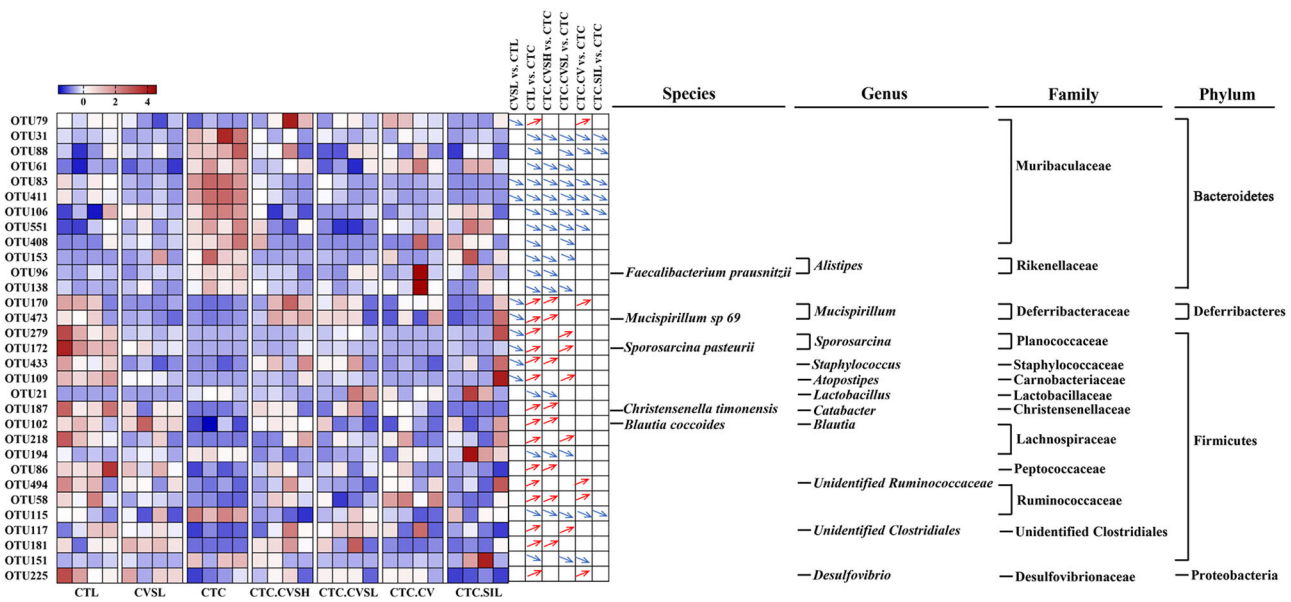

FIGURE 5 | Changes of 31 core operational taxonomic units (OTUs) among different groups. Heatmap showing the relative abundance of 31 core OTUs in each sample among different groups. Red squares represent relatively high abundances, and blue squares represent relatively low abundances. The differentiation and significance of OTU abundances between groups are shown on the right side of the heatmap. For each comparison, a blue down arrow represents the OTU decreased significantly in the front group, and a red up arrow represents the OTU increased significantly in the front group. The taxonomy of 31 core OTUs was annotated on the right side of comparisons. The significances were calculated with Kruskal–Wallis test, and $p \leq 0.05$ was considered significant.

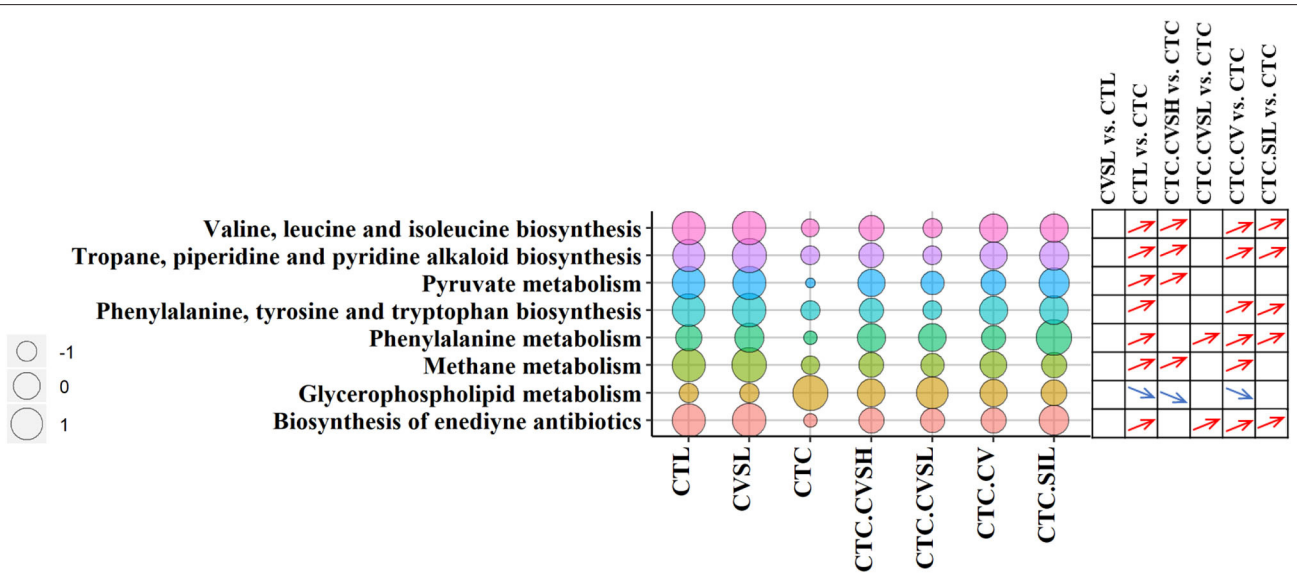

FIGURE 6 | Pathway enrichment in different groups. The bubble chart represents the pathway enrichment predicted by Tax4Fun (37) software among different groups. The size of circulars represents the operational taxonomic unit (OTU) enrichment of pathways, and the different bubble colors represent the different pathways. The differentiation and significance of pathway enrichment between groups are shown on the right side of the bubble chart. For each comparison, a blue down arrow represents the pathway enriched significantly low in the front group, and a red up arrow represents the pathway enriched significantly high in the front group. The significances were calculated with Kruskal–Wallis test, and $p \leq 0.05$ was considered significant.

barley (40). It is reported that *Bacillus subtilis* was isolated from rice vinegar sediments, and the formation of Shanxi aromatic vinegar sediment crystals was caused by supersaturation of calcium oxalate (41). In our study, there was a decoction step before the aging process in CVS production, which was aimed to kill living bacteria. Our qPCR result with amplifier 505F and 806R

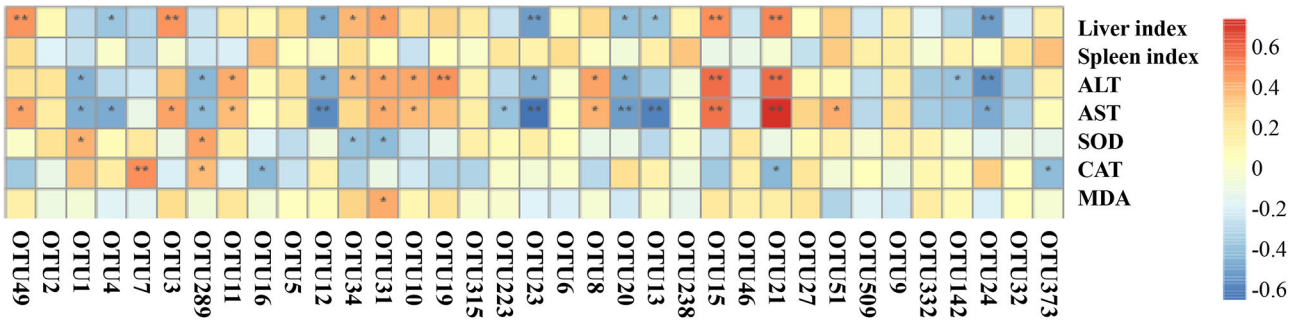

FIGURE 7 | The correlation between operational taxonomic units (OTUs) and physicochemical indices. Heatmap showing the correlations between OTUs and physicochemical indices, the correlations were calculated with Spearman's rank correlation coefficient. Warm colors represent the positive correlation between the OTU and the index, cold colors represent the negative correlation between the OTU and the index. The significances were calculated from Spearman's rank correlation coefficient. The stars represent the significance of correlations: $^{**}p < 0.01$, $^{*}p < 0.05$.

in CVS was negative, neither was Raman spectroscopic result, so there were no bacteria existed in the CVS sample.

It is reported that total polyphenols and total flavonoids were increasing during the Shanxi aged vinegar aging process (39). CVS total polyphenol and total flavonoid contents were relatively higher than Shanxi aged vinegar (42, 43). Qiu et al. (24) reported that oat vinegar showed a strong antioxidant activity than rice vinegar because oat vinegar had higher amounts of polyphenols. Nie et al. (44) demonstrated that the polyphenolic extract from apples, particularly from peels, can be explored as a chemopreventive or chemotherapeutic agent against oxidative-stress-related liver disorders. Flavonoids have been recognized as hepatoprotective compounds. Wang et al. (45) reported that flavonoids extracted from Iris plants showed inhibitory effects on CCl_4-induced rat liver fibrosis. Hu et al. (46) found that purified tartary buckwheat flavonoid fractions, containing 53.6% rutin and 37.2% quercetin, could prevent trimethylamine N-oxide (TMAO)-induced vascular dysfunction and hepatic injury.

The CVS pretreatment could statistically reduce the MDA increasing, SOD decreasing, and CAT decreasing caused by CCl_4 injection. MDA was used as a marker of oxidative stress-induced liver injury. SOD and CAT activities were used to evaluate the changes in the antioxidative system in liver tissues (47). Our results suggested that CVS pretreatment could enhance the efficiency of scavenging free radicals and decomposing hydroxyl radicals in the liver.

Interestingly, as shown in **Supplementary Figure 3**, the different features between the CTC and CTL groups, the CTC and CTC.CVSL groups, the CTC and CVSH groups, and the CTC vs. CTC.SIL groups had common ground. Alphaproteobacteria were relatively low in the CTC group, which indicated the liver injury may affect the gut Alphaproteobacteria (48). *Staphylococcus lentus* had the highest LDA score between the CTC and CTC.SIL groups, however, was not significant in neither the CTL vs. CTC, the CTC vs. CTC.CVSL nor the CTC vs. CTC.CVSH comparisons. This result indicated *Staphylococcus lentus* may respond particularly under silymarin-pretreated acute liver injury mice. Bacteroidia had significant differentiation between CTC and CTL, CTC and CTC.CVSL, and CTC and CTC.CVSH groups but had no significance between CTC and CTC.SIL groups. This result indicated the different regulations to gut microbiota of CVS and silymarin.

Alistipes is a genus that may have protective effects against some diseases, including liver fibrosis, colitis, cancer immunotherapy, and cardiovascular disease (49). According to our result, low-dose CVS intake can significantly increase the relative abundance of *Alistipes*, with CCl_4 administration significantly decreasing the relative abundance of *Alistipes*. Muribaculaceae family belongs to the Bacteroides class, contributes to propionate production, and may have a correlation with longevity enhancement (50). In our study, Muribaculaceae family OTUs significantly increased after CCl_4 administration without pretreatments. However, Muribaculaceae abundances could shift from increasing to relatively stable under either low- and high-dose CVS, or silymarin feeding. Moreover, OTU34 (*Alistipes*) and OTU31 (Muribaculaceae) showed positive correlations with liver ALT, AST levels, and a negative correlation with liver SOD levels. Although there was no direct evidence of CVS had a hepatoprotective effect through the gut–liver axis, OTU34 (*Alistipes*) and OTU31 (Muribaculaceae) were interesting findings that may play important roles in CVS intake response and hepatoprotective effects.

It has been reported that the significant increase of *Lactobacillus* is related to hepatopathy (51) and colitis (52). It is speculated that the hepatoprotective effect of high-dose CVS might be related to the relative abundance of *Lactobacillus, Anaerotruncus,* and *Peptococcus*. By contrast, low-dose CVS could only reverse the relative abundance of *Atopostipes* and *Sporosarcina* of mice with liver injury. *Atopostipes* is a gram-positive bacterium that metabolizes valine and tryptophan into short-chain fatty acids and indole and is positively correlated with phenol, indole, isobutyric acid, and isovaleric acid (53). Perhaps low-dose CVS could enhance the metabolism of valine and tryptophan in the intestine. Vinegar supernatant could significantly reverse the relative abundance of *Desulfovibrio* and *Catabacter* of mice with liver injury, and notably, the latter reversed by high-dose CVS. Silymarin could only reverse the relative abundance of *Jeotgalicoccus* of mice with liver injury.

Cereal vinegar sediment may have some effect on the intestinal mucosal barrier. Among the OTUs affected by low-dose CVS but not altered by high-dose CVS, only 1 OTU and 3 OTUs were identified at the species level and genus level, respectively, namely OTU172 (*Sporosarcina pasteurii*), OTU279 (*Sporosarcina*), OTU109 (*Atopostipes*), and OTU117 (*unidentified_Clostridiales*). A total of 36 OTUs (11 increased, 25 decreased) were altered in healthy mice fed with low-dose CVS, 2 OTUs of which were increased by CCl_4 and decreased after the intervention of CVS (both high- and low-dose), vinegar supernatant, and silymarin. The relative abundance of the 2 OTUs annotated with the Muribaculaceae family in healthy mice treated with low-dose CVS also decreased significantly.

Although the authors measured CVS with multiple methods, there are still several uncertain components inside the CVS like the structure of polysaccharides, the composition of flavonoids, and the composition of insoluble parts. The authors illustrated a potential functional use of CVS, there are several shortages in this study, for example, the number of mice used in 16S rRNA sequencing and the lack of bacteria load measurement. Further studies are needed to clarify the mechanisms of how CVS treatment influences the hepatoprotective effect.

DATA AVAILABILITY STATEMENT

The datasets presented in this study can be found in online repositories. The names of the repository/repositories and accession number(s) can be found in the article/**Supplementary Material**.

ETHICS STATEMENT

The animal study was reviewed and approved by the Institutional Animal Care and Use Committee of Jiangnan University, Wuxi, China.

AUTHOR CONTRIBUTIONS

QG: contributed to methodology, formal analysis, data curation, writing—review and editing, and visualization. TG: involved in investigation and writing original draft. Z-ML: presented conceptualization, validation, and project administration. YG: involved in supervision and methodology. WD: investigated. Y-LR: provided resources. X-JZ: performed methodology. L-JC: validated. J-SS: supervised. Z-HX: contributed to conceptualization, supervision, and funding acquisition. All authors contributed to the article and approved the submitted version.

FUNDING

This study was supported by the National Key R&D Program of China (Grant Nos. 2018YFC1603800 and 2018YFC1603802), the National Natural Science Foundation of China (Grant No. 31771967), and National First-Class Discipline Program of Light Industry Technology and Engineering (Grant No. LITE2018-11).

ACKNOWLEDGMENTS

The authors thank Ms. Theresa M. Kelley from the University of Texas Medical Branch for improving the English writing of the manuscript.

SUPPLEMENTARY MATERIAL

The Supplementary Material for this article can be found online at: https://www.frontiersin.org/articles/10.3389/fnut.2021.798273/full#supplementary-material

Supplementary Figure 1 | Weight change rate of cereal vinegar sediment (CVS) in liver injury mice. Plot showing the body weight changing in different groups. The different colors represent different groups, and error bars represent SD.

Supplementary Figure 2 | Alpha diversity of gut microbiota. **(A)** Rarefaction curves; Alpha diversity indices, including Good's coverage **(B)**, Chao1 **(C)**, ACE **(D)**, Shannon **(E)**, and Simpson **(F)**. Different letters represent a significant difference between groups calculated with the Kruskal–Wallis one-way ANOVA, and error bars represent SD.

Supplementary Figure 3 | Linear discriminant analysis effect size (LEfSe) results based on operational taxonomic unit (OTU) level in different comparisons. **(A)** CTC vs. CTL. Green bars represent OTUs were relatively higher in the CTL group, red bars represent OTUs were relatively higher in the CTC group; **(B)** CTC vs. CTC.SIL. Green bars represent OTUs were relatively higher in the CTC.SIL group, red bars represent OTUs were relatively higher in the CTC group; **(C)** CTC vs. CTC.CVSL. Green bars represent OTUs were relatively higher in the CTC.CVSL group; red bars represent OTUs were relatively higher in the CTC group; **(D)** CTC vs. CTC.CVSH. Green bars represent OTUs were relatively higher in the CTC.CVSH group; red bars represent OTUs were relatively higher in the CTC group.

Supplementary Figure 4 | Operational taxonomic units (OTUs) significantly different between CTL and CTC at "genus" level. **(A)** A genus with relative abundance higher than 0.1%; **(B)** genus with relative abundance <0.1%. Different letters represent a significant difference between groups calculated with the Kruskal–Wallis one-way ANOVA, and error bars represent SD.

Supplementary Figure 5 | Operational taxonomic units (OTUs) significantly different between CTL and CVSL at "genus" level. Different letters represent a significant difference between groups calculated with the Kruskal–Wallis one-way ANOVA, and error bars represent SD.

Supplementary Figure 6 | Relative abundance of operational taxonomic units (OTUs) predicted relating to pentose and glucuronate interconversions pathway. Bar plot showing the relative abundances of selected OTUs in different groups. Different colors represent different groups. Different letters represent a significant difference between groups calculated with the Kruskal–Wallis one-way ANOVA, and error bars represent SD.

Supplementary Figure 7 | Relative abundance of some operational taxonomic units (OTUs) related to physicochemical indices. Bar plot showing the relative abundances of selected OTUs in different groups. Different colors represent different groups. Different letters represent a significant difference between groups calculated with the Kruskal–Wallis one-way ANOVA, and error bars represent SD.

Supplementary Table 1 | Detailed chemical compositions of CVS. *Essential amino acids.

Supplementary Table 2 | Metabolites detected in CVS with LC-MSMS analysis.

Supplementary Table 3 | OTU table generated by vsearch with SILVA 132 database. Sample ids represent groups and replicates.

REFERENCES

1. Fujino T, Kanaya S, Ariyoshi K, Makizumi K, Kaji Y, Tsuda Y, et al. Effects of solid components in brewed vinegar on human serum cholesterol and red cell filtratability. *Kenko Kagaku.* (1990) 12:139–41.
2. Nagano M, Ueno T, Fujii A, Hou D, Fujii M. Anti-hyperglycemic effect of Kurozu moromi powder in type II diabetic model KK-Ay mice. *Nippon Shokuhin Kagaku Kogaku Kaishi.* (2010) 57:346–54. doi: 10.3136/nskkk.57.346
3. Hayashi T, Hasegawa K, Sasaki Y, Sagawa Y, Oka T, Fujii A, et al. Reduction of development of late allergic eosinophilic rhinitis by kurozu moromi powder in BALB/c mice. *Food Sci Technol Res.* (2007) 13:385–90. doi: 10.3136/fstr.13.385
4. Nagano M, Ishihama S, Hayashi K, Kurita M, Kudo I. Effects of kurozu moromi powder on an IgE antigen-mediated dermatitis model. *J Jpn Soc Nutr Food Sci.* (2001) 54:171–3. doi: 10.4327/jsnfs.54.171
5. Kanouchi H, Kakimoto T, Nakano H, Suzuki M, Nakai Y, Shiozaki K, et al. The brewed rice vinegar Kurozu increases HSPA1A expression and ameliorates cognitive dysfunction in aged P8 mice. *PLoS ONE.* (2016) 11:e0150796. doi: 10.1371/journal.pone.0150796
6. Nagano M. Effects of kurozu moromi powder on calcium absorption in ovariectomized osteoporosis model rats. *Jpn Pharmacol Ther.* (2001) 29:635–42. Available online at: https://www.researchgate.net/publication/286747545_Effects_of_kurozu_moromi_powder_on_calcium_absorption_in_ovariectomized_osteoporosis_model_rats
7. Fukuyama N, Jujo S, Ito I, Shizuma T, Myojin K, Ishiwata K, et al. Kurozu moromimatsu inhibits tumor growth of lovo cells in a mouse model *in vivo*. *Nutrition.* (2007) 23:81–6. doi: 10.1016/j.nut.2006.10.004
8. Shizuma T, Ishiwata K, Nagano M, Mori H, Fukuyama N. Protective effects of Kurozu and Kurozu moromimatsu on dextran sulfate sodium-induced experimental colitis. *Dig Dis Sci.* (2011) 56:1387–92. doi: 10.1007/s10620-010-1432-x
9. Shizuma T, Ishiwata K, Nagano M, Mori H, Fukuyama N. Protective effects of fermented rice vinegar sediment (Kurozu moromimatsu) in a diethylnitrosamine-induced hepatocellular carcinoma animal model. *J Clin Biochem Nutr.* (2011) 49:31–5. doi: 10.3164/jcbn.10-112
10. Tripathi A, Debelius J, Brenner DA, Karin M, Loomba R, Schnabl B, et al. The gut–liver axis and the intersection with the microbiome. *Nat Rev Gastroenterol Hepatol.* (2018) 15:397–411. doi: 10.1038/s41575-018-0011-z
11. Albillos A, De Gottardi A, Rescigno M. The gut-liver axis in liver disease: pathophysiological basis for therapy. *J Hepatol.* (2020) 72:558–77. doi: 10.1016/j.jhep.2019.10.003
12. Compare D, Coccoli P, Rocco A, Nardone OM, De Maria S, Carten,ì M, et al. Gut–liver axis: the impact of gut microbiota on non alcoholic fatty liver disease. *Nutr Metab Cardiovasc Dis.* (2012) 22:471–6. doi: 10.1016/j.numecd.2012.02.007
13. Xia T, Zhang B, Duan W, Li Y, Zhang J, Song J, et al. Hepatoprotective efficacy of Shanxi aged vinegar extract against oxidative damage in vitro and in vivo. *J Funct Foods.* (2019) 60:103448. doi: 10.1016/j.jff.2019.103448
14. Zhu S, Guan L, Tan X, Li G, Sun C, Gao M, et al. Hepatoprotective effect and molecular mechanisms of hengshun aromatic vinegar on non-alcoholic fatty liver disease. *Front Pharmacol.* (2020) 11:2034. doi: 10.3389/fphar.2020.585582
15. Xia T, Zhang B, Li S, Fang B, Duan W, Zhang J, et al. Vinegar extract ameliorates alcohol-induced liver damage associated with the modulation of gut microbiota in mice. *Food Funct.* (2020) 11:2898–909. doi: 10.1039/C9FO03015H
16. Song J, Zhang J, Su Y, Zhang X, Li J, Tu L, et al. Monascus vinegar-mediated alternation of gut microbiota and its correlation with lipid metabolism and inflammation in hyperlipidemic rats. *J Funct Foods.* (2020) 74:104152. doi: 10.1016/j.jff.2020.104152
17. Song ZT, Dong XF, Tong JM, Wang ZH. Effects of inclusion of waste vinegar residue in the diet of laying hens on chyme characteristics and gut microflora. *Livest Sci.* (2014) 167:292–6. doi: 10.1016/j.livsci.2014.05.030
18. Wu JJ, Ma YK, Zhang FF, Chen FS. Biodiversity of yeasts, lactic acid bacteria and acetic acid bacteria in the fermentation of "Shanxi aged vinegar", a traditional Chinese vinegar. *Food Microbiol.* (2012) 30:289–97. doi: 10.1016/j.fm.2011.08.010
19. Gardner WH. Water content. *Methods Soil Anal Part 1 Phys Mineral Methods.* (1986) 5:493–544. doi: 10.2136/sssabookser5.1.2ed.c21
20. Helrich, K. (Ed.). (1990). *Official Methods of Analysis of the Association of Official Analytical Chemists*. 15th ed. Arlington, VA.
21. Masuko T, Minami A, Iwasaki N, Majima T, Nishimura SI, Lee YC. Carbohydrate analysis by a phenol–sulfuric acid method in microplate format. *Anal Biochem.* (2005) 339:69–72. doi: 10.1016/j.ab.2004.12.001
22. Aykin E, Budak NH, Güzel-Seydim ZB. Bioactive components of mother vinegar. *J Am Coll Nutr.* (2015) 34:80–9. doi: 10.1080/07315724.2014.896230
23. Corradini E, Foglia P, Giansanti P, Gubbiotti R, Samperi R, Lagana A. Flavonoids: chemical properties and analytical methodologies of identification and quantitation in foods and plants. *Nat Prod Res.* (2011) 25:469–95. doi: 10.1080/14786419.2010.482054
24. Qiu J, Ren C, Fan J, Li Z. Antioxidant activities of aged oat vinegar *in vitro* and in mouse serum and liver. *J Sci Food Agric.* (2010) 90:1951–8. doi: 10.1002/jsfa.4040
25. Shibayama Y, Nagano M, Hashiguchi K, Fujii A, Iseki K. Supplementation of concentrated Kurozu, a Japanese black vinegar, reduces the onset of hepatic steatosis in mice fed with a high-fat diet. *Funct Foods Health Dis.* (2019) 9:276–96. doi: 10.31989/ffhd.v9i4.596
26. Geng Y, Yue Y, Guan Q, Ren Y, Guo L, Fan Y, et al. Cereal vinegar sediment alleviates spontaneous ulcerative colitis in Il-10 deficient mice. *Mol Nutr Food Res.* (2021) 2001227. doi: 10.1002/mnfr.202001227
27. Taniguchi M, Takeuchi T, Nakatsuka R, Watanabe T, Sato K. Molecular process in acute liver injury and regeneration induced by carbon tetrachloride. *Life Sci.* (2004) 75:1539–49. doi: 10.1016/j.lfs.2004.02.030
28. Martin M. Cutadapt removes adapter sequences from high-throughput sequencing reads. *EMBnet J.* (2011) 17:10–2. doi: 10.14806/ej.17.1.200
29. Rognes T, Flouri T, Nichols B, Quince C, Mahé. VSEARCH: A versatile open source tool for metagenomics. *Peer J.* (2016) 4:e2584. doi: 10.7717/peerj.2584
30. Edgar RC. UPARSE: highly accurate OTU sequences from microbial amplicon reads. *Nat Methods.* (2013) 10:996–8. doi: 10.1038/nmeth.2604
31. Quast C, Pruesse E, Yilmaz P, Gerken J, Schweer T, Yarza P, et al. The SILVA ribosomal RNA gene database project: improved data processing and web-based tools. *Nucleic Acids Res.* (2012) 41:D590–6. doi: 10.1093/nar/gks1219
32. Segata N, Izard J, Waldron L, Gevers D, Miropolsky L, Garrett WS, et al. Metagenomic biomarker discovery and explanation. *Genome Biol.* (2011) 12:1–18. doi: 10.1186/gb-2011-12-6-r60
33. Guan Q, Kong W, Zhu D, Zhu W, Dufresne C, Tian J, et al. Comparative proteomics of *Mesembryanthemum crystallinum* guard cells and mesophyll cells in transition from C3 to CAM. *J Proteomics.* (2021) 231:104019. doi: 10.1016/j.jprot.2020.104019
34. Ohkura N, Kihara-Negishi F, Fujii A, Kanouchi H, Oishi K, Atsumi GI, et al. Effects of fermented rice vinegar Kurozu and its sediment on inflammation-induced plasminogen activator inhibitor 1 (PAI-1) increase. *Food Nutr Sci.* (2018) 9:235–46. doi: 10.4236/fns.2018.93018
35. Sandri M, Dal Monego S, Conte G, Sgorlon S, Stefanon B. Raw meat based diet influences faecal microbiome and end products of fermentation in healthy dogs. *BMC Vet Res.* (2016) 13:65. doi: 10.1186/s12917-017-0981-z
36. Walker A, Pfitzner B, Harir M, Schaubeck M, Calasan J, Heinzmann SS, et al. Sulfonolipids as novel metabolite markers of alistipes and odoribacter affected by high-fat diets. *Sci Rep.* (2017) 7:11047. doi: 10.1038/s41598-017-10369-z
37. Aßhauer KP, Wemheuer B, Daniel R, Meinicke P. Tax4Fun: predicting functional profiles from metagenomic 16S rRNA data. *Bioinformatics.* (2015) 31:2882–4. doi: 10.1093/bioinformatics/btv287
38. Boursier J, Mueller O, Barret M, Machado M, Fizanne L, Araujo-Perez F, et al. The severity of nonalcoholic fatty liver disease is associated with gut dysbiosis and shift in the metabolic function of the gut microbiota. *Hepatology.* (2016) 63:764–75. doi: 10.1002/hep.28356
39. Chen SJ, Zhao RH, Kang JJ, Tian JR, Hou JX. Analysis and evaluation of nutritional composition of the sediment in shanxi aged vinegar. *Food Sci.* (2014) 11. Available online at: https://en.cnki.com.cn/Article_en/CJFDTotal-SPKX201411044.htm
40. Pihlava JM. Identification of hordatines and other phenolamides in barley (Hordeum vulgare) and beer by UPLC-QTOF-MS. *J Cereal Sci.* (2014) 60:645–52. doi: 10.1016/j.jcs.2014.07.002
41. Zhang X, Wu Y, Zheng Y, Xu Y, Xia M, Tu L, et al. Unravelling the composition and envisaging the formation of sediments in traditional Chinese vinegar. *Int J Food Sci Technol.* (2019) 54:2927–38. doi: 10.1111/ijfs.14185

42. Xia T, Zhang J, Yao J, Zhang B, Duan W, Zhao C, et al. Shanxi aged vinegar protects against alcohol-induced liver injury via activating nrf2-mediated antioxidant and inhibiting tlr4-induced inflammatory response. *Nutrients.* (2018) 10:805. doi: 10.3390/nu10070805
43. Xie X, Zheng Y, Liu X, Cheng C, Zhang X, Xia T, et al. Antioxidant activity of Chinese Shanxi aged vinegar and its correlation with polyphenols and flavonoids during the brewing process. *J Food Sci.* (2017) 82:2479–86. doi: 10.1111/1750-3841.13914
44. Nie Y, Ren D, Lu X, Sun Y, Yang X. Differential protective effects of polyphenol extracts from apple peels and fleshes against acute CCl 4-induced liver damage in mice. *Food Funct.* (2015) 6:513–24. doi: 10.1039/C4FO00557K
45. Wang YL, Lv HY, Zhang Q. Effect of flavonoid compounds extracted from Iris species in prevention of carbon tetrachloride-induced liver fibrosis in rats. *Genet Mol Res.* (2015) 14:10973–9. doi: 10.4238/2015.September.21.9
46. Hu Y, Zhao Y, Yuan L, Yang X. Protective effects of tartary buckwheat flavonoids on high TMAO diet-induced vascular dysfunction and liver injury in mice. *Food Funct.* (2015) 6:3359–72. doi: 10.1039/C5FO00581G
47. Koyu A, Gokcimen A, Ozguner F, Bayram DS, Kocak A. Evaluation of the effects of cadmium on rat liver. *Mol Cell Biochem.* (2006) 284:81–5. doi: 10.1007/s11010-005-9017-2
48. Betrapally NS, Gillevet PM, Bajaj JS. Changes in the intestinal microbiome and alcoholic and nonalcoholic liver diseases: causes or effects?. *Gastroenterology.* (2016) 150:1745–55. doi: 10.1053/j.gastro.2016.02.073
49. Parker BJ, Wearsch PA, Veloo A, Rodriguez-Palacios A. The genus alistipes: gut bacteria with emerging implications to inflammation, cancer, mental health. *Front Immunol.* (2020) 11:906. doi: 10.3389/fimmu.2020.00906
50. Smith BJ, Miller RA, Ericsson AC, Harrison DC, Strong R, Schmidt TM. Changes in the gut microbiome and fermentation products concurrent with enhanced longevity in acarbose-treated mice. *BMC Microbiol.* (2019) 19:130. doi: 10.1186/s12866-019-1494-7
51. Adolph TE, Grander C, Moschen AR, Tilg H. Liver–microbiome axis in health and disease. *Trends Immunol.* (2018) 39:712–23. doi: 10.1016/j.it.2018.05.002
52. Kedia S, Rampal R, Paul J, Ahuja V. Gut microbiome diversity in acute infective and chronic inflammatory gastrointestinal diseases in North India. *J Gastroenterol.* (2016) 51:660–71. doi: 10.1007/s00535-016-1193-1
53. Cho S, Hwang O, Park S. Effect of dietary protein levels on composition of odorous compounds and bacterial ecology in pig manure. *Asian Austra J Anim Sci.* (2015) 28:1362. doi: 10.5713/ajas.15.0078

Conflict of Interest: The authors declare that the research was conducted in the absence of any commercial or financial relationships that could be construed as a potential conflict of interest.

Publisher's Note: All claims expressed in this article are solely those of the authors and do not necessarily represent those of their affiliated organizations, or those of the publisher, the editors and the reviewers. Any product that may be evaluated in this article, or claim that may be made by its manufacturer, is not guaranteed or endorsed by the publisher.

frontiers in Nutrition

ORIGINAL RESEARCH
published: 04 January 2022
doi: 10.3389/fnut.2021.791886

Novel Millet-Based Flavored Yogurt Enriched With Superoxide Dismutase

Xiankang Fan[1,2], *Xiefei Li*[1,2], *Tao Zhang*[3], *Yuxing Guo*[3], *Zihang Shi*[1,2], *Zhen Wu*[1,2], *Xiaoqun Zeng*[1,2] *and Daodong Pan*[1,2*]

[1] *Key Laboratory of Animal Protein Food Processing Technology of Zhejiang Province, College of Food and Pharmaceutical Sciences, Ningbo University, Ningbo, China,* [2] *State Key Laboratory for Managing Biotic and Chemical Threats to the Quality and Safety of Agro-Products, Ningbo University, Ningbo, China,* [3] *School of Food Science and Pharamaceutical Engineering, Nanjing Normal University, Nanjing, China*

Superoxide dismutase (SOD) is an important antioxidant enzyme with different physiological functions, which can be used as a nutritional fortifier in food. Cereal-based fermented products are becoming popular worldwide. In this study, novel millet-based flavored yogurt enriched with SOD was developed. *Lactiplantibacillus plantarum subsp. plantarum* was screened, which manufactured SOD activity of 2476.21 ± 1.52 U g^{-1}. The SOD content of millet yogurt was 19.827 ± 0.323 U mL^{-1}, which was 63.01, 50.11, and 146.79% higher than that of Bright Dairy Yogurt 1911, Junlebao and Nanjing Weigang, respectively. Fifty-four volatile flavor substances and 22,571 non-volatile flavor substances were found in yogurt. Compared to traditional fermented yogurt, 37 non-volatile metabolites in yogurt with millet enzymatic fermentation broth were significantly upregulated, including 2-phenyl ethanol, hesperidin, N-acetylornithine and L-methionine, which were upregulated by 3169.6, 228.36, 271.22, and 55.67 times, respectively, thereby enriching the sensory and nutritional value of yogurt. Moreover, the manufacture of unpleasant volatile flavor substances was masked, making the product more compatible with consumers' tastes.

Keywords: ***lactic acid bacteria*, superoxide dismutase, yogurt, HPLC-MS, HS-SPME-GC-MS**

OPEN ACCESS

Edited by:
Xiaolong Ji,
Zhengzhou University of Light Industry, China

Reviewed by:
Yanglei Yi,
Northwest A&F University, China
Hongshun Yang,
National University of Singapore, Singapore

***Correspondence:**
Daodong Pan
daodongpan@163.com

Specialty section:
This article was submitted to Food Chemistry, a section of the journal Frontiers in Nutrition

Received: *09 October 2021*
Accepted: *06 December 2021*
Published: *04 January 2022*

Citation:
Fan X, Li X, Zhang T, Guo Y, Shi Z, Wu Z, Zeng X and Pan D (2022) Novel Millet-Based Flavored Yogurt Enriched With Superoxide Dismutase. Front. Nutr. 8:791886. doi: 10.3389/fnut.2021.791886

INTRODUCTION

The probiotic industry has embarked on a new windfall in the post-epidemic era, with market size of $51.2 billion in 2020, and the global probiotic market is expected to grow at a CAGR of 6.9% from 2020 to 2025, while probiotic yogurt accounts for about 78% of the total global probiotic business (1, 2). Yogurt is a traditional dairy product manufactured by *Lactobacillus delbrueckii subsp. bulgaricus* and *Streptococcus thermophilus* by lactic acid fermentation (3). The direction of yogurt development is to develop high quality yogurt enriched with functional factors (4). The fermentation of *Lactobacillus* (LAB) manufactures superoxide dismutase (SOD) and peptides, which make yogurt richer in nutrients, easier to be digested and absorbed by the body (5).

SOD could scavenge superoxide anion free radicals and has various effects, such as anti-aging and anti-inflammatory. Therefore, SOD exhibited various applications in health care products, food and medicine (6). Many scholars have calculated the SOD content in microorganisms, and the results indicate that SOD is widespread in microorganisms. Therefore, the purpose of this study was to screened a strain of LAB with high SOD production to enhance the antioxidant function of yogurt. Some studies have found that using LAB with antioxidant activities can improve the antioxidant function of fermented products. After fermentation using

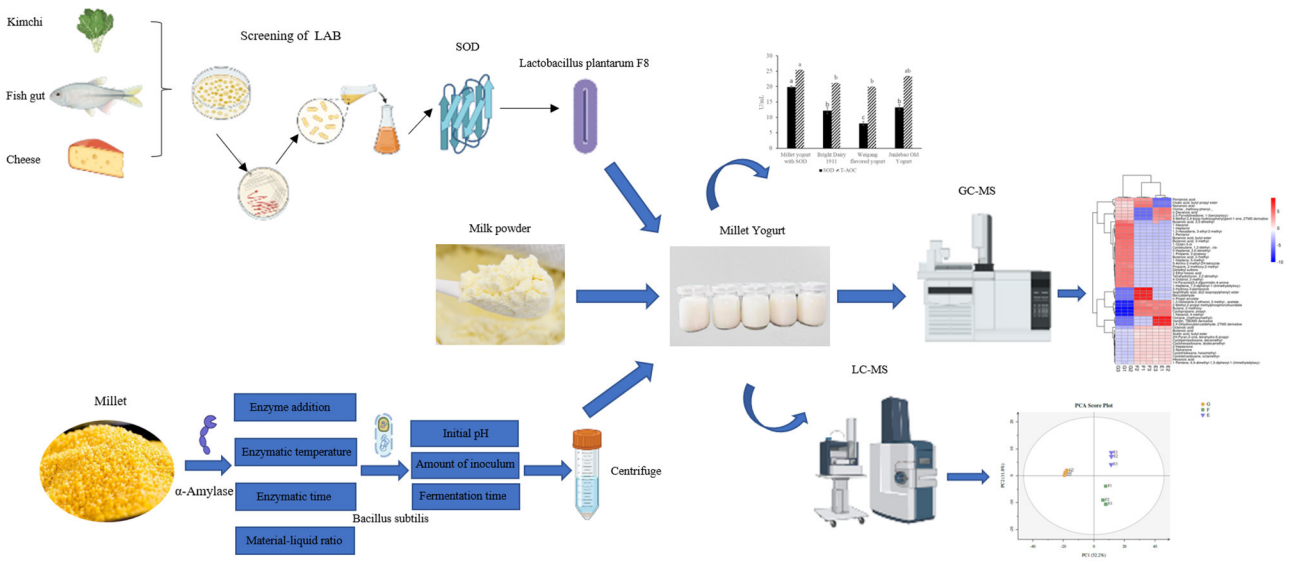

GRAPHICAL ABSTRACT | Novel millet-based flavored yogurt enriched with superoxide dismutase. Simplified experimental protocol for the preparation of SOD-enriched millet flavored yogurt.

the *Lactiplantibacillus plantarum* BCRC 10357, the total phenols and flavonoids in stone lotus increased, leading to improve the superoxide factor, DPPH free-radical scavenging ability, and the T-AOC of stone lotus (7). Soy milk fermented using *Lacticaseibacillus rhamnosus* CRLP81 has a higher T-AOC than the unfermented one, and it can inhibit DNA oxidative damage (8). Clinical studies have discovered that compared with the control group, the SOD activity in the serum of volunteers who ate kelp fermented with *Lactobacillus sp.* BJ20 is higher (9).

Fruit or plant ingredients are often added to yogurt to add sweetness and nutritional value, a practice that can also counteract the natural sourness of the yogurt. For example, pumpkin has been frequently used as a functional food for its antioxidant, antitumor, immunomodulatory, hypoglycemic and hepatoprotective properties (10). Millet contains some active antioxidant substances, such as minerals, vitamins and phenolic compounds (11). Adding millets to acid whey can be used to neutralize acid whey and enable efficient upcycling (12). Xiao Song reported the effect of polymerized whey protein and xanthan gum as thickeners of millet yogurt products on gel and microstructure qualities (13). However, the effect of millet enzymatic fermentation broth on the flavor and antioxidant capacity of yogurt was rarely reported. The treatment of millet was usually done through enzymatic digestion, but it has been improved by inoculating the millet with *Bacillus subtilis* after enzymatic digestion for further fermentation to enhance its utilization and nutritional value in this study. *Bacillus subtilis* is an essential biological leavening agent, many countries and regions use it to make traditional fermented legumes, such as Chinese tempeh and Japanese natto (14). Fermentation of millet enzymatic digests using *Bacillus subtilis* can improve its antioxidant capacity. According to reports, red bean products fermented using *Bacillus subtilis* IMR-NK1 exhibited significant antioxidant activity (15). The fermentation of black soybeans using *Bacillus subtilis*, which can improve the content of total phenols and isoflavones in the fermentation broth, can enhance its antioxidant activity (16). Therefore, we used *Bacillus subtilis* 109047 to ferment millet enzymatic solution, expecting to improve its antioxidant capacity as well as nutritional value.

However, yogurt will eventually be sold to the public, so the senses of yogurt are very crucial. The addition of high SOD-producing LAB and millet fermentation might affect the flavor of yogurt, so it was necessary to detect the flavor. Most of the flavor compounds in yogurt are manufactured by milk fat lipolysis and the microbial conversion of lactose and citrate (17). More than 100 volatile flavors were found in yogurt, including carbonyl compounds, alcohols, acids, esters, hydrocarbons and aromatic compounds (3). HS-SPME-GC-MS and HPLC-MS can be used to determine volatile and non-volatile flavor substances in yogurt, respectively. Erkaya et al. have detected 34 volatile compounds using HS-SPME-GC-MS in yogurt made from the milk of sheep, cows, goats and buffaloes, of which acetaldehyde, diacetyl and acetylene were the major volatile compounds (18). A total of 196 non-volatile metabolites, including nucleosides, amino acids, carbohydrates and lipids, have been evaluated using UPLC-Q-TOF-MS (19).

This paper aimed to develop a millet-flavored yogurt enriched with SOD. Firstly, a LAB strain with high SOD production was screened, and its probiotic properties were investigated. Then, a millet enzyme fermentation broth was prepared and compounded with milk to develop SOD-rich millet yogurt. Finally, the effects of co-fermentation of screened strains with conventional fermenters on metabolites in yogurt and the effects of millet enzymatic fermentation broth on volatile and non-volatile flavor substances in yogurt were analyzed by metabolomics.

MATERIALS AND METHODS

Materials

Kimchi, fish sausage and cheese, the ingredients used to screen for LAB, were purchased from the Nanjing Farmers' Market. Analysis reagents, including methanol, acetonitrile, methyl tert-butyl ether, formic acid and ammonium formate, were all purchased from Thermo. T-AOC kits and peptide assay kits were purchased from Solarbio.

Methods

Screening of LAB With High SOD Production

LAB was isolated from kimchi, fish sausage and cheese by spreading sample diluent on MRS medium that contained bromocresol purple indicator. The pyrogallol autotrophic method was used to determine the SOD enzyme activity of LAB. The strains were identified by 16S rDNA sequencing (20).

Probiotic Potential Evaluation of LAB

The LAB was respectively inoculated into MRS with pH 2.5–8.5 and cultured for 24 h to observe the growth of the bacteria. The activated LAB was inoculated to MRS media with different NaCl content, with NaCl content of 1–8% (w/v) and cultured for 16 h at 37°C to determine their anti-permeable pressure. The LAB was cultured in MRS at pH 7 for 12 h to observe and evaluate the acid production capacity, and cultured in intestinal juice for 8 h and then in gastric juice for 3 h to calculate the survival rate (21). The LAB was successively passaged for 16 generations to determine the genetic stability, and the SOD production ability of the LAB was measured every two generations.

Preparation and Optimization of Millet Enzymatic Hydrolysis Fermentation Broth

The millet powder with a particle size of 80 mesh was prepared, mixed with water and heated at 80°C for 60 min. The gelatinized millet powder was liquefied by alpha-amylase and then boiled. The supernatant was obtained and used to determine the T-AOC and dextrose equivalent (DE) after the gelatinized millet powder had been centrifuged at 8000 ×g for 10 min at 20°C. The solid-liquid ratio (A), with enzyme amount (B), enzymatic digestion time (C) and enzymatic digestion temperature (D) were selected as four factors might affect the quality of millet enzymatic digestion solution for single-factor experiments.

Changing Different Enzymolysis Conditions and the Optimizing Enzymolysis Scheme

The millet enzymatic hydrolysate was fermented with *Bacillus subtilis*109047 at 37°C for a specific period, and then the T-AOC was determined.

$$\mathrm{T-AOC\,(U/mL)} = (\mathrm{x} \times \mathrm{V1}) \div \mathrm{V2} = 34 \times \mathrm{x}$$

Where V1 represents the total volume of the reaction (0.204 mL); V2 represents the volume of the sample in the reaction (0.006 mL), and x is calculated based on the standard curve.

$$DE\,(\%) = (C \times VT) \div (m \times VS) \times 100$$

Where C represents the amount of sugar (mg) based on the standard curve; VT represents the volume of the extract; m represents the mass of the sample, and VS represents the volume (mL) of the sample used in the determination.

Development of Millet Yogurt Rich in SOD

The enzymatic fermentation broth of millet was centrifuged at 8,000 ×g, 4°C for 10 min. The supernatant was mixed with recovered milk and sterilized in a water bath at 95°C for 10 min, then cooled in a water bath at 42°C. Yogurt fermenter (*Lactobacillus delbrueckii subsp. bulgaricus and Streptococcus thermophilus*) with high SOD-producing LAB were inoculated into the above 42°C cooled recovered milk. The recovered milk was homogenized in a sterile environment and then fermented in an incubator at 42°C for 6 h (22). The yogurt with the most SOD content and best sensory were prepared by adding different amounts of starter, using different material-to-liquid ratios, adding different amounts of sucrose, adding phytochemicals and using different fermentation times.

Sensory Evaluation

The sensory evaluation was approved by the Ningbo University Institutional Review Board (NU-IRB). According to Mengdi Yin, sensory evaluation was performed using the quantitative descriptive analysis (QDA) method (23). The sensory evaluation was conducted by a professionally trained panel of 15 males and 15 females. The examined yogurt samples took into account four individual quality characteristics, including organization status, taste, odor and color. As shown in **Table 1**, the descriptors describing the characteristics of the examined samples and their definitions were decided by the panel after the training.

Determination of SOD Content in Yogurt

The pH of the yogurt was adjusted to 4.6 with 2 mol L^{-1} H_3PO_4, and then the yogurt was bathed in water at 38°C for 5–10 min. After the treated yogurt was centrifuged at 7,000 ×g for 10 min, the supernatant was removed and adjusted to pH 6.0 with 0.5 mol L^{-1} NaOH for subsequent SOD content test.

Evaluation of Various Indicators of Yogurt

The pH value of the final yogurt and the content of LAB was measured using a pH meter and the dilution coating method. The differences in T-AOC and peptide content among the final yogurt and Bright Dairy 1911, Junlebao and Nanjing Weigang flavor yogurt were compared.

Analysis of Non-volatile Flavor Substances in Yogurt by HPLC-MS

The yogurt was fermented in a 42°C incubator. The types of yogurts were as follows: traditional starter (Y), traditional starter and *Lactiplantibacillus plantarum subsp. plantarum* F8 (Y-F8), and millet yogurt (Y-F8-M). Non-targeted metabolomics was used to analyze the effect of the addition of *Lactiplantibacillus plantarum subsp. plantarum* F8 and millet enzymatic fermentation broth on non-volatile flavor substances in yogurt (23–25). Metabolites were initially extracted from yogurt samples. Then, all samples were thawed at 4°C, 100 mg

TABLE 1 | Sensory rating scale.

Items	Evaluation criteria	Score
Organizational status	Yogurt has uniform texture, moderate viscosity and no whey precipitation.	20–25
	The yogurt has a relatively uniform texture, moderate viscosity and a small amount of whey precipitation.	15–20
	Yogurt has an uneven texture, low viscosity, and more whey precipitation.	0–15
Taste	The yogurt is moderately sweet and sour, delicate and smooth, and easily accepted.	20–25
	The yogurt is out of proportion to the sweet and sour, and the taste is a little rough but acceptable.	15–20
	Yogurt tastes too sour or too sweet and is not easy to accept.	0–15
Odor	It has the inherent whey flavor and pleasant odor of yogurt.	20–25
	Yogurt has an inherent milky flavor that is relatively light and slightly sour.	15–20
	Yogurt has no creamy flavor, heavy sourness and incongruous odor.	0–15
Color	The yogurt is creamy white and shiny, uniform in color and free of impurities.	20–25
	The yogurt is creamy and slightly shiny, dark in color and free of impurities.	15–20
	Yogurt is milky white and lusterless, dull in color, with impurities.	0–15

of which was transferred into 2 mL centrifuge tubes, added with 200 μL of methanol and 200 μL of MTBE into each centrifuge tube, and shaken for 60 s. Afterward, the samples were centrifuged at 4°C for 10 min at 12,000 rpm, and the supernatant was filtered through a 0.22 μm membrane to obtain the prepared samples for HPLC-MS (Thermo U300; QE). The chromatographic conditions were as follows: a 1.8 μm (2.1×150 mm) chromatographic column was used; injection port temperature of 8°C; flow rate of 0.25 mL min^{-1}; column temperature of 40°C; and a 2 μL injection was used for gradient elution. The mobile phase was positive ion 0.1% formic acid water 0.1% formic acid acetonitrile and negative ion 5 mM ammonium formate water acetonitrile. Finally, a mass spectrometer was used an electrospray ionization source in positive and negative ionization mode with positive and negative ion spray voltages of 3.50 and 2.50 kV, respectively, a sheath gas of 30arb, and an auxiliary gas of 10 arb. The capillary was set at 325°C, and a full scan was performed with a resolution of 70,000, a scan range of 81–1,000, and a secondary cleavage with HCD, with a collision voltage of 30 eV (19, 26, 27).

Analysis of Volatile Flavor Compounds in Yogurt by HS-SPME-GC-MS

The HS-SPME device was used to extract volatile flavor compounds in yogurt for 60 min at 50°C and 350 rpm. The GC-MS instrument make and model was Agilent 8890 GC System+5977B/MSD. The chromatographic conditions were set at an initial temperature of 35°C for 3 min, 4°C min^{-1} to 140°C for 1 min, and 10°C min^{-1} to 250°C for 3 min. The injection temperature was set at 250°C; the carrier gas was He, and the flow rate was 1.0 mL min^{-1}. The mass spectrometry conditions were as follows: ionization mode EI of 70 eV, ion source temperature of 230°C, mass scanning range of 33–650 AMV, and emission voltage of 100 μA (22, 28). Agilent MssHunter Qualitative Analysis B.07.00 software and NIST14.LMS database provided by Agilent were used for data comparison, while we referred to metabolomics analysis methods from other scholars (29–32).

TABLE 2 | SOD content of *lactic acid bacteria* screened.

Bacteria number	SOD (U/g)	Bacteria number	SOD (U/g)
F1	597.48 ± 2.74	F12	2143.97 ± 0.68
F2	363.07 ± 3.68	F13	854.29 ± 6.71
F3	731.47 ± 2.18	F14	1238.99 ± 9.56
F4	682.85 ± 2.25	F15	871.56 ± 2.32
F5	1379.85 ± 1.93	F16	1358.69 ± 7.21
F6	659.46 ± 3.37	F17	587.11 ± 5.79
F7	489.44 ± 3.09	F18	607.05 ± 7.91
F8	2476.21 ± 1.52	F19	563.78 ± 4.23
F9	487.54 ± 4.33	F20	454.26 ± 3.56
F10	963.44 ± 4.37	F21	284.55 ± 5.44
F11	1594.24 ± 5.05		

SOD, Superoxide dismutase.

Statistical Analysis

Differences between samples were analyzed using one-way analysis of variance (ANOVA) and Duncan's multiple range tests using SPSS. A P-value of <0.05 was considered to be statistically significant. All experiments were conducted three times in parallel. Bioinformatics analyses such as PCA plots and heat maps were performed using the OmicStudio tool at https://www.omicstudio.cn/tool.

RESULTS AND DISCUSSION

Screening of LAB With High SOD Production

Twenty-one strains of LAB were screened and their SOD enzyme activities were determined. The results were indicated in **Table 2**, a target strain with high SOD production was screened, and the SOD content of this strain reached 2476.21 ± 1.52 U g^{-1}. This strain had the highest SOD content among the 21 strains of LAB. Based on the 16S rDNA sequence, the screened F8 strain was identified as: *Lactiplantibacillus plantarum subsp. plantarum* (**Figure 1**).

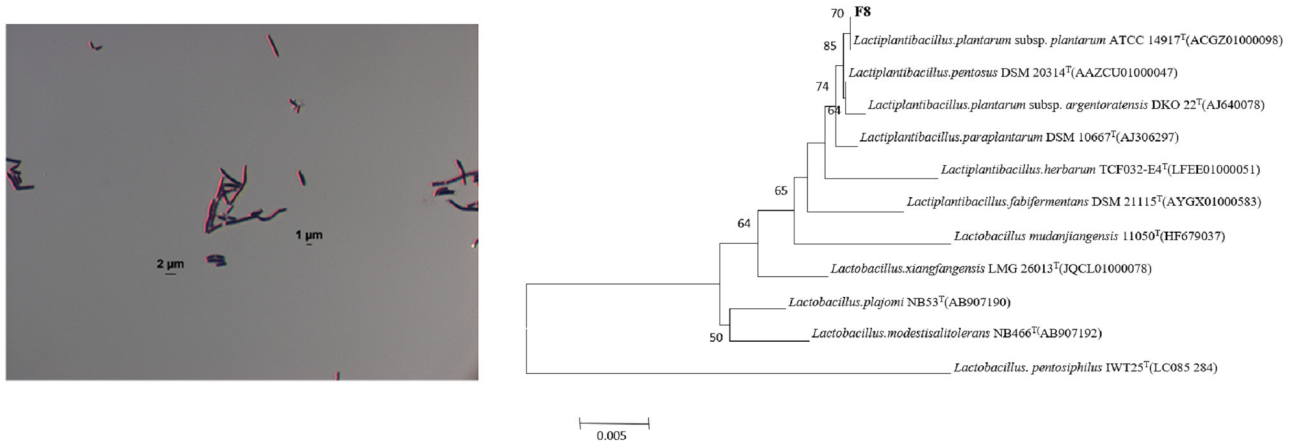

FIGURE 1 | (A) Results of Gram staining of *Lactiplantibacillus plantarum subsp. plantarum F8*. **(B)** Phylogenetic tree of 16S rDNA sequence of the target strain *Lactiplantibacillus plantarum subsp. plantarum F8* and related species.

As indicated in **Figure 2A**, the LAB grew well at a pH of 4, and the LAB needed good acid resistance to maintain their activity in a gastric acid environment (33). **Figure 2B** shows that the bacteria could decrease the pH of the fermentation broth to 4.38 within 12 h, which indicated the high acid production capacity of this LAB. This was close to the results of A H X G screening LAB for fermentation of high-quality yogurt (34). The strain could withstand the osmotic pressure of 8.0% sodium chloride, indicating that the strain might also have application prospects in fermented kimchi and other low-salt pickled foods. The prerequisite that LAB could play a beneficial role in the intestine is to be able to tolerate the gastrointestinal environment and survive (31). As shown in **Figure 2C**, the bacterium exhibited very good tolerance in gastrointestinal fluids, reaching 58.54% survival in intestinal fluids for 8 h and 61.7% survival in gastric fluids for 2 h. This is similar to the result of Wu et al. (35). In addition, the bacterium exhibited excellent genetic stability of SOD (**Figure 2D**), which is similar to Chooruk A's results (36).

Preparation and Optimization of Millet Enzymatic Hydrolysis Fermentation Broth

In the single-factor experiment of millet enzymatic digestion (**Figures 3A–D**), the best enzymatic digestion conditions were as follows: solid-liquid ratio(A) of 1:10 (w/v), amylase addition (B) of 16 U g^{-1}, enzymatic digestion time (C) of 70 min and enzymatic digestion temperature (D) of 65°C. Based on the orthogonal test results (**Table 3**), the order of factors affecting the DE value of millet enzymatic hydrolysate was D>B>C>A. When the T-AOC was used as the standard, the order of factors affecting the T-AOC of millet enzymatic hydrolysate was A>C>B>D. The best combination was obtained from $A_1B_2C_1D_3$. Considering these two factors, the best combination was determined as $A_1B_1C_3D_1$, which is, the ratio of the material to liquid was 1:10 (w/v). The amount of enzyme added was 16 U g^{-1}, the enzymatic hydrolysis time was 80 min and the enzymatic hydrolysis temperature was 65°C. Three repetitive experiments were conducted under this condition. The average DE value was 40.03 ± 0.85% and the T-AOC was 26.24 ± 0.53 U mL^{-1}. The DE value increased by 7.35% and the T-AOC increased by 19.71%. This result was consistent with previous reports that the increased antioxidant capacity of millet enzymatic hydrolysis might be mainly related to the contain of polyphenols and vitamins as well as SOD contained in millet (11).

As indicated in **Figure 3E**, with the extension of fermentation time, the T-AOC of millet enzymatic hydrolysis fermentation broth initially increased and then reduced, reaching the maximum at 36 h. The T-AOC of the fermentation broth continued to rise with the increase in the inoculation amount. When the inoculum amount was 3%, the T-AOC of the fermentation broth was the largest. With the increase of pH, the T-AOC increased and then decreased, reaching a maximum value of 44.53 ± 1.08 U mL^{-1} at pH 7. As the fermentation time was prolonged, the content of *Bacillus subtilis* secreted protease, and other enzymes increased gradually. Large proteins were hydrolyzed into peptides and anti-oxidant substances such as flavonoids and polyphenols, which were found in the millet enzymatic hydrolysate (37). Therefore, it might be that the increase in these antioxidants was what made the T-AOC increased. Afterward, some active peptides were continuously hydrolyzed into free amino acids (38). As time increased, flavonoids and polyphenols continued to decrease, and the T-AOC declined. The amount of inoculation greatly influenced the primary and secondary metabolism of microorganisms (34). When the inoculate volume was at a low level, the enzyme and peptide content in the fermentation broth increased as inoculate volume increases, causing an increase in T-AOC. If the bacteria were cultured in high density, the microorganism's growth and reproduction will be inhibited. Therefore, the enzyme manufactured was relatively small, and the T-AOC was reduced. Therefore, the optimal fermentation conditions were as follows: fermentation time of 36 h, *Bacillus subtilis* addition amount of 3%, and initial pH of 7. Compared with

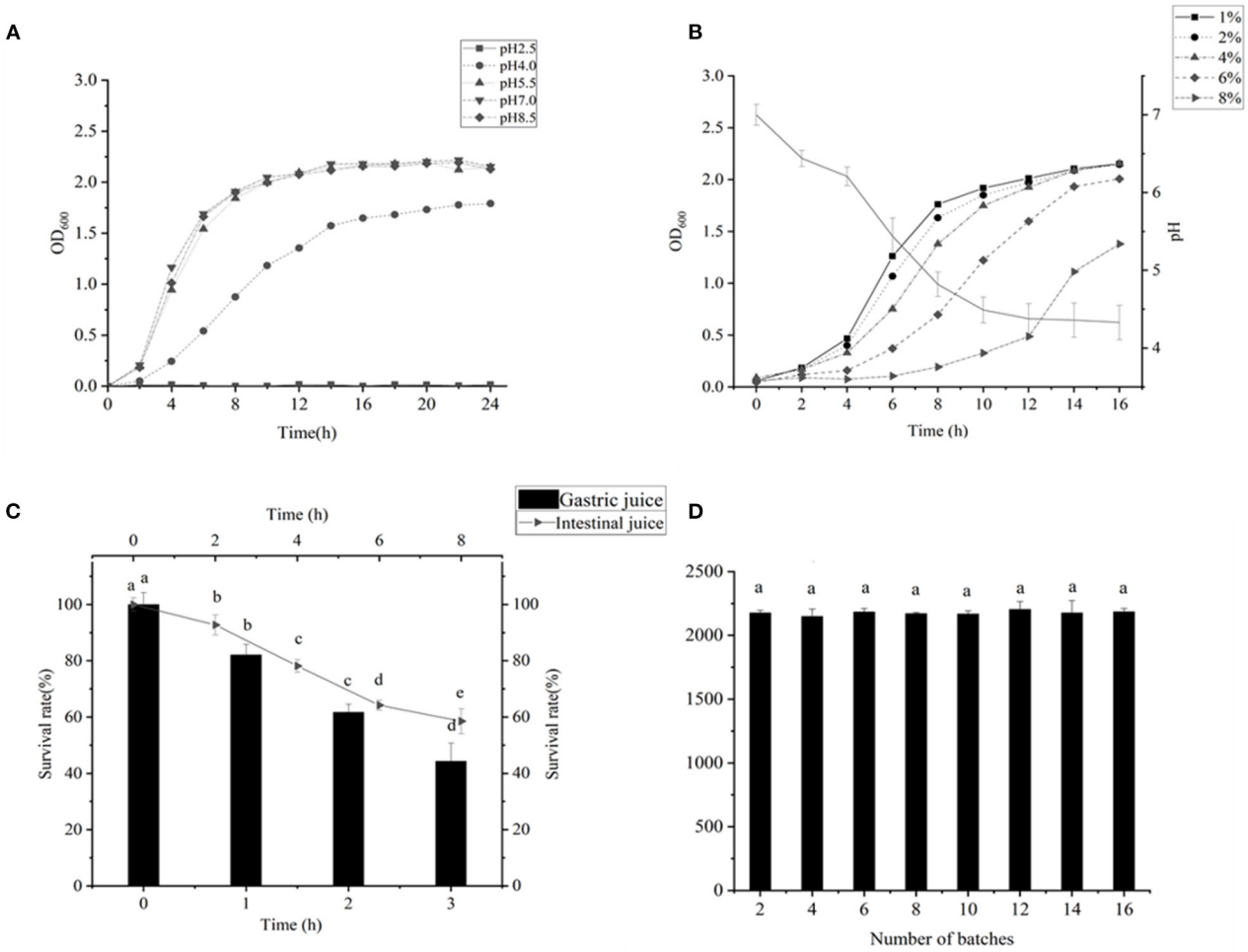

FIGURE 2 | (A) Result of the acid resistance test of *Lactiplantibacillus plantarum subsp. plantarum F8*. **(B)** Determination of acid production capacity; the pH of the medium reduced from 7 to 4.38 within 12 h; 1–8% NaCl was added to the MRS medium, and the growth of the bacteria was measured in 2–16 h. **(C)** Survival rate of LAB in artificial intestinal juice within 8 h. Survival rate of LAB in artificial intestinal juice for 3 h. **(D)** LAB were successively passaged for 16 generations, and the SOD content was measured every two generations. The genetic performance was stable. Significant differences were indicated by the letters a, b and c. Any difference with the same letter was considered not significant ($p > 0.05$) and any difference with a different letter was considered significant ($p < 0.05$).

initial fermentation, the T-AOC of the fermentation broth has increased by 69.7%. *Bacillus subtilis* might improve the nutritional value and antioxidant capacity of millet enzymes by producing nattokinase, SOD, and catalase (37).

Development of Millet Yogurt Rich in SOD

During the fermentation of yogurt, about 20% of sugar and protein was broken down into small molecules and fatty acids, which improved the utilization of nutrients. In addition to retaining all the nutrients of yogurt, lactic acid, amino acids and fatty acids produced by LAB were easily absorbed by the body (39). The SOD content in yogurt reached the maximum at 2:8 (v/v) (**Figure 4A**), and at this time the yogurt had moderate viscosity, no whey precipitation, special yogurt taste, creamy white color and glossy. The SOD content in yogurt reached the maximum at 2:8 (v/v), and at this time the yogurt had moderate viscosity, no whey precipitation, special yogurt taste, creamy white color and glossy. The addition of sucrose had almost no effect on the SOD content in yogurt, but had a great influence on the sensory evaluation score of yogurt taste (**Figure 4B**), which is consistent with previous reports (6).

The SOD content increased significantly with increasing inoculum, reaching a maximum at 4% (v/v) (**Figure 4C**), indicating that the addition of LAB with high SOD production might affect the SOD content of yogurt. This was similar to the results of Wang et al. who fermented stone lotus with *Lactiplantibacillus plantarum* BCRC 10357 (7). As shown in **Figure 4D**, the SOD content gradually increased with the increase of yogurt fermenters, but there was no significant difference. This might be due to the fact that for yogurt fermenters were composed of *Lactobacillus delbrueckii subsp. bulgaricus and Streptococcus thermophilus*, which could also produce small amounts of SOD during fermentation (22). The SOD content in yogurt reached a maximum at 8 h (**Figure 4E**),

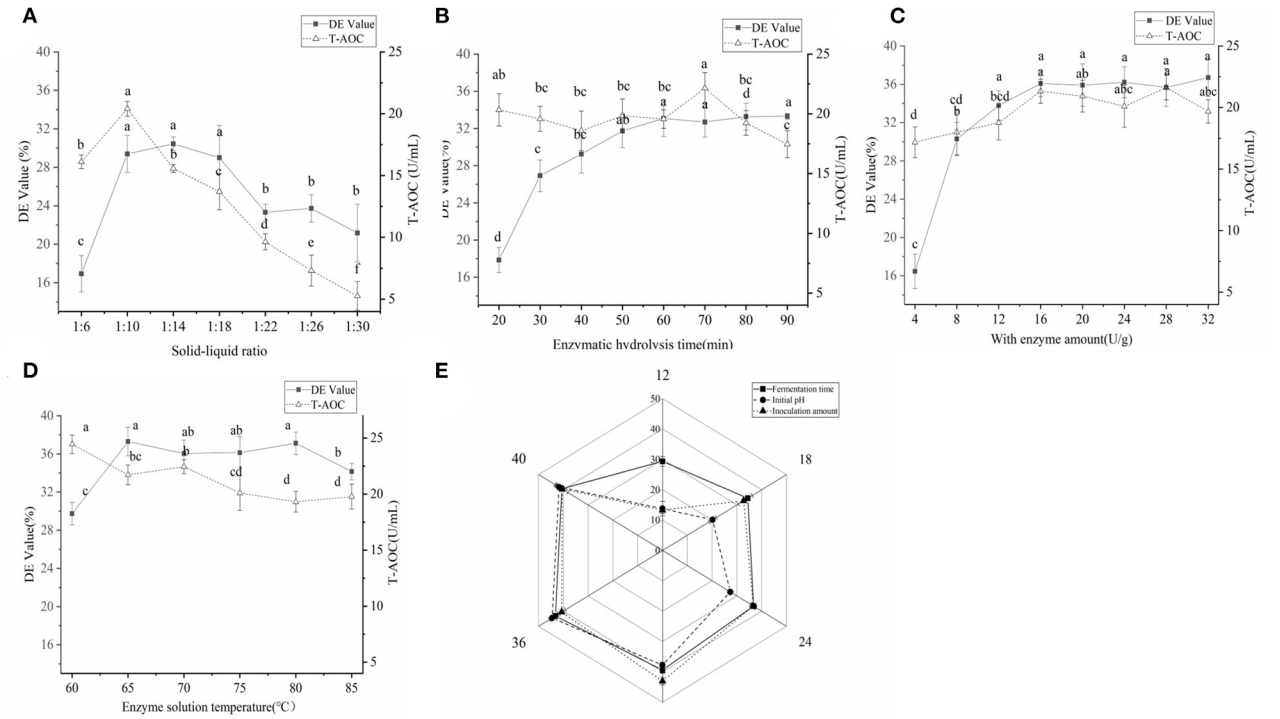

FIGURE 3 | (A) The effect of the material-to-water ratio on the quality of the enzymatic hydrolysate; the material-to-water ratio was set to 1:6, 1:10, 1:14, 1:18, 1:22, 1:26, and 1:30. **(B)** The effect of enzymolysis time on the quality of enzymolysis solution; the enzymolysis time was set to 20–90 min. **(C)** Amount of enzyme added. **(D)** The influence of enzymolysis temperature. **(E)** The effect of fermentation time of *Bacillus subtilis* inoculum and initial pH on the enzymatic hydrolysate of the fermentation broth. Significant differences were indicated by the letters a, b and c. Any difference with the same letter was considered not significant ($p > 0.05$) and any difference with a different letter was considered significant ($p < 0.05$).

TABLE 3 | Analysis table of orthogonal test results.

	Take DE value as standard (%)				Take T-AOC as standard (U/mL)			
K_1	110.81	112.41	108.27	114.39	77.03	71.33	72.59	70.48
K_2	109.86	112.20	108.87	100.92	73.61	72.24	70.09	71.26
K_2	108.48	104.61	112.08	113.91	62.73	69.80	70.69	71.63
k_1	36.94	37.47	36.09	38.13	25.68	23.78	24.20	23.49
k_2	36.62	37.40	36.29	33.64	24.54	24.08	23.36	23.75
k_3	36.16	34.87	37.36	37.97	20.91	23.27	23.56	23.87
R	0.78	2.60	1.27	4.49	4.77	0.81	0.84	0.38
Excellent level	A_1	B_1	C_3	D_1	A_1	B_2	C_1	D_3

DE, Dextrose Equivalent; T-AOC, total antioxidant capacity.

after which it gradually decreased. This could be explained by the gradual decrease in pH with increasing fermentation time, which might affect the SOD production and SOD enzyme activity of LAB (6).

To obtain the best recipe for making millet yogurt, an orthogonal test was conducted. Based on the orthogonal results (**Table 4**), the order of influence on the SOD content in millet yogurt was A>B>D>C. The optimal conditions were as follows: a liquid-to-milk ratio of 2:8 (v/v), amount of added *Lactiplantibacillus plantarum subsp. plantarum* F8 of 3% (v/v), amount of added direct starter of 0.25% (w/v), and fermentation time of 6 h. Re-experiments verified that the SOD content in yogurt was 19.827 ± 0.323 U mL^{-1}, which was increased by 7.25% compared with the previous orthogonal optimization. Feng et al. determined the SOD content in human and certain livestock milk and found that sow milk, dog milk, human milk and cow milk were 69.6, 34.9, 7.1, and 3.2 U mL^{-1}, respectively (40). By contrast, the SOD content of the millet yogurt developed in this experiment was similar to that of dog milk, and it was much higher than that of human milk and cow milk. SOD is the only enzyme known to directly scavenge free radicals, breaking down superoxide dismutase in organisms into oxygen

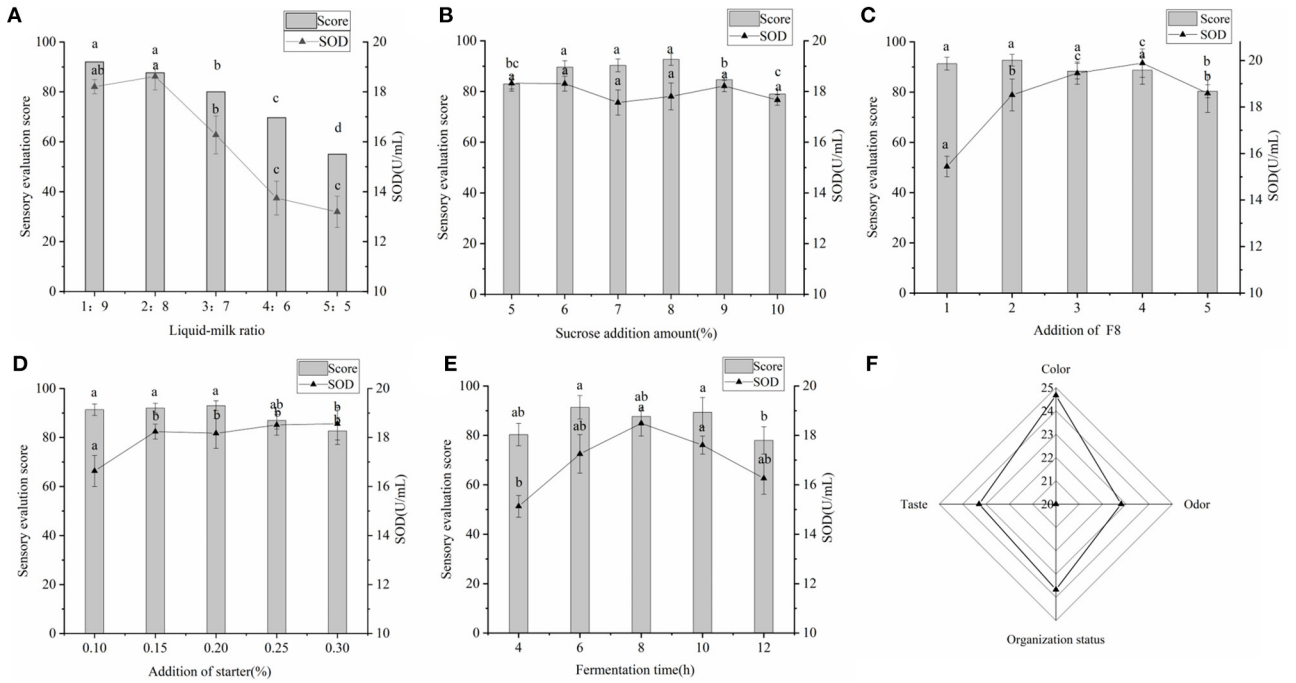

FIGURE 4 | (A) Effects of raw material ratio on SOD content and sensory. The ratio of millet enzymatic fermentation broth and fresh milk was set to 1:9, 2:8, 3:7, 4:6, and 5:5. **(B)** Effects of added sucrose on SOD content and sensory. The amount of sucrose added was set to 5–10%. **(C)** Effects of the amount of *Lactiplantibacillus plantarum subsp. plantarum F8* on SOD content and sensory sense. **(D)** The effect of direct-input starter on the yogurt quality. **(E)** The influence of fermentation time on yogurt. **(F)** Sensory evaluation chart of final yogurt. Significant differences were indicated by the letters a, b and c. Any difference with the same letter was considered not significant ($p > 0.05$) and any difference with a different letter was considered significant ($p < 0.05$).

and hydrogen peroxide with high specificity and efficiency (6). Overexpression of SOD has also been shown to mitigate radiation-induced damage (41). The SOD-rich millet yogurt we have developed was expected to appear in the recipes of people with pre-cancer or to prevent the development of diseases such as cancer.

Figure 4F was drawn from the results of three independent yogurt sensory evaluations. The results indicated that the yogurt was of high quality. The final yogurt was creamy white, glossy, with a pleasant milk flavor, uniform texture and moderate sweetness. The color, odor, texture and taste were 24.7, 22.8, 23.7, and 23.3 points, respectively. The results were similar to those of Yin M et al. for the sensory evaluation of yogurt (23). The pH of the final yogurt ranged from 4.1 to 4.3, the amount of LAB in fermented millet yogurt was 1.43×10^8 CFU mL^{-1} $> 1\times10^6$ CFU mL^{-1}, and no contamination of miscellaneous bacteria was detected in the yogurt. These were in accordance with the regulations for fermented milk (42). The SOD-rich millet yogurt developed by this project was compared with three types of yogurts available on the market. The results were shown in **Table 5**. The SOD content of the final yogurt was 63.01, 50.11, and 146.79% higher than the ordinary yogurt available on the market, including Bright Dairy 1911, Junlebao Old Yogurt and Weigang-flavored yogurt. This might be due to the high SOD-production LAB we used, in addition, the SOD contained in the millet enzymatic hydrolysis fermentation broth also promoted the total SOD in yogurt (6). The T-AOC of the final yogurt was 19.86, 8.67, and 27.24% higher than the aforementioned ordinary yogurt, respectively. This might be because millet yogurt contained antioxidant substances such as polyphenols, flavonoids and vitamin E from millet, and antioxidant enzymes such as SOD and catalase from *Bacillus subtilis* (37). The peptide content was slightly higher than Weigang-flavored yogurt and lower than Bright Dairy 1911 and Junlebao Old Yogurt. These results indicated that yogurt co-fermented with millet enzymatic digest has high-quality properties and significant antioxidant potential, and thus has great potential as a new functional food in the food industry.

Analysis of Non-volatile Flavor Substances in Yogurt by HPLC-MS

Twenty-two thousand five hundred and seventy-one non-volatile flavor substances from traditional starter (Y), traditional starter and *Lactiplantibacillus plantarum subsp. plantarum* F8 (Y-F8), millet yogurt (Y-F8-M) were screened by LC-MS, and the relevant differences among metabolites were determined. The screening conditions were p-value $\leq$ 0.05, VIP $\geq$ 1, and Fold_Change $\geq$ 1.5 or $\leq$0.667. Two hundred differential metabolites were selected (43). Multivariate statistical analysis was conducted to evaluate non-volatile metabolites and identify any potential variability associated with specific conditions. The PCA score was calculated to determine whether the sample

TABLE 4 | $L_9(4^3)$ Orthogonal results of millet yogurt rich in SOD.

Level	Experimental factors				Results
	A	B	C	D	SOD (U/mL)
1	1	1	1	1	16.720 ± 0.200
2	1	2	2	2	17.515 ± 0.745
3	1	3	3	3	18.621 ± 0.227
4	2	1	2	3	17.523 ± 0.175
5	2	2	3	1	19.827 ± 0.323
6	2	3	1	2	17.634 ± 0.540
7	3	1	3	2	15.317 ± 1.326
8	3	2	1	3	16.486 ± 0.361
9	3	3	2	1	17.012 ± 0.027
K_1	53.856	49.560	50.840	53.559	/
K_2	54.984	53.828	52.050	50.466	/
K_3	48.815	53.267	53.765	52.630	/
k_1	17.610	16.520	16.946	17.850	/
k_2	18.328	17.942	17.350	16.822	/
k_3	16.271	17.755	17.921	17.540	/
R	2.057	1.422	0.975	1.031	/
Excellent level	A_2	B_2	C_3	D_1	/

SOD, Superoxide dismutase.

TABLE 5 | Comparison of the contents of various substances in ordinary yogurt.

Category	SOD (U/mL)	T-AOC (U/mL)	Peptide (mg/mL)
Millet yogurt with SOD	19.827 ± 0.323^{a}	25.331 ± 1.691^{a}	1.282 ± 0.049^{c}
Bright Dairy 1911	12.163 ± 1.001^{b}	21.134 ± 1.591^{b}	1.649 ± 0.020^{b}
Weigang flavored yogurt	8.034 ± 0.614^{c}	19.908 ± 2.593^{b}	1.057 ± 0.068^{d}
Junlebao Old Yogurt	13.208 ± 0.892^{b}	23.311 ± 1.207^{ab}	1.881 ± 0.047^{a}

SOD, Superoxide dismutase; T-AOC, total antioxidant capacity. Any difference with the same letter was considered not significant ($p > 0.05$) and any difference with a different letter was considered significant ($p < 0.05$).

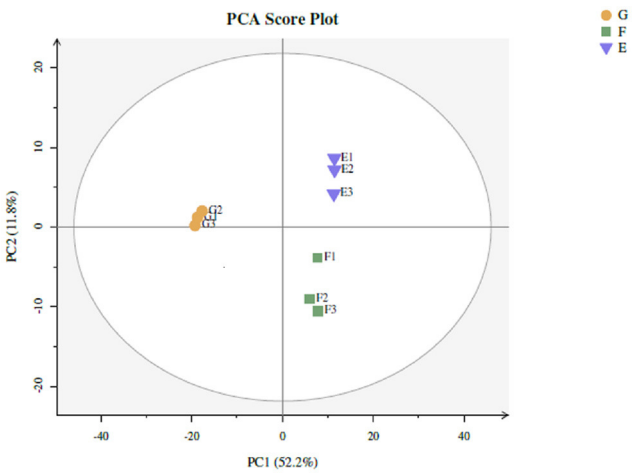

FIGURE 5 | Types of yogurt were as follows: traditional starter (Y), traditional starter and *Lactiplantibacillus plantarum subsp. plantarum F8* (Y-F8), and millet yogurt (Y-F8-M). PCA non-volatile metabolite score for comparison between Y (E), Y-F8 (F), and Y-F8-M (G) (Blue falling triangle: Y, green square: Y-F8, yellow circle: Y-F8-M).

repeatability in the group was sufficiently large (44). As shown in **Figure 5**, the repeatability of the three yogurt samples was better. The distance of the three yogurt samples was relatively close, the difference differed. The three yogurt samples were separated from the PC1 (52.2%), and along the PC2 direction (11.8%).

A Heat-map was drawn to distinguish the three groups of sample metabolites (**Figure 6**). Each small square indicated the metabolic substance content, and the colors indicated the metabolite content. A total of 22,571 non-volatile flavor substances were found in yogurt. Compared with Group E, the change of non-volatile flavor substances in Group F might be mainly related to the 9 metabolic pathways with high significance and high pathway impact in *Lactiplantibacillus plantarum subsp. plantarum* F8. Including 2-Oxocarboxylic acid metabolism, Aminobenzoate degradation, Biosynthesis of alkaloids derived from ornithine, lysine and nicotinic acid, Degradation of aromatic compounds, ABC transporters, Biosynthesis of amino acids, Microbial metabolism in diverse environments and Biosynthesis of secondary metabolites, as shown in **Figure 7A**. Compared with Group E, 12 metabolites were found to be significant upregulated in group F. Among them, the content of 4-Hydroxy-3-methoxybenzenemethanol was increased by 6.48 times. It had milk, cream and coconut aroma, which was a common baked food natural spice (3). The L-Threonine content was increased 5.45 times, which was considered an essential

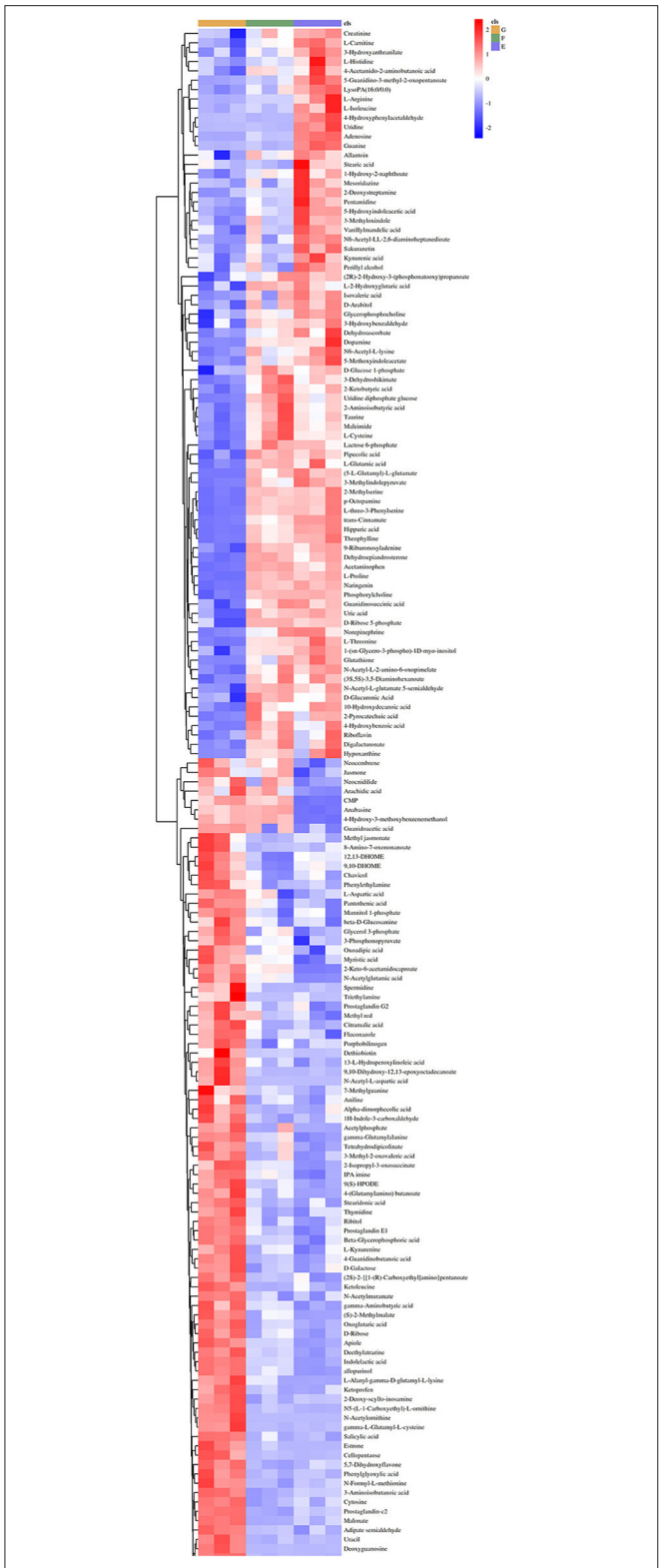

FIGURE 6 | Heat-map and hierarchical clustering of non-volatile metabolite profiles in yogurt. The dendrogram represents sample clusters based on Pearson's correlation coefficient with average linkage. The normalized non-volatile metabolite abundance was visualized by color: red indicates the highest values, and blue indicates the lowest values (E: Y, F: Y-F8, G: Y-F8-M).

amino acid with a slightly sweet taste, and it was produced by the action of threonine synthase with high serine phosphate as a substrate (17). The content of allopurinol increased by 4.57 times, which is an isomer of xanthine. It could reduce the production of oxygen free radicals in ischemic re-injection damage to achieve antioxidant effects, so it was often used in primary and secondary hyperuricemia (45). This might also be partly responsible for the high antioxidant capacity of millet yogurt. Arachidonic acid was increased by 2.01 times, and it was a polyunsaturated fatty acid that might play a role in reducing the prevention of diabetes and tumors. In *Lactiplantibacillus plantarum subsp. plantarum*, it was produced by phosphatidylcholine and H_2O through the arachidonic acid metabolic pathway catalyzed by phospholipase A (46). In addition, nine metabolites were downregulated, with uridine, adenosine and guanine decreasing by 28.57, 4.14, and 4.34 times, respectively. Adenosine is an important intermediate used in the synthesis of adenine, and an increase in purine levels in the body leads to an increase in uric acid, which ultimately leads to hyperuricemia in humans. This was consistent with the reported ability of LAB to absorb and metabolize exogenous nucleosides and purine bases (47). Furthermore, this *Lactiplantibacillus plantarum subsp. plantarum* has a strong nucleoside catabolic capacity and might be applied in the diet of patients with hyperuricemia. The metabolomic analysis indicated that *Lactiplantibacillus plantarum subsp. plantarum* might have a strong probiotic potential and application value.

Compared with Group E, the production of differential non-volatile flavor substances in Group G was related not only to millet enzymatic hydrolysis fermentation broth, but also related to the 13 metabolic pathways with high significance and high pathway impact in *Lactiplantibacillus plantarum subsp. Plantarum* F8. Including Bile secretion, Biosynthesis of alkaloids derived from shikimate pathway, Arginine and proline metabolism, Carbon metabolism, Biosynthesis of alkaloids derived from ornithine, lysine and nicotinic acid, Aminoacyl-tRNA biosynthesis, Central carbon metabolism in cancer, 2-Oxocarboxylic acid metabolism, ABC transporters, Biosynthesis of cofactors, Biosynthesis of plant secondary metabolites, Biosynthesis of amino acids and Biosynthesis of secondary metabolites, as shown in **Figure 7B**. Compared with Group E, the variety of non-volatile flavor substances in Group G increased by two times, mainly due to the addition of millet enzyme fermentation liquid, which greatly ameliorated the flavor of yogurt. Compared with Group E, the non-volatile flavor substances produced by Group G were increased by 37 and reduced by 44. Among them, 2-Phenylethanol was increased 3169.6 times, a colorless liquid organic matter with a rose aroma (44). The content of hesperetin has been increased by 228.36 times, which was a natural flavonoid compound with antioxidant effect and was widely used in fruits, flowers and food (48). The hesperetin in millet yogurt is mainly derived from the added millet enzymatic fermentation broth, which is also consistent with the high antioxidant capacity of the previous yogurt. N-Acetylornithine is an intermediate from L-glutamic acid to L-arginine enzymatic biosynthesis, and the content was increased 271.22 times. L-methionine can be used in synthetic vitamins, which can protect the liver, and it is an essential

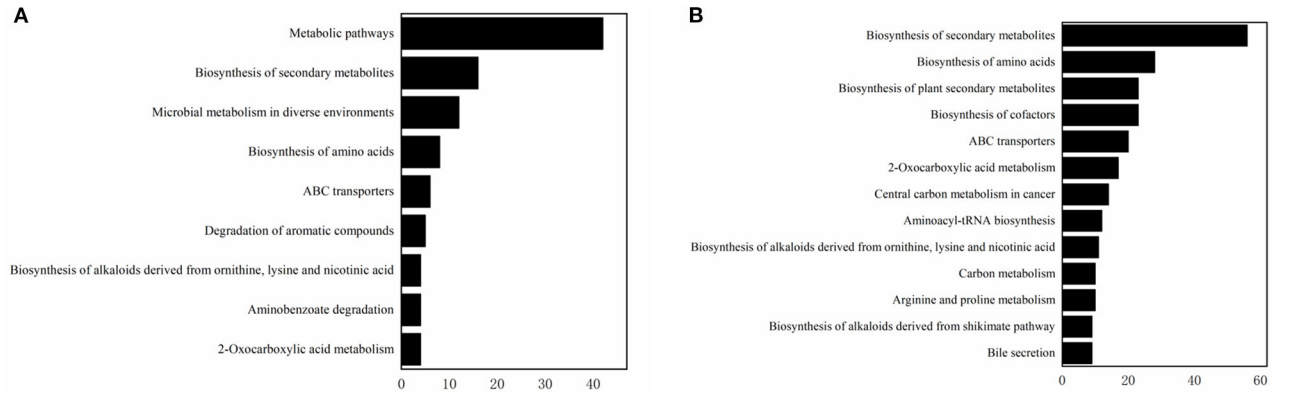

FIGURE 7 | The enriched pathways. **(A)** The enriched pathways involved by significantly increased metabolites when compared group F to group E. **(B)** The enriched pathways involved by significantly increased metabolites when compared group G to group E.

amino acid, which has significant value to the human body (49). L-methionine was increased 55.67 times in non-volatile metabolites. Most flavored compounds in yogurt were because of creamy fat decomposition and microbial transformation of lactose and citrate. The addition of millet enzymatic hydrolysis fermentation broth to yogurt enriched the variety of flavoring substances in yogurt, and this practice could also counteract the natural sourness of yogurt. This was consistent with previous reports that the addition of plant or fruit components might add sweetness or nutritional value of yogurt (50). Compared with ordinary yogurt, adding F8 and millet could improve the flavor and yogurt nutrients. The results of this part of the experiment provide insights into the metabolic mechanisms of *Lactiplantibacillus plantarum subsp. plantarum* F8, mainly related to the biosynthesis of secondary metabolites, amino acid metabolism and nucleotide metabolism. As well as the fingerprinting of the effect of millet enzymatic digest on non-volatile flavor substances in yogurt represents a real advance in the study of metabolites in yogurt.

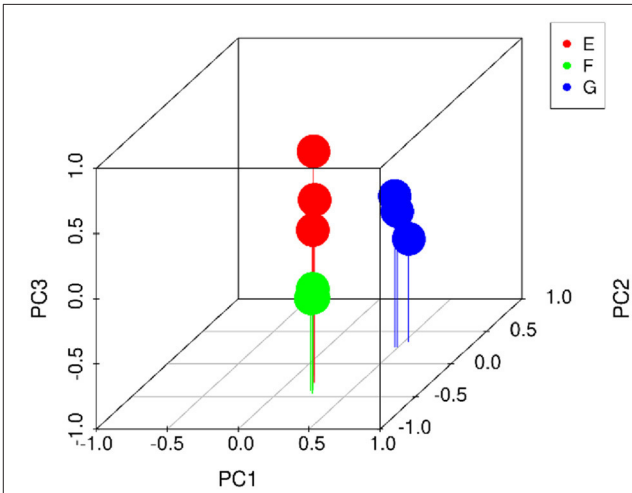

FIGURE 8 | 3D PCA volatile metabolite score was used to compare traditional starter (Y), traditional starter and *Lactiplantibacillus plantarum subsp. plantarum F8* (Y-F8), and millet yogurt (Y-F8-M) (Red circle: Y, green circle: Y-F8, blue circle: Y-F8-M).

Analysis of Volatile Flavor Compounds in Yogurt by HS-SPME-GC-MS

PCA exhibited multiple components with large-to-small contributions (PC1, PC2, PC3…). 3D PCA used the first three dimensions for mapping to observe the distribution of samples in three-dimensional space. As indicated in **Figure 8**, the sample repeatability of the three yogurt groups was good, and the differences among the groups were large. The distance between group E and group F was relatively close, indicating that the addition of *Lactiplantibacillus plantarum subsp. plantarum* F8 affected the volatile flavor compounds of the two yogurts. In contrast, the distance among group G, group F and group E were far, indicating that the amount of added millet remarkably contributed to the volatile flavor of yogurt.

From **Figure 9**, it can be seen that 54 volatile flavor substances were found in yogurt, including alcohols, lipids, organic acids and hydrocarbons. Compared with group E, 12 volatile flavor substances were upregulated, and seven were downregulated in group F. Among these volatile flavor substances, Nonanoic acid was produced in *Lactiplantibacillus plantarum subsp. plantarum* via the fatty acid metabolic pathway and has a fruity flavor (3). Nonanoic acid was also detected and significantly upregulated when Tian studied the effect of four kinds of probiotic LAB on fermented milk flavor substances (51). This indicated that Nonanoic acid might be a typical flavor substance produced by probiotic LAB fermented yogurt. Oxalic acid, butyl propyl ester was produced by esterification in *Lactiplantibacillus plantarum subsp. plantarum* and has an aromatic odor, which was an important component of yogurt aroma (3). 2-Hydroxy-3-pentanone was produced by the conversion of glycerol by *Lactiplantibacillus plantarum subsp. plantarum* through the glycolytic pathway and was commonly used in food flavoring agents (52). Benzaldehyde is an organic

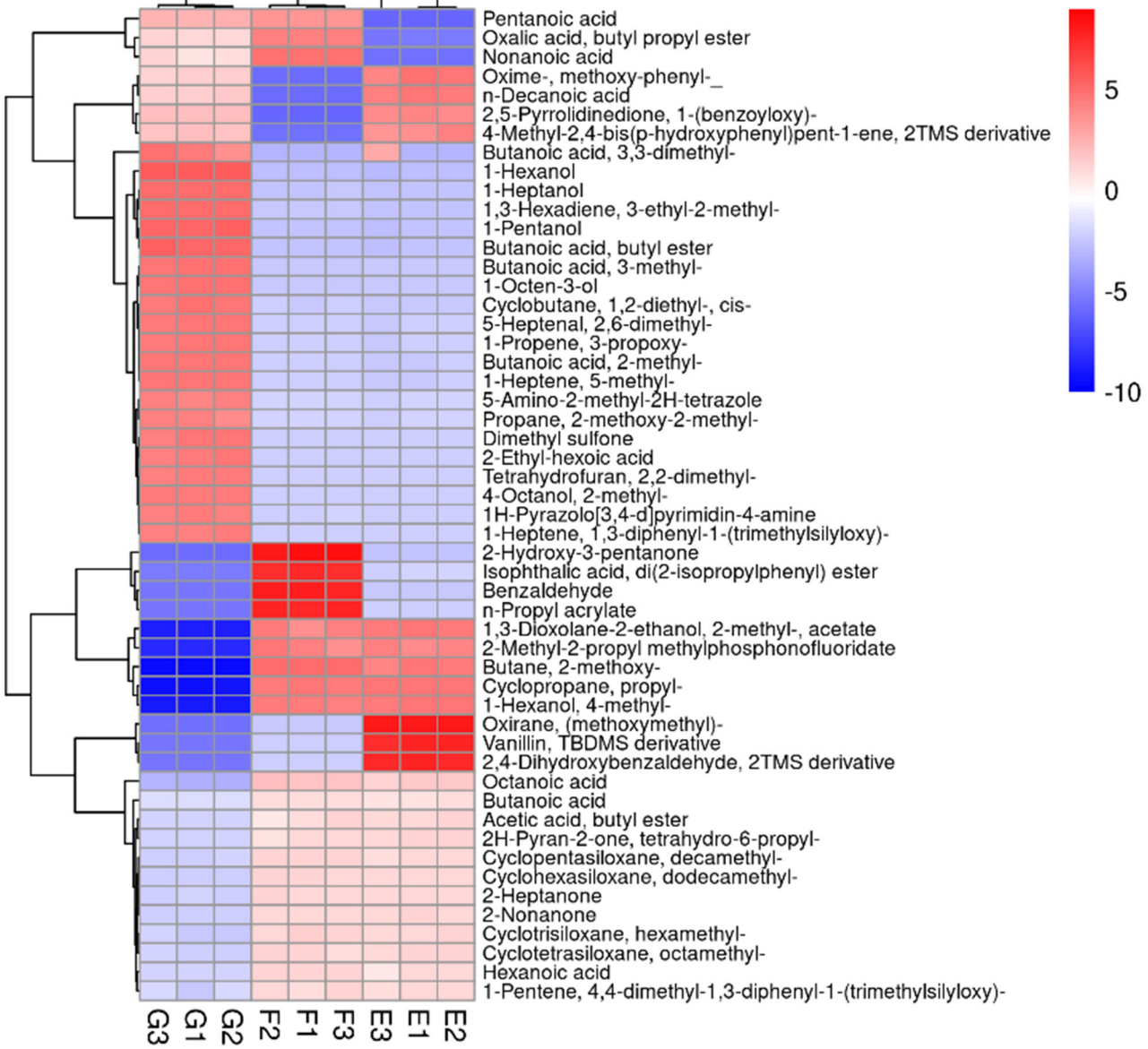

FIGURE 9 | Heat-map and hierarchical clustering of volatile metabolite profiles in yogurt. The normalized volatile metabolite abundance was visualized by color: red indicates the highest values, and blue indicates the lowest values (E: Y, F: Y-F8, G: Y-F8-M).

compound formed when the hydrogen of benzene is replaced by an aldehyde group. It was the most commonly used aromatic aldehyde with a bitter almond, cherry and nutty flavor (53). The current methods of producing benzaldehyde were mainly chemical synthesis or extraction from plants (51). This strain of *Lactiplantibacillus plantarum subsp. plantarum* produced benzaldehyde at relatively high levels and might have the potential to produce benzaldehyde using microbial fermentation. Therefore, the addition of *Lactiplantibacillus plantarum subsp. plantarum* F8 might have a particularly positive effect on the abundance of volatile flavor substances in yogurt.

Compared with group F, 25 volatile flavor substances were upregulated in group G, of which the content of 5-Heptenal, 2,6-dimethyl (with grassy, sweet, cucumber and watermelon aroma), 2-Ethyl-hexoic acid (generally used in barbecues, beverages and sweets and naturally found in wine and beer), 2-Ethyl-hexoic acid

(slightly smelly, used for synthetic spices), 1-Hexanol (with fruity aroma), Butanoic acid, butyl ester (with fresh sweet fruit aroma, similar to banana and pineapple flavor), 1-Pentanol (slightly fruity), 1-Heptanol (with fresh and light oily fat aroma, similar to whiskey and wine-like aroma), n-Decanoic acid (with a rancid taste), Butanoic acid, and 3-methyl (with a strong cheese aroma) was significantly increased (17, 54, 55). The formation of yogurt flavor is a complex and dynamic biochemical process (56). Millet enzymatic fermentation broth were added to enrich the volatile flavor substances in yogurt, mask the production of unpleasant volatile flavor substances, counteract the natural sour taste in yogurt, and make the product more in line with consumer taste. The addition of *Lactiplantibacillus plantarum subsp. plantarum* F8 and the plant-based ingredient millet may make an essential contribution to the flavor of yogurt. Additionally, they promote the formation of volatile metabolites that positively influence the aroma quality of yogurt samples (57). The results of this work provide novel knowledge about the contribution of the isolated strains and the millet enzymatic digests to the flavor profile of yogurt, which will help improve the sensory features of the final product.

CONCLUSIONS

In this study, LAB, namely, *Lactiplantibacillus plantarum subsp. plantarum* F8, was screened, with a SOD yield of $2476.21 \pm 1.52\,\mathrm{U\ g^{-1}}$. Meanwhile, this strain exhibited great potential as a probiotic. When this novel yogurt was used in the millet-based yogurt fermentation, its SOD activity was $19.827 \pm 0.323\,\mathrm{U\ mL^{-1}}$, higher than Bright Dairy 1911, Grand Park Old Yogurt and Weigang Flavored Yogurt Ordinary Yogurt. The addition of *Lactiplantibacillus plantarum subsp. plantarum* F8 significantly upregulated 12 non-volatile metabolites in yogurt, and the addition of millet enzymatic fermentation increased the non-volatile metabolites in yogurt. Thirty-seven species were significantly upregulated, including 2-Phenylethanol, Hesperetin, N-Acetylornithine and L-methionine were upregulated by 3169.6, 228.36, 271.22, and 55.67 times, respectively. The addition of *Lactiplantibacillus plantarum subsp. plantarum* F8 had a specific positive effect on the abundance of volatile flavor substances in yogurt. The addition of millet enzymatic fermentation broth enriched the volatile flavor substances in yogurt. The production of unpleasant volatile flavor substances was masked, making the product more in line with consumer taste.

DATA AVAILABILITY STATEMENT

The original contributions presented in the study are included in the article/supplementary material, further inquiries can be directed to the corresponding author/s.

AUTHOR CONTRIBUTIONS

XF: writing—original draft, data curation, investigation, methodology, and formal analysis. XL: conceptualization, writing—review and editing, data curation, formal analysis, investigation, and project administration. DP: conceptualization, project administration, funding acquisition, validation, and supervision. TZ: data curation, methodology, and supervision. ZW: formal analysis, visualization, resources, and methodology. YG: resources and methodology. XZ: conceptualization and project administration. ZS: conceptualization and formal analysis. All authors contributed to the article and approved the submitted version.

FUNDING

This work was financially supported by Natural Science Funding of China (31972048), Jiangsu Agricultural Science and Technology Innovation Fund [CX(18)3036], Jiangsu Science and Technology Department (BE2018397), the Scientific Research Foundation of Graduate School of Ningbo University (IF2021084).

REFERENCES

1. Macnaughtan J, Figorilli F, García-López E, Lu H, Jalan R. A double-blind, randomized placebo-controlled trial of probiotic lactobacillus casei shirota in stable cirrhotic patients. *Nutrients.* (2020) 12:1651. doi: 10.3390/nu12061651
2. Binda S, Hill C, Johansen E, Obis D, Ouwehand AC. Criteria to qualify microorganisms as "probiotic" in foods and dietary supplements. *Front Microbiol.*(2020) 11:1662. doi: 10.3389/fmicb.2020.01662
3. Aryana KJ, Olson DW. A 100-year review: yogurt and other cultured dairy products. *J Dairy Sci.* (2017) 100:9987–10013. doi: 10.3168/jds.2017-12981
4. Wu Z, Chen T, Pan D, Zeng X, Guo Y, Zhao G. Resveratrol and organic selenium-rich fermented milk reduces D-galactose-induced cognitive dysfunction in mice. *Food Funct.* (2021) 12:1318–26. doi: 10.1039/D0FO02029J
5. Aguirre-Ezkauriatza EJ, Galarza-Gonzalez MG, Uribe-Bujanda AI, Rios-Licea M, Lopez-Pacheco F, Hernandez-Brenes CM, et al. Effect of mixing during fermentation in yogurt manufacturing. *J Dairy Sci.* (2008) 91:4454–65. doi: 10.3168/jds.2008-1140
6. Borgstahl GE, Oberley-Deegan RE. Superoxide Dismutases (SODs) and SOD Mimetics. *Antioxidants.* (2018) 7:156. doi: 10.3390/antiox7110156
7. Wang CY, Wu SJ, Shyu YT. Antioxidant properties of certain cereals as affected by food-grade bacteria fermentation. *J Biosci Bioeng.* (2014) 117:449–56. doi: 10.1016/j.jbiosc.2013.10.002
8. Marazza JA, Nazareno MA, Giori G, Garro MS. Enhancement of the antioxidant capacity of soymilk by fermentation with Lactobacillus rhamnosus. *J Funct Foods.* (2012) 4:594–601. doi: 10.1016/j.jff.2012.03.005
9. Kang YM, Lee BJ, Kim JI, Nam BH, Cha JY, Kim YM. Antioxidant effects of fermented sea tangle (Laminaria japonica) by Lactobacillus brevis BJ20 in individuals with high level of γ-GT: A randomized, double-blind, and placebo-controlled clinical study. *Food Chem Toxicol.* (2012) 50:1166–9. doi: 10.1016/j.fct.2011.11.026
10. Xiaolong J, Baixiang P, Hehui D, Bingbing C, Hui N, Yizhe Y. Purification, structure and biological activity of pumpkin polysaccharides: a review. *Food Rev Int.* (2021). doi: 10.1080/87559129.2021.1904973. [Epub ahead of print].
11. Jhan F, Shah A, Gani A, Ahmad M, Noor N. Nano-reduction of starch from underutilised millets: Effect on structural, thermal, morphological and nutraceutical properties. *Int J Biol Macromol.* (2020) 159:1113–21. doi: 10.1016/j.ijbiomac.2020.05.020
12. Sargun M, Kiruba K, Azlin M. Physical properties of complementary food powder obtained from upcycling of Greek yogurt acid whey with kodo

and proso millets. *J Food Process Eng.* (2021) 44:e13878. doi: 10.1111/jfpe.13878
13. Song X, Sun X, Ban Q, Cheng J, Zhang S, Guo M. Gelation and microstructural properties of a millet–based yogurt–like product using polymerized whey protein and xanthan gum as thickening agents. *J Food Sci.* (2020) 85:3927–33. doi: 10.1111/1750-3841.15504
14. Steinkraus KH. Classification of fermented foods: worldwide review of household fermentation techniques. *Food Control.* (1997) 8:311–31. doi: 10.1016/S0956-7135(97)00050-9
15. Chou ST, Chao WW, Chung YC. Antioxidative activity and safety of 50% ethanolic red bean extract (Phaseolus radiatus L. var Aurea). J *Food Sci.* (2003) 68:21–5. doi: 10.1111/j.1365-2621.2003.tb14108.x
16. Shin EC, Lee JH, Hwang CE, Lee BW, Kim HT, Ko JM, et al. Enhancement of total phenolic and isoflavone-aglycone contents and antioxidant activities during Cheonggukjang fermentation of brown soybeans by the potential probiotic Bacillus subtilis CSY191. *Food Sci Biotechnol.* (2014) 23:531–8. doi: 10.1007/s10068-014-0073-9
17. Chen C, Zhao S, Hao G, Yu H, Tian H, Zhao G. Role of lactic acid bacteria on the yogurt flavour: a review. *Int J Food Properties.* (2017) 20:S316–30. doi: 10.1080/10942912.2017.1295988
18. Erkaya TSENG, Uuml LM. Comparison of volatile compounds in yoghurts made from cowsandrsquo buffaloesandrsquo ewesandrsquo; and goatsandrsquo milks. *Int J Dairy Technol.* (2011) 64:240–6. doi: 10.1111/j.1471-0307.2010.00655.x
19. Gu Y, Li X, Xiao R, Dudu OE, Yang L, Ma Y. Impact of Lactobacillus paracasei IMC502 in coculture with traditional starters on volatile and non-volatile metabolite profiles in yogurt. *Process Biochem.* (2020) 99:61–9. doi: 10.1016/j.procbio.2020.07.003
20. Ofc A, Ahc B, Hs C, Na C, Ht B. Isolation and Identification of lactobacilli from traditional yogurts as potential starter cultures. *LWT.* (2021) 148:111774. doi: 10.1016/j.lwt.2021.111774
21. Fessard A, Bourdon E, Payet B, Remize F. Identification, stress tolerance, and antioxidant activity of lactic acid bacteria isolated from tropically grown fruits and leaves. *Can J Microbiol.* (2016) 62:550–61. doi: 10.1139/cjm,-2015-0624
22. Zhang J, Cai D, Yang M, Hao Y, Zhu Y, Chen Z, et al. Screening of folate-producing lactic acid bacteria and modulatory effects of folate-biofortified yogurt on gut dysbacteriosis of folate-deficient rats. *Food Funct.* (2020) 11:6308–18. doi: 10.1039/D0FO00480D
23. Yin M, Yang D, Lai S, Yang H. Rheological properties of xanthan-modified fish gelatin and its potential to replace mammalian gelatin in low-fat stirred yogurt[J]. *LWT Food Sci Technol.* (2021) 147:111643. doi: 10.1016/j.lwt.2021.111643
24. Xiao F, Ng VK, Marta MK, Yang H. Effects of fish gelatin and tea polyphenol coating on the spoilage and degradation of myofibril in fish fillet during cold storage. *Food Bioprocess Technol.* (2017) 10:89–102. doi: 10.1007/s11947-016-1798-7
25. Chen L, Zhao X, Wu J E, Liu Q, Pang X, Yang H. Metabolic characterisation of eight Escherichia coli strains including 'Big Six' and acidic responses of selected strains revealed by NMR spectroscopy. *Food Microbiol.* (2020) 88:103399. doi: 10.1016/j.fm.2019.103399
26. Dongmo SN, Sacher B, Kollmannsberger H, Becker T. Key volatile aroma compounds of lactic acid fermented malt based beverages–impact of lactic acid bacteria strains. *Food Chem.* (2017) 229:565–73. doi: 10.1016/j.foodchem.2017.02.091
27. Cheng H. Volatile flavor compounds in yogurt: a review. *Crit Rev Food Sci Nutr.* (2010) 50:938–50. doi: 10.1080/10408390903044081
28. Dan T, Wang D, Jin R, Zhang H, Zhou T, Sun T. Characterization of volatile compounds in fermented milk using solid-phase microextraction methods coupled with gas chromatography-mass spectrometry. *J Dairy Sci.* (2017) 100:2488–500. doi: 10.3168/jds.2016-11528
29. Li S, Tian Y, Jiang P, Lin Y, Yang H. Recent advances in the application of metabolomics for food safety control and food quality analyses. *Crit Rev Food Sci Nutr.* (2020) 2020:1–22. doi: 10.1080/10408398.2020.1761287
30. Lin CBJW, Zl A, Qin L, Xue Z, Hya C. Metabolomic analysis of energy regulated germination and sprouting of organic mung bean (Vigna radiata) using NMR spectroscopy. *Food Chem.* (2019) 286:87–97. doi: 10.1016/j.foodchem.2019.01.183
31. Li D, Gao C, Zhang F, Yang R, Lan C, Ma Y, et al. Seven facts and five initiatives for gut microbiome research. *Protein Cell.* (2020) 11:391–400. doi: 10.1007/s13238-020-00697-8
32. Chen L, Zhao X, Wu JE, He Y, Yang H. Metabolic analysis of salicylic acid-induced chilling tolerance of banana using NMR. *Food Res Int.* (2020) 128:108796. doi: 10.1016/j.foodres.2019.108796
33. Kudo H, Sasaki Y. Intracellular pH determination for the study of acid tolerance of lactic acid bacteria. *Methods Mol Biol.* (2019) 1887:33–41. doi: 10.1007/978-1-4939-8907-2_4
34. Gao YX, Xu B, Fan HR, Zhang MR, Li S. 1H NMR-based chemometric metabolomics characterization of soymilk fermented by Bacillus subtilis BSNK-5. *Food Res Int.* (2020) 138(Pt A):109686. doi: 10.1016/j.foodres.2020.109686
35. Wu Z, Wang P, Pan D, Zeng X, Guo Y, Zhao G. Effect of adzuki bean sprout fermented milk enriched in γ-aminobutyric acid on mild depression in a mouse model. *J Dairy Sci.* (2021) 104:78–91. doi: 10.3168/jds.2020-19154
36. Chooruk A, Piwat S, Teanpaisan R. Antioxidant activity of various oral Lactobacillus strains. *J Appl Microbiol.* (2017) 123:271–9. doi: 10.1111/jam.13482
37. Ryu JA, Kim E, Kim MJ, Lee S, Kim HY. Physicochemical characteristics and microbial communities in gochujang, a traditional korean fermented hot pepper paste. *Front Microbiol.* (2021) 11:3543. doi: 10.3389/fmicb.2020.620478
38. Ragaee S, Abdel-Aal E, Noaman M. Antioxidant activity and nutrient composition of selected cereals for food use. (2006) 98:32–8. doi: 10.1016/j.foodchem.2005.04.039
39. Lili Z, Ran F, Fazheng R, Xueying MJL. Addition of buttermilk improves the flavor and volatile compound profiles of low-fat *yogurt*. (2018) 98:9–17. doi: 10.1016/j.lwt.2018.08.029
40. Feng QH, Jin XG, Yu JK, Yuan QS. Detection of superoxide dismutase in milk %. *Food Sci.* (1994) 56–59.
41. Cline JM, Dugan G, Bourland JD, Perry DL, Stitzel JD, Weaver AA, et al. Post-irradiation treatment with a superoxide dismutase mimic, MnTnHex-2-PyP5+, mitigates radiation injury in the lungs of non-human primates after whole-thorax exposure to ionizing radiation. *Antioxidants.* (2018) 7:40. doi: 10.3390/antiox7030040
42. Gao HX, Yu ZL, He Q, Tang SH, ZengWC. A potentially functional yogurt co-fermentation with gnaphalium affine. *LWT.* (2018) 91:423–30. doi: 10.1016/j.lwt.2018.01.085
43. Dan T, Ren W, Liu Y, Tian J, Chen H, Li T, et al. Volatile flavor compounds profile and fermentation characteristics of milk fermented by lactobacillus delbrueckii subsp bulgaricus. *Front Microbiol.* (2019) 10:2183. doi: 10.3389/fmicb.2019.02183
44. Grasso N, Alonso-Miravalles L, O'Mahony JA. Composition, physicochemical and sensorial properties of commercial plant-based yogurts. *Foods.* (2020) 9:252. doi: 10.3390/foods9030252
45. Yang CY, Chen CH, Deng ST, Huang CS, Lin YJ, Chen YJ, et al. Allopurinol use and risk of fatal hypersensitivity reactions: a nationwide population-based study in Taiwan[J]. *JAMA Internal Med.* (2015) 175:1550–7. doi: 10.1001/jamainternmed.2015.3536
46. Lubbers S, Decourcelle N, Vallet N, Guichard E. Flavor release and rheology behavior of strawberry fatfree stirred yogurt during storage. *J Agric Food Chem.* (2004) 52:3077–82. doi: 10.1021/jf0352374
47. Yamanaka H, Taniguchi A, Tsuboi H, Kano H, Asami Y. Hypouricaemic effects of yoghurt containing Lactobacillus gasseri PA-3 in patients with hyperuricaemia and/or gout: a randomised, double-blind, placebo-controlled study. *Modern Rheumatol.* (2019) 29:146–50. doi: 10.1080/14397595.2018.1442183
48. Özcelik S, Kuley E, Özogul F. Formation of lactic, acetic, succinic, propionic, formic and butyric acid by lactic acid bacteria. *LWT.* (2016) 73:536–42. doi: 10.1016/j.lwt.2016.06.066
49. Su N, Ren L, Ye H, Sui Y, Li J, Ye M. Antioxidant activity and flavor compounds of hickory yogurt. *Int J Food Properties.* (2017) 20:1894–903. doi: 10.1080/10942912.2016.1223126
50. Farag MA, Saleh HA, Ahmady E, Elmassry MM Dissecting yogurt: the impact of milk types, probiotics, and selected additives on yogurt quality. *Food Rev Int.*(2021). doi: 10.1080/87559129.2021.1877301. [Epub ahead of print].

51. Tian H, Shen Y, Yu H, He Y, Chen C. Effects of 4 probiotic strains in coculture with traditional starters on the flavor profile of yogurt. *J Food Sci.* (2017) 82:1693–701. doi: 10.1111/1750-3841.13779
52. Turgut T, Cakmakci S. Probiotic strawberry yogurts: microbiological, chemical and sensory properties. *Probiot Antimicrob Proteins.* (2018) 10:64–70. doi: 10.1007/s12602-017-9278-6
53. Le Lay C, Coton E, Le Blay G, Chobert JM, Haertlé T, Choiset Y, et al. Identification and quantification of antifungal compounds produced by lactic acid bacteria and propionibacteria. *Int J Food Microbiol.* (2016) 239:79–85. doi: 10.1016/j.ijfoodmicro.2016.06.020
54. Santis DD, Giacinti G, Chemello G, Frangipane MT. Improvement of the sensory characteristics of goat milk yogurt. *J Food Sci.* (2019) 84:2289–96. doi: 10.1111/1750-3841.14692
55. Yang S, Yan D, Zou Y, Mu D, Wu J. Fermentation temperature affects yogurt quality: a metabolomics study. *Food Biosci.* (2021) 42:101104. doi: 10.1016/j.fbio.2021.101104
56. Tian H, Shi Y, Zhang Y, Yu H, Mu H, Chen C. Screening of aroma–producing lactic acid bacteria and their application in improving the aromatic profile of yogurt[J]. *J Food Biochem.* (2019) 43:e12837. doi: 10.1111/jfbc.12837
57. Das K, Choudhary R, Thompson-Witrick KA. Effects of new technology on the current manufacturing process of yogurt-to increase the overall marketability of yogurt. *LWT.* (2019) 108:69–80. doi: 10.1016/j.lwt.2019.03.058

Conflict of Interest: The authors declare that the research was conducted in the absence of any commercial or financial relationships that could be construed as a potential conflict of interest.

Publisher's Note: All claims expressed in this article are solely those of the authors and do not necessarily represent those of their affiliated organizations, or those of the publisher, the editors and the reviewers. Any product that may be evaluated in this article, or claim that may be made by its manufacturer, is not guaranteed or endorsed by the publisher.

frontiers in Nutrition

ORIGINAL RESEARCH
published: 28 January 2022
doi: 10.3389/fnut.2021.790765

Hulless Black Barley as a Carrier of Probiotics and a Supplement Rich in Phenolics Targeting Against H_2O_2-Induced Oxidative Injuries in Human Hepatocarcinoma Cells

Han Wu[1,2], *Hao-Nan Liu*[1,3], *Chun-Quan Liu*[1], *Jian-Zhong Zhou*[1,3], *Xiao-Li Liu*[1,3]* and *Hong-Zhi Zhang*[1]*

[1] Institute of Agro-Product Processing, Jiangsu Academy of Agricultural Sciences, Nanjing, China, [2] College of Food Science and Technology, Huazhong Agricultural University, Wuhan, China, [3] School of Food and Biological Engineering, Jiangsu University, Zhenjiang, China

OPEN ACCESS

Edited by:
Yu Xiao,
Hunan Agricultural University, China

Reviewed by:
Bin Li,
Shenyang Agricultural University, China
Lu Wang,
Hainan University, China

***Correspondence:**
Xiao-Li Liu
liuxiaoli@jaas.ac.cn
Hong-Zhi Zhang
zhz0731@sina.cn

Specialty section:
This article was submitted to Food Chemistry, a section of the journal Frontiers in Nutrition

Received: 07 October 2021
Accepted: 15 December 2021
Published: 28 January 2022

Citation:
Wu H, Liu H-N, Liu C-Q, Zhou J-Z, Liu X-L and Zhang H-Z (2022) Hulless Black Barley as a Carrier of Probiotics and a Supplement Rich in Phenolics Targeting Against H_2O_2-Induced Oxidative Injuries in Human Hepatocarcinoma Cells. Front. Nutr. 8:790765. doi: 10.3389/fnut.2021.790765

Lactic acid bacteria can provide benefits to human beings and transform phenolic substances to improve their potential functionality. It was of interest to develop black barley as a carrier of probiotics and nutraceutical supplement rich in more antioxidants. Due to fermentation, bacterial counting and free phenolic content in black barley increased to 9.54 ± 0.22 log cfu/mL and 5.61 ± 0.02 mg GAE/mL, respectively. Eleven phenolic compounds, including nine isoflavones and two nitrogenous compounds were characterized using UPLC-QTOF-MS, among which epicatechin, hordatine, and pelargonidin aglycone were largely enriched. Moreover, free phenolic extracts from fermented barley (F-BPE) played a greater role in scavenging DPPH radicals, reducing Fe^{3+} to Fe^{2+}, and increasing oxygen radical absorbance capacity, compared phenolic extracts from unfermented barley [UF-BPE (1.94-, 1.71-, and 1.35-fold at maximum for F-BPE vs. UF-BPE, respectively)]. In hepatocarcinoma cells, F-BPE also better inhibited ROS production and improved cell viability, cell membrane integrity, SOD activity, and non-enzymatic antioxidant GSH redox status (2.85-, 3.28-, 2.05-, 6.42-, and 3.99-fold at maximum for F-BPE vs. UF-BPE, respectively).

Keywords: black barley, lactic acid bacteria, phenolic transformation, antioxidant activity, human hepatocarcinoma cells

HIGHLIGHTS

- *Lactobacillus* improved phenolic content and antioxidant activity of black barley.
- UPLC-QTOF-MS analysis was carried out for phenolic compounds from UFB and FB.
- StrainP-S1016 largely enriched epicatechin, hordatine and pelargonidin aglycone.
- FB phenolics better ameliorated oxidative defense system by a composite mechanism.
- A novel strategy was found to develop barley as carrier of probiotics and therapeutic ingredients.

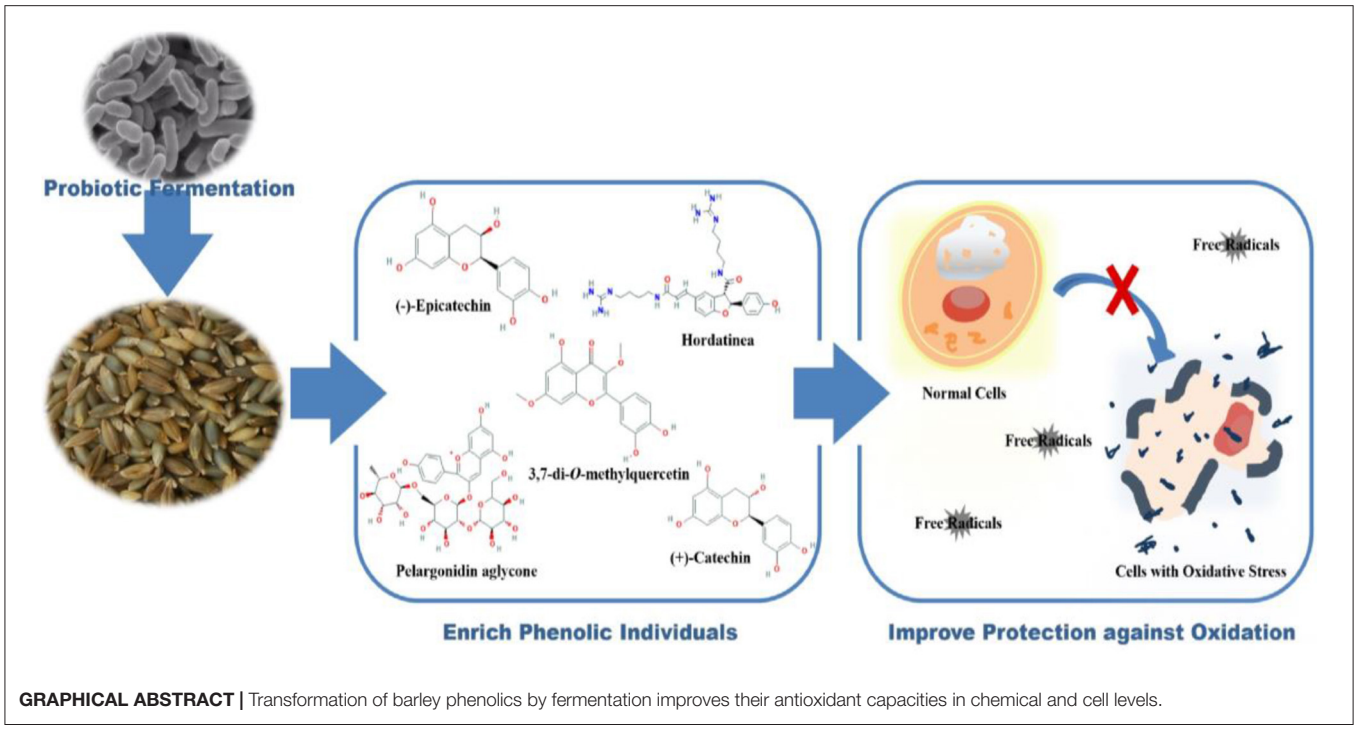

GRAPHICAL ABSTRACT | Transformation of barley phenolics by fermentation improves their antioxidant capacities in chemical and cell levels.

INTRODUCTION

Phenolics are the natural components of plant-based foods and are composed of flavonoids, tannis (hydrolysable and condensed), phenolic acids, stilbenes, lignans, and phenolic aldehydes. As demonstrated in numerous reports, dietary phenolics have some biological effects on scavenging free radicals, regulating digestive enzymes, and chelating metals (1). As previously verified, the optimized ultrasonic-assisted extraction could be used as an eco-friendly technique to better improve the yield and value-adding of phenolic extracts than the stirring-assisted or microwave-assisted extractions (2, 3). Phenolic consumption is considered beneficial for protecting against the oxidation and preventing various chronic diseases, such as ophthalmological, cardiovascular and digestive malfunctions, diabetes, atherosclerosis, allergies, tumorigenesis, and viral infection (4).

Hulless black barley (*Hordeum* spp.) is a special crop that contains valuable sources of minerals, vitamins, and some important bioactive compounds, which grows and matures under arctic–alpine, anoxic, low temperature, and intense ultraviolet conditions. According to epidemiological studies, a negative association exists between metabolic syndrome and the long-term intake of grain foods (5). Commonly, the barley phenolic compounds (PCs) are found in three major forms: soluble free, soluble conjugated that are esterified to sugars and low-molecular-mass components, and insoluble bound states that are covalently bound to structural elements in cell walls, the latter two of which account for the majority of total phenolic content (6). The free PCs can easily be released from plants, whereas the insoluble-bound PCs are not easily extracted due to their interaction with proteins or polysaccharides in cell walls. It is necessary to release the bound phenolics or implement the phenolic transformation before consumption to provide more health advantages to humans (7).

Among different processing techniques, fermentation is one with high specificity, low toxicity, and high performance that facilitates the breaking of covalent bonds and increases the liberation and bioavailability of polyPCs in food materials (8). A presumable mechanism for the fermentation-induced enhancement of phenolic activity in cereal grains is related to the enzymes present in fermenting microbes, causing the transformation of substances, the structural breakdown of cell-wall matrix, and hydrolyzing PCs to separate them from their glycosides or other conjugates (9, 10). Wang et al. (11) confirmed that the leaves of *Psidium guajava* L. had a decreased content of insoluble-bound polyphenol components after being cofermented with *Monascus anka* and *Bacillus* sp., and the soluble PCs exhibited greater protective effects against DNA oxidative damage compared with the insoluble-bound PCs. Similarly, Bei et al. (12) also revealed that the total phenolic content, especially free phenolic content (FPC), was significantly increased by bioprocessing. Considering that lactic acid bacteria (LAB) is generally recognized as safe (GRAS) and possessed the ability to produce various enzymes, such as glycosyl hydrolases, esterases, tannin hydrolases, reductases, and decarboxylases (13), a *Lactobacillus plantarum* strain isolated from plant-based material was used in the present study.

Generally, oxidative stress is manifested by the excessive production of reactive oxygen species and is an insufficient or defective antioxidant defense system involved in aging (1).

Until now, many studies have employed fermentation to increase the content of free PCs in cereal products to enhance their antioxidant activity (14, 15). However, only a few researchers paid attention to study the role of microorganisms in improving the antioxidant activity of hulless black barley, and even less, established a cell model to interpret the mechanisms through which the phenolics from fermented black barley protect against the oxidative stress-induced damage. According to Lima et al. (16), HepG2 cells, a human hepatoma cell line, could be adopted as an excellent model to investigate the intracellular mechanisms. H_2O_2 is a major factor implicated in the free-radical theory of aging. It can induce oxidative stress and damage biomacromolecules in cells, including nucleic acids, membrane lipids, and proteins (17). On this basis, the influences of fermentation with LAB on the cytoprotection of barley phenolics targeting the H_2O_2-induced HepG2 cells were further studied.

In this study, the phenolic transformation of the major individual compounds from the unfermented barley (UFB) to the barley fermented with *L. plantarum* P-S1016 were investigated. The antioxidant capacities of phenolics were then examined using a series of experiments at the chemical and cell levels. Meanwhile, a principal component analysis was performed to learn the correlative relationships among different indexes, including the viable bacterial number, FPC, and different antioxidant variables, and to reveal the effects of fermentation on these indexes. This manuscript focused on the development of hulless black barley as a novel carrier of LAB and nutraceutical supplement rich in antioxidants. The ultimate objective was to extensively realize the comprehensive utilization of hulless black barley and interpret the mechanism by which LAB enhanced the protective effects of PCs against H_2O_2-induced oxidative stress in liver cells.

MATERIALS AND METHODS

Materials, Microorganisms, and Chemicals

Black barley was obtained from Jiangsu Coastal Area Institute of Agriculture Sciences, China, and *L. plantarum* P-S1016 was conserved in Jiangsu Academy of Agricultural Sciences, China. Methanol and acetonitrile were purchased from TEDIA (Fairfield, OH, USA) with purifies of > 95.00%. The 2,2-diphenyl-1-picrylhydrazyl (DPPH) and 2,4,6-tris (2-pyridyl)-S-triazine (TPTZ) were purchased from Sigma-Aldrich (St. Louis, MO, USA), 6-hydroxy-2,5,7,8-tetramethylchromate-2-carboxylic acid (Trolox), and 2,2'-azobis (2-methylpropionamide)-dihydrochloride (AAPH) were, respectively, obtained from Acros Organics (Morris Plains, NJ, USA) and J&K Chemical (Beijing, China). A human hepatocarcinoma cell (HepG2) line was obtained from Taide Biological Technology (Nanjing, China). Dulbecco's modified eagle medium (DMEM) and fetal bovine serum (FBS) were obtained from Gibco/Invitrogen (Shanghai, China). MTT cell proliferation and cytotoxicity assay kit, reactive oxygen species (ROS) assay kit, lactate dehydrogenase (LDH) release assay kit, total superoxide dismutase (SOD) assay kit with WST-8, and glutathione (GSH and GSSH) assay kit were purchased from Beyotime Biotechnology (Shanghai, China).

Inoculum Preparation and Fermentation of Black Barley

The strain was prepared for two successive transfers in de Man-Rogosa and Sharp broth (MRS, pH 6.20 ± 0.20, UK) at 30.0°C for 24.0 h and 12.0 h. The activated microorganisms were collected by centrifugation at 5,000 *g* at 4.0°C for 15.0 min (3K15, Sigma-Laborzentrifugen, Osterode am Harz, Germany) and washed twice with sterilized physiological saline (18, 19). Black barley was dispersed in 5-fold distilled water to make a slurry and sterilized at 121.0°C for 20 min before *L. plantarum* P-S1016 inoculation (3.00%, v/v) at 37.0°C. As previously determined, the fermentation continued for 36.0 h, where the viable counting number had a maximum value. The prepared UFB and fermented barley (FB) were stored at 4.0°C for future use.

Microbiological Analysis

Viable bacterial count was determined by the plate count method (20). Briefly, for the harvested UFB and FB, 1.00 mL of each sample was homogenized aseptically with 9.00 mL of sterile physiological saline (0.85%, w/w) before a series of 10-fold dilutions. MRS agar (pH 6.20 ± 0.20) was used for bacterial growth at 37.0°C for 48.0 h. The confirmed colonies were counted and their numbers were expressed as log cfu/mL.

pH Measurement

A total of 20.00 mL of each sample of UFB and FB was fetched and shaken in a blender to measure their pH values with an IS128 pH meter (Insmark Instrument Technology, Shanghai, China) (21).

Phenolic Extraction

The preparation of phenolic extracts was according to the method of Xiao et al. (15) with a slight modification. Equal weight of the dried samples of UFB and FB of were extracted with 10-fold 80.0% (v/v) ethanol in a water bath at 40.0°C for 3.0 h (DKZ-450B, Sengxin Ultrasonic Instruments, Shanghai, China). The extracted solution was then centrifuged at 10,000 *g* at 4.0°C for 15 min. The supernatant was evaporated to dryness and its substances were reconstituted with distilled water to be lyophilized (Powerdry LL3000, Thermo, Massachusetts, USA). The prepared free unfermented barley phenolic extract (UF-BPE) and fermented barley phenolic extract (F-BPE) powders were sealed and stored at −18.0°C for antioxidant analysis.

FPC and Insoluble-Bound Phenolic Content Detection

Following the water-bath phenolic extraction, phenolic contents were determined using the Folin–Ciocalteu colorimetric method (22, 23). Briefly, each of the dried samples of UFB and FB weighted 1.00 g, and their relevant supernatants were evaporated, and finally 1.00 mL 80.0% (v/v) ethanol was added to obtain a constant volume. A total of 0.40 mL of each free phenolic solution was oxidized with 2.00 mL 0.50 mol/L Folin–Ciocalteu reagent at room temperature for 4.0 min. Then, the reaction was neutralized by adding 2.00 mL of 75.00 g/L saturated sodium carbonate.

After 2.0 h of incubation in the dark, the absorbance at 760 nm was recorded using a spectrophotometer (UV 5500, Metash Instruments, Shanghai, China). The FPC results were expressed as gallic acid equivalent (GAE), i.e., mg GAE/g. Furthermore, the residue from the above extraction was hydrolyzed directly with 50.00 mL of 4.00 M NaOH solution for 4.0 h with shaking. The mixture was adjusted to pH 2.00 with concentrated HCl and extracted with ethylacetate (11). The relevant supernatant was evaporated and finally 1.00 mL of 80.0% (v/v) ethanol was added to a constant volume. The IBPC was measured as above and also expressed as mg GAE/g.

UPLC-QTOF-MS Analysis

The phenolic extracts were analyzed by HPLC-MS (G2-XS QTOF, Waters Corporation, Massachusetts, USA). Two microliters of phenolic solution was injected into the UPLC column (2.1 × 100 mm ACQUITY UPLC BEH C18 column containing 1.7 μm particles) with a flow rate of 0.35 mL/min. Buffer A consisted of 0.1% formic acid in water and buffer B contained 0.1% formic acid in acetonitrile. The gradient was 5% buffer B for 0.5 min, 5.0–40.0% buffer B over 20.0 min, and 40.0–95.0% buffer B over 2.0 min (24, 25). Mass spectrometry was performed using electrospray source in positive ion mode with MSe continnum acquisition mode, with a selected mass range of 50–1,200 m/z. The capillary voltage was 2.0 kV, collision energy was 10–40 eV, source temperature was 120.0°C, and desolvation gas temperature was 400.0°C.

In vitro Antioxidant Activity Assays

DPPH Radical Scavenging Activity Detection

The DPPH radical scavenging activity of black barley extracts (UF-BPE and F-BPE) was determined according to the method of Shimada et al. (26) and Lee et al. (27). Specifically, 2.00 mL of each sample at different concentrations (0–20 μg/mL) was added to 2.00 mL DPPH solution (0.2 mmol/L) previously dissolved in 80.0% (v/v) methanol. The mixture was shaken and allowed to stand in the dark for 30.0 min. The absorbance was then recorded at 517 nm. The activity was calculated as follows: DPPH radical scavenging activity (%) = [1-absorbance of sample/absorbance of control] × 100%.

Ferric Reducing Antioxidant Power Detection

The FRAP was evaluated using the method of Benzie and Strain (28) and Qin et al. (29) with slight modifications. A 100.00 mL aliquot of 0.30 mol/L acetate buffer, 10.00 mL of 10.0 mmol/L TPTZ solution in 40.0 mmol/L HCl, and 10.00 mL of 20.0 mmol/L ferric chloride was mixed to prepare the FRAP reagent. A total of 1.00 mL of each sample at different concentrations (0–20 μg/mL) was added to 5.00 mL of FRAP solution, and the mixture was placed in the dark at 37.0°C for 20.0 min. The absorbance was measured at 593 nm. The results were expressed as Fe(II) equivalent antioxidant capacity, i.e., μmol Fe(II)/L, by plotting the standard curve of ferrous sulfate.

Oxygen Radical Absorbance Capacity Detection

As for ORAC assay, the reaction was completed at 37.0°C in pH 7.40 phosphate buffer. One hundred microliters of each sample at different concentrations and 50 μL of 0.2 μmol/L fluorescein were mixed in a 96-well microplate. After preincubation at 37.0°C for 15.0 min, 50 μL of 80.0 mmol/L AAPH solution was added immediately. The fluorescence was recorded by an LB 941 TriStar Microplate Reader (Berthold Technologies, Bad Wildbad, Germany) with 485-P excitation and 535-P emission filters every minute during a 100.0-min process (30). The results were expressed as Trolox equivalent antioxidant capacity, i.e., mol Trolox/g.

Antioxidant Activity Assays in Oxidative-Damaged HepG2 Cells

HepG2 Cell Culture and Treatment

HepG2 cells were cultured in DMEM supplemented with 10.00% FBS, 1.00% streptomycin and penicillin, and 1.00% 1.00 mol/L HEPS buffer at 37.0°C in a 5.0% CO_2 humidified incubator (MIR-254, Sanyo Denki, Shanghai, China) (31). Before the experiment, the cells were quiesced in a reduced serum medium for 4.0 h and then seeded at a concentration of 200,000 cells/mL. According to our preliminary experiment, HepG2 cells were first treated with UF-BPE or F-BPE at different concentrations (1–10 μg/mL) for 6.0 h. Then, 2.40 mmol/L H_2O_2 was added to induce oxidative stress and stimulate the cells for 2.0 h. A normal cell group with neither sample pretreatment nor H_2O_2 stimulation was used as the control. A group of H_2O_2-induced cells was applied as the oxidative model.

Cell Viability Measurement

HepG2 cells were cultured according to the treatment above, and cell viability was determined by the MTT method (32). Detailly, the cells were cultured with 20 μL of 5.0 mg/mL MTT for 4.0 h, followed by the removal of the incubation medium. The formazan crystals were dissolved by the addition of 150 μL of dimethyl sulfoxide (DMSO) and slowly shaken for 10.0 min. After the absorbance measurement at 490 nm on an LB 941 TriStar Microplate Reader, the cell viability levels were calculated as follows: viability level (fold increase) = OD value of oxidative-model or sample group/OD value of control group.

ROS Detection

A dichlorodihydrofluorescein diacetate (DCFH-DA) detection kit was used to evaluate ROS level in HepG2 cells. The cultured cells were washed with phosphate buffered saline (PBS), and 0.01 mmol/L DCFH-DA was added to each well to start the reaction at 37.0°C for 20.0 min (33). After being washed thoroughly with PBS to remove the DCFH-DA so that it does not enter the cells, the HepG2 cells were collected and suspended in PBS and seeded in the 96-well black plates. The fluorescence was immediately determined by an LB 941 TriStar Microplate Reader with 485-P excitation and 535-P emission filters. The ROS levels of cells were calculated as follows: ROS release level (fold increase) = [cell fluorescence intensity of oxidative-model or sample group/the corresponding cell viability]/[cell fluorescence intensity of control group/the corresponding cell viability].

LDH, SOD, GSH, and GSSG Detections

The supernatants of cultured cells with different treatments were collected for LDH activity release analysis, and the lysates of cells were used for SOD activity, and GSH and GSSG content detections. The experiments were all executed using the Assay Kit (Beyotime) and according to the manufacturer's instructions. Firstly, the extracellular and intracellular proteins in each of supernatants and cell sediments were quantified, respectively, using a BCA Protein Assay Kit. Then, as for LDH detection, 10.0% (v/v) LDH releasing agent was added to each well for 1 h before the collection of cells, and then 60 μL of LDH detecting agent, including 2-p-iodophenyl-3-nitropheyltetrazolium chloride (INT) and other chemicals were added to the cell supernatant obtained from each well. After incubation for 30.0 min, the absorbance of each sample was measured at 490 nm (34). LDH release level (fold increase) = LDH activity in protein of the control or oxidative-model or sample group/LDH activity in protein of the release group. The SOD was detected using the WST-8 method. A 20-μL of cell sediment obtained from each well was mixed with 160 μL WST-8/enzyme reagent and 20 μL reaction starter, and incubated for 30.0 min at 37.0°C. The absorbance of each sample was measured at 450 nm (35). SOD release level (fold increase) = SOD activity in protein of the oxidative-model or sample group/SOD activity in protein of the control group. To evaluate the GSH and GSSH levels, the cells were trypsinized, added to deproteinized solution, and inserted into a 96-well plate. A 150-μL of working assay mixture was added in each well for incubation for 5.0 min. Afterward, 50 μL NADPH solutions were also rapidly mixed with each of the reaction products several times. The results were measured with absorbance at 412 nm (36). The GSH and GSSG were expressed as ratios of their contents relative to the corresponding protein contents, i.e., mol/g protein.

Statistical Analysis

The data was presented as mean ± standard deviation (SD) of five independent experiments. OriginPro® 2021 (OriginLab, Northampton, Massachusetts, USA) was used to plot the figures and calculate the area under fluorescence decay curves. One-way analysis of variance (ANOVA) and Duncan's multiple comparison tests were determined by using IBM SPSS Version 22.0 (SPSS, Chicago, IL, USA). Principal component analysis (PCA) was conducted using SIMCA-P Version 11.5 (Umetrics, Malmö, Sweden). The difference at $p < 0.05$ was considered to be statistically significant.

RESULTS AND DISCUSSION

Changes in Microbial Growth, Free and Insoluble-Bound Phenolic Contents

Figure 1 shows the viable bacterial counts and pH values of UFB and FB samples, respectively. After 36.0 h of fermentation, the LAB population significantly increased from 6.94 ± 0.07 to 9.54 ± 0.22 log cfu/mL ($P < 0.01$). Conversely, the pH value had a downward trend, dropping from 6.78 ± 0.08 to 3.84 ± 0.04 ($P < 0.01$). As shown in **Figure 1**, the FPC of FB was 5.61 ± 0.02 mg GAE/g, which was significantly higher than that of UFB

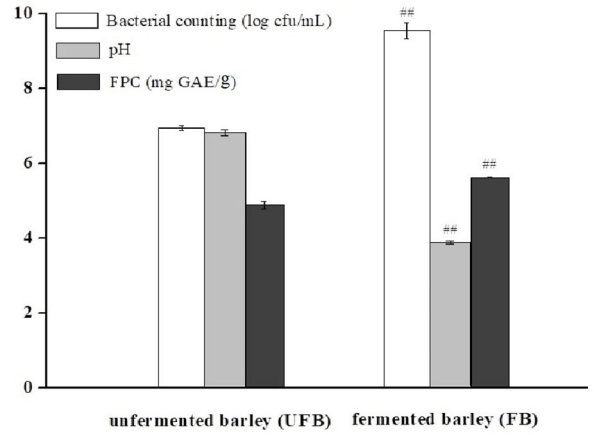

FIGURE 1 | Bacterial counting, pH, and free phenolic content (FPC) of unfermented barley (UFB) and fermented barley (FB). Bars represented mean values ± SD ($n = 5.00$). For the same index, ## indicated significant difference at the level of $P < 0.01$ between UFB and FB.

(4.87 ± 0.01 mg GAE/g) ($p < 0.01$). The content of insoluble-bound phenolic fraction was previously determined as well, and it showed a significant decrease from 3.43 ± 0.01 to 2.16 ± 0.01 mg GAE/g during the whole fermentation process ($p < 0.01$). In this way, the total phenolic content of fermented black barley was slightly improved by approximately 10% compared with that of the unfermented one.

For LAB, the pH decline tendency indicated the growth performance of microorganisms (37). The hydrolytic process of *L. plantarum* P-S1016 enriched the total phenolics and might also lead to the enhancement of cereal bioactivity. It was implied that the increase of total and FPCs were in basic synchronization with the growth of microorganisms. Kaprasob et al. (38) focused on the LAB-based biotransformation of cashew apple juice (CAJ) and also found that *Lactobacillus* spp. improved the TPC in CAJ to a value of 0.13 mg GAE/mL. The results of Wang et al. (11) also showed a significant influence of cofermentation by strater microorganisms on the development of polyphenols from *P. guajava* L. leaves. Consistently, due to fermentation, the total phenolic content in oat increased to 6.04 GAE mg/g, and the FPC in particular, changed with an upward trend (3.27 GAE mg/g) and contributed the majority of the total phenolic content (12). The PCs generally conjugated and insolubly combined with cell wall polymers, such as cellulose, hemicellulose, and lipid moieties through β-glycoside bonds, or other hydrogen and ionic bonds. There might be three reasons why microbial fermentation could increase the content of free phenolics from black barley. One was that the polyphenols in barley mainly existed in the form of bound phenolics, which could be released and transformed into free-form phenolics by alkali, acid, or specific microorganism-derived enzyme system (39, 40). Secondly, microbial metabolism could modify the bioactive substances in barley, leading to the synthesis of new substances such as PCs. Thirdly, *L. plantarum* P-S1016 reduced the pH value and to some extent promoted the

TABLE 1 | Identification of phenolic compounds in the unfermented and fermented barleys using the spectral characteristic in UPLC and ion fragment information in UPLC-QTOF-MS.

Compound name	Empirical formula	RT[a] (min)	λ_{max} (nm)	MW[b]	[MS-][c] (*m/z*)	[MS-MS-][d] (*m/z*)	Change ratio[e]
B-type Procyanidin dimer	$C_{30}H_{26}O_{12}$	3.25	282	578.50	579	291, 409, 427	−84.39%
(+)-Catechin	$C_{15}H_{14}O_6$	3.58	272	290.27	291	147	+52.64%
p-Coumaroylagmatine	$C_{14}H_{20}N_4O_2$	4.09	290	276.33	277	147, 217	−88.64%
(-)-Epicatechin	$C_{15}H_{14}O_6$	4.97	281	290.27	291	139	+5686.67%
Isovitexin-7-*O*-glucoside	$C_{27}H_{30}O_{15}$	6.07	328	594.50	595	162, 313, 433	−68.15%
Hordatine A	$C_{28}H_{38}N_8O_4$	6.20	291	550.70	551	291	+121.83%
Apigenin-6-C-glucoside-8-C-arabinoside	$C_{26}H_{28}O_{14}$	6.35	329	564.50	565	403, 547	−62.01%
Peonidin-3-*O*-sophoroside	$C_{28}H_{33}O^+_{16}$	6.51	520	625.60	625	301	−69.38%
Isoscoparin-2" -*O*-glucoside	$C_{28}H_{32}O_{16}$	7.60	323	624.50	625	343, 445	−71.39%
Pelargonidin-3-*O*-glucosyl-rutinoside	$C_{33}H_{41}O^+_{19}$	8.32	520	741.70	741	271, 433	+88.40%
3,7-Di-*O*-methylquercetin	$C_{17}H_{14}O_7$	14.26	275	330.29	331	301, 315	+70.10%

[a] *RT was retention time of UPLC-QTOF-MS.*
[b] *MW was molecular weight of each compound.*
[c] *[MS-]was mass spectrometry ions.*
[d] *[MS-MS-] was mass spectrometry-mass spectrometry ions.*
[e] *Values of change ratio with "–" and "+" indicated the decrease and increase in contents of individual phenolic compounds from black barley due to fermentation with L. plantarum P-S1016, respectively.*

release of oat core cell wall degrading enzymes to accelerate the intra-cell compounds releasing (7).

Identification and Comparison of PCs

The total ion chromatographies of free phenolic extracts, UF-BPE, and F-BPE are presented in **Supplementary Figure 1**, displaying the apparent amplitude of variation. As detected by UPLC-QTOF-MS, the FB sample contained PCs with more species and more abundance than the UFB sample. Eleven PCs were identified in the black barley. The phenolic identification was conducted by comparing their spectral characteristics in ultraperformance liquid chromatography with diode array detection (UPLC-DAD), and parent and daughter ion information in UPLC-QTOF-MS, with previously reported literature data (**Supplementary Figures 2–12**) (41–45). According to the classification by KEGG Database (https://www.kegg.jp/kegg/brite.html), these compounds included one proanthocyanidin (*B*-type procyanidin dimer), eight flavonoids (two flavan-3-ols, three flavones, two anthocyanidins, and one flavonol), and two amino-acid-related compounds (*p*-coumaroylagmatine and hordatine A) (**Table 1**). The flavan-3-ols were composed of (+)-catechin (3.58 min) and (-)-epicatechin (4.97 min), which were two isomerides with $[M+H]^+$ at *m/z* 291, and were separated by using the individual standards in UPLC-QTOF-MS detection. The dimer procyanidin *B* ($[M+H]^+$ *m/z* 579) involves the monomeric unit of catechin or epicatechin, and thus it produced the dominant product ions at *m/z* 409 and *m/z* 291 upon fragmentation. Among the flavones group, compounds were all in the glycosylated form, which were assigned as isovitexin-7-*O*-glucoside, apigenin-6-C-glucoside-8-C-arabinoside, isoscoparin-2" -*O*-glucoside. Moreover, two anthocyanidins were also confirmed in the colored barley, through comparing the characteristic product ions of anthocyanin aglycones. The peak with $[M+H]^+$ at *m/z* 625 was peonidin (*m/z* 301) glycosylated by the sugar moiety of sophorose (*m/z* 324), and that with $[M+H]^+$ at *m/z* 625 was pelargonidin (*m/z* 271) conjugated with the sugar moieties of glucose (*m/z* 162) and rutinose (*m/z* 326). The *p*-coumaroylagmatine was with a protonated molecule $[M+H]^+$ at *m/z* 277 and MS/MS fragments at *m/z* 217 and 147 $[M+H-130]^+$, corresponding to loss of residue agmatine ($C_5H_{14}N_4$), and is a member of the class of cinnamamides obtained by formal condensation of the carboxy group of 4-coumaric acid with the primary amino group of agmatine. The hordatine A, a dimer of *p*-coumaroylagmatine, is defined as a phenolamide typical to barley (*Hordeum vulgare*), possessing a critical role in plant development, response to abiotic stress, and defense systems against pathogens and herbivores (41).

Moreover, the relative contents of individual PCs were compared between unfermented and fermented black barley. The percentages of five compounds were enlarged due to LAB fermentation, including catechin, epicatechin, hordatine, pelargonidin aglycone and 3,7-di-*O*-methylquercetin. Similarly, the aglycones' content in soybean was promoted by *Aspergillus oryzae* and *Monascus purpureus*, as some microorganisms produce key enzymes that destroy the β-glycoside bonds between isoflavones and proteins/polysaccharides in the cell walls in herbal plants (39, 46). The enrichment of certain PCs could also be explained according to others' previous work (41, 47), which indicated that carbohydrate metabolism is the source of the synthesis and transformation of plant secondary metabolites, providing precursors and energy for the subsequent transformation. PCs are a large group of secondary metabolites produced through the phenylpropanoid pathway, where amino acid phenylalanine is the primary starting molecule. As reported, most biosynthesis of aromatic polyketides consist of repeated Claisen condensations of acetyl-coenzyme A (CoA) and malonyl-CoA units, catalyzed by polyketide synthase type.

During the biosynthesis of polyketides, polyphenols result from directed cyclocondensations of poly-β-keto intermediates or only partially reduced polyketides chains produced by iterative polyketide synthases (48). Specifically, in the first step of hordatine A biosynthesis, agmatine coumaroyltransferase (ACT) catalyzes agmatine conjugates from pcoumaroyl-CoA, and then the hydroxycinnamic acid agmatines are further oxidatively dimerized to hordatine. The phenolic type and content differences between our unfermented and fermented hulless black barleys might be ascribed to the influence on the substrate environment caused by strain *L. plantarum* P-S1016, and also to the released microbial enzymes acting on the critical points of phenolic metabolite pathways. It was worth mentioning that flavan-3-ols and flavonols possess the conjugated double bonds and multiple hydroxyl groups, attributing to their higher antioxidant activity compared to hydroxycinnamic acids, and the increased anthocyanin not only affects the sensory characteristic and color of barley, but also improves the barley antioxidant activity (49, 50).

In vitro Antioxidant Activities

Antioxidants are endogenous or exogenous molecules that mitigate any form of oxidative/nitrosative stress of its consequences. According to others' report, the primary protective role of antioxidants in bodies is through their reaction with free radicals (51). In this study, different assays were used to study the antioxidant effects of hulless barley extracts because *in vitro* antioxidant activity should not be determined using a single antioxidant test model. The DPPH radical is a stable lipophilic free radical that is commonly employed to evaluate the free radical scavenging potential of plant extracts (15). **Figure 2A** showed the dose-response curves for various concentrations of F-BPE and UF-BPE on the DPPH radical scavenging activity. It was observed that the free radical inhibitory activities continued to increase and reached percentages of 90.30% ± 2.34% and 98.15% ± 1.12% for UF-BPE and F-BPE, respectively. At different concentrations (1, 2, 5, 10, 15, 20 μg/mL), F-BPE always performed better in scavenging DPPH radicals than UF-BPE. Here, during the fermentation of barley, the higher antioxidant ability might be attributed to the enrichment in PCs, which reacted with the free radicals and terminated the radical chain reactions (15).

The FRAP had a similar tendency of variation to the DPPH scavenging activity and was enhanced along with the elevated concentrations of phenolic extracts. As Vadivel et al. (52) revealed, the presence of phenolics in extracts caused the reduction of TPTZ-Fe^{3+} complex to TPTZ-Fe^{2+} form and displayed the FRAP. The higher FRAP obtained from the FB might be associated with the release of iron-chelated compounds during fermentation. **Figure 2B** demonstrated the dose-response curves for various concentrations of F-BPE and UF-BPE on the FRAP. The highest FRAP values for UF-BPE and F-BPE were 436.12 ± 12.01 and 586.02 ± 23.00 μmol Fe(II)/L, respectively. The fermentation process contributed to ameliorating the ferric reducing antioxidant power of barley-derived polyphenols.

Additionally, ORAC may be one of the most suitable methods to assess the *in vitro* antioxidant activity because it utilizes a biologically relevant radical source (1). The ORAC assay was performed to explore the activity of PCs, combining both the time and degree of inhibition. The result indicated that the barley extract's overall antioxidant activity was elevated from 9.66 ± 0.37 to 11.60 ± 0.41 mol Trolox/g ($p < 0.05$) due to fermentation. Our results were consistent with those of others who studied the fermented maize-based product and koji from millet. The studies showed that the general increases in antioxidant activity of fermented foods were attributed to a release of insoluble-bound PC due to activities of hydrolytic enzymes during bioprocessing (53, 54). The discrepancy in antioxidant activities in different studies might be attributed to three significant factors: the microbial strain, the fermentation type, and the fermentation substrate (41). As mentioned above, black barley contained

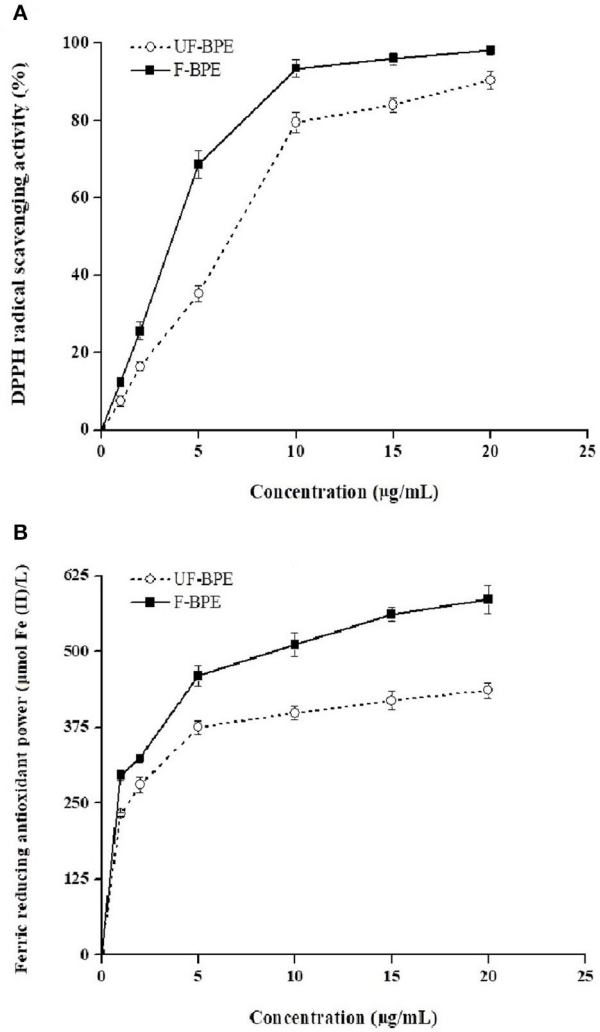

FIGURE 2 | Effects of unfermented barley phenolic extracts (UF-BPE) and fermented barley phenolic extracts (F-BPE) at different concentrations (0.00–20.0 μg/mL) on **(A)** DPPH radical scavenging activity and **(B)** ferric reducing antioxidant power (FRAP). Bars represented mean values ± SD (n = 5.00).

substantial amounts of phenolic antioxidants, and the increased antioxidant activities were positively related with the enrichment in PCs in the FB (55). Due to the potential enhancement of different spectrophotometric antioxidant activities by *L. plantarum* P-S1016 fermentation, a H_2O_2-induced oxidative stress in HepG2 cell was further established for in-depth study.

Antioxidant Activities in Oxidative-Damaged HepG2 Cells

Cytotoxicity of Phenolic Extracts in Cells

To estimate the cytotoxicity of phenolic extracts, they were added at different concentrations in HepG2 cells without H_2O_2 stimulation. Compared with the control group, the viability levels of cells pretreated with 1–10 μg/mL extracts ranged between 1.03 ± 0.04- and 1.53 ± 0.06-fold ($p > 0.05$, $P < 0.01$) (**Figure 3A**). The UF-BPE and F-BPE were proved to have no cytotoxicity on cells and even elevate the cell viability under the normal environment.

Protective Effects Against H_2O_2-Induced Cytotoxicity, ROS Production in Cells

A potential mechanism by which PCs confer antioxidant activity involves the induction of detoxification mechanisms through phase II conjugation reactions, which prevents the formation of carcinogens from precursors as well as by blocking the reaction of carcinogens with critical cellular macromolecules (56). The phenolics also modify some cellular signaling processes and donate an electron/transfer hydrogen atom to free radicals, activate endogenous antioxidant mechanisms, which increases the levels of antioxidant enzymes, and act as chelators of trace metals involved in free radical protection (57). The oxidative damage should be restricted by intervention of efficient antioxidant-defense mechanisms; however, ROS levels increase and the antioxidant levels decrease in aging tissues (31). In the current study, H_2O_2 generated the ROS overproduction, serving as an important biomarker for the assessment of oxidative stress level. As for **Figure 3B**, it was indicated that pretreatment with UF-BPE and F-BPE (1, 2, 5, 10 μg/mL) for 6.0 h increased the viability of oxidatively injured cells. As for the incubation of UF-BPE prior to H_2O_2 induction, the cell viability levels were 0.78 ± 0.02-, 0.89 ± 0.02-, 0.98 ± 0.02- and 0.94 ± 0.04-fold of the control, which were increased by 27.71%, 45.92%, 60.70%, and 54.12% than those in the oxidative model group ($p < 0.05$, $p < 0.01$, $p < 0.01$, $p < 0.01$), respectively. Compared with UF-BPE, F-PBE exhibited a more pronounced ability to reduce the cytotoxic effect of H_2O_2 on cells. The cell viabilities of the F-BPE-pretreated groups were 51.21, 57.00, 63.52, and 74.51% greater than those of the oxidative model group (all $P < 0.01$). Consistently, this result demonstrated that *L. plantarum* P-S1016 enhanced the antioxidant activity of barley phenolics.

The fluorescence probe DCFH-DA was used to detect the intracellular ROS level. Here in **Figure 3C**, H_2O_2 significantly increased the ROS level in HepG2 cells by 49.20% ($p < 0.01$ vs. the control group), whereas incubation with phenolic extracts effectively decreased the H_2O_2-induced ROS level. Moreover, there existed a dose–effect relationship between the phenolic concentrations and the ROS release levels. When the concentrations of BPE were 1, 2, 5, and 10 μg/mL, the production of H_2O_2-induced ROS was significantly inhibited by 7.98, 7.51, 12.71, and 19.95%, respectively, for UF-BPE ($p > 0.05$, $p < 0.05$, $p < 0.05$, $p < 0.01$ vs. the oxidative model group), and 7.04, 8.98, 20.20, and 25.51%, respectively, for F-BPE ($p < 0.05$, $p < 0.05$, $p < 0.01$, $p < 0.01$ vs. the oxidative model group). Our results indicated that the PCs from FB had a better performance in impairing the overproduction of ROS in cells under oxidative stress. As previously reported, ROS had the destructive actions on both proteins and DNA and are therefore regarded in pathogenesis, resulting in cellular death and arterial disease (58). The reduction in ROS was relevant to the amelioration of some side effects, such as DNA mutation and genetic instability. Thus, the fermentation of black barley with *L. plantarum* P-S1016 improved the antioxidant activity of barley.

Effects on LDH and SOD Activities in Cells

Moreover, when cell apoptosis or necrosis occurs, the cytoplasmic enzyme LDH is released rapidly following plasma membrane damage. The LSG leakage assay is usually utilized to indicate the cell membrane's integrity for further assessing the cell damage caused by oxidative stress (59). SOD is another antioxidant enzyme, which catalyzes the transformation of toxic superoxide radicals into ordinary molecular oxygen or hydrogen peroxide and plays an important role in cell protection in response to H_2O_2-induced oxidative stress (31). In this study, triton X-100 was used as the releasing agent, and the activity level of LDH completely released was considered one (**Figure 3D**). After exposure to 2.40 mmol/L H_2O_2, LDH activity in the cell culture supernatant increased from 0.36 ± 0.07- to 0.67 ± 0.02-fold (1.86-fold, $P < 0.01$ vs. the control group). The higher LDH release level suggested that serious cell injury was generated. However, UF-PBE and F-PBE attenuated LDH release in a positive concentration-dependent manner. The inhibitory rates for UF-BPE and F-BPE (2–10 μg/mL) were 16.50–42.91% and 21.46–56.42% ($p < 0.05$ or $p < 0.01$ vs. the oxidative model group), respectively. For the F-BPE at concentrations of 8 and 10 μg/mL, the LDH release levels were not significantly different from those of the control group ($p > 0.05$). The LDH activities in supernatants of BPE-protected cells were greatly decreased compared with those in the H_2O_2-induced oxidative model. Consistently, F-PBE displayed a better capacity to repair the injured cells and protect cells from oxidative damage induced by H_2O_2.

As shown in **Figure 3E**, the SOD activity in cells stimulated by H_2O_2 for 2.0 h was significantly reduced (0.42 ± 0.04-fold, $p < 0.01$ vs. the control group), probably related to the dramatic decrease in both viability and LDH release in cells induced by H_2O_2. Moreover, BPEs at different concentrations possessed diverse abilities to improve the intracellular SOD levels. UF-BPE (5 and 10 μg/mL) significantly increased SOD activities by 51.02 and 80.70%, respectively ($p < 0.05$ and $p < 0.01$ vs. the oxidative model group). F-BPE showed a more pronounced influence on protection against oxidative stress in H_2O_2-treated HepG2 cells. F-BPEs at different concentrations (2, 5, and 10 μg/mL) significantly promoted the production of SOD in a dose-dependent manner, and correspondingly, the

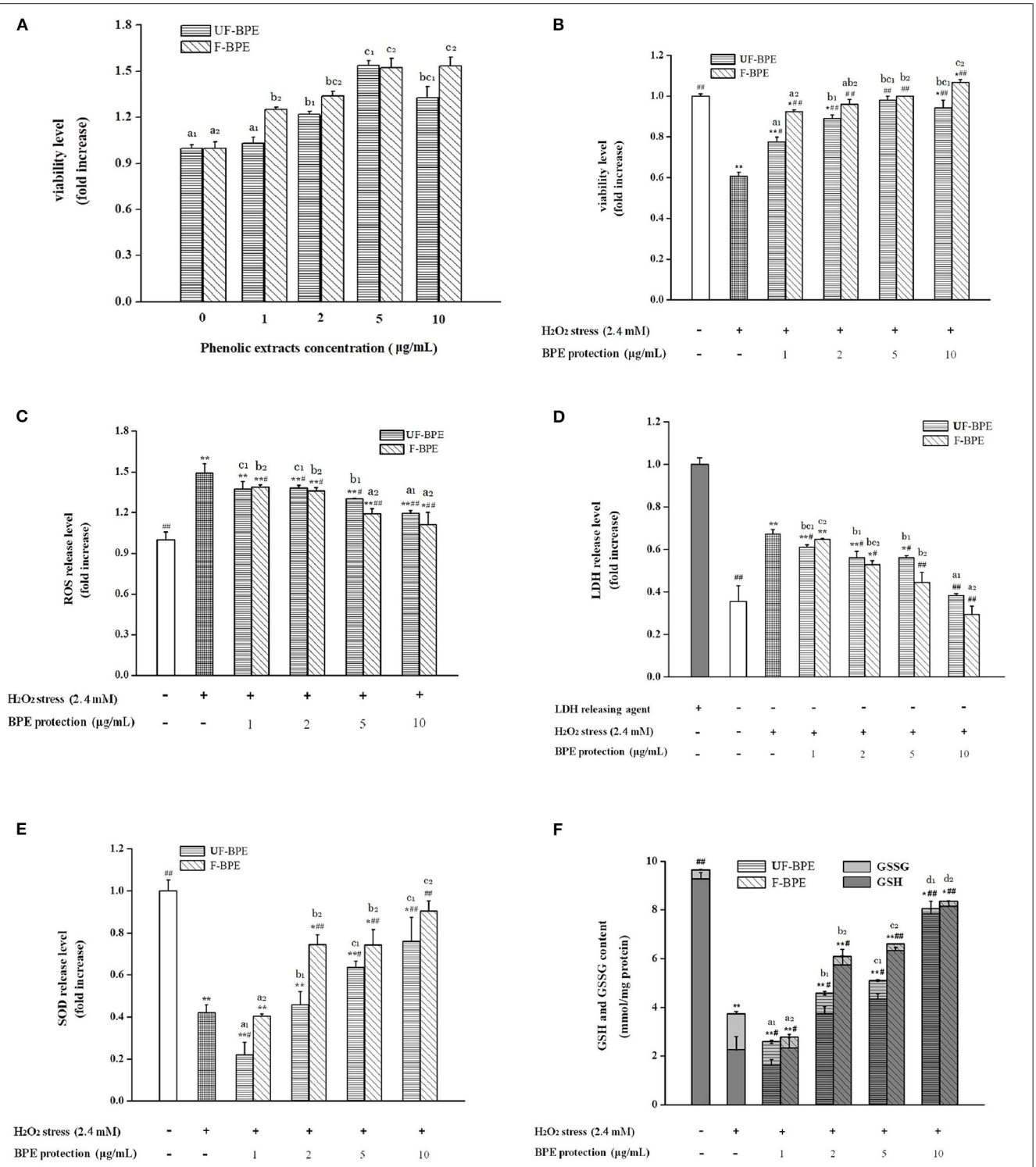

FIGURE 3 | Effects of UF-BPE and F-BPE at different concentrations (1.00–10.0 μg/mL) on **(A)** cytotoxicity, **(B)** cell viability, **(C)** ROS release level, **(D)** LDH release level, **(E)** SOD release level, and **(F)** GSH and GSSG contents in different HepG2 cell groups. Bars represented mean values ± SD ($n = 5.00$). * and ** indicated significant differences at the levels of $P < 0.05$ and $P < 0.01$, respectively, between control group and other groups; # and ## indicated significant differences at the levels of $P < 0.05$ and $P < 0.01$, respectively, between oxidative model group and other groups. Mean values of the same extract with different lowercase letters were significantly different at the level of $P < 0.05$.

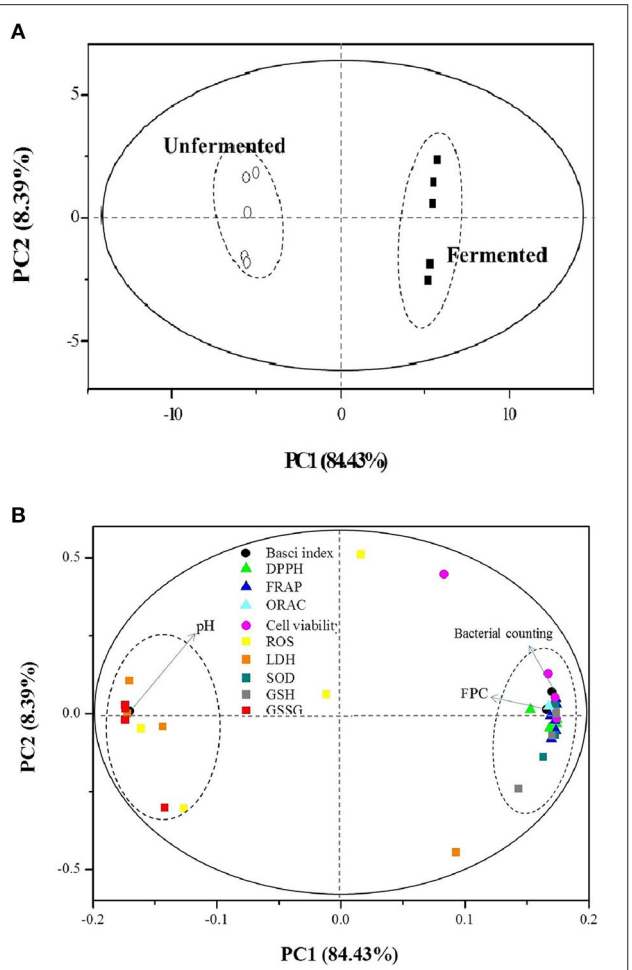

FIGURE 4 | Plots of **(A)** sample scores and **(B)** parameter loadings of principal component analysis (PCA) involving 12 variables on UF-BPE and F-BPE.

SOD activities were augmented by 77.21, 76.78, and 115.02% (all $p < 0.01$ vs. the oxidative model group). Due to the higher SOD activities exhibited in cells of the BPE-treated groups than those of the oxidative model group, phenolics, particularly from barley fermented with *L. plantarum* P-S1016, defensed against the cellular oxidative damage.

Effects on GSH and GSSH Contents in Cells

As an important intracellular non-enzymatic antioxidant, glutathione is the most abundant non-protein thiol in eukaryotic cells. Reduced glutathione (GSH) usually served as an electron donor to detoxify endogenous peroxides, leading to the formation of oxidized glutathione (GSSG) (31). The glutathione redox status level, namely, the GSH/GSSG ratio, might be also a critical indicator of oxidative stress in cells and organisms (60). Contents of GSH and GSSG were measured to assess the change in glutathione redox status in HepG2 cells with different BPE treatments. As indicated, glutathione existed mainly in the reduced form in the control group cells, where GSH accounted for 96.20% of the total (**Figure 3F**). The induction of H_2O_2 for 2.0 h caused a reduction in the total contents of GSH and GSSG in cells, and a distinct reversal occurred. The GSH content decreased from 9.29 ± 0.25 to 2.26 ± 0.53 mmol/mg protein and that of GSSG was raised from 0.37 ± 0.02 to 1.47 ± 0.09 mmol/mg protein. The decline in GSH/GSSG ratio clearly indicated a cellular peroxide dominant status. However, **Figure 3F** also showed that the phenolic extracts from barley induced the regeneration of GSH from GSSG under H_2O_2-induced condition. With the protection of BPE (2, 5, and 10 μg/mL), the total glutathione content was significantly higher than that in the oxidative model group ($p < 0.05$ or $p < 0.01$), and the GSH/GSSG ratio in cells was augmented progressively. As for UF-BPE and F-BPE treatments, the GSHs were determined to be 0.65–2.46- and 1.54–2.61-fold higher, respectively ($p < 0.05$ or $p < 0.01$ vs. the oxidative model group), whereas the GSSG was notably lost by 0.34–0.85- and 0.69–0.86-fold, respectively ($p < 0.05$ or $p < 0.01$ vs. the oxidative model group). These findings declared that BPE turned the cellular environment into that with a relatively lower degree of oxidative stress. Compared with UF-PBE, F-PBE displayed an enhanced performance in GSH production and peroxide inhibition, consequently supporting its more protective effects on H_2O_2-damaged HepG2 cells.

Overall, the barley extracts exhibited positive effects on cell oxidative defense system through enzymatic and non-enzymatic mechanisms. Compared with UF-BPE, F-BPE was better at increasing cell viability and membrane integrity, scavenging ROS, enhancing the activity level of the key intracellular antioxidant enzyme SOD, and the status of glutathione redox system. Our results were consistent with that reported by Granado-Serrano et al. (61), who found that quercetin contributed to preventing potential oxidation in HepG2 cells and the liver. Also, microorganisms were helpful for boosting the potent activity of PCs from mulberry and blackberry to protect cells against oxidative injury and facilitate cell growth or proliferation again (62). The F-BPE showed more advantages in resisting oxidation than UF-BPE in both the chemical tests and the HepG2 cells. The transformed phenolics from fermented black barley were able to protect cells more effectively against H_2O_2-induced damage by a composite antioxidant mechanism.

PCA Analysis

The PCA provided valuable information on LAB fermentation's influence on various parameters, especially on the antioxidant capacities. There were two principal components (PC1 and PC2), clarifying up to 92.83% of the total variance. The score plot (**Figure 4A**) showed that the unfermented and fermented samples were distributed on the left (PC1 < 0.00) and right (PC1 > 0.00), respectively. The converse dimension indicated that *L. plantarum* P-S1016 fermentation could make a noticeable difference in barley, taking into account their antioxidant activities. Moreover, **Figure 4B** divided the 12 parameters into two categories. The bacterial counting, FPC, DPPH, FRAP, ORAC, cell viability under BPE protection, SOD, and GSH were well correlated to each other according to their high loadings on PC1, which reflected the mutual relevance between FPC and other indexes involving the

antioxidant activities, antioxidant enzyme, and non-enzymatic antioxidant in cells. The results demonstrated that the PCs from black barley could modify some cellular signaling processes and donate an electron/transfer hydrogen atom to free radicals, activate endogenous antioxidant mechanisms, thus increasing the levels of antioxidant enzymes and acting as chelators of trace metals involved in free radical protection (63). Consistent with the results related to antioxidant performance of barley extracts, PCA also revealed that fermentation by *Lactobacillus plantarum* was an effective tool to produce barley rich in phenolics possessing superior antioxidant activity.

As we all know, to exert the health benefits, PCs need be bioavailable. One key step in bioavailability is bioaccessibility: the release of bioactive compounds in the gastro-intestinal tract and the solubility of these compounds in the digestive fluid which could be determined by *in vitro* digestion (64). Once the phenolics are released and dissolved in intestinal juices, they are potentially accessible for absorption by the epithelial cells of the intestinal wall into the blood stream and available for use. However, these compounds are susceptible to binding with other diet elements released during digestion, like minerals, carbohydrates, dietary fiber, or proteins that affect the solubility and bioaccessibility of PCs (65). If the phenolics bind with other components to form substances that have large molecular masses under the relatively high pH in the intestinal tract, such molecules cannot pass through the dialysis tube and lead to a lower bioavailability (66).

Compared with the soluble free phenolics, the insoluble-bound phenolics are commonly of lower bioaccessibility during digestion (67). Corona-Leo et al. (68) found that the recovery and bioaccessibility index of FPC in apples ranged from 7.23 to 26.61%, and 20.79 to 81.43%, respectively for the gastric and intestinal steps (68). Gong et al. (69) also reported that the FPCs of digested cereal grains ranged from 2.89 (wheat) to 4.23 (corn). In our study, the microbial fermentation resulted in a variation of FPC from 4.87 mg GAE/g to 5.61 mg GAE/g, which was consistent with these above reports. The release and solubilization of phenolics from black barley by microbial enzymes in our study could further take advantage of the potential health benefits of phenolics, as only those phenolics that are soluble can be potentially bioaccessible.

It was found that the phenolic acids in cereals and the products of cereal had a very low bioavailability of substance in human body, with figures as low as 3% (70). Mateo Anson et al. (71) demonstrated that in a dynamic *in vitro* system, the bioavailability of phenolics from bran and aleurone was lower than 1%, assuming that the sole free fraction is a significant contributor. Recently, the Dietary Guidelines for Americans recommended a consumption of at least 3 ounce equivalents of whole meal cereals per day for an adult (72). In this case, it was hypothesized that our black barley-based fermented product could contribute to approximately more than 10 ng/g PCs that are ultimately absorbed after the dietary intake of product. This result was in accordance with others' findings obtained by using *in vivo* experiments. For example, the anthocyanins, representative substance of the PCs, have been confirmed to have protective effects against H_2O_2-induced oxidative injury in human cells, and their accumulated concentration was detected to be 0.709 ng/g in pigs and 115 ng/g in rats, respectively (73).

CONCLUSIONS

The present study investigated the biotransformation of black barley phenolics and evaluated the amelioration of antioxidant activity of phenolics at the chemical and cellular levels. After fermentation, the bacterial counting and the total and FPCs of barley considerably increased. The phenolics from FB performed better on chromatographic profile than those from UFB. Eleven PCs were then identified and quantitatively compared, among which two flavan-3-ols, one flavonol, hordatine A, and pelargonidin-3-*O*-glucosyl-rutinoside were enriched by fermentation. Furthermore, F-BPE possessed better activity in scavenging DPPH radicals and improving FRAP and ORAC, and also had a more remarkable influence on ameliorating the oxidative defense system in HepG2 cells. As concluded, *Lactobacillus* accelerated the release of barley phenolics accessible for absorption, improved their phenolic composition, and largely enriched the compounds such as epicatechin, pelargonidin aglycone, etc. The cytoprotective effects of phenolics were therefore enhanced and performed through a composite mechanism, attributing to the fermentation by *Lactobacillus*. LAB fermentation could be considered a novel approach to develop barley as a source of cereal-derived therapeutic ingredients. In the next study, the recovery and bioacccessibility of phenolics from this black barley-based fermented product should be further investigated, and the bioavailability of phenolics and their health benefits would be studied *in vivo* as well.

DATA AVAILABILITY STATEMENT

The original contributions presented in the study are included in the article/**Supplementary Material**, further inquiries can be directed to the corresponding author/s.

AUTHOR CONTRIBUTIONS

Conceptualization was done by HW and X-LL. Data curation was done by HW and C-QL. Formal analysis was done by H-NL and C-QL. Funding acquisition was done by HW, X-LL, and H-ZZ. HW and H-NL performed the investigation. The methodology was given by J-ZZ, the project administration by HW, the resources by X-LL, and software by J-ZZ. The supervision was done by X-LL and validation by HW. Visualization was done by HW and C-QL, writing the original

draft by HW, and writing-review and editing by HW, X-LL, and H-ZZ. All authors contributed to the article and approved the submitted version.

FUNDING

This work was financially supported by the Science and Technology Plan Program of Yangzhou City (Grant No. YZ2020045) and Institute Research Fund of Jiangsu Academy of Agricultural Sciences (Grant No. 013036611703).

SUPPLEMENTARY MATERIAL

The Supplementary Material for this article can be found online at: https://www.frontiersin.org/articles/10.3389/fnut.2021.790765/full#supplementary-material

REFERENCES

1. Huang WY, Zhang HC, Liu WX, Li CY. Survey of antioxidant capacity and phenolic composition of blueberry, blackberry, and strawberry in Nanjing. *J Zhejiang Univ-SC B.* (2012) 13:94–102. doi: 10.1631/jzus.B1100137
2. Lin X, Wu LF, Wang X, Yao LL, Wang L. Ultrasonic-assisted extraction for flavonoid compounds content and antioxidant activities of India *Moringa oleifera* L. leaves: Simultaneous optimization, HPLC characterization and comparison with other methods. *J Appl Res Med Aroma.* (2020) 20:100284. doi: 10.1016/j.jarmap.2020.100284
3. Wang RM, He RP, Li ZH, Li SJ, Li CF, Wang L. Tailor-made deep eutectic solvents-based green extraction of natural antioxidants from partridge leaf-tea (*Mallotus furetianus* L.). *Sep Purif Technol.* (2021) 275:119159. doi: 10.1016/j.seppur.2021.119159
4. Khalifa I, Zhu W, Li KK, Li CM. Polyphenols of mulberry fruits as multifaceted compounds: Compositions, metabolism, health benefits, and stability-A structural review. *J Funct Foods.* (2018) 40:28–43. doi: 10.1016/j.jff.2017.10.041
5. Zhao L, Zhang F, Ding X, Wu G, Lam YY, Wang X, et al. Gut bacteria selectively promoted by dietary fibers alleviate type 2 diabetes. *Science.* (2018) 359:1151–6. doi: 10.1126/science.aao5774
6. Ayoub M, de Camargo AC, Shahidi F. Antioxidants and bioactivities of free, esterified and insoluble-bound phenolics from berry seed meals. *Food Chem.* (2016) 197:221–32. doi: 10.1016/j.foodchem.2015.10.107
7. Acosta-Estrada BA, Gutierrez-Uribe JA, Serna-Saldívar SO. Bound phenolics in foods, a review. *Food Chem.* (2014) 152:46–55. doi: 10.1016/j.foodchem.2013.11.093
8. Xiao Y, Huang YX, Chen YL, Fan ZY, Chen RY, He C, et al. Effects of solid-state fermentation with Eurotium cristatum YL-1 on the nutritional value, total phenolics, isoflavones, antioxidant activity, and volatile organic compounds of black soybeans. *Agronomy.* (2021) 11:1029. doi: 10.3390/agronomy11061029
9. Dordević TM, Siler-Marinković SS, Dimitrijević-Branković SI. Effect of fermentation on antioxidant properties of some cereals and pseudo cereals. *Food Chem.* (2010) 119:957–63. doi: 10.1016/j.foodchem.2009.07.049
10. Chen YL, Wang YL, Chen JX, Tang H, Wang CH, Li ZJ, et al. Bioprocessing of soybeans (*Glycine max* L.) by solid-state fermentation with Eurotium cristatum YL-1 improves total phenolic content, isoflavone aglycones, antioxidant activity. *RSC Adv.* (2020) 10:16928–41. doi: 10.1039/C9RA10344A
11. Wang L, Bei Q, Wu YN, Liao WZ, Wu ZQ. Characterization of soluble and insoluble-bound polyphenols from *Psidium guajava* L. leaves co-fermented with Monascus anka and Bacillus sp. and their bio-activities. *J Funct Foods.* (2017) 32:149–59. doi: 10.1016/j.jff.2017.02.029
12. Bei Q, Liu Y, Wang L, Chen G, Wu ZQ. Improving free, conjugated, and bound phenolic fractions in fermented oats (*Avena sativa* L.) with Monascus anka and their antioxidant activity. *J Funct Foods.* (2017) 32:185–94. doi: 10.1016/j.jff.2017.02.028
13. Gänzle MG. Enzymatic and bacterial conversions during sourdough fermentation. *Food Microbiol.* (2014) 37:2–10. doi: 10.1016/j.fm.2013.04.007
14. Cai SB, Wang O, Wu W, Zhu SJ, Zhou F, Ji BP, et al. Comparative study of the effects of solid-state fermentation with three filamentous fungi on the total phenolics content (TPC), flavonoids, and antioxidant activities of subfractions from oats (*Avena sativa* L.). *J Agr Food Chem.* (2011) 60:507–13. doi: 10.1021/jf204163a
15. Xiao Y, Rui X, Xing GL, Wu H, Li W, Chen XH, et al. Solid state fermentation with Cordyceps militaris SN-18 enhanced antioxidant capacity and DNA damage protective effect of oats (*Avena sativa* L.). *J Funct Foods.* (2015) 16:58–73. doi: 10.1016/j.jff.2015.04.032
16. Lima CF, Fernandes-Ferreira M, Pereira-Wilson C. Phenolic compounds protect HepG2 cells from oxidative damage: Relevance of glutathione levels. *Life Sci.* (2006) 79:2056–68. doi: 10.1016/j.lfs.2006.06.042
17. Kich DM, Bitencourt S, Caye B, Faleiro D, Alves C, Silva J, et al. Lymphocyte genotoxicity and protective effect of Calyptranthes tricona (Myrtaceae) against H2O2-induced cell death in MCF-7 cells. *Mol Cell Biochem.* (2017) 424:35–43. doi: 10.1007/s11010-016-2840-9
18. Wu H, Rui X, Chen XH, Jiang M, Dong MS. Mung bean (Vigna radiata) as probiotic food through fermentation with Lactobacillus plantarum B1-6. *LWT-Food Sci Technol.* (2015) 63:445–51. doi: 10.1016/j.lwt.2015.03.011
19. Rui X, Wen DL, Li W, Chen XH, Jiang M, Dong MS. Enrichment of ACE inhibitory peptides in navy bean (*Phaseolus vulgaris*) using lactic acid bacteria. *Food Funct.* (2015) 6:622–9. doi: 10.1039/C4FO00730A
20. Li CC, Li W, Chen XH, Feng XM, Rui X, Jiang M, et al. Microbiological, physicochemical and rheological properties of fermented soymilk produced with exopolysaccharide (EPS) producing lactic acid bacteria strains. *LWT-Food Sci Technol.* (2014) 57:447–85. doi: 10.1016/j.lwt.2014.02.025
21. Wu H, Rui X, Li W, Xiao Y, Zhou JZ, Dong MS. Whole-grain oats (*Avena sativa* L.) as a carrier of lactic acid bacteria and a supplement rich in angiotensin I-converting enzyme inhibitory peptides through solid-state fermentation. *Food Funct.* (2018) 9:2270–81. doi: 10.1039/C7FO01578J
22. Xiao Y, Xing GL, Rui X, Li W, Chen XH, Jiang M, et al. Enhancement of the antioxidant capacity of chickpeas by solid state fermentation with Cordyceps militaris SN-18. *J Funct Foods.* (2014) 10:210–22. doi: 10.1016/j.jff.2014.06.008
23. Baba SA, Malik SA. Determination of total phenolic and flavonoid content, antimicrobial and antioxidant activity of a root extract of *Arisaema jacquemontii* Blume. *J Taibah Univ Sci.* (2015) 9:449–54. doi: 10.1016/j.jtusci.2014.11.001
24. Rocchetti G, Lucini L, Lorenzo Rodriguez JM, Barba FJ, Giuberti G. Gluten-free flours from cereals, pseudocereals and legumes: Phenolic fingerprints and in vitro antioxidant properties. *Food Chem.* (2019) 271:157–64. doi: 10.1016/j.foodchem.2018.07.176
25. Xiao Y, Wu X, Yao XS, Chen YL, Ho CT, He C, et al. Metabolite profiling, antioxidant and α-glucosidase inhibitory activities of buckwheat processed by solid-state fermentation with Eurotium cristatum YL-1. *Food Res Int.* (2021) 143:110262. doi: 10.1016/j.foodres.2021.110262
26. Shimada K, Fujikawa K, Yahara K, Nakamura T. Antioxidative properties of xanthan on the autoxidation of soybean oil in cyclodextrin emulsion. *J Agr Food Chem.* (1992) 40:945–8. doi: 10.1021/jf00018a005
27. Lee YL, Yang JH, Mau JL. Antioxidant properties of water extracts from Monascus fermented soybeans. *Food Chem.* (2008) 106:1128–37. doi: 10.1016/j.foodchem.2007.07.047
28. Benzie IFF, Strain JJ. The ferric reducing ability of plasma (FRAP) as a measure of "antioxidant power": the FRAP assay. *Anal Biochem.* (1996) 239:70–6. doi: 10.1006/abio.1996.0292
29. Qin Y, Jin XN, Park Heui D. Comparison of antioxidant activities in black soybean preparations fermented with various microorganisms. *Agr Sci China.* (2010) 9:1065–71. doi: 10.1016/S1671-2927(09)60191-7
30. Li CY, Huang WY, Wang XN, Liu WX. Oxygen radical absorbance capacity of different varieties of strawberry and the antioxidant stability in storage. *Molecules.* (2013) 18:1528–39. doi: 10.3390/molecules18021528
31. Huang WY, Wu H, Li DJ, Song JF, Xiao YD, Liu CQ, et al. Protective effects of blueberry anthocyanins against H2O2-induced oxidative injuries

in human retinal pigment epithelial cells. *J Agr Food Chem.* (2018) 66:1638–48. doi: 10.1021/acs.jafc.7b06135
32. Zhu C, Dong YC, Liu HL, Ren H, Cui ZH. Hesperetin protects against H2O2-triggered oxidative damage via upregulation of the Keap1-Nrf2/HO-1 signal pathway in ARPE-19 cells. *Biomed Pharmacother.* (2017) 88:124–33. doi: 10.1016/j.biopha.2016.11.089
33. Kaczara P, Sarna T, Burke JM. Dynamics of H2O2 availability to ARPE-19 cultures in models of oxidative stress. *Free Rad Biol Med.* (2010) 48:1064–70. doi: 10.1016/j.freeradbiomed.2010.01.022
34. Vincent A, Thauvin M, Quévrain E, Mathieu E, Layani S, Seksik P, et al. Evaluation of the compounds commonly known as superoxide dismutase and catalase mimics in cellular models. *J Inorg Biochem.* (2021) 219:111431. doi: 10.1016/j.jinorgbio.2021.111431
35. Shi XC, Yang JJ, Wen XT, Tian FL, Li CY. Oxygen vacancy enhanced biomimetic superoxide dismutase activity of CeO2-Gd nanozymes. *J Rare Earth.* (2020) 39:1108–16. doi: 10.1016/j.jre.2020.06.019
36. Zhang WJ, Gao JL, Lu L, Bold T, Li X, Wang S, et al. Intracellular GSH/GST antioxidants system change as an earlier biomarker for toxicity evaluation of iron oxide nanoparticles. *NanoImpact.* (2021) 23:100338. doi: 10.1016/j.impact.2021.100338
37. Zhang ST, Shi Y, Zhang SL, Shang W, Gao XQ, Wang HK. Whole soybean as probiotic lactic acid bacteria carrier food in solid-state fermentation. *Food Control.* (2014) 41:1–6. doi: 10.1016/j.foodcont.2013.12.026
38. Kaprasob R, Kerdchoechuen O, Laohakunjit N, Sarkar D, Shetty K. Fermentation-based biotransformation of bioactive phenolics and volatile compounds from cashew apple juice by select lactic acid bacteria. *Process Biochem.* (2017) 59:141–9. doi: 10.1016/j.procbio.2017.05.019
39. Bhanja T, Kumari A, Banerjee R. Enrichment of phenolics and free radical scavenging property of wheat koji prepared with two filamentous fungi. *Bioresource Technol.* (2009) 100:2861–6. doi: 10.1016/j.biortech.2008.12.055
40. Wang L, Wei W, Tian X, Shi K, Wu Z. Improving bioactivities of polyphenol extracts from *Psidium guajava* L. leaves through co-fermentation of Monascus anka GIM 3.592 and Saccharomyces cerevisiae GIM 2.139. *Ind Crop Prod.* (2016) 94:206–15. doi: 10.1016/j.indcrop.2016.08.043
41. Pihlava JM. Identification of hordatines and other phenolamides in barley (Hordeum vulgare) and beer by UPLC-QTOF-MS. *J Cereal Sci.* (2014) 60:645–52. doi: 10.1016/j.jcs.2014.07.002
42. Rao S, Santhakumar AB, Chinkwo KA, Blanchard CL. Q-TOF LC/MS identification and UHPLC-Online ABTS antioxidant activity guided mapping of barley polyphenols. *Food Chem.* (2018) 266:323–8. doi: 10.1016/j.foodchem.2018.06.011
43. Gangopadhyay N, Rai DK, Brunton NP, Gallagher E, Hossain MB. Antioxidant-guided isolation and mass spectrometric identification of the major polyphenols in barleys (Hordeum vulgare) grain. *Food Chem.* (2016) 210:212–20. doi: 10.1016/j.foodchem.2016.04.098
44. Krupa-Małkiewicz M, Oszmiański J, Lachowicz S, Szczepanek M, Jaśkiewicz B, Pachnowska K, et al. Effect of nanosilver (nAg) on disinfection, growth, and chemical composition of young barley leaves under *in vitro* conditions. *J Integr Agr.* (2019) 18:1871–81. doi: 10.1016/S2095-3119(18)62146-X
45. Rocchetti G, Giuberti G, Lucini L. Gluten-free cereal-based food products: the potential of metabolomics to investigate changes in phenolics profile and their in vitro bioaccessibility. *Curr Opin Food Sci.* (2018) 22:1–8. doi: 10.1016/j.cofs.2017.10.007
46. Handa CL, Couto UR, Vicensoti AH, Georgetti SR, Ida EI. Optimisation of soy flour fermentation parameters to produce β-glucosidase for bioconversion into aglycones. *Food Chem.* (2014) 152:56–65. doi: 10.1016/j.foodchem.2013.11.101
47. Boudet AM. Evolution and current status of research in phenolic compounds. *Phytochemistry.* (2007) 68:2722–35. doi: 10.1016/j.phytochem.2007.06.012
48. Schümann J, Hertweck C. Advances in cloning, functional analysis and heterologous expression of fungal polyketide synthase genes. *J Biotechnol.* (2006) 124:690–703. doi: 10.1016/j.jbiotec.2006.03.046
49. Juan MY, Chou CC. Enhancement of antioxidant activity, total phenolic and? avonoid content of black soybeans by solid state fermentation with Bacillus subtilis BCRC 14715. *Food Microbiol.* (2010) 27:586–91. doi: 10.1016/j.fm.2009.11.002
50. Lachowicz S, Oszmiański J, Pluta S. The composition of bioactive compounds and antioxidant activity of Saskatoon berry (Amelanchier alnifolia Nutt.) genotypes grown in central Poland. *Food Chem.* (2017) 235:234–43. doi: 10.1016/j.foodchem.2017.05.050
51. Kurutas EB. The importance of antioxidants which play the role in cellular response against oxidative/nitrosative stress: Current state. *Nutr J.* (2016) 15:71–92. doi: 10.1186/s12937-016-0186-5
52. Vadivel V, Stuetz W, Scherbaum V, Biesalski HK. Total free phenolic content and health relevant functionality of Indian wild legume grains: Effect of indigenous processing methods. *J Food Compos Anal.* (2011) 24:935–43. doi: 10.1016/j.jfca.2011.04.001
53. Salar RK, Certik M, Brezova V. Modulation of phenolic content and antioxidant activity of maize by solid state fermentation with Thamnidium elegans CCF 1456. *Biotechnol Bioprocess Eng.* (2012) 17:109–16. doi: 10.1007/s12257-011-0455-2
54. Salar RJ, Purewal SS, Bhatti MS. Optimization of extraction conditions and enhancement of phenolic content and antioxidant activity of pearl millet fermented with Aspergillus awamori MTCC-54. *Resour Effic Technol.* (2016) 2:148–57. doi: 10.1016/j.reffit.2016.08.002
55. Wu H, Chai Z, Hutabarat RP, Zeng QL, Niu LY, Li DJ, et al. Blueberry leaves from 73 different cultivars in southeastern China as nutraceutical supplements rich in antioxidants. *Food Res Int.* (2019) 122:548–60. doi: 10.1016/j.foodres.2019.05.015
56. Slavin J. Why whole grains are protective: Biological mechanisms. *Proc Nutr Soc.* (2003) 62:129–34. doi: 10.1079/PNS2002221
57. Ghasemzadeh A, Ghasemzadeh N. Flavonoids and phenolic acids: Role and biochemical activity in plants and human. *J Med Plants Res.* (2011) 5:6697–703. doi: 10.5897/JMPR11.1404
58. Pelicano H, Carney D, Huang P. ROS stress in cancer cells and therapeutic implications. *Drug Resist.* (2004) 7:97–110. doi: 10.1016/j.drup.2004.01.004
59. Abdel-Latif L, Murray BK, Renberg RL, O'Neill KL, Porter H, Jensen JB, et al. Cell death in bovine parvovirus-infected embryonic bovine tracheal cells is mediated by necrosis rather than apoptosis. *J Gen Virol.* (2006) 87:2539–48. doi: 10.1099/vir.0.81915-0
60. Kaneko T, Iuchi Y, Kawachiya S, Fujii T, Saito H, Kurachi H, et al. Alteration of glutathione reductase expression in the female reproductive organs during the estrous cycle. *Biol Reprod.* (2001) 65:1410–6. doi: 10.1095/biolreprod65.5.1410
61. Granado-Serrano AB, Martín MA, Bravo L, Goya L, Ramos S. Quercetin modulates Nrf2 and glutathione-related defense in HepG2 cells: Involvement of p38. *Chem-Biol Interact.* (2012) 195:154–64. doi: 10.1016/j.cbi.2011.12.005
62. Gowd V, Bao T, Chen W. Antioxidant potential and phenolic profile of blackberry anthocyanin extract followed by human gut microbiota fermentation. *Food Res Int.* (2019) 120:523–33. doi: 10.1016/j.foodres.2018.11.001
63. Sevgi K, Tepe B, Sarikurkcu C. Antioxidant and DNA damage protection potentials of selected phenolic acids. *Food Chem Toxicol.* (2015) 77:12–21. doi: 10.1016/j.fct.2014.12.006
64. Holst B, Williamson G. Nutrients and phytochemicals: From bioavailability to bioefficacy beyond antioxidants. *Curr Opin Biotech.* (2008) 19:73–82. doi: 10.1016/j.copbio.2008.03.003
65. Chen GL, Chen SG, Chen F, Xie YQ, Han MD, Luo CX, et al. Nutraceutical potential and antioxidant benefits of selected fruit seeds subjected to an *in vitro* digestion. *J Funct Foods.* (2016) 20:317–331. doi: 10.1016/j.jff.2015.11.003
66. Saura-Calixto F, Serrano J, Goni I. Intake and bioaccessibility of total polyphenols in a whole diet. *Food Chem.* (2007) 101:492–501. doi: 10.1016/j.foodchem.2006.02.006
67. Liu RH. Whole grain phytochemicals and health. *J Cereal Sci.* (2007) 46:207–19. doi: 10.1016/j.jcs.2007.06.010
68. Corona-Leo LS, Meza-Marquez OG, Hernandez-Martinez DM. Effect of *in vitro* digestion on phenolic compounds and antioxidant capacity of different apple (Malus domestica) varieties harvested in Mexico. *Food Biosci.* (2021) 43:101311. doi: 10.1016/j.fbio.2021.101311
69. Gong ES, Gao N, Li T, Chen H, Wang Y, Si X, et al. Effect of *in vitro* digestion on phytochemical profiles and cellular antioxidant activity of whole grains. *J Agr Food Chem.* (2019) 67:7016–24. doi: 10.1021/acs.jafc.9b02245
70. Kern SM, Bennett RN, Mellon FA, Kroon PA, GarciaConesa MT. Absorption of hydroxycinnamates in humans after highbran cereal consumption. *J Agric Food Chem.* (2003) 51:6050–5. doi: 10.1021/jf0302299

71. Mateo Anson N, van den Berg R, Havenaar R, Bast A, Haenen GRMM. Bioavailability of ferulic acid is determined by its bioaccessibility. *J Cereal Sci.* (2009) 49:296–300. doi: 10.1016/j.jcs.2008.12.001
72. U.S. Department of Agriculture and U.S. Department of Health and Human Services. *Dietary Guidelines for Americans, 7th ed.* Washington, DC: U.S. Government Printing Office (2010).
73. Kalt W, Blumberg J, McDonald J, Vinqvist-Tymchuk M, Fillmore S, Graf B, et al. Identification of anthocyanins in the liver, eye, and brain of blueberry-fed pigs. *J Agric Food Chem.* (2008) 56:705–12. doi: 10.1021/jf071998l

Conflict of Interest: The authors declare that the research was conducted in the absence of any commercial or financial relationships that could be construed as a potential conflict of interest.

Publisher's Note: All claims expressed in this article are solely those of the authors and do not necessarily represent those of their affiliated organizations, or those of the publisher, the editors and the reviewers. Any product that may be evaluated in this article, or claim that may be made by its manufacturer, is not guaranteed or endorsed by the publisher.

frontiers in Nutrition

ORIGINAL RESEARCH
published: 08 February 2022
doi: 10.3389/fnut.2021.794231

Changes in Physicochemical Properties, Volatile Profiles, and Antioxidant Activities of Black Apple During High-Temperature Fermentation Processing

Zuoyi Zhu, Yu Zhang, Wei Wang*, Suling Sun, Junhong Wang, Xue Li, Fen Dai and Yunzhu Jiang*

Institute of Agro-Product Safety and Nutrition, Zhejiang Academy of Agricultural Science, Hangzhou, China

Black apple is a new elaborated product obtained from whole fresh apple through fermentation at controlled high temperature (60∼90°C) and humidity (relative humidity of 50∼90%). The appearance, color, texture, and taste of black apple changed dramatically compared with those of fresh apple. In this study, changes in the physicochemical and phytochemical properties, volatile profiles, and antioxidant capacity of apple during the fermentation process were investigated. Results showed that the browning intensity and color difference increased continuously during the whole 65-day fermentation process ($p < 0.05$). Sugars decreased in the whole fermentation process ($p < 0.05$), whereas the contents of organic acids increased first and then decreased with prolonged 35 days of fermentation ($p < 0.05$). Total polyphenol content of black apple showed an increase of 1.5-fold as that of fresh apple, whereas 12 common polyphenolic compounds present in fresh apple decreased dramatically in the whole fermentation process ($p < 0.05$). The analysis of flavor volatiles showed that high-temperature fermentation decreased the levels of alcohols and esters and resulted in the formation of furanic and pyranic compounds, which are the main products of Maillard reaction (MR). Antioxidant activities of black apple were enhanced compared with those of fresh apple, and results indicated that the enhancement of antioxidant activities was related to the polyphenols and products of MR.

Keywords: apple, high-temperature fermentation processing, physicochemical properties, volatile profiles, antioxidant activity

OPEN ACCESS

Edited by:
Xiaolong Ji,
Zhengzhou University of Light Industry, China

Reviewed by:
Jixun Zhan,
Utah State University, United States
Guohua Zhang,
Shanxi University, China

****Correspondence:***
Yu Zhang
zhyu7711@163.com
Wei Wang
wangwei5228345@126.com

Specialty section:
This article was submitted to Food Chemistry, a section of the journal Frontiers in Nutrition

Received: *13 October 2021*
Accepted: *29 October 2021*
Published: *08 February 2022*

Citation:
Zhu Z, Zhang Y, Wang W, Sun S, Wang J, Li X, Dai F and Jiang Y (2022) Changes in Physicochemical Properties, Volatile Profiles, and Antioxidant Activities of Black Apple During High-Temperature Fermentation Processing. Front. Nutr. 8:794231. doi: 10.3389/fnut.2021.794231

INTRODUCTION

Nowadays, apple is one of the most consumed fruits worldwide. The popularity of apple all over the world is not only due to its pleasant flavor and nutritional value, but also a due to a significant source of dietary bioactive compounds (1). The dietary intake of apple has been shown to have significant benefits to human health, including lowering the risk of cancer, cardiovascular diseases, obesity, type-2 diabetes, and inflammatory disorders (2–5). Recently, China has become the largest apple producer among the world, with apple planting area and yield accounting for approximately 50% of the world. The production of apple in China was 42.43 million tons in 2019. However, the

main consumption way of apple is fresh fruit. Dried apple, apple juice, and cider make up only a small proportion of the apple consumption (6, 7). With the expansion of apple planting scale, market saturation, and lack of deep processing technology, apple supply in excess of demand happens all the time, leading to serious economic losses of fruit farmers. In addition, in the process of apple cultivation, due to the planting technology, management, climate, and environment etc., a part of the apples have defects in shape, color, and appearance. Such defects greatly affect the sale of fresh apples. Therefore, it is of great significance to develop advanced processing technologies for apple.

Thermal processes are commonly used in food manufacturing to improve the sensory quality of foods, such as colors, textures, and tastes, as well as to improve the storage performance of foods. This will cause chemical changes to form new compounds that are not originally present in foods. Black garlic is a thermal-processed product, which is prepared through natural fermentation of fresh garlic cloves at high temperature and humidity for a long time (8). Black garlic has been a popular food particularly in China, Korea, and Japan (9). After high-temperature fermentation processing (HTFP), the garlic cloves change from white to black with the texture becoming soft and elastic. The taste of black garlic is sweeter without the pungent odor (10). Many studies have shown that black garlic exhibits a variety of biological activities, such as antioxidant, hepatoprotective, neuroprotective, antiallergic, antidiabetic, and anticancer activities (11–15). Although the application of HTFP on garlic has been intensively studied and widely used, HTFP on other plant foods such as onion, potato, apple, and peach has not been tried yet. In view of the high-quality health benefits of black garlic, HTFP can be a potential alternative to traditional thermal processing technologies to develop safe, tasty, nutritive, and functional food products.

In our previous study, the HTFP technology of black garlic was carried out on apple as reference (16). A new fermented product with characteristic black appearance, named as black apple, was obtained. The texture of the final products becomes soft and sticky, with a sweet-sour flavor. At the same time, many nonenzymatic reactions such as Maillard reaction (MR) and caramelization reaction, occurred during the HTFP process of apple. These reactions will definitely cause changes in the physicochemical properties and biological activities of apple. To the best of our knowledge, there is no information available about the changes of apple during the HTFP process. However, the influences of thermal process on the physicochemical properties, bioactive compounds, volatile profiles, and biological activities of apple are still unknown. Therefore, the objective of this study was to investigate the changes in the physicochemical and phytochemical properties of apple, including color, browning intensity, pH, the contents of moisture, sugars, organic acids, phenolic and volatile compounds, during the 65-day HTFP process. The antioxidant activities of apple during the HTFP process were also studied by 2,2′-azino-bis(3-ethylbenzothiazoline-6-sulfonic acid) diammonium salt (ABTS), 2,2′-diphenyl-1-picrylhydrazyl (DPPH), hydroxyl radicals, FRAP, and Fe^{2+}-chelating assays. Furthermore, the correlation between physicochemical properties and antioxidant activities of processed apple was also evaluated.

MATERIALS AND METHODS

Chemicals

2,2′-Azino-bis(3-ethylbenzothiazoline-6-sulfonic acid) diammonium salt, DPPH, 2,3,5-triphenyltetrazolium chloride (TPTZ), 6-hydroxy-2,5,7,8-tetramethylchromane-2-carboxylic acid (Trolox), 3-nonanone as internal standard (IS), and ferrozine were purchased from Sigma Chemical Co. (St. Louis, MO, United States). Sorbitol, glucose, fructose, sucrose, formic acid, acetic acid, lactic acid, malic acid, citric acid, gallic acid (GA), protocatechualdehyde (PRO), (+)-catechin (CAT), chlorogenic acid (CHL), caffeic acid (CAF), syringic acid (SYR), epicatechin (EPI), *p*-coumaric acid (*p*-CUM), rutin (RUT), phlorizin (PRI), quercetin (QUE), and phloretin (PRE) were purchased from Shanghai Yuanye Biotechnology Co., Ltd. (Shanghai, China). All other reagents used were of analytical grade.

Samples

Apple samples were kindly provided by Zhejiang Shengyuan Agricultural Science & Technology Co., Ltd. The whole fresh Fuji apples were cleaned and fermented with activated lactic acid bacteria for 24 h and then manufactured in a fermentation bin at controlled temperature (60∼90°C) and humidity (relative humidity of 50∼90%) for 65 days. The fresh apples were used as the reference blank. Samples were removed after 5, 15, 30, 45, and 65 days of high-temperature fermentation treatment. Moisture content, color, and pH values were determined immediately after sample removing. Then, each sample was divided into two subsamples. One was lyophilized using a freeze dryer and then ground into powder by a high-speed grinding powder machine. The other was frozen with liquid nitrogen and stored at −80°C until volatile profile analysis.

Determination of Color

The apples were sliced and the inside color was measured using a portable CR-410T colorimeter (Konica Minolta, Japan). The total color difference (ΔE) was calculated by the following formula (17):

$$\Delta E = (\Delta L)^2 + (\Delta a)^2 + (\Delta b)^2$$

where ΔL, Δa, and Δb represent the difference between processed apple and fresh apple sample (0 day) on L, a, and b values, respectively.

Moisture Contents Measurement

Moisture contents were measured according to the vacuum drying method described in Chinese standard GB5009.3-2016 (18) with a DZF-6050 vacuum drying oven (Shanghai Yiheng Scientific Instrument Co., Ltd., China).

Determination of pH Values

Five grams of the homogenized sample was added to 20 mL distilled water and vortexed at a speed of 2,000 rpm for 3 min.

Then, the homogeneous samples were filtered before the pH measurement. A digital pH meter (PHS−3C, Shanghai Precision Instrument Co., Ltd, China) was used to measure the pH values of samples.

Sample Pretreatment

One gram of lyophilized sample was extracted with 100 mL distilled water by ultrasonic extraction at 25°C for 60 min. The mixture was then centrifuged at 4,000 g for 10 min. The liquid supernatant was collected and diluted for further browning intensity, sugars, and organic acids determination and antioxidant analysis.

Determination of Browning Intensity

The browning intensity (K420) of apple samples was determined by the method described by Lertittikul et al. (19). The absorption values of apple samples at 420 nm were measured against a blank (distilled water) by a N5000 spectrophotometer (Shanghai Youke Instrument Co., Ltd, China).

Determination of Sorbitol, Glucose, Fructose, and Sucrose

The contents of sugars were determined by ion chromatography with pulsed amperometric detection (IC-PAD). The determination was performed on a Thermo Fisher Scientific (Sunnyvale, CA, United States) ICS-3000 ion chromatograph. CarboPac PA10 guard column (50 mm × 4 mm i.d., 10 μm) and analytical column (250 mm × 4 mm i.d., 10 μm) were used for separation. The elution mode was as follows: 15 mM NaOH from 0 to 12 min; 100 mM NaOH from 12.1 to 17 min; and 15 mM NaOH from 17.1 to 22 min. The flow rate was 1.0 mL/min. Column temperature was set at 30°C. The conditions of PAD were the same as the published method (20). The results were expressed as g/100 g of dry matter (DM).

Determination of Organic Acids

The contents of organic acids were determined by IC with conductivity detection. The determination was also performed on a Thermo Fisher Scientific ICS-3000 ion chromatograph. Guard column (IonPac AG11-HC, 50 mm × 4 mm i.d., 9 μm) and analytical column (IonPac AS11-HC, 250 mm × 4 mm i.d., 9 μm) were used for separation. Gradient elution mode was employed as follows: 1 mM NaOH from 0 to 7 min; 1–30 mM NaOH from 7.1 to 25 min; keeping at 30 mM NaOH from 25.1 to 30 min, and 1 mM NaOH from 30.1 to 35 min. Suppression current was set at 75 mA. The flow rate was 1.0 mL/min, and the column temperature was set at 30°C. The results were expressed as g/kg of DM.

Total Polyphenol Content (TPC) and Polyphenolic Compounds

The Folin-Ciocalteu method was used to measure the TPC of apple samples. Briefly, 1 g of lyophilized sample was ultrasonically extracted with 10 mL of acetic acid–water–methanol (1:29:70, v/v/v) for 60 min. The mixture was then centrifuged at 4,000 g for 5 min and the liquid supernatant was collected. A re-extraction of the residue was performed. The supernatants were combined and made up to 20 mL with water. The apple extract (1 mL) was mixed with 5 mL of Folin-Ciocalteu reagent. After 5 min, 4 mL of 7.5% Na_2CO_3 was added. The mixture was left to react for 60 min in the dark. The absorbance was measured at 765 nm. Gallic acid (10–100 mg/L) was used as standard for the quantification of TPC. The content of TPC was expressed as mg GA equivalents per g of DM (mg GAE/g).

High-performance liquid chromatography-electrochemical detection (HPLC-ECD) was used to determine the polyphenols in apple samples followed by a prior study carried out in our laboratory (21), with minor modifications. Four milliliters of the extraction solution above was evaporated using a stream of nitrogen to 1 mL before injection. The analytical column was an Agilent XDB C18 column (250 mm x 4.6 mm i.d., 5 μm) maintained at 35°C. The mobile phase consisted of phosphoric acid (0.05%, v/v) as solvent A and methanol as solvent B. The gradient program was as follows: 0 min (95% A + 5% B); 20 min (80% A + 20% B); 40 min (70% A + 30% B); 50 min (55% A + 45% B) and kept for 15 min; 65–70 min (95% A + 5% B). The flow rate was 1.0 mL/min. ECD was performed on a glassy carbon electrode and was set at 1.0 V in oxidative mode. The results were expressed as μg/g of DM.

Determination of the Volatile Profile

Headspace solid-phase microextraction followed by gas chromatography-tandem mass spectrometry (HS-SPME/GC-MS/MS) was used to determine the volatile compounds. Frozen samples were melted and homogenized. Weighed samples (equivalents of 0.5 g DM) were transferred to a 20-mL headspace vial. Distilled water was added to 10 mL, and then 2 g of NaCl and 5 μL of internal standard (IS, 3-nonanone/methanol at 1:50,000, v:v) were added. The solution was heated for 20 min at 40°C with constant stirring, and then a 65-μm DVB/CAR/PDMS fiber (Supelco, PA, United States) was exposed to the headspace of the sample for 20 min at 50°C for SPME extraction.

The Agilent 8890 GC system was interfaced with an Agilent 7000D triple quadrupole mass spectrometer (Agilent, CA, United States). A HP-5 (30 m × 0.25 mm i.d. × 0.25 μm)-fused silica capillary column (Agilent, CA, United States) was used for separation. After HS-SPME extraction, the fiber was introduced into the GC injector port for the thermal desorption of analytes at 250°C for 6 min. A split injection was used with the split ratio of 2:1. The following chromatographic program was used: 40°C kept for 5 min, increased 2°C/min−60°C and kept for 2 min, increased 3°C/min−120°C, increased 5°C/min−150°C, and then increased 8°C/min−250°C with 5-min hold, with a total run time of 60 min. The flow rate was kept at 1 mL/min with helium as carrier gas. The quadrupole mass detector, ion source, and transfer line temperatures were set at 150, 230, and 250°C, respectively. MS acquisition was carried out in full scan mode (in the range m/z 50–500 amu) with electronic impact (EI) mode at 70 eV. The identification of volatile compounds was performed by matching the mass spectra with the NIST17 data library with a similarity higher than 80% and by comparing the Kovats index (KI) values (22) with the values reported in the NIST library. The relative content (RC) of each volatile compound was calculated by the ratio between the peak area of volatile compound and IS.

Antioxidant Activity

ABTS Radicals Assay

The ABTS radical scavenging activity was evaluated as follows (23). Briefly, ABTS radicals were produced by reacting 7 mM ABTS stock solution with 2.45 mM potassium persulfate. The mixture was left in the dark for 12–16 h before use. The ABTS solution was diluted with 5 mM phosphate-buffered saline (pH 7.4) to an absorbance of 0.70 ± 0.02 at 730 nm. Twenty microliters of sample solution was added to 280 μL of the diluted ABTS solution on a transparent 96-well polystyrene microplate. The absorbance was measured after 20 min using an AMR-100 microplate reader (Hangzhou Allsheng Instrument Co., Ltd, China). ABTS radical scavenging activity was calculated as follows: scavenging rate (%) = [1– (A_1-A_2)/A_0] × 100, where A_0 was the absorbance of ABTS solution, A_1 was the absorbance in the presence of sample and ABTS radicals, and A_2 was the background absorbance of sample.

The DPPH Radical Assay

The DPPH radical scavenging activity was measured according to the method reported by Braca et al. (24) with a slight modification. Briefly, 0.1 mL of sample solution was mixed with 2.9 mL of 0.2 mM DPPH–ethanol solution. The mixture was left in the dark for 10 min. Absorbance was measured at 517 nm using N5000 spectrophotometer. DPPH radical scavenging activity was calculated as follows: Scavenging rate (%) = [1– (A_1-A_2)/A_0] × 100, where A_0 is the absorbance of DPPH solution, A_1 is the absorbance in the presence of sample and DPPH radicals, and A_2 is the background absorbance of sample.

Hydroxyl Radical Assay

The hydroxyl radical scavenging activity was determined according to the method published by Chen et al. (25). The reaction mixture consisted of 0.1 mL of H_2O_2 (20 mM), 0.1 mL of $FeSO_4$ (10 mM), 0.1 mL of salicylic acid–ethanol solution (10 mM), 2.5 mL deionized water, and 0.2 mL of sample solution. The mixture was incubated at 37°C for 1 h, and the absorbance was measured at 510 nm. The hydroxyl radical scavenging activity was calculated as follows: scavenging rate (%) = [1– (A_1-A_2)/A_0] × 100, where A_0 is the absorbance of hydroxyl radicals, A_1 is the absorbance in the presence of sample and hydroxyl radicals, and A_2 is the background absorbance of sample.

The FRAP Assay

The FRAP ability was estimated according to the procedure described in the study by Benzie and Strain (26) with a slight modification. The FRAP reagent consisted of 2.5 mL of 10 mM TPTZ solution in 40 mM HCl, 2.5 mL of 20 mM $FeCl_3.6H_2O$, and 25 mL of 0.3 M acetate buffer at pH 3.6. In brief, 280 μL of FRAP reagent was mixed with 20 μL of sample. The mixture was left in the dark for 10 min. The absorbance of the mixture was measured at 595 nm using AMR-100 microplate reader. Trolox solutions (0.1–1.0 mM) were used to perform the calibration curve. Results were expressed as μM equivalents of Trolox per g sample (DM).

Measurement of Fe^{2+}-Chelating Ability

The Fe^{2+}-chelating ability was determined according to the method published by Decker and Welch (27). In brief, 0.5 mL of the sample solution was added to 0.1 mL of 0.2 mM $FeCl_2$ and 0.2 mL of 0.5 mM ferrozine solutions. After reaction for 10 min, the absorbance at 562 nm was measured. The Fe^{2+}-chelating ability was calculated as follows: Chelating rate (%) = [1– (A_1-A_2)/A_0] × 100, where A_0 is the absorbance of the blank control group, A_1 is the absorbance of the test group, and A_2 is the background absorbance of the sample.

Statistical Analysis

All experiments in this study were performed three times. Experimental data were reported as mean values with SD. A $p < 0.05$ was used to indicate significant differences, and a $p < 0.01$ was used to indicate extremely significant differences. The statistical program SPSS 19.0 (Armonk, NY, United States) was used to analyze the data.

RESULTS AND DISCUSSION

Changes in Appearance, Color, Moisture Content, pH, and Browning Intensity

When fresh apple underwent high-temperature fermentation, the color of apple turned brown first and then changed to dark brown and black gradually (**Figure 1**). This change was mainly due to the nonenzymatic browning reactions and the formation of high molecular weight (MW) compounds, such as melanoidins, resulting from MR. The apples became soft at day 15 of fermentation since the texture began to change. After that, wrinkles appeared on the surface of apple due to the moisture loss. The texture of black apple finally became sticky and chewy. The total color difference (ΔE) increased from 22.74 ± 1.21 to 61.87 ± 1.74 over fermentation time of 5–65 days. The moisture content of apple decreased slowly in the first 15 days due to the high relative humidity of HTFP and then decreased dramatically from 79.7 ± 0.6% to 22.0 ± 0.5% of the final products. The pH value did not vary much throughout the whole fermentation process. The pH value of raw apple was 4.27 and decreased eventually to 3.96 of the final products. The pH decrease of black apple was not as apparent as that of black garlic. According to the reported study by Zhang et al. (9), the pH value decreased from 6.25 to 4.25 with whole heating process. The decrease of pH was probably due to the organic acids developed by the fermentation and produced a sour taste mouthfeel of black apple. The browning intensity (K420) of apple extract showed a sustained increase with the increasing HTFP time. In the initial stage of 30 days, it increased slowly from 0.07 ± 0.003 to 0.33 ± 0.01, whereas it increased sharply from 0.33 ± 0.01 to 1.53 ± 0.02 in the latter stage. As reported, the K420 is an important index of MR and is known to correlate with the antioxidant activity of MR systems (28). These results indicated that vigorous MR occurred in the latter stage of HTFP, leading to the formation of high MW compounds like melanoidins.

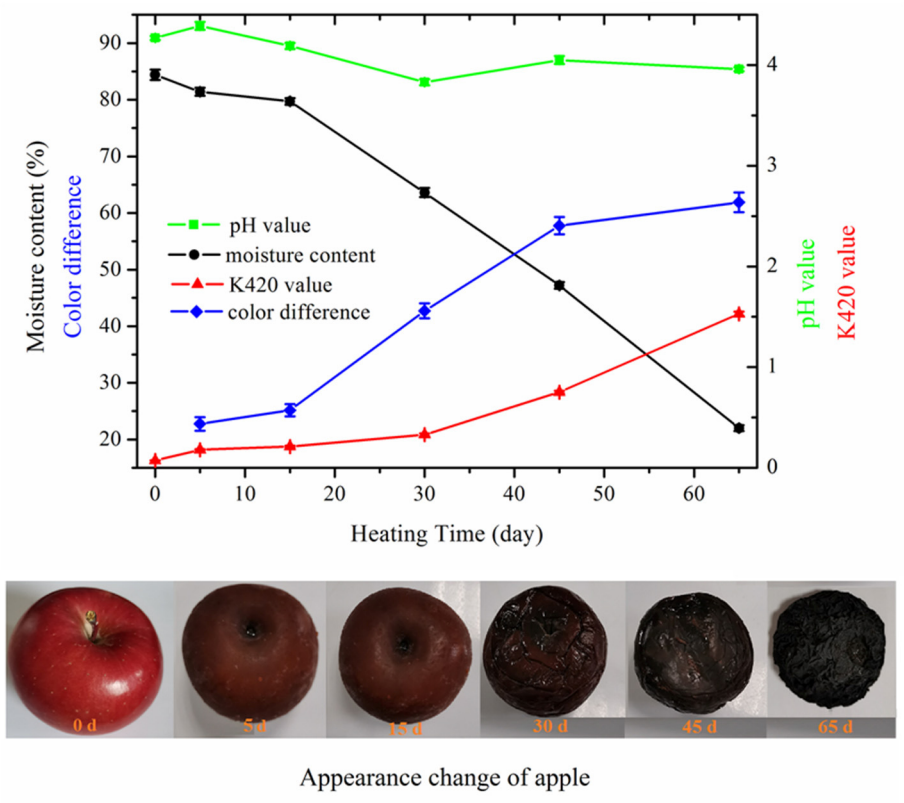

FIGURE 1 | Changes in appearance, moisture content, color difference, browning intensity, and pH of apple during 65-day HTFP process.

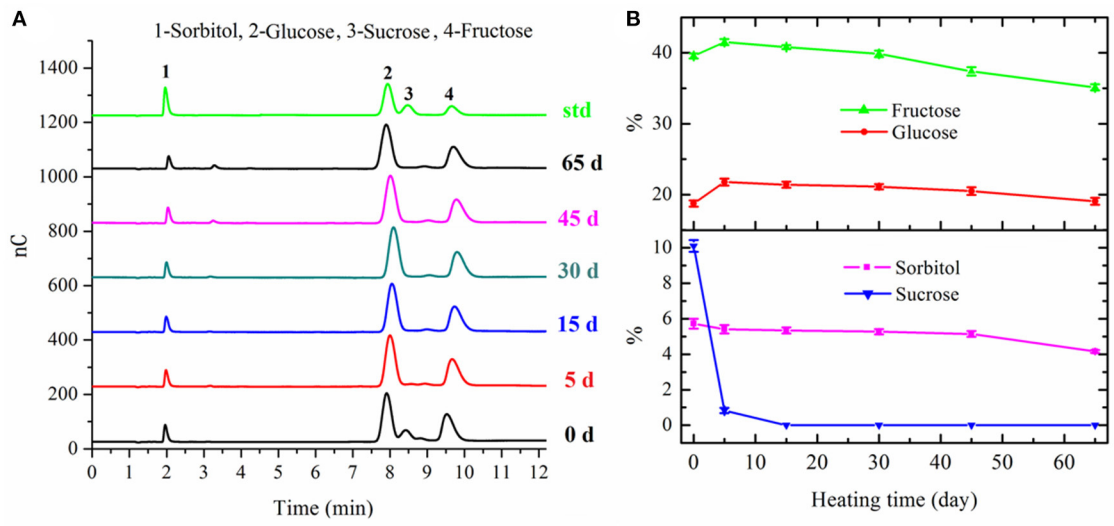

FIGURE 2 | Chromatograms of sugars in apple samples with different fermentation days **(A)** and changes in sugars of apple during 65-day HTFP process **(B)**.

Changes in Sugars

The sugars in fresh apple mainly consisted of sorbitol (5.72 ± 0.28 g/100 g DM), fructose (39.55 ± 0.34 g/100 g DM), glucose (18.75 ± 0.43 g/100 g DM), and sucrose (10.10 ± 0.33 g/100 g DM), respectively. With regard to sucrose, the content of this disaccharide decreased extremely to 0.83 ± 0.15 g/100 g DM in apple after 5 days' fermentation, and then degraded into fructose and glucose completely after 15 days' fermentation

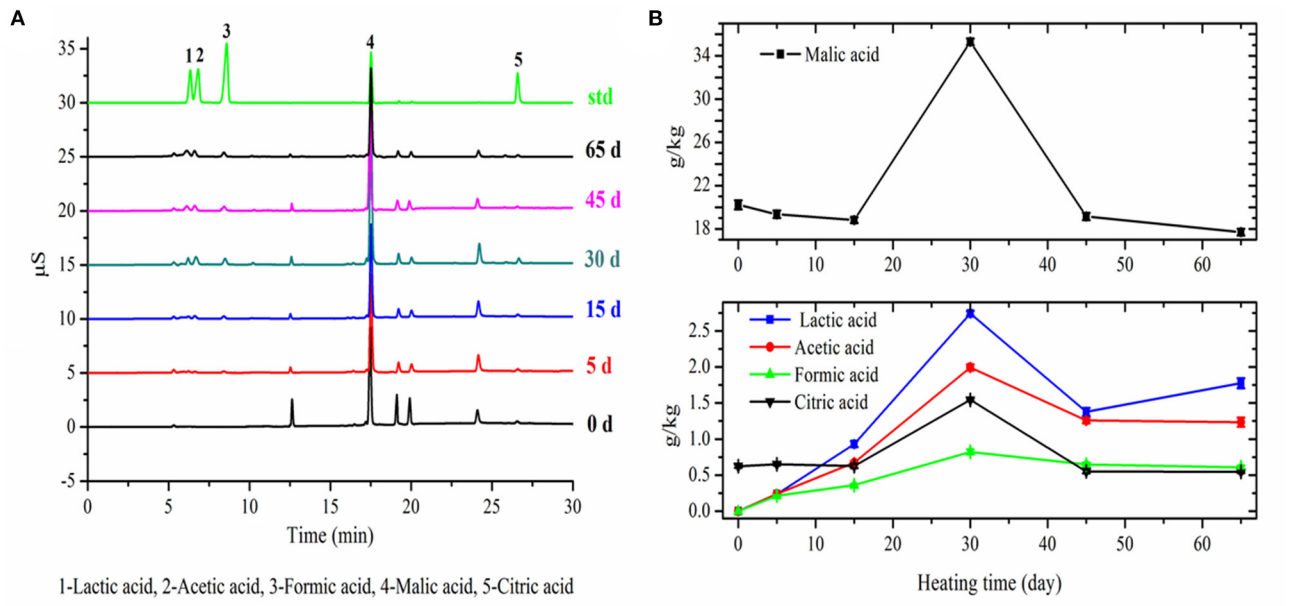

FIGURE 3 | Chromatograms of organic aids in apple samples with different fermentation days **(A)** and changes in organic aids of apple during 65-day HTFP process **(B)**.

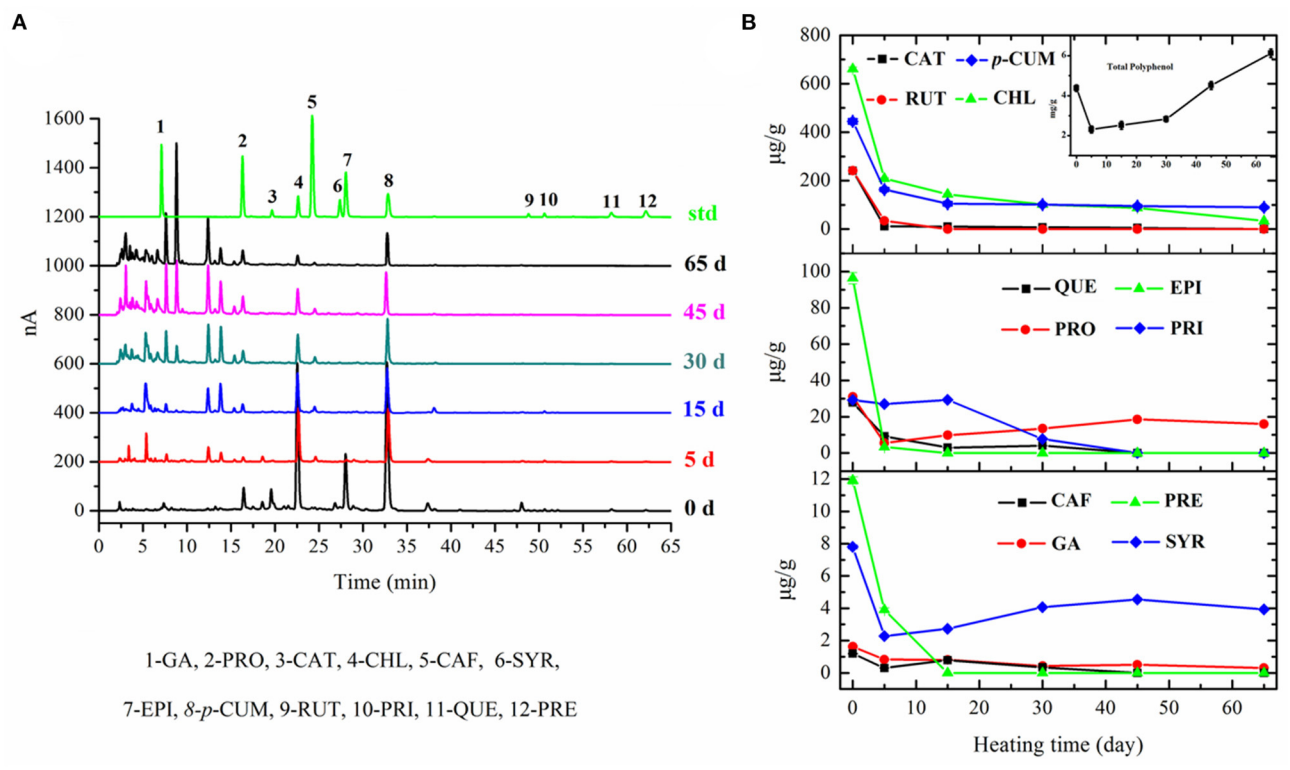

FIGURE 4 | Chromatograms of polyphenols in apple samples with different fermentation days **(A)** and changes in TPC (inset) and polyphenolic profiles of apple during 65-day HTFP process **(B)**.

(**Figure 2**). The degradation of sucrose and other polysaccharides resulted in an increase for both fructose and glucose after 5 days' fermentation. After that, both the contents of fructose and glucose decreased gradually in the following fermentation process. The content of fructose decreased to 35.12 ± 0.44 g/100 g DM in the final black apple product. However, the content of glucose in the final black apple product increased a little bit compared with that of fresh apple. The consumption of fructose and glucose in apple during the fermentation process could mainly be ascribed to MR and bioconversion of sugars into organic acids. These results also suggested that the reactivity of fructose was higher than that of glucose, presumably because fructose had a higher proportion of open chain form than glucose (29). As shown in **Figure 2**, a slight decrease in the content of sorbitol was observed during 0–45 days of fermentation. The content of sorbitol decreased from 5.14 ± 0.16 g/100 g DM to 4.16 ± 0.08 g/100 g DM during the last 20 days' fermentation.

Changes in Organic Acids

The variation trends of five organic acids' contents in apple with fermentation time were similar (**Figure 3**). Among them, lactic acid, acetic acid, and formic acid were not present in fresh apples. The contents of these three organic acids were remarkably increased to a maximum of 2.74 ± 0.056 g/kg DM, 1.99 ± 0.044 g/kg DM, and 0.82 ± 0.033 g/kg DM in apples within 30 days' fermentation, respectively, and then, there was an obvious decrease at day 45 of fermentation. The content of malic acid ranged from 20.23 ± 0.43 g/kg DM in fresh apple to 17.70 ± 0.31 g/kg DM in the final black apple. The content of malic acid decreased slowly during the first 15 days, remarkably increased to a maximum of 35.30 ± 0.32 g/kg DM at 30 days' fermentation, and then decreased sharply. The content of citric acid in apple was extremely low compared with malic acid, and its variation trend in apple with fermentation time was similar as malic acid. The increase of the organic acids during the first half-stage of fermentation could be attributed to the bioconversion of sugars into organic acids and the decrease during the latter half stage of fermentation could be attributed to the volatilization and degradation of organic acids under high temperature and lower relative humidity. The results of organic acids were in agreement with the pH results.

Changes in TPC and Polyphenolic Profiles

The results showed that the TPC of fresh apple was 4.27 ± 0.16 mg GAE/g DM. The TPC of apple decreased to 2.31 ± 0.17 mg GAE/g DM after the initial 5 days' fermentation, increased slowly in the following 25 days, and then increased sharply during the latter half-stage of fermentation (inset of **Figure 4**). The TPC in black apple was 6.22 ± 0.21 mg GAE/g DM and showed an increase of 1.5-fold as that in fresh apple. Previous black garlic studies have described an increase in polyphenol content of about 3-fold, compared to raw garlic (30).

The transformation process of fresh apple into black apple also caused changes in the phenolic acid and flavonoid profiles. According to the results in **Figure 4**, the main polyphenols present in fresh apple are CHL (660.98 ± 18.29 μg/g DM), *p*-CUM (440.86 ± 10.23 μg/g DM), RUT (240.90 ± 10.66 μg/g DM), CAT (240.47 ± 5.87 μg/g DM), and EPI (96.36 ± 6.11 μg/g DM). There was a great loss for almost all 12 polyphenols after 5 days' fermentation when compared with fresh apple, except PRI. The levels of most compounds were continuously decreased in apples as the increasing fermentation time to day 30, and then kept nearly at a constant in the following fermentation time to the final products, except PRO and SYR. The amount of PRI was basically unchanged in the initial 15 days of fermentation and then decreased to zero at day 45. Only *p*-CUM, CHL, PRO, and SYR existed in the final black apple products with contents of 89.60 ± 4.21 μg/g DM, 33.63 ± 2.14 μg/g DM, 15.99 ± 0.39 μg/g DM, and 3.93 ± 0.23 μg/g DM, respectively. Regarding the decrease in phenolic acids, the results of some studies about black garlic are in accordance with ours (31). Studies of citrus peel extract also showed that the thermal process decreased the total phenolic acids content (32). The decreased concentration of phenolic acids in black apple can be due to the fact that some phenolic acids are unstable when they undergo a thermal process. However, the results of flavonoids in this study were different from those reported by Martinez-Casas et al. (31). The contents of flavonoids decreased during the HTFP process in our study. As reported, an increase of EPI was observed in the black garlic and no difference was found in the amount of apigenin between black garlic and raw garlic. In fact, some flavonoids, like RUT, break down easily in the light and high temperature. The evolution of phenolic compounds in foods during the thermal process is ambiguous, with great differences depending on the products. The contents of 12 analyzed polyphenolic compounds originally found in fresh apples decreased dramatically in the black apple, whereas the TPC of black apple increased compared with that of fresh apple. This may be due to the fact that large amounts of new polyphenolic compounds were produced. According to the HPLC chromatograms of the processed apple, a lot of unidentified peaks appeared, which remain to be identified by HPLC-MS in our following research study.

Volatile Profiles

Forty-eight volatile compounds were identified in apples and were classified into nine groups: alcohols, esters, acids, and carbonyl, terpenoid, furanic, pyranic, pyrrole, pyridine compounds (**Table 1**). In fresh apple, 30 volatile compounds consisting of eight alcohols (42.02%), 14 esters (26.78%), four carbonyl compounds (11.20%), and four terpenoid compounds (20.00%) were detected. These results were in good agreement with those reported by Aprea et al. (33). Processed apple presented significant differences in the volatile profiles regarding fresh apple. Only three alcohols and five esters remained at day 5 of fermentation, and most of them showed continuous decreasing as fermentation progressed, except phenylcarbinol, 2-phenylethanol, and 3-methylcyclopentyl acetate. The contents of these three compounds in apple increased first at day 5 of fermentation and then decreased. The temporary increase could be due to the fact that high temperature caused the disruption of the cell wall, resulting in a release of them in the apple. Only 2-ethyl-1-hexanol and 3-methylcyclopentyl acetate were

TABLE 1 | Volatile compounds identified in apples with different fermentation time and their relative contents.

Chemical families	Compounds	Formula	KI^{a}_{CAL}	KI^{b}_{NIST}	RC_{0d}	RC_{5d}	RC_{15d}	RC_{30d}	RC_{45d}	RC_{65d}
Alcohols	2-methyl-1-butanol	$C_5H_{12}O$	734	739	1.764 ± 0.145	–	–	–	–	–
	3-methyl-1-butanol	$C_5H_{12}O$	735	736	0.172 ± 0.016	–	–	–	–	–
	3-(methylthio)-1-propanol	$C_4H_{10}OS$	976	981	0.169 ± 0.012	–	–	–	–	–
	2-methyl-6-hepten-1-ol	$C_8H_{16}O$	995	994	0.131 ± 0.009	–	–	–	–	–
	2-ethyl-1-hexanol	$C_8H_{18}O$	1,034	1,030	0.648 ± 0.072	0.365 ± 0.029	0.305 ± 0.041	0.250 ± 0.036	0.062 ± 0.005	0.043 ± 0.004
	Phenylcarbinol	C_7H_8O	1,036	1,036	0.043 ± 0.005	0.608 ± 0.038	0.342 ± 0.041	–	–	–
	2-phenylethanol	$C_8H_{10}O$	1,112	1,116	0.084 ± 0.006	0.216 ± 0.026	0.260 ± 0.023	0.102 ± 0.011	–	–
	2-phenoxy-ethanol	$C_8H_{10}O_2$	1,219	1,225	0.019 ± 0.003	–	–	–	–	–
Esters	Butyl acetate	$C_6H_{12}O_2$	817	812	0.006 ± 0.001	–	–	–	–	–
	2-methylbutyl acetate	$C_7H_{14}O_2$	881	880	1.082 ± 0.112	–	–	–	–	–
	3-methylcyclopentyl acetate	$C_8H_{14}O_2$	902	905	0.148 ± 0.023	0.748 ± 0.052	0.614 ± 0.056	0.299 ± 0.024	0.216 ± 0.024	0.092 ± 0.011
	Methyl hexanoate	$C_7H_{14}O_2$	926	925	0.054 ± 0.006	0.016 ± 0.002	–	–	–	–
	Ethyl hexanoate	$C_8H_{16}O_2$	1,003	1,000	0.039 ± 0.005	0.027 ± 0.003	–	–	–	–
	Hexyl acetate	$C_8H_{16}O_2$	1,019	1,011	0.360 ± 0.023	–	–	–	–	–
	Methyl octanoate	$C_9H_{18}O_2$	1,128	1,126	0.132 ± 0.017	–	–	–	–	–
	Diethyl succinate	$C_8H_{14}O_4$	1,186	1,182	0.044 ± 0.006	0.023 ± 0.002	0.044 ± 0.033	0.026 ± 0.003	–	–
	Methyl salicylate	$C_8H_8O_3$	1,192	1,192	0.006 ± 0.001	0.006 ± 0.001	0.002 ± 0.0003	–	–	–
	Butyl hexanoate	$C_{10}H_{20}O_2$	1,194	1,189	0.113 ± 0.020	–	–	–	–	–
	Methyl nonanoate	$C_{10}H_{20}O_2$	1,227	1,225	0.029 ± 0.004	–	–	–	–	–
	n-hexyl-2-methylbutanoate	$C_{11}H_{22}O_2$	1,240	1,236	0.014 ± 0.002	–	–	–	–	–
	Isopentyl hexanoate	$C_{11}H_{22}O_2$	1,255	1,252	0.013 ± 0.002	–	–	–	–	–
	2-methylbutyl octanoate	$C_{13}H_{26}O_2$	1,453	1,449	0.011 ± 0.001	–	–	–	–	–
Carbonyl compounds	Hexanal	$C_6H_{12}O$	803	800	0.172 ± 0.021	0.062 ± 0.005	0.045 ± 0.005	0.037 ± 0.005	0.027 ± 0.003	
	4-cyclopentene-1,3-dione	$C_5H_4O_2$	884	881	–	–	–	0.033 ± 0.004	0.062 ± 0.005	0.141 ± 0.020
	6-methyl-5-hepten-2-one	$C_8H_{14}O$	988	986	0.294 ± 0.034	–	–	–	–	–
	(E)-2-octenal	$C_8H_{14}O$	1,061	1,060	0.363 ± 0.027	–	–	–	–	–
	(E)-2-nonenal	$C_9H_{16}O$	1,162	1,162	0.029 ± 0.004	–	–	–	–	–
	β-damascenone	$C_{13}H_{18}O$	1,386	1,386	–	0.013 ± 0.002	0.005 ± 0.001	0.009 ± 0.001	0.005 ± 0.001	0.006 ± 0.001
Terpenoid compounds	D-limonene	$C_{10}H_{16}$	1,028	1,018	1.166 ± 0.078	1.605 ± 0.192	2.770 ± 0.223	1.258 ± 0.021	0.081 ± 0.007	0.090 ± 0.008
	γ-terpinene	$C_{10}H_{16}$	1,060	1,060	–	0.034 ± 0.004	0.043 ± 0.004	0.022 ± 0.003	–	–
	α-cedrene	$C_{15}H_{24}$	1,411	1,411	0.044 ± 0.005	0.035 ± 0.003	0.034 ± 0.003	0.023 ± 0.004	0.016 ± 0.002	0.011 ± 0.002
	α-farnesene	$C_{15}H_{24}$	1,511	1,508	0.322 ± 0.036	0.113 ± 0.014	0.081 ± 0.005	0.013 ± 0.001	0.011 ± 0.001	0.004 ± 0.0003
	Cedrol	$C_{15}H_{26}O$	1,606	1,598	0.189 ± 0.015	0.181 ± 0.021	0.052 ± 0.006	0.025 ± 0.003	–	–
Acids	2-methyl-butanoic acid	$C_5H_{10}O_2$	864	861	–	0.193 ± 0.023	0.156 ± 0.021	0.087 ± 0.009	0.058 ± 0.007	0.056 ± 0.007
Furanic compounds	3-furaldehyde	$C_5H_4O_2$	831	832	–	1.304 ± 0.141	4.526 ± 0.237	6.123 ± 0.412	11.569 ± 0.572	25.121 ± 1.460
	1-(2-furanyl)-ethanone	$C_6H_6O_2$	911	911	–	0.039 ± 0.003	0.083 ± 0.007	0.134 ± 0.015	0.212 ± 0.019	0.734 ± 0.065

(Continued)

TABLE 1 | Continued

Chemical families	Compounds	Formula	KI^{a}_{CAL}	KI^{b}_{NIST}	RC_{0d}	RC_{5d}	RC_{15d}	RC_{30d}	RC_{45d}	RC_{65d}
	5-methyl-2-furancarboxaldehyde	$C_6H_6O_2$	960	965	–	0.037 ± 0.005	0.163 ± 0.013	0.476 ± 0.052	0.866 ± 0.056	3.998 ± 0.312
	2-acetyl-5-methylfuran	$C_7H_8O_2$	1,039	1,039	–	0.007 ± 0.001	0.008 ± 0.001	0.011 ± 0.002	0.014 ± 0.002	0.028 ± 0.003
	2,5-diformylfuran	$C_6H_4O_3$	1,079	1,076	–	0.024 ± 0.003	0.124 ± 0.014	0.241 ± 0.032	0.334 ± 0.041	0.349 ± 0.044
	1-(2-furanyl)-2-hydroxy-ethanone	$C_6H_6O_3$	1,081	1,087	–	0.086 ± 0.009	0.582 ± 0.067	0.916 ± 0.064	1.104 ± 0.130	1.599 ± 0.018
	2-methyl-benzofuran	C_9H_8O	1,103	1,109	–	–	–	–	–	0.013 ± 0.002
	2-furfuryl-5-methylfuran	$C_{10}H_{10}O_2$	1,183	1,190	–	–	–	–	–	0.004 ± 0.0006
	5-hydroxymethylfurfural	$C_6H_6O_3$	1,229	1,233	–	0.091 ± 0.007	3.039 ± 0.291	9.246 ± 0.451	12.335 ± 0.774	13.511 ± 0.824
Pyranic compounds	2,3-dihydro-3,5-dihydroxy-6-methyl-4(H)-pyran-4-one	$C_6H_8O_4$	1,141	1,151	–	–	0.046 ± 0.005	0.124 ± 0.015	0.118 ± 0.023	0.181 ± 0.023
	Maltol	$C_6H_6O_3$	1,109	1,110	–	–	–	0.105 ± 0.009	0.081 ± 0.007	0.062 ± 0.008
Pyrrole	1H-pyrrole-2-carboxaldehyde	C_5H_5NO	1,011	1,015	–	–	–	0.047 ± 0.005	0.100 ± 0.009	0.115 ± 0.014
	2-acetyl pyrrole	C_6H_7NO	1,063	1,064	–	–	–	0.032 ± 0.003	0.056 ± 0.007	0.175 ± 0.015
Pyridine	3-butyl-pridine	$C_9H_{13}N$	1,104	1,101	–	–	–	–	–	0.012 ± 0.002

–: Not detected.

[a]*Kovats index relative n-alkanes (C_8 to C_{20}) on a HP-5 capillary column.*

[b]*Kovats index relative reported in the NIST database.*

present in the final black apple products. For the four carbonyl compounds found in fresh apple, only hexanal was still detected in apple at day 5 of fermentation and its amount continuously decreased. Besides, β-damascenone was first found at day 5 of fermentation in apple and its content fluctuated in the following fermentation time. 4-cyclopentene-1,3-dione was detected at day 30 of fermentation of apple and its contents showed an increase in the following fermentation time. Four terpenoid compounds, namely, D-limonene, α-cedrene, α-farnesene, and cedrol, were found in fresh apple. The content of D-limonene increased in the initial 15 days of fermentation and then decreased in the latter stage of fermentation. The contents of the other three compounds decreased during the whole fermentation process. Another terpenoid compound, γ-terpinene, was first detected at day 5 of fermentation of apple, whereas it was not found in the final black apple as cedrol. For acids, only 2-methyl-butanoic acid was detected in apple from the fifth day of fermentation with its content decreasing during the fermentation process. Nine furanic compounds, as the main products of MR, were detected in the fermentation process of apple. Among them, seven furanic compounds were first detected at day 5 of fermentation in apple and their concentrations increased as fermentation progressed. Except 2-acetyl-5-methylfuran, the contents of the other six furanic compounds increased sharply as fermentation progressed. The contents of 5-hydroxymethylfurfural, 5-methyl-2-furancarboxaldehyde, 3-furaldehyde, 1-(2-furanyl)-ethanone, 1-(2-furanyl)-2-hydroxy-ethanone, and 2,5-diformylfuran in the final black apple products were 148.5-fold, 108.1-fold, 19.3-fold, 18.8-fold, 18.6-fold, and 14.5-fold compared with those in apples at day 5, respectively. These results are in agreement with those from Molina-Calle et al. (34), who demonstrated that 5-hydroxymethylfurfural increased its concentration with garlic fermentation, confirming the development of MR during garlic fermentation. 2-Methyl-benzofuran and 2-furfuryl-5-methylfuran were only detected in the final products with low amounts. Except furanic compounds, pyranic, pyrrole, and pyridine compounds were also detected in the latter stage of fermentation as the products of MR and only maltol decreased with increasing fermentation time. These new generated volatiles might contribute to the flavor and aroma of baking in black apple.

Antioxidant Activities

Hydroxyl Radical Scavenging Activity

The scavenging activities of apple at various fermentation times against the hydroxyl radicals are shown in **Figure 5**. The fresh apple showed high hydroxyl radical scavenging activity of 80.2 ± 2.8%, and then, the scavenging activity of apple decreased to 60.6 ± 2.1% after 15 days' fermentation. After that, the scavenging activity of processed apple increased continuously. The scavenging rate of final black apple was 84.8 ± 3.0%. Results suggested that the hydroxyl radical scavenging activity of the black apple increased slightly compared with that of the fresh apple. The results in this study were different from those of black garlic reported by Zhang et al. (9). As reported, the black garlic showed a significantly

higher scavenging activity of hydroxyl radicals than that of raw garlic.

DPPH Radical Scavenging Activity

The scavenging rate of DPPH radicals decreased sharply from 61.8 ± 2.1% to 43.0 ± 2.0% during the initial 5 days, increased continuously in the following fermentation stage, and then came to a maximum of 85.6 ± 2.0% with the final products. The variation trend of DPPH radical scavenging ability with fermentation time was similar as that of TPC, suggesting that a correlation existed between the two due to the demonstrated antioxidant power of polyphenols.

ABTS Radical Scavenging Activity

The fresh apple showed low ABTS scavenging activity of 13.7 ± 0.5%, and then the scavenging ability of processed apple increased continually to 68.2 ± 2.2% as fermentation time increased from 0 to 65 days. The ABTS radical scavenging rate of the black apple was 5-fold higher than that of the fresh apple. This result was in agreement with those of black garlic obtained by Angeles et al. (30). As reported, a higher increase of 6.5- to 9.5-folds in the antioxidant capacity of black garlic was observed.

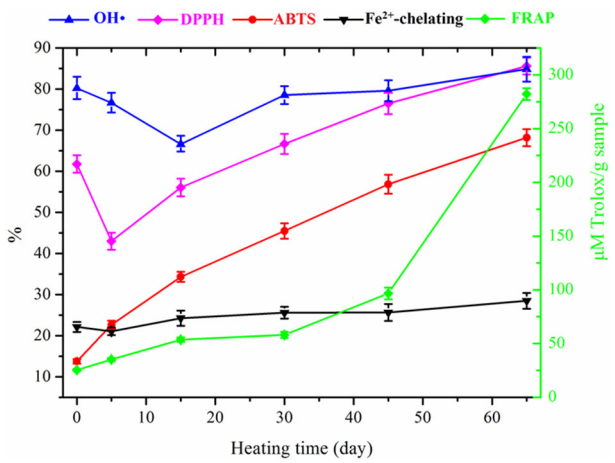

FIGURE 5 | Changes in antioxidant activities of apple during 65-day HTFP process.

FRAP Ability

As shown in **Figure 5**, the FRAP values of processed apple increased slowly in the initial 45 days of fermentation and then increased sharply in the last 20 days. The FRAP value of the fresh apple was 25.4 μM Trolox/g sample (DM), whereas the reducing power of the final black apple was 282.1 μM Trolox/g sample (DM). This result indicated that the reducing power of apple was significantly enhanced during the thermal processing, as the FRAP value of black apple was approximately 10-fold higher than that of fresh apple. This increase mainly occurred in the later phase of the nonenzymatic browning reaction as reported (31).

Fe^{2+}-Chelating Ability

Results showed that the Fe^{2+}-chelating ability of apple increased slowly with the increased heating time. The Fe^{2+}-chelating rates of fresh apple and black apple were 22.1 ± 1.2% and 28.5 ± 1.9%, respectively. Compared with the Fe^{2+}-chelating activity of fresh apple, the slight increase in the Fe^{2+}-chelating activity of black apple was probably ascribed to the high MW products of nonenzymatic browning reactions such as melanoidins, which were shown to have the ability of chelating for Fe^{2+} (35).

In general, the antioxidant activities of black apple were increased compared with those of fresh apple. The increase in the antioxidant activities was statistically correlated with the TPC, physicochemical properties (K420 and ΔE), and products of MR (**Table 2**). Therefore, the representative antioxidant compounds in black apple could be the polyphenols. Furthermore, in the thermal process, a number of furanic compounds with high antioxidant power such as 5-hydroxymethylfurfural were generated through nonenzymatic browning reactions (36, 37). Antioxidant activities are closely related to the product's components and their structure; thus, elucidating correlative antioxidant activities with structural characteristics is of great significance (38).

CONCLUSION

The high-temperature fermentation processing of apple caused significant changes in the physicochemical and phytochemical properties of apple, including the color, browning intensity, pH, moisture content, sugars, organic acids, polyphenolic, and volatile profiles. The antioxidant activities of black apple based on ABTS, DPPH, hydroxyl radical scavenging activity, FRAP and Fe^{2+}-chelating ability were higher than those of fresh apple. The increased antioxidant activities of black apple could be

TABLE 2 | Correlation analysis between physiochemical characteristics and antioxidant activities.

Correlation coefficients	TPC	K420	ΔE	Furanic compounds	Pyranic compounds	Pyrrole compounds
ABTS	0.589*	0.891**	0.975	0.966*	0.921	0.920**
DPPH	0.866**	0.839**	0.733*	0.894**	0.836**	0.900**
•OH	0.758**	0.603**	0.383*	0.547**	0.498	0.674**
FRAP	0.802*	0.980*	0.737	0.933*	0.673	0.943*
Fe^{2+}-chelating	0.660**	0.866**	0.854	0.950	0.908	0.896**

*The marks * and ** indicate statistically significant difference ($p < 0.05$) and statistically extremely significant difference ($p < 0.01$), respectively.*

ascribed to the polyphenols and products of MR. In summary, HTFP can be considered as a promising method of apple processing. It is valuable to carry out the identification of other biologically active compounds in black apple in the future study.

DATA AVAILABILITY STATEMENT

The original contributions presented in the study are included in the article/supplementary material, further inquiries can be directed to the corresponding authors.

AUTHOR CONTRIBUTIONS

ZZ involved in data curation, writing the original draft, writing the review, and editing. YZ involved in formal analysis, investigation, and methodology. WW involved in conceptualization, methodology, and supervision. SS involved in formal analysis. JW involved in data curation and validation. XL and FD involved in writing-review and editing. YJ involved in data curation and formal analysis. All authors contributed to the article and approved the submitted version.

REFERENCES

1. Laaksonen O, Kuldjarv R, Paalme T, Virkki M, Yang B. Impact of apple cultivar, ripening stage, fermentation type and yeast strain on phenolic composition of apple ciders. *Food Chem.* (2017) 233:29–37. doi: 10.1016/j.foodchem.2017.04.067
2. Bondonno NP, Bondonno CP, Ward NC, Hodgson JM, Croft KD. The cardiovascular health benefits of apples: whole fruit vs. isolated compounds. *Trends Food Sci Tech.* (2017) 69:243–56. doi: 10.1016/j.tifs.2017.04.012
3. Chen L, Yang X, Liu R, Liu L, Zhao D, Liu J, et al. Thinned young apple polysaccharide improves hepatic metabolic disorder in high-fat diet-induced obese mice by activating mitochondrial respiratory functions. *J Funct Foods.* (2017) 33:396–407. doi: 10.1016/j.jff.2017.03.055
4. Li D, Yang Y, Sun L, Fang Z, Chen L, Zhao P, et al. Effect of young apple (*Malus domestica Borkh. cv Red Fuji*) polyphenols on alleviating insulin resistance. *Food Biosci.* (2020) 36:100637. doi: 10.1016/j.fbio.2020.100637
5. Tu S-H, Chen L-C, Ho Y-S. An apple a day to prevent cancer formation: reducing cancer risk with flavonoids. *J Food Drug Anal.* (2017) 25:119–24. doi: 10.1016/j.jfda.2016.10.016
6. Lorenzini M, Simonato B, Slaghenaufi D, Ugliano M, Zapparoli G. Assessment of yeasts for apple juice fermentation and production of cider volatile compounds. *LWT.* (2019) 99:224–30. doi: 10.1016/j.lwt.2018.09.075
7. Wu C, Li T, Qi J, Jiang T, Xu H, Lei H. Effects of lactic acid fermentation-based biotransformation on phenolic profiles, antioxidant capacity and flavor volatiles of apple juice. *LWT.* (2020) 122:109064. doi: 10.1016/j.lwt.2020.109064
8. Ryu JH, Kang D. Physicochemical properties, biological activity, health benefits, and general limitations of aged black garlic: a review. *Molecules.* (2017) 22:919. doi: 10.3390/molecules22060919
9. Zhang Z, Lei M, Liu R, Gao Y, Xu M, Zhang M. Evaluation of alliin, saccharide contents and antioxidant activities of black garlic during thermal processing. *J Food Biochem.* (2015) 39:39–47. doi: 10.1111/jfbc.12102
10. Molina-Calle M, de Medina VS, Priego-Capote F, de Castro MDL. Establishing compositional differences between fresh and black garlic by a metabolomics approach based on LC-QTOF MS/MS analysis. *J Food Compos Anal.* (2017) 62:155–63. doi: 10.1016/j.jfca.2017.05.004
11. Al-Shehri SA. Efficacy of black garlic extract on anti-tumor and anti-oxidant activity enhancement in rats. *Clin Nutr Open Sci.* (2021) 36:126–39. doi: 10.1016/j.nutos.2021.03.005
12. Dong M, Yang G, Liu H, Liu X, Lin S, Sun D, et al. Aged black garlic extract inhibits Ht29 colon cancer cell growth via the PI3K/Akt signaling pathway. *Biomed Rep.* (2014) 2:250–4. doi: 10.3892/br.2014.226
13. Hermawati E, Sari DCR, Partadiredja G. The effects of black garlic ethanol extract on the spatial memory and estimated total number of pyramidal cells of the hippocampus of monosodium glutamate-exposed adolescent male Wistar rats. *Anat Sci Int.* (2015) 90:275–86. doi: 10.1007/s12565-014-0262-x
14. Kim MH, Kim MJ, Lee JH, Han JI, Kim JH, Sok D-E, et al. Hepatoprotective effect of aged black garlic on chronic alcohol-induced liver injury in rats. *J Med Food.* (2011) 14:732–8. doi: 10.1089/jmf.2010.1454
15. Yoo J-M, Sok D-E, Kim MR. Anti-allergic action of aged black garlic extract in RBL-2H3 cells and passive cutaneous anaphylaxis reaction in mice. *J Med Food.* (2014) 17:92–102. doi: 10.1089/jmf.2013.2927
16. Zhu Z, Zhang Y, Wang W, Huang Z, Wang J, Li X, et al. Structural characterisation and antioxidant activity of melanoidins from high-temperature fermented apple. *Int J Food Sci Technol.* (2021) 56:2471–80. doi: 10.1111/ijfs.14881
17. Ibarz A, Pagán J, Garza S. Kinetic models for colour changes in pear puree during heating at relatively high temperatures. *J Food Eng.* (1999) 39:415–22. doi: 10.1016/s0260-8774(99)00032-1
18. China. *Chinese standard GB 5009.3-2016. Determination of moisture in foods*. Beijing: The standard Press of RP China (2016).
19. Lertittikul W, Benjakul S, Tanaka M. Characteristics and antioxidative activity of Maillard reaction products from a porcine plasma protein-glucose model system as influenced by pH. *Food Chem.* (2007) 100:669–77. doi: 10.1016/j.foodchem.2005.09.085
20. Zhu Z, Zhang Y, Wang J, Li X, Wang W, Huang Z. Characterization of sugar composition in Chinese royal jelly by ion chromatography with pulsed amperometric detection. *J Food Compos Anal.* (2019) 78:101–7. doi: 10.1016/j.jfca.2019.01.003
21. Zhu Z, Zhang Y, Wang J, Li X, Wang W, Huang Z. Sugaring-out assisted liquid-liquid extraction coupled with high performance liquid chromatography-electrochemical detection for the determination of 17 phenolic compounds in honey. *J Chromatogr A.* (2019) 1601:104–14. doi: 10.1016/j.chroma.2019.06.023
22. van Den Dool, H, Dec Kratz P. A generalization of the retention index system including linear temperature programmed gas-liquid partition chromatography. *J Chromatogr A.* (1963) 11:463–71. doi: 10.1016/s0021-9673(01)80947-x
23. Jiménez-Escrig A, Dragsted LO, Daneshvar B, Pulido R, Saura-Calixto F. *In vitro* antioxidant activities of edible artichoke (*Cynara scolymus* L.) and effect on biomarkers of antioxidants in rats. *J Agric Food Chem.* (2003) 51:5540–5. doi: 10.1021/jf030047e
24. Braca A, De-Tommasi N, Di-Bari L, Pizza C, Politi M, Morelli I. Antioxidant principles from Bauhinia tarapotensis. *J Nat Prod.* (2001) 64:892–5. doi: 10.1021/np0100845
25. Chen X, Wu G, Huang Z. Structural analysis and antioxidant activities of polysaccharides from cultured *Cordyceps militaris*. *Int J Biol Macromol.* (2013) 58:18–22. doi: 10.1016/j.ijbiomac.2013.03.041
26. Benzie IFF, Strain JJ. The ferric reducing ability of plasma (FRAP) as a measure of "antioxidant power": the FRAP assay. *Anal Biochem.* (1996) 239:70–6. doi: 10.1006/abio.1996.0292
27. Decker EA, Welch B. Role of ferritin as a lipid oxidation catalyst in muscle food. *J Agric Food Chem.* (1990) 38:674–7. doi: 10.1021/jf00093a019
28. Kanzler C, Schestkowa H, Haase PT, Kroh LW. Formation of reactive intermediates, color, and antioxidant activity in the Maillard reaction of maltose in comparison to D-glucose. *J Agric Food Chem.* (2017) 65:8957–65. doi: 10.1021/acs.jafc.7b04105
29. Benjakul S, Lertittikul W, Bauer F. Antioxidant activity of Maillard reaction products from a porcine plasma protein-sugar model system. *Food Chem.* (2004) 93:189–96. doi: 10.1016/j.foodchem.2004.10.019

30. Angeles TMM, Jesus PA, Rafael MR, Tania MA. Evolution of some physicochemical and antioxidant properties of black garlic whole bulbs and peeled cloves. *Food Chem.* (2016) 199:135–9. doi: 10.1016/j.foodchem.2015.11.128
31. Martinez-Casas L, Lage-Yusty M, Lopez-Hernandez J. Changes in the aromatic profile, sugars, and bioactive compounds when purple garlic is transformed into black garlic. *J Agric Food Chem.* (2017) 65:10804–11. doi: 10.1021/acs.jafc.7b04423
32. Xu G, Ye X, Chen J, Liu D. Effect of heat treatment on the phenolic compounds and antioxidant capacity of citrus peel extract. *J Agric Food Chem.* (2007) 55:330–5. doi: 10.1021/jf062517l
33. Aprea E, Gika H, Carlin S, Theodoridis G, Vrhovsek U, Mattivi F. Metabolite profiling on apple volatile content based on solid phase microextraction and gas-chromatography time of flight mass spectrometry. *J Chromatogr A.* (2011) 1218:4517–24. doi: 10.1016/j.chroma.2011.05.019
34. Molina-Calle M, Medina VSD, Calderon-Santiago M, Priego-Capote F, Castro MDLD. Untargeted analysis to monitor metabolic changes of garlic along heat treatment by LC-QTOF MS/MS. *Electrophoresis.* (2017) 38:2349–60. doi: 10.1002/elps.201700062
35. Yoshimura Y, Iijima T, Watanabe T, Nakazawa H. Antioxidative effect of Maillard reaction products using glucose-glycine model system. *J Agric Food Chem.* (1997) 45:4106–9. doi: 10.1021/jf9609845
36. Hwang IG, Kim HY, Woo KS, Lee J, Jeong HS. Biological activities of Maillard reaction products (MRPs) in a sugar-amino acid model system. *Food Chem.* (2011) 126:221–7. doi: 10.1016/j.foodchem.2010.10.103
37. Wang H, Yang J, Yang M, Ji W. Antioxidant activity of Maillard reaction products from a Yak casein-glucose model system. *Int Dairy J.* (2018) 91:55–63. doi: 10.1016/j.idairyj.2018.12.010
38. Ji X, Peng B, Ding H, Cui B, Nie H, Yan Y. Purification, structure and biological activity of pumpkin (*Cucurbita moschata*) polysaccharides: a review. *Food Rev Int.* (2021). doi: 10.1080/87559129.2021.1904973. [Epub ahead of print].

Conflict of Interest: The authors declare that the research was conducted in the absence of any commercial or financial relationships that could be construed as a potential conflict of interest.

Publisher's Note: All claims expressed in this article are solely those of the authors and do not necessarily represent those of their affiliated organizations, or those of the publisher, the editors and the reviewers. Any product that may be evaluated in this article, or claim that may be made by its manufacturer, is not guaranteed or endorsed by the publisher.

frontiers in Nutrition

ORIGINAL RESEARCH
published: 09 February 2022
doi: 10.3389/fnut.2022.833906

Fermentation and Storage Characteristics of "Fuji" Apple Juice Using *Lactobacillus acidophilus*, *Lactobacillus casei* and *Lactobacillus plantarum*: Microbial Growth, Metabolism of Bioactives and *in vitro* Bioactivities

Jie Yang[1,2], *Yue Sun*[1,2], *Tengqi Gao*[1,2], *Yue Wu*[3], *Hao Sun*[1,2], *Qingzheng Zhu*[1,2], *Chunsheng Liu*[1,2], *Chuang Zhou*[4], *Yongbin Han*[5] *and Yang Tao*[5]*

[1] *Jiangsu Key Laboratory of Marine Bioresources and Environment/Jiangsu Key Laboratory of Marine Biotechnology, Jiangsu Ocean University, Lianyungang, China,* [2] *Co-Innovation Center of Jiangsu Marine Bio-industry Technology, Jiangsu Ocean University, Lianyungang, China,* [3] *Sonochemistry Group, School of Chemistry, The University of Melbourne, Parkville, VIC, Australia,* [4] *Department of Animal Husbandry and Veterinary Medicine, Jiangsu Vocational College of Agriculture and Forestry, Jurong, China,* [5] *College of Food Science and Technology, Whole Grain Food Engineering Research Center, Nanjing Agricultural University, Nanjing, China*

OPEN ACCESS

Edited by:
Yu Xiao,
Hunan Agricultural University, China

Reviewed by:
Hossein Kiani,
University of Tehran, Iran
Kit Wayne Chew,
Xiamen University Malaysia, Malaysia

***Correspondence:**
Yang Tao
yang.tao@njau.edu.cn

Specialty section:
This article was submitted to Food Chemistry, a section of the journal Frontiers in Nutrition

Received: *12 December 2021*
Accepted: *17 January 2022*
Published: *09 February 2022*

Citation:
Yang J, Sun Y, Gao T, Wu Y, Sun H, Zhu Q, Liu C, Zhou C, Han Y and Tao Y (2022) Fermentation and Storage Characteristics of "Fuji" Apple Juice Using Lactobacillus acidophilus, Lactobacillus casei and Lactobacillus plantarum: Microbial Growth, Metabolism of Bioactives and in vitro Bioactivities. Front. Nutr. 9:833906. doi: 10.3389/fnut.2022.833906

Fruit juices have been widely used as the substrates for probiotic delivery in non-dairy products. In this study, three lactic acid bacteria (LAB) strains, including *Lactobacillus acidophilus*, *Lactobacillus casei* and *Lactobacillus plantarum,* were selected to ferment apple juice. During 72-h of fermentation, these LAB strains grew well in the apple juice with significant increases in viable cell counts (from 7.5 log CFU/mL to 8.3 log CFU/mL) and lactic acid content (from 0 to 4.2 g/L), and a reduction of pH value (from 5.5 to around 3.8). In addition, the antioxidant and antibacterial capacities of fermented apple juice *in vitro* were significantly improved through the phenolic and organic acid metabolisms. After storage at 4°C for 30 days, the total amino acid content of fermented apple juice was significantly increased, although the viable cell counts and total phenolic content were decreased ($p < 0.05$). Furthermore, the stored fermented apple juices still possessed antibacterial and *in vitro* antioxidant activities. Overall, all the selected LAB strains could be suitable for apple juice fermentation and can effectively improve their biological activities.

Keywords: lactic acid bacteria, apple juice, fermentation, physicochemical properties, bioactivities

INTRODUCTION

Probiotics are living microorganisms and potential functional foods, which have a positive impact on the human body by improving the microbial balance in the human intestine (1). Lactic acid bacteria (LAB) are important probiotics, and they are often used in yogurt and other dairy products. In recent years, the researches on fermented fruit and vegetable juices by lactic acid bacteria have gradually emerged. Meanwhile, the related products in the Chinese market are still limited, which

could not meet the consumer's demand. After the fermentation of fruit and vegetable juices by LAB strains, their nutritional and functional values are improved, which not only gives fruit and vegetable juice a special taste and taste, but also extends their shelf life (2, 3).

Apple is one of the most consumed fruits in the world, especially in "fuji" and related varieties which are widely accepted by consumers because of its excellent sensory properties (4, 5). They are characterized by high sugar content and low acidity (6). With the improvement of living standards, consumers are more concerned about the freshness, originality, physicochemical properties, and nutritional values of food products including fruit juice (7). Apple juice has some positive impacts on human health due to its rich contents of polyphenols such as isoflavones, flavonoids and phenolic acids (8). Although fruit juices are rich in minerals, sugars and vitamins, they contain low amounts of free peptides and amino acids, which is adverse to the growth and metabolism of human intestinal microorganisms (9). To address this problem, LAB strains are widely used for the fermentation of fruit and vegetable substrates due to their excellent tolerability in acidic environments. In addition, the nutrients of apples are retained due to the fermentation by probiotics, resulting in unique flavor and efficacy (8). In the literature, Chen et al. (10) studied the effect of four LAB strains on the flavors of fermented apple juice. The results showed that the total acid concentration and microbial activity under the fermentation of lactic acid bacteria increased markedly, and new volatile compounds with important flavors were produced. Kwaw et al. (11) reported that the effects of lactic acid bacteria on the color, phenolics (such as anthocyanins) and antioxidant activity of mulberry juice. The results found that lactic acid fermentation can enrich the bioactive components in mulberry juice. Similarly, Vivek et al. (12) found an increase trend of antioxidant activity, total phenolic and anthocyanin contents in "Sohiong" juice fermented by *L. plantarum*, confirming the suitability and feasibility of developing a non-dairy based probiotic drinks from Sohiong juice. Kaprasob et al. (13) also reported an increase in phenolic compounds, vitamin C and other antioxidants in cashew apple juices fermented by *L. casei, L. plantarum* and *L. acidophilus*. In theory, by using the selected three lactic acid bacteria, apple juice can be processed into value-added products. However, there is still limited researches about the effect of LAB on the fermentation and preservation of apple juice.

In this study, three potential probiotics, *L. plantarum*, *L. acidophilus* and *L. casei*, were selected to ferment apple juice. The changes of organic acids, sugars, free amino acids, and phenolics during fermentation and storage (4°C for 30 days) were evaluated. Finally, this study can provide the basic knowledge of the biotransformation of relevant components in apples by LAB fermentation, and guide the development of fermented apple juice products with high nutritional value and safety.

MATERIALS AND METHODS

Materials and Chemicals

Fresh apple was provided by Xuanwu Fruit Store, Nanjing, Jiangsu Province. Ethanol, acetonitrile, Folin-Ciocalteu reagent, organic acid standards (oxalate acid, pyruvic acid, malic acid, citric acid, succinic acid and lactic acid), phenolic acid standards (gallic acid, protocatechuic acid, catechin, procyanidin B_2, chlorogenic acid, hydroxybenzoic acid, caffeic acid, ferulic acid, rutin and quercetin), amino acid standards (Asp, Thr, Ser, Glu, Gly, Ala, Cys, Val, Met, Ile, Leu, Tyr, Phe, Lys, His, Arg, Pro) and sugar standards (fructose, sorbitol, glucose and sucrose) were all bought from Yuanye Biotechnology Co., Ltd (Shanghai, China).

Lactic Acid Bacteria Strains and Inoculum Preparation

Three commercial LAB strains *L. acidophilus* BNCC 185342, *L. casei* ATCC 393, *L. plantarum* BNCC 337796 were provided by Beijing Beina Chuanglian Biotechnology Research Institute (Beijing, China). All stains were activated in MRS broth (Bo Microbiology Technology Co., Ltd. Shanghai) at 37°C for 24 h to achieve a final concentration at 9.0 log CFU/mL.

Preparation of Apple Juice and Fermentation

Fresh apples ("Red Fuji" apple from Xuanwu Fruit Store, Nanjing, Jiangsu Province) were washed, peeled, nucleated, and cut into small pieces. Next, 0.15% (w/w) ascorbic acid (also known as vitamin C) was added during crushing. Then, apple slurries were filtered through four layers of gauze and centrifuged at 6,000 × *g* for 20 min. The supernatant was collected, and the soluble solid content and pH were adjusted to 13% using glucose and 6.5 using 1N NaOH, separately.

Apple juice was sterilized at 110°C for 10 min before fermentation. After cooling to room temperature, 8 mL of inoculum containing various LAB strains were added into 400 mL of apple juice, respectively. The initial viable bacterial count in apple juice was about 7.5 log CFU/mL. Next, apple juice with different LAB strains were placed into an incubator to ferment for 72 h at 37°C. After that, fermented juices were immediately stored at 4°C for 30 days. Unfermented apple juice was selected as a control group. Samples were collected for analysis during fermentation at 0, 12, 24, 48, 72 h and storage at 10, 20, 30 d. Before the physicochemical analysis, the collected samples were centrifuged at 4°C and 12,000 × *g* for 15 min.

Determination of Viable Cell and pH

The number of viable bacteria was determined by the plate counting method. Specifically, 1 mL fermented juices were diluted serially with sterile saline to 10^4-10^{10} dilutions. Inoculation of 0.1 mL of the diluted samples were plated on the MRS agar. The plates were incubated at 37°C for 36–48 h. Plates containing 30–300 colonies were counted and recorded as log CFU/mL (14). The pH of fermented apple juice was monitored by a digital pH meter (PHS-3C, Shanghai INESA Scientific Instrument Co., Ltd, Shanghai, China).

Determination of the Browning Index

The browning index of unfermented and fermented apple juice samples were measured referring to Tiwari et al. (15). 3 mL of centrifuged apple juice was thoroughly mixed with 3 mL of anhydrous ethanol, and then the mixture was centrifuged at 4°C

and 12,000 × *g* for 15 min. The supernatant was collected, and its absorbance was measured at 420 nm in a spectrophotometer (LabTech UV9100, USA).

Determination of Organic Acid Contents

Organic acids were determined by a LC-2010A system (Shimadzu Company, Japan) according to the previously reported method (16). The mobile phase is KH_2PO_4 (0.08 mol/L, pH 2.9). An Agilent TC-C18 chromatographic column (250 × 4.6 mm i.d., 5 mm) was applied for the separation of organic acids and it was maintained at 30°C. The injection volumes of the samples or standards were 20 μL, and the flow rate was 0.7 mL/min. Organic acids were detected using an ultraviolet detector (DAD) at 210 nm. The content of each organic acid was expressed as mg/L.

Determination of Sugar Contents

The sugars were determined by a HPLC-ELSD system (Agilent Technologies, USA., Alltech-ELSD 3300 evaporative light scattering detector: Otai Technology, USA) coupled with a Grace Prevail Carbohydrate ES column (250 × 4.6 mm i.d., 5 mm) according to the previously reported method (17). The mobile phase consisted of 25% (v/v) H_2O and 75% (v/v) acetonitrile. The solvent flow rate was 1.0 mL/min and the injection volume was 10 μL. The column temperature was maintained at 30°C. The drift tube temperature of the ELSD detector was 80°C, the flow rate of nitrogen gas was 1.5 L/min. The content of each sugar was expressed as mg/L.

Determination of Free Amino Acids Contents

The apple juice collected at different time intervals was filtered through 0.45 μm membranes. The amino acids were analyzed by a L-8900 automatic amino acid analyzer (Hitachi Technology Company, Japan). The content of each free amino acid was expressed as mg/L.

Determination of the Contents of Total Phenolics and Individual Phenolic Compounds

The method for the determination of total phenols was the Folin-Ciocalteu method (18). Specifically, 0.2 mL of diluted apple juice sample was mixed with 1.5 mL of 7.5% (w/v) Na_2CO_3 and 1.5 mL of Folin-Ciocalteu (10-fold dilution). After standing at 25°C in darkness for 40 min, and the absorbance was measured at 765 nm. The total phenolic content was standardized against gallic acid and expressed as gallic acid equivalents/L.

The phenolic substances were analyzed using a Shimadzu-HPLC system coupled with an Inertsil ODS-3 column (250 × 4.6 mm i.d., 5 mm) (LC-2010A, Shimadzu Corporation, Japan) according to the previously reported method (19, 20). The column was maintained at 25°C, and the injection volume was 20 μL. The binary mobile phase consisted of (A) glacial acetic acid aqueous (1%, v/v) and (B) glacial acetic acid methanol (1%, v/v). The samples were eluted at a flow rate of 0.6 mL/min with the following gradients: 0–10 min, 10–26% B; 10–25 min, 10–26% B; 25–45 min, 40–65% B; 45–55 min, 65–95% B; 55–58 min, 95–100% B; 58–65 min, 100% B. Flavonoids and phenolic acids in samples were detected at 350 and 280 nm respectively. The results were expressed in mg/L.

Determination of Antioxidant Activities *in vitro*

The free radical scavenging activity of apple juice was assessed by the $ABTS^{\cdot+}$ method, as described in previous paper (21). The calibration curve was made using Trolox as the standard, and the results were expressed as mmol Trolox/L. Ferric reducing antioxidant power (FRAP) was determined according to our previously reported method (21). $FeSO_4$ was employed as the standard to obtain the calibration curve, and the results were expressed as mmol Fe^{2+}/L.

Statistical Analysis

The experiments were repeated three times. The test data were analyzed by Excel, Origin 8.0, Minitab, and SPSS 20.0 software. Significance was defined at $p < 0.05$, and Duncan's test was used.

RESULTS AND DISCUSSION

Bacterial Growth and Change in pH During LAB Fermentation and Storage

Changes in viable cell counts and pH value of apple juice fermented with *L. acidophilus*, *L. casei* and *L. plantarum* during 72-h fermentation and the subsequent 30-day storage are shown in **Figure 1**, which can reflect the growth status of these strains. As can be seen from **Figure 1A**, *L. acidophilus*, *L. casei* and *L. plantarum* all grew well in the apple juice, and there was no significant difference in their viable cell count during the fermentation process ($p \geq 0.05$). At the latter period of fermentation (from 48 to 72 h), the viable cell counts of *L. acidophilus*, *L. casei* and *L. plantarum* were still above 8.3 log CFU/mL. This result demonstrates that the growth of *L. acidophilus*, *L. casei* and *L. plantarum* metabolized vigorously. Meanwhile, this result also confirmed that apple juice can be a suitable substrate for the fermentation of the selected strains. Additionally, the viable cell counts of three LAB strains were maintained above 8.0 log CFU/mL in apple juice during the first 20 days of storage at 4°C. However, during the storage of 20–30 days, the viable cell counts of *L. casei* decreased rapidly to 5.4 ± 0.04 log CFU/mL, following *L. acidophilus* (5.6 ± 0.13 log CFU/mL) and *L. plantarum* (5.7 ± 0.04 log CFU/mL). These results are in line with the findings reported by Yoon et al. (22), which states that *L. casei* and *L. plantarum* were able to grow in cabbage juice without supplementing nutrients. With the increase of storage time, the substances that can be used by LAB in the apple juice were dramatically reduced with a marked accumulation of the metabolites (13). Eventually, the growth of the LAB reached the death phase, when the viable cell counts of LAB rapidly decreased.

LAB strains can metabolize sugar and produce organic acids, thus changing the pH value of apple juice during fermentation and storage (23). The change in pH values of apple juice fermented with *L. acidophilus*, *L. casei* and *L. plantarum* is shown

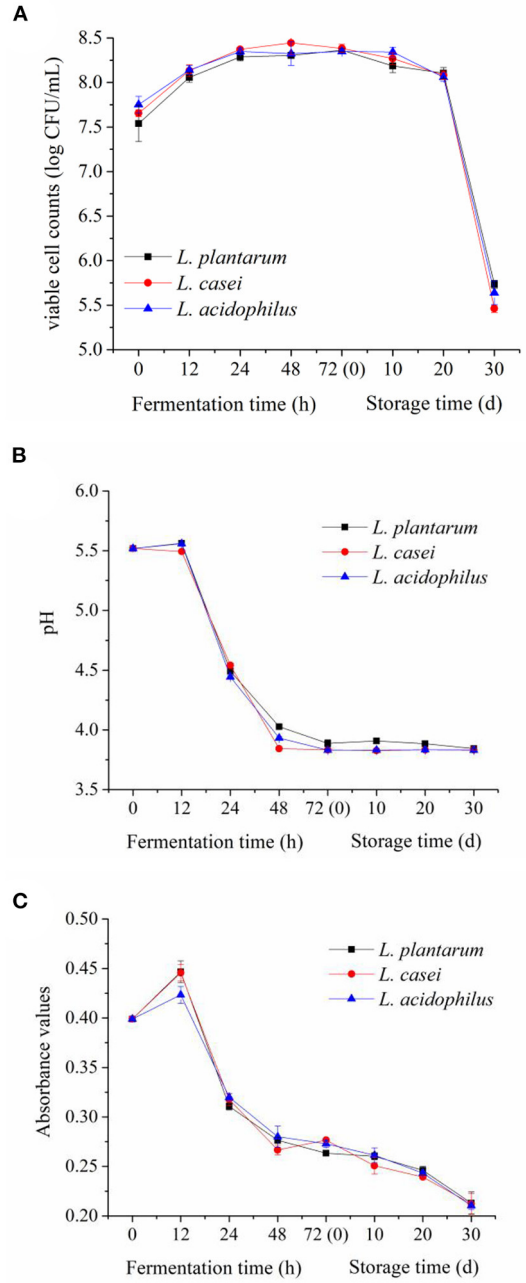

FIGURE 1 | Evolutions of viable cell counts **(A)**, pH value **(B)** and browning index **(C)** in apple juices fermented by the three LAB strains during fermentation and refrigerated storage (4°C, 30 days).

in **Figure 1B**. The pH values of apple juice fermented by the three LAB strains had a minor change in the first 12 h of fermentation, and then experienced a rapid drop between 12 and 72 h (from 5.5∼4.0). To be specific, after 48-h fermentation, the maximum reduction of pH value was obtained in apple juice fermented with *L. casei* (3.8 ± 0.02), following that fermented with *L. acidophilus* (3.9 ± 0.01) and *L. plantarum* (4.0 ± 0.02). In the storage period, the pH value remained stable, and there was no significant difference among the juices fermented by the three different strains ($p \geq 0.05$). The variations of the pH values were consistent with the report of Chen et al. (10), who studied the effects of four LAB strains on the flavor characteristics of fermented apple juice.

Change in Browning Index During LAB Fermentation and Storage

Color is an important quality indicator for apple juice, and the fermentation of LAB in fruit and vegetable substrates can change their color (11). The change in color of apple juice fermented with *L. acidophilus*, *L. casei* and *L. plantarum* during the 72-h fermentation and the subsequent 30-day storage are shown in **Figure 1C**. The Browning Index value of apple juice increased slightly during the first 12 h of fermentation, and then decreased rapidly during the fermentation between 12 and 24 h, which was consistent with the variation of pH. The Browning Index value showed a downward trend during the period of 24-h fermentation and 30-day storage at 4°C. This may be due to the metabolism of phenolics in apple juice caused by LAB fermentation and the decrease of pH in apple juice, which inhibited the color change caused by Maillard reaction (24).

Changes in Organic Acids and Sugars Contents During LAB Fermentation and Storage

The changes in organic aicds and sugars in apple juice fermented with *L. acidophilus*, *L. casei* and *L. plantarum* during the 72-h fermentation and the subsequent 30-day storage are summarized in **Supplementary Table 1**. Organic acids are important products derived from LAB metabolism, which can improve the flavor and palatability of fruit juices (25). Meanwhile, organic acids can increase the acidity of the juice and inhibit the growth of spoilage and pathogen microorganisms. Therefore, organic acids have a profound influence on the storage characteristics and flavor of fermented fruit and vegetable juices (25). As shown in **Supplementary Table 1**, six organic acids including oxalic acid, pyruvic acid, malic acid, lactic acid, citric acid, and succinic acid can be identified in the fermented apple juice with *L. acidophilus*, *L. casei* and *L. plantarum*.

Lactic acid content was increased significantly after fermentation owing to the biosynthesis pathway of LAB metabolism, and the highest concentration was 4,191.6 ± 31.6 mg/L by *L. casei*. Malic acid is the main source of sour flavor in unfermented apple juice. Before fermentation, it had the highest content of 1,166.5 ± 14.7 mg/L in apple juice (26, 27). Malic acid can be bio-transferred to lactic acid under the catalysis of the malolactic enzyme produced by LAB, thus weakening the acidity and providing a mildly sour taste of apple juice (28). The existence of this metabolic pathway can be confirmed by the similarity between the increasing amount of lactic acid content and the decreasing amount of malic acid content.

Citric acid content (730.7 ± 13.1 mg/L in unfermented juice) was decreased after lactic acid fermentation as a result of its decomposition into various products, such as diacetyl, lactic acid, and acetic acid (29). Pyruvate is an intermediate product of the

basic metabolic pathways of organisms such as tricarboxylic acid cycle, glycolysis, and other metabolic pathways. The pyruvic acid content experienced an increasing trend and reached a maximum concentration of 130.2 ± 1.4 mg/L after fermentation by *L. plantarum* for 24 h, and then followed a decreasing trend. It has been confirmed that pyruvic acid can be produced from glucose through glycolysis, which may be related to the rising phase of pyruvic acid. In addition, pyruvic acid can also be used to form the amino acid alanine and converted into lactic acid or ethanol via fermentation, which may be associated with its decline at the end of fermentation (30). The trends in the content of oxalic acid and succinic acid in fermented apple juice were similar to that of pyruvic acid. In addition, the content of total organic acids increased during fermentation and then remained stable during the storage period, which may be due to the inhibition of the metabolism of lactic acid bacteria at low temperatures.

Before fermentation, fructose is the major sugar (52.0 ± 2.3 mg/L) in apple juice. During the fermentation process, the content of glucose in all fermented samples experienced a continuous decrease from 17.7 ± 0.8 mg/L to about 11.7 ± 0.1 mg/L, although there was no significant difference in the content of glucose among the apple juice fermented with different microbial strains ($p \geq 0.05$). This trend can be explained by the reason that the fermentation of the selected LAB strains is facultative heterologous fermentation, and glucose and fructose are converted into lactic acid through the Embden-Meyerhof pathway. The content of sucrose in apple juice fermented with *L. acidophilus*, *L. casei* and *L. plantarum* was reduced continuously, which can be attributed to the hydrolysis of sucrose by galactosidase in LAB strains. This trend is consistent with the results of Wang et al. (31) who used LAB strains to ferment soy milk. The contents of glucose, fructose and sorbitol were also increased significantly ($P < 0.05$) during storage. This may be due to the inhibition of the respiration of LAB strains by monosaccharides in an environment of low temperature and high acidity. Meanwhile, the degradation of sucrose by galactosidase may also take place in LAB strains (32–34).

Change of Free Amino Acids During LAB Fermentation and Storage

Amino acids are important flavoring compounds and their compositions have a profound influence on the evaluation of sensory properties of apple juice (35). For LAB fermentation, amino acids may first undergo decarboxylation, deamination, transamination, and desulfurization reactions, followed by amine conversion. Eventually, the aldehydes generated from amino acid metabolism are oxidized or reduced to the corresponding carboxylic acids and alcohols (36). Seventeen free amino acids could be detected in the apple juice samples fermented by the three LAB strains. Among them, Thr possessed the highest amount in unfermented samples (695.3 ± 13.2 mg/L). To clarify the effect of LAB strains on the metabolism of amino acids, two-dimensional analysis of the principal component analysis (PCA) was used to analyze the profile of free amino acids during 72-h fermentation. Meanwhile, the original data about the content of each amino acid are prepared in **Table 1**. Two principal components, PC1 and PC2, were extracted that accounted for 67.7% and 19.7% of the total variance in seventeen variable systems, respectively. The unfermented sample was distributed on the negative side of PC1. During 72-h fermentation, a significant shift of the distribution could be observed among fermented apple juice (**Figure 2A**). This phenomenon indicates that the profile of amino acids in apple juice changed obviously during 72-h fermentation. For example, the PC1 value of unfermented apple juice was−7.31. After fermentation for 72 h, the PC1 values for apple juice fermented with *L. acidophilus*, *L. plantarum*, and *L. casei* increased to 2.42, 2.49, and 2.47. According to the loading plot (**Figure 2B**), Leu, Ala, Val, His, Ile, Met, Thr and Phe distributed on the negative side of PC1, and Tyr, Lys, Pro, Arg, Glu, Asp, Cys and Gly distributed on the positive side. These amino acids placed to the right such as Pro, Cys and Gly in the loading plot were close and positively correlated. However, amino acids on the negative side were negatively correlated. In addition, some amino acids including Leu, Val, Ala, His, Ile, Met, Thr, Phe, Pro, Cys, Gly and Asp distributed far from the origin of the first PC. Therefore, LAB fermentation of apple juice may have a higher influence on the content of these amino acids. Based on the locations of samples and the attributes, it can be found that the contents of Leu, Ala, Val, His, Ile, Met, Thr and Phe in apple juice were generally decreased with fermentation. In contrast, the lactic acid fermentation led to the increment of the amounts of Tyr, Lys, Pro, Arg, Glu, Asp, Cys and Gly. Besides, it can be observed that the fermented apple juice by the three microbial strains at the same stage had similar PC1 values, indicating that PC2 is mainly responsible for the discrimination of the samples fermented by different strains. For example, after 72-h fermentation, the contents of Asp, Cys and Gly in apple juice fermented with *L. acidophilus*, *L. plantarum*, and *L. casei* were 979.4 ± 1.0 mg/L, 972.9 ± 1.0 mg/L, 969.3 ± 16.8 mg/L; 6.2 ± 0 mg/L, 6.2 ± 0.2 mg/L, 5.8 ± 0.1 mg/L and 80.3 ± 1.2 mg/L, 86.9 ± 1.7 mg/L, 85.3 ± 1.2 mg/L, respectively. And the PC2 values of Asp, Cys and Gly were−0.17, 0.17, and 0.10 (**Figure 2B**). This result implies that different strains have different capacities to metabolize some amino acids such as Asp, Cys and Gly and others.

The contents of Asp and Gly were increased significantly during fermentation ($P < 0.05$), which may improve the flavor of fermented apple juice (37). LAB can metabolize threonine to pyruvate and ammonia through threonine dehydratase, resulting in a significant decrease in threonine content ($P < 0.05$) during the first 24-h fermentation. It has been reported that lactic acid bacteria can alleviate environmental acid stress by increasing the expression of enzymes consuming cytoplasm (38). Ammonia produced by amino acid metabolism can accept protons and promote acid-base balance in microbial cells (29), which is confirmed by the increase in ammonia contents from 3.5 ± 0.1 mg/L to 121.0 ± 0.2 mg/L, 121.0 ± 2.4 mg/L, 120.2 ± 0.01 mg/L during fermented by *L. acidophilus*, *L. plantarum*, and *L. casei*, respectively. Moreover, the contents of Phe, Val, Ile and Met also showed a downward trend throughout fermentation, which may be related to the decarboxylase (4) and transaminase (39, 40) produced by LAB. Decarboxylase decomposes free amino acids to produce primary amine and release carbon dioxide, while

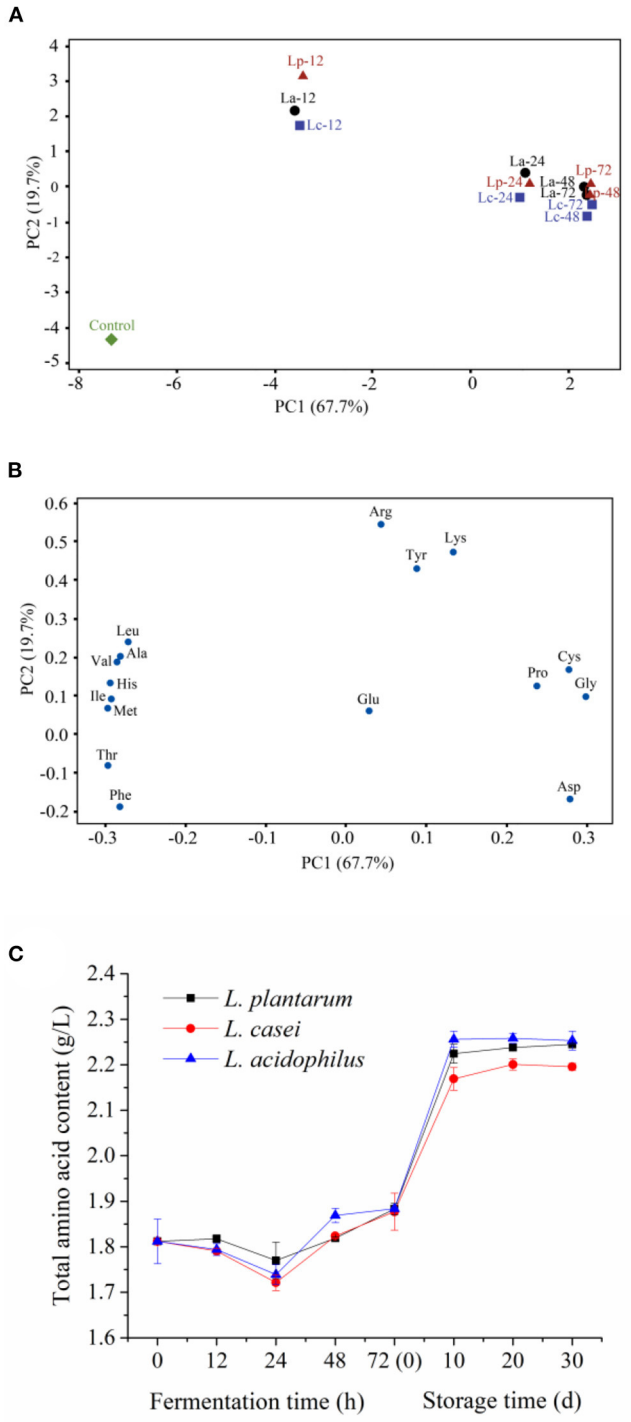

FIGURE 2 | Principal component analysis of free amino acid profile in apple juice during fermentation by the three LAB strains [**(A)**, score plot; **(B)**, loading plot] and changes in total free amino acids **(C)**. "Control," Unfermented apple juice; "La," Apple juice fermented by *L. acidophilus*; "Lp", Apple juice fermented by *L. plantarum*; "Lc", Apple juice fermented by *L. casei*. In **(A)**, the number followed with the name of strain indicated the time of fermentation.

transaminases can catalyze the inter-conversion of amino acids into alpha-ketonic acid (38) and the transamination reaction between branched-chain amino acids (i.e., leucine) and alpha-keto-beta-methyl valerate/alpha-keto isopropionate (41).

During storage, almost all the mentioned amino acids were increased significantly during the first 10-day storage ($P < 0.05$). To be specific, the contents of Asp, Phe and Gly in apple juice fermented by *L. plantarum* increased from about 972.9 ± 1.0 mg/L, 7.2 ± 0.1 mg/L and 86.9 ± 1.7 mg/L to approximately 1496.4 ± 20.2 mg/L, 11.7 ± 0.1 mg/L and 106.8 ± 1.6 mg/L, respectively. Meanwhile, the contents of Met, Ile, Leu had no obvious changes in the early period of storage. In the contrast, the content of Thr was decreased from 370.6 mg/L to below 1 mg/L. In the subsequent storage period, there was no significant change in the content of all the amino acids ($P \geq 0.05$).

Besides, the content of total amino acids in apple juice fermented by three LAB strains was studied. The results are shown in **Figure 2C**. The total amino acid content in fermented apple juice was decreased slightly in the first 24 h of fermentation, and then increased gradually. During the first 10 days of storage at 4°C, the content of total amino acids in apple juice fermented by *L. acidophilus*, *L. plantarum*, and *L. casei* were increased from 1.88 ± 0.002 g/L, 1.88 ± 0.01, and 1.88 ± 0.04 g/L to 2.26 ± 0.02 g/L, 2.22 ± 0.02 g/L, and 2.27 ± 0.03 g/L, respectively. Then maintained at this level until the end of storage.

Evolution of Phenolic Profile During LAB Fermentation and Storage

Gallic acid, protocatechuic acid, catechin, proanthocyanidin B_2, chlorogenic acid, *p*-hydroxybenzoic acid, coffee acid, syringic acid, phloxic acid, *p*-coumaric acid, ferulic acid, cinnamaldehyde, *p*-vinyl guaiacol, rutin and quercitrin can be tentatively identified in the fermented apple juice. Gallic acid, protocatechuic acid, catechin, proanthocyanidin B_2, caffeic acid, rutin ferulate and quercetin were the main phenolic substances in fermented apple juice, and their contents were summarized in **Table 2**. After 48-h fermentation by *L. acidophilus*, *L. plantarum*, and *L. casei*, the content of ferulic acid was declined by 11.1, 18.5, and 11.1%, and the caffeic acid content was reduced by 41.7, 50, and 50%, respectively. These results indicated that the selected LAB strains were able to biotransform ferulic acid and caffeic acid. This phenomenon can be explained by two possible pathways. One is that phenolic acid decarboxylases synthesized by LAB can catalyze the non-oxidative decarboxylation of phenolic acids to generate their corresponding *p*-vinyl derivatives (42). Another reason is that ferulic acid and caffeic acid could be transformed to dihydrocaffeic acid and dihydroferulic acids through the side chain hydrogenation (43–46). The ferulic acid content in apple juice fermented by *L. plantarum* was decreased faster than those fermented by *L. acidophilus* and *L. casei* ($P < 0.05$), guessing that *L. plantarum* was more capable to synthesize the enzymes involved in the metabolism of ferulic acid.

The content of ferulic acid was significantly decreased from around 4.7 mg/L to about 0.8 mg/L ($P < 0.05$) after storage for

TABLE 1 | Changes in the contents of free amino acids (mg/L) of apple juice during lactic acid fermentation and the subsequent refrigerated storage period (4°C, 30 days).

Amino acid	Strains	Time							
		Fermentation for 0 h	Fermentation for 12 h	Fermentation for 24 h	Fermentation for 48 h	Fermentation for 72 h (Storage for 0 d)	Storage for 10 d	Storage for 20 d	Storage for 30 d
Asp	*L. acidophilus*	678.8 ± 31.8^{Ad}	662.3 ± 1.9^{Bd}	834.4 ± 15.7^{Ac}	974.1 ± 14.2^{Ab}	979.4 ± 1.0^{Ab}	1,529.7 ± 12.5^{Aa}	1522.8 ± 1.6^{Aa}	1512 ± 4.5^{Aa}
	L. casei	678.8 ± 31.8^{Ad}	672.4 ± 7.3^{ABd}	835.3 ± 17^{Ac}	933.4 ± 5.7^{Bb}	969.3 ± 16.8^{Ab}	1,443 ± 20.9^{Ba}	1460.3 ± 6.2^{Ba}	1,458.2 ± 2.5^{Ca}
	L. plantarum	678.8 ± 31.8^{Ad}	676.6 ± 1.5^{Ad}	852.9 ± 33.6^{Ac}	926.7 ± 7.2^{Bb}	972.9 ± 1.0^{Ab}	1,496.4 ± 20.2^{ABa}	1492.7 ± 17.4^{ABa}	1,489.3 ± 9.8^{Ba}
Thr	*L. acidophilus*	695.3 ± 13.2^{Aa}	522.7 ± 2.7^{Ab}	404.3 ± 6.2^{Ac}	385.5 ± 1.8^{Ad}	373.9 ± 2.6^{Ad}	ND	ND	ND
	L. casei	695.3 ± 13.2^{Aa}	521.5 ± 4.6^{Ab}	400.2 ± 0.3^{Ac}	379.4 ± 2.3^{Ad}	371.4 ± 2.9^{Ad}	ND	ND	ND
	L. plantarum	695.3 ± 13.2^{Aa}	533.6 ± 8.2^{Ab}	412.9 ± 8.6^{Ac}	378.2 ± 5.3^{Ad}	370.6 ± 6.8^{Ad}	ND	ND	ND
Ser	*L. acidophilus*	ND	ND	ND	ND	ND	ND	ND	ND
	L. casei	ND	ND	ND	ND	ND	ND	ND	ND
	L. plantarum	ND	ND	ND	ND	ND	ND	ND	ND
Glu	*L. acidophilus*	200.9 ± 3.2^{Ad}	213.4 ± 2.5^{Ac}	184.6 ± 0.8^{Ae}	205.3 ± 1.5^{Bd}	218.4 ± 1.6^{Bb}	292.2 ± 3.1^{Aa}	294.7 ± 1.3^{Ba}	294.1 ± 0.4^{Ba}
	L. casei	200.9 ± 3.2^{Ad}	211.2 ± 1.1^{Ac}	185 ± 2.3^{Ae}	212 ± 0.6^{Ac}	227.7 ± 1.7^{Ab}	293.7 ± 6.1^{Aa}	300.5 ± 2.2^{Aa}	299.9 ± 2.4^{Aa}
	L. plantarum	200.9 ± 3.2^{Ad}	210.1 ± 1.8^{Ac}	189.6 ± 4.8^{Ae}	206.1 ± 2.8^{Bcd}	224.3 ± 0.5^{Ab}	298.9 ± 1.1^{Aa}	300.1 ± 0.5^{Aa}	301.1 ± 1.1^{Aa}
Gly	*L. acidophilus*	4 ± 0.1^{Af}	47 ± 0^{Be}	72.5 ± 0.9^{Bd}	77.8 ± 1.6^{Bc}	80.3 ± 1.2^{Bb}	100.2 ± 0.6^{Ba}	100.1 ± 1.3^{Ba}	101.3 ± 1.2^{Ba}
	L. casei	4 ± 0.1^{Ae}	46.9 ± 0.2^{Bd}	76.8 ± 1.8^{ABc}	83 ± 1.4^{Ab}	85.3 ± 1.2^{Ab}	104.9 ± 2^{ABa}	106.2 ± 1.9^{Aa}	106.5 ± 1.2^{Aa}
	L. plantarum	4 ± 0.1^{Ae}	48.2 ± 0.1^{Ad}	77.6 ± 1.7^{Ac}	84.8 ± 1.4^{Ab}	86.9 ± 1.7^{Ab}	106.8 ± 1.6^{Aa}	107.7 ± 1.7^{Aa}	108.9 ± 1.8^{Aa}
Ala	*L. acidophilus*	33.3 ± 0.1^{Ab}	37.8 ± 0.9^{Aa}	8.3 ± 0.8^{Ac}	1.9 ± 0.2^{Ad}	1.9 ± 0^{Ad}	ND	ND	ND
	L. casei	33.3 ± 0.1^{Ab}	36.8 ± 0.9^{Aa}	7.7 ± 0.4^{Ac}	1.9 ± 0^{Ad}	1.9 ± 0.2^{Ad}	ND	ND	ND
	L. plantarum	33.3 ± 0.1^{Ab}	39 ± 1.1^{Aa}	9.9 ± 1^{Ac}	2 ± 0.2^{Ad}	1.9 ± 0.1^{Ad}	ND	ND	ND
Cys	*L. acidophilus*	3.1 ± 0.1^{Ad}	5.1 ± 0^{Ac}	6.5 ± 0.3^{Aab}	6.5 ± 0^{Aa}	6.2 ± 0^{Ab}	ND	ND	ND
	L. casei	3.1 ± 0.1^{Ad}	5 ± 0^{Ac}	6 ± 0.1^{Aa}	5.9 ± 0^{Bab}	5.8 ± 0.1^{Bb}	ND	ND	ND
	L. plantarum	3.1 ± 0.1^{Ac}	5.2 ± 0^{Ab}	6.4 ± 0.4^{Aa}	6.4 ± 0.2^{Aa}	6.2 ± 0.2^{Aa}	ND	ND	ND
Val	*L. acidophilus*	31.5 ± 0.1^{Ab}	35.3 ± 0.3^{Aa}	8.7 ± 0.9^{Ac}	2.1 ± 0.2^{Ad}	2.7 ± 0.2^{Ad}	8.4 ± 0.4^{Ac}	6.9 ± 3.5^{Ac}	8.2 ± 0.7^{Ac}
	L. casei	31.5 ± 0.1^{Ab}	34.2 ± 0.4^{Aa}	6 ± 0.3^{Bd}	1.5 ± 0.1^{Be}	2.2 ± 0.2^{Ae}	7.5 ± 0.4^{Ac}	8 ± 0.4^{Ac}	7.7 ± 0.7^{Ac}
	L. plantarum	31.5 ± 0.1^{Ab}	34.8 ± 0.5^{Aa}	7.7 ± 0.8^{ABc}	1.7 ± 0^{Be}	2.3 ± 0.2^{Ae}	4.1 ± 0.3^{Bde}	6.3 ± 3.4^{Acd}	8.3 ± 0.5^{Ac}
Met	*L. acidophilus*	10.4 ± 0.5^{Aa}	8 ± 0^{Aab}	2.9 ± 1^{Abc}	1.1 ± 0.5^{Ac}	1.2 ± 0.3^{ABc}	4.3 ± 1.1^{Abc}	4.7 ± 1.3^{Abc}	11.4 ± 6.4^{Aa}
	L. casei	10.4 ± 0.5^{Aab}	7.7 ± 0^{Bb}	0.9 ± 0.5^{Ac}	0.6 ± 0^{Ac}	0.9 ± 0^{Bc}	9.7 ± 3.8^{Aab}	13 ± 1.1^{Aa}	10.3 ± 5^{Aab}
	L. plantarum	10.4 ± 0.5^{Aab}	7.9 ± 0.2^{ABabc}	1.3 ± 0^{Ac}	1.1 ± 0.5^{Ac}	1.5 ± 0^{Ac}	3.5 ± 0.1^{Abc}	9.6 ± 8.8^{Aab}	13.8 ± 2.2^{Aa}
Ile	*L. acidophilus*	59.6 ± 1.6^{Aa}	49.1 ± 0.5^{Ab}	7.4 ± 0.3^{Ac}	1.4 ± 0.1^{Ad}	1.8 ± 0.2^{Ad}	2.4 ± 0.6^{Ad}	3.9 ± 3.1^{Acd}	4 ± 2.6^{Acd}
	L. casei	59.6 ± 1.6^{Aa}	46.9 ± 0.6^{Ab}	3.9 ± 0.2^{Bc}	0.7 ± 0.1^{Bd}	1.2 ± 0.1^{Ad}	0.9 ± 0.2^{Bd}	1.6 ± 1^{Ad}	1.8 ± 0.6^{Ad}
	L. plantarum	59.6 ± 1.6^{Aa}	48.4 ± 1.1^{Ab}	5.9 ± 0.9^{Ac}	0.9 ± 0.3^{ABd}	1.5 ± 0.3^{Ad}	1.3 ± 0.3^{ABd}	3.4 ± 3.2^{Acd}	3.4 ± 3.2^{Acd}
Leu	*L. acidophilus*	16.7 ± 0.3^{Ab}	22.6 ± 0.4^{Aa}	4.1 ± 0.1^{Acd}	1.8 ± 0.3^{Ad}	2.6 ± 0.3^{Ad}	3.9 ± 0.4^{Acd}	7.1 ± 2.8^{Ac}	6.5 ± 3.1^{Ac}
	L. casei	16.7 ± 0.3^{Ab}	21.8 ± 0.5^{Aa}	3.1 ± 0.2^{Bc}	0 ± 0^{Bf}	1.2 ± 0.6^{Ae}	2.2 ± 0.5^{Ad}	2.2 ± 0.5^{Ad}	2.4 ± 0.1^{Acd}
	L. plantarum	16.7 ± 0.3^{Ab}	22.4 ± 0.2^{Aa}	3.9 ± 0.3^{Acde}	1.4 ± 0.5^{Ae}	2.1 ± 0.6^{Ade}	3.4 ± 0.7^{Acde}	5.8 ± 4.1^{Acd}	6.7 ± 2.9^{Ac}
Tyr	*L. acidophilus*	ND	3.2 ± 0.1^{Aa}	3.5 ± 0.2^{Aa}	3.9 ± 0.1^{Aa}	4 ± 0^{Aa}	ND	3.6 ± 0.6^{Aa}	2 ± 2.8^{Aab}
	L. casei	ND	3 ± 0^{Ad}	3.7 ± 0.1^{Ab}	3.4 ± 0.1^{Bc}	4.1 ± 0.2^{Aa}	ND	ND	ND
	L. plantarum	ND	7.9 ± 7^{Aa}	3.3 ± 0^{Aab}	3.9 ± 0.1^{Aab}	3.9 ± 0^{Aab}	ND	2 ± 2.9^{Aab}	3.7 ± 0.4^{Aab}
Phe	*L. acidophilus*	12.9 ± 0.1^{Aa}	8.9 ± 0.3^{Ac}	7.1 ± 0^{Ad}	7.1 ± 0.1^{Ad}	7.2 ± 0.1^{Ad}	12 ± 0.3^{Ab}	12.1 ± 0.1^{Ab}	11.8 ± 0^{Bb}
	L. casei	12.9 ± 0.1^{Aa}	8.9 ± 0.3^{Ac}	7.2 ± 0.1^{Ad}	6.8 ± 0.1^{Be}	7.1 ± 0.2^{Ade}	11.7 ± 0.1^{Ab}	11.8 ± 0.1^{ABb}	11.9 ± 0^{Ab}
	L. plantarum	12.9 ± 0.1^{Aa}	9 ± 0.4^{Ac}	7.2 ± 0^{Ad}	7 ± 0^{Ad}	7.2 ± 0.1^{Ad}	11.7 ± 0.1^{Ab}	11.7 ± 0.1^{Bb}	11.9 ± 0.1^{ABb}
Lys	*L. acidophilus*	25.4 ± 0.1^{Ad}	51 ± 0.7^{Ab}	51.8 ± 0.6^{Ab}	46.9 ± 0.1^{ABc}	46 ± 0.1^{Ac}	60.9 ± 0.8^{Aa}	61.1 ± 0.5^{Aa}	60.6 ± 0.2^{Aa}
	L. casei	25.4 ± 0.1^{Ad}	49.9 ± 0.7^{Ab}	49.6 ± 0.1^{Ab}	44.8 ± 0.4^{Bc}	44 ± 0.5^{Ac}	57.8 ± 0.6^{Aa}	58.2 ± 1^{Aa}	58 ± 0.1^{Aa}
	L. plantarum	25.4 ± 0.1^{Ac}	50.1 ± 0.5^{Ab}	49.4 ± 3.9^{Ab}	47.4 ± 1.3^{Ab}	46.5 ± 1.4^{Ab}	60.9 ± 1.7^{Aa}	61.1 ± 1.5^{Aa}	60.7 ± 1.9^{Aa}
His	*L. acidophilus*	26 ± 0.1^{Aa}	25.5 ± 0.2^{Ab}	21.1 ± 0.1^{Ad}	19.4 ± 0^{Ae}	19.5 ± 0^{Ae}	24 ± 0.3^{Ac}	24.1 ± 0.1^{Ac}	24 ± 0.1^{Ac}
	L. casei	26 ± 0.1^{Aa}	25 ± 0.2^{Ab}	20.5 ± 0.2^{Ad}	18.8 ± 0.1^{Be}	19 ± 0.1^{Be}	23 ± 0.2^{Bc}	23.3 ± 0.4^{Bc}	23.3 ± 0.2^{Bc}
	L. plantarum	26 ± 0.1^{Aa}	25.4 ± 0.2^{Ab}	20.8 ± 0.5^{Ad}	19.3 ± 0.1^{Ae}	19.4 ± 0.2^{ABe}	23.6 ± 0.2^{ABc}	23.6 ± 0.1^{ABc}	23.6 ± 0.1^{ABc}
Arg	*L. acidophilus*	10.8 ± 0.1^{Ae}	45.3 ± 0.7^{Aa}	36.3 ± 0.4^{Ac}	33.5 ± 0.3^{Ad}	34.2 ± 0.5^{Ad}	40.7 ± 0.8^{Ab}	41.6 ± 0.5^{Ab}	41.2 ± 0.2^{Ab}

(Continued)

TABLE 1 | Continued

Amino acid	Strains	Time							
		Fermentation for 0 h	Fermentation for 12 h	Fermentation for 24 h	Fermentation for 48 h	Fermentation for 72 h (Storage for 0 d)	Storage for 10 d	Storage for 20 d	Storage for 30 d
	L. casei	10.8 ± 0.1^{Ae}	44.4 ± 0.7^{Aa}	34.9 ± 0.2^{Ac}	32.3 ± 0.5^{Ad}	32.9 ± 0.4^{Ad}	38.9 ± 0.6^{Ab}	39.5 ± 1^{Ab}	39.5 ± 0.4^{Bb}
	L. plantarum	10.8 ± 0.1^{Ae}	44.4 ± 0.6^{Aa}	35.4 ± 1^{Ac}	32.9 ± 0.4^{Ad}	33.3 ± 0.7^{Ad}	39.9 ± 0.5^{Ab}	40.1 ± 0.5^{Ab}	39.8 ± 0.8^{ABb}
Pro	*L. acidophilus*	ND	6.3 ± 0.6^{Ac}	6.7 ± 0.1^{Ac}	9.9 ± 0.6^{Ab}	11.1 ± 0.6^{Ab}	53.7 ± 0.1^{Aa}	54.8 ± 2.8^{Aa}	55.1 ± 0.4^{Aa}
	L. casei	ND	5.8 ± 0.3^{Acd}	2.6 ± 3.7^{Ade}	9 ± 0.2^{Abc}	10.7 ± 0.5^{Ab}	55.5 ± 2.2^{Aa}	56 ± 0.4^{Aa}	56 ± 0.3^{Aa}
	L. plantarum	ND	5.8 ± 0.7^{Ac}	6.9 ± 0.3^{Ac}	8.9 ± 0.9^{Ab}	10.4 ± 0.9^{Ab}	53.5 ± 1.7^{Aa}	53.9 ± 0.7^{Aa}	53.4 ± 0.4^{Ba}

Results are expressed as mean ± standard deviation from the three replicates. ND refers to not detected. Values with different letters indicated a significant difference ($p < 0.05$).

10 days, which may also be related to the metabolism of ferulic acid into 4-vinyl guaiacol and other substances (43). Also, caffeic acid content increased rapidly, which could be attributed to the conversion of dihydrocaffeic acid to caffeic acid (47). Meanwhile, the content of catechin in apple juice fermented by *L. acidophilus*, *L. plantarum*, and *L. casei* were increased from 10.1 ± 0.1 mg/L, 9.9 ± 0.3 mg/L, 10.5 ± 0.4 mg/L to 12.6 ± 0.9 mg/L, 14.0 ± 0.5 mg/L, and 14.7 ± 0.3 mg/L while the content of protocatechuic acid were decreased from 24.4 ± 0.09 mg/L, 22.8 ± 2.6 mg/L, 25.1 ± 0.3 mg/L to 16.2 ± 0.8 mg/L, 18.9 ± 2.5 mg/L, and 18.2 ± 0.6 mg/L in the first 10-day storage. It has been reported that LAB can metabolize protocatechuic acid to catechin through the decarboxylation reaction (48). The study of Annalisa et al. also demonstrated the metabolic correlation between protocatechuic acid and catechin (49). It was also found that the changes of rutin and quercetin were almost the same during fermentation and storage at 4°C. Moreover, the contents of rutin and quercetin were almost stable throughout fermentation and there was no significant difference among the three LAB fermented samples ($P \geq 0.05$). However, the contents of rutin and quercetin in all the samples decreased significantly after storage for 10 days ($P < 0.05$), which may be attributed to the uncoupling of beta-glucosidase in lactic acid bacteria (50). Meanwile, rutin and quercetin could be biotransformed to low molecular weight metabolites, such as 2-(3,4-dihydroxyphenyl) acetic acid, 2-(3-hydroxyphenyl) acetic acid, 3,4-dihydroxybenzoic acid and others (51). The gallic acid content was increased during 72-h fermentation, but decreased during storage at 4°C for 30 days. In contrast, the content of proanthocyanidin B_2 was decreased rapidly within the first 12 h of fermentation and then stayed stable in the following 36 h of fermentation. Similar to gallic acid, the proanthocyanidin B_2 content was decreased significantly during storage.

The changes of individual phenolic compounds during 72-h fermentation were analyzed by PCA (**Figures 3A,B**). PC1 and PC2 explained 94% of the total variance of all the "fuji" apple juices. According to **Figure 3A**, the unfermented sample was located on the positive side of PC1. And apple juices fermented with *L. acidophilus*, *L. plantarum*, and *L. casei* at different stage were distributed on the different PC1 region, implying that PC1 can be considered as a contributor to distinguish the unfermented and fermented samples. In the loading plot of phenolic acids (**Figure 3B**), three phenolics, including cinnamaldehyde, phloretin, and *p*-vinyl guaiacol, were located on the negative side of PC1. In contrast, the other 13 phenolic acids were located on the positive side of PC1. Among them, *p*-vinyl guaiacol, phloretin, cinnamaldehyde, quercetin and ferulic acid were placed nearby the origin of first PC. Therefore, LAB fermentation may have minor effects on these phenolic acids. However, protocatechuic acid, gallic acid, *p*-hydroxybenzoic acid, *p*-coumaric acid, chlorogenic acid and syringic acid were all placed far from the origin of first PC and positively correlated. This result implied that LAB fermentation has some positive effects on the phenolic acids in apple juice.

The changes in total phenolic content in apple juices fermented by the three LAB strains are shown in **Figure 3C**. Overall, the total phenolic content was declined after 72-h fermentation ($P < 0.05$). During the first 12 h of fermentation, the total phenolic contents of apple juice fermented with different strains all declined from 1.37 g/L to around 1.27 g/L. However, the total phenolic content in apple juice fermented by *L. casei* was increased to 1.35 ± 0.01 g/L after 72 h of fermentation ($P < 0.05$), while that in apple juice fermented by *L. plantarum* was decreased to 1.27 ± 0.02 g/L. The loss of phenolics may be due to the interaction between phenolics and proteins in apple juice during fermentation, which could produce insoluble complexes (4). Another potential reason is that phenolics are the inhibitors of the growth of *L. plantarum*, and LAB can synthetize a series of enzymes (benzyl alcohol dehydrogenase, decarboxylase, tannase) to degrade phenolics (42, 52). The total phenolic contents in apple juice fermented by the three LAB strains were close after fermentation. In the first 10 day of storage, the total phenolic content decreased continuously to about 0.95 g/L. After that, no significant change in the total phenolic content was observed in the subsequent 20-day storage. Similar results were found by Wang et al. (53), the total phenolic content of fermented mango juice experienced a rapid decrease during the first 10-d storage and then stable. This phenomenon may be caused by the presence of dissolved oxygen which resulted in the oxidation of phenolic compounds during the

TABLE 2 | Changes in the contents of individual phenolic compounds (mg/L) of apple juices during lactic acid fermentation and the subsequent refrigerated storage period (4°C, 30 days).

organic	strains	Time							
		Fermentation for 0 h	**Fermentation for 12 h**	**Fermentation for 24 h**	**Fermentation for 48 h**	**Fermentation for 72 h (Storage for 0 d)**	**Storage for 10 d**	**Storage for 20 d**	**Storage for 30 d**
Gallic acid	*L. acidophilus*	15.4 ± 0.06^{ef}	12.8 ± 0.54^{de}	16.8 ± 0.11^{f}	19.8 ± 0.10^{gh}	21.3 ± 0.23^{h}	9.9 ± 2.23^{c}	4.5 ± 0.45^{a}	3.2 ± 0.13^{a}
	L. casei	15.4 ± 0.06^{ef}	14.3 ± 1.94^{ef}	16.5 ± 0.11^{f}	19.6 ± 0.05^{gh}	21.6 ± 0.16^{h}	10.5 ± 2.57^{cd}	4.3 ± 0.63^{a}	2.8 ± 0.42^{a}
	L. plantarum	15.4 ± 0.06^{ef}	12.2 ± 0.37^{d}	16.5 ± 0.32^{f}	18.9 ± 0.14^{g}	20.8 ± 0.14^{gh}	7.5 ± 1.57^{b}	3.2 ± 0.52^{a}	2.9 ± 0.15^{a}
Protocatechuic acid	*L. acidophilus*	17.1 ± 0.50^{ab}	16.0 ± 1.45^{c}	24.9 ± 0.40^{c}	23.9 ± 0.87^{c}	24.4 ± 0.09^{c}	16.2 ± 0.84^{ab}	18.8 ± 1.19^{b}	17.4 ± 1.02^{ab}
	L. casei	17.1 ± 0.50^{ab}	20.1 ± 1.70^{bc}	23.0 ± 2.31^{c}	24.4 ± 0.73^{c}	25.1 ± 0.31^{c}	18.2 ± 0.60^{ab}	19.9 ± 1.23^{bc}	17.9 ± 0.68^{ab}
	L. plantarum	17.1 ± 0.50^{ab}	17.4 ± 0.95^{ab}	20.0 ± 0.97^{bc}	22.5 ± 2.69^{c}	22.8 ± 2.57^{c}	18.9 ± 2.50^{b}	19.4 ± 0.37^{b}	18.1 ± 1.24^{ab}
Catechin	*L. acidophilus*	8.9 ± 0.08^{a}	8.6 ± 1.73^{a}	10.3 ± 0.16^{c}	9.6 ± 0.35^{bc}	10.1 ± 0.14^{bc}	12.6 ± 0.89^{d}	13.5 ± 0.65^{de}	12.6 ± 0.68^{d}
	L. casei	8.9 ± 0.08^{a}	9.7 ± 0.27^{bc}	9.9 ± 0.14^{bc}	9.7 ± 0.36^{bc}	10.5 ± 0.37^{c}	14.7 ± 0.29^{e}	13.5 ± 0.18^{de}	12.9 ± 0.35^{de}
	L. plantarum	8.9 ± 0.08^{a}	7.7 ± 0.18^{a}	9.6 ± 1.17^{bc}	9.0 ± 0.77^{b}	9.9 ± 0.27^{bc}	14.0 ± 0.48^{e}	13.7 ± 0.17^{de}	12.8 ± 0.63^{d}
Procyanidin B2	*L. acidophilus*	78.7 ± 6.78^{f}	43.1 ± 8.73^{c}	58.9 ± 1.08^{e}	56.5 ± 2.40^{de}	57.4 ± 0.38^{de}	28.4 ± 1.77	27.7 ± 1.58^{ab}	24.9 ± 1.59^{ab}
	L. casei	78.7 ± 6.78^{f}	52.3 ± 0.73^{d}	57.4 ± 1.43^{de}	57.6 ± 1.65^{de}	59.4 ± 0.49^{e}	31.9 ± 1.47^{b}	28.1 ± 0.73^{ab}	24.7 ± 1.34^{ab}
	L. plantarum	78.7 ± 6.78^{f}	42.7 ± 0.99^{c}	56.9 ± 3.48^{de}	55.8 ± 2.29^{de}	57.8 ± 0.60^{de}	30.0 ± 0.88^{b}	28.1 ± 0.54^{ab}	23.9 ± 2.67^{a}
Chlorogenic acid	*L. acidophilus*	116.0 ± 0.26^{g}	97.8 ± 2.66^{c}	111.0 ± 0.43^{e}	107.8 ± 1.25^{de}	106.8 ± 0.32^{de}	99.0 ± 2.90^{ab}	98.7 ± 1.76^{ab}	96.3 ± 0.89^{ab}
	L. casei	116.0 ± 0.26^{g}	99.7 ± 0.53^{d}	110.5 ± 0.57^{de}	108.7 ± 1.10^{de}	107.9 ± 0.31^{e}	105.2 ± 2.65^{b}	97.9 ± 0.36^{ab}	95.8 ± 0.79^{ab}
	L. plantarum	116.0 ± 0.26^{g}	94.2 ± 0.76^{c}	110.0 ± 2.08^{de}	107.4 ± 1.48^{de}	106.9 ± 0.52^{de}	100.9 ± 1.59^{b}	98.2 ± 0.49^{ab}	96.1 ± 1.09^{a}
P-hydroxybenzoic acid	*L. acidophilus*	19.3 ± 0.18^{d}	15.0 ± 1.64^{a}	18.2 ± 0.15^{cd}	20.1 ± 2.36^{de}	21.4 ± 0.14^{e}	15.2 ± 0.82^{a}	15.8 ± 0.42^{bc}	15.2 ± 0.50^{a}
	L. casei	19.3 ± 0.18^{d}	15.9 ± 0.17^{bc}	17.8 ± 0.22^{c}	21.6 ± 0.50^{e}	21.5 ± 0.19^{e}	16.9 ± 0.43^{c}	15.7 ± 0.17^{bc}	15.3 ± 0.27^{b}
	L. plantarum	19.3 ± 0.18^{d}	13.7 ± 0.14^{a}	17.4 ± 0.96^{c}	20.6 ± 1.20^{de}	21.2 ± 0.10^{e}	16.3 ± 0.43^{bc}	15.9 ± 0.12^{bc}	15.4 ± 0.42^{bc}
Caffeic acid	*L. acidophilus*	1.2 ± 0.27^{b}	1.0 ± 0.81^{b}	1.2 ± 0.09^{b}	0.7 ± 0.42^{ab}	1.6 ± 0.07^{bc}	2.0 ± 0.50^{c}	3.0 ± 0.22^{d}	3.0 ± 0.42^{d}
	L. casei	1.2 ± 0.27^{b}	1.6 ± 0.15^{bc}	1.0 ± 0.11^{b}	0.6 ± 0.29^{ab}	2.0 ± 0.09^{c}	3.0 ± 0.13^{d}	3.1 ± 0.08^{d}	3.2 ± 0.26^{d}
	L. plantarum	1.2 ± 0.27^{b}	0.0 ± 0.05^{a}	0.4 ± 0.58^{ab}	0.6 ± 0.42^{ab}	1.9 ± 0.04^{c}	3.0 ± 0.19^{d}	3.3 ± 0.12^{d}	3.0 ± 0.34^{d}
Ferulic acid	*L. acidophilus*	5.4 ± 0.08^{e}	5.1 ± 0.93^{d}	5.0 ± 0.05^{d}	4.8 ± 0.05^{cd}	4.6 ± 0.19^{cd}	0.4 ± 0.19^{a}	0.8 ± 0.10^{a}	0.7 ± 0.18^{a}
	L. casei	5.4 ± 0.08^{e}	5.4 ± 0.32^{d}	4.9 ± 0.02^{cd}	4.8 ± 0.06^{cd}	4.8 ± 0.04^{cd}	0.9 ± 0.02^{a}	0.9 ± 0.03^{a}	0.8 ± 0.11^{a}
	L. plantarum	5.4 ± 0.08^{e}	3.7 ± 0.00^{b}	4.4 ± 0.56^{c}	4.4 ± 0.53^{c}	4.7 ± 0.04^{cd}	0.8 ± 0.12^{a}	0.9 ± 0.03^{a}	0.8 ± 0.03^{a}
Rutin	*L. acidophilus*	2.3 ± 0.00^{bc}	2.2 ± 0.05^{b}	2.5 ± 0.27^{c}	2.4 ± 0.19^{c}	2.6 ± 0.24^{c}	0.3 ± 0.02^{a}	0.3 ± 0.05^{a}	0.3 ± 0.02^{a}
	L. casei	2.3 ± 0.00^{bc}	2.3 ± 0.08^{bc}	2.2 ± 0.01^{bc}	2.3 ± 0.02^{bc}	2.3 ± 0.01^{bc}	0.3 ± 0.02^{a}	0.3 ± 0.02^{a}	0.3 ± 0.03^{a}
	L. plantarum	2.3 ± 0.00^{bc}	2.2 ± 0.02^{bc}	2.2 ± 0.01^{bc}	2.3 ± 0.02^{bc}	2.3 ± 0.00^{bc}	0.4 ± 0.19^{a}	0.3 ± 0.00^{a}	0.3 ± 0.20^{a}
Quercetin	*L. acidophilus*	2.1 ± 0.00^{bc}	2.1 ± 0.12^{bc}	2.2 ± 0.21^{c}	2.2 ± 0.18^{bc}	2.2 ± 0.19^{c}	0.2 ± 0.01^{a}	0.2 ± 0.03^{a}	0.2 ± 0.02^{a}
	L. casei	2.1 ± 0.00^{bc}	2.0 ± 0.01^{b}	2.1 ± 0.01^{bc}	2.1 ± 0.01^{bc}	2.1 ± 0.01^{bc}	0.2 ± 0.01^{a}	0.2 ± 0.01^{a}	0.2 ± 0.02^{a}
	L. plantarum	2.1 ± 0.00^{bc}	2.0 ± 0.02^{bc}	2.1 ± 0.01^{bc}	2.1 ± 0.02^{bc}	2.1 ± 0.01^{bc}	0.2 ± 0.04^{a}	0.2 ± 0.03^{a}	0.2 ± 0.05^{a}

Results are expressed as mean ± standard deviation from the three replicates. Values with different letters indicate a significant difference ($p < 0.05$).

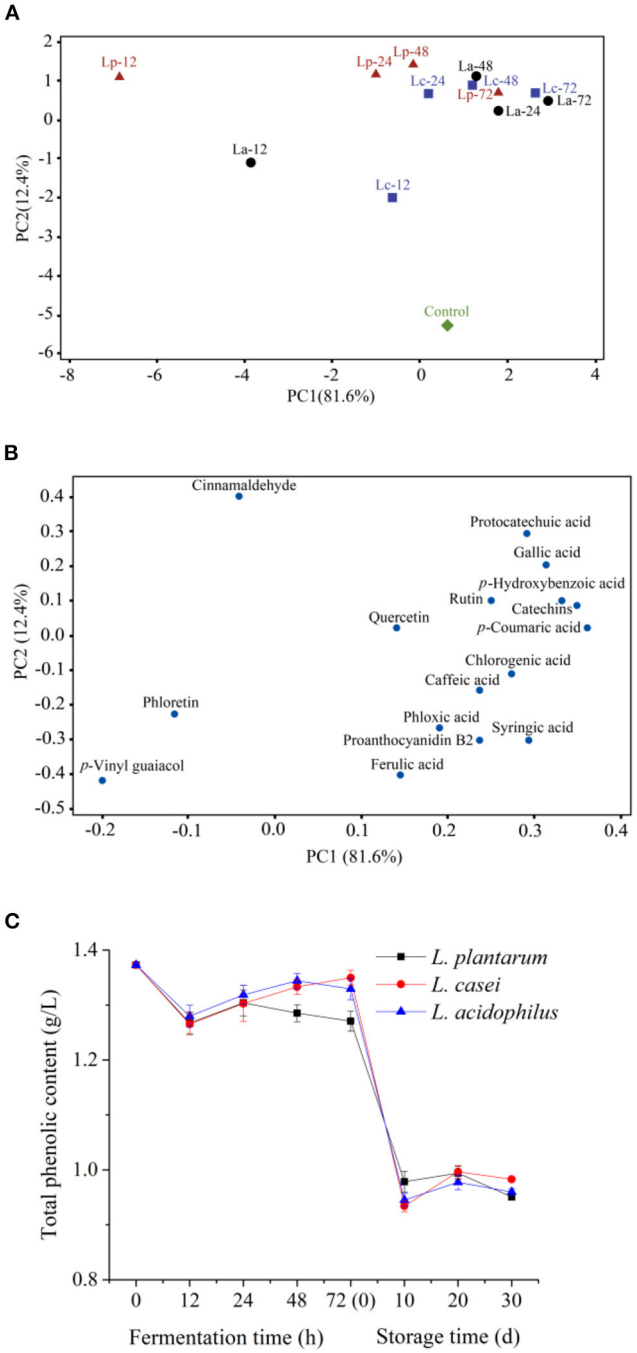

FIGURE 3 | Principal component analysis of phenolic profile in apple juice during fermentation by the three LAB strains [**(A)**, the score plots; **(B)**, the loading plots] and changes in total phenolic content **(C)**. "Control," Unfermented apple juice; "La," Apple juice fermented by *L. acidophilus*; "Lp", Apple juice fermented by *L. plantarum*; "Lc", Apple juice fermented by *L. casei*. The number followed with the name of strain indicated the time of fermentation.

first 10-d storage (54). However, phenolic compounds were more stable with the consumption of oxygen during the later storage stage.

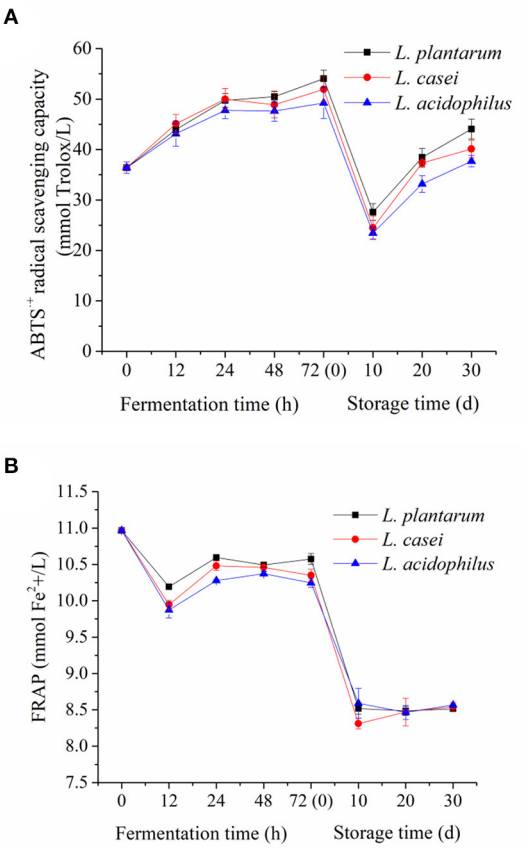

FIGURE 4 | The antioxidant activity of unfermented and LAB-fermented apple juice *in vitro*. **(A)** $ABTS^{\cdot+}$ radical scavenging activity, **(B)** ferric reducing antioxidant power.

Change in the Antioxidant and Antimicrobial Activities *in vitro* During LAB Fermentation and Storage

The antioxidant properties of apple juice are mainly related to vitamin C and phenolics (55, 56). $ABTS^{\cdot+}$ method (free radical scavenging capacity) and FRAP method (iron reduction capacity) were used to evaluate the effect of LAB fermentation on the antioxidant activity of apple juice *in vitro*. The results of antioxidant activity of fermented apple juice are shown in **Figure 4**. Generally, LAB fermentation enhanced the $ABTS^{\cdot+}$ radical scavenging capacity of the apple juice fermented by *L. acidophilus*, *L. plantarum*, and *L. casei* were increased from 36.41 ± 1.1 mmol Trolox/L to 49.22 ± 3.0 mmol Trolox/L, 54.03 ± 1.7 mmol Trolox/L, 51.94 ± 2.4 mmol Trolox/L, which was consistence with the trend in pomegranate juice (57) and jussara pulp (58) fermented by LAB. On the other hand, both $ABTS^{\cdot+}$ radical scavenging capacity and ferric reducing power of fermented apple juice declined significantly during the first 10-day storage, which could be related to the aforementioned decrease of total phenolic content in fermented apple juice. In the next 20-day storage, their trends have different performance.

The ferric reducing power was stable, whereas the $ABTS^{\cdot+}$ radical scavenging capacity was even increased. Overall, the ferric reducing ability of fermented apple juice has similar trend with the change of total phenolic acid content whereas the $ABTS^{\cdot+}$ radical scavenging capacity of fermented apple juice were increased during fermentation. Such inconsistent changes in ferric reducing ability and $ABTS^{\cdot+}$ radical scavenging capacity of fermented juice were also found by Wang et al. (9) who used LAB to ferment apple juice. There are two possible reasons for this phenomenon. First one is that the dissolved oxygen and microbial strains can affect the $ABTS^{\cdot+}$ radical scavenging capacity of fermented apple juice (9). Another one is that the bioconversion of phenolic acids during fermentation (59). Ozgen et al. (60) compared the $ABTS^{\cdot+}$ radical scavenging activities of four phenolic acids (gallic acid, chlorogenic acid, caffeic acid and ascorbic acid), and reported that gallic acid had the highest $ABTS^{\cdot+}$ radical scavenging activities, followed by caffeic acid. Zhang et al. (61) illustrated that gallic acid and caffeic acid had more contribution to the $ABTS^{\cdot+}$ radical scavenging activity as compared to ferulic acid. And in our study, we also found an increase in these phenolic acid contents (gallic acid, caffeic acid and so on).

In addition, microbial contamination is an important reason of food spoilage. *E. coli* (G^-) and *S. aureus* (G^+) are the most common microorganisms in contaminated food (62). In this study, the antimicrobial activities of unfermented and fermented apple juice against the growth of *E. coli* and *S. aureus* were evaluated, and the results are shown in **Figure 5**. Before fermentation, the samples had weak antibacterial activities. After 72-h fermentation, the diameters of the inhibition circles against *E. coli* and *S. aureus* were 23.78 ± 0.1 mm and 17.53 ± 1.0 mm for the apple juice fermented by *L. plantarum*, 23.74 ± 1.1 mm and 16.81 ± 0.6 mm for the juice fermented by *L. casei*, and 23.76 ± 0.9 mm and 17.13 ± 0.8 mm for the juice fermented by *L. acidophilus*. It is supposed that the antibacterial properties of fermented apple juice may be related to bacteriocin, diacetyl, organic acid and hydrogen peroxide produced by lactic acid bacteria metabolism (63). Although LAB fermentation improved the antimicrobial activities, there was no significant difference in the areas of inhibition zone of apple juice fermented by the three LAB strains after 72-h fermentation. Interestingly, after storage for 30 days, the diameter of the inhibition circle against *E. coli* for all the juices even increased. The apple juice fermented with *L. acidophilus* had the largest inhibition circles (26.41 ± 0.3 mm) followed by those fermented with *L. plantarum* (25.03 ± 0.6 mm) and *L. casei* (24.31 ± 0.9 mm). In addition, the diameter of the inhibition circle against *S. aureus* for the samples fermented with *L. acidophilus* did not change significantly after 30-day storage, whereas the antimicrobial ability of samples fermented with *L. casei* and *L. plantarum* against *S. aureus* got weakened with storage. Generally, the antimicrobial activities of unfermented and fermented apple juice can be contributed by the acid production, these acids can lower pH and create an unfavorable environment for pathogens and deteriorating microorganisms (64). Additionally, LAB can produce some antimicrobial compounds such as H_2O_2 and bacteriocin, which can inhibit microbial growth (21). Therefore, such changes in antimicrobial activities after fermentation and storage may be influenced by the change of organic acids and viable cell counts of LAB.

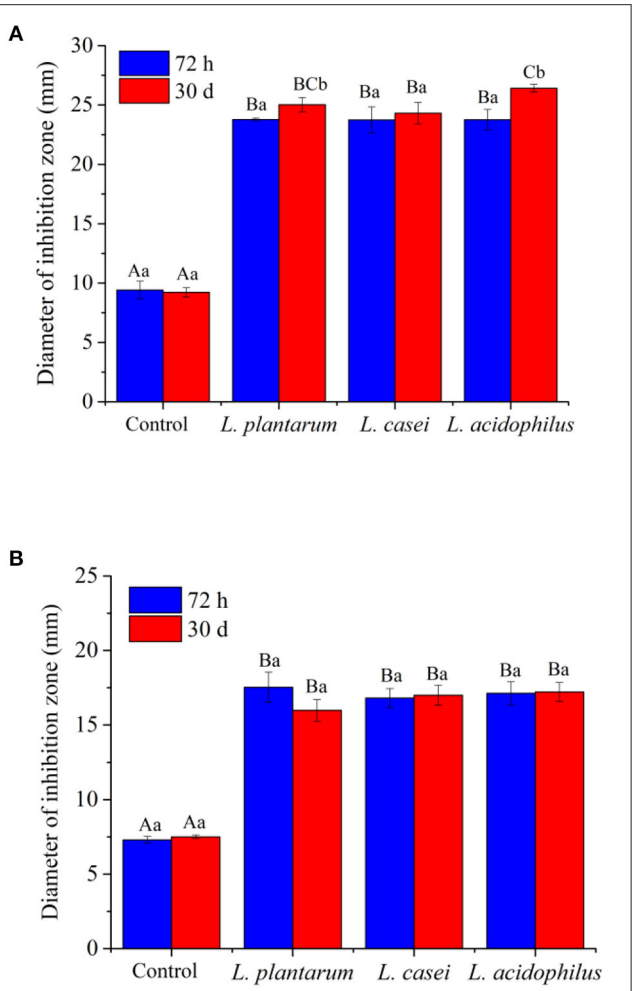

FIGURE 5 | The antimicrobial activity of unfermented and LAB-fermented apple juice against the growths of **(A)** *E. coli* and **(B)** *S. aureus in vitro*. Values with different letters within each samples indicated a significant difference in content ($p < 0.05$).

CONCLUSION

In this study, three commercial LAB strains including *L. acidophilus*, *L. casei*, and *L. plantarum* were utilized to ferment apple juice. All the microbial strains presented satisfactory growth capacities in the studied apple juice environment. In general, LAB fermentation improved the antioxidant and antimicrobial capacities by metabolizing phenolics and producing lactic acid. In addition, the changes in the physicochemical properties of fermented apple juice during storage at 4°C for 30 days was also evaluated. The results showed that the total amino acid content was significantly increased, but the total phenolic content was significantly decreased. Overall, these results prove that lactic acid

fermentation is a useful method to enhance the nutritional value of apple juice.

DATA AVAILABILITY STATEMENT

The original contributions presented in the study are included in the article/**Supplementary Material**, further inquiries can be directed to the corresponding author/s.

AUTHOR CONTRIBUTIONS

JY performed the experiments, analyzed the data, and wrote the manuscript. YS, TG, and YW analyzed the data and wrote the manuscript. HS, QZ, and CL analyzed and discussed the data. CZ, YH, and YT provided samples and discussed the data. YT designed the research content, analyzed the data, and modified the manuscript. All authors read and approved the final manuscript.

FUNDING

This work was financially supported by grants from the National Natural Science Foundation of China (No. 32100037), Natural Science Research General Project of Jiangsu Higher Education Institutions (No. 20KJB550008), Science and Technology Program of Kizilsu Kirghiz Autonomous Prefecture in 2021 (No. 3-25), Jiangsu Planned Projects for Postdoctoral Research Funds (No. 2019K015), Priority Academic Program Development of Jiangsu Higher Education Institutions (PAPD), and the Research and Practice Innovation Program for College Graduates of Jiangsu Province (No. KYCX20_2888).

SUPPLEMENTARY MATERIAL

The Supplementary Material for this article can be found online at: https://www.frontiersin.org/articles/10.3389/fnut.2022.833906/full#supplementary-material

REFERENCES

1. Yuasa M, Shimada A, Matsuzaki A, Eguchi A, Tominaga M. Chemical composition and sensory properties of fermented citrus juice using probiotic lactic acid bacteria. *Food Biosci.* (2020) 39:100810. doi: 10.1016/j.fbio.2020.100810
2. Dogan K, Akman PK, Tornuk F. Role of non-thermal treatments and fermentation with probiotic *Lactobacillus plantarum* on in vitro bioaccessibility of bioactives from vegetable juice. *J Sci Food Agr.* (2021) 101:4779–88. doi: 10.1002/jsfa.11124
3. Wang Z, Feng Y, Yang N, Jiang T, Xu H, Lei H. Fermentation of kiwifruit juice from two cultivars by probiotic bacteria: bioactive phenolics, antioxidant activities and flavor volatiles. *Food Chem.* (2022) 373:131455. doi: 10.1016/j.foodchem.2021.131455
4. Ankolekar C, Johnson K, Pinto M, Johnson D, Labbe RG, Greene D, et al. Fermentation of whole apple juice using *lactobacillus acidophilus* for potential dietary management of hyperglycemia, hypertension, and modulation of beneficial bacterial responses. *J Food Biochem.* (2012) 36:718–38. doi: 10.1111/j.1745-4514.2011.00596.x
5. Varela P, Salvador A, Fiszman S. Shelf-life estimation of 'Fuji' apples: Sensory characteristics and consumer acceptability. *Postharvest Biol Tec.* (2005) 38:18–24. doi: 10.1016/j.postharvbio.2005.05.009
6. Zhu G, Tian C. Determining sugar content and firmness of "Fuji' apples by using portable near-infrared spectrometer and diffuse transmittance spectroscopy. *J Food Process Eng.* (2018) 41:e12810.1–10. doi: 10.1111/jfpe.12810
7. Ross JA, Kasum CM. Dietary flavonoids: bioavailability, metabolic effects, and safety. *Annu Rev Nutr.* (2002) 22:19–34. doi: 10.1146/annurev.nutr.22.111401.144957
8. Wang X, Han M, Zhang M, Wang Y, Ren Y, Yue T, et al. *In vitro* evaluation of the hypoglycemic properties of lactic acid bacteria and its fermentation adaptability in apple juice. *LWT- Food Sci Technol.* (2021) 136:110363. doi: 10.1016/j.lwt.2020.110363
9. Wang H, Tao Y, Li Y, Wu S, Li D, Liu X, et al. Application of ultrasonication at different microbial growth stages during apple juice fermentation by *Lactobacillus plantarum*: Investigation on the metabolic response. *Ultrason Sonochem.* (2021) 73:105486. doi: 10.1016/j.ultsonch.2021.105486
10. Chen C, Lu Y, Yu H, Chen Z, Tian H. Influence of 4 lactic acid bacteria on the flavor profile of fermented apple juice. *Food Biosci.* (2019) 27:30–6. doi: 10.1016/j.fbio.2018.11.006
11. Kwaw E, Ma YK, Tchabo W, Apaliya MT, Wu M, Sackey AS. Effect of *lactobacillus strains* on phenolic profile, color attributes and antioxidant activities of lactic-acid-fermented mulberry juice. *Food Chem.* (2018) 250:148–54. doi: 10.1016/j.foodchem.2018.01.009
12. Vivek K, Mishra S, Pradhan RC, Jayabalan R. Effect of probiotification with *Lactobacillus plantarum* MCC 2974 on quality of Sohiong juice. *LWT-Food Sci Technol.* (2019) 108:55–60. doi: 10.1016/j.lwt.2019.03.046
13. Kaprasob R, Kerdchoechuen O, Laohakunjit N, Sarkar D, Shetty K. Fermentation-based biotransformation of bioactive phenolics and volatile compounds from cashew apple juice by select lactic acid bacteria. *Process Biochem.* (2017) 59:141–9. doi: 10.1016/j.procbio.2017.05.019
14. Balestra GM, Misaghi IJ. Increasing the efficiency of the plate counting method for estimating bacterial diversity. *J Microbiol Methods.* (1997) 30:111–7. doi: 10.1016/S0167-7012(97)00056-0
15. Tiwari BK, Muthukumarappan K, Odonnell CP. Colour degradation and quality parameters of sonicated orange juice using response surface methodology. *LWT-Food Sci Technol.* (2008) 41:1876–83. doi: 10.1016/j.lwt.2007.11.016
16. Lima M, Silani I, Toaldo IM, Correa LC, Biasoto ACT, Pereira GE. Phenolic compounds, organic acids and antioxidant activity of grape juices produced from new Brazilian varieties planted in the northeast region of Brazil. *Food Chem.* (2014) 161:94–103. doi: 10.1016/j.foodchem.2014.03.109
17. Wasik A, Mccourt J, Buchgraber M. Simultaneous determination of nine intense sweeteners in foodstuffs by high performance liquid chromatography and evaporative light scattering detection—Development and single-laboratory validation. *J Chromatogr A.* (2007) 1157:187–96. doi: 10.1016/j.chroma.2007.04.068
18. A MRR, B RCB. Quantification of total phenols in bio-oil using the Folin–Ciocalteu method–sciencedirect. *J Anal Appl Pyrol.* (2013) 104:366–71. doi: 10.1016/j.jaap.2013.06.011
19. Zhang W, Han F, He J, Duan C. HPLC-DAD-ESI-MS/MS analysis and antioxidant activities of nonanthocyanin phenolics in mulberry (Morus alba L). *J Food Sci.* (2008) 73:C512–518. doi: 10.1111/j.1750-3841.2008.00854.x
20. Abid M, Jabbar DS, Wu T, Hashim MM, Hu B, Lei S. Sonication enhances polyphenolic compounds, sugars, carotenoids and mineral elements of apple juice. *Ultrason Sonochem.* (2013) 21:93–7. doi: 10.1016/j.ultsonch.2013.06.002
21. Wang Y, Tao Y, Zhang X, Shao S, Han Y, Chu DT. Metabolic profile of ginkgo kernel juice fermented with lactic aicd bacteria: a potential way to degrade ginkgolic acids and enrich terpene lactones and phenolics. *Process Biochem.* (2019) 76:25–33. doi: 10.1016/j.procbio.2018.11.006
22. Yoon KY, Woodams EE, Hang YD. Production of probiotic cabbage juice by lactic acid bacteria. *Bioresour Technol.* (2006) 97:1427–30. doi: 10.1016/j.biortech.2005.06.018

23. Ricci A, Cirlini M, Levante A. Volatile profile of elderberry juice: Effect of lactic acid fermentation using *L. plantarum, L rhamnosus* and *L casei* strains. *Food Res Int.* (2018) 105:412–22. doi: 10.1016/j.foodres.2017.11.042
24. Verardo V, Moreno-Trujillo TR, Caboni MF, Garcia-Villanova B, Guerra-Hernandez EJ. Influence of infant cereal formulation on phenolic compounds and formation of Maillard reaction products. *J Food Compos Anal.* (2021) 104:104187. doi: 10.1016/j.jfca.2021.104187
25. Pimentel TC, Madrona GS, Garcia S, Prudencio SH. Probiotic viability, physicochemical characteristics and acceptability during refrigerated storage of clarified apple juice supplemented with *Lactobacillus paracasei* ssp. paracasei and oligofructose in different package type. *LWT-Food Sci Technol.* (2015) 63:415–22. doi: 10.1016/j.lwt.2015.03.009
26. Toit M, Engelbrecht L, Lerm E, Krieger-Weber S. *Lactobacillus*: the next generation of malolactic fermentation starter cultures—an overview. *Food Bioprocess Tech.* (2011) 4:876–906. doi: 10.1007/s11947-010-0448-8
27. Ye M, Yue T, Yuan Y. Polyphenols and organic acids evolution during apple cider fermentation. *J Sci Food Agr.* (2014) 94:2951–7. doi: 10.1002/jsfa.6639
28. Zhang H, Zhou F, Ji B, Nout RMJ, Yang FZ. Determination of organic acids evolution during apple cider fermentation using an improved HPLC analysis method. *Eur Food Res Technol.* (2008) 22:1183–90. doi: 10.1007/s00217-008-0835-9
29. Dudley EG, Steele JL. Succinate production and citrate catabolism by cheddar cheese nonstarter *lactobacilli*. *J Appl Microbiol.* (2010) 98:14–23. doi: 10.1111/j.1365-2672.2004.02440.x
30. Abdelrahman MA, Tashiro Y, Sonomoto K. Recent advances in lactic acid production by microbial fermentation processes. *Biotechnol Adv.* (2013) 31:877–902. doi: 10.1016/j.biotechadv.2013.04.002
31. Wang YC, Yu RC, Yang HY, Chou CC. Sugar and acid contents in soymilk fermented with lactic acid bacteria alone or simultaneously with *bifidobacteria*. *Food Microbiol.* (2003) 20:333–8. doi: 10.1016/S0740-0020(02)00125-9
32. Ortiz-Cortés LY, Ventura-Canseco L, Abud-Archila M, Ruíz-Valdiviezo VM, Velázquez-Ríos IO, Alvarez-Gutiérrez PE. Evaluation of temperature, pH and nutrient conditions in bacterial growth and extracellular hydrolytic activities of two alicyclobacillus spp. *strains Arch Microbiol.* (2021) 203:1–14. doi: 10.1007/s00203-021-02332-4
33. Hughes DB, Hoover DG. Viability and enzymatic activity of *Bifidobacteria* in Milk. *J Dairy Sci.* (1995) 78:268–76. doi: 10.3168/jds.S0022-0302(95)76634-6
34. KMital B, Shallenberger RH, Steinkraus K. α-Galactosidase activity of *Lactobacilli*. *J Appl Microbiol.* (1973) 26:783–8. doi: 10.1128/am.26.5.783-788.1973
35. Bermdez R, Franco D, Carballo J. Influence of muscle type on the evolution of free amino acids and sarcoplasmic and myofibrillar proteins through the manufacturing process of Celta dry-cured ham. *Food Res Int.* (2014) 56:226–35. doi: 10.1016/j.foodres.2013.12.023
36. Mcsweeney P, Sousa M. Biochemical pathways for the production of flavour compounds in cheeses during ripening: a review. *Lait.* (2000) 80:293–324. doi: 10.1051/lait:2000127
37. Mau JL, Tseng YH. Nonvolatile taste components of three strains of *Agrocybe cylindracea*. *J Agr Food Chem.* (1998) 46:2071–4. doi: 10.1021/jf971016k
38. Zuljan FA, Mortera P, Alarcón SH, Blancato VS, Espariz M, Magni C. Lactic acid bacteria decarboxylation reactions in cheese. *Inter Dairy J.* (2016) 62:53–62. doi: 10.1016/j.idairyj.2016.07.007
39. Liesbeth R, Mireille Y, Richard van K, Pascal C, Annette V, Emilie C, et al. Lactococcal aminotransferases Arat and Bcat are key enzymes for the formation of aroma compounds from amino acids in cheese. *Int Dairy J.* (2003) 13:805–12. doi: 10.1016/S0958-6946(03)00102-X
40. Tanous C, Gori A, Rijnen L, Chambellon E, Yvon M. Pathways for -ketoglutarate formation by *Lactococcus lactis* and their role in amino acid catabolism. *Int Dairy J.* (2004) 15:759–70. doi: 10.1016/j.idairyj.2004.09.011
41. Thierry A, Mailard MB, Yvon M. Conversion of L-Leucine to isovaleric acid by *Propionibacterium freudenreichii* TL 34 and itgp23. *Appl Environ Microb.* (2002) 68:608–15. doi: 10.1128/AEM.68.2.608-615.2002
42. Rodriguez H, Curiel JA, Landete JM. Food phenolics and lactic acid bacteria. *Int J Food Microbiol.* (2009) 132:79–90. doi: 10.1016/j.ijfoodmicro.2009.03.025
43. Knockaert D, Raes K, Wille C, Struijs K, Camp JV. Metabolism of ferulic acid during growth of *Lactobacillus plantarum* and *Lactobacillus collinoides*. *J Sci Food Agr.* (2012) 92:2291–6. doi: 10.1002/jsfa.5623
44. Filannino P, Bai Y, Cagno R, Gobbetti M, Gaenzle MG. Metabolism of phenolic compounds by *Lactobacillus spp*. during fermentation of cherry juice and broccoli puree. *Food Microbiol.* (2014) 46:272–9. doi: 10.1016/j.fm.2014.08.018
45. Sanchez-Maldonado AF, Schieber A, Ganzie MG. Structure-function relationships of the antibacterial activity of phenolic acids and their metabolism by lactic acid bacteria. *J Appl Microbiol.* (2011) 111:1176–84. doi: 10.1111/j.1365-2672.2011.05141.x
46. Huang J, Depaulis T, May J. Antioxidant effects of dihydrocaffeic acid in human EA. hy926 endothelial cells. *J Nutr Biochem.* (2005) 15:722–9. doi: 10.1016/j.jnutbio.2004.07.002
47. Ricci A, Cirlini M, Calani L. In vitro metabolism of elderberry juice polyphenols by lactic acid bacteria. *Food Chem.* (2019) 276:692–9. doi: 10.1016/j.foodchem.2018.10.046
48. Tabasco R. Snchez-pat NF, Monagas M, Bartolome B, Moreno-Arribas MV, Pelaez C. Effect of grape polyphenols on lactic acid bacteria and bifidobacteria growth: Resistance and metabolism. *Food Microbiol.* (2011) 28:1345–52. doi: 10.1016/j.fm.2011.06.005
49. He L, Xu H, Liu X, He WH, Yuan F, Hou ZQ, et al. Identification of phenolic compounds from pomegranate (*Punica granatum* L) seed residues and investigation into their antioxidant capacities by HPLC–ABTS^{+} assay. *Food Res Int.* (2011) 44:1161–7. doi: 10.1016/j.foodres.2010.05.023
50. Svensson L, Sekwati-monang B, Lopeslutz D, Schieber AG, Nzle MG. Phenolic acids and flavonoids in nonfermented and fermented red Sorghum (Sorghum bicolor L Moench). *J Agr Food Chem.* (2010) 58:9214–20. doi: 10.1021/jf101504v
51. Attri S, Sharma K, Raigond P, Goel G. Colonic fermentation of polyphenolics from sea buckthorn (*Hippophae rhamnoides*) berries: assessment of effects on microbial diversity by principal component analysis. *Food Res Int.* (2018) 105:324–32. doi: 10.1016/j.foodres.2017.11.032
52. Hashemi SMB, Khaneghah AM, Barbaf FJ, Nemati Z, Shokofti SS, Alizadeh F. Fermented sweet lemon juice (*Citrus limetta*) using *Lactobacillus plantarum* LS5: chemical composition, antioxidant and antibacterial activities. *J Functional Foods.* (2017) 38:409–14. doi: 10.1016/j.jff.2017.09.040
53. Wang J, Xie B, Sun Z. Quality parameters and bioactive compound bioaccessibility changes in probiotics fermented mango juice using ultraviolet-assisted ultrasonic pre-treatment during cold storage. *LWT-Food Sci Technol.* (2021) 137:110438. doi: 10.1016/j.lwt.2020.110438
54. Filho A, Freitas HV, Rodrigues S, Virgínia Kelly Gonalves Abreu, Pereira A. Production and stability of probiotic cocoa juice with sucralose as sugar substitute during refrigerated storage. *LWT-Food Sci Technol.* (2019) 99:371–8. doi: 10.1016/j.lwt.2018.10.007
55. Queirozc C, Lopes M, Fialho E, Valente-Mesquita VL. Changes in bioactive compounds and antioxidant capacity of fresh-cut cashew apple. *Food Res Int.* (2011) 44:1459–62. doi: 10.1016/j.foodres.2011.03.021
56. Xiao Y, Wu X, Yao X, Chen Y, Ho CT, He C, et al. Metabolite profiling, antioxidant and α-glucosidase inhibitory activities of buckwheat processed by solid-state fermentation with *Eurotium cristatum* YL-1. *Food Res Int.* (2021) 143:110262. doi: 10.1016/j.foodres.2021.110262
57. Mousavi Z, Mousavi M, Razavi S, Hadinejad M, Emam-Djomeh Z, Mirzapour M. Effect of Fermentation of pomegranate Juice by *Lactobacillus plantarum* and *Lactobacillus acidophilus* on the antioxidant activity and metabolism of sugars, organic acids and phenolic compounds. *Food Biotechnol.* (2013) 27:1–13. doi: 10.1080/08905436.2012.724037
58. Braga A, Mesquita L, Martins P, Habu S, Rosso VD. *Lactobacillus* fermentation of jussara pulp leads to the enzymatic conversion of anthocyanins increasing antioxidant activity. *J Food Compos Anal.* (2018) 69:162–70. doi: 10.1016/j.jfca.2017.12.030
59. Wu Y, Li S, Tao Y, Li D, Han Y, Show PL. et al. Fermentation of blueberry and blackberry juices using *Lactobacillus plantarum, Streptococcus thermophilus* and *Bifidobacterium bifidum*: Growth of probiotics, metabolism of phenolics, antioxidant capacity in vitro and sensory evaluation. *Food Chem.* (2021) 348:129083. doi: 10.1016/j.foodchem.2021.129083
60. Ozgen M, Reese RN, Tulio AZ, Scheerens JC, Miller AR. Modified 2,2-azino-bis-3-ethylbenzothiazoline-6-sulfonic acid (ABTS) method to measure

antioxidant capacity of selected small fruits and comparison to ferric reducing antioxidant power (FRAP) and 2,2'-diphenyl-1-picrylhydrazyl (DPPH) methods. *J Agri Food Chem.* (2006) 54:1151–7. doi: 10.1021/jf051960d

61. Zhang B, Xia T, Duan W, Zhang Z, Wang M. Effects of organic acids, amino acids and phenolic compounds on antioxidant characteristic of Zhenjiang aromatic vinegar. *Molecules.* (2019) 24:3799. doi: 10.3390/molecules24203799
62. Thuibaut S, Caillon J, Huart C, Grandjean G, Lombrail P, Potel G. Susceptibility to the main antibiotics of *Escherichia coli* and *Staphylococcus aureus* strains identified in community acquired infections in France (MedQual, 2004–2007). *Med Mal Al Infec.* (2010) 40:74–80. doi: 10.1016/j.medmal.2009.01.011
63. Reis JA, Paula AT, Casarotti S, Penna A. Lactic acid bacteria antimicrobial compounds: characteristics and applications. *Food Eng Rev.* (2012) 4:124–40. doi: 10.1007/s12393-012-9051-2
64. Pereira A, Maciel TC, Rodrigues S. Probiotic beverage from cashew apple juice fermented with *Lactobacillus casei*. *Food Res Int.* (2011) 44:1276–83. doi: 10.1016/j.foodres.2010.11.035

Conflict of Interest: The authors declare that the research was conducted in the absence of any commercial or financial relationships that could be construed as a potential conflict of interest.

frontiers in Nutrition

ORIGINAL RESEARCH
published: 22 February 2022
doi: 10.3389/fnut.2022.824525

Antifatigue Effect of *Panax Notoginseng* Leaves Fermented With Microorganisms: *In-vitro* and *In-vivo* Evaluation

Min Yang[1,2†], *Liang Tao*[1,2,3†], *Cun-Chao Zhao*[2,3], *Zi-Lin Wang*[1,2], *Zhi-Jin Yu*[1,3], *Wen Zhou*[1], *Yan-Long Wen*[1,2], *Ling-Fei Li*[1,2*], *Yang Tian*[1,2,3*] and *Jun Sheng*[2,4*]

[1] College of Food Science and Technology, Yunnan Agricultural University, Kunming, China, [2] Engineering Research Center of Development and Utilization of Food and Drug Homologous Resources, Ministry of Education, Yunnan Agricultural University, Kunming, China, [3] National Research and Development Professional Center for Moringa Processing Technology, Yunnan Agricultural University, Kunming, China, [4] Key Laboratory of Pu-erh Tea Science, Ministry of Education, Yunnan Agricultural University, Kunming, China

OPEN ACCESS

Edited by:
Xiudong Xia,
Jiangsu Academy of Agricultural Sciences (JAAS), China

Reviewed by:
Xiao Xu,
Shaoxing University, China
Juanmei Zhang,
Henan University, China

***Correspondence:**
Ling-Fei Li
lingfeili@163.com
Yang Tian
tianyang1208@163.com
Jun Sheng
shengj@ynau.edu.cn

[†] These authors have contributed equally to this work

Specialty section:
This article was submitted to Food Chemistry, a section of the journal Frontiers in Nutrition

Received: 29 November 2021
Accepted: 25 January 2022
Published: 22 February 2022

Citation:
Yang M, Tao L, Zhao C-C, Wang Z-L, Yu Z-J, Zhou W, Wen Y-L, Li L-F, Tian Y and Sheng J (2022) Antifatigue Effect of Panax Notoginseng Leaves Fermented With Microorganisms: In-vitro and In-vivo Evaluation. Front. Nutr. 9:824525. doi: 10.3389/fnut.2022.824525

Fatigue is a common physiological phenomenon caused by many complicated factors. Excessive fatigue will lead to a series of uncomfortable reactions and damage body health. *Panax notoginseng* leaves (PNL) is a new resource food that good for soothing nerves, nourishing the heart, and strengthening the spleen. Microbial fermentation could increase the content of bio-ingredients and produce new active ingredients. However, the effect of fermented *P. notoginseng* leaves (FPNL) on antifatigue and the molecular mechanisms remain to be elucidated. Thus, in this study, we evaluated the antifatigue effect of co-fermented *P. notoginseng* leaves by *Saccharomyces cerevisiae* and *Bacillus subtilis in-vitro* and *in-vivo*, and its mechanism was further elucidated. The results showed that FPNL exhibited higher saponins, organic phenolic acids content, and antioxidant activity than PNL. FPNL improved ISO-induced H9c2 myocardial cell damage by alleviating apoptosis (modulating Bax and Bcl-2 protein expression) and reducing antioxidant activity *in-vitro*. Moreover, *in-vivo* experiment showed that FPNL significantly prolonged the weight-loading swimming time of mice. After gavaged FPNL, the levels of liver glycogen (LG) and serum lactate dehydrogenase (LDH) activity were increased in mice. In contrast, the levels of blood urea nitrogen (BUN), lactate acid, and malondialdehyde (MDA) were decreased. In summary, our results indicated that FPNL showed a good antifatigue effect *in-vivo* and *in-vitro*.

Keywords: *Panax notoginseng* leaves, microbial, fermentation, weight-loading swimming, antifatigue, antioxidant

INTRODUCTION

Fatigue refers to a physiological state in which the body cannot maintain a certain level of function or an organ cannot maintain a predetermined exercise intensity. This phenomenon is mainly caused by excessive energy consumption in the body and the accumulation of metabolic waste such as lactic malondialdehyde (1). Fatigue can be divided into secondary fatigue, physiological fatigue, or chronic fatigue. Secondary fatigue is due to sleep disorders, depression, overwork, or drug side effects. Physiological fatigue is caused by lack of rest, physical labor, or mental reasons.

Chronic fatigue refers to fatigue that persists for more than 6 months. All types of fatigue can lead to health damage (2). In addition, fatigue is also divided into central fatigue and peripheral fatigue. Central fatigue is triggered by factors related to the central nervous system, brain, spinal cord, and motor neurons, while peripheral fatigue is related to muscle weakness caused by changes in the neuromuscular junction or distal end (3). The accumulation of lactic acid (LD) and ammonia metabolites, blood sugar, and tissue glycogen consumption are the leading cause of peripheral fatigue (4). However, the continuous supply of energy resources and the elimination of metabolites could alleviate peripheral fatigue (5). Fatigue is becoming increasingly severe in modern society, leading to aging, cancer, depression, multiple sclerosis, Parkinson's syndrome, and other diseases. Research has shown that antifatigue drugs may cause adverse reactions or toxic effects (6). While regular exercise and a balanced diet are considered healthy methods to relieve fatigue. However, people are also looking for other antifatigue methods. Some studies have shown that herbal medicine has unique advantages in eliminating fatigue. Therefore, developing natural antifatigue products to improve exercise ability and relieve fatigue is a common concern in the future.

Panax notoginseng is a perennial herb that showed a good function at promoting blood circulation, relieving swelling, and protecting the human liver (7). The primary chemical constituents of *P. notoginseng* are saponins, which can be classified into four types depending on the glycine content: 20 (S)—protopanoxadiol types (PPD), 20 (S)—protopanaxatriol types (PPT), C17 side chain variation types and other kinds types. For a long time, *P. notoginseng* has been involved in a wide range of medical fields. With the continuous utilization of natural resources, *P. notoginseng* leaves (PNL) as a new food material have been gradually discovered and used by many studies. Studies have found that PNL is rich in various active ingredients, such as promoting blood circulation, eliminating stasis, relieving pain, reducing inflammation, and promoting digestion (8–10). In addition, PNL contains seven kinds of essential amino acids and is rich in vitamin C, nicotinamide, folic acid, biotin (8). Meanwhile, the saponin content of PNL was approximately 9%. These saponins had different biological activities (11). Therefore, the development and utilization of PNL have become a research hotspot.

Microbial fermentation could secret various biological enzymes to decompose the structure of plant cells (12), increase the content of active ingredients in plants (13). In this process, microorganisms metabolize macromolecules into small molecules for easy absorb. Therefore, microbial metabolism could improve the utilization rate of active ingredients (14). A lot of foods are fermented or enriched in probiotics to be evaluated as possible carriers of these beneficial microorganisms. Several species of *Lactobacillus* and *Bifidobacterium* have become the most commonly used probiotic strains in these food products. Other microorganisms such as *Saccharomyces cerevisiae*, *Enterococcus*, *Bacillus*, and *Escherichia* are also applied in functional food (15). It was shown that after fermenting by *Bacillus subtilis*, the ginsenoside Rh4 of *P. notoginseng* roots was obtained (16). *Panax notoginseng* leaves fermented by microorganisms were increased polysaccharide contents and significantly showed antiinflammatory effects (17). Moreover, PNL fermented by *Lactobacillus* significantly improved the anti-liver cancer activity (14). Therefore, fermentation is one of the most convenient techniques in biocatalytic processes. During fermentation, microbial metabolism can transform raw materials into products with specific health-promoting properties.

This study investigated the contents of total saponins, total polyphenols, and organic phenolic acids in PNL and fermented *P. notoginseng* leaves (FPNL). The stability of bioactive substances from FPNL has been studied with ABTS and 2,2-diphenyl-1-picrylhydrazyl (DPPH) analysis. Then a fatigue injury model of H9c2 cardiomyocytes was constructed with isoproterenol (ISO), and the protective effects of FPNL and PNL on H9c2 cells were investigated. Furthermore, the antifatigue effect of FPNL was studied by a weight-loading swimming experiment in mice. Finally, the swimming time and antifatigue-related biochemical indices were detected to evaluate the antifatigue of FPNL *in-vivo and in-vitro*.

Abbreviations: BUN, blood urea nitrogen; LD, lactic acid; LDH, lactate dehydrogenase; LG, liver glycogen; MDA, malondialdehyde; Bcl-2, B-cell lymphoma 2; ABTS, 2,2-azino-bis-3-ethylbenzthiazoline-6-sulphonic salt; DPPH, 2,2-diphenyl-1-picrylhydrazyl; HPLC, high-performance liquid chromatography; DMEM, Dulbecco's modified Eagle's medium; DMSO, dimethyl sulfoxide; PBS, phosphate buffered saline; PPT, protopanaxatriol; PPD, protopanaxadiol; PNL, *Panax notoginseng* leaves; FPNL, fermented *P. notoginseng* leaves.

MATERIALS AND METHODS

Plant Materials and Reagents

Panax notoginseng leaves were collected from the organic *P. notoginseng* planting base at Yunnan Agricultural University (Lan Cang, Yunnan, China). *Lactobacillus acidophilus* (CICC 20710), *Lactobacillus reuteri* (CICC 6226), *Lactobacillus plantarum* (CICC 194165), *Pichia kluyveri* (CICC 32845), *S. cerevisiae* (CICC 31393), and *B. subtilis* (CICC 22459) were purchased from the China Center of Industrial Culture Collection; *S. cerevisiae* (GIM2.43) and *Rhizopus oryzae* (CICC 41441) were purchased from Guangdong Microbial Culture Collection Center. All strains were stored at −80°C; 3-4,5-dimethylthiazole-z-yl-3,5-diphenyltetrazolium bromide (MTT), trypsin, dimethyl sulfoxide (DMSO), and phosphate-buffered saline (PBS) were purchased from Solarbio Technology Co., Ltd. (Beijing, China) and stored at −20°C; DMEM and fetal bovine serum (FBS) were obtained from Invitrogen Technology (Gaithersburg, USA). BCA protein quantitative kit was acquired from Beyotime Biotechnology Co., Ltd. (Shanghai, China). Antibodies against Bax and Bcl-2 were acquired from Cell Signaling Technology (Beverly, USA); rabbit and mouse antibodies were acquired from Abcam (NY, USA). A liver glycogen (LG) assay kit (A043-1-1), LD assay kit (A019-2-1), lactate dehydrogenase (LDH) assay kit (A020-2-2), malondialdehyde (MDA) assay kit (A003-1-2), and urea assay (BUN) kit (C013-2-1) were purchased from Nanjing Jiancheng Bioengineering Institute (Jiangsu, China).

Preparation of FPNL

The strains were cultured in MRS medium for 24 h, then sub-cultured all strains three times. Strains of *Lactobacillus* spp. were cultured under anaerobic conditions in a Bugbox anaerobic chamber (Ruskin Technology, USA). The PNL were dried in an oven, crushed, and screened for 40 mesh. *Panax notoginseng* leaves was extracted by microwave-assisted method (18). The PNL powder (10 g) was immersed in 200 ml UP water, ultrasonicated (200 W) at 110°C for 15 min, then 1% glucose was added, sterilized at 121°C for 20 min, and cooled for reserve. The strains (1.0×10^9 CFU/ml) were added to the fermentation medium of PNL, mixed well, and then incubated in an incubator at the controlled temperature (30°C) and humidity (relative humidity of 80%) for 144 h. The fermentation products were centrifuged at 4,000 rpm at 4°C for 15 min, freeze-dried at −50°C and 7–10 MPa, and then stored at −80°C until use. The suitable strains were screened to FPNL according to the previous research (**Supplementary Table 1**; **Supplementary Figure 1**). Finally, *S. cerevisiae* (CICC 31393) and *B. subtilis* (CICC 22459) were co-inoculated to ferment PNL in this research.

Total Saponin in PNL and FPNL

The total saponins content of PNL and FPNL were assayed by the vanillin and glacial acetic acid method (19). 1.5 mg ginsenoside Re standard was weighed and added to a 6 ml methanol solution to dissolve entirely. The absorbance was measured at a wavelength of 560 nm, and the standard curve of *P. notoginseng* saponin was drawn. The content of *P. notoginseng* saponins in ample solutions was determined according to the standard curve drawing method.

Total Polyphenols in PNL and FPNL

The total phenolic content of PNL and FPNL was assessed using the Folin–Ciocalteu reagent (FCR) method (20). The sample (100 μl) was added to a solution containing FCR (100 μl), sodium carbonate (100 μl; 20% w/v), and methanol (100 μl). The sample–reagent mixture was allowed to react in the dark for 20 min, and then it was centrifuged at 13,000 rpm for 3 min. The absorbance was monitored at 760 nm using gallic acid as a standard, while methanol was used as a blank. The results were calculated as μg of gallic acid equivalent per gram of dry weight.

Total Flavonoids in PNL and FPNL

The total flavonoids content of PNL and FPNL were assayed by $AlCl_3$ colorimetry (21), which is based on the reaction of aluminum ions with flavonoid molecules under primary conditions. A total of 1.5 ml of the extract was added to 450 μl of 5.3% $NaNO_2$, 900 μl of 10% $AlCl_3$-H_2O, and 4 ml of 1 M NaOH. The mixture was stirred and allowed to rest for 5 min before each addition. The absorbance was measured at 510 nm.

Antioxidant Activities in PNL and FPNL

Changes of antioxidant capacity in PNL and FPNL under external environmental stimulation were determined as described by Rakmai et al. (22) with a slight modification. The oxidative stimulation of PNL and FPNL was simulated by UV irradiation for a week. The retention of antioxidant activity of PNL and FPNL under external environmental stimulation were then measured daily from the supernatant after UV irradiation. The antioxidant activity of FPNL and PNL was determined by using a DPPH and ABTS radical scavenging assay (23). 2,2-Diphenyl-1-picrylhydrazyl powder was dissolved in 100 ml methanol to prepare the 0.05 mM DPPH solution for the method. The prepared solution was stored at 4°C. 0.1 ml of sample solution was mixed with 3.9 ml DPPH solution and incubated for 30 min in the dark. 2,2-Diphenyl-1-picrylhydrazyl solution (3.9 ml) and 0.1 ml of 70% methanol aqueous solution were used as negative controls. Then, the absorbance was measured at 517 nm. The scavenging activity (SC) of the samples was expressed using the following formula:

$$\text{The DPPH sactivity } (100\%) = [A_0 - (A_1 - A_2)/A_0] \times 100\%$$

where A_0, A_1, and A_2 represent the absorbance of the blank control, sample, and negative control, respectively.

The ABTS radicals scavenging was reacting ABTS and potassium persulfate (23). The mixture was incubated in the dark at room temperature. 0.2 ml FPNL and PNL were mixed with ABTS radical cation solution, then incubated for 15 min in the dark. The absorbance was measured at 734 nm. The ABTS activity of the samples was expressed using the following formula:

$$\text{The ABTS activity } (100\%) = [A_0 - (A_1 - A_2)/A_0] \times 100\%$$

where A_0, A_1, and A_2 represent the absorbance of the blank control, sample, and negative control, respectively.

Analysis of Saponins by High Performance Liquid Chromatography

The contents of different saponins in PNL and FPNL were analyzed by the high performance liquid chromatograph (HPLC) method described in a previous study (24, 25). High performance liquid chromatograph-grade methanol and acetonitrile were purchased from Merck (Darmstadt, Germany). Deionized water was purified by a Milli-Q purification system (Millipore, Bedford, MA, USA). Four standard substances (ginsenoside R1, Rg1, Rb1, and Rb3) were purchased from the National Institute for the Control of Pharmaceutical and Biological Products (Beijing, PR China) according to the National Standards of the People's Republic of China (GBT19086-2008).

The sample was dissolved in 70% methanol (v/v) and filtered using Millipore Amicon Ultra UFC900396 (Millipore, Bedford, MA, USA). The centrifugal liquid was filtered by 0.22 μm (Millipore, Bedford, MA, USA) prior to HPLC analysis.

The quantitative analysis of saponins was performed on an Agilent 1260 series HPLC (Santa Clara, CA, USA) equipped with an Agilent Zorbax SB-C18 column (250 × 4.6 mm, 5 μm). The gradient elution system consisted of water (A) and acetonitrile (B). Separation was achieved using the following gradient: 0–6 min, 20–30% B; 6–14 min, 30–40% B; 14–20 min, 40–30% B; and 20–30 min, 20% B. The flow rate was 1.0 ml/min, and the injection volume was 10 μl. The UV detection wavelength was carried out at 203 nm. The column temperature was maintained at 36°C. The contents for ginsenosides in samples were calculated by their respective peak areas (25).

Metabolomic Analysis by LC-MS/MS

FPNL and PNL (20 mg) were put into EP tube, 1,000 μl solution (acetonitrile:methanol:water = 2:2:1, with the isotopically labeled internal standard mixture) was added. After 30 s mixing, the samples were homogenized at 35 Hz for 4 min and sonicated for 5 min on ice. The homogenization and sonication cycle was repeated 3 times. Then, the samples were incubated for 1 h at −40°C and centrifuged at 12,000 rpm for 15 min at 4°C. The resulting supernatant was transferred to a fresh glass vial for LC/MS analysis. High performance liquid chromatograph separation was carried out using a 1290 Infinity series UHPLC System (Agilent Technologies) with a UPLC BEH Amide column (2.1 × 100 mm, 1.7 μm, Waters). The mobile phase consisted of 25 mmol/L ammonium acetate and 25 mmol/L ammonia hydroxide in water (pH = 9.75) (A) and acetonitrile (B). The analysis was carried out with an elution gradient as follows: 0–0.5 min, 95% B; 0.5–7.0 min, 95–65% B; 7.0–8.0 min, 65–40% B; 8.0–9.0 min, 40% B; 9.0–9.1 min, 40–95% B; 9.1–12.0 min, 95% B. The column temperature was 25°C. The autosampler temperature was 4°C, and the injection volume was 3 μL. A QE mass spectrometer was used for its ability to acquire MS/MS spectra in information-dependent acquisition (IDA) mode in the control of the acquisition software (Xcalibur 4.0.27, Thermo). In this mode, the acquisition software continuously evaluates the full scan MS spectrum. The ESI source conditions were set as follows: sheath gas flow rate of 45 Arb, aux gas flow rate of 15 Arb, capillary temperature of 400°C, full MS resolution of 70,000, MS/MS resolution of 17,500, collision energy of 10/30/60 eV in mode.

Cell Lines and Culture

Cardiomyocyte H9c2 cell lines were obtained from Kunming Cell Bank of the Typical Culture Preservation Committee, Chinese Academy of Sciences. Cells were cultured in DMEM (HyClone, CA, United States). All cells were cultured in a humidified atmosphere with 5% CO_2 at 37°C. All media were supplemented with 10% FBS and 1% penicillin-streptomycin mixture.

MTT Test

H9c2 cells in the logarithmic phase were seeded in 96-well plates. The cell concentration was adjusted to 10,000 cells per well and inoculated with 200 μl (26). Cells were cultured for 24 h and then divided into seven groups: the control group (normal medium and the corresponding volume of DMSO), model group (10 μmol/L ISO), FPNL group (10, 20, 40, 80, 160 μg/ml), and PNL group (10, 20, 40, 80, 160 μg/ml). All groups were incubated for 48 h, then the cells were incubated with 10 μmol/L ISO for 1 h. 5 μg/ml MTT solution was added to each well and continuously incubated for 4 h. Media were replaced with DMSO, and the optical densities (ODs) were measured at 490 nm wavelength using a microplate reader. The inhibition rate was calculated according to the following equation:

$$\text{The inhibition rate of tumor cell proliferation} = 1 - (\text{OD drug treatment group}/\text{OD cell control group}) \times 100\%$$

In-vivo Animal Swimming Model

To determine the effects of PNL and FPNL on mice *in-vivo*, 4-week-old male C57/BL6 mice (weight 20 g ± 2 g) were fed in an SPF environment (27). All of the animal experiments were performed under protocols approved by the Institutional Animal Ethical Committee of Yunnan Agricultural University (YNAU-201911017). All mice were then randomly divided into five groups (six mice per group): the control group (distilled water), low-dose group (50 mg/kg FPNL), medium-dose group (100 mg/kg FPNL), high-dose group (200 mg/kg FPNL), and not fermentation group (200 mg/kg PNL). The drug was administered by gavage every day. Each group was gavaged continuously for 30 days. Body weights and total food intake of mice were measured every 4 days.

Weight-Loading Swimming Test

After treatment with FPNL and PNL, all mice rested for 30 min and were then subjected to a weight-loading swimming test (28). Mice were placed in a swimming pool, strapped with 5% of their own body, and swam every week in a swimming tank with a water temperature of 25 ± 1°C and a water depth of 30 cm. The time from the start of swimming to the fatigue of the mice was recorded.

Serum Indices

After swimming with loaded, mice were killed to collect blood and organs. Blood samples were collected through a heparinization tube for eyeball blood collection and centrifuged at 3,500 rpm for 30 min, and all organs (heart, liver, lungs, spleen, kidney) were frozen in liquid nitrogen (27). The serum contents of LG, LD, LDH, MDA, and blood urea nitrogen (BUN) were investigated by ELISA kits according to the kit instructions. All samples were stored at −80°C.

Western Blot Analysis

Cells were treated with a water extract of PNL or FPNL for 48 h, and then washed twice with cold PBS. Total cell protein was extracted by RIPA buffer (Beyotime, Shanghai, China), and protein concentrations were assessed by the BCA assay kit (Beyotime, Shanghai, China) (29). Target protein samples were separated by 10% SDS-PAGE and transferred by electroblotting to polyvinylidene difluoride (PVDF) membranes. After blocking with 5% skim milk for 2 h, proteins were incubated with primary antibodies against Bax, Bcl-2, and β-actin overnight at 4°C. The PVDF membranes were washed three times with Tris HCl Tween (TBST) for nearly 8 min each time and then incubated with goat anti-rabbit HRP or goat anti-mouse HRP (1:10,000, Abcam, MA,

TABLE 1 | Contents of total polyphenols, flavonoids, and saponins in PNL and FPNL.

Name	Total polyphenol content (mg GAE/g)	flavonoid content (mg/g)	total saponins content (mg/g)
PNL	38.26 ± 3.57	25 ± 4.87	161.584 ± 3.13
FPNL	63.75 ± 4.16	54.72 ± 2.85	192.861 ± 2.82

United States) for 1 h. The protein signal was detected using ECL Western blotting substrate and analyzed by *ImageJ*.

Statistical Analysis

All data were analyzed using GraphPad Prism 7.0. Values are expressed as the mean ± standard error of the mean (SEM). The results comparisons were performed using one-way analysis of variance (ANOVA). $^{*}p < 0.05$, $^{**}p < 0.01$, $^{***}p < 0.001$, and $^{****}p < 0.0001$; $^{\#}p < 0.05$, $^{\#\#}p < 0.01$, and $^{\#\#\#}p < 0.001$ were considered to indicate statistically significant differences. Single factors texts were used to determine the significant differences between means ($P < 0.05$) using SPSS version 17.0 (Chicago, USA). Three replicates ($n = 3$) for *in-vitro* texts, Six replicates ($n = 6$) for *in-vivo* texts.

Principal component analysis (PCA) pattern recognition was performed with SIMCA software (V15.02, Sartorius Stedim Data Analytics AB, Umea, Sweden). Metabolites with VIP values >1.0 were considered differential metabolites for potential discrimination of samples in the OPLS-DA models. We used Student's *t*-test to analyze these models, which is commonly used for metabolomics statistical analysis. $P < 0.05$ was considered statistically significant.

RESULTS

Contents of Total Polyphenols, Flavonoids, and Saponins in PNL and FPNL

Our previous research found that the highest content of total saponins was obtained from the co-fermentation of PNL by *S. cerevisiae* CICC 31393 and *B. subtilis* CICC 22459 (the ratio of the two microorganisms was 1:1) (**Supplementary Table 1**;

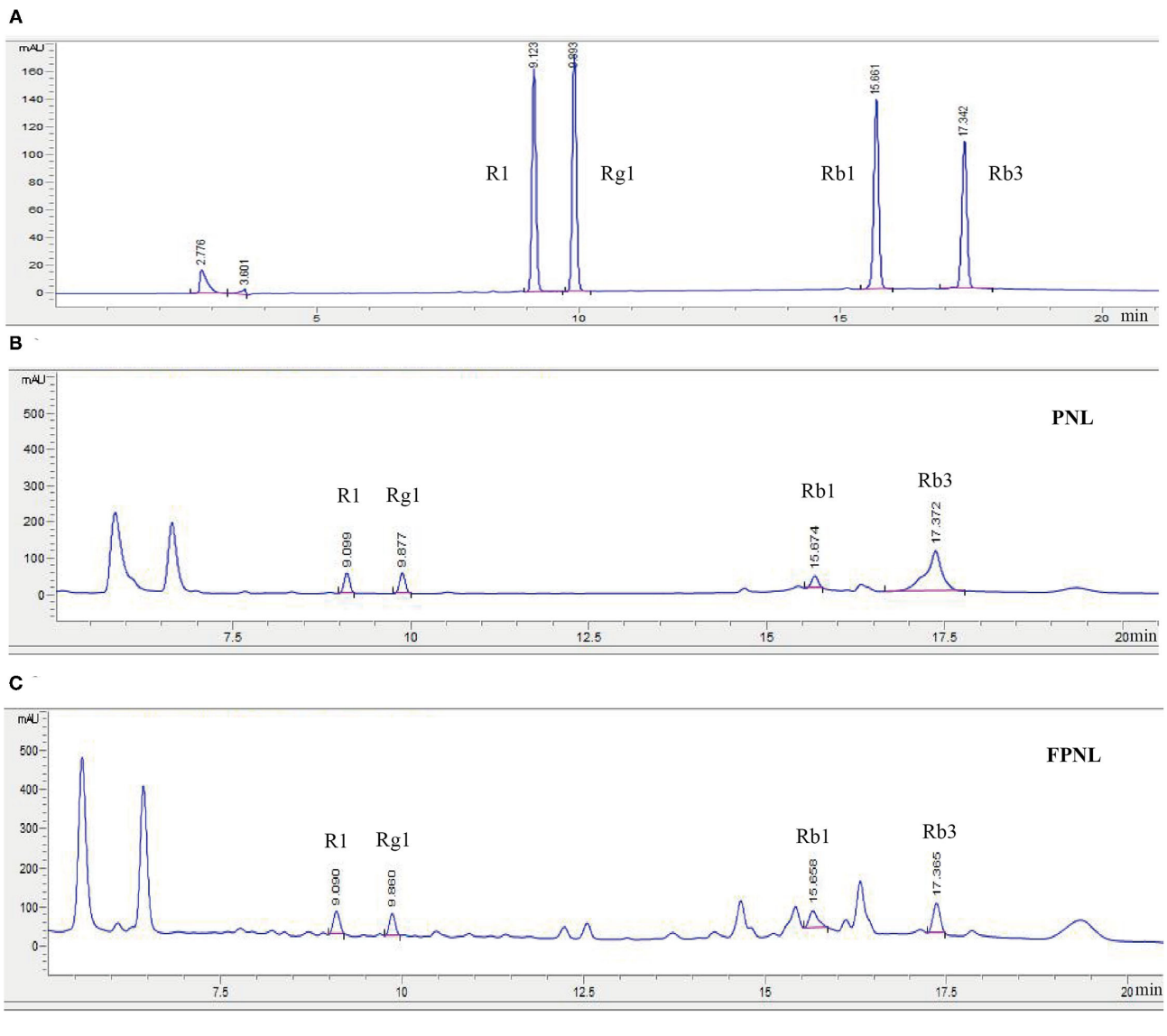

FIGURE 1 | HPLC analysis of different saponins content in PNL and FPNL. **(A)** A stander mixture of four saponins. **(B)** The four saponins in PNL. **(C)** The four saponins in FPNL.

Supplementary Figure 1). Therefore, *S. cerevisiae* CICC 31393 and *B. subtilis* CICC 22459 were used to co-fermented PNL for subsequent studies. The results showed that the total polyphenols, flavonoids, and saponins in FPNL were 1.6, 2.1, and 1.2 times higher than PNL (**Table 1**). High-performance liquid chromatography analysis showed that after fermentation, the composition of saponins was changed. In particular, compared with the PNL, the PPT type of R1 and Rg1 increased in FPNL, while protopanaxadiol types of Rb1 and Rb3 decreased slightly, indicating that biological transformation of saponins in PNL occurred after fermentation (**Figure 1**; **Supplementary Tables 2**, **3**).

Antioxidant Stability in PNL and FPNL

Most active substances do not work well due to the influence of water solubility and stability. Therefore, a stability test could be used to compare the stability of active substances produced by fermentation. The oxidative stimulation of PNL and FPNL was performed by UV irradiation. The antioxidant stability of PNL and FPNL was determined by DPPH and ABTS radical scavenging for different days (0–7 days). The results showed that although both DPPH radical scavenging ability and ABTS radical scavenging ability of PNL and FPNL were decreased after UV treatment in time-dependent. The ABTS scavenging ability of PNL decreased rapidly to 5.11%. While, the ABTS scavenging ability of FPNL was relatively stable in the first 4 days and then decreased to 26.34% on the last day (**Figure 2A**). Similarly, the DPPH radical scavenging ability of PNL was significantly decreased from 72.31 to 10.09%. However, FPNL decreased relatively slowly and still kept at 35.1% on the last day (**Figure 2B**). In addition, the antioxidant activities of FPNL were also better than PNL between these 7 days. It indicated that FPNL might show significantly antioxidant stability than PNL. These results showed that the active substances in FPNL could be more fully released, and the stability of the active substances could be enhanced to avoid the loss of active substances by the external environment, such as UV, to some extent.

Change of the Metabolites of PNL After Co-fermented

To further to explore the differences in metabolites between PNL and FPNL, LC-MS/MS was used in this study, with the PNL group as a control. As shown in **Figure 3**, all samples are within the 95% confidence interval. Principal component analysis (**Figure 3A**) and orthogonal partial least squares discriminant analysis (OPLS-DA) plot scores and volcano plot showed that samples of FPNL and PNL were in different locations, indicating that both models were valid (**Figures 3B–D**).

Next, we obtained a comprehensive metabolites view of PNL after fermentation, then mapped these different metabolites into their biochemical pathways (**Figures 4A,B**). The results of metabolic enrichment and pathway analyses based on the KEGG database and MetaboAnalyst showed significantly changed in the pathways of the citrate cycle (TCA), glyoxylate and dicarboxylate metabolism, arginine, and proline metabolism (**Figure 4A**; **Supplement Figure 2**). Moreover, two kinds of essential AAs (Isoleucine, Leucine) and six kinds of unessential AAs (Tyrosine, Valine Leucine Alanine, Glutamate Proline) pathways were enriched in FPNL (**Figure 4B**). As shown in the string map and heat map (**Figures 4C,D**), some active metabolites were rich in FPNL, too. A total of 31 different metabolites were selected based on variable importance in the projection (VIP) values >1 and *p*-values <0.05. The significantly different metabolites with known nutritional functions identified in the FPNL are shown in **Table 2**. These metabolites mainly include phenolic acids, amino acids, and pyrimidines. In this study, the contents of organic phenolic acids such as pyrocatechol, citric acid, benzoic acid, shikimic acid, and the contents of AAs such as Isoleucine, Leucine, Proline in FPNL were significantly increased.

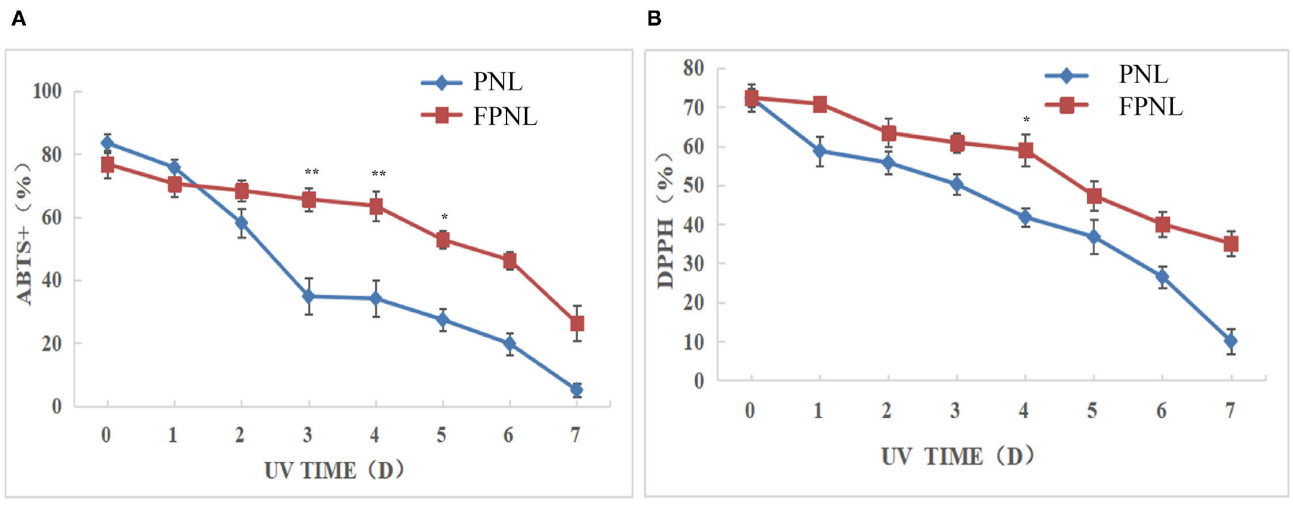

FIGURE 2 | Changes of ABTS and DPPH free radical scavenging rates of PNL and FPNL. **(A)** Changes in ABTS rates of PNL and FPNL. **(B)** Changes in DPPH rates of PNL and FPNL. *$P < 0.05$, **$P < 0.01$ vs. PNL group.

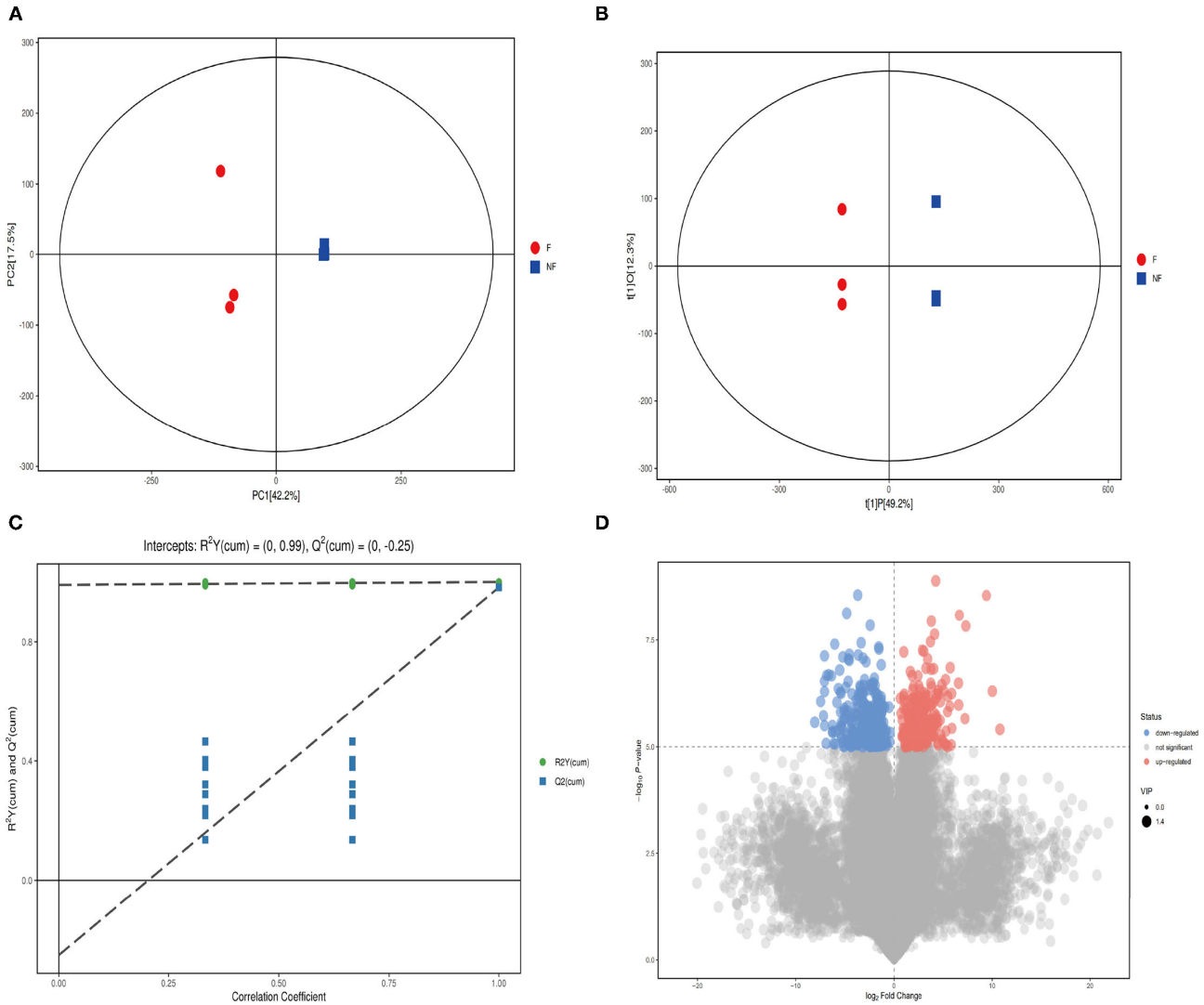

FIGURE 3 | Identification of discriminating biomarkers of fermented *P. notoginseng* leaves metabolomics analysis. **(A)** The OPLS-DA score plot in ion mode. **(B)** The PCA score plot in ion mode. **(C)** The H volcanic figure plot in ion mode. **(D)** The validation plot for the OPLS-DA model is built for negative, the slope of R2 is greater than 0, and the intercept of Q2 on the Y-axis is less than 0.05, indicating a valid model, the scattered shape and color of Figure. Three represent disparate studied groups.

FPNL Alleviate Myocardial Cell Failure

To determine the antifatigue effect of FPNL, H9c2 cells were treated with different concentrations of aqueous extracts of PNL and FPNL for 48 h, and then treated with ISO for 1 h. MTT assay showed that, compared with the control group, the ISO-treatment group showed lower cell viability (**Figures 5A,B**). The viability of cells in the FPNL group (**Figure 5A**) and PNL group was increased significantly and showed less toxicity on H9c2 cells (**Figure 5B**). Moreover, compared with the PNL group, the FPNL group had a significant antifatigue effect on H9c2 cells. Based on these results, 40, 80, and 160 μg/ml concentrations for FPNL and PNL were selected for subsequent experiments.

The Effect of FPNL on Myocardial Cell Apoptosis

To detecte whether FPNL affects apoptosis in H9c2 cells, the expression of the apoptosis-related proteins Bax and Bcl-2 was examined by Western blot. The results showed that the expression of pro-apoptotic protein Bax was decreased (**Figures 5C,D**) when the concentration was 160 μg/ml, the expression of Bax in the FPNL group was better than that in the PNL group, and the expression of anti-apoptotic protein Bcl-2 was significantly increased (**Figures 5C,E**). It was suggested that the antifatigue effect of FPNL on the ISO-induced cells might be driven by the intrinsic apoptotic pathway.

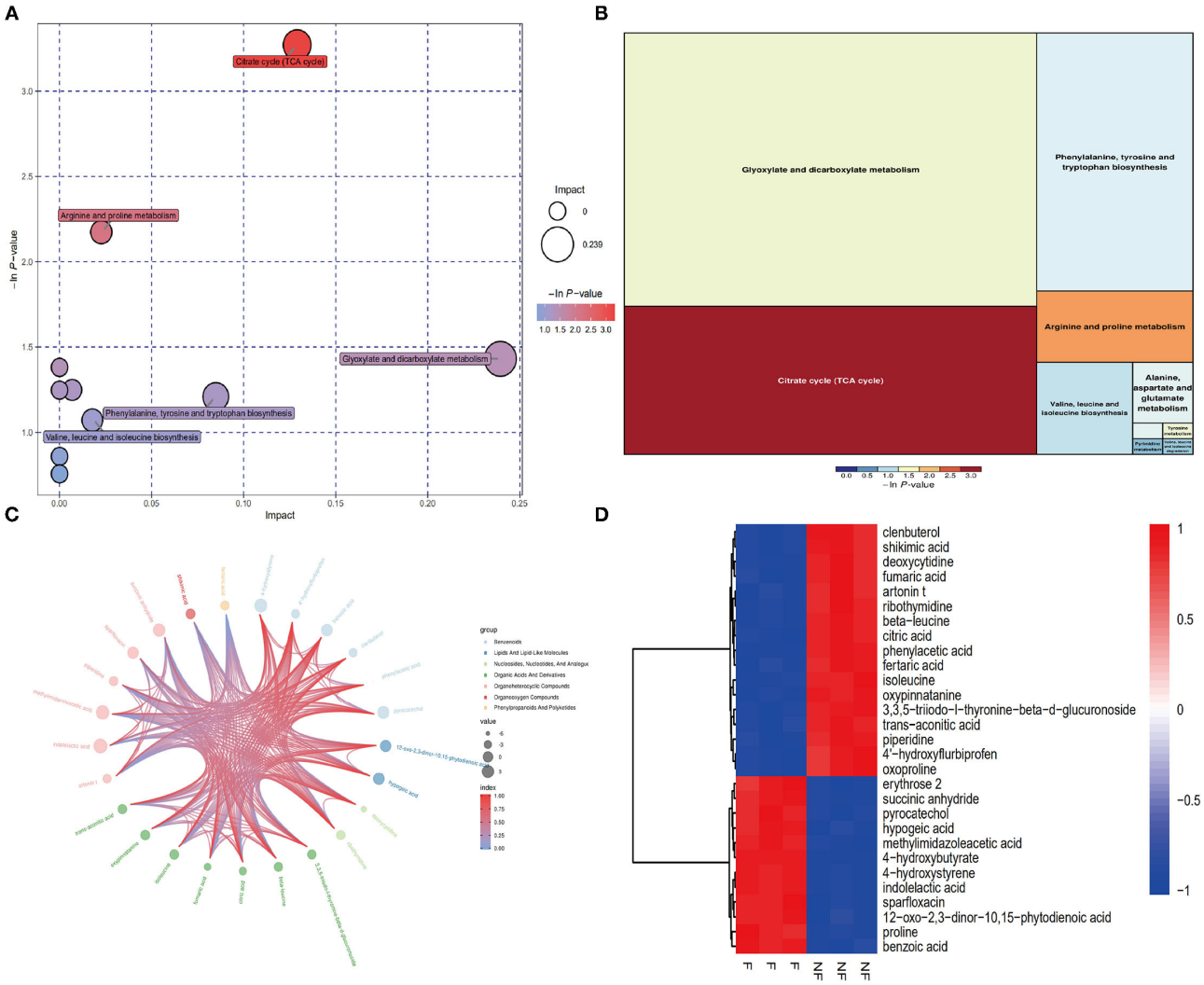

FIGURE 4 | Improvement of different metabolites of PNL and FPNL. **(A)** Bubble plot displays the increasing impact of the enrichment analysis of metabolic pathways, with key bubbles reflecting that the metabolic pathways were significantly altered by fermentation. **(B)** Heatmap clearly shows the relationship in potential biomarkers after fermentation. **(C)** Chord diagram of metabolic differences. **(D)** Metabolites differential enrichment map.

The Effect of FPNL on Weight-Loading Swimming Mice

The animal swimming experiment is one of the important indices to evaluate the antifatigue effect of healthy food (30). Therefore, we evaluated the swimming ability of mice after gavaging FPNL and PNL (**Figure 6A**). The results showed that the swimming time of mice with 100 and 200 mg/kg FPNL and 200 mg/kg PNL groups was significantly longer than the control group ($P < 0.05$). Moreover, the FPNL groups showed significantly longer swimming time than the PNL groups in a dose-dependent manner. The swimming time increased by 1.96 times in FPNL group (200 mg/kg) compared with PNL group (200 mg/kg) (**Figure 6B**) ($P < 0.05$). These results indicated that FPNL showed a significantly relieving fatigue effect *in-vivo*. As shown in **Figure 6C**, after 30 days of gavage, the average body weights of mice in the control group, FPNL (50, 100, and 200 mg/kg) groups, and PNL (200 mg/kg) groups were 22.94, 23.51, 22.73, and 22.16 g, respectively. The organ weight of the mice did not significantly change (**Table 3**). These results suggested that FPNL may improve the antifatigue function and exhibit no toxicity in the mice in the dose range used in this study.

The Effect of FPNL on LG, MDA, and BUN Levels

Liver glycogen content is one of the indicators of physical fatigue. After weight-loading swimming, the LG of mice was consumed, which makes fatigue occur. As shown in **Figure 7A**, the LG levels of mice in the FPNL and PNL were significantly higher than those in the control group ($P < 0.05$). Furthermore, the LG levels of

TABLE 2 | The variations in *P. notoginseng* leaves metabolites after fermented.

Name	VIP	*P*-value	Fold	Log
4′Hydroxyflurbiprofen	1.4236	0.000322	0.2550	−1.9712
Beta-leucine	1.4254	0.000140	0.2909	−1.7812
4-Hydroxystyrene	1.4244	0.00031	14.1641	3.8241
Deoxycytidine	1.4163	0.00027	0.0351	−4.8291
Piperidine	1.4214	0.00030	0.3596	−1.4752
Pyrocatechol	1.4226	0.000319	5.1849	2.3742
Artonin t	1.4218	0.000362	0.2299	−2.1204
3,3,5-Triiodothyronine-beta-glucuronoside	1.4214	0.00210	0.3509	−1.5107
Clenbuterol	1.4236	0.0002367	0.20421	−2.29187
Methylimidazoleacetic acid	1.3927	0.0001182	29.4480	4.8809
Proline	1.4248	0.0002815	3.46094	1.79116
Oxoproline	1.4214	0.0002703	0.16272	−2.61946
Citric acid	1.4212	0.0001197	0.118788	−3.07352
Ribothymidine	1.4240	0.0002998	0.32737	−1.61098
Hypogeic acid	1.4232	0.0002173	3.26973	1.70917
Fumaric acid	1.4107	0.0002565	0.067328	−3.89263
Isoleucine	1.1699	0.0002199	0.48346	−1.04850
Indolelactic acid	1.4203	0.0000845	53.38945	5.73841
Phenylacetic acid	1.4241	0.0001078	0.008551	−6.86956
Benzoic acid	1.4235	0.0002099	3.448989	1.786173
Oxypinnatanine	1.4225	0.0001560	0.457686	−1.275697
Shikimic acid	1.4244	0.0002616	0.583155	−0.778048
4-Hydroxybutyrate	1.2262	0.0000176	682.8043	9.41532
Sparfloxacin	1.4233	0.0002161	2.82629	1.49891
Erythrose 2	1.4237	0.0003457	4.366523	2.12648
Trans-aconitic acid	1.4185	0.0002928	0.359388	−1.476384
Succinic anhydride	1.4244	0.0001543	7.521064	2.910931
Fertaric acid	1.4232	0.00018291	0.272257	−1.876595
12-Oxo-2,3-dinor 10,15-phytodienoic acid	1.4191	0.00029548	2.504321	1.32443
Analyte	1.4247	0.00012273	0.09360	−3.417341

FPNL were significantly higher than PNL at the same dose (200 mg/kg) ($P < 0.05$).

The effects of FPNL and PNL on BUN and MDA levels in mice after swimming are shown in **Figures 7B,C**. The BUN level of the mice in the FPNL groups was significantly lower than the control group ($P < 0.05$). Additionally, compared to the PNL groups, the BUN level in the mice of the FPNL group at 200 mg/kg significantly decreased (**Figure 7B**). Malondialdehyde levels in the FPNL groups were also reduced significantly compared with the control group ($P < 0.05$) (**Figure 7C**), although there was no significant difference at concentrations of 50 and 100 mg/kg.

The Effect of FPNL on LD and LDH Levels in Mice

Lactic acid was produced after fatigue exercise. Compared with the control group, the LD level in the FPNL and PNL groups significantly decreased ($P < 0.05$) (**Figure 8A**). Moreover, the LD level of the FPNL groups was dramatically lower than the PNL at the same dose (200 mg/kg). The results illuminated that FPNL effectively impeded the accumulation of LD with a dose-dependent decrease and played a positive role in delaying fatigue.

Lactate dehydrogenase is a glycolytic enzyme that oxidizes LD into pyruvate. Therefore, LDH can be used as an indicator of fatigue level. The results showed that compared with the control group, the LDH content in mice with high- and medium-dose FPNL and PNL groups was significantly increased (**Figure 8B**). Furthermore, compared with the PNL, the LDH level of FPNL was significantly increased at the same dose (200 mg/kg). These results indicated that the FPNL could significantly increase the activity of LDH, accelerate the removal of LD, and improve the antifatigue ability of mice.

DISCUSSION

Panax notoginseng leaves as a new resource food approved by the China Ministry of Health, widely used in food processing. It showed the different effects of antioxidant, antidiabetes, and immunity (31–33). In this study, we reported for the first time that the co-fermentation of PNL by fungi and bacteria was enriched with saponins, phenolic acids, and amino acids, and found that FPNL may have strong antifatigue and antioxidant capacity. Moreover, FPNL could reduce ISO-induced damage to H9c2 myocardial cells by regulating the apoptotic pathway, prolong the weight-loading swimming time of mice, and exhibit antifatigue effects *in intro* and *in-vivo*.

Microbial fermentation is a common way to improve the nutrition and quality of foods (34, 35). Fermentation by a single strain can lead to a large accumulation of microbial metabolites, which in turn feedback to inhibit the synthesis of related enzymes and affect fermentation effectiveness. Although mixed fermentation was coordinated in growth and metabolism, some microorganisms such as yeasts can use metabolites to increase growth and eliminate feedback inhibition (36). In this study, single and mixed strains were used to ferment PNL. The results showed that the total saponin content of PNL was highest with co-fermented by *S. cerevisiae* and *B. subtilis* (**Supplementary Table 1**; **Supplementary Figure 1**). *S. cerevisiae* and *B. subtilis* are widely used as safety microorganisms in fermented foods. However, the long growth cycle of *S. cerevisiae* affects the supply and synthesis efficiency of food-grade functional factors, while *B. subtilis* has the advantages of a short growth period and fast growth rate. This implies that *B. subtilis* and *S. cerevisiae* have a synergistic and symbiotic effect during co-fermentation (37). *Bacillus subtilis* can secrete biological enzymes such as cellulase, amylase, and protease, which can decompose cellulose and other carbohydrates in plants. The oligosaccharides and monosaccharides produced after decomposition can be utilized by *S. cerevisiae*, thus eliminating the influence of the glucose inhibition effect and improving the fermentation efficiency. Meanwhile, co-fermentation can produce abundant metabolites that not only degrade macromolecular proteins into small peptides or amino acids, but also produce proteins that are more conducive to digestion and absorption (38). Therefore, in

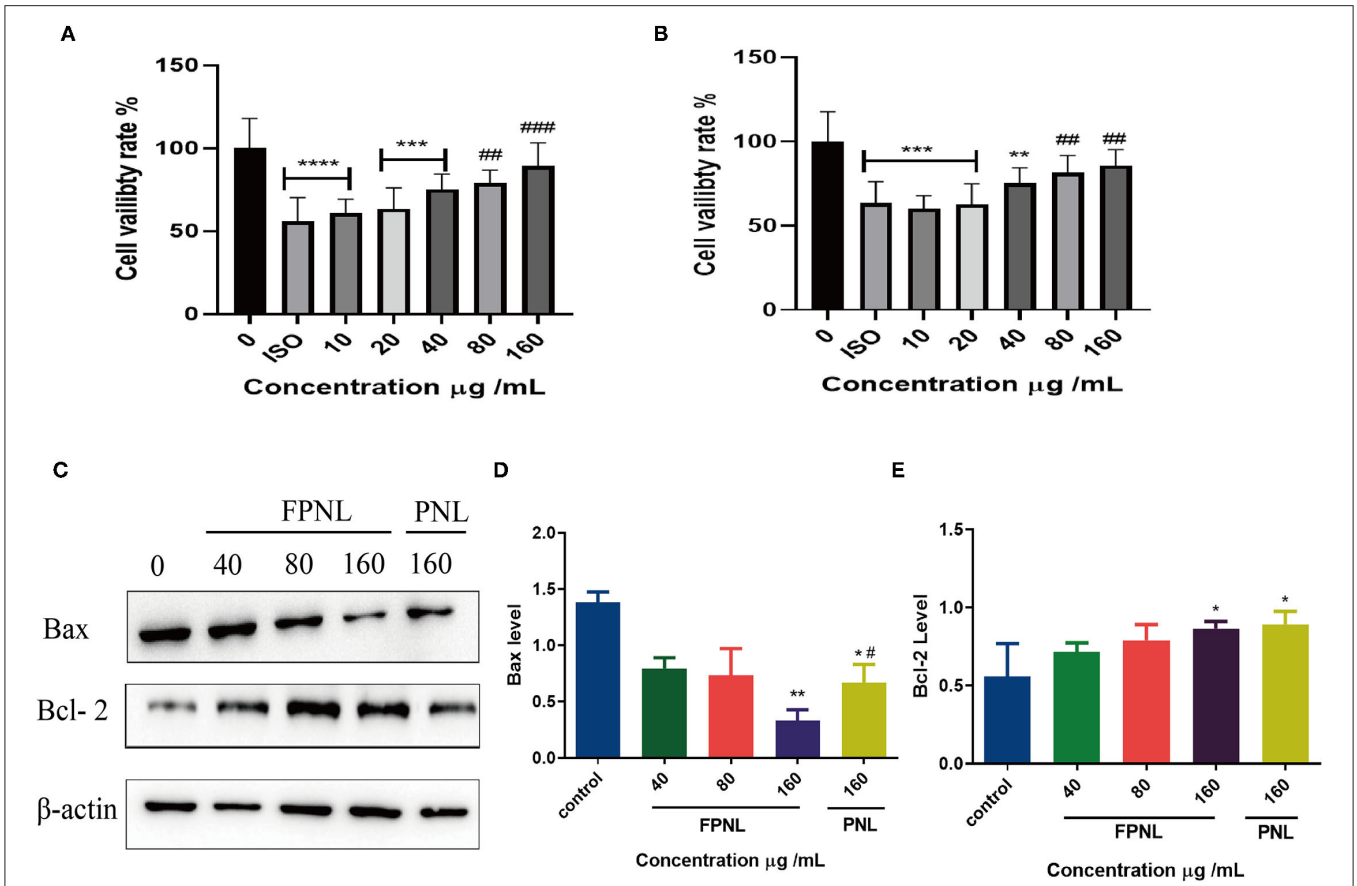

FIGURE 5 | The effect of PNL and FPNL on ISO-induced H9c2 cell apoptosis. **(A)** Alleviated of the proliferation of H9c2 cells by different concentrations of FPNL. **(B)** Alleviated of the proliferation of H9c2 cells by different concentrations of PNL. **(C–E)** Expression of apoptotic proteins (Bax, Bcl-2) in HCT116 cells. Data are expressed as mean ± SEM from three independent experiments ($n = 3$). $^{*}P < 0.05$, $^{**}P < 0.01$, $^{***}P < 0.001$, $^{****}P < 0.0001$ vs. control. $^{\#}P < 0.05$, $^{\#\#}P < 0.01$, $^{\#\#\#}P < 0.001$ vs. FPNL (160 μg/ml) group.

this study, *S. cerevisiae* and *B. subtilis* were used to co-ferment PNL to assess the antifatigue *in-vitro* and *in-vivo*.

Microbial fermentation not only secretes more enzymes to destroy plant cells and release active components, but it is also accompanied by the modification and transformation of plant active components. Some plant components can stimulate microorganisms to produce secondary metabolites. Through fermentation, various biomolecules such as phenolic compounds, saponins, flavor substances, organic acids, and pigments can be produced or enriched (34). As reported by Xia et al. (39), the antioxidant activities of soymilk are significantly enhanced due to the increase in phenolics and aglucone flavone after microbial fermentation. In the present study, organic phenolic acids in PNL, such as pyrocatechol, citric acid, benzoic acid, shikimic acid, were significantly increased by co-fermentation (**Table 2**), thus increasing the types and contents of phenolic acids in the FPNL. Studies have shown that these different phenolic acids have antifatigue effects (31, 32). In particular, pyrocatechol (40, 41) and citric acid (42) could significantly alleviate exercise fatigue by improving the antioxidant capacity.

Also, LC-MS/MS results showed that microorganisms also biotransformed the active substances in PNL through TCA cycle, glucose-alanine cycle and amino acid cycle (**Figure 4**). Specifically, two essential AAs (Isoleucine, Leucine) and six kinds of unessential AAs (Tyrosine, Valine Leucine Alanine, Glutamate Proline) were enriched during all the fermentation processes (**Table 2**). Previous studies have also shown that fermentation leads to changes in the amino acid content of *P. notoginseng* (43, 44). Thus, these changes in components of FPNL may improve its antifatigue effect.

In addition, microbial fermentation has shown significant advantages in the biosynthesis of triterpenoid saponins. It was shown that the level of saponins C-K increased six-fold in PNL after fermentation by *Lactobacillus brevis* M3 (45). Kim et al. (46) FPNL with *L. plantarum* M1 and found that the total ginsenosides content increased to 176.8 mg/g after 4 days. Our results also demonstrated that co-fermentation increased total saponins content in PNL (**Table 1**). The total saponins in PNL also showed potent antifatigue activity that prolonged the exhaustive swimming time of mice (27). In addition, some saponins of FPNL were altered in this study. The levles of

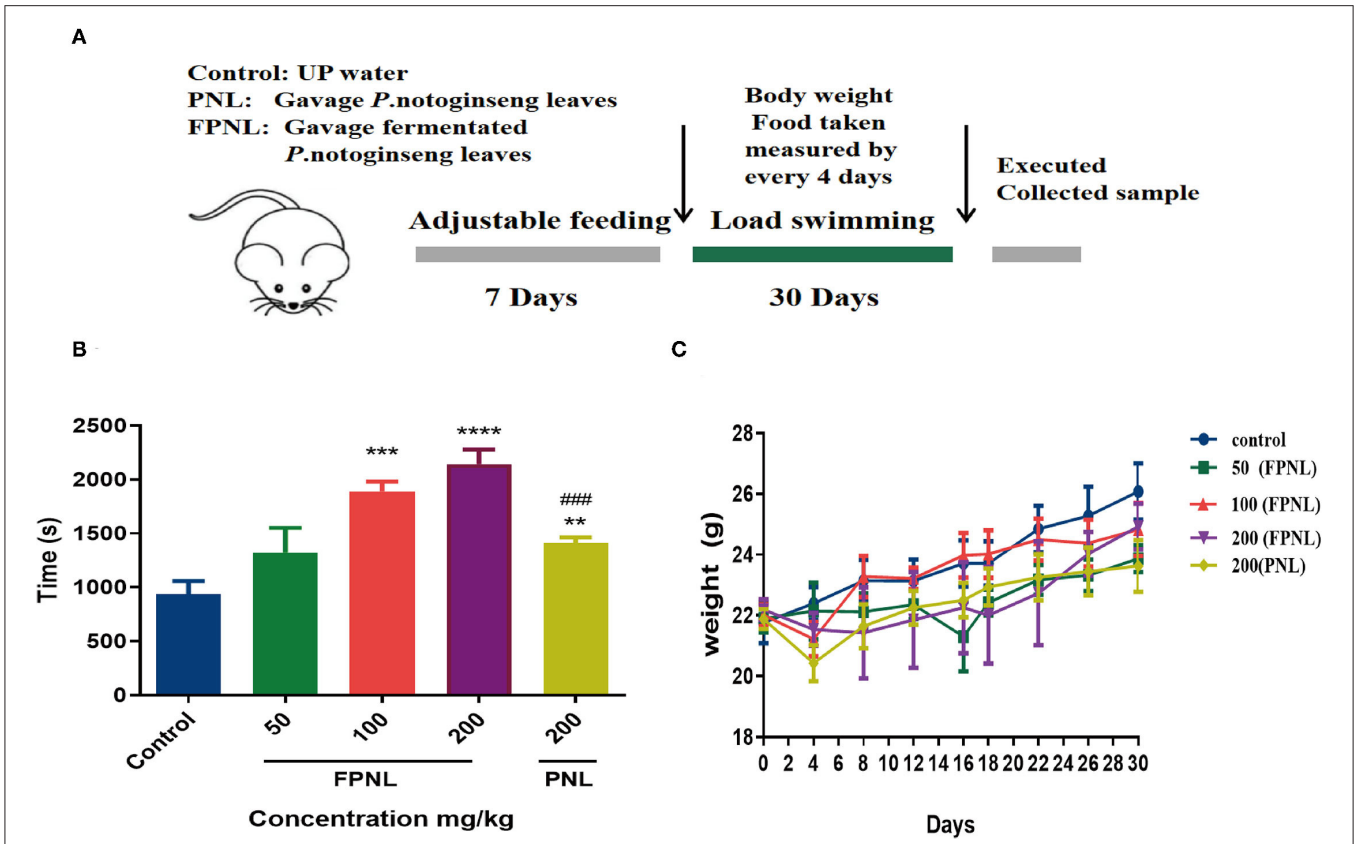

FIGURE 6 | Fermented *P. notoginseng* leaves alleviates fatigues in swimming mice. **(A)** Loading swimming experimental design. **(B)** Swimming time with weight loading after gavage PNL and FPNL. **(C)** Body weight, measured every 4 days. Data are expressed as mean ± SEM from six independent parallel experiments ($n = 6$). $^{**}P < 0.01$, $^{***}P < 0.001$, $^{****}P < 0.0001$ vs. control. $^{\#\#\#}P < 0.001$ vs. FPNL (200 mg/kg) group.

TABLE 3 | Organ weight of mice.

Orange weight	Control	FPNL		PNL	
(g)		50 (mg/kg)	100 (mg/kg)	200 (mg/kg)	200 (mg/kg)
Heart	0.23 ± 0.20	0.22 ± 0.13	0.21 ± 0.13	0.25 ± 0.12	0.24 ± 0.22
Liver	1.62 ± 0.1	1.65 ± 0.08	1.64 ± 0.14	1.67 ± 0.13	1.63 ± 0.17
Lungs	0.31 ± 0.15	0.33 ± 0.11	0.35 ± 0.16	0.38 ± 0.15	0.35 ± 0.18
Spleen	0.16 ± 0.2	0.19 ± 0.07	0.15 ± 0.11	0.17 ± 0.17	0.18 ± 0.15
Kidney	0.58 ± 0.13	0.60 ± 0.20	0.61 ± 0.12	0.63 ± 0.21	0.56 ± 0.14

R1 and Rg1 were increased, while the levels of Rb1 and Rb3 were decreased (**Figures 1B,C**; **Supplementary Table 2**). Some studies reported that Rb1 and Rg1 had significant antifatigue effects on hypoxia mice (28). Interestingly, R1 and Rg1 were 20 (S)—protopanaxatriol types (PPT), Rb1 and Rb3 were 20 (S)—protopanaxadiol types (PPD). Rb1 could be converted to R1 and Rg1, and Rg1 could be converted to Rb1 by biotransformation pathway after fermentation (47). Studies have shown that either PPT or PPD could improve the antifatigue ability of mice and prolong exercise time by modulating the levels of corticosterone, LD, and creatinine. However, the protective effect of the PPT was stronger than that of PPD (48). Our results also showed that R1 and Rg1 increased in FPNL (**Figure 1**; **Supplementary Table 2**).

Furthermore, plant components can also activate gene expression by altering microbial secondary metabolism pathways to produce new secondary metabolites. Wang et al. (25) found that *P. notoginseng* by steaming significantly altered the composition of saponins. After treatment, new saponins as 20S/R-Rh1, Rk3, Rh4, 20S/R-Rg3, Rk1, and Rg5 appeared. These new saponins are promising to improve hyperlipidemia. The Rg3 content of *P. notoginseng* roots was changed after fermentation (49). Similarly, changes were found in this study by HPLC result. Compared with the PNL group, some new

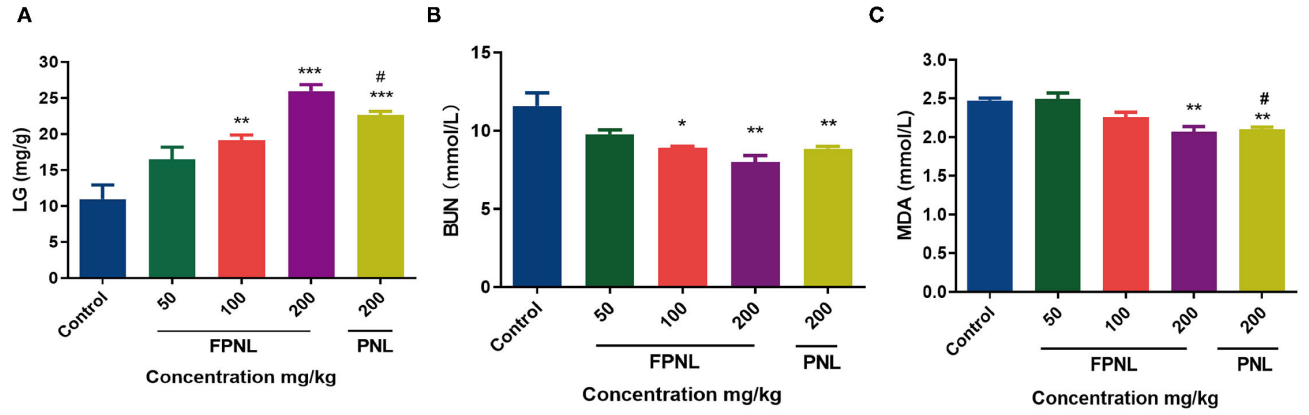

FIGURE 7 | Effect of fermented *P. notoginseng* leaves and *P. notoginseng* leaves on LG BUN, MDA level in serum. **(A)** The LG level in mice serum after swimming. **(B)** The BUN level in mice serum after swimming. **(C)** The MDA level in mice serum after swimming. Data are expressed as mean ± SEM from six independent experiments ($n = 6$). $^{*}P < 0.05$, $^{**}P < 0.01$, $^{***}P < 0.001$ vs. control. $^{\#}P < 0.05$ vs. FPNL (200 mg/kg) group.

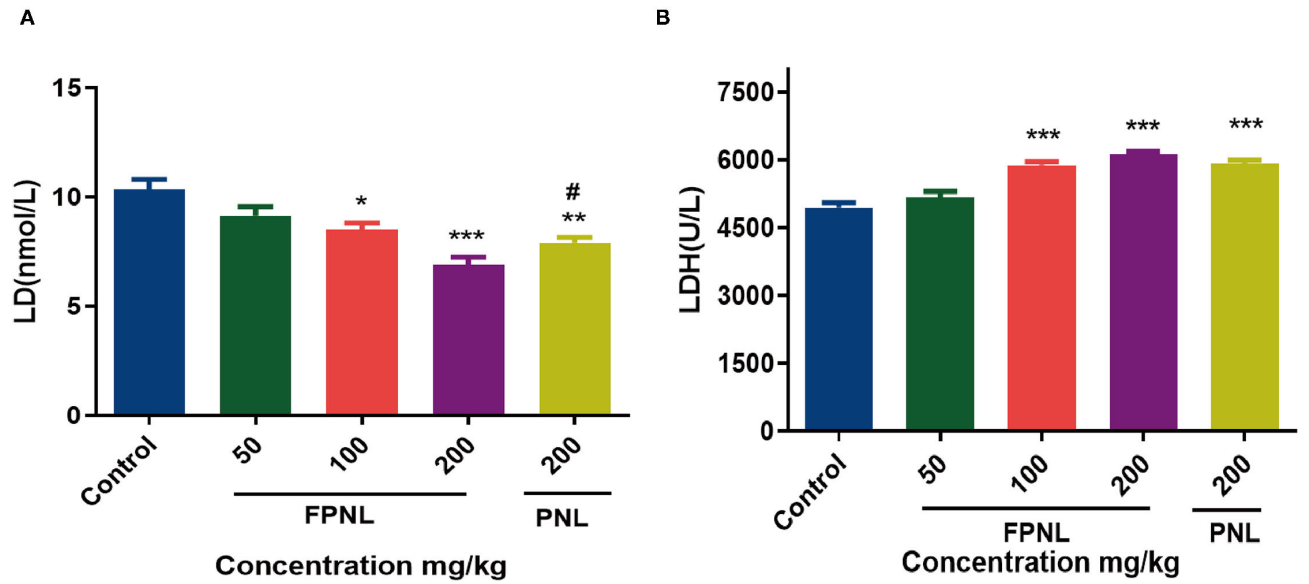

FIGURE 8 | Effect of fermented *P. notoginseng* leaves and *P. notoginseng* leaves on LD, LDH level in serum. **(A)** The LD level in mice serum after swimming. **(B)** The LDH level in mice serum after swimming. Data are expressed as mean ± SEM from six independent experiments ($n = 6$). $^{*}P < 0.05$, $^{**}P < 0.01$, $^{***}P < 0.001$ vs. control. $^{\#}P < 0.05$ vs. FPNL (200 mg/kg) group.

peak patterns appeared around the four saponins in the FPNL group, and these new peaks may be the saponins produced by biotransformation after co-fermentation (**Figure 1B**). Therefore, we can further determine the structures of these saponins by NMR spectrometry and spectrum technology, and explore the molecular mechanisms between saponins and antifatigue properties by molecular docking techniques in the future.

When oxidative factors rise, or the efficacy of antioxidant defenses falls in cells, oxidative stress increases, and oxidative stress negatively affects muscle contractility. Fatigue has been demonstrated to be closely related to free radicals (50). Oxidative stress in muscles severely interferes with muscle activity during exercise, reducing exercise performance or increasing fatigue (51). Our results showed that FPNL showed better oxidation stability than PNL (**Figure 2**). Isoproterenol is a catecholamine that can enhance cardiac contractility and cardiovascular systolic blood pressure by oxidative damage (52). Therefore, ISO is often used to induce myocardial fibrosis and heart failure models (53). *Panax notoginseng* leaves could protect against LPS-induced astrocyte damage by activating the Nrf2 pathway and antioxidant system to inhibit ROS, and showed no toxicity of cells (54). Jin et al. indicated that PNL (0–80 μg/ml) could protect H9c2 cells against hypoxia-reoxygenation-induced cell damage, accompanied by increased cell viability, reduced cell

apoptosis, and downregulation of LDH and MDA (55). Our study also found that different concentrations of FPNL significantly repaired ISO-induced damage in the $H9_C2$ myocardial cell model. Compared with the PNL group, the FPNL group showed a significant antifatigue effect on H9c2 cells. Moreover, the cell survival rate was above 80%, indicating that FPNL exhibited low toxicity to H9c2 cells (**Figures 5A,B**). Furthermore, the expression of the pro-apoptotic protein Bax in the cells tended to decrease. In contrast, the expression of the anti-apoptotic protein Bcl-2 was significantly increased in the FPNL group (**Figures 5C,D**). These results suggested that FPNL alleviated ISO-induced damage possibly driven by reducing oxidative damage and regulating the intrinsic apoptotic pathway.

In addition, the improvement of exercise-related endurance is the most visual indicator for the antifatigue effect of functional foods. The weight-loading swimming test has been widely used to evaluate exercise ability and validate the antifatigue effects of natural functional foods (56–58). Zhou et al. (28) found that PNL at dose of 0.42, 1.11, and 11.53 g/kg showed a significant effect on improving swimming time, and there was no apparent toxic effect on mice. Other studies have also suggested that PNL with gavage doses of 20–80 mg/kg showed antifatigue activity, prolonging the exhaustive swimming time in mice (27). Moreover, Yang et al. (59) gavaged mice at 1 or 2 g/kg/day for 30 days, and found that none of the mice died. In this study, FPNL showed a significant antifatigue effect on weight-loading swimming mice at the dose of 50–200 mg/kg (**Figure 6A**). In addition, each group had normal living habits, and there were no significant changes in organs or bodyweight of mice (**Figure 6C**; **Table 3**). It indicated that FPNL showed no toxicity on the mice and displayed harmless effects (**Figure 6**).

The primary energy used by organisms for exercise comes from decomposition fats and carbohydrates. Glycogen is the primary energy resource for the body during exercise (56). Glycogen is excess glucose in the body that accumulates and is stored in the liver. When the body needs energy, glycogen decomposes into glucose to produce energy (60). The increase in LG consumption has been associated with increased fatigue (27). In this study, 200 mg/kg of FPNL significantly improved LG reserve and slowed down the duration of fatigue in mice (**Figure 7A**). Blood urea nitrogen is the final ammonia product of human protein metabolism. Our study showed that the BUN levels in FPNL groups were significantly lower than those in PNL groups (**Figure 7B**). Several studies have shown that strenuous exercise could accelerate the production of free radicals and further induce oxidative damage. Malondialdehyde level is a typical indicator of the degree of lipid peroxidation (5). In this study, FPNL significantly reduced the MDA levels compared with the control and PNL groups, suggesting that FPNL could retarding MDA production. The overaccumulation of ammonia produced by amino acid metabolism could reduce endurance and lead to fatigue (**Figure 7C**). Lactic acid and LDH are the primary metabolites of glycolysis during exercise, which are the key indicators of physical fatigue (61). Excess LD could decrease the pH value and weaken muscle contraction strength. LDH could consume LD to relieve fatigue (62). In this study, we found that FPNL significantly reduced LD levels (**Figure 8A**). In contrast, FPNL increased LDH levels to clearance the LD in mice after exercise (**Figure 8B**). These results showed that FPNL shows a strong antifatigue effect by regulating oxidative factors *in-vivo*.

CONCLUSION

In this study, it was found that the contents of saponins, phenolic acids, flavonoids, and other active substances in PNL were significantly increased and showed good antioxidant stability capacity after co-fermentation by *S. cerevisiae* and *B. subtilis*. Moreover, FPNL could repair ISO-induced damage in H9c2 myocardial cells by reducing the expression of Bax and improving the expression of Bcl-2 to avoid cell apoptosis *in-vitro*. *In-vivo* experiments showed that FPNL could significantly improved the swimming-loading time and enhanced metabolic ability in mice by reducing the levels of BUN, MDA, and LD, and improving the levels of LG and LDH. This study strongly indicated that PNL co-fermented with *S. cerevisiae* and *B. subtilis* could improve exercise-related energy storage and alleviate fatigue.

DATA AVAILABILITY STATEMENT

The original contributions presented in the study are included in the article/**Supplementary Materials**, further inquiries can be directed to the corresponding author/s.

ETHICS STATEMENT

The animal study was reviewed and approved by Institutional Animal Ethical Committee of Yunnan Agricultural University (YNAU-201911017).

AUTHOR CONTRIBUTIONS

JS and YT supervised the study. YT, L-FL, LT, and MY designed experiments. MY, LT, C-CZ, Z-LW, Z-JY, WZ, and Y-LW performed experiments. MY wrote the manuscript. YT, L-FL, and LT reviewed the results and the manuscript. All authors contributed to the article and approved the submitted version.

FUNDING

This work was supported by Major Project of Science and Technology Department of Yunnan Province (202002AA100005 and 202102AE090027), YEFICRC Project of Yunnan Provincial Key Programs (2019ZG009), and Yunnan Province Young and Middle-aged Academic and Technical Leaders Reserve Talents Project (2018HB040).

SUPPLEMENTARY MATERIAL

The Supplementary Material for this article can be found online at: https://www.frontiersin.org/articles/10.3389/fnut.2022.824525/full#supplementary-material

REFERENCES

1. Huang LZ, Huang BK, Ye Q, Qin LP. Bioactivity-guided fractionation for anti-fatigue property of Acanthopanax senticosus. *J Ethnopharmacol.* (2011) 133:213–9. doi: 10.1016/j.jep.2010.09.032
2. Yang Q, Jin W, Lv X, Dai P, Ao Y, Wu M, et al. Effects of macamides on endurance capacity and anti-fatigue property in prolonged swimming mice. *Pharm Biol.* (2016) 54:827–34. doi: 10.3109/13880209.2015.1087036
3. Chen YM, Tsai YH, Tsai TY, Chiu YS, Wei L, Chen WC, et al. Fucoidan supplementation improves exercise performance and exhibits anti-fatigue action in mice. *Nutrients.* (2014) 7:239–52. doi: 10.3390/nu7010239
4. Huang WC, Chiu WC, Chuang HL, Tang DW, Lee ZM, Wei L, et al. Effect of curcumin supplementation on physiological fatigue and physical performance in mice. *Nutrients.* (2015) 7:905–21. doi: 10.3390/nu7020905
5. Narkhede AN, Jagtap SD, Nirmal PS, Giramkar SA, Nagarkar BE, Kulkarni OP, et al. Anti-fatigue effect of Amarkand on endurance exercise capacity in rats. *BMC Complement Altern Med.* (2016) 16:23. doi: 10.1186/s12906-016-0995-2
6. Yang Z, Sunil C, Jayachandran M, Zheng X, Cui K, Su Y, et al. Anti-fatigue effect of aqueous extract of Hechong (*Tylorrhynchus heterochaetus*) via AMPK linked pathway. *Food Chem Toxicol.* (2020) 135:111043. doi: 10.1016/j.fct.2019.111043
7. Yang Y, Ju Z, Yang Y, Zhang Y, Yang L, Wang Z. Phytochemical analysis of *Panax* species: a review. *J Ginseng Res.* (2021) 45:1–21. doi: 10.1016/j.jgr.2019.12.009
8. Liang W, Ge S, Yang L, Yang M, Ye Z, Yan M, et al. Ginsenosides Rb1 and Rg1 promote proliferation and expression of neurotrophic factors in primary Schwann cell cultures. *Brain Res.* (2010) 1357:19–25. doi: 10.1016/j.brainres.2010.07.091
9. Yang L, Deng Y, Xu S, Zeng X. *In vivo* pharmacokinetic and metabolism studies of *ginsenoside* Rd. *J Chromatogr B Analyt Technol Biomed Life Sci.* (2007) 854:77–84. doi: 10.1016/j.jchromb.2007.04.014
10. Ma J, Li W, Tian R, Lei W. *Ginsenoside* Rg1 promotes peripheral nerve regeneration in rat model of nerve crush injury. *Neurosci Lett.* (2010) 478:66–71. doi: 10.1016/j.neulet.2010.04.064
11. Lee YC, Wong WT, Li LH, Chu LJ, Menon MP, Ho CL, et al. Ginsenoside M1 induces apoptosis and inhibits the migration of human oral cancer cells. *Int J Mol Sci.* (2020) 21. doi: 10.3390/ijms21249704
12. Xia Y, Oyunsuren E, Yang Y, Shuang Q. Comparative metabolomics and microbial communities associated network analysis of black and white horse- sourced koumiss. *Food Chem.* (2021) 370:130996. doi: 10.1016/j.foodchem.2021.130996
13. Jia Y, Niu CT, Xu X, Zheng FY, Liu CF, Wang JJ, et al. Metabolic potential of microbial community and distribution mechanism of Staphylococcus species during broad bean paste fermentation. *Food Res Int.* (2021) 148:110533. doi: 10.1016/j.foodres.2021.110533
14. Lin YW, Mou YC, Su CC, Chiang BH. Antihepatocarcinoma activity of lactic acid bacteria fermented *Panax notoginseng*. *J Agric Food Chem.* (2010) 58:8528–34. doi: 10.1021/jf101543k
15. Nguyen BT, Bujna E, Fekete N, Tran ATM, Rezessy-Szabo JM, Prasad R, et al. Probiotic beverage from pineapple juice fermented with *Lactobacillus* and *Bifidobacterium Strains*. *Front Nutr.* (2019) 6:54. doi: 10.3389/fnut.2019.00054
16. Li Q, Wang Y, Cai G, Kong F, Wang X, Liu Y, et al. Antifatigue activity of liquid cultured *Tricholoma matsutake* mycelium partially via regulation of antioxidant pathway in mouse. *Biomed Res Int.* (2015) 2015:562345. doi: 10.1155/2015/562345
17. Kim KM, Yu KW, Kang DH, Suh HJ. Anti-stress and anti-fatigue effect of fermented rice bran. *Phytother Res.* (2002) 16:700–2. doi: 10.1002/ptr.1019
18. Vongsangnak W, Gua J, Chauvatcharin S, Zhong J-J. Towards efficient extraction of notoginseng saponins from cultured cells of *Panax notoginseng*. *Biochem Eng J.* (2004) 18:115–20. doi: 10.1016/s1369-703x(03)00197-9
19. Nascimento RPD, Machado A, Lima VS, Moya A, Reguengo LM, Bogusz Junior S, et al. Chemoprevention with a tea from hawthorn (*Crataegus oxyacantha*) leaves and flowers attenuates colitis in rats by reducing inflammation and oxidative stress. *Food Chem X.* (2021) 12:100139. doi: 10.1016/j.fochx.2021.100139
20. Tsikrika K, Muldoon A, O'Brien NM, Rai DK. High-pressure processing on whole and peeled potatoes: influence on polyphenol oxidase, antioxidants, and glycaemic indices. *Foods.* (2021) 10:2425. doi: 10.3390/foods10102425
21. Moreno Gracia B, Laya Reig D, Rubio-Cabetas MJ, Sanz Garcia MA. Study of phenolic compounds and antioxidant capacity of spanish almonds. *Foods.* (2021) 10:2334. doi: 10.3390/foods10102334
22. Rakmai J, Cheirsilp B, Mejuto JC, Torrado-Agrasar A, Simal-Gándara J. Physico-chemical characterization and evaluation of bio-efficacies of black pepper essential oil encapsulated in hydroxypropyl-beta-cyclodextrin. *Food Hydrocoll.* (2017) 65:157–64. doi: 10.1016/j.foodhyd.2016.11.014
23. Zhang Y, Wu X, Wang X, Zeng Y, Liao Y, Zhang R, et al. Grey relational analysis combined with network pharmacology to identify antioxidant components and uncover its mechanism from moutan cortex. *Front Pharmacol.* (2021) 12:748501. doi: 10.3389/fphar.2021.748501
24. Wan J-B, Li P, Yang R-L, Zhang Q-W, Wang Y-T. SEPARATION AND PURIFICATION OF 5 SAPONINS FROM *PANAX NOTOGINSENG* BY PREPARATIVE HIGH-PERFORMANCE LIQUID CHROMATOGRAPHY. *J Liq Chromatogr Relat Technol.* (2013) 36:406–17. doi: 10.1080/10826076.2012.657736
25. Wang Q, Mu RF, Liu X, Zhou HM, Xu YH, Qin WY, et al. Steaming changes the composition of saponins of *Panax notoginseng* (Burk) FH Chen that function in treatment of hyperlipidemia and obesity. *J Agric Food Chem.* (2020) 68:4865–75. doi: 10.1021/acs.jafc.0c00746
26. Chen X, Ma L, Shao M, Wang Q, Jiang Q, Guo D, et al. Exploring the protective effects of PNS on acute myocardial ischaemia-induced heart failure by Transcriptome analysis. *J Ethnopharmacol.* (2021) 271:113823. doi: 10.1016/j.jep.2021.113823
27. Yong-xin X, Jian-jun Z. Evaluation of anti-fatigue activity of total saponins of Radix notoginseng. *Indian J Med Res.* (2013) 137:151–5. doi: 10.1051/jp4:2004118040
28. Zhou S, Wang Y, Tian H, Huang Q, Gao Y, Zhang G. Anti-fatigue effects of *Panax notoginseng* in simulation plateau-condition mice. *Pharmacogn Mag.* (2012) 8:197–201. doi: 10.4103/0973-1296.99284
29. Yang M, Li WY, Xie J, Wang ZL, Wen YL, Zhao CC, et al. Astragalin inhibits the proliferation and migration of human colon cancer HCT116 Cells by regulating the NF-kappaB signaling pathway. *Front Pharmacol.* (2021) 12:639256. doi: 10.3389/fphar.2021.639256
30. Kacem M, Borji R, Sahli S, Rebai H. The disturbing effect of neuromuscular fatigue on postural control is accentuated in the premenstrual phase in female athletes. *Front Physiol.* (2021) 12:736211. doi: 10.3389/fphys.2021.736211
31. Jiang DQ, Guo Y, Xu DH, Huang YS, Yuan K, Lv ZQ. Antioxidant and anti-fatigue effects of anthocyanins of mulberry juice purification (MJP) and mulberry marc purification (MMP) from different varieties mulberry fruit in China. *Food Chem Toxicol.* (2013) 59:1–7. doi: 10.1016/j.fct.2013.05.023
32. Wu C, Chen R, Wang XS, Shen B, Yue W, Wu Q. Antioxidant and anti-fatigue activities of phenolic extract from the seed coat of Euryale ferox Salisb. and identification of three phenolic compounds by LC-ESI-MS/MS. *Molecules.* (2013) 18:11003–21. doi: 10.3390/molecules180911003
33. Dai CY, Liu PF, Liao PR, Qu Y, Wang CX, Yang Y, et al. Optimization of flavonoids extraction process in *Panax notoginseng* stem leaf and a study of antioxidant activity and its effects on mouse melanoma B16 cells. *Molecules.* (2018) 23:2219. doi: 10.3390/molecules23092219
34. Yin L, Zhang Y, Wang L, Wu H, Azi F, Tekliye M, et al. Neuroprotective potency of a soy whey fermented by *Cordyceps militaris* SN-18 against hydrogen peroxide-induced oxidative injury in PC12 cells. *Eur J Nutr.* (2021) 61:115–61. doi: 10.1007/s00394-021-02679-w
35. Wu H, Liu H-N, Ma -M, Zhou J-Z, Xia X-D. Synergetic effects of *Lactobacillus plantarum* and *Rhizopus oryzae* on physicochemical, nutritional and antioxidant properties of whole-grain oats (*Avena sativa* L.) during solid-state fermentation. *Lwt.* (2022) 154:112687. doi: 10.1016/j.lwt.2021.112687
36. Kalyani D, Lee K-M, Kim T-S, Li J, Dhiman SS, Kang YC, et al. Microbial consortia for saccharification of woody biomass and ethanol fermentation. *Fuel.* (2013) 107:815–22. doi: 10.1016/j.fuel.2013.01.037
37. Liu Y, Su A, Tian R, Li J, Liu L, Du G. Developing rapid growing *Bacillus subtilis* for improved biochemical and recombinant protein production. *Metab Eng Commun.* (2020) 11:e00141. doi: 10.1016/j.mec.2020.e00141
38. Pagana I, Morawicki R, Hager TJ. Lactic acid production using waste generated from sweet potato processing. *Int J Food Sci Technol.* (2014) 49:641–9. doi: 10.1111/ijfs.12347

39. Xia X, Dai Y, Wu H, Liu X, Wang Y, Yin L, et al. Kombucha fermentation enhances the health-promoting properties of soymilk beverage. *J Funct Foods.* (2019) 62:103549. doi: 10.1016/j.jff.2019.103549
40. Haramizu S, Ota N, Hase T, Murase T. Catechins suppress muscle inflammation and hasten performance recovery after exercise. *Med Sci Sports Exerc.* (2013) 45:1694–702. doi: 10.1249/MSS.0b013e31828de99f
41. Chen S, Minegishi Y, Hasumura T, Shimotoyodome A, Ota N. Involvement of ammonia metabolism in the improvement of endurance performance by tea catechins in mice. *Sci Rep.* (2020) 10:6065. doi: 10.1038/s41598-020-63139-9
42. Sugino T, Aoyagi S, Shirai T, Kajimoto Y, Kajimoto O. Effects of citric acid and l-carnitine on physical fatigue. *J Clin Biochem Nutr.* (2007) 41:224–30. doi: 10.3164/jcbn.2007032
43. Jowko E, Sadowski J, Dlugolecka B, Gierczuk D, Opaszowski B, Cieslinski I. Effects of *Rhodiola rosea* supplementation on mental performance, physical capacity, and oxidative stress biomarkers in healthy men. *J Sport Health Sci.* (2018) 7:473–80. doi: 10.1016/j.jshs.2016.05.005
44. Messina OD, Vidal Wilman M, Vidal Neira LF. Nutrition, osteoarthritis and cartilage metabolism. *Aging Clin Exp Res.* (2019) 31:807–13. doi: 10.1007/s40520-019-01191-w
45. Kim SH, Kim SY, Lee H, Ra KS, Suh HJ, Kim SY, et al. Transformation of ginsenoside-rich fraction isolated from ginseng (*Panax ginseng)* leaves induces compound K. *Food Sci Biotechnol.* (2011) 20:1179–86. doi: 10.1007/s10068-011-0163-x
46. Kim B-G, Choi S-Y, Kim M-R, Suh HJ, Park HJ. Changes of ginsenosides in Korean red ginseng (*Panax ginseng*) fermented by *Lactobacillus plantarum* M1. *Process Biochemistry.* (2010) 45:1319–24. doi: 10.1016/j.procbio.2010.04.026
47. Zhou X, Chen LL, Xie RF, Lam W, Zhang ZJ, Jiang ZL, et al. Chemosynthesis pathway and bioactivities comparison of saponins in radix and flower of *Panax notoginseng* (Burk) FH Chen. *J Ethnopharmacol.* (2017) 201:56–72. doi: 10.1016/j.jep.2016.11.008
48. Oh HA, Kim DE, Choi HJ, Kim NJ, Kim DH. Anti-fatigue effects of 20(S)-protopanaxadiol and 20(S)-protopanaxatriol in mice. *Biol Pharm Bull.* (2015) 38:1415–9. doi: 10.1248/bpb.b15-00230
49. Shin NR, Bose S, Choi Y, Kim YM, Chin YW, Song EJ, et al. Anti-obesity effect of fermented *Panax notoginseng* is mediated via modulation of appetite and gut microbial population. *Front Pharmacol.* (2021) 12:665881. doi: 10.3389/fphar.2021.665881
50. Chen X, Liang D, Huang Z, Jia G, Zhao H, Liu G. Anti-fatigue effect of quercetin on enhancing muscle function and antioxidant capacity. *J Food Biochem.* (2021) 45:e13968. doi: 10.1111/jfbc.13968
51. Xiaoming W, Ling L, Jinghang Z. Antioxidant and anti-fatigue activities of flavonoids from *Puerariae radix*. *Afr J Tradit Complement Altern Med.* (2012) 9:221–7. doi: 10.4314/ajtcam.v9i2.6
52. Li Y, Ma L, Gu S, Tian J, Cao Y, Jin Z, et al. UBE3A alleviates isoproterenol-induced cardiac hypertrophy through the inhibition of the TLR4/MMP-9 signaling pathway. *Acta Biochim Biophys Sin (Shanghai).* (2020) 52:58–63. doi: 10.1093/abbs/gmz119
53. Jensen BC, O'Connell TD, Simpson PC. Alpha-1-adrenergic receptors in heart failure: the adaptive arm of the cardiac response to chronic catecholamine stimulation. *J Cardiovasc Pharmacol.* (2014) 63:291–301. doi: 10.1097/FJC.0000000000000032
54. Zhou N, Tang Y, Keep RF, Ma X, Xiang J. Antioxidative effects of *Panax notoginseng* saponins in brain cells. *Phytomedicine.* (2014) 21:1189–95. doi: 10.1016/j.phymed.2014.05.004
55. Jin Z, Gan C, Luo G, Hu G, Yang X, Qian Z, et al. Notoginsenoside R1 protects hypoxia-reoxygenation deprivation-induced injury by upregulation of miR-132 in H9c2 cells. *Hum Exp Toxicol.* (2021) 40:S29–38. doi: 10.1177/09603271211025589
56. Tan W, Yu KQ, Liu YY, Ouyang MZ, Yan MH, Luo R, et al. Anti-fatigue activity of polysaccharides extract from Radix Rehmanniae Preparata. *Int J Biol Macromol.* (2012) 50:59–62. doi: 10.1016/j.ijbiomac.2011.09.019
57. Qiang F. Effect of malate-oligosaccharide solution on antioxidant capacity of endurance athletes. *Open Biomed Eng J.* (2015) 9:326–9. doi: 10.2174/1874120701509010326
58. Yang BZ, Mallory JM, Roe DS, Brivet M, Strobel GD, Jones KM, et al. Carnitine/acylcarnitine translocase deficiency (neonatal phenotype): successful prenatal and postmortem diagnosis associated with a novel mutation in a single family. *Mol Genet Metab.* (2001) 73:64–70. doi: 10.1006/mgme.2001.3162
59. Yang YQ, Li YQ, Yu LP, Li X, Mu JK, Shang J, et al. Muscle fatigue-alleviating effects of a prescription composed of Polygonati rhizoma and notoginseng radix et rhizoma. *Biomed Res Int.* (2020) 2020:3963045. doi: 10.1155/2020/3963045
60. Loureiro LMR, Dos Santos Neto E, Molina GE, Amato AA, Arruda SF, Reis CEG, et al. Coffee increases post-exercise muscle glycogen recovery in endurance athletes: a randomized clinical trial. *Nutrients.* (2021) 13:3335. doi: 10.3390/nu13103335
61. Wang X, Qu Y, Zhang Y, Li S, Sun Y, Chen Z, et al. Antifatigue potential activity of *Sarcodon imbricatus* in acute excise-treated and chronic fatigue syndrome in mice via regulation of Nrf2-mediated oxidative stress. *Oxid Med Cell Longev.* (2018) 2018:9140896. doi: 10.1155/2018/9140896
62. Zhong L, Zhao L, Yang F, Yang W, Sun Y, Hu Q. Evaluation of anti-fatigue property of the extruded product of cereal grains mixed with Cordyceps militaris on mice. *J Int Soc Sports Nutr.* (2017) 14:15. doi: 10.1186/s12970-017-0171-1

Conflict of Interest: The authors declare that the research was conducted in the absence of any commercial or financial relationships that could be construed as a potential conflict of interest.

Publisher's Note: All claims expressed in this article are solely those of the authors and do not necessarily represent those of their affiliated organizations, or those of the publisher, the editors and the reviewers. Any product that may be evaluated in this article, or claim that may be made by its manufacturer, is not guaranteed or endorsed by the publisher.

frontiers in Nutrition

ORIGINAL RESEARCH
published: 28 February 2022
doi: 10.3389/fnut.2022.831243

Integrated Microbiomic and Metabolomic Dynamics of Fermented Corn and Soybean By-Product Mixed Substrate

Cheng Wang[1,2,3,4,5], *Siyu Wei*[1,2,3,4,5], *Mingliang Jin*[1,2,3,4,5], *Bojing Liu*[1,2,3,4,5], *Min Yue*[6] *and Yizhen Wang*[1,2,3,4,5*]

[1] National Engineering Laboratory for Feed Safety and Pollution Prevention and Controlling, Hangzhou, China, [2] Key Laboratory of Molecular Animal Nutrition, Ministry of Education, Hangzhou, China, [3] Key Laboratory of Animal Nutrition and Feed Science (Eastern of China), Ministry of Agriculture and Rural Affairs, Hangzhou, China, [4] Key Laboratory of Animal Feed and Nutrition of Zhejiang Province, Hangzhou, China, [5] Institute of Feed Science, Zhejiang University, Hangzhou, China, [6] Institute of Preventive Veterinary Sciences and Department of Veterinary Medicine, Zhejiang University College of Animal Sciences, Hangzhou, China

OPEN ACCESS

Edited by:
Yu Xiao,
Hunan Agricultural University, China

Reviewed by:
Fei Xia,
Shaanxi University of Science and Technology, China
Dingfu Xiao,
Independent Researcher, Changsha, China
Liang Zhao,
Washington State University, United States
Xi Ma,
China Agricultural University, China

***Correspondence:**
Yizhen Wang
yizhenwang321@zju.edu.cn

Specialty section:
This article was submitted to Food Chemistry, a section of the journal Frontiers in Nutrition

Received: *08 December 2021*
Accepted: *21 January 2022*
Published: *28 February 2022*

Citation:
Wang C, Wei S, Jin M, Liu B, Yue M and Wang Y (2022) Integrated Microbiomic and Metabolomic Dynamics of Fermented Corn and Soybean By-Product Mixed Substrate. Front. Nutr. 9:831243. doi: 10.3389/fnut.2022.831243

Microbes and their metabolites produced in fermented food have been considered as critical contributors to the quality of the final products, but the comprehensive understanding of the microbiomic and metabolomic dynamics in plant-based food during solid-state fermentation remains unclear. Here, the probiotics of *Bacillus subtilis* and *Enterococcus faecalis* were inoculated into corn and defatted soybean to achieve the two-stage solid-state fermentation. A 16S sequencing and liquid chromatography–tandem mass spectrometry were applied to investigate the dynamics of microbiota, metabolites, and their integrated correlations during fermentation. The results showed that the predominant bacteria changed from *Streptophyta and Rickettsiales* at 0 h to *Bacillus* and *Pseudomonas* in aerobic stage and then to *Bacillus*, *Enterococcus*, and *Pseudomonas* in anaerobic stage. In total, 229 notably different metabolites were identified at different fermentation times, and protein degradation, amino acid synthesis, and carbohydrate metabolism were the main metabolic pathways during the fermentation. Notably, phenylalanine metabolism was the most important metabolic pathway in the fermentation process. Further analysis of the correlations among the microbiota, metabolites, and physicochemical characteristics indicated that *Bacillus* spp. was significantly correlated with amino acids and carbohydrate metabolism in aerobic stage, and *Enterococcus* spp. was remarkably associated with amino acids metabolism and lactic acid production in the anaerobic stage. The present study provides new insights into the dynamic changes in the metabolism underlying the metabolic and microbial profiles at different fermentation stages, and are expected to be useful for future studies on the quality of fermented plant-based food.

Keywords: fermentation, metabolomic analyses, dynamics, microbiomic data, plant-based food by-product

INTRODUCTION

Corn is one of the main grains produced worldwide, providing 30% of food calories for more than 4.5 billion people worldwide, and is considered to be the main staple food in most countries (1, 2). Whereas, compared with other cereal crops, the nutritional value of corn is low, lacking essential amino acids and lysine (3). Soy-derived foods have been consumed for centuries, especially in Asian diets. But soy products contain isoflavones, antigen proteins, and fiber substances that are not easy to be absorbed, which affect their bioavailability (4, 5). Therefore, many processing technologies like physical and chemical methods have been applied to corn and soybean-based foods to enhance the nutritional value of the final products. However, these processing tools are un-environmental friendly and lose nutrients (6).

Fermentation is one of the traditional biotechnologies in the food field because it makes a solid foundation for the development of safe food with better nutrition and functions. It is a natural way to preserve food, increase nutritional value and digestibility, and reduce anti-nutritional factors. Fermenting microbes like *Bacillus* and *Aspergillus* can degrade anti-nutritional factors and improve food quality (7, 8). Lactic acid bacteria can produce organic acids, improve food flavor, and lengthen storage time (9, 10). In the past few years, many studies have been conducted on fermentation to obtain fermented corn-based products that are beneficial to human health (11–13). In addition, fermentation has been used to improve the bioavailability of protein, vitamins, minerals, and isoflavones in soybeans, as well as to change their flavor, improve stability, and even create novel foods (14–17). Natto, fermented bean curd, Miso, and soy sauce have a long history in the Asian diet. It has been reported that these traditional fermented soybean-based foods can improve bone health, reduce the risk of cancer, and prevent the progression of diabetes (18).

Fermentation is conducted through the action of various microorganisms under open or semi-open conditions, including starters and local microorganisms, and plays important roles in anti-nutritional factor degradation, nutrition improvement, and flavor production (19, 20). At present, high-throughput sequencing provides a reliable method for the comprehensive description of microbial community dynamics and expands our understanding of the microbial community structure of fermented corn and soybean products. The latest research showed that *Lactococcus*, *Streptococcus*, *Enterobacter*, *Acinetobacter,* and fungi such as *Trichosporon* and *Aspergillus* are common fermenting microbes in Sufu flora (21). In addition, microbial abundance is mainly related to nutritional characteristics. Besides, metabolomics methods such as gas chromatography (GC), mass spectrometry (MS), and high-performance liquid chromatography (HPLC) have been applied to determine the metabolite profiles of fermented foods (22, 23). However, the comprehensive dynamic changes of microbes and metabolites during plant-based food fermentation still lack understanding, especially in corn and defatted soybean. Here, corn and defatted soybean were carried out with a two-stage solid-state fermentation inoculating with *Bacillus subtilis* and *Enterococcus faecalis*. A 16S rRNA sequencing and liquid chromatography–mass spectrometry (LC/MS) were used to explore the microbial and metabolic dynamics during the fermentation. The evidence will expand our knowledge of improving the quality of fermented plant-based food from an integrated microbiomic and metabolomic perspective.

MATERIALS AND METHODS

Experimental Design and Sampling

Bacillus subtilis (NCBI Accession No. MH885533, CGMCC No:12825) and *Enterococcus faecalis* (NCBI Accession No. MN038173, CGMCC 1.15424) were cultured, respectively, in Luria broth and de Man, Rogosa, and Sharpe liquid medium at 37°C, as described in detail by Wang et al. (24). About 200 g of the substrates contained 40% of defatted soybean, 40% of corn, and 20% of yellow wine lees were transferred into a 500 mL Erlenmeyer flask. Sterilized water was added to achieve a 40% moisture concentration. *B. subtilis* (1×10^7 CFU/g) was inoculated in the mixed substrate at 37°C for 24 h in aerobic fermentation, and then *E. faecalis* (2×10^7 CFU/g) was inoculated in the fermented substrate with an anaerobic fermentation at 37°C until 48 h. Samples were collected at 0, 12, 24, and 48 h. The nutrition determination of the fermented matrix is shown in **Supplementary Table S1**.

The Measurement of Nutritional Content

Moist samples (∼100 g) at 0, 12, 24, and 48 h were collected to determine the numbers of microorganisms and microbial metabolites and for 16S rRNA gene sequencing, and the remaining samples were dried at 60°C for 24 h, cooled, ground, and subjected to physicochemical analysis. Dried samples were collected for further analysis of the crude protein (CP), neutral detergent fiber (NDF), acid detergent fiber (ADF), and amylose contents using AOAC International guidelines (25). The content of phytate phosphorus was analyzed according to the method described by Shi et al. (26). The pH of the fermented product was determined with a pH meter (Mettler Toledo, Switzerland) according to a previous study (27). Lactate was detected using a lactic acid assay kit (Nanjing Jiancheng Bioengineering Institute, Nanjing) following the manufacturer's instructions. The contents of antigenic protein were analyzed using a commercial kit (Jiangsu Meibiao Biological Technology Co., Jiangsu, China).

Liquid Chromatography–Mass Spectrometry Analysis and Data Processing

A 50 mg of the sample was weighted to an EP tube, and 1,000 μL extract solution (methanol:acetonitrile:water = 2:2:1, with isotopically labeled internal standard mixture) was added. Then the samples were homogenized at 35 Hz for 4 min and sonicated for 5 min in ice water bath. The homogenization and sonication cycle was repeated 3 times. Then the samples were incubated for 1 h at −40°C and centrifuged at 12,000 rpm for 15 min at 4°C. The resulting supernatant was transferred to a fresh glass vial for analysis. The quality control (QC) sample was prepared

by mixing an equal aliquot of the supernatants from all of the samples.

LC–MS/MS analyses were performed using a UHPLC system (Vanquish, Thermo Fisher Scientific) with a UPLC BEH Amide column (2.1 mm × 100 mm, 1.7 μm) coupled to Q Exactive HFX mass spectrometer (Orbitrap MS, Thermo). The mobile phase consisted of 25 mmol/L ammonium acetate and 25 ammonia hydroxide in water (pH = 9.75) (A) and acetonitrile (B). The auto-sampler temperature was 4°C, and the injection volume was 3 μL. The QE HFX mass spectrometer was used for its ability to acquire MS/MS spectra on information-dependent acquisition (IDA) mode in the control of the acquisition software (Xcalibur, Thermo). In this mode, the acquisition software continuously evaluates the full scan MS spectrum. The ESI source conditions were set as follows: sheath gas flow rate as 30 Arb, Aux gas flow rate as 25 Arb, capillary temperature 350°C, full MS resolution as 60,000, MS/MS resolution as 7,500, collision energy as 10/30/60 in NCE mode, spray Voltage as 3.6 kV (positive) or −3.2 kV (negative), respectively.

The raw data were converted to the mzXML format using ProteoWizard and processed with an in-house program, which was developed using R and based on XCMS, for peak detection, extraction, alignment, and integration. Then an in-house MS2 database (BiotreeDB) was applied in metabolite annotation. The cutoff for annotation was set at 0.3. The obtained data were conducted to principal component analysis (PCA), Partial Least Squares Discriminant Analysis (PLS-DA), and orthogonal partial least squares discriminant analysis (OPLS-DA). The goodness-of-fit parameter (R2) and the predictive ability parameter (Q2) were used to evaluate the quality of PLS-DA and OPLS-DA models. Variable importance projection (VIP) > 1.0 and $P < 0.05$ were identified as the differential metabolites. To further interpret the biological significance of metabolites, metabolic pathway analyses were performed by an online analysis platform in the MetaboAnalyst 5.0 (https://www.metaboanalyst.ca/). KEGG analysis has been conducted by enrichment analysis sections of MetaboAnalyst.

Bioinformatics Analysis of Sequencing Data

Total DNA was extracted from 16 samples using the E.Z.N.A. soil DNA kit (Omega Bio-Tek, Norcross, GA, United States). A NanoDrop 2,000 UV–vis spectrophotometer (Thermo Scientific, Wilmington, DE, United States) and 1% agarose gel electrophoresis were used to analyze DNA content and quality.

The MiSeq platform (Personal Biotechnology Co., Ltd, Shanghai, China) was used to describe the bacterial community based on the gene segment from the the V3-V4 gene regions of the bacterial 16S rRNA gene primers 338F (5′-ACTCCTACGGGAGGCAGCAG-3′) and 806R (5′-GGACTACHVGGGTWTCTAAT-3′). PCR was conducted as follows: 3 min of denaturation at 95°C; 27 cycles of 30 s at 95°C, 30 s for annealing at 55°C, and 45 s for elongation at 72°C; and a final extension at 72°C for 10 min. The AxyPrep DNA gel extraction kit (Axygen Biosciences, Union City, CA, United States) and QuantiFluor-ST instrument (Promega, United States) were used to further extract, purify, and quantify the PCR products. Subsequently, raw Illumina FASTQ files were demultiplexed, quality filtered, and analyzed using Quantitative Insights into Microbial Ecology (QIIME v1.9.1). Raw fastq files were quality filtered by Trichromatic and merged by FLASH. OTUs were clustered with a 97% similarity cutoff using UPARSE (version 7.1). The taxonomy of each 16S rRNA gene sequence was analyzed using the RDP Classifier algorithm (http://rdp.cme.msu.edu/) against the Silvia 16S rRNA database using a confidence threshold of 70%. The assembled MiSeq sequences were submitted to the NCBI's Sequence Read Archive (SRA BioProject no. PRJNA552228) for open access. Estimates of diversity values for these samples using the Chao1, Shannon, and Simpson indexes for diversity estimation were calculated by rarefaction analysis. Nonmetric Multidimensional Scaling (NMDS) and cluster analysis with the ANOSIM method were conducted using the Web server tool METAGENassist based on unweighted UniFrac distances.

The main differentially abundant genera were selected by the LEfSe method (https://huttenhower.sph.harvard.edu/galaxy/). To predict metabolic genes during the process, PICRUSt (https://huttenhower.sph.harvard.edu/galaxy/) was applied to obtain a functional profile from the 16S rRNA data. Before metagenome prediction, the OTUs of 16S rRNA sequences were analyzed using PICRUSt. PICRUSt and KEGG were used to obtain functions for the genes that were predicted to be present in the samples and to assign the genes into metabolic pathways.

Spearman's rank correlation coefficient was calculated with R version 3.6.3 to evaluate the relationship among physicochemical characteristics, microbiota, and metabolites.

Statistical Analysis

All the data were presented as means ± SEM ($N = 4$ for chemical and microbial analysis, $N = 6$ for metabolic analysis). The data were analyzed applying the SPSS software (version 26.0, SPSS Inc. Chicago, IL, United States). Statistical differences between different fermentation stages were determined by Student's *t*-tests and one-way ANOVA followed by Duncan's multiple-range test. The *P*-values of the metabolomics and microbiome data were corrected using Welch's test and the Benjamini–Hochberg false-discovery rate (FDR). *P*-values < 0.05 indicate statistically significant differences. Bar plots were generated in GraphPad Prism 8 (San Diego, CA, United States).

RESULTS

The Change of Physicochemical Parameters and Microbial Community

The nutrients are presented in **Supplementary Table S1**. The pH value showed a dramatic decrease from aerobic to anaerobic fermentation stage while the content of lactic acid increased approximately three-fold range at 48 h. The crude protein (CP) content significantly increased from 28.21 to 31.54%, and a sharp increase was observed in small peptides (SP). Notably, similar significantly downward trends were observed for the levels of amylose, NDF, phytate phosphorus, glycinin, and β-conglycinin during the whole process of fermentation.

The composition of the bacterial community during corn and defatted soybean fermentation is shown in **Figure 1**.

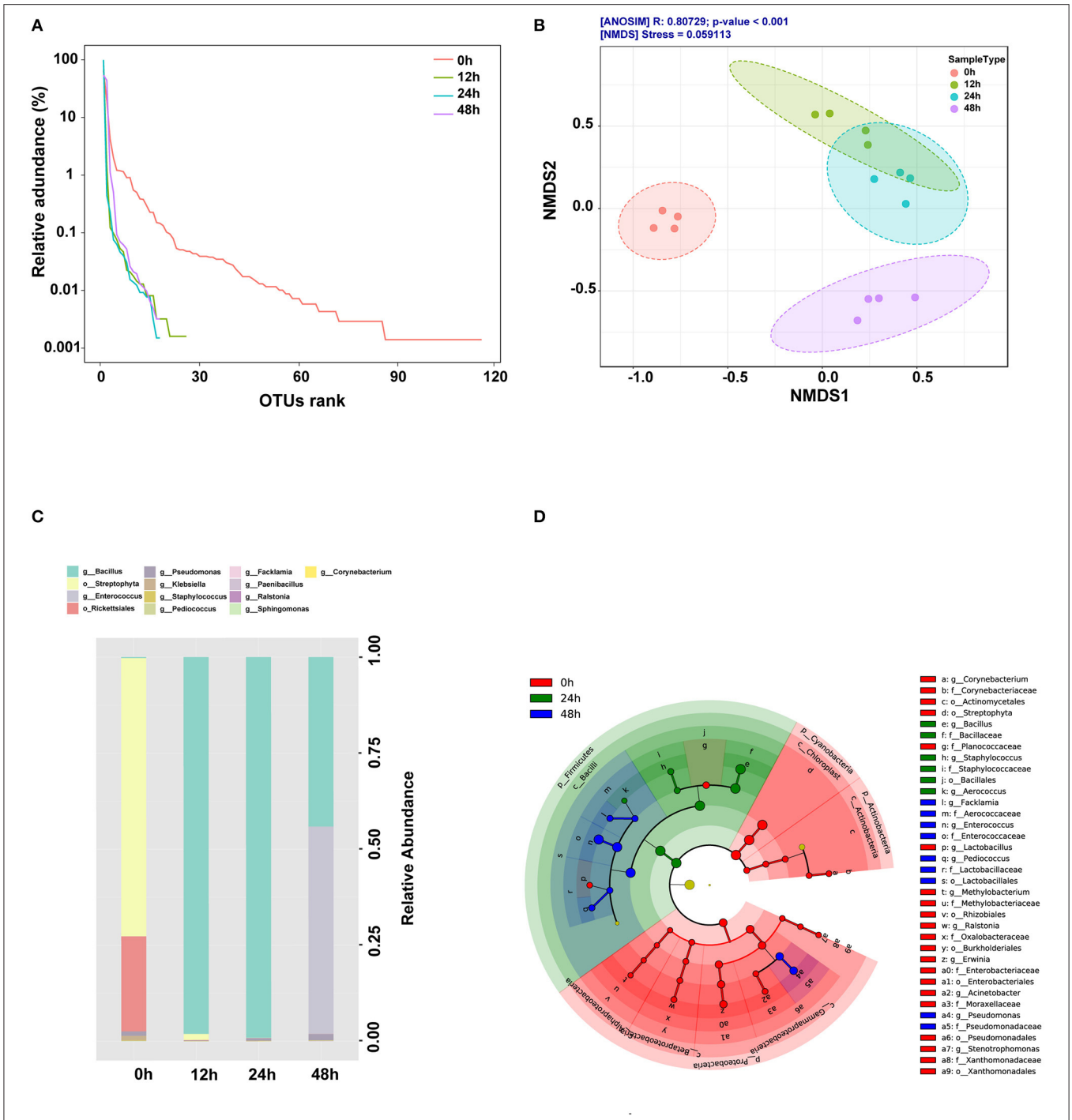

FIGURE 1 | Changes of microbial community during fermentation. **(A)** OTU rank curve during fermentation. **(B)** β-diversity was performed using the ordination-based Nonmetric Multidimensional Scaling (NMDS) based on the Jaccard index distance method and analysis of group similarities (ANOSIM) at the species level. **(C)** Genus-level compositions of the bacterial community during fermentation. **(D)** Cladogram plot of significant genera based on LEfSe analysis (LDA scores >3.0).

α-Diversity is used to measure the diversity within a sample or an ecosystem. The two most commonly used alpha-diversity measurements are Richness (count) and Evenness (distribution). The rank-curve generated by OTU ranks and their relative abundance illustrated that α-diversity reduced during the initial 24 h after *B. subtilis* treatment, whereas increased at the anaerobic fermentation stage (**Figure 1A**). β-Diversity represents the explicit comparison of microbial communities (in-between) based on their composition and provides a measure of the distance or dissimilarity between each sample pair. The

result showed that microbial β-diversity based on NMDS and Jaccard index distance method was distinct at different time points since the structures of microbial communities were separated into four clusters (**Figure 1B**). The results showed that the predominant bacteria changed from Streptophyta and Rickettsiales at 0 h to Bacillus and Pseudomonas in the aerobic stage and then to Bacillus, Enterococcus, and Pseudomonas in the anaerobic stage (**Figure 1C**). Significantly different bacteria from order to genus level among different fermentation time points were identified by the linear discriminant analysis effect size (LEfSe) (**Figure 1D**). The abundance of *Bacillus*, *Staphylococcus,* and *Aerococcus* increased significantly at 24 h. *Enterococcus*, *Pseudomonas*, *Pediococcus,* and *Facklamia* were the predominant genus at 48 h.

Cluster Analysis of Metabolites at Different Fermentation Time Points

Unsupervised mode of the PCA can reveal the variation between and within groups, and reflect the tendency of distribution as well as possible discrete points. The first principal component (PC1 = 67.0%) and the second principal component (PC2 = 16.5%) directly showed the similarities and differences between groups (**Supplementary Figure S1A**). The result showed that fermentation samples at 0, 12, 24, and 48 h were separated, especially by the first principal component, and all samples fell within a 95% confidence ellipse. The accurate differences between samples could not be completely interpreted according to the visual distinctions generated by the PCA plot, because PCA is an unsupervised model and belongs to exploratory analysis. Therefore, supervised classification models of Partial Least Squares Discriminant Analysis (PLS-DA) and Orthogonal Partial Least Squares Discriminant Analysis (OPLS-DA) were implemented to confirm the transformation degree of metabolites with fermentation time. The results showed obvious separation between different fermentation groups indicating that it could be used to identify the metabolic differences in the fermentation process of the substrates (**Supplementary Figures S1B,C**). A further cluster analysis was to determine whether metabolites differences existed during the fermentation. The chart showed that all the samples were clustered into four groups, and each cluster with samples belonged to the same time points (**Supplementary Figure S1D**). These results suggested that good stability and reproducibility were obtained, and the change of metabolites during fermentation was time dependent.

The Changes of Metabolic Composition at Different Levels

Metabolome analysis revealed that nucleosides, nucleotides, and analogs; lipids and lipid-like molecules; carbohydrates; amino acids, peptides, and proteins were the main abundant metabolites during the whole fermentation stage (**Figure 2A**). The relative abundance of amino acids, peptides, and proteins in the process of fermentation constantly increased ($P < 0.05$), whereas the abundance of nucleosides, nucleotides, and analogs and lipids and lipid-like molecules maintained decreasing ($P < 0.05$). Carbohydrates decreased from 0 to 12 h and then remained in a relatively stable state. To find the specific change of the related metabolites, we explored the next level of top 20 metabolites (**Figure 2B**). At 0 h, daidzin, lysoPC(16:0), glycerophosphocholine, lysoPC[18:2(9Z,12Z)], and 5-aminopentanoic acid were the main metabolites. The top 5 metabolites at 12 h were daidzin, norvaline, lysoPC[18:2(9Z,12Z)], 2′-O-methyladenosine, and 5-aminopentanoic acid. Norvaline, 3,3,5-triiodo-L-thyronine-beta-D-glucuronoside, 5-aminopentanoic acid, imidazole-4-acetaldehyde, lysoPC[18:2(9Z,12Z)], and 2′-O-methyladenosine were the dominant substances at 24 h. Notably, the concentration of metabolites was sharply elevated in the anaerobic stage. Phenylacetaldehyde dramatically raised in the anaerobic stage and became the predominant metabolites. 3,3,5-Triiodo-L-thyronine-beta-D-glucuronoside and norvaline in samples at 48 h were higher relative to that in 24 h. During the whole fermentation stage, daidzin continued to reduce while 5-aminopentanoic acid persistently increased.

Different Metabolites in the Process of Fermentation

The main metabolites based on the variable importance for the projection (VIP) were selected and sorted to better understand the changes of the primary different metabolites. Totally 229 metabolites were identified after annotation, and these metabolites have individual metabolic features at different time points after fermentation. Top 35 significantly different metabolites during fermentation were selected (**Figure 3A**), and the VIP values of these 35 metabolites based on the PLS-DA model were shown (**Figure 3B**). The main significantly different metabolites enriched in 0 h were trimethylamine N–oxide, 1,3,5–trihydroxybenzene, cytidine 2′,3′–cyclic phosphate, isoferulic acid 3-sulfate, N'–hydroxyneosaxitoxin, kojibiose, cyclic AMP, and apigenin 7–O–(6″–O-acetylglucoside). These eight metabolites slightly reduced from 0 to 12 h while remarkably decreased in 24 and 48 h ($P < 0.05$). Fumigaclavine, deterrol stearate, and fumitremorgin B were the metabolic biomarkers at 24 h. A total of 24 metabolites were significantly up-regulated at 48 h, in particular, nnal-N-oxide, 4-(nitrosoamino)-1-(3-pyridinyl)-1-butanone, and 9,10-epoxyoctadecanoic acid were the top 3 substrates, which had the high VIP scores. Phenylalanyl–asparagine, (E)−4–[5–(4–hydroxyphenoxy)-3-penten-1-ynyl] phenol, 9,10–epoxyoctadecanoic acid, cinnzeylanine [10]–dehydrogingerdione, (x)−2–heptanol glucoside, and blumenol C glucoside were the most abundant compounds identified at 48 h.

Prediction of Metabolic Pathways by Identifying Significantly Different Metabolites

KEGG databases were used to explore the metabolism pathway and elucidate the mechanism of metabolic changes during fermentation. Thus, enrichment analysis and topological analysis were performed to find the key pathways that were most relevant to the metabolites. A total of 22 metabolic pathways involving 229 different metabolites were sorted out throughout the fermentation process (**Supplementary Tables S2**, **S3**).

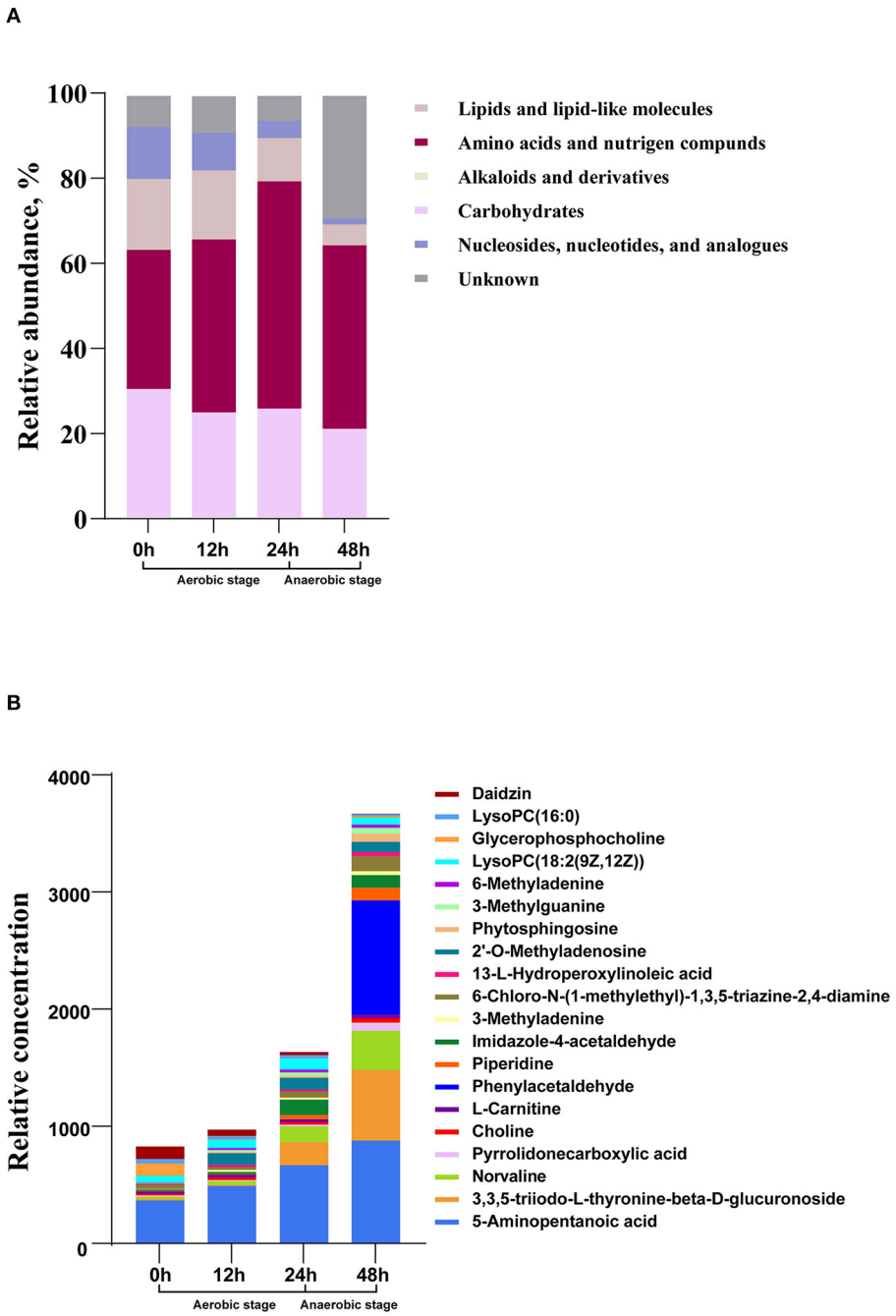

FIGURE 2 | The changes of metabolic composition at different levels in the process of fermentation. **(A)** Relative compositions of the main metabolites. **(B)** Top 20 metabolites at different fermentation times.

To more intuitively and directly compare the differences of metabolic pathways at different fermentation time points, the first 20 metabolic pathways were retained (**Figure 4**). Metabolites mapped to phenylalanine metabolism, starch and sucrose metabolism, taurine and hypotaurine metabolism, biotin metabolism, and cysteine and methionine metabolism were the main metabolism pathways in the whole fermentation process. Starch and sucrose metabolism and purine metabolism enriched in 0 h and decreased until the end of fermentation. Taurine and hypotaurine metabolism, glycerolipid metabolism, and glycerophospholipid metabolism were significantly upregulated in 24 h. A total of 15 significantly different metabolic pathways were remarkably increased in 48 h, including phenylalanine metabolism, biotin metabolism, cysteine and methionine metabolism, arginine biosynthesis, and glutathione metabolism etc. These findings suggested the succession of different

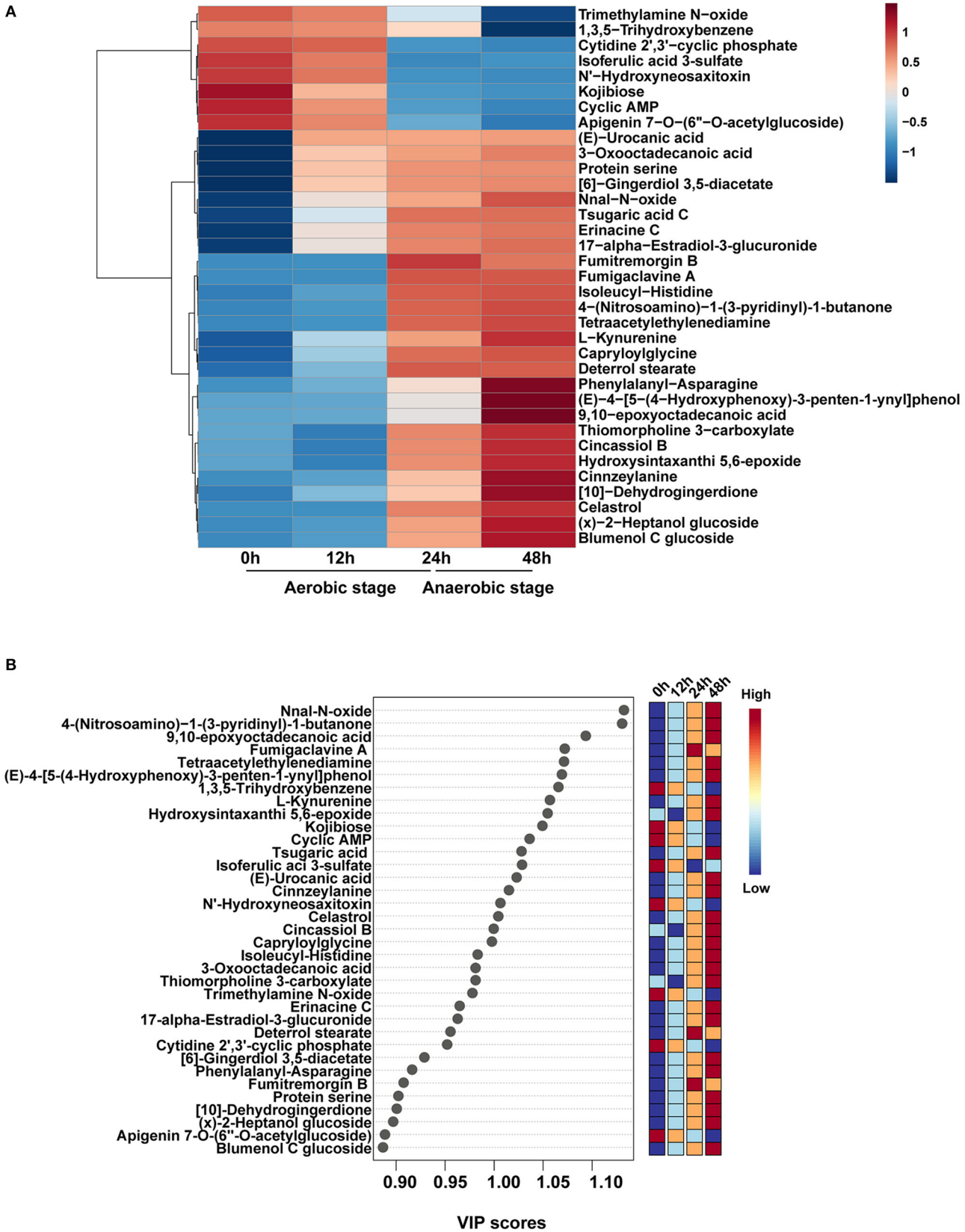

FIGURE 3 | Significantly different metabolites during fermentation. **(A)** Top 35 significantly different metabolites. **(B)** A scatter plot of the top 35 distinct metabolites was identified by applying variable importance projection (VIP).

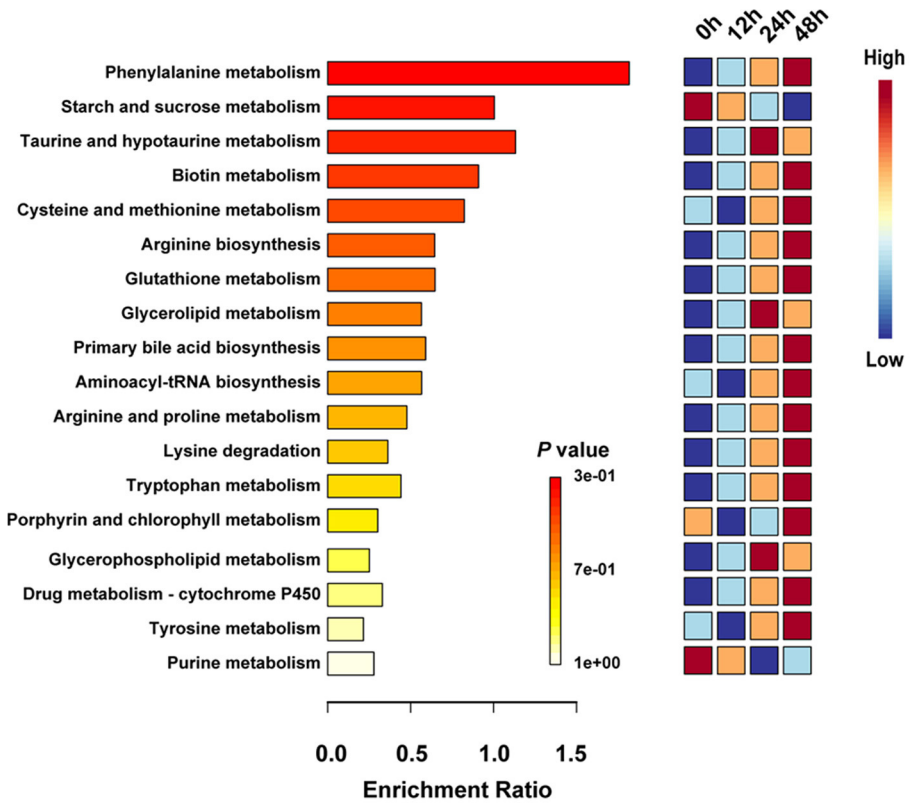

FIGURE 4 | Prediction of metabolic pathways by identifying significantly different metabolites. The significantly different metabolites are based on the variable importance for the projection (VIP) >1 and $P < 0.05$.

metabolic pathways during the process of fermentation, especially the transformation of related metabolism caused by the change of fermentation condition.

Correlations Among the Significantly Different Microbiota, Nutritional Value, Metabolites, and Metabolic Pathways During Fermentation

To further investigate the observations regarding the impact of the changes in the bacteria, nutritional indexes, metabolites, and metabolic pathways, correlation analyses were performed. *Bacillus*, *Staphylococcus,* and *Aerococcus* which increased at 24 h had the opposite relations with nutritional value and metabolites, compared with that of 0 h enriched microbes. *Bacillus*, *Staphylococcus,* and *Aerococcus* were positively related with amino acids and nitrogen compounds and negatively correlated with lipids and nucleosides, and contributed to the nutritional value of the substrates (**Figure 5A**). Notably, *Bacillus* was negatively related to carbohydrates. Correlations among the metabolites, microbiota, and nutrients in the anaerobic stage are shown in **Figure 5B**. *Enterococcus* and *Facklamia* had positive correlations with crude protein, small peptides, and lactic acids, and were negatively correlated with most of the metabolites. The correlations between microbes and metabolic pathways were further conducted. *Bacillus* was negatively related to starch and sucrose metabolism and positively correlated with most of the amino acid metabolism in the aerobic stage (**Figure 5C**). In the anaerobic stage, *Enterococcus* was positively related to amino acid metabolism (**Figure 5D**).

Integrated Microbiomic and Metabolomic Changes of Functional Pathways During Fermentation

The integrated metabolic pathways are shown in the metabolome view map (**Figure 6**). A total of 6 microbial metabolism pathways based on KEGG database at level 1 were identified, including carbohydrate metabolism, lipid metabolism, amino acid metabolism, metabolism of cofactors and vitamins, metabolism of other amino acids, and glycan biosynthesis and metabolism. Carbohydrates metabolism consistently increased from the aerobic to anaerobic stages, while the metabolism of cofactors and vitamins, glycan biosynthesis, and metabolism decreased from 0 to 48 h. Lipid metabolism and metabolism of other amino acids were enriched at 12 h, amino acid metabolism increased to a high level at 24 h. At level 2, starch and sucrose metabolism and glyoxylate and dicarboxylate metabolism showed an opposite expression trend of change. Primary bile acid biosynthesis and glycerolipid metabolism consistently increased, but glycerophospholipid metabolism decreased

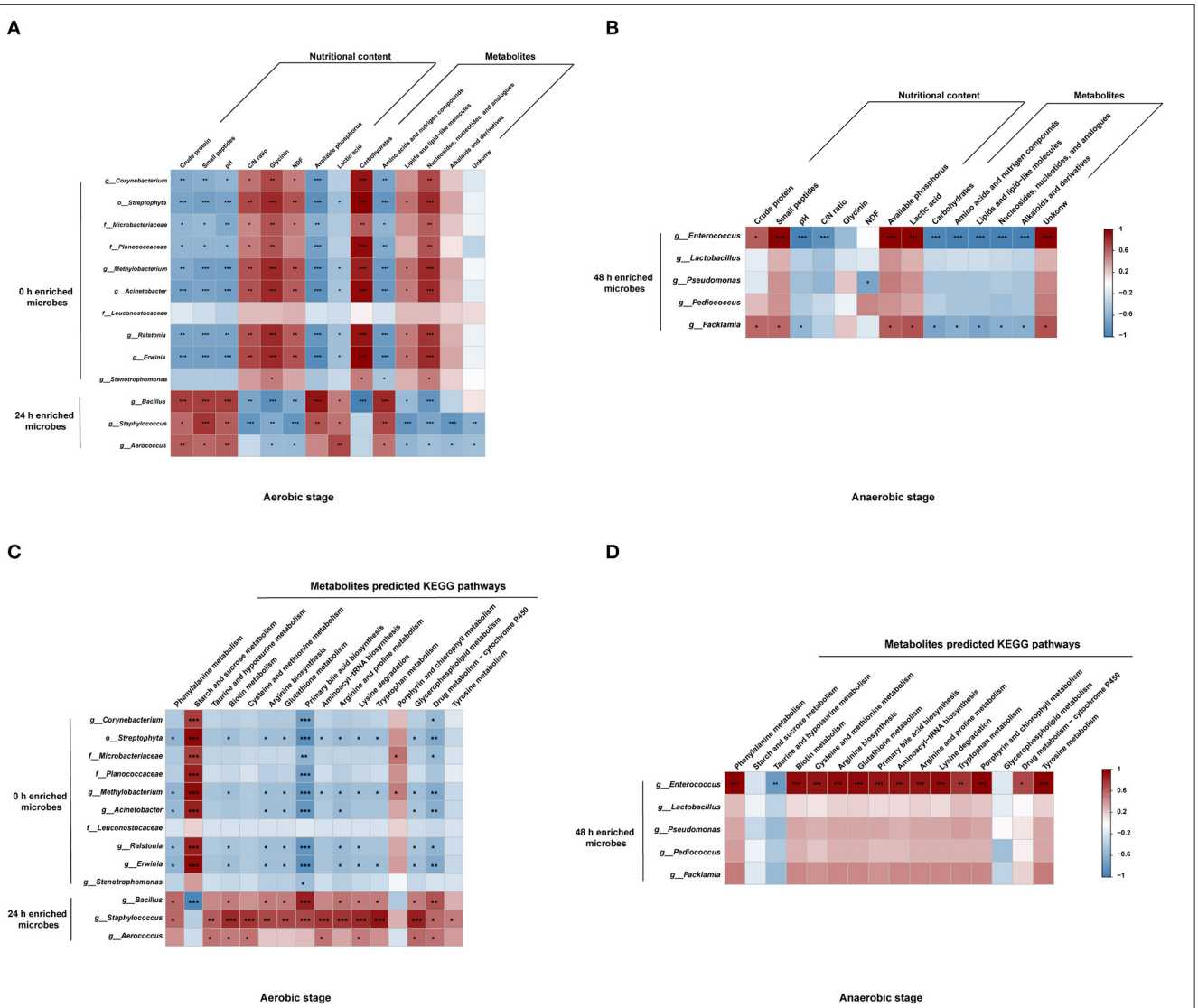

FIGURE 5 | Relationships among the microbiota, metabolites, nutritional value, and KEGG pathways. Relationships among the microbiota, metabolites, and nutritional value in aerobic stage **(A)** and anaerobic stage **(B)**. Relationships between the microbiota and metabolite predicted KEGG pathways in the aerobic stage **(C)** and the anaerobic stage **(D)**. ***$P < 0.001$, **$0.001 < P < 0.01$, *$0.01 < P < 0.05$, respectively.

from 0 to 48 h. C-lysine was the product of three major metabolic pathways involving carbohydrate metabolism, lipid metabolism, and amino acid metabolism, and then could be converted into 5-amino-levulinate in porphyrin and chlorophyll metabolism. Phosphatidyl-ethanolamine was produced by glycerophospholipid metabolism, and further generaterd ethanolamonephosphate which was higher at 12 h. The content of L-cysteine and taurocholate was down-regulated, and L-cysteine was the precursor of taurine which can be converted into taurocholate.

DISCUSSION

In recent years, fermented plant-based foods have gained attention due to their potential health benefits (28, 29). Fermented corn and soy-based foods such as fermented corn flour, Natto, Sufu, Miso, Douchi, and soy sauce are popular because they are important plant-derived food for humans and have a huge global consumption. Many research studies have reported that fermentation is capable of reducing anti-nutritional factors, making the original substrate more flavorful and nutritional. However, few studies spotlight the dynamics of fermented corn and soybean by-products by appling microbiome and matebolome. The present study indicated the temporal changes during microbial fermentation of fermented corn and defatted soybean based on using a multi-omics approach. *Bacillus*, *Enterococcus,* and *Pseudomonas* were mainly involved in the maturation of the fermented corn and defatted soybean. Importantly, phenylalanine metabolism was the main and vital metabolism pathway in the anaerobic fermentation stage.

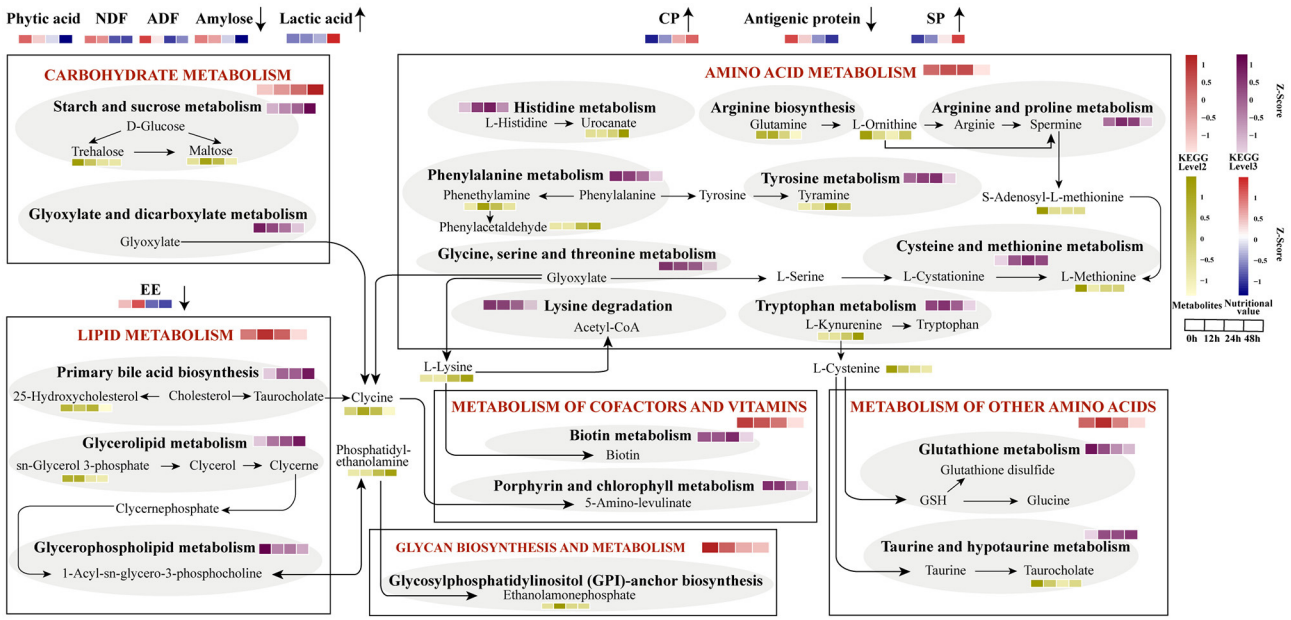

FIGURE 6 | Integrated microbiomic and metabolomic changes of functional pathways. The KEGG level2 was selected based on significantly different metabolic data. The abundance of KEGG level2 and 3 were predicted by 16S data.

Correlation analysis suggested a strong relationship between *Bacillus* and amino acids in the aerobic stage, and *Enterococcus* mainly acted as an acid and amino acids producer at the anaerobic stage of fermentation.

The changes of metabolites were found to be time dependent during fermentation by adapting a two-step fermentation method. PLS-DA analysis and the structure of metabolites showed that metabolic profiles were significantly different among the groups. The microbial analysis also revealed that the dynamic changes of microbial community occurred during this two-stage solid-state fermentation process. These findings suggest that the change of metabolites during fermentation may be caused by the change of microbial niche at different stages. A recent study reported that different fermented soy foods had various soluble and volatile metabolites (30). Besides, fermenting microbes and metabolites contributes to the taste and flavor of Sufu (31). These findings have implications for considering the metabolites as a way to assess the fermented plant-based food and the metabolites can be used to understand the fermentation stages.

Metabolites annotation further indicated that metabolic activities of carbohydrates, amino acids, and lipid metabolism were dominant during fermentation, which is in agreement with previous studies about fermented soybean paste (32, 33). Amino acids, peptides, and proteins increased, whereas lipids and lipid-like molecules, and carbohydrates decreased during fermentation in our study. These results were consistent with the changes in nutrients as the content of antigenic protein, NDF, ADF, amylose, and crude fat reduced, and the level of crude protein raised during the anaerobic fermentation stage. For individual metabolites, daidzin, a natural organic compound in soybean (34), is elementary for the oxidation of acetaldehyde derived from ethanol metabolism and can be converted by resident bacteria for secondary metabolism (35). Soybean and soybean-based products are rich in daidzin, which is poorly absorbed in the human gut (36). The decrease of daidzin during the fermentation process in our study indicates that fermentation improves the bioavailability of isoflavones and assists in the digestion of protein. 5-Aminopentanoic acid is a lysine degradation product, which could be produced by bacterial catabolism of lysine (37). Nontargeted urine metabolomics analysis showed that 5-aminopentanoic acid was a biomarker, which played a role in protective and therapeutic effects on high-fat feed-induced hyperlipidemia in rats (38). The increase of 5-aminopentanoic acid suggests that the fermentation up-regulates potential benefit of the substrates. Notably, the dramatic increase in phenylacetaldehyde was observed at 48 h. Phenylacetaldehyde is a typical fragrant compound in traditional Chinese-type soy sauce and alcohol-free beers (39, 40). These results provide an evidence that important contribution of these flavor compounds to the value of fermented corn and defatted soybean.

The identification of significantly different metabolites further confirmed that fermentation caused significant changes in various metabolites. Previous studies reported that several bacterial species (*Bacillus* and *Pseudomonas)* metabolically degraded trimethylamine oxide (TMAO) in food fermentation (41). Clinical evidence supported that there is a strong association between elevated TMAO levels with increased risk of developing diseases such as atherosclerosis and thrombosis (42). The present study demonstrated that the level of TMAO continued to decrease, and *Bacillus* and *Pseudomonas* were rich in the fermentation stage. These findings are consistent with previous reports and suggested that fermentation reduces

harmful substances. The source of dipeptides and free amino acids is mainly caused by protease secreted by microorganisms that decompose the protein components of a Thai fermented soybean (43). Jin et al. (44) found that L-theanine, glutamine, and glutamic acid enriched in the fermented corn, defatted soybean, and bran incubated with a combination of probiotics. Studies showed that the concentrations of most amino compounds gradually increased during fermentation with soybean as substrate (32, 45). The concentration of phenylalanyl-asparagine, protein serine, and isoleucyl-histidine showed a steady increase over time, which supports the notion of a previous study. Phenylalanyl-asparagine and isoleucyl-histidine are incomplete breakdown products of protein digestion or protein catabolism. Phenylalanine, isoleucine, and histidine are essential amino-acids. Serine, a health-promoting compound, is functionally important in many proteins which are involved in the metabolism of fats, fatty acids, cell membranes, and a healthy immune system. These metabolites outcomes directly implied the degradation of protein during fermentation and the production of amino acids, peptides, and analogs occurred and may play essential roles in quality improvement of the fermented corn and defatted soybean.

To reveal the specific effect of the significantly different metabolites during fermentation, KEGG databases were used to characterize the most influential pathways. The level of phenylalanine and glutamine was improved during the fermentation of soybean (46, 47). Tyrosine is considered to be an indispensable dietary amino acid in humans and animals, and a diet supplemented with phenylalanine is a common way of compensating it (48). Glutathione is a major antioxidant, which is metabolized in multiple ways leading to the biosynthesis of glutamate, glycine, cysteine, and other amino acids (49). The present study showed that phenylalanine metabolism, glutathione metabolism, cysteine, and methionine metabolism were the top 3 important metabolism pathways during fermentation. Our previous study also demonstrated that the content of amino acid metabolism gradually increased as fermentation progressed in terms of the predicted microbial function (24). These results indicated that the metabolism of amino acids was active and the number of amino acids increased in the fermentation of corn and defatted soybean. In addition, phenylalanine metabolism is a major pathway for anthocyanin biosynthesis (50). Anthocyanin aroused a wide public concern as a potent beneficial metabolite due to its antioxidant activity, antimicrobial, antiviral, and antithrombotic characteristics (51, 52). Anthocyanin was detected after fermentation as well, suggesting that fermentation may improve the nutritional value of the fermented substances. Therefore, these affected metabolic pathways are closely related to the fermented corn and defatted soybean and provide clues for further study on the effect of two-stage fermentation on its metabolites.

Complex microbial–ecological interactions influence the production of metabolites. In the first-stage aerobic fermentation, *Bacillus* rapidly proliferated. Relevant studies reported that *Bacillus* was the predominant fermentative bacteria responsible for the natural fermentation of protein-rich food, production of flavor substances, conversion of complex food compounds in small components in the fermentation of west African seed condiments (53). In a Nigerian fermented soybean condiment, *Bacillus* was the dominant species occurring throughout the fermentation (54). *Bacillus* was positively related to amino acids and nitrogen compounds revealing that the proteolysis of *Bacillus* results in the increase of peptides, amino acids, and ammonia from proteins. In addition, the degradation of complex carbohydrates from the enzymes secreted by *Bacillus*, such as amylase, galactanase, galactosidase, glucosidase, and fructofuranosidase, interpreted the positive correlation between *Bacillus* and carbohydrates in the aerobic stage. *Enterococcus*, a lactate-producing bacteria as well as an acid-tolerant bacteria (55, 56), plays important roles in food production, particularly they can accelerate the ripening of food and improve the taste and flavor through proteolysis, lipolysis, carbohydrates breakdown, and the production of aromatic compounds (57). *Enterococcus* was the most dominant genus in the anaerobic fermentation stage. The enzyme secreted by *Enterococcus* and *Bacillus* played important roles in hydrolyzing proteins, and the accumulation of amino acids and related substances occurred in the whole process, resulting in a positive correlation between *Enterococcus* and amino acids. Small peptides in foods are generally easy to be absorbed and utilized by the gut, and most of them have specific biological functions (58–60), such as improving gut health and immunity. The relationships of microbes and metabolic pathways further confirmed the effects on protein and carbohydrates breakdown of *Bacillus* and amino acid synthesis of *Enterococcus*. A detailed understanding of the fermentation microbiota and their unique functional characteristics is fundamental to developing high-quality and safe fermented products and enhancing specifically adapted starter cultures. These results implied that *Bacillus* and *Enterococcus* were critical bacteria in corn and defatted soybean fermentation and suggested that they may be the optimized selective strains used in the two-stage fermentation.

The overview of the metabolic pathways map will help to further explain the causes of the differences in these metabolites and to explore the metabolic mechanism. Interestingly, the content of amino acid metabolism increased at the aerobic phase but declined abruptly at 48 h, and the consistent increase of carbohydrates was observed according to the predicted microbial functions. These findings were distinct from the metabolomics analysis, suggesting the limitation and deviation of the analysis of the dynamics during the fermentation based solely on microbial data. In the first stage, bacteria like *Bacillus* which directly participated in amino acid metabolism resulted in increased metabolic capacity. With the proliferation of carbohydrate-degrading bacteria and the increased acidification in the second stage, the main metabolism of fermentation gradually changes to carbohydrate metabolism. Therefore, the distinctive dominant metabolic functions at different fermentation stages were further interpreted. The physicochemical features were consistent with the change of metabolites, verified the metabolism differences caused by the significantly different bacteria in the two-stage fermentation. The metabolic process of fermented plant-based food is complex, and the specific metabolic mechanisms of these metabolites identified in our study are still not fully

understood. Thus, future studies should focus on the secondary metabolites and establish standardized metabolic fingerprints for the fermentation.

CONCLUSIONS

In summary, the dynamic changes in the nutritional properties, microbial composition, and metabolites during the corn and defatted soybean fermentation were systematically studied. Phenylalanine metabolism, glutathione metabolism, and cysteine and methionine metabolism were considered to be the important metabolic pathways affecting the quality of fermented corn and defatted soybean. The results further unraveled that *Bacillus* spp. was the predominant genera that mainly participated in the breakdown of protein and carbohydrates in the aerobic stage, and *Enterococcus* spp. was associated with amino acid metabolism and lactic acid production toward the end of fermentation. This study potentially serves as a foundation for increasing the nutrition of corn and defatted soybean food and guides the underlying fermenting mechanism of solid-state fermentation of plant-based food.

DATA AVAILABILITY STATEMENT

The datasets presented in this study can be found in online repositories. The names of the repository/repositories and accession number(s) can be found in the article/**Supplementary Material**.

AUTHOR CONTRIBUTIONS

CW and YW conceived the project and designed the experiments. CW and SW analyzed the nutritional value, 16S rRNA sequencing data and metabolic data, and wrote the manuscript. MJ, MY, and YW help review, revise, and approve the manuscript. BL assisted the nutritional value analyses and contributed to revise and approve the manuscript. All authors contributed to the article and approved the submitted version.

FUNDING

This work was funded by China Agriculture Research System of MOF and MARA (CARS-35).

ACKNOWLEDGMENTS

We are grateful to Shanghai Biotree Biotech Co., Ltd. and Yan Wang for their contributions to the LC-MS/MS analyses using their UHPLC system metabolite annotation and related bioinformatics analysis.

SUPPLEMENTARY MATERIAL

The Supplementary Material for this article can be found online at: https://www.frontiersin.org/articles/10.3389/fnut.2022.831243/full#supplementary-material

Supplementary Figure S1 | Dimension reduction analysis and clustering of dynamic metabolome. **(A)** Principal component analysis (PCA) plot of compounds in fermented mixed substances. **(B)** Partial Least Squares Discriminant Analysis (PLS-DA) plot of compounds in fermented mixed substances. The accuracy, goodness-of-fit (R2), and goodness-of-prediction (Q2) were 1.0, 0.999, and 0.991, respectively. **(C)** Orthogonal partial least-squares discrimination analysis (OPLS-DA) plot of compounds in fermented mixed substances; R2X, R2Y, and Q2 were 0.098, 0.883, and 0.523, respectively. **(D)** Cluster analysis of different fermentation times.

Supplementary Table S1 | Determined nutrient contents of fermented corn and defatted soybean at 0, 12, 24, and 48 h.

Supplementary Table S2 | Identification of significantly different metabolites during fermentation.

Supplementary Table S3 | Enrichment pathways of significantly different metabolites in fermented mixed substances.

REFERENCES

1. Nguyen H, Mwangomba W, Nyirenda EM. Delving into possible missing links for attainment of food security in Central Malawi: farmers' perceptions and long term dynamics in maize (*Zea mays* L) production. *Heliyon.* (2021) 7:e07130. doi: 10.1016/j.heliyon.2021.e07130
2. Jones RB, Berger PK, Plows JF, Alderete TL, Millstein J, Fogel J, et al. Lactose-reduced infant formula with added corn syrup solids is associated with a distinct gut microbiota in Hispanic infants. *Gut Microbes.* (2020) 12:1813534. doi: 10.1080/19490976.2020.1813534
3. Terefe ZK, Omwamba MN, Nduko JM. Effect of solid state fermentation on proximate composition, antinutritional factors and in vitro protein digestibility of maize flour. *Food Sci Nutr.* (2021) 9:6343–52. doi: 10.1002/fsn3.2599
4. Cao ZH, Green-Johnson JM, Buckley ND, Lin QY. Bioactivity of soy-based fermented foods: a review. *Biotechnol Adv.* (2019) 37:223–38. doi: 10.1016/j.biotechadv.2018.12.001
5. Fernandez-Raudales D, Hoeflinger JL, Bringe NA, Cox SB, Dowd SE, Miller MJ, et al. Consumption of different soymilk formulations differentially affects the gut microbiomes of overweight and obese men. *Gut Microbes.* (2012) 3:490–500. doi: 10.4161/gmic.21578
6. Adebo OA, Oyedeji AB, Adebiyi JA, Chinma CE, Oyeyinka SA, Olatunde OO, et al. Kinetics of phenolic compounds modification during maize flour fermentation. *Molecules*. (2021) 26:6702 doi: 10.3390/molecules 26216702
7. Kimura K, Yokoyama S. Trends in the application of Bacillus in fermented foods. *Curr Opin Biotechnol.* (2019) 56:36–42. doi: 10.1016/j.copbio.2018.09.001
8. Zhang D, Wang Y, Shen SN, Hou Y, Chen YY, Wang TT. The mycobiota of the human body: a spark can start a prairie fire. *Gut Microbes.* (2020) 11:655–79. doi: 10.1080/19490976.2020.1731287
9. Rathod NB, Phadke GG, Tabanelli G, Mane A, Ranveer RC, Pagarkar A, et al. Recent advances in bio-preservatives impacts of lactic acid bacteria and their metabolites on aquatic food products. *Food Biosci.* (2021) 44:101440. doi: 10.1016/j.fbio.2021.101440
10. Feng T, Wang J. Oxidative stress tolerance and antioxidant capacity of lactic acid bacteria as probiotic: a systematic review. *Gut Microbes.* (2020) 12:1801944. doi: 10.1080/19490976.2020.1801944
11. Cui L, Li DJ, Liu CQ. Effect of fermentation on the nutritive value of maize. *Int J Food Sci Tech.* (2012) 47:755–60. doi: 10.1111/j.1365-2621.2011.02904.x
12. Forsido SF, Hordofa AA, Ayelign A, Belachew T, Hensel O. Effects of fermentation and malt addition on the physicochemical properties

of cereal based complementary foods in Ethiopia. *Heliyon.* (2020) 6:e04606. doi: 10.1016/j.heliyon.2020.e04606
13. Hiran P, Kerdchoechuen O, Laohakunjit N. Combined effects of fermentation and germination on nutritional compositions, functional properties and volatiles of maize seeds. *J Cereal Sci.* (2016) 10:2566. doi: 10.1016/j.jcs.2016.09.001
14. Chiang SS, Pan TM. Antiosteoporotic effects of *Lactobacillus*-fermented soy skim milk on bone mineral density and the microstructure of femoral bone in ovariectomized Mice. *J Agric Food Chem.* (2011) 59:7734–42. doi: 10.1021/jf2013716
15. Ikeda Y, Iki M, Morita A, Kajita E, Kagamimori S, Kagawa Y, et al. Intake of fermented soybeans, natto, is associated with reduced bone loss in postmenopausal women: Japanese Population-Based Osteoporosis (JPOS) Study. *J Nutr.* (2006) 136:1323–8. doi: 10.1093/jn/136.5.1323
16. Rekha CR, Vijayalakshmi G. Bioconversion of isoflavone glycosides to aglycones, mineral bioavailability and vitamin B complex in fermented soymilk by probiotic bacteria and yeast. *J Appl Microbiol.* (2010) 109:1198–208. doi: 10.1111/j.1365-2672.2010.04745.x
17. Singh P, Kumar R, Sabapathy SN, Bawa AS. Functional and edible uses of soy protein products. *Compr Rev Food Sci F.* (2008) 7:14–28. doi: 10.1111/j.1541-4337.2007.00025.x
18. Kwon DY, Daily JW, Kim HJ, Park S. Antidiabetic effects of fermented soybean products on type 2 diabetes. *Nutr Res.* (2010) 30:1–13. doi: 10.1016/j.nutres.2009.11.004
19. Oh NS, Joung JY, Lee JY, Song JG, Oh S, Kim Y, et al. Glycated milk protein fermented with *Lactobacillus rhamnosus* ameliorates the cognitive health of mice under mild-stress condition. *Gut Microbes*. (2020) 11:1643-61. doi: 10.1080/19490976.2020.1756690
20. Hwang JH, Wu SJ, Wu PL, Shih YY, Chan YC. Neuroprotective effect of tempeh against lipopolysaccharide-induced damage in BV-2 microglial cells. *Nutr Neurosci.* (2019) 22:840–9. doi: 10.1080/1028415X.2018.1456040
21. Wan HF, Wang LP, Zhao Y, Li L. Analysis of microorganisms in two kinds of Jiajiang sufu based on high-throughput sequencing. *J. Chin. Inst. Food Sci.Technol.* (2020) 20, 278–285. doi: 10.16429/j.1009-7848.2020.08.034
22. Beaumont M, Paës C, Mussard E, Knudsen C, Cauquil L, Aymard P, et al. Gut microbiota derived metabolites contribute to intestinal barrier maturation at the suckling-to-weaning transition. *Gut Microbes.* (2020) 11:1268–86. doi: 10.1080/19490976.2020.1747335
23. Moy YS, Chou CC. Changes in the contents of sugars and organic acids during the ripening and storage of Sufu, a traditional oriental fermented product of soybean cubes. *J Agric Food Chem.* (2010) 58:12790–3. doi: 10.1021/jf1033653
24. Wang C, Shi C, Su W, Jin M, Xu B, Hao L, et al. Dynamics of the physicochemical characteristics, microbiota, and metabolic functions of soybean meal and corn mixed substrates during two-stage solid-state fermentation. *mSystems.* (2020) 5:e00501–19. doi: 10.1128/mSystems.00501-19
25. Feldsine P, Abeyta C, Andrews WH, Committee AIM. AOAC International methods committee guidelines for validation of qualitative and quantitative food microbiological official methods of analysis. *J AOAC Int.* (2002) 85:1187–200. doi: 10.1093/jaoac/85.5.1187
26. Shi C, Zhang Y, Yin Y, Wang C, Lu Z, Wang F, et al. Amino acid and phosphorus digestibility of fermented corn-soybean meal mixed feed with *Bacillus subtilis* and *Enterococcus faecium* fed to pigs. *J Anim Sci.* (2017) 95:3996–4004. doi: 10.2527/jas.2017.1516
27. Yoshihara T, Oikawa Y, Kato T, Kessoku T, Kobayashi T, Kato S, et al. The protective effect of *Bifidobacterium bifidum* G9-1 against mucus degradation by *Akkermansia muciniphila* following small intestine injury caused by a proton pump inhibitor and aspirin. *Gut Microbes.* (2020) 11:1385–404. doi: 10.1080/19490976.2020.1758290
28. Masia C, Geppel A, Jensen PE, Buldo P. Effect of *Lactobacillus rhamnosus* on physicochemical properties of fermented plant-based raw materials. *Foods.* (2021) 10:573. doi: 10.3390/foods10030573
29. Wuyts S, Van Beeck W, Allonsius CN, Van Den Broek MFL, Lebeer S. Applications of plant-based fermented foods and their microbes. *Curr Opin Biotechnol.* (2020) 61:45–52. doi: 10.1016/j.copbio.2019.09.023
30. Lee SH, Lee S, Lee SH, Kim HJ, Singh D, Lee CH. Integrated metabolomics and volatolomics for comparative evaluation of fermented soy products. *Foods.* (2021) 10:2516. doi: 10.3390/foods10112516
31. Yao D, Xu L, Wu MN, Wang XY, Wang K, Li ZJ, et al. Microbial community succession and metabolite changes during fermentation of BS Sufu, the fermented black soybean curd by *Rhizopus microsporus*, *Rhizopus oryzae*, and *Actinomucor elegans*. *Front Microbiol.* (2021) 12:665826. doi: 10.3389/fmicb.2021.665826
32. An FY, Li M, Zhao Y, Zhang Y, Mu DL, Hu XY, et al. Metatranscriptome-based investigation of flavor-producing core microbiota in different fermentation stages of dajiang, a traditional fermented soybean paste of Northeast China. *Food Chem.* (2021) 343:128509. doi: 10.1016/j.foodchem.2020.128509
33. Wu JR, Tian T, Liu YM, Shi YX, Tao DB, Wu RN, et al. The dynamic changes of chemical components and microbiota during the natural fermentation process in Da-Jiang, a Chinese popular traditional fermented condiment. *Food Res Int.* (2018) 112:457–67. doi: 10.1016/j.foodres.2018.06.021
34. Chiang CM, Wang DS, Chang TS. Improving free radical scavenging activity of soy isoflavone glycosides daidzin and genistin by 3'-Hydroxylation using recombinant *Escherichia coli*. *Molecules.* (2016) 21:1723. doi: 10.3390/molecules21121723
35. Rafii F. The role of colonic bacteria in the metabolism of the natural isoflavone daidzin to equol. *Metabolites.* (2015) 5:56–73. doi: 10.3390/metabo5010056
36. Mustafa SE, Mustafa S, Abas F, Manap MYABD, Ismail A, Amid M, et al. Optimization of culture conditions of soymilk for equol production by *Bifidobacterium* breve 15700 and *Bifidobacterium longum* BB536. *Food Chem.* (2019) 278:767–72. doi: 10.1016/j.foodchem.2018.11.107
37. Cheng J, Luo Q, Duan HC, Peng H, Zhang Y, Hu JP, et al. Efficient whole-cell catalysis for 5-aminovalerate production from L-lysine by using engineered *Escherichia coli* with ethanol pretreatment. *Sci Rep*. (2020) 10:990. doi: 10.1038/s41598-020-57752-x
38. Zeng W, Huang KE, Luo Y, Li DX, Chen W, Yu XQ, et al. Nontargeted urine metabolomics analysis of the protective and therapeutic effects of Citri Reticulatae Chachiensis Pericarpium on high-fat feed-induced hyperlipidemia in rats. *Biomed Chromatogr.* (2020) 34:e4795. doi: 10.1002/bmc.4795
39. Piornos JA, Balagiannis DP, Methven L, Koussissi E, Brouwer E, Parker JK. Elucidating the odor-active aroma compounds in alcohol-free beer and their contribution to the worty flavor. *J Agr Food Chem.* (2020) 68:10088–96. doi: 10.1021/acs.jafc.0c03902
40. Zhao GZ, Ding LL, Hadiatullah H, Li S, Wang XW, Yao YP, et al. Characterization of the typical fragrant compounds in traditional Chinese-type soy sauce. *Food Chem.* (2020) 312:126054. doi: 10.1016/j.foodchem.2019.126054
41. Osimani A, Ferrocino I, Agnolucci M, Cocolin L, Giovannetti M, Cristani C, et al. Unveiling hakarl: a study of the microbiota of the traditional Icelandic fermented fish. *Food Microbiol.* (2019) 82:560–72. doi: 10.1016/j.fm.2019.03.027
42. Simo C, Garcia-Canas V. Dietary bioactive ingredients to modulate the gut microbiota-derived metabolite TMAO. New opportunities for functional food development. *Food Funct.* (2020) 11:6745–76. doi: 10.1039/D0FO01237H
43. Dajanta K, Apichartsrangkoon A, Chukeatirote E, Frazier RA. Free-amino acid profiles of thua nao, a Thai fermented soybean. *Food Chem.* (2011) 125:342–7. doi: 10.1016/j.foodchem.2010.09.002
44. Jin W, Zhang Z, Zhu K, Xue Y, Xie F, Mao S. Comprehensive understanding of the bacterial populations and metabolites profile of fermented feed by 16S rRNA gene sequencing and liquid chromatography-mass spectrometry. *Metabolites.* (2019) 9:239. doi: 10.3390/metabo9100239
45. Xu D, Wang P, Zhang X, Zhang J, Sun Y, Gao L, et al. High-throughput sequencing approach to characterize dynamic changes of the fungal and bacterial communities during the production of sufu, a traditional Chinese fermented soybean food. *Food Microbiol.* (2020) 86:103340. doi: 10.1016/j.fm.2019.103340
46. Namgung HJ, Park HJ, Cho IH, Choi HK, Kwon DY, Shim SM, et al. Metabolite profiling of doenjang, fermented soybean paste, during fermentation. *J Sci Food Agric.* (2010) 90:1926–35. doi: 10.1002/jsfa.4036
47. Shahzad R, Shehzad A, Bilal S, Lee IJ. *Bacillus amyloliquefaciens* RWL-1 as a new potential strain for augmenting biochemical and nutritional composition of fermented soybean. *Molecules.* (2020) 25:2346. doi: 10.3390/molecules25102346
48. Roberts SA, Ball RO, Filler R, Moore AM, Pencharz PB. Phenylalanine and tyrosine metabolism in neonates receiving

parenteral nutrition differing in pattern of amino acids. *Pediatr Res.* (1998) 44:907–14. doi: 10.1203/00006450-199812000-00014
49. Kiriyama K, Hara KY, Kondo A. Oxidized glutathione fermentation using *Saccharomyces cerevisiae* engineered for glutathione metabolism. *Appl Microbiol Biot.* (2013) 97:7399–404. doi: 10.1007/s00253-013-5074-8
50. Perin EC, Messias RD, Borowski JM, Crizel RL, Schott IB, Carvalho IR, et al. ABA-dependent salt and drought stress improve strawberry fruit quality. *Food Chem.* (2019) 271:516–26. doi: 10.1016/j.foodchem.2018.07.213
51. Ai J, Wu QX, Battino M, Bai WB, Tian L. M. Using untargeted metabolomics to profile the changes in roselle (*Hibiscus sabdariffa* L) anthocyanins during wine fermentation. *Food Chem.* (2021) 364:130425. doi: 10.1016/j.foodchem.2021.130425
52. Coklo M, Maslov DR, Kraljević Pavelić S. Modulation of gut microbiota in healthy rats after exposure to nutritional supplements. *Gut Microbes.* (2020) 12:1–28. doi: 10.1080/19490976.2020.1779002
53. Owusu-Kwarteng J, Parkouda C, Adewumi GA, Ouoba LII, Jespersen L. Technologically relevant *Bacillus* species and microbial safety of west African traditional alkaline fermented seed condiments. *Crit Rev Food Sci Nutr.* (2020) 1–18. doi: 10.1080/10408398.2020.1830026
54. Ezeokoli O, Gupta A, Popoola T, Bezuidenhout C. Molecular analysis of bacterial community dynamics during the fermentation of soy-daddawa condiment. *Food Sci Biotechnol.* (2016) 25:1081–6. doi: 10.1007/s10068-016-0174-8
55. Hou, Q.C., Zhao, F.Y., Liu, W.J., Lv, R.R., Khine, W.W.T., Han, J., et al. (2020). Probiotic-directed modulation of gut microbiota is basal microbiome dependent. Gut Microbes. 2020, 12:1736974. doi: 10.1080/19490976.2020.1736974
56. Hu YL, Dun YH, Li SN, Zhang DX, Peng N, Zhao SM, et al. Dietary *Enterococcus faecalis* LAB31 improves growth performance, reduces diarrhea, and increases fecal *Lactobacillus* number of weaned piglets. *PLoS ONE.* (2015) 10:e0116635. doi: 10.1371/journal.pone.0116635
57. Foulquie Moreno MR, Sarantinopoulos P, Tsakalidou E, De Vuyst L. The role and application of enterococci in food and health. *Int J Food Microbiol.* (2006) 106:1–24. doi: 10.1016/j.ijfoodmicro.2005.06.026
58. Lopez-Gonzalez JA, Suarez-Estrella F, Vargas-Garcia MC, Lopez MJ, Jurado MM, Moreno J. Dynamics of bacterial microbiota during lignocellulosic waste composting: Studies upon its structure, functionality and biodiversity. *Bioresour Technol.* (2015) 175:406–16. doi: 10.1016/j.biortech.2014.10.123
59. Xie WC, Song LY, Wang XY, Xu YG, Liu ZS, Zhao DF, et al. A bovine lactoferricin-lactoferrampin-encoding *Lactobacillus reuteri* CO21 regulates the intestinal mucosal immunity and enhances the protection of piglets against enterotoxigenic *Escherichia coli* K88 challenge. *Gut Microbes.* (2021) 13:1956281. doi: 10.1080/19490976.2021.1956281
60. Zong X, Fu J, Xu BC, Wang YZ, Jin ML. Interplay between gut microbiota and antimicrobial peptides. *Anim Nutr.* (2020) 6:389–96. doi: 10.1016/j.aninu.2020.09.002

Conflict of Interest: The authors declare that the research was conducted in the absence of any commercial or financial relationships that could be construed as a potential conflict of interest.

Publisher's Note: All claims expressed in this article are solely those of the authors and do not necessarily represent those of their affiliated organizations, or those of the publisher, the editors and the reviewers. Any product that may be evaluated in this article, or claim that may be made by its manufacturer, is not guaranteed or endorsed by the publisher.

frontiers in Nutrition

ORIGINAL RESEARCH
published: 08 March 2022
doi: 10.3389/fnut.2022.833555

Soybean Whey Bio-Processed Using *Weissella hellenica* D1501 Protects Neuronal PC12 Cells Against Oxidative Damage

Liqing Yin[1,2†], *Yongzhu Zhang*[3†], *Fidelis Azi*[2], *Mekonen Tekliye*[2,4], *Jianzhong Zhou*[1,2,5], *Xiaonan Li*[1,5], *Zhuang Xu*[1,5], *Mingsheng Dong*[2] *and Xiudong Xia*[1,5*]

[1] *Institute of Agricultural Product Processing, Jiangsu Academy of Agricultural Sciences, Nanjing, China,* [2] *College of Food Science and Technology, Nanjing Agricultural University, Nanjing, China,* [3] *Institute of Food Safety and Nutrition, Jiangsu Academy of Agricultural Sciences, Nanjing, China,* [4] *Faculty of Chemical and Food Engineering, Bahir Dar Institute of Technology, Bahir Dar University, Bahir Dar, Ethiopia,* [5] *School of Food and Biological Engineering, Jiangsu University, Zhenjiang, China*

OPEN ACCESS

Edited by:
Sandrina A. Heleno, Polytechnic Institute of Bragança (IPB), Portugal

Reviewed by:
Viduranga Y. Waisundara, Australian College of Business and Technology, Sri Lanka
Miryam Amigo-Benavent, University of Limerick, Ireland

***Correspondence:**
Xiudong Xia
86084056@163.com

†These authors have contributed equally to this work and share first authorship

Specialty section:
This article was submitted to Food Chemistry, a section of the journal Frontiers in Nutrition

Received: *11 December 2021*
Accepted: *11 February 2022*
Published: *08 March 2022*

Citation:
Yin L, Zhang Y, Azi F, Tekliye M, Zhou J, Li X, Xu Z, Dong M and Xia X (2022) Soybean Whey Bio-Processed Using Weissella hellenica D1501 Protects Neuronal PC12 Cells Against Oxidative Damage. Front. Nutr. 9:833555. doi: 10.3389/fnut.2022.833555

Soybean whey, as a byproduct of soybean industry, has caused considerable concern recently because of its abundant nutrients. To further utilize soybean whey, it was fermented with *Weissella hellenica* D1501, and the neuroprotective potency of this beverage was studied in the present work. The phenolic profile and antioxidant capacity of fermented soybean whey (FSBW) were analyzed. The neuroprotective effects were evaluated based on the hydrogen peroxide-stimulated oxidative damage model in a neural-like cell (PC12). Results demonstrated that soybean whey's phenolic contents and antioxidant activities were markedly improved after fermentation. Glycoside isoflavones were efficiently converted into aglycones by *W. hellenica* D1501. FSBW extract apparently increased cell viability, decreased reactive oxide species levels, and protected antioxidant enzymes in oxidative damage. Furthermore, FSBW effectively reduced apoptosis rate by inhibiting Bax protein and improving Bcl-2 and Bcl-xL proteins. FSBW ameliorated the cell cycle through the decrease of p21 protein and an increase of cyclin A protein. The findings of this study thus suggested that *W. hellenica* D1501-fermented soybean whey could potentially protect nerve cells against oxidative damage.

Keywords: phenolic profile, antioxidant enzyme, apoptosis rate, nerve cell, beverage

INTRODUCTION

Soybean products are popular worldwide that are linked to various high-quality nutrition and associated health-promoting effects (1, 2). Large quantities of soybean whey are generated during processing soybean-derived food products, and it is generally discarded as waste, resulting in environmental problems (3, 4). Reports have shown that soybean whey is rich in various useful compounds, including phenolics, common isoflavones (glycitin, daidzin, genistin, glycitein, daidzein, and genistein), and oligosaccharides, which benefit human health (5, 6). Instead of treating soybean whey as a waste, it has been utilized as a potential resource in

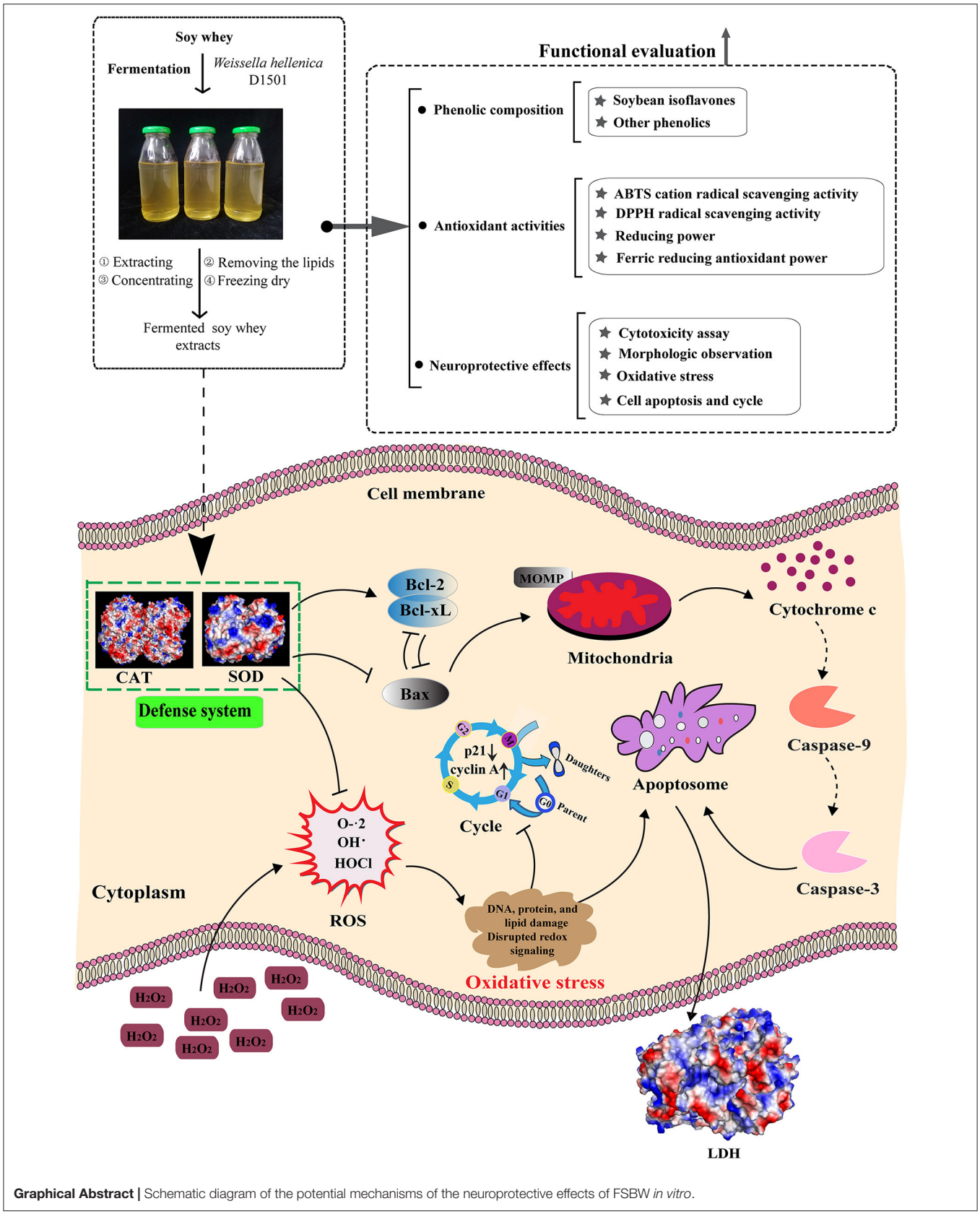

Graphical Abstract | Schematic diagram of the potential mechanisms of the neuroprotective effects of FSBW *in vitro*.

a variety of ways. Soybean whey can be used as a useful substrate for probiotics to produce a beverage with a potential *in vitro* antihypertensive bioactivity (3). Soybean whey bio-processed with *Lactobacillus amylolyticus* can be served as a coagulant for tofu production (6). Soybean whey can also be directly biotransformed into a novel functional alcoholic beverage with high content of free isoflavones after *Saccharomyces cerevisiae*-fermentation (4). Furthermore, isoflavone glycosides (glycitin, daidzin, and genistin) in soybean whey can be efficiently hydrolyzed into its corresponding aglycones (glycitein, daidzein, and genistein) with high bioactivity during fermentation (7–9).

Neurodegenerative diseases have drawn much attention recently due to their damage to the human lifespan (10, 11). The overproduction of reactive oxygen species (ROS) can oxidize biomacromolecules, destroy mitochondrial function, and promote neuronal apoptosis, consequently causing neurodegenerative diseases (12, 13). Plant polyphenols are widely believed to be a potent free radical scavenger to attenuate oxidative stress (14). There is increasing evidence that polyphenolic extracts, especially soybean isoflavones, are effective in the mice model of Alzheimer's and Parkinson's diseases (15, 16). Fermented soybean whey (FSBW) with lactic acid bacteria has been reported to be rich in phenolics, especially aglycone isoflavones (6, 7). Nevertheless, the information involved in the protective effects of lactic acid bacteria-fermented soybean whey on nerve cells and the underlying mechanisms is still unclear.

PC12 cells were derived from rat pheochromocytoma cells and commonly used as an *in vitro* model for studying neuronal apoptosis, oxygen sensor mechanisms, and neuronal differentiation (17). In this study, the neuroprotective effects of soybean whey bio-processed with *W. hellenica* D1501 on preventing hydrogen peroxide (H_2O_2)-stimulated oxidative damage were evaluated in PC12 cells. We also identified the phenolic composition and investigated the antioxidant activity of FSBW. The present study aimed to develop FSBW as a potential beverage to protect brain neurons from oxidative damage.

MATERIALS AND METHODS

Bacteria

The strain *W. hellenica* D1501 (Genbank: FJ654461) was first cultured in MRS (pH 6.2) at 37°C for 24 h and then expanded under the same condition for 16 h. The cells were obtained after centrifugation at 5,000 × *g* for 10 min and then resuspended using sterilized physiological saline (0.85% g/v) for soybean whey fermentation.

Soybean Whey Fermentation and Extraction

Soybean whey was first sterilized under 108°C for 15 min. Then, 1% (v/v) of the sterilized physiological saline containing *W. hellenica* D1501 (OD_{600nm} 1.0) was inoculated into soybean whey. The mixture was cultivated in a constant temperature incubator at 37°C for 24 h to obtain FSBW. After fermentation, FSBW was extracted with 80% (v/v) ethanol in an ultrasonic bath and then centrifuged at 10,000 × *g* for 20 min. Subsequently, the supernatant was filtered using a 0.45 μm syringe filter and treated with hexanes to remove the lipids. The filtrate was freeze-dried at−50°C for further study. The unfermented soybean whey (USBW) was treated under the same conditions except *W. hellenica* D1501 fermentation and served as a control.

Phenolic Composition and Antioxidant Capacity

Samples were dissolved in 80% (v/v) methanol. A 0.22 μm syringe filter was used to remove solid particles. The phenolic composition was analyzed using high-performance liquid chromatography (HPLC) equipped with the ZORBAX Eclipse Plus C18 reversed-phase analytical column (4.60 × 250 mm, 5 μm, Agilent). 0.4% (v/v) acetic acid in water (buffer A) and acetonitrile (buffer B) were the mobile phases. Detailed elution was conducted as the report of our previous work (18). The total phenolic content (TPC) was measured using Folin-Ciocalteau assay as Xiao et al. (7). The antioxidant capacities, including DPPH radical scavenging activity, ABTS radical cation scavenging activity, reducing power (RP), and ferric reducing antioxidant power (FRAP), were also performed according to Yin et al. (18).

Influence of USBW and FSBW on Oxidative Damage

Cell Culture and Cytotoxicity

PC12 cells were cultivated in DMEM (Gibco, USA) added with streptomycin (100 μg/mL), penicillin (100 U/mL), and fetal bovine serum (10%, Gibco, USA) inactivated by heat. Cells were kept in a 5% CO_2 incubator at 37°C for at least 2 days before further study. Cell viability was measured according to the method provided by Zhang et al. (19). Briefly, 1.8×10^4 cells were seeded in each well of 96-well plate for 12 h. And then the cells were treated with H_2O_2 or the extracts of USBW and FSBW at different concentrations for 4 h. The plate was supplemented with MTT solution and maintained at 37°C for 4 h. Subsequently, the reaction product of MTT was extracted in dimethylsulfoxide (DMSO) (150 μL) after the culture was removed. The optical density was spectrophotometrically read at 490 nm.

Influence of USBW and FSBW on H_2O_2-Stimulated Loss of Cell Viability

A density of 1.8×10^4 cells/well was seeded in a 96-well plate at 37°C for 12 h and then stimulated with H_2O_2 (550 μM) for

Abbreviations: USBW, Unfermented Soybean Whey; FSBW, Fermented Soybean Whey; HPLC, High-Performance Liquid Chromatography; ABTS, 2,2-azinobis(3-ethylbenzothiazoline-6-sulfonic acid) diammonium salt; DPPH, 2,2-diphenyl-1-picrylhydrazyl; RP, Reducing Powder; FRAP, Ferric Reducing Antioxidant Power; TPC, Total Phenolic Content; H_2O_2, hydrogen peroxide; LDH, Lactic Dehydrogenase; MTT, 3-(4,5-dimethylthiazol-2-yl)-2,5-diphenyl tetrazolium bromide; CAT, catalase; SOD, Superoxide Dismutase; ROS, Reactive Oxygen Species; DMEM, Dulbecco's modified Eagle's Medium; GAE, Gallic Acid Equivalent; GSH-Px, glutathione peroxidase.

4 h and with or without different concentrations of USBW and FSBW extracts. After incubation, cell viability was determined using MTT assay as described above.

Influence of USBW and FSBW on LDH Level in Culture Medium

A density of 3.6×10^5 cells/well was seeded in a 6-well plate at 37°C for 12 h. Subsequently, cells were stimulated using H_2O_2 (550 μM) and with or without different concentrations of USBW and FSBW extracts for 4 h. According to its instruction, an LDH assay kit (Beyotime, China) was used to determine the LDH levels. Furthermore, the cell morphology of PC12 cells was examined using an inverted microscope (ECLIPSE TE2000-S, Nikon, Japan).

Influence of USBW and FSBW on ROS Production

A density of 3.6×10^5 cells/well was seeded in a 6-well plate for 12 h. Subsequently, cells were stimulated using H_2O_2 (550 μM) and with or without USBW and FSBW extracts at 3 mg/mL for 4 h. A ROS assay kit (Beyotime, China) was used to measure the ROS level according to its instruction. In brief, the adherent cells were collected using trypsin and then mixed with 10 μM DCFH-DA at 37°C for 20 min. The cells were resuspended in a cell culture medium without serum. The production of ROS was monitored using a flow cytometer (Accuri C6 Plus, BD, USA).

Influence of USBW and FSBW on Catalase, Superoxide Dismutase, and Glutathione Peroxidase

After treatment as described above, cells were collected using trypsin and treated with an ultrasonic cell disruption system. After centrifugation at 10,000 × *g* for 20 min, the supernatant obtained was applied to determine antioxidant enzyme activities using catalase (CAT), superoxide dismutase (SOD), and glutathione peroxidase (GSH-Px) kits (Beyotime, China) based on their instructions. The protein content in the lysate was quantified according to the BCA method.

Influence of USBW and FSBW on Cell Apoptosis

PC12 cells were treated as above and harvested by trypsin. Cell apoptosis rates were determined based on the instruction of a cell apoptosis kit (Beyotime, China). In brief, cells were washed, resuspended with annexin V-FITC binding buffer, and then incubated with Annexin V-FITC and prodium iodide (1:2, v/v) at room temperature for 20 min. The fluorescence was quantified using a flow cytometer (Accuri C6 Plus, BD, USA).

Influence of USBW and FSBW on Cell Cycle

PC12 cells were treated as above and harvested by trypsin. The cell cycle was determined based on the instruction of a cell cycle kit (Beyotime, China). Shortly, PC12 cells were washed and fixed using 70% ethanol (v/v). And then cells were washed again and dyed using a prodium iodide staining reagent. The fluorescence intensity was quantified using a flow cytometer (Accuri C6 Plus, BD, USA).

Western Blot Analysis

The western blot analysis was performed following Zhang et al. (19). Shortly, PC12 cells were harvested and lysed using RIPA buffer. The lysate was centrifuged to collect the supernatant. The protein content was quantified with the BCA method. Protein (30 μg/lane) was loaded into 10% or 15% SDS-PAGE gel. After electrophoresis, the protein bands were transferred to a PVDF membrane (Bio-Rad, USA). The membranes were incubated with antibodies against Bax, Bcl-2, Bcl-xL, cyclin A, p21, and β-tubulin proteins. Afterward, the protein signals were enhanced by HRP-conjugated secondary antibody. And then the membrane was treated with an ECL reagent and analyzed by a detection system (ImageQuant LAS4000mini, GE, USA). The densitometric semi-quantifications of the western blot results were determined using ImageJ software.

Statistical Analysis

All experiments were repeated at least three independent times. Each value was represented as mean ± standard deviation. Data were analyzed by one-way ANOVA (Duncan's *post-hoc* multiple comparisons) in SPSS. The treatment effect was considered significant at $p < 0.05$.

RESULTS

Phenolic Compositions of USBW and FSBW

As shown in **Table 1**, the TPC of soybean whey significantly ($p < 0.05$) increased after *W. hellenica* D1501 fermentation, wherein the TPC of FSBW extract was 18.36% higher than that of USBW. *W. hellenica* D1501 fermentation also showed a significant effect on the phenolic compositions of soybean whey. This study investigated eleven phenolics in soybean whey (**Table 1**, **Supplementary Figure 1**). Six soybean isoflavones, including glycitein, genistein, daidzein, glycitin, daidzin, and genistin, were the major phenolic components in soybean whey and accounted for 81.32% of the TPC in USBW and 73.41% of the TPC in FSBW. The glycosidic isoflavones were efficiently transformed into their corresponding aglycones during fermentation. The total glycosidic isoflavone, including glycitin, daidzin, and genistin, was 528.49 mg/100 g extract in USBW, which made up 83.35% of the total soybean isoflavones. The aglycone isoflavone, including glycitein, genistein, and daidzein, was 637.30 mg/100 g extract in FSBW, which made up 94.08% of the total soybean isoflavones. Phenolics like chlorogenic acid, vanillic acid, caffeic acid, ferulic acid, and quercetin were also analyzed by HPLC after fermentation (**Table 1**). Results showed no effects on chlorogenic acid and vanillic acid, and the others were not detected. Meanwhile, the detected TPC was higher than that obtained from HPLC analysis. This was possibly due to the fact that some phenolic compounds in small concentrations were not detected by HPLC (7).

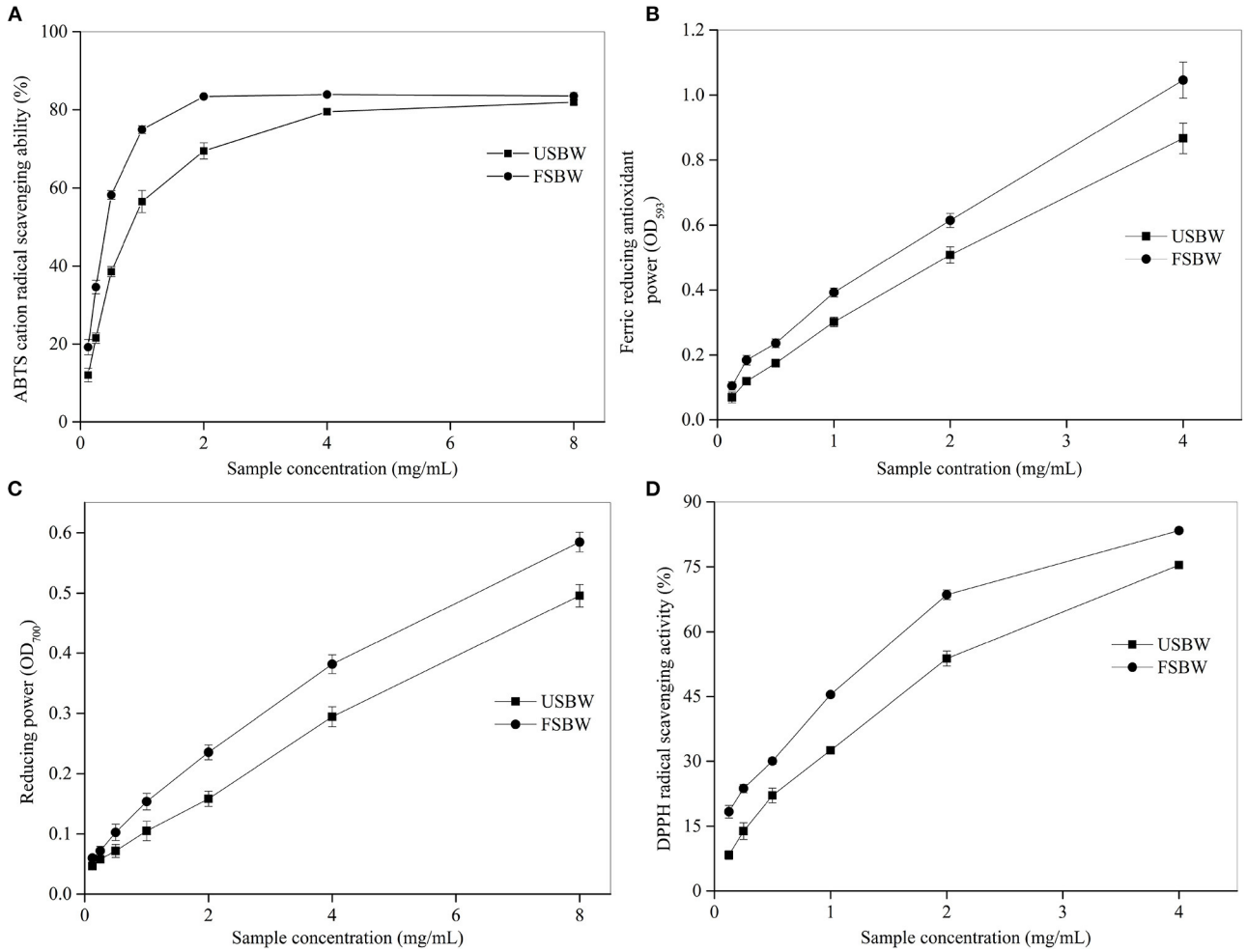

FIGURE 1 | Antioxidant capacity of USBW and FSBW extracts. **(A)** ABTS·$^+$ scavenging capacity; **(B)** ferric reducing antioxidant power; **(C)** reducing power; **(D)** DPPH radical scavenging capacity.

Antioxidant Properties of USBW and FSBW

The antioxidant activities of foods are up to the composition and concentrations of their antioxidant compounds. Different antioxidants show their radical scavenging activities through different mechanisms (20). Consequently, four assays were chosen to appraise the antioxidant ability of USBW and FSBW in this study. Soybean whey's ABTS·$^+$ scavenging ability was significantly enhanced after fermentation (**Figure 1A**). For instance, when the extract concentration was 0.5 mg/mL, the ABTS·$^+$ scavenging ability of FSBW was 58.19%, which was 1.51 times that for USBW. The ABTS·$^+$ scavenging ability of USBW and FSBW also exhibited an apparent dose-dependent effect with the increased extract concentration. Furthermore, a similar trend was also observed in FRAP, RP, and DPPH (**Figures 1B–D**). The half-efficiency concentration (EC_{50}) is generally used to express the antioxidant activity of compounds, and its value is inversely related to the antioxidant activity (19). In the present work, EC_{50} values of USBW and FSBW were also analyzed in **Supplementary Table 1**. The result showed that the EC_{50} values of soybean whey were all significantly decreased after fermentation. The EC_{50} values for ABTS$\bullet^+$ scavenging ability, DPPH scavenging ability, and RP of FSBW, respectively, decreased by 48.91, 40.19, and 20.50% compared with those of USBW.

Effects of USBW and FSBW on H_2O_2-Induced Oxidative Injury

Cytotoxicity Evaluation

In this study, PC12 cells were incubated with various concentrations of H_2O_2 ranging from 50 to 700 μM for 4 h. As shown in **Figure 2A**, the H_2O_2-induced injury was in a clear dose-dependent manner. The PC12 cell viability held steady when H_2O_2 was below 300 μM, and then a rapid decrease was observed (>300 μM). Exposure to 550 μM H_2O_2 for 4 h led to a 47.07% decrease in the cell viability of PC12 cells. So 550 μM H_2O_2 was chosen to stimulate oxidative injury in the following treatment. The safe dose of the USBW and FSBW extracts was also investigated in this study. The USBW and FSBW extracts

TABLE 1 | Phenolic profile of USBW and FSBW.

Peak	Phenolic compound (mg/100 g)	USBW	FSBW
1	Chlorogenic acid	4.69 ± 0.38^{Ea}	4.72 ± 0.33^{Da}
2	Vanillic acid	16.50 ± 0.96^{DEa}	15.26 ± 0.67^{CDa}
3	Caffeic acid	N.D.	N.D.
4	Daidzin	318.97 ± 27.75^{Aa}	8.62 ± 1.22^{Db}
5	Glycitin	65.84 ± 6.54^{Ca}	29.03 ± 2.47^{Cb}
6	Ferulic acid	N.D.	N.D.
7	Genistin	143.68 ± 9.70^{Ba}	2.48 ± 0.12^{Db}
8	Daidzein	26.20 ± 2.29^{Db}	208.52 ± 24.88^{Ba}
9	Glycitein	63.80 ± 7.08^{Cb}	236.00 ± 11.50^{Aa}
10	Quercetin	N.D.	N.D.
11	Genistein	15.56 ± 1.15^{DEb}	192.78 ± 5.90^{Ba}
	TPC (mg GAE/100 g)	779.70 ± 31.62^{b}	922.86 ± 22.51^{a}

N.D., not detected; TPC, total phenolic content; GAE, gallic acid equivalent. $p < 0.05$ was considered as the significant level. The different small letters a and b were used to show the significant difference between USBW and FSBW for the same component where "a" indicates a significantly higher yield than "b". The different capital letters within a column indicate the significant difference and the ordering of results.

below 3 mg/mL were non-cytotoxic to PC12 cells (**Figure 2B**). However, cell viability exhibited an obvious decrease when PC12 cells were exposed to a higher dose (4 mg/mL) of FSBW extract (**Figure 2B**). Therefore, the safe dose (<4 mg/mL) of samples for PC12 cells was chosen for further study.

Protection of USBW and FSBW on PC12 Cell Viability

Cells were stimulated with 550 μM H_2O_2, treated with or without the USBW, and FSBW extracts at nontoxic concentrations (0.5–3 mg/mL) for 4 h. As shown in **Figure 2C**, cell viability treated with only H_2O_2 apparently decreased to 52.93% of the untreated group. However, incubation with soybean whey extracts significantly reduced the cell damage induced by oxidative injury. Additionally, FSBW exhibited higher protection on PC12 cells than USBW. The FSBW extract at 3 mg/mL presented the highest protection on PC12 cells against the H_2O_2 damage by increasing the cell viability from 52.93 to 86.66%, which was 1.19 times that of the USBW extract-treated group. Furthermore, USBW and FSBW extracts also significantly reduced the LDH release (**Figure 2D**) and improved cell morphology (**Figure 2E**).

Attenuation of USBW and FSBW on H_2O_2-Induced Oxidative Stress

ROS played an essential role in H_2O_2-stimulated oxidative damage (21). As shown in **Figures 3A,B**, H_2O_2 treatment resulted in an obvious increase in ROS production in PC12 cells. ROS levels in PC12 cells exposed to only H_2O_2 increased by 291.45% of that in the untreated control. However, ROS production was significantly ($p < 0.05$) repressed when PC12 cells were cultured with the USBW and FSBW extracts at 3 mg/mL, decreasing ROS level from 391.45 to 262.10% and 175.40% compared with that of the H_2O_2-treated control, respectively. The defense mechanism composed of antioxidant enzymes, such as CAT and SOD, plays a crucial role in preventing oxidative damage caused by ROS (22). As shown in **Figures 3C–E**, the intracellular CAT, SOD, and GSH-Px activities in PC12 cells stimulated with 550 μM H_2O_2 exhibited a significant decrease, only 29.82, 36.10, and 44.27% compared with those in the untreated control, respectively. This effect of H_2O_2 on intracellular antioxidant enzyme activities was in agreement with the report of Tang et al. (22). However, treatment with the soybean whey extracts at a range of 0.5 mg/mL-3 mg/mL apparently promoted CAT, SOD, and GSH-Px activities in a dose-dependent way (**Figures 3C–E**). Furthermore, FSBW showed a more vital ability to induce the production of CAT, SOD, and GSH-Px. For example, the enzyme activities of CAT, SOD, and GSH-Px in the FSBW-treated group at 3 mg/mL were 1.26, 1.14, and 1.21 times those in the USBW-treated group, respectively.

Influence of USBW and FSBW on Cell Apoptosis

As shown in **Figure 4**, H_2O_2 treatment remarkably increased the PC12 cell apoptosis rate. The early and late apoptotic cells, respectively, distributed in Q3 and Q2 regions. The total apoptosis rate of H_2O_2-treated cells (38.71%) was 8.66-fold higher than that in the untreated control (4.47%). However, this increase of the PC12 cell apoptosis was significantly attenuated by USBW extract at 3 mg/mL (28.01%), with a 27.64% decrease in the cell apoptosis ratio compared with that in the H_2O_2-treated control (**Figures 4A,B**). FSBW also significantly decreased the cell apoptosis by 48.72% compared with H_2O_2-treated control. Furthermore, FSBW showed a stronger ability to decrease PC12 cell apoptosis. The total apoptosis rate in the FSBW-treated group was only 70.87% of that in the USBW-treated control.

The Bcl-2 and Bcl-xL proteins are crucial anti-apoptotic cytokines, and Bax is an apoptosis-promoter closely related to cell death, which usually forms a complex with Bcl-2 (23). To further study the protective mechanisms of USBW and FSBW, Influence on the expression levels of Bcl-2, Bcl-xL, and Bax protein, was investigated. **Figures 4C,D** showed that H_2O_2 treatment significantly ($p < 0.05$) up-regulated the pro-apoptotic protein Bax level. Inversely, the induced decreases by H_2O_2 in anti-apoptotic protein levels of Bcl-2 and Bcl-xL were markedly inhibited after USBW or FSBW treatments (**Figures 4C,E,F**), wherein the Bcl-2 and Bcl-xL protein levels in FSBW-treated cells, respectively, increased by 70.11 and 81.01% ($p < 0.05$). Therefore, FSBW effectively protected PC12 cells against oxidative injury-induced apoptosis by up-regulating the anti-apoptotic protein levels of Bcl-2 and Bcl-xL and down-regulating the pro-apoptotic protein level of Bax.

Influence of USBW and FSBW on Cell Cycle

As shown in **Figures 5A,B**, H_2O_2 inhibited PC12 cell proliferation by inducing S phase cell cycle arrest. H_2O_2 stimulation significantly ($p < 0.05$) increased the cell number at the S phase (43.28%) compared with the untreated control (25.43%), and the G1 phase cell reduced from 57.68% to 34.05%. The cell cycle arrest induced by H_2O_2 was inhibited by USBW extract, and this protection was improved after *W. hellenica* D1501 fermentation. For instance, the S phase cell significantly decreased from 43.28 to 36.05% in the USBW-treated group and

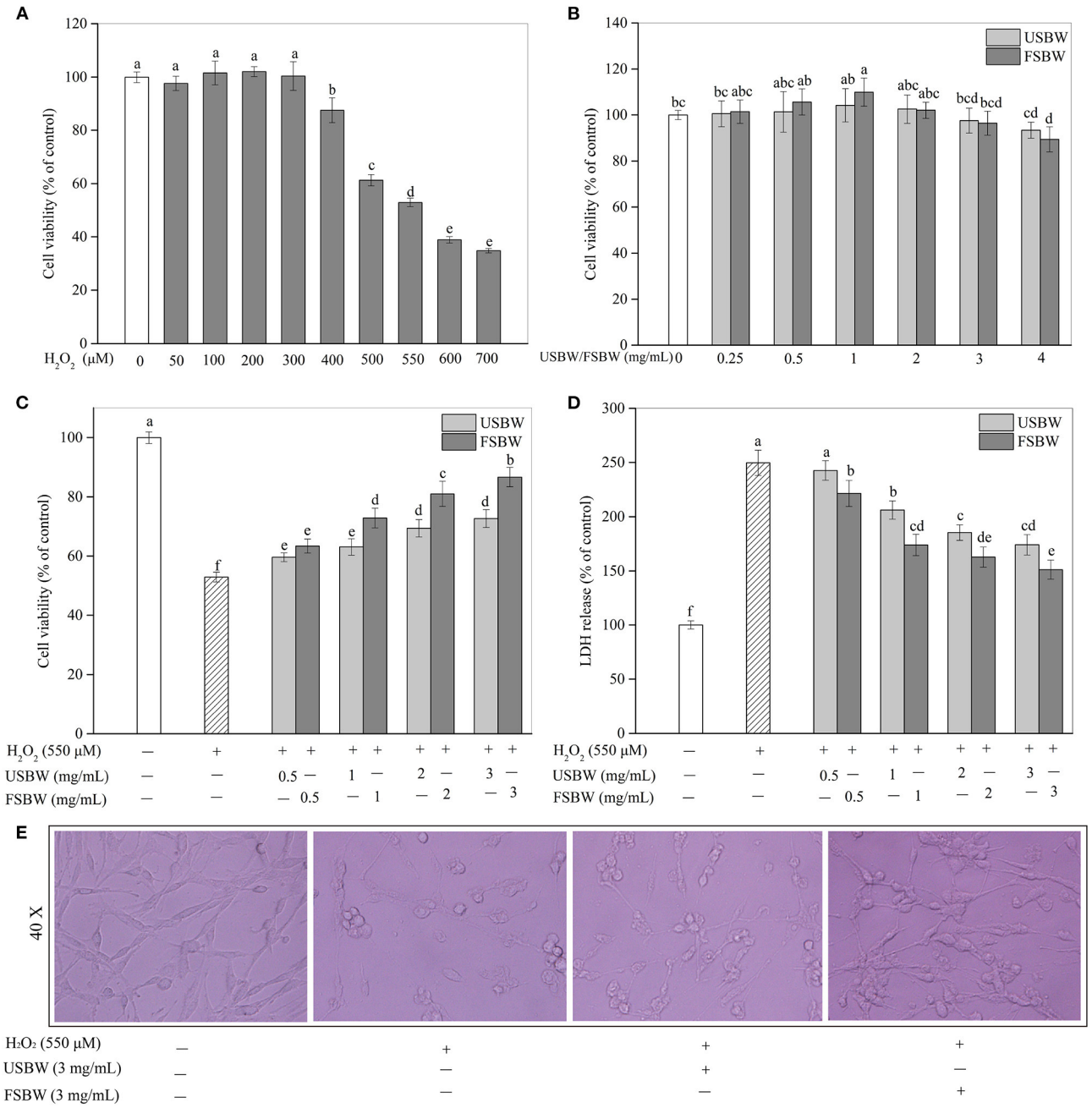

FIGURE 2 | Cytotoxicity and the protection of USBW and FSBW extracts on H_2O_2-induced oxidative damage. **(A)** Cytotoxicity of H_2O_2; **(B)** Cytotoxicity of USBW and FSBW extracts; **(C)** Cell viability; **(D)** LDH levels; **(E)** PC12 cell morphology. $p < 0.05$ was considered as the significant level. The small letters were used to indicate the significant difference and the ordering of results.

31.81% in the FSBW-treated group compared with the H_2O_2-treated control, and the G1 phase cell increased from 34.05 to 44.87% and 52.63%, respectively. The important proteins cyclin A and p21 participated in the cell cycle were measured to investigate the cellular mechanisms (**Figures 5C–E**). The level of cyclin A protein in PC12 cells suffered a significant decrease after H_2O_2 treatment, which was reduced by 34.71% compared to control. At the same time, an apparent increase in p21 protein level was also observed in the H_2O_2-treated group. The observed S phase cell cycle arrest induced by H_2O_2 was significantly attenuated by USBW or FSBW extracts through significant increase of the cyclin A protein level and decrease of the p21 protein level in PC12 cells. FSBW exhibited a more significant inhibitory effect on H_2O_2-induced S phase arrest than USBW

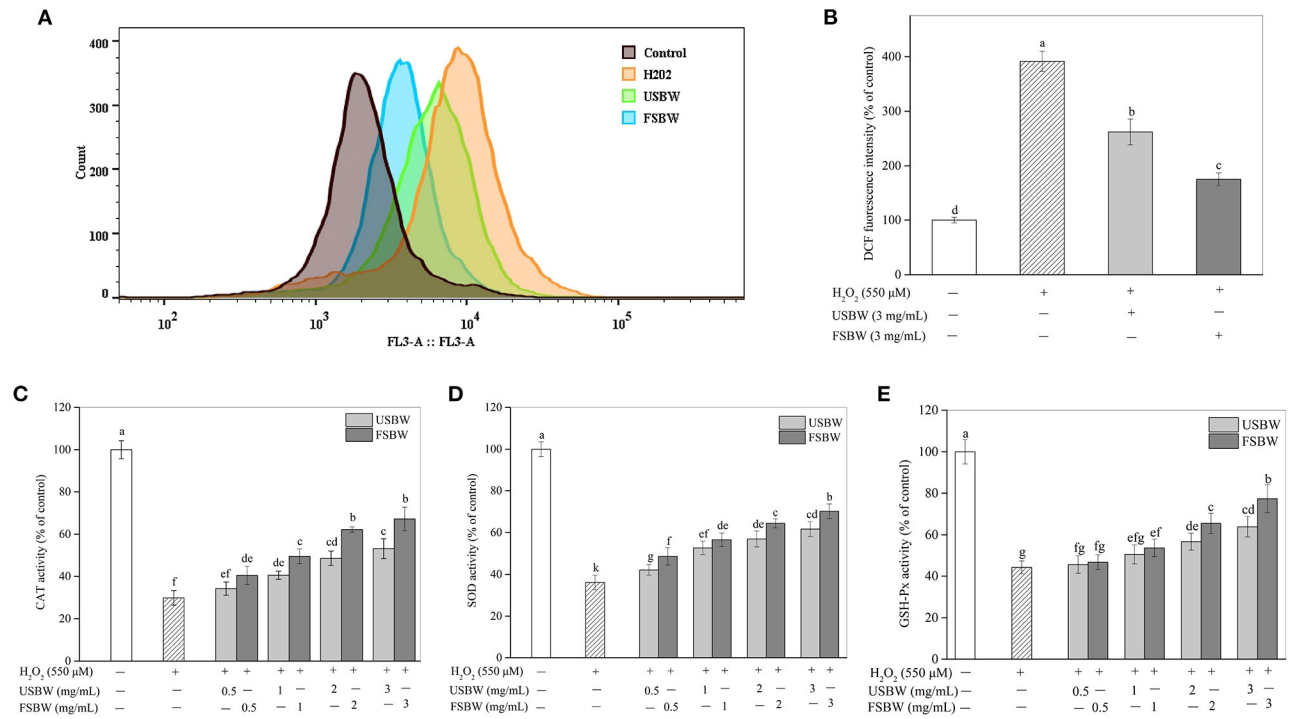

FIGURE 3 | Influence of USBW and FSBW on oxidative stress. **(A)** ROS production; **(B)** Statistical histogram in **(A)**; **(C)** Catalase (CAT) activity; **(D)** Superoxide dismutase (SOD) activity. **(E)** Glutathione peroxidase (GSH-Px) activity. $p < 0.05$ was considered as the significant level. The small letters were used to indicate the significant difference and the ordering of results.

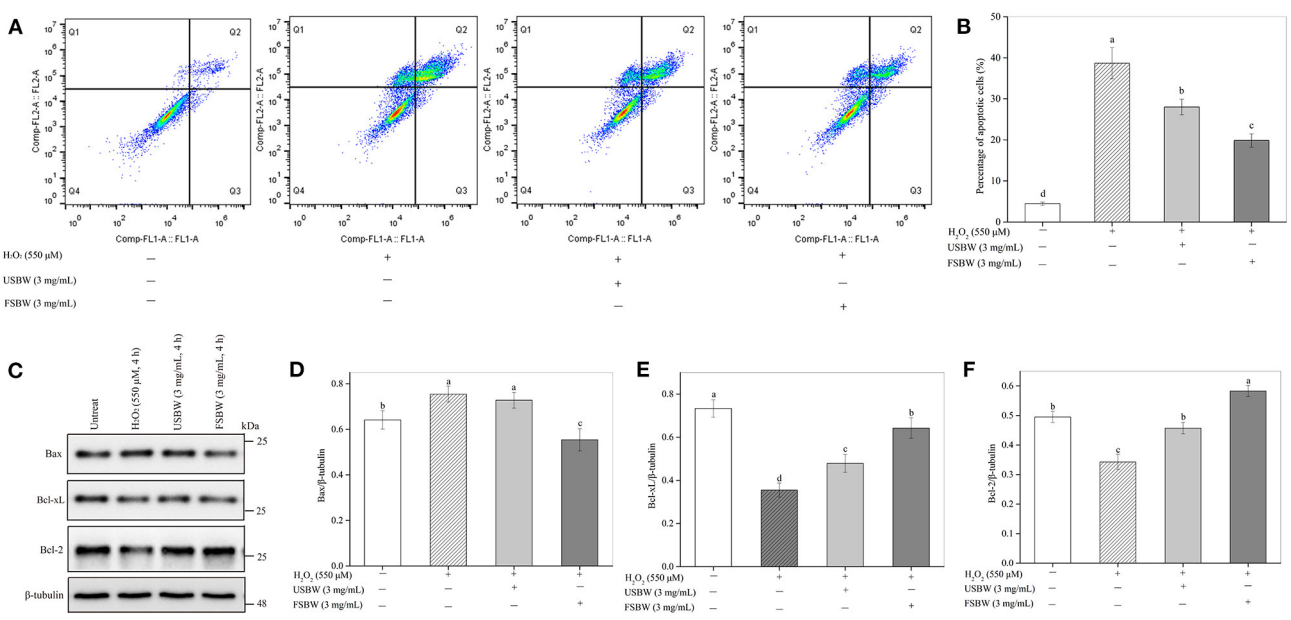

FIGURE 4 | Influence of the USBW and FSBW extracts on H_2O_2-induced cell apoptosis. **(A)** Cell apoptosis detected using a flow cytometer; **(B)** Statistical histogram in **(A)**; **(C)** Bcl-xL, Bax, and Bcl-2 levels; **(D–F)** Statistical histogram in **(C)**. $p < 0.05$ was considered as the significant level. The small letters were used to indicate the significant difference and the ordering of results.

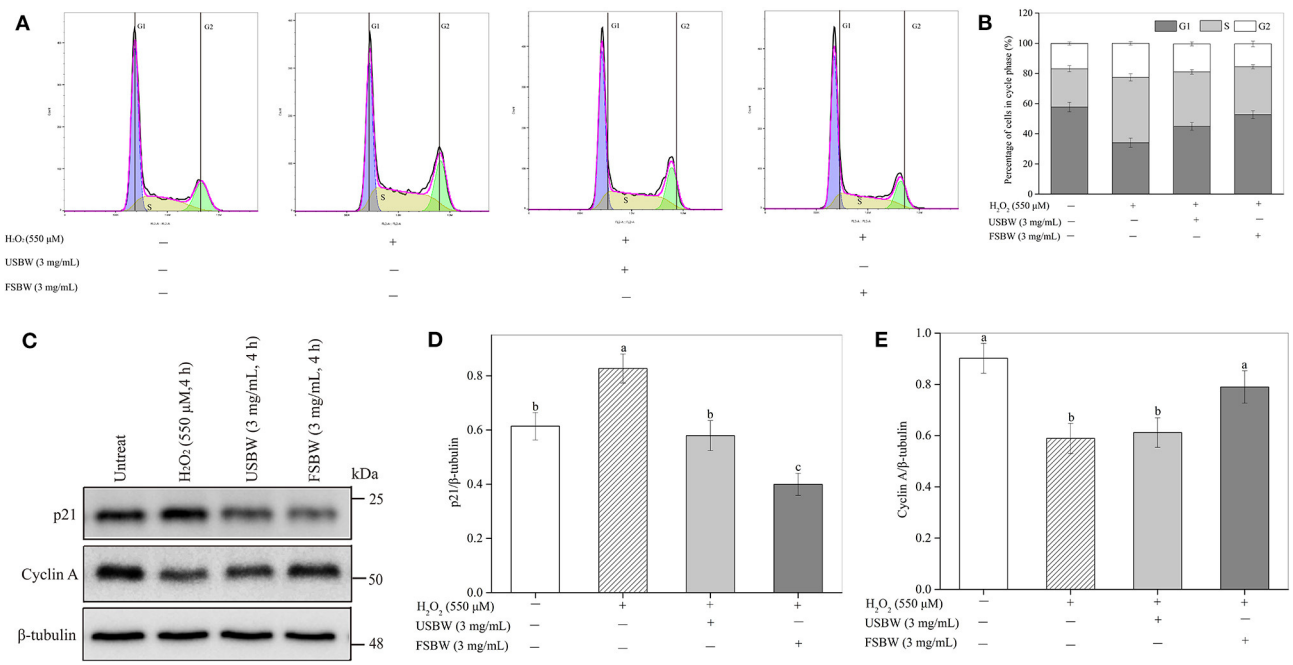

FIGURE 5 | Influence of USBW and FSBW in H_2O_2-induced cell cycle arrest. **(A)** Cell cycle detected using a flow cytometer; **(B)** Statistical histogram in **(A)**; **(C)** Cyclin A and p21 levels; **(D,E)** Statistical histogram in **(C)**. $p < 0.05$ was considered as the significant level. The small letters were used to indicate the significant difference and the ordering of results.

through improving a higher expression level of cyclin A protein and limiting p21 protein expression.

DISCUSSION

Soybean foods are a vital source of dietary polyphenols because of their abundant isoflavone content, which mainly exist as glucosides and aglycones (5, 6). It has been reported that isoflavones can ameliorate various diseases, including cardiovascular disease, tumor, and nervous disorder (15, 16, 24). Several reports have described that abundant soybean isoflavones are mostly transferred to soybean whey in the process of soybean foods (6, 7). In this study, the total content of 634.05 mg/100 g extract soybean isoflavones has existed in USBW, which indicated that soybean whey could serve as a good source for isoflavones. However, as a by-product of soybean products in large amounts every year, soybean whey is generally discarded by the food industry, thus resulting in environmental problems (3).

Microbial fermentation has been an efficient strategy to fully utilize soybean whey. Tu et al. (25) showed that soybean whey was a suitable substrate for water kefir to produce a new type of biomedical beverage due to its high phenolic content after fermentation. Chua et al. (4) found that *Saccharomyces cerevisiae*-fermentation can efficiently transform low bioactivity glucoside isoflavone to the corresponding high bioactivity aglycones and enhance the antioxidant capacity of soybean whey, obtaining an alcoholic beverage with fruity and floral notes. In this study, *W. hellenica* D1501 fermentation also significantly affected the phenolic content and composition. TPC in soybean whey significantly ($p < 0.05$) increased after fermentation and most isoflavone glucosides were converted into their corresponding aglycones. Most natural phenolic compounds generally occur as bound forms by forming covalent bonds with sugars and proteins, which are difficult to use for humans (5, 26). The enzymes produced by microorganisms, such as protease, cellulase, and glucosidase, can release bound phenolic acids, which well explains the increased TPC and aglycone isoflavone content of soybean whey after fermentation in this study (18). Plant phenolics exhibit a strong antioxidant ability to scavenge free radicals and form chelate complexes with prooxidant metals (27). Isoflavones in aglycone form exhibit higher antioxidant activity and are absorbed faster by cells than their corresponding glucosides because of their higher lipophilicity and smaller molecular weight (7–9). Therefore, the soybean whey's antioxidant activity, such as the free radical scavenging capacity of ABTS·+ and DPPH and the reduced power on Fe^{3+}, significantly ($p < 0.05$) increased after *W. hellenica* D1501 fermentation. Our results demonstrated that *W. hellenica* D1501 fermentation effectively produced a soybean whey beverage with high antioxidant activity.

The overproduction of ROS can oxidize biomacromolecules, break mitochondrial function, and promote neuronal apoptosis, consequently causing neurodegenerative diseases (12). Soybean whey was found to be rich in phenolics, especially isoflavones, which had a strong ability to scavenge free radicals (14). Consequently, the neuroprotective effect of FSBW against oxidative injury in PC12 cells was further studied. The study

indicated that H_2O_2 caused a strong oxidative injury in PC12 cells by significantly increasing ROS levels. The overproduction of ROS induced by H_2O_2 broke down the membrane integrity, caused cell morphological abnormality, damaged antioxidant enzyme, and resulted in cell apoptosis and cell cycle arrest, thereby presenting a significant decrease in PC12 cell viability. Evidence shows that antioxidants can protect cells against various stressors, concluding oxidative stress through their antioxidant action (28). In the present study, we found that soybean whey protected PC12 cells from H_2O_2-induced oxidative damage by maintaining cell viability, inhibiting the overproduction of ROS, reducing the loss of antioxidant enzymes, and attenuating cell apoptosis and cell cycle arrest. Furthermore, we found that USBW and FSBW extracts protected PC12 cells from oxidative injury-induced apoptosis through regulation of Bax, Bcl-2 and Bcl-xL proteins. In addition, USBW and FSBW notably reduced the S phase cell cycle by inhibiting the expression of p21 protein and improving the expression of cyclin A protein. Cho et al. (29) demonstrated that the leaf extract with a high phenolic content exhibits a strong antioxidant capacity and can significantly increase PC12 cell viability and membrane integrity, and reduce intracellular oxidative stress in a dose-dependent manner. Im et al. (30) presented that the phenolic compounds in romaine lettuce could help neuronal PC12 cells withstand oxidative stress by maintaining the integrity of cell membrane. Ma et al. (31) indicated that soybean isoflavone genistein could effectively recover PC12 cells' redox balance by decreasing the ROS production induced by Aβ25-35. Liu et al. (32) also found that H_2O_2-stimulated damage was effectively attenuated by the flavonoid extract derived from *Rosa laevigata Michx* fruit. Accordingly, the protective effects of soybean whey on PC12 cells were possibly attributed to its abundant phenolic component, especially the isoflavones, which can effectively enhance the ROS scavenging ability of PC12 cells.

The protection of soybean whey on PC12 cells was remarkably promoted by *W. hellenica* D1501 fermentation. This finding might be attributed to the increased phenolics and aglycone isoflavones in soybean whey after fermentation, which exhibited stronger antioxidant activity to scavenge H_2O_2-induced ROS, resulting in higher cell viability in the FSBW-treated group than that in the USBW-treated group. This was in agreement with the previous study results that fermented Kudzu root with higher flavonoid content showed stronger bioactivity to protect PC12 cells against H_2O_2-induced injury than non-fermented (33). Furthermore, soybean isoflavone glucosides were converted to their corresponding aglycones with high biological activity. The aglycones were more fastly absorbed by the cells culminating in a more effective activation of the antioxidant mechanism to remove ROS in cells (8). Di Cagno et al. (9) also found that fermented soybean milk rich in isoflavone aglycones exhibits higher bioactivity to protect the human intestinal Caco-2 cells against toxin-induced damage. The present study indicated that FSBW could potentially protect nerve cells from oxidative damage, thereby contributing to consumer's health.

In soybean industry, soy whey is a by-product from the preparation of soybean products such as tofu, and soy protein isolate, among others. Large amounts of soy whey are produced every year, and these are generally discarded and considered as waste, which have aggravated burden of the industry on sewage treatment and also a wastage of this resource (34). Based on our findings, these soy whey can be processed into a functional beverage with high antioxidant activity and potential neuroprotective effects by fermentation with *W. hellenica* D1501. Furthermore, this processing method has the advantages of short cycle (not more than 24 h), simple equipment, and low cost, which is very suitable for industrial mass production. Hence, our study provided a good strategy for the full utilization of soybean whey in industry. Of course, the present work was at the initial stage and not ready for trials in humans. Further studies will be performed in a mice model of Alzheimer's disease to explore the potential neuroprotective mechanism of FSBW.

CONCLUSIONS

W. hellenica D1501 fermentation was a good strategy to promote the biological activity of soybean whey. The total phenolic content of soybean whey was significantly increased after fermentation, consequently obtaining a higher antioxidant activity. Glycosides soybean isoflavones were efficiently converted to their corresponding aglycones by *W. hellenica* D1501. Soybean whey fermented with *W. hellenica* D1501 could significantly protect PC12 cells from H_2O_2-stimulated oxidative injury through enhancing cell viability, inhibiting ROS production, reducing the loss of antioxidant enzyme, attenuating cell cycle arrest, thus repressing cell apoptosis. The present study suggested that soybean whey fermented with *W. hellenica* D1501 could be used as a soybean beverage with potential health-promoting effects.

DATA AVAILABILITY STATEMENT

The raw data supporting the conclusions of this article will be made available by the authors, without undue reservation.

AUTHOR CONTRIBUTIONS

LY and YZ: investigation, methodology, formal analysis, writing-original draft, and visualization. FA and MT: methodology, data curation, and writing-review and editing. JZ, XL, ZX, and MD: resources, validation, and supervision. XX: conceptualization, data curation, funding acquisition, and writing-review and editing. All authors contributed to the article and approved the submitted version.

FUNDING

The financial support from Jiangsu Agriculture Science and Technology Innovation Fund (Grant No. CX(21)2003), Yangzhou Science and Technology Plan (Grant No. YZ2020044), and National Natural Science Foundation of China (Grant No. 31501460) are gratefully acknowledged.

ACKNOWLEDGMENTS

Thanks for Dr. Ning Wang and Dr. Wei Han in Central laboratory in Jiangsu Academy of Agricultural Sciences for their help in this work.

SUPPLEMENTARY MATERIAL

The Supplementary Material for this article can be found online at: https://www.frontiersin.org/articles/10.3389/fnut.2022.833555/full#supplementary-material

REFERENCES

1. Xia X, Dai Y, Wu H, Liu X, Wang Y, Yin L, et al. Kombucha fermentation enhances the health-promoting properties of soymilk beverage. *J Funct Foods.* (2019) 62:103549. doi: 10.1016/j.jff.2019.103549
2. Corzo-Martínez M, García-Campos G, Montilla A, Moreno FJ. Tofu whey permeate is an efficient source to enzymatically produce prebiotic fructooligosaccharides and novel fructosylated α-galactosides. *J Agri Food Chem.* (2016) 64:4346–52. doi: 10.1021/acs.jafc.6b00779
3. Fung WY, Liong MT. Evaluation of proteolytic and ACE-inhibitory activity of *Lactobacillus acidophilus* in soy whey growth medium via response surface methodology. *LWT-Food Sci Technol.* (2010) 43:563–7. doi: 10.1016/j.lwt.2009.10.004
4. Chua JY, Lu Y, Liu SQ. Biotransformation of soy whey into soybean alcoholic beverage by four commercial strains of *Saccharomyces cerevisiae*. *Int J Food Microbiol.* (2017) 262:14–22. doi: 10.1016/j.ijfoodmicro.2017.09.007
5. Azi F, Tu C, Meng L, Li Z, Cherinet MT, Ahmadullah Z, et al. Metabolite dynamics and phytochemistry of a soy whey-based beverage bio-transformed by water kefir consortium. *Food Chem.* (2020) 342:128225. doi: 10.1016/j.foodchem.2020.128225
6. Fei Y, Liu L, Liu D, Chen L, Tan B, Fu L, et al. Investigation on the safety of *Lactobacillus amylolyticus* L6 and its fermentation properties of tofu whey. *LWT-Food Sci Technol.* (2017) 84:314–22. doi: 10.1016/j.lwt.2017.05.072
7. Xiao Y, Wang L, Rui X, Li W, Chen X, Jiang M, et al. Enhancement of the antioxidant capacity of soy whey by fermentation with *Lactobacillus plantarum* B1-6. *J Funct Foods.* (2015) 12:33–44. doi: 10.1016/j.jff.2014.10.033
8. Izumi T, Piskula MK, Osawa S, Obata A, Tobe K, Saito M, et al. Soy isoflavone aglycones are absorbed faster and in higher amounts than their glucosides in humans. *J Nutr.* (2000) 130:1695–9. doi: 10.1093/jn/130.7.1695
9. Di Cagno R, Mazzacane F, Rizzello CG, Vincentini O, Silano M, Giuliani G, et al. Synthesis of isoflavone aglycones and equol in soy milks fermented by food-related lactic acid bacteria and their effect on human intestinal Caco-2 cells. *J Agric Food Chem.* (2010) 58:10338–46. doi: 10.1021/jf101513r
10. Dohrmann DD, Putnik P, Bursać Kovačević D, Simal-Gandara J, Lorenzo JM, Barba FJ. Japanese, mediterranean and argentinean diets and their potential roles in neurodegenerative diseases. *Food Res Int.* (2018) 120:464–77. doi: 10.1016/j.foodres.2018.10.090
11. Schimidt HL, Garcia A, Martins A, Mello-Carpes PB, Carpes FP. Green tea supplementation produces better neuroprotective effects than red and black tea in alzheimer-like rat model. *Food Res Int.* (2017) 100:442–8. doi: 10.1016/j.foodres.2017.07.026
12. Manoharan S, Guillemin GJ, Abiramasundari RS, Essa MM, Akbar M, Akbar MD. The role of reactive oxygen species in the pathogenesis of Alzheimer's disease, Parkinson's disease, and huntington's disease: a mini review. *Oxid Med Cell Longev.* (2016) 2016:8590578. doi: 10.1155/2016/8590578
13. Butterfield DA, Boyd-Kimball D, Perry G, Avila J, Zhu X. Oxidative stress, amyloid-β peptide, and altered key molecular pathways in the pathogenesis and progression of Alzheimer's disease. *J Alzheimers Dis.* (2018) 62:1345–67. doi: 10.3233/JAD-170543
14. Yoon G, Park S. Antioxidant action of soy isoflavones on oxidative stress and antioxidant enzyme activities in exercised rats. *Nutr Res Pract.* (2014) 8:618–24. doi: 10.4162/nrp.2014.8.6.618
15. Devi KP, Shanmuganathan B, Manayi A, Nabavi SF, Nabavi SM. Molecular and therapeutic targets of genistein in Alzheimer's disease. *Mol Neurobiol.* (2016) 54:7028–41. doi: 10.1007/s12035-016-0215-6
16. Essawy AE, Abdou HM, Ibrahim HM, Bouthahab NM. Soybean isoflavone ameliorates cognitive impairment, neuroinflammation, and amyloid β accumulation in a rat model of Alzheimer's disease. *Environ Sci Pollut Res.* (2019) 26:26060–70. doi: 10.1007/s11356-019-05862-z
17. Greene LA. Nerve growth factor prevents the death and stimulates the neuronal differentiation of clonal PC12 pheochromocytoma cells in serum-free medium. *J Cell Biol.* (1978) 78:747–55. doi: 10.1083/jcb.78.3.747
18. Yin L, Zhang Y, Wu H, Wang Z, Dai Y, Zhou J, et al. Improvement of the phenolic content, antioxidant activity, and nutritional quality of tofu fermented with *Actinomucor elegans*. *LWT Food Sci Technol.* (2020) 133:110087. doi: 10.1016/j.lwt.2020.110087
19. Zhang Y, Yin L, Huang L, Tekliye M, Dong M. Composition, antioxidant activity, and neuroprotective effects of anthocyanin-rich extract from purple highland barley bran and its promotion on autophagy. *Food Chem.* (2020) 339:127849. doi: 10.1016/j.foodchem.2020.127849
20. Shahidi F, Zhong Y. Measurement of antioxidant activity. *J Funct Foods.* (2015) 18:757–81. doi: 10.1016/j.jff.2015.01.047
21. Yao J, Zhang B, Ge C, Peng S, Fang J. Xanthohumol, a polyphenol chalcone present in hops, activating Nrf2 enzymes to confer protection against oxidative damage in PC12 cells. *J Agric Food Chem.* (2015) 63:1521–31. doi: 10.1021/jf505075n
22. Tang J, Yan Y, Ran L, Mi J, Sun Y, Lu L, et al. Isolation, antioxidant property and protective effect on PC12 cell of the main anthocyanin in fruit of *Lycium ruthenicum* Murray. *J Funct Foods.* (2017) 30:97–107. doi: 10.1016/j.jff.2017.01.015
23. Yang T, Zhu H, Zhou H, Lin Q, Li W, Liu J. Rice protein hydrolysate attenuates hydrogen peroxide induced apoptosis of myocardiocytes H9c2 through the Bcl-2/Bax pathway. *Food Res Int.* (2012) 48:736–41. doi: 10.1016/j.foodres.2012.06.017
24. Nagarajan S. Mechanisms of anti-atherosclerotic functions of soy-based diets. *J Nutr Biochemist.* (2010) 21:255–60. doi: 10.1016/j.jnutbio.2009.09.002
25. Tu C, Azi F, Huang J, Xu X, Xing G, Dong M. Quality and metagenomic evaluation of a novel functional beverage produced from soy whey using water kefir grains. *LWT Food Sci Technol.* (2019) 113:108258. doi: 10.1016/j.lwt.2019.108258
26. Bei Q, Liu Y, Wang L, Chen G, Wu Z. Improving free. conjugated, and bound phenolic fractions in fermented oats (Avena sativa L) with Monascus anka and their antioxidant activity. *J Func Food.* (2017) 32:185–94. doi: 10.1016/j.jff.2017.02.028
27. Olszowy M. What is responsible for antioxidant properties of polyphenolic compounds from plants? *Plant Physiol Biochemist.* (2019) 144:135–43. doi: 10.1016/j.plaphy.2019.09.039
28. Sonee M, Sum T, Wang C, Mukherjee SK. The soy isoflavone, genistein, protects human cortical neuronal cells from oxidative stress. *Neurotoxicology.* (2004) 25:885–91. doi: 10.1016/j.neuro.2003.11.001
29. Cho CH, Jang H, Lee M, Kang H, Heo HJ, Kim DO. Sea buckthorn (*Hippophae rhamnoides* L.) leaf extracts protect neuronal PC-12 cells from oxidative stress. *J Microbiol Biotechnol.* (2017) 28:1257–65. doi: 10.4014/jmb.1704.04033
30. Im SE, Yoon H, Nam TG, Heo HJ, Lee CY, Kim DO. Antineuro-degenerative effect of phenolic extracts and caffeic acid derivatives in romaine lettuce on neuron-like PC-12 cells. *J Med Food.* (2010) 13:779–84. doi: 10.1089/jmf.2009.1204
31. Ma W, Yuan L, Yu H, Ding B, Xi Y, Feng J, et al. Genistein as a neuroprotective antioxidant attenuates redox imbalance induced by β-amyloid peptides 25–35 in PC12 cells. *Int J Dev Neurosci.* (2010) 28:289–95. doi: 10.1016/j.ijdevneu.2010.03.003
32. Liu M, Xu Y, Han X, Liang C, Yin L, Xu L, et al. Potent effects of flavonoid-rich extract from *Rosa laevigata* michx fruit against hydrogen peroxide-induced damage in PC12 cells via attenuation of oxidative stress, inflammation

and apoptosis. *Molecules*. (2014) 19:11816–32. doi: 10.3390/molecules190811816

33. Zhang B, Li W, Dong M. Flavonoids of Kudzu root fermented by *Eurtotium cristatum* protected rat pheochromocytoma line 12 (PC12) cells against H2O2-induced apoptosis. *Int J Mol Sci*. (2017) 18:2754. doi: 10.3390/ijms18122754
34. Penas E, Préstamo G, Polo F, Gomez R. Enzymatic proteolysis, under high pressure of soybean whey: analysis of peptides and the allergen Gly m 1 in the hydrolysates. *Food Chem*. (2006) 99:569–73. doi: 10.1016/j.foodchem.2005.08.028

Conflict of Interest: The authors declare that the research was conducted in the absence of any commercial or financial relationships that could be construed as a potential conflict of interest.

Publisher's Note: All claims expressed in this article are solely those of the authors and do not necessarily represent those of their affiliated organizations, or those of the publisher, the editors and the reviewers. Any product that may be evaluated in this article, or claim that may be made by its manufacturer, is not guaranteed or endorsed by the publisher.

frontiers in Nutrition

ORIGINAL RESEARCH
published: 11 March 2022
doi: 10.3389/fnut.2022.847064

Mechanism of Longevity Extension of *Caenorhabditis elegans* Induced by *Schizophyllum commune* Fermented Supernatant With Added Radix Puerariae

Yongfei Deng[1,2,3], *Han Liu*[2], *Qian Huang*[1], *Lingyun Tu*[1,2,3], *Lu Hu*[2], *Bisheng Zheng*[4], *Huaiqing Sun*[2], *Dengjun Lu*[3]*, *Chaowan Guo*[2]* and *Lin Zhou*[1]*

[1] Guangdong Province Key Laboratory for Biotechnology Drug Candidates, School of Biosciences and Biopharmaceutics, Guangdong Pharmaceutical University, Guangzhou, China, [2] Research and Development Center, Guangdong Marubi Biotechnology Co., Ltd., Guangzhou, China, [3] School of Light Industry and Food Engineering, Guangxi University, Nanning, China, [4] School of Food Science and Engineering, South China University of Technology, Guangzhou, China

OPEN ACCESS

Edited by:
Xiudong Xia,
Jiangsu Academy of Agricultural Sciences (JAAS), China

Reviewed by:
Swapnil Pandey,
University of Florida, United States
Chatrawee Duangjan,
University of Southern California, United States
Xiaodong Cui,
Shanxi University, China

***Correspondence:**
Lin Zhou
zhoulin@gdpu.edu.cn
Chaowan Guo
guo.chaowan@marubi.cn
Dengjun Lu
dj6688@126.com

Specialty section:
This article was submitted to Food Chemistry, a section of the journal Frontiers in Nutrition

Received: 01 January 2022
Accepted: 07 February 2022
Published: 11 March 2022

Citation:
Deng Y, Liu H, Huang Q, Tu L, Hu L, Zheng B, Sun H, Lu D, Guo C and Zhou L (2022) Mechanism of Longevity Extension of Caenorhabditis elegans Induced by Schizophyllum commune Fermented Supernatant With Added Radix Puerariae. Front. Nutr. 9:847064. doi: 10.3389/fnut.2022.847064

Schizophyllum commune (*S. commune*) fermented supernatant with added Radix Puerariae (SC-RP) showed significant antioxidant activity in our previous work. However, the possible lifespan and healthspan extending the capacity of *Caenorhabditis elegans* (*C. elegans*) and the underlying mechanism were not illuminated. In this study, the effect of SC-RP on extending the lifespan and improving stress resistance of *C. elegans* were examined. Additionally, the underlying lifespan extending molecular mechanisms of SC-RP were explored. Treated with SC-RP at 10 μg/mL, the lifespan of *C. elegans* increased by 24.89% ($P < 0.01$). Also, SC-RP prolonged the healthspan of the nematode, including reducing lipofuscin levels, improving mobility and enhancing resistance to oxidative stress and heat shock. Moreover, superoxide dismutase and catalase activities were increased for SC-RP treated *C. elegans.* Meantime the intracellular levels of thiobarbituric acid reactive substances (TBARS) and reactive oxygen species (ROS) were attenuated. Express levels of eight genes including *daf-2, daf-16*, *sod-3*, *skn-1, gst-4, clk-1, age-1 and mev-1* were analyzed by RT-PCR method for possible *C. elegan* anti-aging mechanisms of SC-RP. Expression levels of key genes *daf-2, gst-4 and sod-3* were up-regulated, while that of *daf-16*, *skn-1,* and *clk-1* were down-regulated. The results suggest that SC-RP could extend the lifespan and healthspan of *C. elegans* significantly, and the IIS pathway, SKN-1/Nrf2 pathway and mitochondrial metabolism pathway were primarily considered associated. Thus, SC-RP is a potential component to improve aging and aging-related symptoms as new functional materials.

Keywords: anti-aging activity, *Schizophyllum commune*, Radix puerariae, stress resistance, *Caenorhabditis elegans*

INTRODUCTION

Aging is a physiological phenomenon that occurs in all living organisms, and can lead to behavioral defects and signaling pathway dysfunction such as decreased resistance and physiological decline (1–3). Aging and age-related pathologies are becoming a major global issue because of the aging population (4). Nonetheless, growing evidence has demonstrated that consuming foods rich in

polysaccharides, polyphenols and other active compounds from natural sources such as fungi and plants that possess excellent antioxidant properties may protect or reduce the effects of aging on organisms (5–8). Therefore, research on the use of natural active ingredients with excellent antioxidant activity to prevent aging and age-related diseases has received great attention over the last decade.

Recently, fermentation has been applied to extract and enrich the active ingredients in edible plants and fungi and improve their antioxidant/anti-aging capacity (9). As a wellknown edible white-rot fungus, *Schizophyllum commune* (*S. commune*) is popular because this fungus produces exopolysaccharide schizophyllan (SPG), which is used in vaccines and anti-cancer therapies, in oxygen-impermeable films, as an antibacterial hydrogel for food preservation and as an anti-inflammatory agent (10–12). Apart from SPG, other metabolites such as phenolics from *S. commune* may scavenge for free radicals and thus be suitable for use in food and cosmeceuticals industries (13). Furthermore, the fermentation liquid of *S. commune* contains various enzymes, including lignocellulase, xylanase and cellulose (14). A previous study illustrated that *S. commune* can biotransform sophoricoside in *Fructus sophorae* to synthesize new active substances with outstanding toxicity toward MCF-7 cells, thus revealing that *S. commune* has the potential to enrich active ingredients of fermented products and enhance antioxidant, anti-aging or biological properties of phytochemicals in fermentation substrates (15). Therefore, the fermentation system of *S. commune* is a practical platform for improving the biological activity of food or traditional Chinese medicinal materials. Radix Puerariae (RP) is rich in isoflavones, which are primary polyphenolic antioxidants found in medicinal and edible plants (16, 17). Our previous study have confirmed that adding RP to the *S. commune* fermentation system can increase the antioxidant activity of the fermented supernatant, and these antioxidant activities are mainly contributed by the puerarin from RP and some new ingredients synthesized during fermentation such as resveratrol (18). Furthermore, the above results proves the feasibility of *Schizophyllum* liquid fermentation system as a bioreactor and provides a reference for the biotransformation of edible medicinal fungi such as *Cordyceps militaris* and *Ganoderma lucidum* et al.

Caenorhabditis elegans (*C. elegans*) has a simple physiological structure, is easily cultured, has a short life cycle, the genetic pathways are well known and there are 60 to 80% of the genomic sequences in *C. elegans* show homology to sequences in the human genome (19). Based on these advantages, *C. elegans* has been used widely to evaluate the anti-aging properties of substances (20–22). In *C. elegans*, signaling pathways regulating aging have been studied extensively, including the insulin/insulin-like growth factor signaling (IIS) pathway, SKN-1/Nrf2 pathway and mitochondrial electron transport chain pathway. These signaling pathways are associated with lifespan and stress resistance (23–25). Research efforts use nematodes as an *in vivo* model to study the anti-aging activities and molecular mechanisms of natural products. Ibe et al. found that fermented soybean extracts can extend the lifespan, provide resistance to oxidation and heat shock and delay lipofuscin accumulation in *C. elegans* (26). Moreover, Shi et al. found that Monascin formed *Monascus*-fermented products enhances oxidative stress resistance *via* regulation of the DAF-16/FOXO-dependent pathway (27). Furthermore, rice kefiran also induces anti-aging effects and upregulates the thermal stress tolerance of *C. elegans* through the IIS pathway by activating the DAF-16 transcription factor (28).

The antioxidant activity *in vitro* of fermented supernatant cultured from *S. commune* in RP supplemented medium was verified (18). However, whether the significant antioxidant activity of SC-RP can play an anti-aging effect remains unclear. In the present study, we used *C. elegans* as an *in vivo* model to systematically survey the longevity effect and mechanisms of action of SC-RP. Our results showed that SC-RP prolonged the lifespan significantly, promoted healthspan behaviors, improved the activities of antioxidant enzymes and enhanced stress resistance of *C. elegans* by regulating multiple mechanisms, including the IIS pathway, SKN-1 pathway and mitochondrial metabolism pathway. These results provide a meaningful understanding of the antioxidant and anti-aging effect of SC-RP, thus facilitating the development and application of SC-RP as a functional food or new pharmaceutical raw material.

MATERIALS AND METHODS

Materials and Reagents

Superoxide dismutase (SOD; A001-2), catalase (CAT; A007-1) and thiobarbituric acid reactive substances (TBARS; A003-1) assay kits were purchased from Nanjing Jiancheng Bioengineering Research Institute (Nanjing, China). 2′, 7′-Dichlorofluorescein diacetate (DCFH-DA) and methyl viologen dichloride (paraquat, 98%) were purchased from Sigma-Aldrich Chemical Co. (St Louis, MO, USA). All other chemicals and solvents were of analytical grade or higher.

Preparation of SC-RP

The seed medium for *S. commune* 5.43: Glucose 30.0 g, KH_2PO_4 1.0 g, $MgSO_4$ $7H_2O$ 0.5 g, Yeast extract 3.0 g, and these ingredients were dissolved into 1000 mL deionized water at natural pH (about 6.0). Then sterilized at 121°C for 20 min. The *S. commune* strain was cultured initially in a seed medium as a fermented seed at 28°C for 3 days. The seed culture was inoculated with a 10.0 % inoculum size (v/v) to fermentation medium containing 12.80 g/L RP, and cultivation was carried out on a rotary shaker (ZAZY-78BN, ZHICHU, China) at 160 rpm and 28°C. After 7.0 d fermentation, the fermentation broth was used a centrifuge (GL-21M, CENCE, China) at 15000 g for 10 min to separate the fungi and supernatant, and the SC-RP was sterilized through a 0.22-μm filter membrane and collected for further study (18).

Determination of Total Phenolic and Flavonoid Contents

Total phenolics were determined by the Folin-Ciocalteu colorimetric method as described previously (29) using gallic acid (GA) as the standard. Total flavonoid content was measured using the sodium borohydride/chloranil method (30), and

catechin hydrate (CE) was used as a standard. Data are reported as milligram GA equivalents per 100 g fresh weight (mg GAE/100 g, FW) and milligram CE equivalents per 100 g FW (mg CE/100 g, FW).

Determination of Polysaccharides and Total Protein Contents

Polysaccharides were determined by the phenol-sulfuric acid method as described previously (31), using glucose as the standard. The reducing sugar content in a sample was determined by the DNS method. On the basis of the manufacturer's instructions, the total protein content was measured using the BCA protein assay kit (A045-4-2; Nanjing Jiancheng Bioengineering Research Institute, Nanjing, China).

Nematodes Strains and Maintenance

The *C. elegans* strains used in this study were provided by the *Caenorhabditis Genetics* Center (CGC, University of Minnesota, Minneapolis, MN, USA): wild-type Bristol N2, *daf-16* (mgDf50), *age-1* (hx546) I, *mev-1* (zIs356 IV.) II, *clk-1* (e2519) II, *skn-1*(zu135) IV, LD1:ldIs7[*skn-1* b/c::GFP *rol-6 (su100)*], CF1553 {*muIs84* [pAD76 (SOD-3::GFP)]} and TJ356 [*zIs356* IV (p*daf-16-daf-16*::GFP; *rol-6*)]. Worms were raised and maintained at 20°C on nematode growth media (NGM) seeded with *E. coli* OP50 bacteria as a food source starting from the first day of hatching, except where indicated. The SC-RP solutions (1.0 mg/mL in ultrapure water) were diluted into different concentrations by *E. coli* OP50 based on the antioxidant capacity of SC-RP (final concentrations: 5, 10, 20 μg/mL). The utilization of water as a substitute for SC-RP was the control group.

Lifespan Assay

Age-synchronized N2 nematodes (32) were used for the lifespan assay. The eggs were allowed to hatch on the NGM plates with *E. coli* OP50 until the L4 stage. L4 worms were transferred to NGM Petri dishes containing appropriate working doses of SC-RP (0, 5, 10, and 20 μg/mL). During the reproductive period, worms were scored daily and transferred to new treatment dishes every other day. Worms that failed to move by gentle prodding with a needle were scored as dead. Worms that burrowed into or escaped from the agar or died were removed immediately during the counting process. All assays were performed in three independent trials, and each experimental group included at least 50 worms.

Reproduction Assay

Age-synchronized L4 stage worms (32) were allowed to lay eggs and transferred to fresh-treated plates every day during the progeny production period. The original plates were stored at 20°C for another day to allow viable eggs to hatch before scoring. The oviposition number of each worm in the breeding time (around 5 to 7 days) was counted, as described by Liu et al. (33).

Movement Assay

A sinusoidal motion was defined as a one-wavelength shift relative to the long axis of the body (30 individuals in total). The head swing was defined as swinging of the head from one side to the other and then back (30 individuals in total). Locomotivity classes were determined as follows (60 individuals per repetition): the highly mobile worms, which we designated as class A, moved spontaneously and smoothly; members of class B did not move unless prodded and left tracks that were non-sinusoidal; and class C worms did not move forward or backward, but oscillated their nose or tails in response to touch (33). Worms were placed on NGM and allowed to move freely for 1 min before observation.

Analysis of Lipofuscin Accumulation

Age-synchronized L4 stage Worms (32) were treated with SC-RP as described above to determine the lipofuscin levels. On days 5, 10 and 15 after treated with SC-RP, the worms were placed on 2% (w/v) agarose pads on glass slides and anesthetized with sodium azide (10 mM) (34). The worms were visualized under a fluorescence microscope (MF54-N, Mshot, Guangzhou, China). The fluorescence intensity of the worms was measured using Image J software 8.0 (National Institutes of Health, Bethesda, USA).

Activities of Superoxide Dismutase (SOD) and Catalase (CAT), and Contents of Thiobarbituric Acid Reactive Substances (TBARS) and Intracellular Reactive Oxygen Species (ROS)

The activities of SOD and CAT and TBARS levels in the supernatant were determined using commercial kits on the basis of the manufacturer's instructions. Endogenous ROS levels in nematodes were measured using a modified DCFH-DA assay (7). In brief, SC-RP-treated worms (∼1,000 worms) were crushed by a biological grinder. After centrifugation, the supernatant (50 μL) and DCFH-DA (50 μL) were mixed in a 96-well plate. Fluorescence was immediately quantified by a microplate reader (SPARK 10M, TECAN, Switzerland) at an excitation/emission wavelength of 485/535 nm. Final results were normalized to protein levels obtained using the BCA protein assay kit.

Stress Resistance Assays

At least 150 Age-synchronized L4 stage worms (32) treated or not treated with SC-RP for 5 days were used to perform three independent biological replicates. Subsequently, worms were exposed to various stresses until all worms died.

H_2O_2-induced oxidative stress assay. This assay was performed according to a method described by Lin with minor modifications (6). The worms were transferred to freshly prepared NGM containing 0.1 of 10% H_2O_2. The vitality of the worms was examined every 30 min.

Paraquat-induced oxidative stress assay. The assay was performed according to the method reported previously (34). Briefly, survival was monitored every 24 h after the worms were subjected to plates containing 10 mM paraquat.

Heat shock assay. The assay was performed according to the method reported previously (34). The number of dead worms was recorded every hour after the worms were transferred from a 20°C culture environment to a 35°C culture environment.

Nuclear DAF-16::GFP and SKN-1::GFP Quantitation

For the translocation assay, age-synchronized L4 stage worms (32) pretreated with SC-RP for 5 days at 20°C were transferred onto one microscope slide coated with a 2% (w/v) agarose pad, followed by anesthetization with 10 mM sodium azide for 2 min (33). The worms were observed under a confocal microscope (Nikon Eclipse 80i Microscope SOP, Tokyo, Japan). The distribution of DAF-16::GFP and SKN-1::GFP was identified by the following principles: "cytoplasmic," "intermediate" and "nuclear," which represents the percentage in each treated group. All trials were conducted in triplicate using 20–30 worms per group.

SOD-3::GFP Fluorescence Quantification Assay

CF1553 (SOD-3::GFP) transgenic strains were used to detect the expression of SOD-3. Age-synchronized L4 stage worms (32) were treated with SC-RP for 5 days at 20°C. Subsequently, the worms were transferred onto one microscope slide coated with a 2% (w/v) agarose pad, followed by anesthetization with 10 mM sodium azide for 2 min (34). Images were captured using a fluorescence microscope (MF54-N, Mshot, Guangzhou, China).

Quantitative Real-Time Polymerase Chain Reaction (qRT-PCR) Assay

Total RNA was isolated from ∼1,000 worms (treated for 5 days) by TRIzol® reagent (Invitrogen, Carlsbad, CA, USA) (7), and then these total RNA were synthesized to cDNA using the PrimeScript™ RT Reagent Kit (Takara Biotechnology, Dalian, China). Subsequently, RT-qPCR was conducted using the Bio-Rad Mini Option™ Real-Time PCR Detection System (BioRad, Hercules, CA, USA) with SYBR® Green Supermix fluorescence dye. The expression levels of genes were analyzed using the $2^{-\Delta\Delta Ct}$ method, and *β-actin-1* was the reference gene. The primers used for RT-qPCR are listed in **Supplementary Table 1**.

Statistical Analysis

All data were expressed as mean ± SD ($n = 3$). Survival analyses were performed using the Kaplan–Meier method by GraphPad Prism 8.0 software (San Diego, CA, USA), and statistical analyses were conducted using IBM SPSS 25.0 (SPSS Inc., Chicago, IL, USA). Statistical significance was determined by one-way ANOVA with Duncan's multiple comparison post-test, and differences were considered significant at $P < 0.05$.

RESULTS

Chemical Composition of SC-RP

As shown in **Table 1**, the total phenolics and total flavonoids of SC-RP were 3,731.56 ± 54.07 mg GAE/100 g, FW and 27.97 ± 0.41 mg CE/100 g, FW, respectively. SC-RP also contains 6.76 ± 0.47 mg/mL schizophyllan and 4.66 ± 0.05 mg/mL total protein (18). Moreover, the addition of RP introduces puerarin into the fermentation products, with a content of 56.45 ± 3.26 mg/100 g, FW. This result illustrated that fermented supernatant cultured from *S. commune* in RP-supplemented medium is rich in phytochemical components, which may be the main source of anti-aging activity. Therefore, the anti-aging activity of SC-RP was further evaluated.

TABLE 1 | Chemical compositions of SC-RP.

Active substance	Contents[a]
Total phenolics (mg GAE/100g, FW)	3,731.56 ± 54.07
Total flavonoids (mg CE/100g, FW)	27.97 ± 0.41
Puerarin (mg/100g, FW)	56.45 ± 3.26
Schizophyllan (mg/mL)	6.76 ± 0.47
Total protein (mg/mL)	4.66 ± 0.05

[a] *Data were expressed as the mean ± SD (n = 3).*

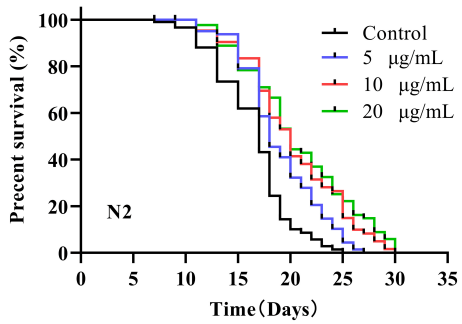

FIGURE 1 | Survival of wild-type *C. elegans* treated with *Schizophyllum commune* fermented supernatant with added Radix Puerariae (SC-RP). *C. elegans* (N2) were treated with final concentrations of 0 (control), 5, 10, or 20 μg/mL SC-RP starting from the L4 stage (day 0). During the reproductive period, worms were scored daily and transferred to new treatment dishes every other day. The survivals were recorded every other day, until all of the worms died. There were at least three independent biological replicates ($n \geq 50$). The log-rank (Mantel–Cox) test was used for statistical analysis, showing that 5, 10, and 20 μg/mL SC-RP resulted in significant survival curves compared to the control ($P < 0.001$).

SC-RP Increased the Lifespan of *C. elegans*

A previous study reported that the mean lifespan of wild-type N2 worms was 2–3 weeks at 20°C (7). The average lifespan of N2 control worms under our laboratory conditions was 16.27 ± 1.34 days (**Figure 1**). After testing 5, 10 and 20 μg/mL SC-RP, the median lifespan of worms increased to 18.88 ± 0.54, 20.32 ± 0.88 and 20.38 ± 1.30 days, respectively, and the corresponding increments compared with the control group were 16.04, 24.89, and 25.26%, respectively (**Table 2**). This result clearly showed that SC-RP prolongs the lifespan of *C. elegans* significantly at SC-RP doses of 10 and 20 μg/mL ($P < 0.05$).

SC-RP Reduced Reproduction Capacity of the Nematode

Previous research has shown that life expectancy is positively correlated with a decrease in infertility (35). The number of offspring from each worm was counted to investigate whether the increase in lifespan was accompanied by an improvement

TABLE 2 | Effect of SC-RP on the lifespan of *C. elegans*. (mean ± SD, $n = 3$).

Group	Mean Lifespan (Days)	Maximum Lifespan (Days)	Number	Mean fold Increase %[a]
Control	16.27 ± 1.34	23.50 ± 2.12	115/150	–
SC-RP (5 μg/mL)	18.88 ± 0.54	26.50 ± 0.71	127/150	16.04
SC-RP (10 μg/mL)	20.32 ± 0.88**	30.00 ± 1.00**	123/150	24.89
SC-RP (20 μg/mL)	20.38 ± 1.30*	31.00 ± 0.00***	113/150	25.26

*$P < 0.05$; **$P < 0.01$; ***$P < 0.001$. [a]Percentage of mean fold increase is relative to the control.

in fertility (**Figure 2A**). The number of offspring per worm in the control group was 259 ± 10 eggs/worm. After administering SC-RP, the total offspring decreased to 247 ± 7 eggs/worm (5 μg/mL group), 236 ± 7 eggs/worm (10 μg/mL group) and 217 ± 10 eggs/worm (20 μg/mL group). These results indicated that SC-RP reduced the fertility of the nematode at doses of 10 and 20 μg/mL and this observation was statistically significant ($P < 0.05$). According to the conservation of energy, it seems plausible that SC-RP prolongs the lifespan and this increase is related to changes in spawning. Nonetheless, extending the lifespan without affecting reproduction remains the most desirable outcome.

SC-RP Improved the Mobility of the Nematode

Behavioral changes of *C. elegans* and their response to external mechanical stimulation may be associated with the aging process (2). Movement behavior was evaluated using three indicators: head swing (**Figure 2B**), sinusoidal motion (**Figure 2C**) and locomotivity (**Figure 2D**) at the early, mid and mid-late life stages (on days 5, 10, and 15, respectively). In terms of head bend frequency and sinusoidal motion, the worms treated with 20 μg/mL SC-RP exhibited a significant increase in these activities ($P < 0.05$) but 10 μg/mL SC-RP was the most effective concentration on day 10. The decline in motility on day 10 and 15 was markedly delayed in a dose-dependent manner for worms treated with different doses of SC-RP (**Figure 2D**). Moreover, on day 5, most worms in all groups continued to move freely (class A), and only 6.67% of worms were scored as class B in the control group. On day 10, 84.44% of the worms in the control group were class A, whereas 97.78% of the worms were class A in the groups treated with 10 μg/mL SC-RP. By day 15, SC-RP-treated groups still maintained better motility and presented highly significant dose-dependent differences ($P < 0.05$). The ratio of class A worms administrated with the highest dose was 62.22%, whereas the control group was only 6.64%. Taken together, worms treated with 20 μg/mL SC-RP showed the greatest improvement in mobility and the highest increase in lifespan among the three treatment groups.

Effects of SC-RP on Lipofuscin Accumulation in *C. elegans* at Different Stages

Lipofuscin accumulation is an essential feature of aging. We determined the effects of SC-RP on lipofuscin accumulation in nematodes by fluorescence intensity measurements (**Figure 3**). On day 5, no significant difference in age pigment accumulation was observed in all groups, with only a 3.47% reduction in lipofuscin content at high doses of SC-RP. Increasing the SC-RP concentration reduced the accumulation of lipofuscin in nematodes significantly in the mid-late stages ($P < 0.05$), with lipofuscin content in the SC-RP-treated groups decreasing by 7.80% (5 μg/mL group), 10.28% (10 μg/mL group) and 11.37% (20 μg/mL group) when compared with that of the control group on day 10. By day 15, the age pigment accumulation in nematodes for the SC-RP-treated groups still showed a reduction at doses of 10 and 20 μg/mL SC-RP. Moreover, lipofuscin accumulation in worms treated with 20 μg/mL was markedly decreased by 8.36% when compared with that of the control group ($P < 0.05$). Consequently, SC-RP may weaken the accumulation of lipofuscin to improve health indicators.

SC-RP Rendered *C. elegans* Resistant to Stress

As depicted in **Figure 4A**, treatment with SC-RP significantly augmented the survival time of N2 worms under H_2O_2-induced oxidative conditions when compared with that of the control group. The longest median lifespan was observed for the group treated with 10 μg/mL SC-RP (6.06 ± 0.52 h), which was a significant increase by 65.09% when compared with that of the control group ($P < 0.01$). As depicted in **Figure 4B**, the mean lifespan of control nematodes was 4.27 ± 0.04 days, whereas those treated with 10 μg/mL SC-RP had a mean lifespan of 5.18 ± 0.32 days, which is a significant increase in the mean lifespan of nematodes by 21.31% ($P < 0.05$). The results indicated that oxidative tolerance was enhanced significantly by SC-RP treatment. Furthermore, the survival time for N2 worms pretreated with 5, 10, and 20 μg/mL SC-RP was increased by 5.53, 14.44, and 7.69%, respectively, when compared with that of the control group in the thermal shock stress test (**Figure 4C**; **Table 3**). These results suggest that SC-RP reduced oxidative stress and markedly enhanced the thermotolerance of the nematodes ($P < 0.05$).

SC-RP Increased Antioxidant Enzyme Activities and Decreased the Accumulation of TBARS and ROS

At 5, 10 and 20 μg/mL SC-RP, SOD activity in worms was observed to increase significantly by 16.56, 26.38, and 38.33%, respectively (**Figure 5A**, $P < 0.05$). The same tendency was also observed for CAT activity (**Figure 5B**). The high dose (20 μg/mL) SC-RP treatment group resulted in an 80.42% increase in CAT activity when compared with that of the control group ($P < 0.001$). In addition, the TBARS content in the high dose (20 μg/mL) group was reduced by 70.39% when compared with that of the control group ($P < 0.001$). Furthermore, the ROS level was reduced by 6.71, 25.76, and 13.56% in the 5, 10, and 20 μg/mL SC-RP treatment groups, respectively, when compared with that of the control group (**Figure 6**, $P < 0.05$). Clearly, SC-RP showed significant antioxidant potential by enhancing the

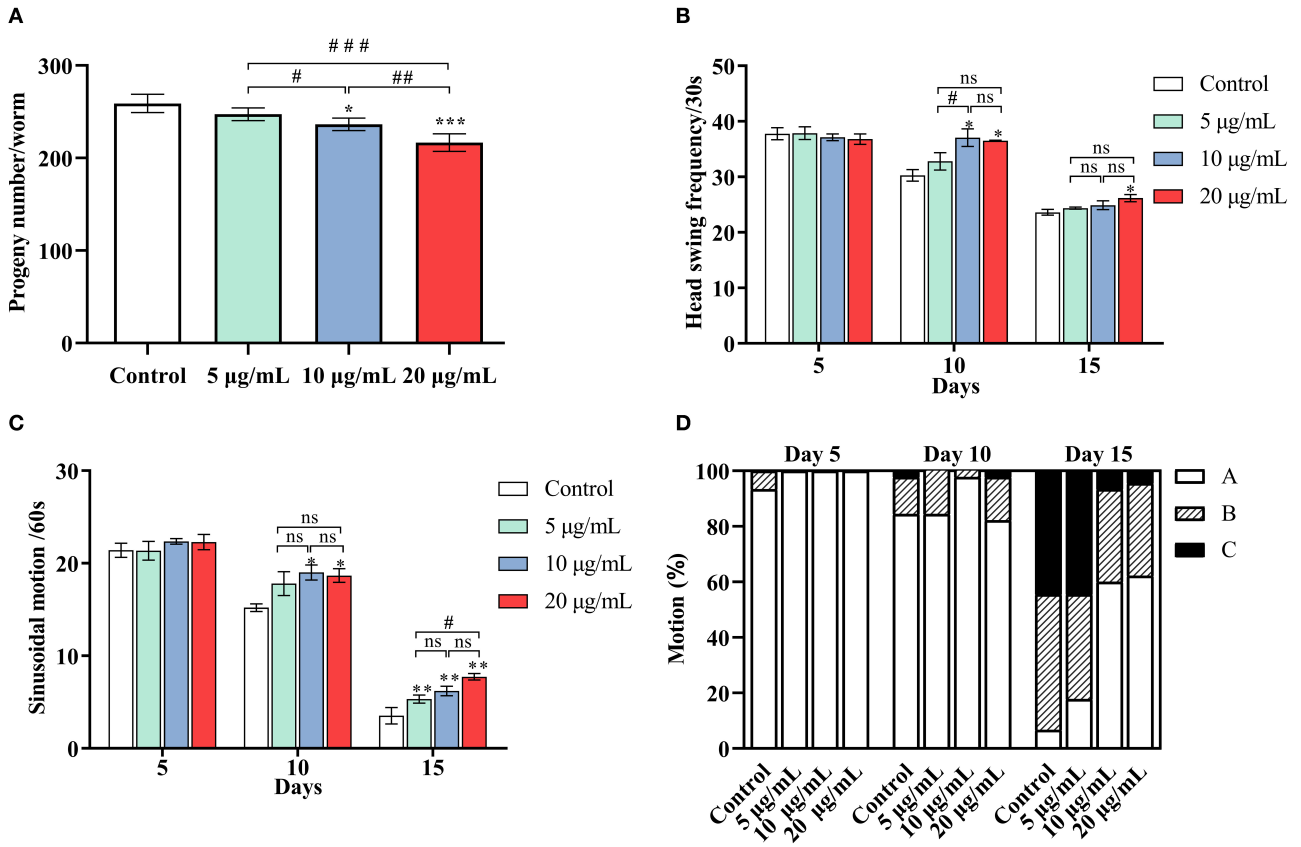

FIGURE 2 | Effect of SC-RP on the physiological functions of *C. elegans*. **(A)** The progeny number of each worm was counted until the parental worms were dead or stopped producing progeny. **(B)** The frequency of the head swing, **(C)** The sinusoidal locomotion, and **(D)** Three levels of locomotivity were performed on days 5, 10, and 15 of the worms. There were at least three independent biological replicates (n ≥ 10 for progeny rate and n ≥ 30 for mobile ability). $^{*}P < 0.05$, $^{**}P < 0.01$, and $^{***}P < 0.001$ indicated statistical significance with control group. $^{\#}P < 0.05$, $^{\#\#}P < 0.01$, and $^{\#\#\#}P < 0.001$ indicated statistical significance in different SC-RP treated groups.

activities of SOD and CAT and reducing the levels of TBARS and intracellular ROS.

SC-RP Regulated the Insulin/IGF-1 Signaling (IIS) Pathway

We investigated the lifespan of *daf-16* mutant and upstream gene *age-1* mutant to assess whether the IIS pathway was associated with extending the lifespan of SC-RP-treated nematodes. We found that 10 μg/mL SC-RP treatment did not extend the lifespan of *daf-16* mutant but prolonged the lifespan of *age-1* mutant (**Figures 7A,B**; **Table 4**), demonstrating that the IIS pathway is required and the *daf-16* gene may play a role in increasing the lifespan of nematodes treated with SC-RP. In addition, the localization of DAF-16 in nuclei is an essential prerequisite for activating target gene transcription by this protein. We next used the TJ356 strain containing a GFP::DAF-16 transgene to further determine the effect of SC-RP on DAF-16 subcellular localization. As shown in **Figure 8A**, the TJ356 green fluorescent protein subcellar distribution can be divided into cytosolic (top), intermediate (middle) and nuclear (bottom). The results showed that the nuclear fraction increased from (22.11 ± 3.65) to (55.76 ± 3.23)%, whereas the cytosolic location of DAF-16 reduced from (33.95 ± 3.54) to (10.15± 1.19)% (**Figure 8B**). This finding suggested that SC-RP may directly activate DAF-16 or molecules located upstream of DAF-16.

The expression levels of the *daf-16* gene and its upstream/downstream genes were examined to explore the underlying anti-aging mechanisms of SC-RP further. After treatment with 10 μg/mL SC-RP, the relative expression level of *daf-16* decreased to 0.12-fold, and the levels of *age-1, daf-2 and sod-3* increased by 1.08 ± 0.03, 6.24 ± 0.92, and 4.47 ± 0.04 times, respectively (**Figure 11A**). Moreover, we also observed significant expression in the mean fluorescence intensity of *SOD-3*p::GFP following SC-RP treatment (**Figures 9A,B**, $P < 0.001$), which further indicated that SC-RP may reduce oxidative stress by regulating the expression of *daf-16*-related genes. Taken together, these results indicated that SC-RP extended the healthspan of *C. elegans* through modulation of the IIS signaling pathway.

SC-RP Regulated the SKN-1/Nrf2 Pathway

The decrease in the activity of the IIS signaling pathway directly promotes SKN-1 nuclear accumulation in the intestine and

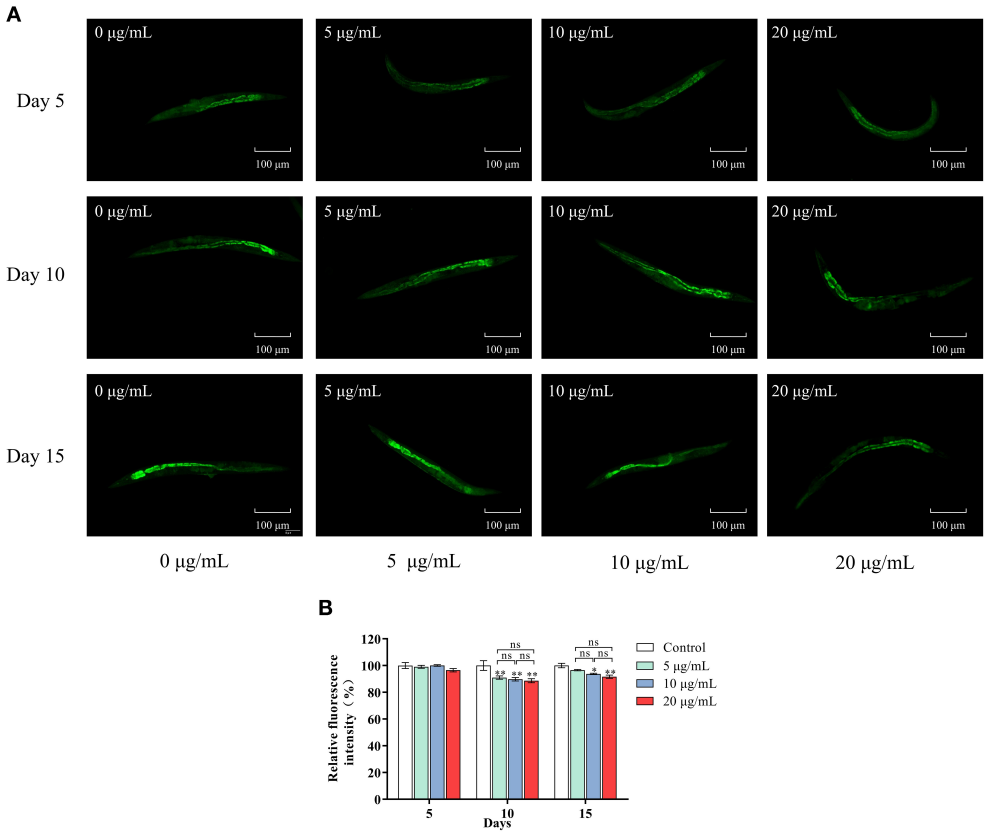

FIGURE 3 | Effect of SC-RP on lipofuscin accumulation in *C. elegans*. **(A)** On days 5, 10 and 15 after hatching, the worms in different SC-RP treated groups were placed on 2% (w/v) agarose pads on glass slides and anesthetized with sodium azide (10 mM). The lipofuscin accumulation of worms was visualized under a fluorescence microscope. **(B)** The relative fluorescence intensity of lipofuscin were quantitated by image J. Data were expressed as the mean ± SD ($n = 3$). $^{*}P < 0.05$, $^{**}P < 0.01$, and $^{***}P < 0.001$ indicated statistical significance with control group.

activates downstream target genes, which is parallel to DAF-16 activity. A lifespan assay of the *skn-1* (zu135) mutant was performed to determine whether SKN-1 affects the healthspan of SC-RP-treated nematodes. Treatment with 10 μg/mL SC-RP showed no effect in prolonging the lifespan in the *skn-1* mutant, indicating that SC-RP extends the lifespan of the nematode in a *skn-1*-independent manner (**Figure 7C**; **Table 4**).

The localization of SKN-1::GFP was measured using the transgenic strain LD1 to study further the role of SKN-1 in extending the nematode lifespan (**Figures 10A,B**). The results showed that nuclear translocation of SKN-1 in the intestine increased from (25.00 ± 3.21) to (44.46 ± 0.99)% and cytosolic localization of SKN-1 decreased from (34.09 ± 3.21) to (21.12 ± 5.78)% (**Figure 10B**), indicating that SC-RP promotes translocation of SKN-1 into the nucleus significantly. In addition, we explored the effect of SC-RP on the expression of *skn-1* and its downstream gene glutathione-S transferase-4 (*gst-4*). The results showed that compared with the control group, the mRNA expression level of *skn-1* decreased to 0.63 ± 0.07-fold, and the expression level of *gst-4* increased by 4.68 ± 0.75-fold (**Figure 11A**), suggesting that SKN-1 may play an essential role in regulating the lifespan of nematodes treated with SC-RP.

SC-RP Regulated the Mitochondrial Electron Transport Chain Pathway

Oxidative stress is a key factor of aging and ROS is primarily generated from mitochondrial metabolism (36). However, whether SC-RP extends the lifespan through the mitochondrial electron transport chain pathway is unknown. Thus, the anti-aging effect of SC-RP on *mev-1* and *clk-1* worms was evaluated. SC-RP treatment was observed to extend the mean survival time by 24.6% in *mev-1* mutant, demonstrating that SC-RP improves survival during mild oxidative stress (**Figure 7D**; **Table 4**). We then measured the *clk-1* mutant lifespan, and the results revealed no increase in the median lifespan, demonstrating that SC-RP may act independently of *clk-1* (**Figure 7E**; **Table 4**). Moreover, quantitative real-time PCR results showed that the mRNA level of *mev-1* and *clk-1* was

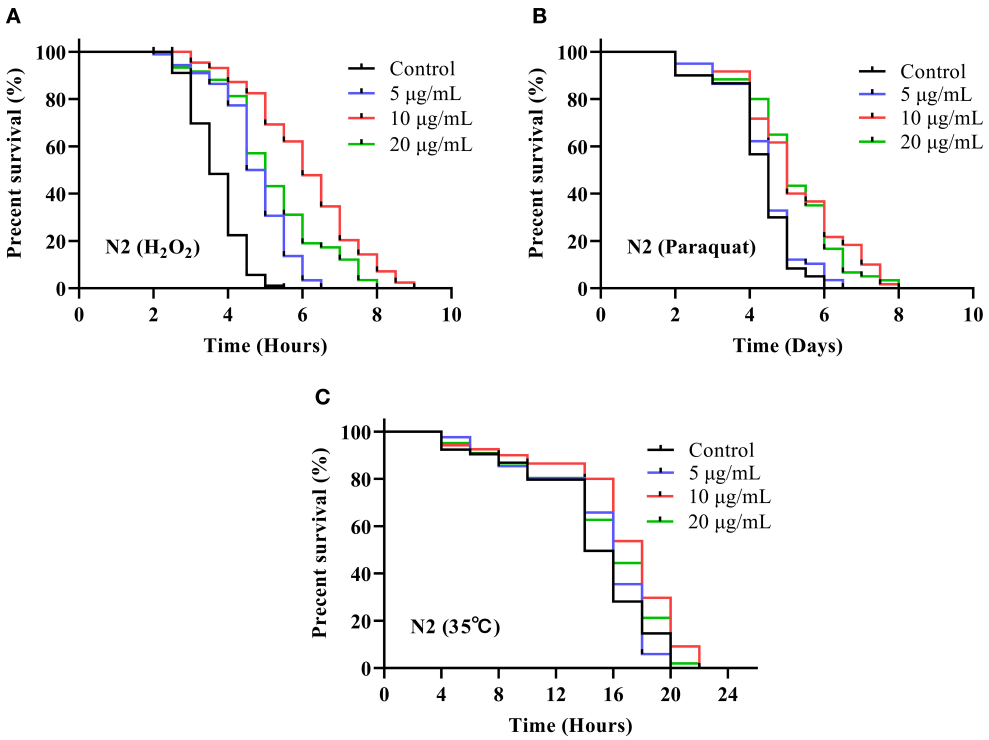

FIGURE 4 | Effect of SC-RP on stress resistance in *C. elegans*. Survival curve of the *C. elegans* N2 strain under **(A)** H_2O_2-induced oxidative stress, **(B)** paraquat-induced oxidative stress, and **(C)** heat shock stress. During the reproductive period, worms were scored daily and transferred to new treatment dishes every other day. The survivals were recorded every other day, until all of the worms died. There were at least three independent biological replicates ($n \geq 50$).

TABLE 3 | Effect of SC-RP on stress resistance to oxidative stress and thermal shock in *C. elegans* (mean ± SD, $n = 3$).

Genotype and Condition	Treatment	Meanlifespan	Maximum Lifespan	Number	Mean fold Increase %[a]
N2 (H_2O_2, 20°C, Hours)	0 μg/mL	3.67 ± 0.07	5.17 ± 0.29	120/150	–
	5 μg/mL	4.73 ± 0.10	6.33 ± 0.29**	118/150	28.89
	10 μg/mL	6.06 ± 0.52***	8.50 ± 0.50***	114/150	65.12
	20 μg/mL	5.18 ± 0.43*	7.75 ± 0.35***	116/150	41.14
N2 (paraquat, 20°C, Days)	0 μg/mL	4.27 ± 0.04	5.75 ± 0.35	119/150	–
	5 μg/mL	4.41 ± 0.03	6.50 ± 0.00**	118/150	3.28
	10 μg/mL	5.18 ± 0.32*	7.75 ± 0.35***	120/150	21.31
	20 μg/mL	5.11 ± 0.25*	7.75 ± 0.46***	120/150	19.67
N2 (35°C, Hours)	0 μg/mL	13.93 ± 0.80	20.00 ± 0.00	112/150	–
	5 μg/mL	14.70 ± 1.18	20.00 ± 1.36	116/150	5.53
	10 μg/mL	15.93 ± 0.89**	22.00 ± 0.46**	119/150	14.44
	20 μg/mL	15.00 ± 0.54	21.33 ± 1.15	113/150	7.69

*$P < 0.05$; **$P < 0.01$; ***$P < 0.001$. [a]Percentage of mean fold increase is relative to the control.

reduced by 0.90 ± 0.01- and 0.11 ± 0.02-fold, respectively (**Figure 11A**).

In summary, SC-RP treatment was dependent on CLK-1 activity but acted independently of MEV-1. Thus, the mitochondrial electron transport chain is partially associated with extending the lifespan of SC-RP-treated nematodes.

DISCUSSION

Numerous studies have shown that compounds and extracts derived from edible plants containing polysaccharides and polyphenols can extend the lifespan and healthspan of a variety of species (6, 37). In our previous research, RP acted as the exogenous additive in a submerged culture of *S. Commune*,

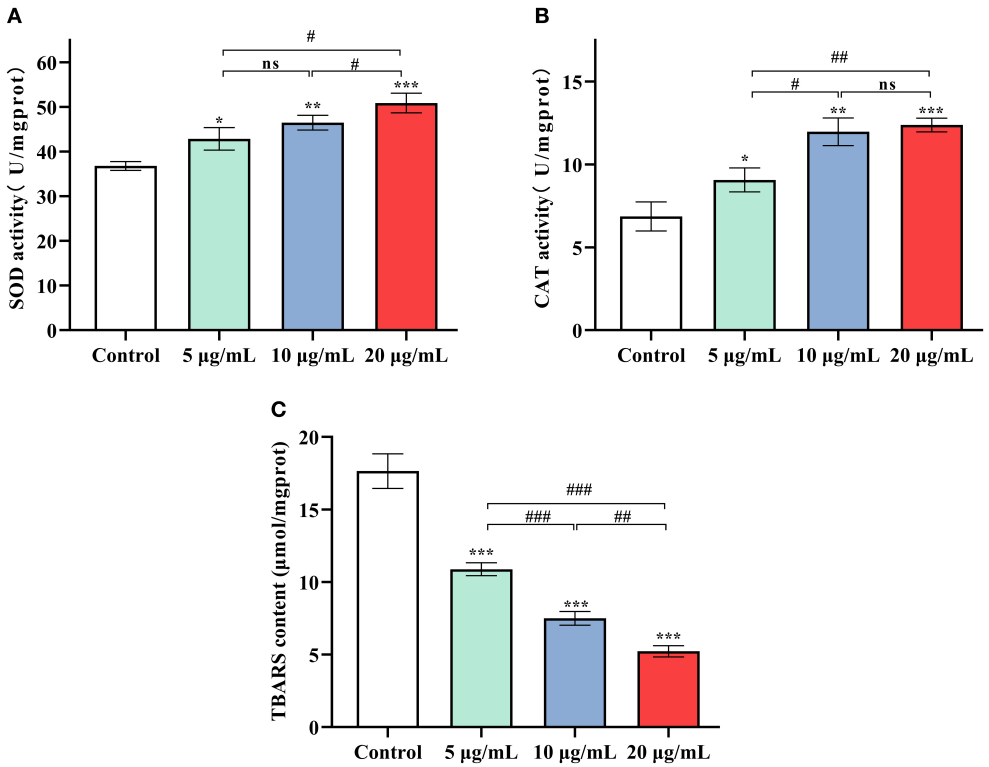

FIGURE 5 | Effect of SC-RP on the activities of antioxidant enzymes SOD **(A)** and CAT **(B)**, and the level of TBARS **(C)** in *C. elegans*. The activities of SOD and CAT and TBARS levels in the supernatant were determined using commercial kits on the basis of the manufacturer's instructions. Final results were normalized to protein levels obtained using the BCA protein assay kit. Data were expressed as the mean ± SD ($n = 3$). $^{*}P < 0.05$, $^{**}P < 0.01$, and $^{***}P < 0.001$ indicated statistical significance with control group. $^{\#}P < 0.05$, $^{\#\#}P < 0.01$, and $^{\#\#\#}P < 0.001$ indicated statistical significance in different SC-RP treated groups.

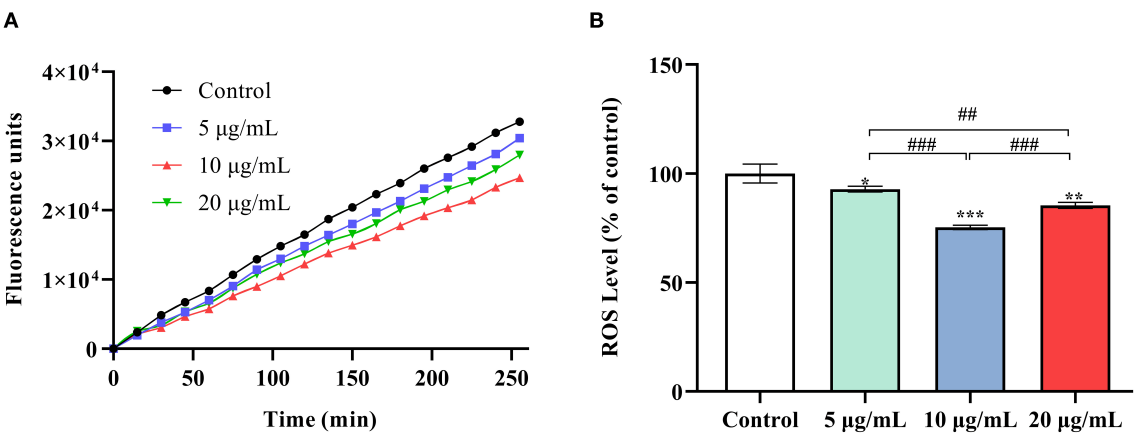

FIGURE 6 | Effect of SC-RP on the oxidative stress sensitivity of wild-type N2 worms. Relative formation of ROS after 96 h of exposure to SC-RP (0, 5, 10, or 20 μg/mL). SC-RP-treated worms (~1000 worms) were crushed by a biological grinder. Endogenous ROS levels in nematodes were measured using a modified DCFH-DA assay. **(A)** The curve showed the accumulation of the fluorescence intensity of ROS in the nematodes. **(B)** The ROS accumulation level in nematodes. Final results were normalized to protein levels obtained using the BCA protein assay kit. Values are means ± SD ($n = 3$). $^{*}P < 0.05$, $^{**}P < 0.01$, and $^{***}P < 0.001$ indicated statistical significance with control group. $^{\#}P < 0.05$, $^{\#\#}P < 0.01$, and $^{\#\#\#}P < 0.001$ indicated statistical significance in different SC-RP treated groups.

with the resulting fermented supernatant (SC-RP) containing a considerable phytochemical composition (18). The phenolic content of SC-RP was 8- to 18-times higher when compared with that of a blueberry extract (38), which suggests that SC-RP is a potentially abundant source of phytochemicals. In this study, we initially found that fermented supernatant cultured

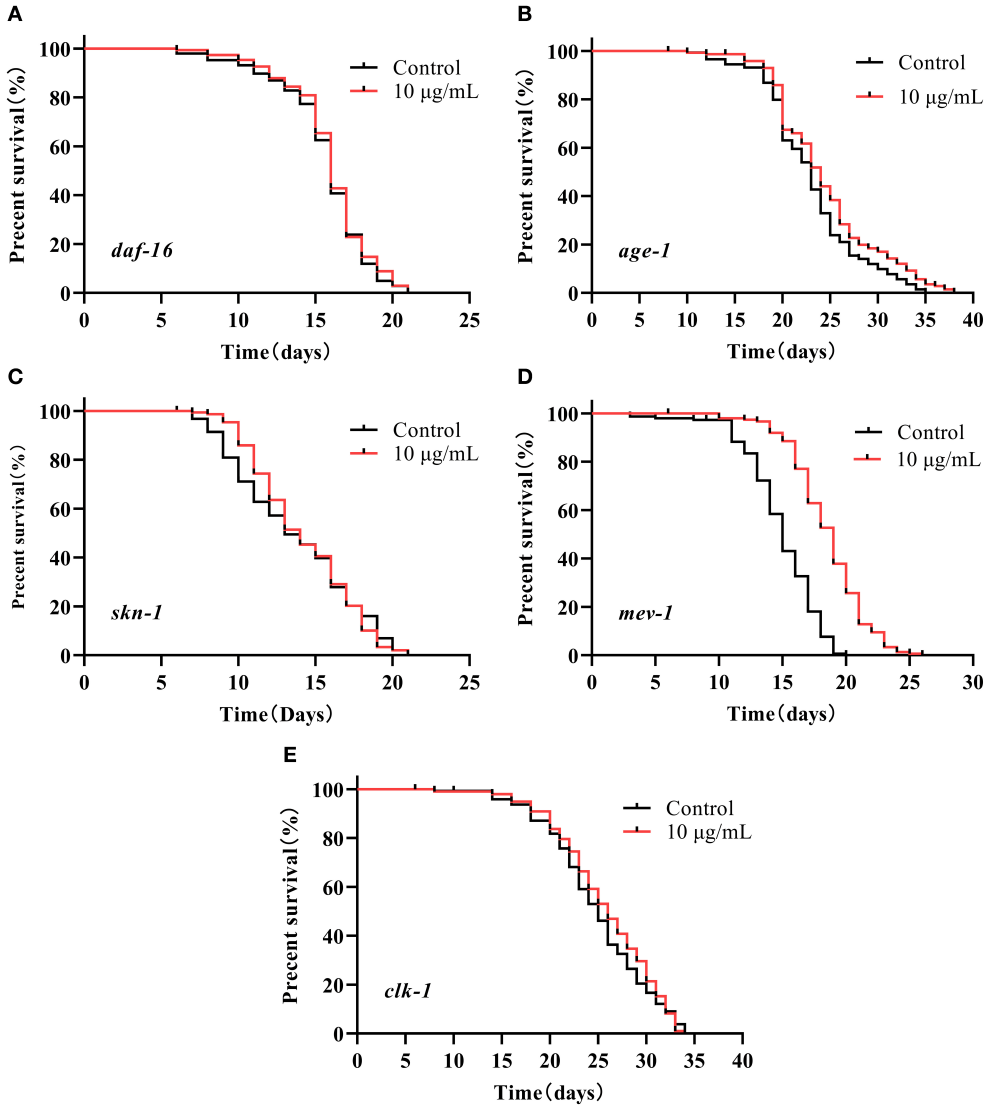

FIGURE 7 | Survival of several mutant strains treated with SC-RP (representative results). **(A–E)** Loss-of-function mutant strains in several genes related to lifespan regulation were treated with final concentrations of 0 (control) or 10 μg/mL SC-RP starting from the L4 stage (day 0). The survivals were recorded until all of the mutants died (n = 134–150 worms/treatment). The log-rank (Mantel–Cox) test was used for statistical analysis.

from an RP-supplemented medium extends the lifespan and healthspan of *C. elegans*. And, we also founded that SC-RP are not dose-dependent to exert an antiaging effect, which may highly have related to the SPG's higher viscosity to binds tightly to phenolics and flavonoids. Notably, a dose of 10 μg/mL SC-RP prolonged the mean lifespan of *C. elegans* (by 24.89%) to a greater extent when compared with different kinds of fermented products (**Figure 1**; **Table 2**) (26, 28) and polysaccharides from *notoginseng* (5), and even reached comparable levels of activity observed previously in crude extracts of edible plants such as a *Rhodiola* extract and the synergistic effects of apple peel and blueberry extract (37, 39). In contrast to the mycelial water extract (MWE) from fermented mycelia of *Cordyceps sobolifera* (40). SC-RP also markedly prolonged the mean survival time of *C. elegans* by ∼24%. Furthermore, we found that SC-RP exhibited a similar effect on extending the lifespan of *C. elegans* when compared with that of MWE when the working dose (10 μg/mL) is only one percent of MWE (1 mg/mL), demonstrating that biotransformation can efficiently enrich active substances. Moreover, various research efforts have confirmed that the biological activity of plants and herbal medicines can be enhanced by fermentation because of the biotransformation interactions among multiple phytochemicals and microorganisms (41, 42). Therefore, we propose that the magnitude of the mean lifespan extension of *C. elegans* treated with SC-RP rather than with a single composition may be attributed to interactions among various compounds such as puerarin, SPG and some phenolics or flavonoids in

TABLE 4 | Effect of SC-RP on the lifespan of *daf-16 (mgDf50)* mutants, *age-1 (hx546)* mutants, *clk-1(e2519)* mutants, *mev-1(kn1)* mutants, and *skn-1(zu135)* mutants (mean ± SD, $n = 3$).

Genotype and condition	Treatment	Meanslifespan	Maximum lifespan	Number	Mean fold increase%/ Genetic requirement[a]
daf-16 (mgDf50)(20°C, Days)	0 μg/mL	15.56 ± 0.18	20.33 ± 0.71	147/150	yes
	10 μg/mL	15.84 ± 0.05	20.67 ± 0.58	150/150	
age-1 (hx546)(20°C, Days)	0 μg/mL	22.98 ± 0.57	34.33 ± 1.15	150/150	-
	10 μg/mL	24.47 ± 0.56*	37.67 ± 0.54***	147/150	6.48
clk-1(e2519)(20°C, Days)	0 μg/mL	24.90 ± 0.06	34.00 ± 0.00	134/150	yes
	10 μg/mL	24.88 ± 0.12	32.33 ± 0.58*	147/150	
mev-1(kn1)(20°C, Days)	0 μg/mL	14.89 ± 0.26	19.33 ± 0.58	145/150	-
	10 μg/mL	18.55 ± 0.56***	25.00 ± 1.00***	148/150	24.58
skn-1(zu135)(20°C, Days)	0 μg/mL	14.49 ± 0.72	21.00 ± 0.00	141/150	yes
	10 μg/mL	15.01 ± 0.50	20.67 ± 0.58	146/150	

*$P < 0.05$; ***$P < 0.001$. [a]Percentage of mean fold increase is relative to the control.

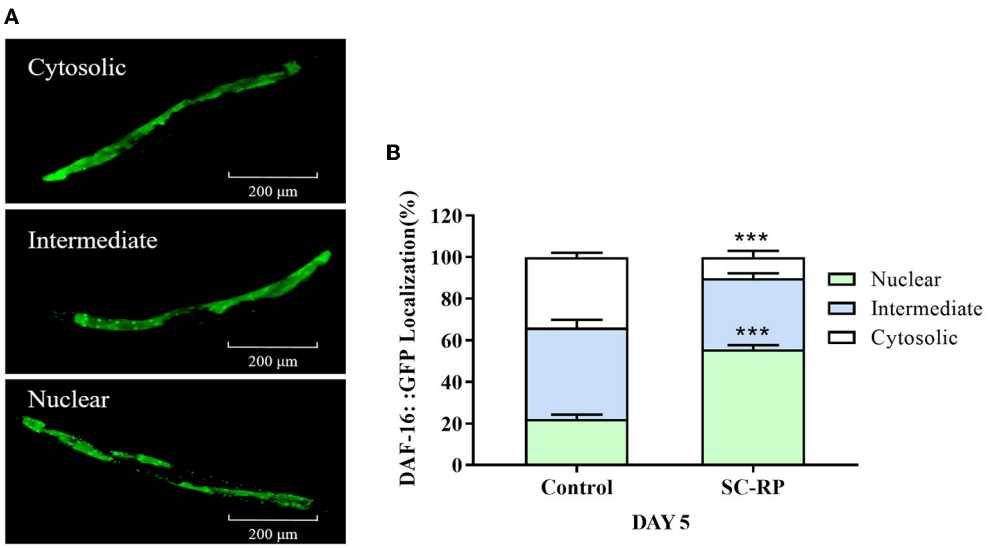

FIGURE 8 | Effect of SC-RP on subcellular localization of DAF-16. **(A)** Representative fluorescence images of TJ356 worms with cytosolic (top), intermediate (middle), and nuclear (bottom) DAF-16::GFP localization. **(B)** The number of transgenic TJ356 worms of each category was measured ($N > 20$). Data were expressed as the mean ± SD ($n = 3$). *$P < 0.05$, **$P < 0.01$, and ***$P < 0.001$ indicated statistical significance with control group.

SC-RP. Characterization of these interactions requires further investigation. In addition, SC-RP contains various active ingredients listed above, it is possible the SC-RP extended the lifespan *via* restricting bacterial growth. To verify this idea, we cultured *E. coli* OP50 in LB medium with SC-RP at a working solution (5, 10, and 20 μg/mL). And SC-RP did not inhibit the growth of *E. coli* OP50 in any bacterial growth (data not shown). Therefore, the SC-RP did not extend the lifespan through antimicrobial effect. Besides, low doses of SC-RP (5 μg/mL) did not extend the lifespan of nematodes (**Table 2**). Alive E. coli *OP50* has poor metabolic capacity at 20°C, thus the influence of killed-E. coli *OP50* or alive E. coli *OP50* to SC-RP was not significant in our test.

Intracellular ROS imbalance can cause aging, which may cause many chronic diseases such as coronary heart disease, osteoporosis, and diabetes (4, 43, 44). The free radical theory of aging proposes that with aging, the accumulation of ROS exceeds the clearance rate by the body, thereby disrupting the redox balance of cells, which leads to the accumulation of oxidative stress and accelerates the aging process (45). Endogenous oxidative stress represents the main factor of aging. Stress in nematodes affects signaling pathways and related genes that play a crucial role in regulating lifespan and various diseases. Various studies have shown that extending *C. elegans* lifespan is associated with enhancing and improving stress resistance (7, 46). In this study, *C. elegans* exhibited increased tolerance against abiotic stress (heat shock) and oxidative stress after supplementing with SC-RP (**Figure 4**; **Table 3**). As byproducts of aerobic metabolism, ROS can damage the body. Our previous results showed that SC-RP exhibits good antioxidant activity at the chemical and

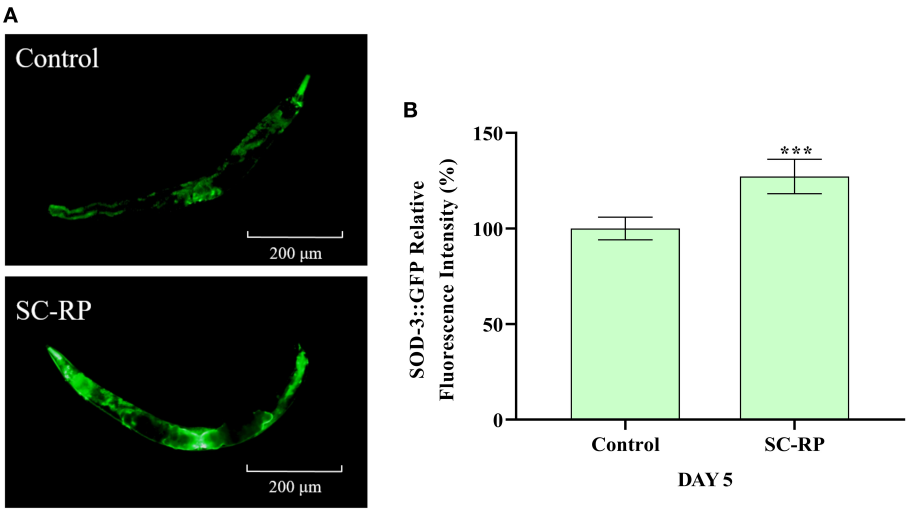

FIGURE 9 | Effect of SC-RP on the relative fluorescence intensity of SOD-3::GFP **(A,B)**. The relative fluorescence intensity of SOD-3::GFP was quantified using Image J software ($N > 20$). Data were expressed as the mean ± SD ($n = 3$). $^{*}P < 0.05$, $^{**}P < 0.01$, and $^{***}P < 0.001$ indicated statistical significance with control group.

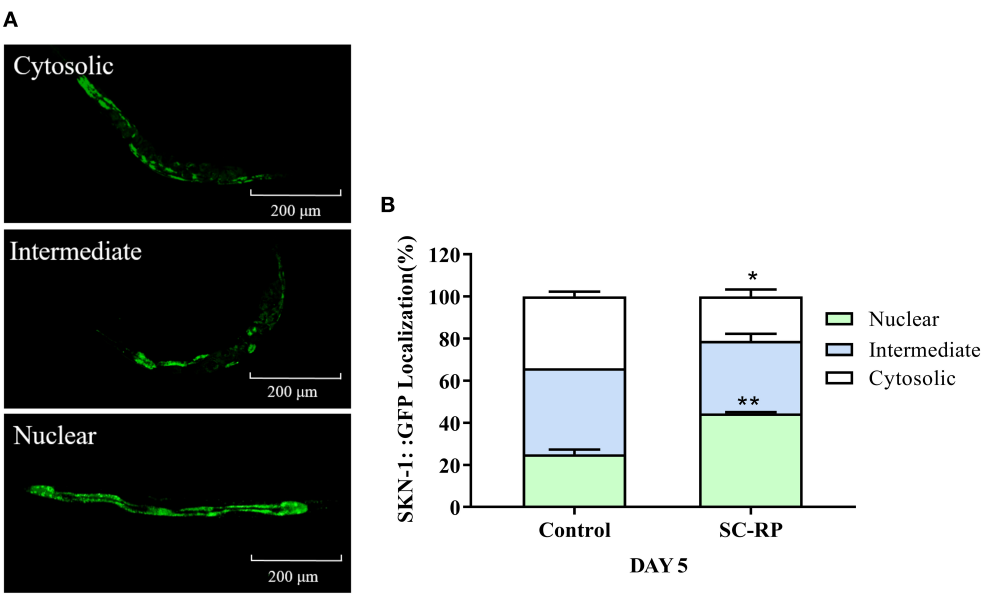

FIGURE 10 | Effect of SC-RP on subcellular localization of SKN-1. **(A)** Representative fluorescence images of SKN-1 worms with cytosolic (top), intermediate (middle), and nuclear (bottom) SKN-1:: GFP localization. **(B)** The number of transgenic SKN-1 worms of each category was measured ($N > 20$). Data were expressed as the mean ± SD ($n = 3$). $^{*}P < 0.05$, $^{**}P < 0.01$, and $^{***}P < 0.001$ indicated statistical significance with control group.

cellular level when compared with fermented supernatant cultured from a regular medium (SC) at the same concentration of SPG (data not shown), which may be related to puerarin and other active substances present in SC-RP. The present results showed that SC-RP may exert oxidative stress resistance and anti-aging effects by increasing the antioxidant activity *in vivo*. Our present results showed that SC-RP noticeably reduces the ROS and TBARS levels and promotes the activities of antioxidant enzymes such as SOD and CAT (**Figures 5**, **6**), suggesting that the antioxidant activity of SC-RP may contribute strongly to its anti-aging effect. In addition, we found that SC and SPG do not extend the lifespan of *C. elegans* (**Supplementary Figure 2**; **Supplementary Table 2**). Therefore, we hypothesize that components of RP such as puerarin and substances produced by biotransformation like phenolics and flavonoids play a key role in the anti-aging effect and characterizing the role of these compounds will be the focus of future research efforts.

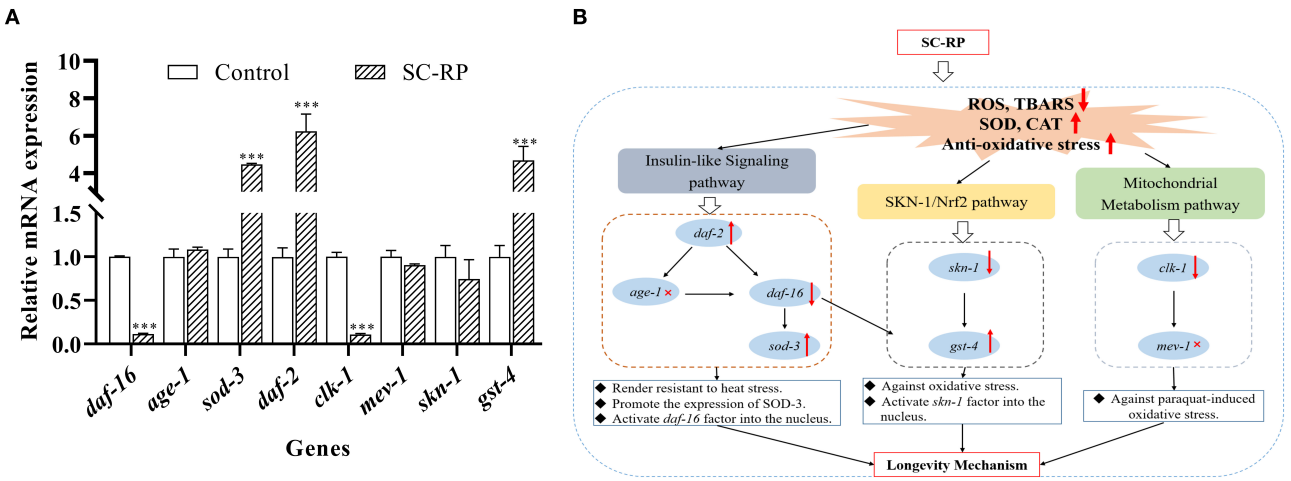

FIGURE 11 | Molecular mechanism of SC-RP in the anti-aging effect. **(A)** The mRNA levels of *daf-16, age-1, sod-3, daf-2, skn-1, gst-4, clk-1, and mev-1* were determined by quantitative real-time RT-PCR and normalized to the expression of *β-actin-1*. **(B)** The up and down arrows respectively represent the up and down expression of genes, and these gene-related pathways play important roles in the regulation of aging. The gene with a red cross was showed no relation to the SC-RP's regulation of aging by measuring the lifespan of mutant nematodes and the aging-related gene expression of nematodes. The above results reveal the possible mode of action for the longevity extension mediated by SC-RP. Data were expressed as the mean ± SD ($n = 3$). $^{*}P < 0.05$, $^{**}P < 0.01$, and $^{***}P < 0.001$ indicated statistical significance with control group.

Our results revealed that SC-RP improved both healthspan and lifespan. Thus, the effect of SC-RP on the transcriptional expression of key genes and mutants was examined. In *C. elegans*, many genetic manipulations and pathways affect aging, including insulin/IGF-1 signaling, SKN-1/Nrf2 signaling and the mitochondrial respiration pathway (24, 33, 47). The IIS pathway is linked to diet, metabolism, growth, development, longevity and behavior in *C. elegans*. Inhibition of the insulin/IGF receptor DAF-2 reduces the activity of the phosphoinositide 3-kinase (PI3K)/Akt kinase cascade, which, in turn, dephosphorylates and activates the transcription factor DAF-16/FOXO by enhancing DAF-16 translocation from the cytoplasm to the nucleus, where it controls the expression of various genes that contribute to stress resistance and longevity (48). Nematodes with reduced IIS pathway activity are resistant to heat and oxidative stress, indicating that increasing the prevention or repair of oxidative damage can extend the lifespan of *C. elegans* (28, 49). In the current study, SC-RP prolonged the lifespan of *C. elegans via* activation of the insulin/IGF-1 pathway by regulating *daf-16* and *daf-2* but not *age-1* (**Figures 7A,B**, **11A**; **Table 4**). Moreover, oxidative stress may inhibit IIS-induced phosphorylation and promote the translocation of DAF-16 into the nucleus. As SC-RP extended the lifespan of *C. elegans via daf-16* (**Figures 7A**, **8**; **Table 4**), it may reduce insulin-like signaling, thus activating DAF-16 and promoting the transcriptional activation of genes targeted by DAF-16. A previous study reported that the lifespan extension and DAF-16 translocation coincide may not necessarily be causally connected (50). Therefore, we inferred that the inconsistent behavior of *daf-16* gene expression and translocation in this experiment may be influenced by upstream related factors thus forming a negative feedback regulation and also occurred in *skn-1* gene in our research. In addition, we confirmed the upregulation of *sod-3* expression by qRT-PCR, which plays an important role in oxidative stress and regulating the transcription activity of DAF-16 (**Figure 9**; **Figure 11A**).

Therefore, we conclude that the longevity effect of SC-RP in *C. elegans* involves the IIS pathway.

Activation of SKN-1 is also vital in mediating longevity and antioxidant activities in *C. elegans*. SKN-1 of *C. elegans* is the functional ortholog of the mammalian transcription factor Nrf2, which accumulates in the intestinal nucleus and activation expression of phase 2 detoxification genes such as *gst-4* in response to stress. Similar to the IIS pathway, *skn-1* is involved in various genetic and pharmacologic interventions and thus promotes longevity of *C. elegans* (47). The current study indicated that SC-RP promoted the downregulation of *skn-1* expression and abolished the extension of the lifespan of *skn-1 (zu135)* mutant (**Figure 7C**; **Table 4**). Furthermore, SC-RP promoted nuclear translocation of SKN-1 into the nucleus and *gst-4* expression (**Figure 11A**). These findings suggest that SKN-1 plays a key role in extending the lifespan of SC-RP-treated *C. elegans*.

Mitochondrial respiration plays a major role in energy production and mediates the aging process. ROS are the main byproducts generated from mitochondrial metabolism, which can damage mitochondria and thus affect the lifespan of *C. elegans* (51). Thus, we evaluated the possible role of mitochondrial function in extending the lifespan and the anti-aging effect by studying *mev-1* and *clk-1* worms. The *mev-1* strain produces above-average levels of ROS in mitochondria because of incomplete reduction of O_2 in the electron transporter chain, which indirectly leads to a reduced lifespan of the worm (52). *clk-1* encodes an evolutionarily conserved enzyme required for the biosynthesis of ubiquinone (UQ; co-enzyme

Q; CoQ). The long-lived *clk-1* mutant lacks the endogenous form of coenzyme Q10, which carries electrons and protons from mitochondrial complexes I and II to complex III (53). We illustrated that SC-RP extends the life span of the *mev-1* mutant but did not affect the lifespan of the *clk-1* mutant (**Figures 7D,E**; **Table 4**). Moreover, SC-RP downregulated the expression of *clk-1* significantly, showing that SC-RP may function in a *clk-1*-dependent manner but is independent of *mev-1* for extending the longevity of *C. elegans*.

In summary, insulin/IGF-1 signaling, SKN-1/Nrf2 and mitochondrial metabolism pathways were affected by SC-RP treatment and therefore are partly responsible for extending the healthspan of *C. elegans*. The current findings indicated that SC-RP enhances the expression of *daf-2*, *sod-3* and *gst-4* genes and downregulates the expression of *daf-16*, *skn-1* and *clk-1* genes (**Figure 11A**). Therefore, we propose that the longevity effect of SC-RP involves the IIS pathway, SKN-1/Nrf-2 pathway and mitochondrial metabolism pathway (**Figure 11B**). Moreover, the specific regulation pathway of SC-RP will be verified in future work.

CONCLUSIONS

The current study showed that SC-RP synergistically decreased age-related behaviors and increased the mean lifespan of *C. elegans*, and improved the resistance of *C. elegans* to stress. The lifespan of nematodes treated with SC-RP was extended by 24.89% when compared with that of non-treated (control) nematodes ($P < 0.01$). SC-RP also markedly promoted the activities of antioxidant enzymes (SOD and CAT) and reduced TBARS and ROS levels in cells ($P < 0.05$), indicating that SC-RP contributes to the anti-aging effect by enhancing the activity of antioxidant enzymes. Moreover, mutant assays illustrated that SC-RP-mediated life extension is related to *daf-16*, *skn-1* and *clk-1* expression levels. SC-RP was found to extend longevity by upregulation of *daf-2*, *sod-3* and *gst-4* expression and downregulation of *daf-16* and *clk-1* expression. In addition, SC-RP stimulated the migration of DAF-16 and SKN-1 into the nucleus and increased SOD-3 activity. Our finding indicated that the IIS pathway, SKN-1/Nrf-2 pathway and mitochondrial metabolism pathway are associated with the longevity afforded by SC-RP. The present findings provide a scientific basis for using SC-RP as an anti-aging agent, and SC-RP may be suitable for developing functional foods and nutraceuticals products. This study also provides a reference for biotransformation and application of edible medicinal fungi such as *Cordyceps militaris* and *Ganoderma lucidum* et al.

DATA AVAILABILITY STATEMENT

The original contributions presented in the study are included in the article/**Supplementary Material**, further inquiries can be directed to the corresponding author/s.

AUTHOR CONTRIBUTIONS

YD responsible for the methodology, data curation, formal analysis, investigation, and draft of the manuscript. HL responsible for methodology and software and validation. QH: analysis summary and discussion. LT and LH: assisted testing. BZ and HS: formal analysis. DL and CG: formal analysis and supervision. LZ: organized, supervised, and provided overall guidance of the project. All authors contributed to the article and approved the submitted version.

FUNDING

The authors are grateful for the financial support from the Guangdong Pharmaceutical University Research Project (43255098), Marubi Joint Research Project Fund (YB202109131043), and Guangzhou Science and Technology Plan Project Fund (202103000055).

ACKNOWLEDGMENTS

We thank Liwen Bianji (Edanz) (www.liwenbianji.cn/), for editing the English text of a draft of this manuscript.

SUPPLEMENTARY MATERIAL

The Supplementary Material for this article can be found online at: https://www.frontiersin.org/articles/10.3389/fnut.2022.847064/full#supplementary-material

REFERENCES

1. El Assar M, Angulo J, Rodríguez-Mañas L. Oxidative stress and vascular inflammation in aging. *Free Radical Bio Med.* (2013) 65:380–401. doi: 10.1016/j.freeradbiomed.2013.07.003
2. Golden TR, Hubbard A, Dando C, Herren MA, Melov S. Age-related behaviors have distinct transcriptional profiles in *Caenorhabditis elegans*. *Aging Cell.* (2008) 7:850–65. doi: 10.1111/j.1474-9726.2008.00433.x
3. Niccoli T, Partridge L. Aging as a risk factor for disease. *Curr Biol.* (2012) 22:R741–52. doi: 10.1016/j.cub.2012.07.024
4. López-Otín C, Blasco MA, Partridge L, Serrano M, Kroemer G. The hallmarks of aging. *Cell.* (2013) 153:1194–217. doi: 10.1016/j.cell.2013.05.039
5. Feng S, Cheng H, Xu Z, Yuan M, Huang Y, Liao J, et al. *Panax notoginseng* polysaccharide increases stress resistance and extends lifespan in *Caenorhabditis elegans*. *J Funct Foods.* (2018) 45:15–23. doi: 10.1016/j.jff.2018.03.034
6. Lin C, Su Z, Luo J, Jiang L, Shen S, Zheng W, et al. Polysaccharide extracted from the leaves of *Cyclocarya paliurus* (*Batal.*) Iljinskaja enhanced stress resistance in *Caenorhabditis elegans via skn-1* and *hsf-1*. *Int J Biol Macromol.* (2020) 143:243–54. doi: 10.1016/j.ijbiomac.2019.12.023
7. Wang H, Liu J, Li T, Liu RH. Blueberry extract promotes longevity and stress tolerance *via* DAF-16 in *Caenorhabditis elegans*. *Food Funct.* (2018) 9:5273-82. PubMed PMID:30238944. doi: 10.1039/C8FO01680A
8. Wei C, Yu C, Yen P, Lin H, Chang S, Hsu F, et al. Antioxidant activity, delayed aging, and reduced amyloid-β toxicity of methanol extracts of tea seed pomace fromcamellia tenuifolia. *J Agr Food Chem.* (2014) 62:10701–7. doi: 10.1021/jf503192x

9. Das G, Paramithiotis S, Sundaram Sivamaruthi B, Wijaya CH, Suharta S, Sanlier N, et al. Traditional fermented foods with anti-aging effect: a concentric review. *Food Res Int.* (2020) 134:109269. doi: 10.1016/j.foodres.2020.109269
10. Zhang Y, Kong H, Fang Y, Nishinari K, Phillips GO. Schizophyllan: a review on its structure, properties, bioactivities and recent developments. *Bioactive Carbohydrat Dietary Fiber.* (2013) 1:53–71. doi: 10.1016/j.bcdf.2013.01.002
11. Hamedi S, Shojaosadati SA, Najafi V, Alizadeh V. A novel double-network antibacterial hydrogel based on aminated bacterial cellulose and schizophyllan. *Carbohyd Polym.* (2020) 229:115383. doi: 10.1016/j.carbpol.2019.115383
12. Takedatsu H, Mitsuyama K, Mochizuki S, Kobayashi T, Sakurai K, Takeda H, et al. A new therapeutic approach using a schizophyllan-based drug delivery system for inflammatory bowel disease. *Mol Ther.* (2012) 20:1234–41. doi: 10.1038/mt.2012.24
13. Abd Razak DL, Mohd Fadzil NH, Jamaluddin A, Abd Rashid NY, Sani NA, Abdul Manan M. Effects of different extracting conditions on anti-tyrosinase and antioxidant activities of schizophyllum commune fruit bodies. *Biocatalysis Agricult Biotechnol.* (2019) 19:101116. doi: 10.1016/j.bcab.2019.101116
14. Metreveli E, Kachlishvili E, Singer SW, Elisashvili V. Alteration of white-rot basidiomycetes cellulase and xylanase activities in the submerged co-cultivation and optimization of enzyme production by Irpex lacteus and *Schizophyllum commune*. *Bioresource Technol.* (2017) 241:652–60. doi: 10.1016/j.biortech.2017.05.148
15. Wu J, Yang X, Ge J, Zhang Y, Wu L, Liu J, et al. Biotransformation of sophoricoside in *Fructus sophorae* by the fungus *Schizophyllum commune*. *Bioresource Technol.* (2012) 111:496–9. doi: 10.1016/j.biortech.2012.02.038
16. Wenli Y, Yaping Z, Bo S. The radical scavenging activities of radix puerariae isoflavonoids: a chemiluminescence study. *Food Chem.* (2004) 86:525–9. doi: 10.1016/j.foodchem.2003.09.005
17. Huang Q, Zhang H, Xue D. Enhancement of antioxidant activity of radix puerariae and red yeast rice by mixed fermentation with *Monascus purpureus*. *Food Chem.* (2017) 226:89–94. doi: 10.1016/j.foodchem.2017.01.021
18. Deng Y, Huang Q, Hu L, Liu T, Zheng B, Lu D, et al. Enhanced exopolysaccharide yield and antioxidant activities of *Schizophyllum commune* fermented products by the addition of radix puerariae. *Rsc Adv.* (2021) 11:38219–34. doi: 10.1039/D1RA06314F
19. Kaletta T, Hengartner MO. Finding function in novel targets: *C.* elegans as a model organism. nature reviews. *Drug discov.* (2006) 5:387–99. doi: 10.1038/nrd2031
20. Liao VH. Use of *Caenorhabditis elegans* to study the potential bioactivity of natural compounds. *J Agr Food Chem.* (2018) 66:1737–42. doi: 10.1021/acs.jafc.7b05700
21. Matsunami K. Frailty and caenorhabditis elegans as a benchtop animal model for screening drugs including natural herbs. *Front Nutri.* (2018) 5:11. doi: 10.3389/fnut.2018.00111
22. Luo X, Wang J, Chen H, Zhou A, Song M, Zhong Q, et al. Identification of flavoanoids from finger citron and evaluation on their antioxidative and antiaging activities. *Front Nutri.* (2020) 7:900. doi: 10.3389/fnut.2020.584900
23. Ye Y, Gu Q, Sun X. Potential of *Caenorhabditis elegans* as an antiaging evaluation model for dietary phytochemicals: a review. *Compr Rev Food Sci F.* (2020) 19:3084–105. doi: 10.1111/1541-4337.12654
24. Slack C, Partridge L. Genes, pathways and metabolism in aging. *Drug Discovery Today: Disease Models.* (2013) 10:e87–93. doi: 10.1016/j.ddmod.2013.01.002
25. Peng Y, Sun Q, Gao R, Park Y. AAK-2 and SKN-1 are involved in chicoric-acid-induced lifespan extension in *Caenorhabditis elegans*. *J Agr Food Chem.* (2019) 67:9178–86. doi: 10.1021/acs.jafc.9b00705
26. Ibe S, Kumada K, Yoshida K, Otobe K. Natto (fermented soybean) extract extends the adult lifespan of *Caenorhabditis elegans*. *Biosci Biotechnol Biochem.* (2013) 77:392–4. PubMed PMID:23391920. doi: 10.1271/bbb.120726
27. Shi Y, Pan T, Liao VH. Monascin from *Monascus*-fermented products reduces oxidative stress and amyloid-β Toxicity *via* DAF-16/FOXO in *Caenorhabditis elegans*. *J Agr Food Chem.* (2016) 64:7114–20. doi: 10.1021/acs.jafc.6b02779
28. Sugawara T, Furuhashi T, Shibata K, Abe M, Kikuchi K, Arai M, et al. Fermented product of rice with *Lactobacillus kefiranofaciens* induces anti-aging effects and heat stress tolerance in nematodes *via* DAF-16. *Biosci Biotechnol Biochemistr.* (2019) 83:1484–9. doi: 10.1080/09168451.2019.1606696
29. Zhou L, Lin X, Abbasi AM, Zheng B. Phytochemical contents and antioxidant and antiproliferative activities of selected black and white sesame seeds. *Biomed Res Int.* (2016) 2016:1–9. doi: 10.1155/2016/8495630
30. Pandey S, Tiwari S, Kumar A, Niranjan A, Chand J, Lehri A, et al. Antioxidant and anti-aging potential of juniper berry (*Juniperus communis* L.) essential oil in *Caenorhabditis elegans* model system. *Ind Crop Prod.* (2018) 120:113–22. doi: 10.1016/j.indcrop.2018.04.066
31. Chen S, Huang H, Huang G. Extraction, derivatization and antioxidant activity of cucumber polysaccharide. *Int J Biol Macromol.* (2019) 140:1047–53. doi: 10.1016/j.ijbiomac.2019.08.203
32. Karengera A, Bao C, Riksen JAG, van Veelen HPJ, Sterken MG, Kammenga JE, et al. Development of a transcription-based bioanalytical tool to quantify the toxic potencies of hydrophilic compounds in water using the nematode caenorhabditis elegans. *Ecotox Environ Safe.* (2021) 227:112923. doi: 10.1016/j.ecoenv.2021.112923
33. Liu X, Liu H, Chen Z, Xiao J, Cao Y. DAF-16 acts as the "hub" of astaxanthin's anti-aging mechanism to improve aging-related physiological functions in *Caenorhabditis elegans*. *Food Funct.* (2021) doi: 10.1039/D1FO01069G
34. Lin C, Zhang X, Xiao J, Zhong Q, Kuang Y, Cao Y, et al. Effects on longevity extension and mechanism of action of carnosic acid in *Caenorhabditis elegans*. *Food Funct.* (2019) 10:1398–410. doi: 10.1039/C8FO02371A
35. Arantes-Oliveira N, Berman JR, Kenyon C. Healthy animals with extreme longevity. *Science.* (2003) 302:611. doi: 10.1126/science.1089169
36. Labuschagne CF, Brenkman AB. Current methods in quantifying ROS and oxidative damage in *caenorhabditis elegans* and other model organism of aging. *Aging Res Rev.* (2013) 12:918–30. doi: 10.1016/j.arr.2013.09.003
37. Jiang S, Deng N, Zheng B, Li T, Liu RH. *Rhodiola* extract promotes longevity and stress resistance of *Caenorhabditis elegans via* DAF-16 and SKN-1. *Food Funct.* (2021) 12:4471–83. doi: 10.1039/D0FO02974B
38. Wang H, Guo X, Hu X, Li T, Fu X, Liu RH. Comparison of phytochemical profiles, antioxidant and cellular antioxidant activities of different varieties of blueberry (*Vaccinium spp.*). *Food Chem.* (2017) 217:773–81. doi: 10.1016/j.foodchem.2016.09.002
39. Song B, Wang H, Xia W, Zheng B, Li T, Liu RH. Combination of apple peel and blueberry extracts synergistically induced lifespan extension *via* DAF-16 in *Caenorhabditis elegans*. *Food Funct.* (2020) 11:6170–85. doi: 10.1039/D0FO00718H
40. Lin QY, Long LK, Zhuang ZH, Wu LL, Wu SL, Zhang WM. Antioxidant activity of water extract from fermented mycelia of cordyceps sobolifera (Ascomycetes) in caenorhabditis elegans. *Int J Med Mushrooms.* (2018) 20:61–70. doi: 10.1615/IntJMedMushrooms.2018025324
41. Shi YC, Yu CW, Liao VH, Pan TM. *Monascus*-fermented dioscorea enhances oxidative stress resistance *via* DAF-16/FOXO in *Caenorhabditis elegans*. *Plos ONE.* (2012) 7:e39515. doi: 10.1371/journal.pone.0039515
42. Hur SJ, Lee SY, Kim Y, Choi I, Kim G. Effect of fermentation on the antioxidant activity in plant-based foods. *Food Chem.* (2014) 160:346–56. doi: 10.1016/j.foodchem.2014.03.112
43. Bou-Teen D, Kaludercic N, Weissman D, Turan B, Maack C, Di Lisa F, et al. Mitochondrial ROS and mitochondria-targeted antioxidants in the aged heart. *Free Radical Bio Med.* (2021) 167:109–24. doi: 10.1016/j.freeradbiomed.2021.02.043
44. Ames BN, Shigenaga MK, Hagen TM. Oxidants, antioxidants, and the degenerative diseases of aging. *Proc Natl Acad Sci U S A.* (1993) 90:7915–22. doi: 10.1073/pnas.90.17.7915
45. Sohal RS, Mockett RJ, Orr WC. Mechanisms of aging: an appraisal of the oxidative stress hypothesis. *Free Radic Biol Med.* (2002) 33:575–86. doi: 10.1016/S0891-5849(02)00886-9
46. Xiong L, Deng N, Zheng B, Li T, Liu RH. HSF-1 and SIR-2.1 linked insulin-like signaling is involved in goji berry (*Lycium spp.*) extracts promoting lifespan extension of *Caenorhabditis elegans*. *Food Funct.* (2021) 12:7851–66. doi: 10.1039/D0FO03300F

47. Blackwell TK, Steinbaugh MJ, Hourihan JM, Ewald CY, Isik M. SKN-1/Nrf, stress responses, and aging in *Caenorhabditis elegans*. *Free Radical Bio Med.* (2015) 88:290–301. doi: 10.1016/j.freeradbiomed.2015.06.008
48. Zečić A, Braeckman BP. DAF-16/FoxO in *Caenorhabditis elegans* and its role in metabolic remodeling. *Cells-Basel.* (2020) 9:109. doi: 10.3390/cells9010109
49. Satoh T, Sakamoto K. Fermented brown sugar residue prolongs the *Caenorhabditis elegans* Lifespan *via* DAF-16. *Food Nutri Sci.* (2017) 08:855–64. doi: 10.4236/fns.2017.89061
50. Pietsch K, Saul N, Menzel R, Sturzenbaum SR, Steinberg CE. Quercetin mediated lifespan extension in *Caenorhabditis elega*ns is modulated *by age-1, daf-2, sek*-1 an*d unc*-43. *Biogerontology.* (2009) 10:565–78. doi: 10.1007/s10522-008-9199-6
51. Dancy BM, Sedensky MM, Morgan PG. Effects of the mitochondrial respiratory chain on longevity in *C. elegans*. *Exp Gerontol.* (2014) 56:245–55. doi: 10.1016/j.exger.2014.03.028
52. Soares ATG, Rodrigues LBL, Salgueiro WG, Dal Forno AHDC, Rodrigues CF, Sacramento M, et al. Organoselenotriazoles attenuate oxidative damage induced by mitochondrial dysfunction in *mev-1 Caenorhabditis elegans* mutants. *J Trace Elem Med Bio.* (2019) 53:34–40. doi: 10.1016/j.jtemb.2019.01.017
53. Stepanyan Z, Hughes B, Cliche DO, Camp D, Hekimi S. Genetic and molecular characterization of CLK-1/mCLK1, a conserved determinant of the rate of aging. *Exp Gerontol.* (2006) 41:940–51. doi: 10.1016/j.exger.2006.06.041

Conflict of Interest: YD and LT are graduate students jointly trained by Guangxi University and Guangdong Pharmaceutical University. CG, LH, HS, and HL is employed by Guangdong Marubi Biotechnology Co., Ltd, and the experimental part of this research was completed in the R&D laboratory of Guangdong Marubi Biotechnology Co., Ltd.

The remaining authors declare that the research was conducted in the absence of any commercial or financial relationships that could be construed as a potential conflict of interest.

frontiers in Nutrition

METHODS
published: 17 March 2022
doi: 10.3389/fnut.2022.842766

Optimization of the *Artemisia* Polysaccharide Fermentation Process by *Aspergillus niger*

Ali Tao, Xuehua Feng, Yajing Sheng and Zurong Song*

College of Pharmacy, Anhui Xinhua University, Hefei, China

In order to investigate the fermentation process of *Artemisia* polysaccharides, this paper showcases an investigation into the effects of fermentation time, fermentation temperature, strain inoculum, *Artemisia annua* addition, and shaker speed on the polysaccharides production of *Artemisia annua*. The yield of *Artemisia* polysaccharides content was determined based on the optimization of single-factor test, and then a response surface test was conducted with temperature, inoculum, and time as response variables and the yield of *Artemisia* polysaccharides as response values. The fermentation process was then optimized and the antioxidant activity of *Artemisia* polysaccharides was monitored using DPPH, $ABTS^{+}$, OH, and total reducing power. The optimum fermentation process was determined by the test to be 5% inoculum of *Aspergillus niger*, temperature 36°C, time 2 d, shaker speed 180 r/min, and 4% addition of *Artemisia annua*, and the extraction of *Artemisia* polysaccharides was up to 17.04% by this condition of fermentation. The polysaccharides from *Artemisia annua* fermented by *Aspergillus Niger* had scavenging effects on DPPH, ABTS, and OH free radicals.

Keywords: *Aspergillus niger*, *Artemisia annua* polysaccharide, optimization, fermentation process, single factor, response surface

OPEN ACCESS

Edited by:
Xiaolong Ji,
Zhengzhou University of Light Industry, China

Reviewed by:
Baoming Tian,
Zhejiang University of Technology, China
Xuefeng Zeng,
Guizhou University, China

****Correspondence:***
Xuehua Feng
fengxuehua@axhu.edu.cn

Specialty section:
This article was submitted to Food Chemistry, a section of the journal Frontiers in Nutrition

Received: *24 December 2021*
Accepted: *28 January 2022*
Published: *17 March 2022*

Citation:
Tao A, Feng X, Sheng Y and Song Z (2022) Optimization of the Artemisia Polysaccharide Fermentation Process by Aspergillus niger. Front. Nutr. 9:842766. doi: 10.3389/fnut.2022.842766

INTRODUCTION

Polysaccharide is a natural biological macromolecular substance with anti-inflammatory (1), anti-tumor, anti-radiation, hypoglycemic, hypolipidemic, and immune-enhancing effects (2). Studies have shown that some plant polysaccharides composed of galacturonic acid and glucuronic acid (3) and can enter the colon and exhibit probiotic properties (4), which may alter specific microbial populations and protect the gastrointestinal tract (5, 6). *Artemisia annua L.* is an annual, strongly scented herb commonly found in Chahar and northern Suiyuan provinces of China at altitudes of 1,000–1,500 m (7). It has been found to have anti-inflammatory, antibacterial, antihypertensive, antimalarial, antioxidant, antiparasitic, immunosuppressive, and collagen-induced arthritic effects (8). It is used clinically for the treatment of respiratory, digestive, skin, endocrine, and febrile diseases (9). The discovery of Artemisinin by Tu Youyou and her team is the first natural drug in China to be internationally recognized (10). It contains sesquiterpene lactones with intracyclic peroxide bonds (11). It is the drug of choice for the treatment of malaria. The main chemical components of *Artemisia annua*, flavonoids, coumarins, sesquiterpenes, and volatile oils, have been extensively reported (12) in large quantities. Although *Artemisia* polysaccharide is one of the active components of *Artemisia*, little research has been carried out on it and its extraction process. In recent years, it has been found that *Artemisia* polysaccharides have an anti-inflammatory effect (13). It can induce apoptosis of cancer cells, improve immunity,

and show anti-liver cancer properties (14). Therefore, we can focus on its extraction research. The traditional extraction method of polysaccharides is hot water or boiling water extraction (15), now the extraction methods of polysaccharides from *Artemisia annua* are mostly: ultrasonic leaching method (16), *papain* extraction method (17), and microwave-assisted extraction method (18).

Microbial fermentation can effectively improve the yield of active ingredients of herbal medicines, and some studies have shown that the fermentation of *Aspergillus niger* can produce *cellulase*, decompose plant cell walls, and promote the release of active ingredients (19). In Tao et al. (20) the fermentation of *Astragalus* membranaceus using *Aspergillus niger* resulted in a significant increase in the free berberine content. In Liu et al. (21) the fermentation of *Astragalus* membranaceus using *Aspergillus niger* resulted in a significant increase in the extraction of *Astragalus* polysaccharides after process optimization. In recent years, although microbial fermentation has been widely studied for its low cost and simple operation, it is rarely mentioned for *Artemisia* polysaccharides. Therefore, in this paper, *Aspergillus niger* was selected to ferment *Artemisia annua*, and the process of extracting *Artemisia* polysaccharides was investigated.

MATERIALS AND METHODS

Materials

Aspergillus niger (provided by the laboratory of School of Pharmacy, Anhui Xinhua College), dried ground part of *Artemisia annua* (Hefei Chinese herbal market), other reagents were analytically pure.

Instrumentations

UV2300 Ultraviolet Spectrophotometer (Shanghai Prism Technology Co., Ltd.), Ultra Clean Bench (Haier Co., Ltd.), AL104 Electronic Balance (Shanghai Mettler Toledo Instruments Co., Ltd.), HBM-103 Flow-through Crusher (Hanbo Mechatronics Co., Ltd).

Test Methods

Medium Formulation

Oblique seed medium: the potatoes were peeled and washed, weighed to 200 g and cut into pieces, boiled for 30 min, gauze filtered, then 20 g of glucose was added, along with 15–20 g of agar, which was dissolved and supplemented with enough water to reach 1,000 ml and a natural pH, sterilized at 115°C for 20 min.

Seed medium: a liquid PDA medium without agar.

The bottle of seed medium was shaken: the seed medium was prepared and sealed with eight layers of gauze, sterilized at 121°C for 20 min, cooled to room temperature, and 3∼4 pieces of 0.5∼1.0 cm^2 slant strains of surface mycelium (without medium) were inserted into the triangular bottle with liquid volume 50 or 250 ml and incubated 28°C (150 r/min) for 48 h.

Fermentation medium: sucrose 0.15 g, magnesium sulfate 0.021 g, dipotassium hydrogen phosphate 0.1 g, calcium chloride 0.027 g, water in the appropriate amount, sterilized at 121°C for 20 min.

Activation and Culture of *Aspergillus niger*

Strain activation: slant seed medium was prepared and sterilized at 121°C for 20 min. The slant medium was made, each sample was slanted into 0.5∼1.0 cm^2 blocks and incubated at 28°C for 72 h. The mycelium evenly grew all over the slant.

Strain culture: *Aspergillus niger* was inoculated in the medium, incubated in the thermostat 30°C until *Aspergillus niger* spores were growing uniformly, then moved to 4°C refrigerator storage spare.

Single-Factor Experimental Design

The effects of inoculum, temperature, time, shaker speed, and *Artemisia annua* addition on the yield of *Artemisia* polysaccharides using *Aspergillus niger* and *Artemisia annua* as raw materials were investigated by deep fermentation.

Selection of the Optimal Inoculum of Aspergillus niger

The fermentation medium with *Artemisia annua* added at 4% and distilled water 100 ml was inoculated with 3, 4, 5, 6, and 7% *Aspergillus niger,* respectively, and another medium without *Aspergillus niger* inoculation was set as the control group and fermented at 36°C and set to 180 r/min in a shaking bed for 4 d.

Selection of the Optimal Temperature

The fermentation medium with *Artemisia annua* was added at 4%, inoculum at 5%, with 100 ml of distilled water, and another medium without *Aspergillus niger* inoculation was set as the control group, and the temperature was set at 32°C, 34°C, 36°C, 38 °C, and 40°C, in order of gradient, and fermented in a shaking bed at 180 r/min for 4 d.

Best Time to Visit

The fermentation medium with *Artemisia annua* added at 4%, inoculum 5%, with 100 ml of distilled water, and another medium without *Aspergillus niger* inoculation was taken as the control group, and fermented at 36°C, 180 r/min in a shaking bed for 1 d, 2 d, 3 d, 4 d, 5 d, respectively.

Optimal Shaker Speed

The fermentation medium of *Artemisia annua* with an additional amount of 4%, inoculation amount of 5%, with 100 ml of distilled water, and a medium without *Aspergillus niger* was set as the control group, at 36°C, according to the gradient setting of 120 r/min, 150 r/min, 180 r/min, 210 r/min, 240 r/min, shaker fermentation for 4 d.

Selection of Optimal Artemisia annua Addition

The fermentation mediums with 5% inoculum and 100 ml of distilled water were added to 2, 3, 4, 5, and 6 %, respectively, and another medium without *Aspergillus niger* was set as the control group and fermented in a shaking bed at 36°C, 180 r/min for 4 d.

Response Surface Optimization Tests

Based on the results of the single-factor test, the inoculum amount, temperature, *Artemisia annua* addition, and fermentation time were determined as the main influencing factors with the yield of *Artemisia* polysaccharide as the index. Based on the Box-Behnken (BBD) central combination design

TABLE 1 | Response surface test factors and levels.

Factor	Level		
	−1	0	1
A Inoculum amount/%	4	5	6
B Temperature/°C	35	36	37
C Fermentation time/d	1	2	3
D *Artemisia annua* addition/%	3	4	5

principle, the inoculum amount, temperature, *Artemisia annua* addition and fermentation time were selected as independent variables, and the yield of *Artemisia* polysaccharides was set as the response value, and a four-factor, three-level test was set up, and the data were processed by Design-Expert 12.0 software. The experimental factors and levels are shown in **Table 1**.

Artemisia Polysaccharide Sample Preparation

Artemisia annua was crushed and sifted through 60 mesh to get uniform powder. Four gram of *Artemisia annua* powder was weighed precisely in a 25 ml colorimetric tube, a certain volume of water was added, sonicated, filtered, and water was added to fix the volume to 50 ml to obtain the sample solution of *Artemisia annua* polysaccharides.

Determination of *Artemisia* Polysaccharides Content

Artemisia polysaccharide is a water-soluble polysaccharide, so the colorimetric method of phenol sulfate was chosen for the determination (22). The content of *Artemisia* polysaccharides was determined by the colorimetric method of phenol sulfate. The basic principle is that the polysaccharide is hydrolyzed by concentrated sulfuric acid to produce monosaccharide, and the glyoxal derivatives generated immediately after dehydration react with phenol under the action of strong acid to produce an orange-yellow substance, and the absorbance value A is linearly correlated with the sugar concentration c at a wavelength of 490 nm and within a certain concentration range.

Standard Curve Plotting

After precisely aspirating 0.1mg/ml glucose standard solution of 0.2, 0.4, 0.6, 0.8, 1.0, 1.2, 1.4 ml, respectively into seven test tubes, distilled water was added to make the volume up to 2.0 ml, and 5% phenol was also added at 1.0 ml each and shaken well, before quickly adding concentrated sulfuric acid 5.0 ml, shaking well again, placing the solution in a boiling water bath 15 for min, then in cold water to bring it to room temperature. The absorbance was measured at 490 nm and 2.0 ml of distilled water was used as a control.

Sample Content Determination

0.6 ml of the sample solution of *Artemisia annua* was drawn up precisely in a 50 ml volumetric flask, water was added to the mark, 2.0 ml of the diluted solution was taken, and the absorbance was measured as described above Standard Curve Plotting to calculate the polysaccharide yield (23).

Polysaccharide yield (%) = concentration measured by cuvette (μg/ml) × dilution times × volume of solution (ml)/mass of experimental material (g) × 100%.

Preparation of *Artemisia annua* Polysaccharides

Fermentation Method

Fermentation was carried out by using the optimized process of a single factor experiment. The control group and the experimental group were centrifuged at 10,000 r/min for 10 min, the supernatant was concentrated to 200 ml, added with 4 times the volume of anhydrous ethanol for alcohol precipitation, and then moved to the refrigerator for storage. After 24 h suction filtration, the precipitate is the crude polysaccharide of *Artemisia annua*.

Hot Water Method

The hot water method was used to extract the polysaccharides from *Artemisia annua* as the reference extraction method. The final conditions were selected at the time of 4 h, the temperature of 90°C, and the addition of *Artemisia annua* 4%. The treated samples were placed in distilled water for water bath extraction. After extraction, the method of Preparation of *Artemisia annua* Polysaccharides was used to obtain *Artemisia annua* polysaccharide.

Artemisia annua Polysaccharide Refining

After the crude polysaccharide of *Artemisia annua* was dissolved in water, it was mixed with 4 times the volume of Sevage reagent (chloroform:n-butanol = 4:1), shaken for 30 min, centrifuged at 4,000 r/min for 10 min, before collecting the supernatant and repeating twice (24). After deproteinization, the crude polysaccharide solution was decolorized by AB-8 macroporous adsorption resin method, shaken for 2 h, suction filtered, the filtrate was concentrated to a certain volume, 4 times the volume of anhydrous ethanol was added, then it was moved to a 4°C refrigerator overnight, 10,000 r/min for 10 min, and the pellet was in deionized water. 8,000–14,000 dialysis bags were used for dialysis, the water was changed several times during the dialysis, and the dialysate was freeze-dried after 48 h to obtain the polysaccharide powder of *Artemisia annua* by fermentation method and the polysaccharide powder of *Artemisia annua* by hot water method, which were used for the determination of antioxidant activity.

Determination of Antioxidant Activity of *Artemisia* Polysaccharides

$DPPH^-$ Free Radical Scavenging Rate

Weighed 5 mg of DPPH dissolved with anhydrous ethanol and fixed the volume into a 100ml volumetric flask, stored it away from light for use right after it was ready (25). Added 2.0 ml of DPPH solution to 2.0 ml of Preparation of *Artemisia annua* Polysaccharides. *Artemisia annua* polysaccharides aqueous solution was prepared at different concentrations, shaken well, and let stand for 30 min away from light, and the absorbance was detected at 517 nm. The same volume of deionized water was used as a blank group, the same volume of DPPH was used as background control and the same concentration of ascorbic acid

was used as positive control. The scavenging rate of free radicals was calculated as follows.

$$\text{Clearance (\%)} = (1 - (A_{\text{sample}} - A_{\text{back}}))/A_{\text{empty}}$$

$ABTS^+$ Free Radical Scavenging Rate

Seven millimoles per liter methanolic solution of ABTS was mixed with sodium persulfate and incubated in the dark 16 for h to form ATBS radicals (26). $ABTS^+$ was diluted overnight in methanol to obtain an $ABTS^+$ solution with an absorbance of 0.70 ± 0.02 measured at 734 nm. The 15.0 ml $ABTS^+$ solution prepared by this method was mixed with 2.0 ml of *Artemisia* polysaccharide solution at different concentrations, stirred, and reacted for 10 min at 30°C protected from light, and the absorbance was measured at 734 nm. The same volume of deionized water was used as blank, the same volume of methanol as background control, and the same concentration of ascorbic acid as positive control.

$$\textit{Clearance}\ (\%) = (1 - (A_{\text{sample}} - A_{\text{back}}))/A_{\text{empty}}$$

OH^- Radical Scavenging Rate

In turn, 1 ml of 9 mol/L ferrous sulfate solution and 2.0 ml of 9 mol/L salicylate alcohol solution was mixed well in a 10 ml colorimetric tube, 1.0 ml of 0.01% hydrogen peroxide solution and 2.0 ml of different concentrations of *Artemisia* polysaccharide aqueous solution were then added (27). The absorbance was measured at 510 nm in a constant temperature water bath at 36°C for 1 h. The same volume of water was used instead of *Artemisia* polysaccharide solution as a blank group, the same volume of water instead of hydrogen peroxide solution as a background control, and the same concentration of ascorbic acid as a positive control, the clearance of hydroxyl groups was calculated as follows.

$$\text{Clearance (\%)} = (1 - (A_{\text{sample}} - A_{\text{back}}))/A_{\text{empty}}$$

Total Reducing Power Determination

1.0 ml of *Artemisia* polysaccharide solution was added to 2.5 ml of phosphate buffer solution (pH = 6.6, 0.2 mol/L) and 2.5 ml of 1% potassium ferricyanide solution, mixed well, and reacted in a constant temperature water bath at 50°C for 30 min (28). 2.5 ml of 10% trichloroacetic acid was added, centrifuged at 3,000 r/min for 10 min, The supernatant was taken at 2.5 ml and 2.5 ml of deionized water was added, as well as 0.5 ml of 0.1% ferric chloride solution. The absorbance was measured at 700 nm after 30 min.

Data Statistics and Analysis

The above experiments were repeated three times and the average value was used as the final test data. Design Expert 12.0 was used for response surface design.

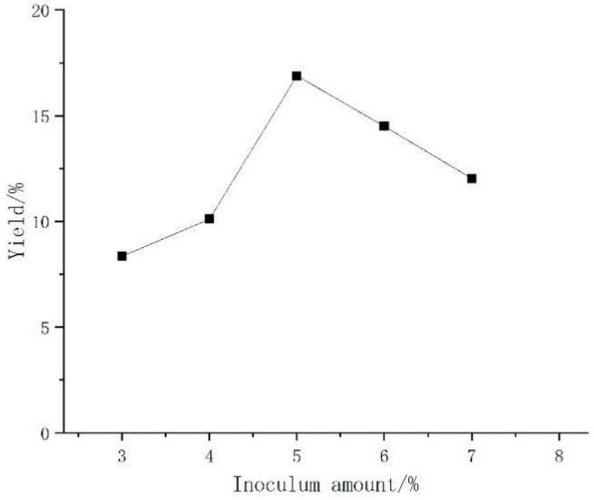

FIGURE 1 | Effect of *Aspergillus niger* inoculum on the yield of *Artemisia* polysaccharides.

RESULTS AND ANALYSIS

One-Factor Test

Effect of *Aspergillus niger* Inoculum on the Yield of *Artemisia* Polysaccharides

Artemisia polysaccharide changed pattern as shown in **Figure 1**, polysaccharide yield with the increase in the inoculum first increased, then decreased in trend, peaking at the inoculum amount of 5% polysaccharide yield, and then tending to decline. The reason may be that due to the fermentation of *Aspergillus niger* in the early stage, polysaccharide production had increased, but because *Aspergillus niger* was aerobic bacteria, the amount of bacteria in the medium was too much, so that the nutrient consumption was too fast, and the polysaccharide yield decreased. Therefore, the inoculum amount of 5% was selected for the follow-up test.

Effect of Temperature on the Yield of *Artemisia* Polysaccharides

The bacterium needed suitable temperature for reproduction, and when it was too high or low, the enzyme production activity as well as metabolism of the bacterium were affected and the growth of the bacterium was inhibited. In **Figure 2**, it can be seen that the temperature of the polysaccharide yield had a significant impact. A too high and too low temperature decreased the polysaccharide yield. At more than 38°C, the decline was particularly obvious. The results show that high and low temperatures were not suitable for *Aspergillus niger* fermentation, so 36°C was chosen as the best temperature.

Effect of Time on the Yield of *Artemisia* Polysaccharides

Figure 3 shows the effect of different fermentation times on the polysaccharide yield. The bacterium grew logarithmically in the early stage of fermentation, accumulated metabolites in

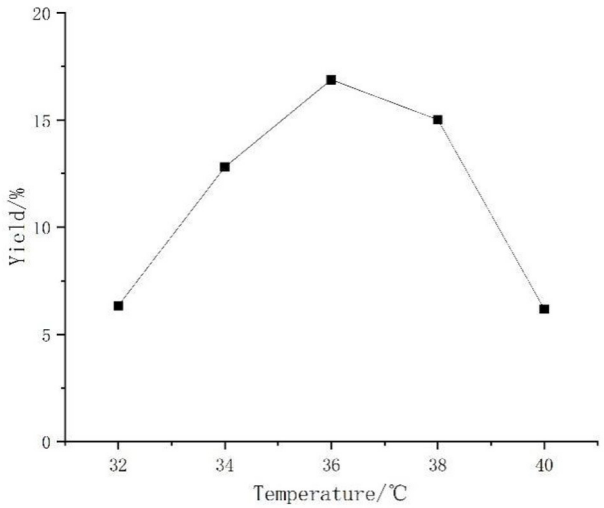

FIGURE 2 | Effect of temperature on the yield of *Artemisia* polysaccharides.

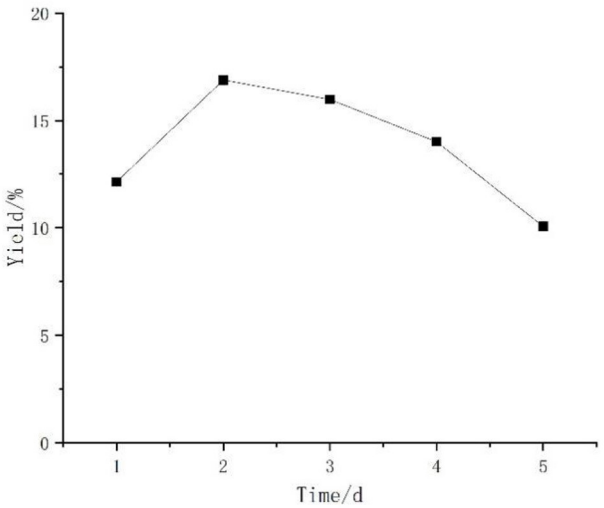

FIGURE 3 | Effect of time on the yield of *Artemisia* polysaccharides.

the middle and late stage, and then gradually senesced when the growth of the bacterium was stable. The polysaccharide yield in the fermentation broth increased with the increase of fermentation time before 2 d and reached the highest at 2 d. After 2 d, the polysaccharide yield began to decrease, probably due to insufficient nutrient supply and because the consumption of polysaccharide was greater than the production. The results showed that the optimal fermentation time was 2 d.

Effect of Shaking Bed Speed on the Yield of *Artemisia* Polysaccharides

Aspergillus niger is aerobic bacteria, the shaker speed was responsible for regulating the amount of dissolved oxygen. Under the same premise, if the speed was too high or too low, it

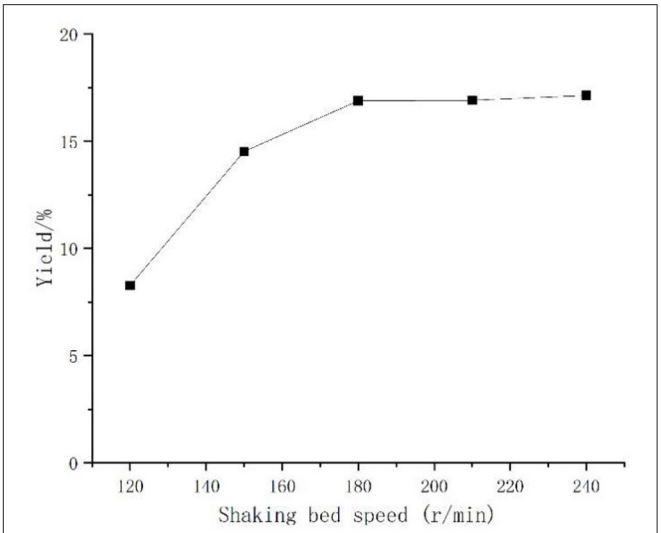

FIGURE 4 | Effect of shaking bed speed on the yield of *Artemisia* polysaccharides.

was not conducive to the growth and reproduction of the bacterium. Observations in **Figure 4** found that with the increase of shaking bed speed, the polysaccharide yield rose, but when the speed exceeded 180 r/min, the polysaccharide yield rise was not obvious, considering the actual operation. One hundred eighty revolutions per minute was selected as the best shaking bed speed for *Aspergillus niger* fermentation.

Effect of *Artemisia annua* Addition on the Yield of *Artemisia* Polysaccharides

The enzymes produced by *Aspergillus niger* fermented *Artemisia*, and when too much *Artemisia* was added, the polysaccharide yield might be affected due to insufficient enzyme production by *Aspergillus niger*. The effect of *Artemisia annua* addition on the yield of polysaccharide was shown in **Figure 5**, the overall change was relatively gentle, first with the increase of *Artemisia* addition and then slowly increasing, reaching the peak at 4%, after which there was an obvious decline. Therefore, the 4% addition of *Artemisia annua* was the best addition.

Response Surface Testing

Based on the results of the single-factor test, a Box-Behnken experimental design was conducted with inoculum, temperature, and time as independent variables and *Artemisia* polysaccharide yield as response values, and the results were shown in **Table 2.**

Applying Design-Expert 12.0 software to fit the **Table 2** to a multiple regression analysis, the regression equation was obtained.

$$Y = 16.94 - 0.29A - 0.07B + 0.24C + 0.63D - 0.06AB - 0.06AC + 0.33AD - 0.19BC + 0.19BD + 0.53CD - 0.78A^2 - 0.90B^2 - 1.2C^2 - 0.98D^2$$

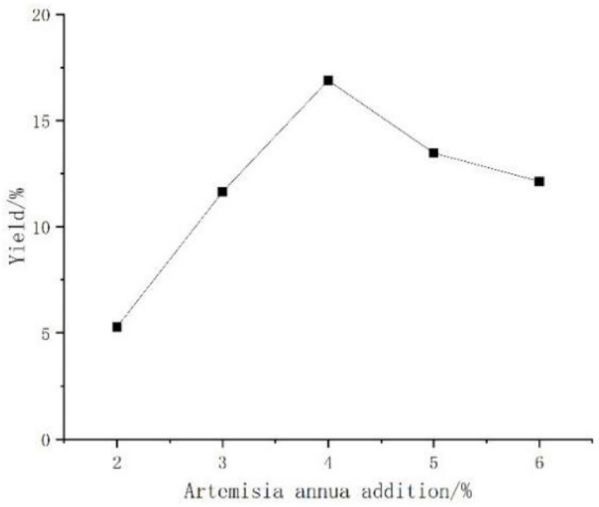

FIGURE 5 | Effect of *Artemisia annua* addition on the yield of *Artemisia* polysaccharides.

The regression model significance test and anova were performed and the results were shown in **Table 3**.

As seen through the above table, the regression model was highly significant (P model < 0.0001), the polysaccharide yield misfit term was not significant ($P = 0.2445 > 0.05$), the model had a good fit, and the experimental error was small. The coefficient of determination, $R^2 = 0.9604$, indicated a good correlation between the measured and predicted values of Y. Over 96.04% of the experimental values could be explained by this equation. The factors affected the degree of *Artemisia* polysaccharide extraction differently, the primary term affected D (<0.0001) > C (0.0076) > A (0.0023) > B (0.384), the interaction AB, AC, AD, BC, BD were not significant ($P > 0.05$), CD was significant ($P < 0.005$), the secondary terms A^2, B^2, C^2, D^2 were extremely significant ($P < 0.00001$).

Response Surface Interaction

To further investigate the effects of inoculum, temperature, and time on the yield of *Artemisia* polysaccharide, response surface and contour plots were made according to the regression equation, see **Figures 6–11**. The steeper the curve trend, the stronger the interaction and the greater the effect on the yield of *Artemisia* polysaccharides, and the contour plot visually reflected the significant degree of the interaction between the factors. With the increase of any two variables the yield of *Artemisia* showed an increasing trend, and after the peak of the interaction between the two, the surface decreased. The interaction between time and *Artemisia* addition was the most significant, with the steepest curve and an elliptical contour line.

Response Surface Results Optimization

After the analysis of the regression model equation, it was obtained that the best process for the fermentation of *Artemisia* polysaccharides by *Aspergillus niger* was 4.882% inoculum, time 2.181 d, temperature 35.98°C, 4.352% *Artemisia* addition, and the yield of *Artemisia* polysaccharides under this condition was 17.087%. Considering the feasibility of practical operation, it was modified and the fermentation process was determined as 5% inoculum, temperature 36°C, time 2 d, shaker speed 180 r/min, and 4% *Artemisia annua* addition. According to the above conditions, the test was repeated three times and the average worth of *Artemisia* polysaccharide extraction was taken as 17.04 %, which was 0.047% from the theoretical value, indicating that the model is credible and the regression equation can be used for the fermentation of *Artemisia* polysaccharide by *Aspergillus niger*.

TABLE 2 | Response surface test design and results.

Test number	Inoculum amount/%	Temperature/°C	Time/d	*Artemisia annua* addition (%)	Yield/%
1	0	1	−1	0	14.72
2	0	−1	0	1	15.40
3	−1	0	0	1	15.86
4	0	0	0	0	16.88
5	0	−1	1	0	15.55
6	0	1	0	1	15.63
7	0	0	1	−1	13.85
8	1	−1	0	0	15.01
9	0	1	0	−1	14.05
10	0	0	0	0	16.68
11	0	0	−1	−1	14.14
12	1	0	1	0	14.64
13	1	0	0	−1	14.10
14	0	1	1	0	14.92
15	−1	1	0	0	15.70
16	0	0	0	0	16.84
17	−1	0	1	0	15.04
18	−1	0	−1	0	14.82
19	0	−1	0	−1	14.56
20	0	−1	−1	0	14.59
21	1	1	0	0	14.86
22	0	0	1	1	16.47
23	−1	0	0	−1	15.49
24	0	0	0	0	17.16
25	1	0	−1	0	14.65
26	1	0	0	1	15.78
27	−1	−1	0	0	15.61
28	0	0	0	0	17.12
29	0	0	−1	1	14.64

Determination of Polysaccharide Content

The standard curve equation is: $A = 0.0614c - 0.0034$, $R^2 = 0.9978$.

Where c is the polysaccharide concentration (μg/ml) and A is the absorbance value. Put $A = 0.575$ into the equation, and get $c = 9.420$, so the purity of polysaccharide after purification: $9.420/10 \times 100\% = 94.20\%$.

Table 4 shows the yield of polysaccharides extracted by the fermentation method and the yield of polysaccharides

TABLE 3 | Response surface regression model analysis of variance.

Source	Sum of squares	DF	Mean square	F-value	*P*-value	Significance
Model	24.73	14	1.77	24.26	<0.0001	Extremely significant
A	1.01	1	1.01	13.86	0.0023	Significant
B	0.0588	1	0.0588	0.8077	0.384	Non-significant
C	0.7057	1	0.7057	9.69	0.0076	Significant
D	4.8	1	4.8	65.95	< 0.0001	Extremely significant
AB	0.0144	1	0.0144	0.1978	0.6633	Non-significant
AC	0.0132	1	0.0132	0.1817	0.6764	Non-significant
AD	0.429	1	0.429	5.89	0.0293	Non-significant
BC	0.1444	1	0.1444	1.98	0.1808	Non-significant
BD	0.1369	1	0.1369	1.88	0.1918	Non-significant
CD	1.12	1	1.12	15.44	0.0015	Significant
A^2	3.91	1	3.91	53.7	<0.0001	Extremely significant
B^2	5.21	1	5.21	71.59	<0.0001	Extremely significant
C^2	9.62	1	9.62	132.1	<0.0001	Extremely significant
D^2	6.17	1	6.17	84.72	<0.0001	Extremely significant
Residual	1.02	14	0.0728			
Lack of fit	0.8572	10	0.0857	2.12	0.2445	non-significant
Pure error	0.1619	4	0.0405			
Cor total	25.74	28				
$R^2 = 0.9604$	R^2 adj = 0.9208	R^2 pre = 0.7984				
Adeq precision	16.0412					

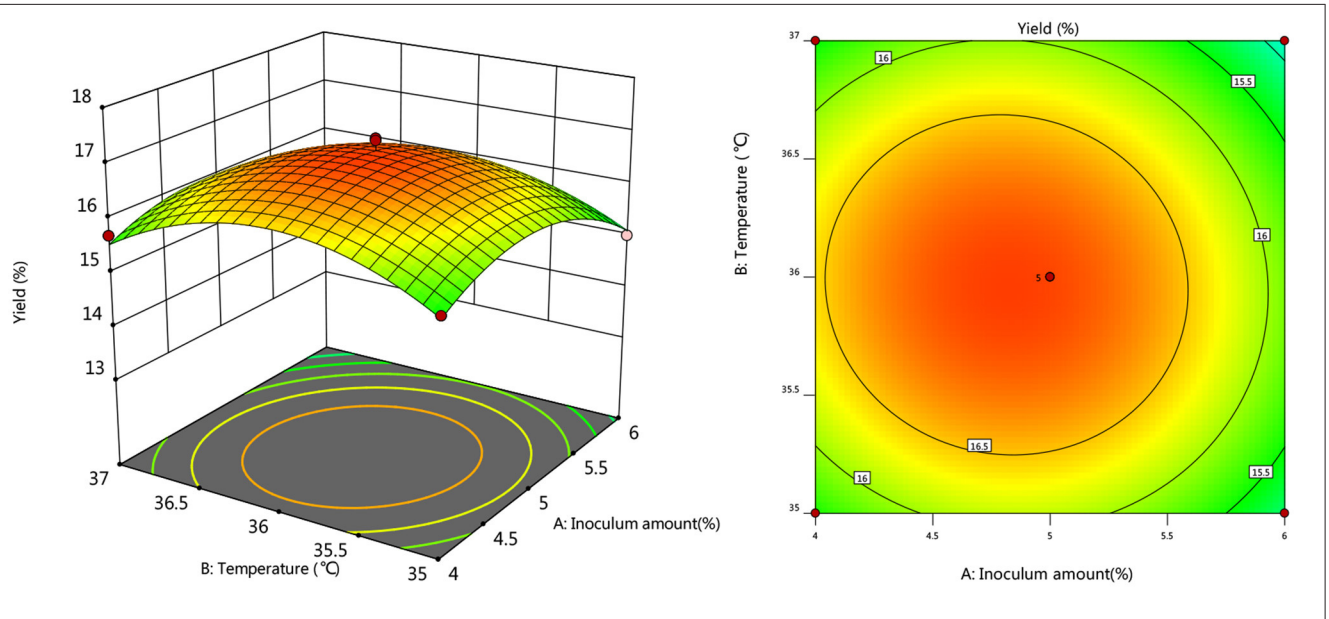

FIGURE 6 | Response plot of the interaction between inoculum and temperature on yield.

extracted by the traditional hot water method. Compared with the traditional hot water method, the fermentation method takes a long time, but requires low temperature and low energy consumption. It is mainly destroyed by extracellular enzymes produced by the fermentation of *Aspergillus niger*. *Artemisia annua* cells promote polysaccharide release.

Analysis of the Results of Antioxidant Experiments

The test was carried out to examine the antioxidant of *Artemisia* polysaccharides using ascorbic acid as a positive control, as shown in **Figure 12**. *Artemisia* polysaccharides and ascorbic acid showed a scavenging effect on DPPH, $ABTS^+$, and OH radicals and there was a dose-dependent relationship. The free

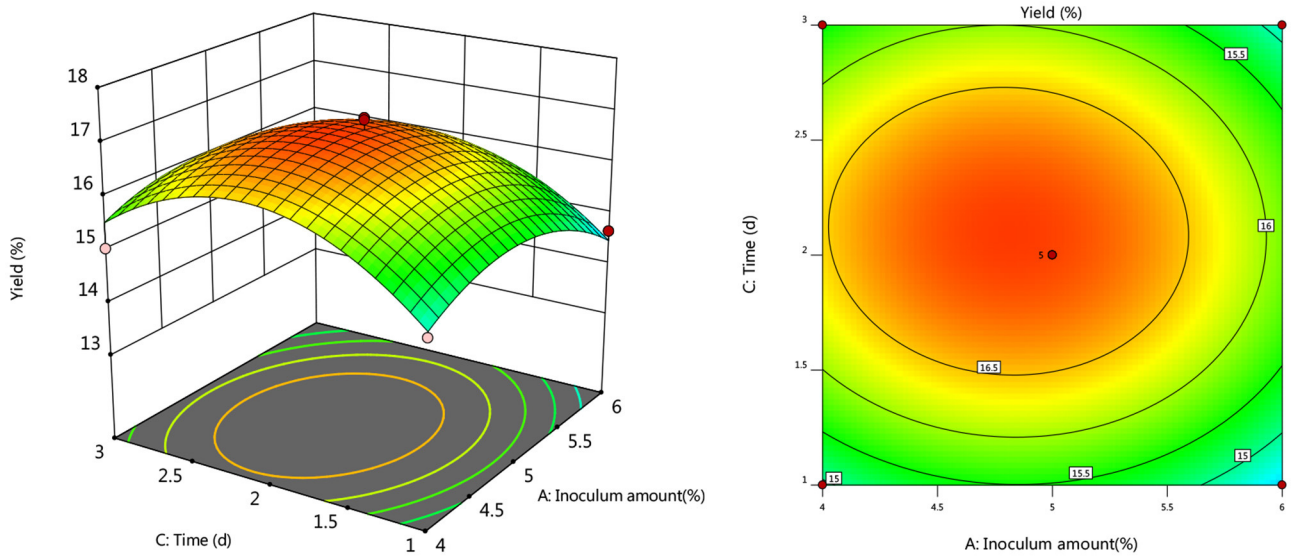

FIGURE 7 | Response plots for the interaction of inoculation volume and time on yield.

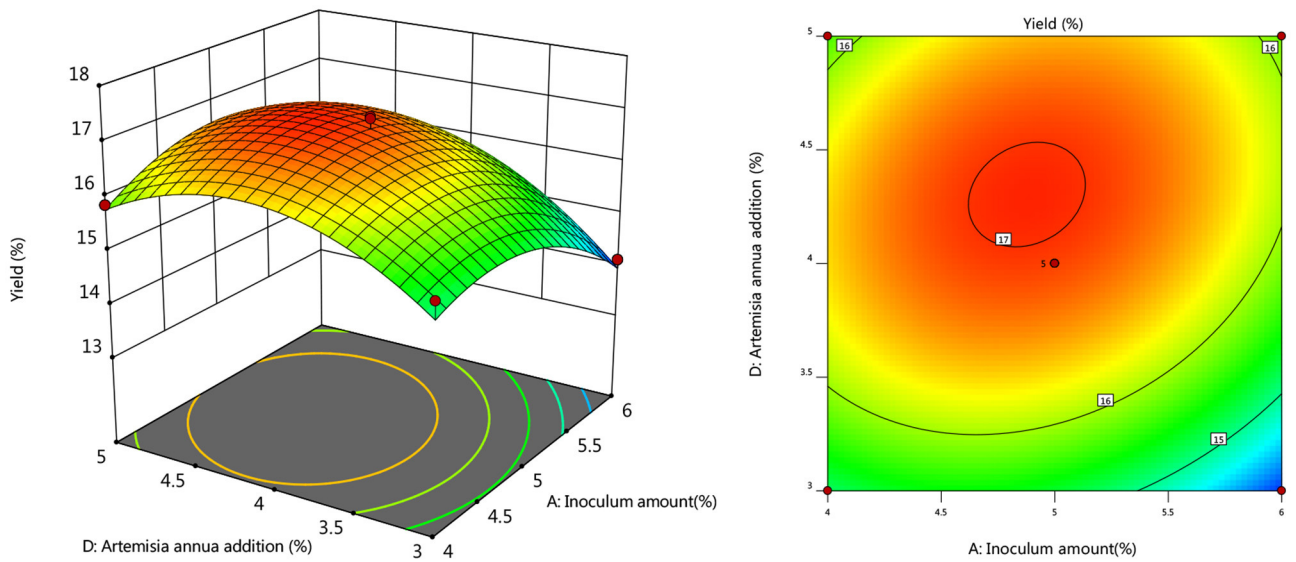

FIGURE 8 | Response plot of the interaction between inoculum and *Artemisia annua* addition on yield.

radical scavenging rate increased continuously with increasing polysaccharide mass concentration. At the same concentration, the scavenging rate of DPPH, $ABTS^{+}$, and OH radicals by *Artemisia* polysaccharide was weaker than that by ascorbic acid.

DISCUSSION

Some polysaccharides can participate in cell metabolism for physiological regulation, resulting in a variety of biological functions, such as anti-tumor, anti-virus, anti-oxidation, and immune enhancement, and are widely used as drug delivery carriers because of their non-toxicity and good biocompatibility (29). Deng et al. (30) found that *Artemisia annua* has a high sugar content, but there are not many studies on its extraction.

Li (31) used *Fusarium* rot, *Penicillium chrysogenum*, and *Aspergillus niger* to ferment *Poria*, and found that the water-soluble polysaccharide content of *Poria* fermented by *Aspergillus niger* was the highest, reaching 2.66%, which was 3.86 times that of *Fusarium rot*., and 2.89 times that of *Penicillium flavus*. Gong et al. (32) found that the content of water-soluble tea polysaccharides increased by 5.7 times during the solid-state

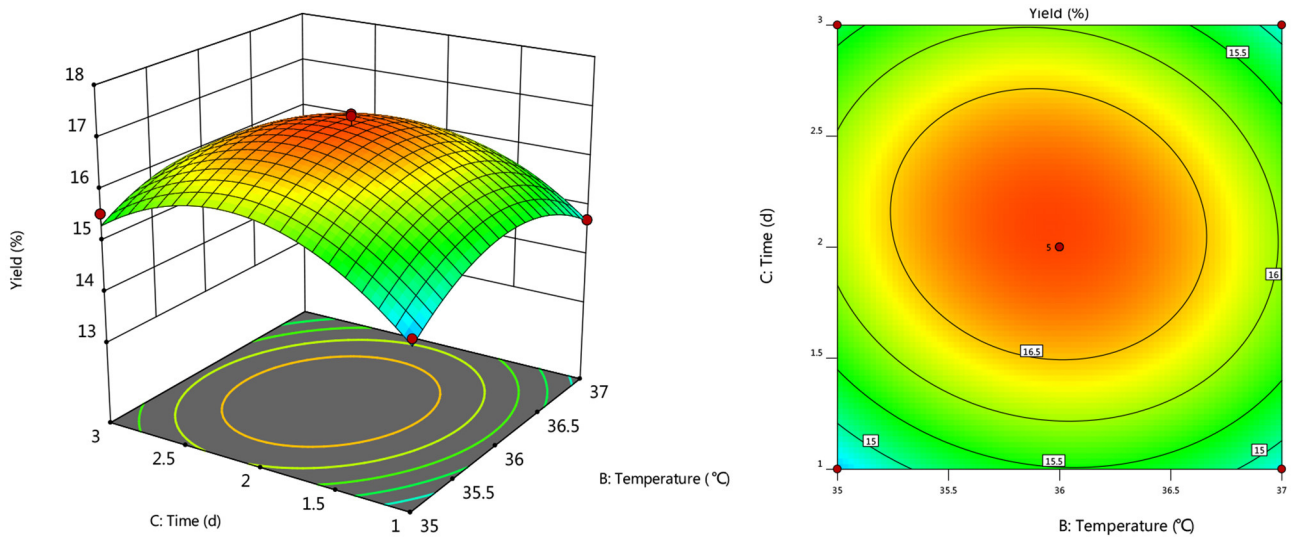

FIGURE 9 | Plot of the response of temperature and time on the interaction of yield.

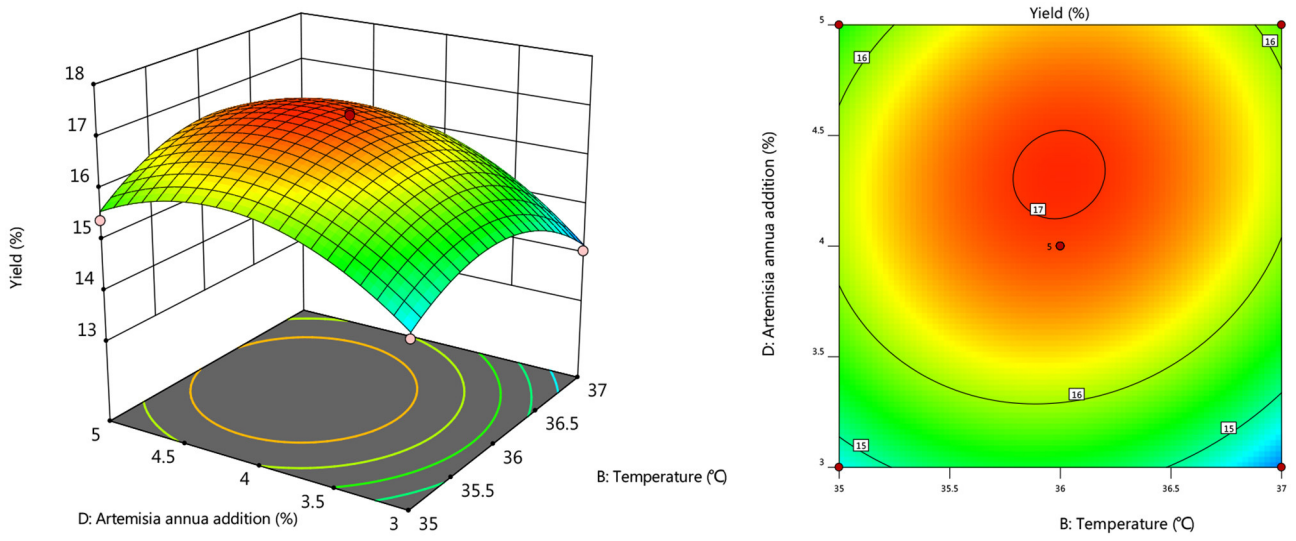

FIGURE 10 | Response plot of the interaction between temperature and *Artemisia annua* addition on yield.

fermentation process, while polyphenols, flavonoids, catechins, and water-soluble oligosaccharides increased. Sugar content decreased. Using *Aspergillus niger* for fermentation, given the best conditions, the fermentation cycle is short and the growth is vigorous, which can increase the production of enzymes during the fermentation process, thereby destroying the polysaccharide structure of the cell wall (33), and promoting the release of active polysaccharide components, and solid-state fermentation is suitable for filamentous fungi, as it grows in low moisture (34), so *Aspergillus niger* is used for fermentation.

Microbial fermentation can produce enzymes to destroy cell walls, increase active ingredients, reduce toxicity, and regulate the metabolism of reactants to achieve controllable production of products (35). The extraction of polysaccharides by this method is mild and controllable, the operation is simple, and there is no reagent pollution, but the time is relatively long. The ultrasonic extraction method is a physical method for enhanced extraction. The principle is that ultrasonic waves produce a cavitation process in the medium. When the cavitation bubbles collapse, accompanied by high heat, high pressure, and strong shock waves, the cells are ruptured and the active ingredients are released (36). This method extracts polysaccharides. It takes a short time, moderate amount of solvent, produces a high yield, and is a convenient operation, but may lead to the change of polysaccharide structure (37) Zheng et al. (16) extracted polysaccharide from *Artemisia annua* with ultrasonic

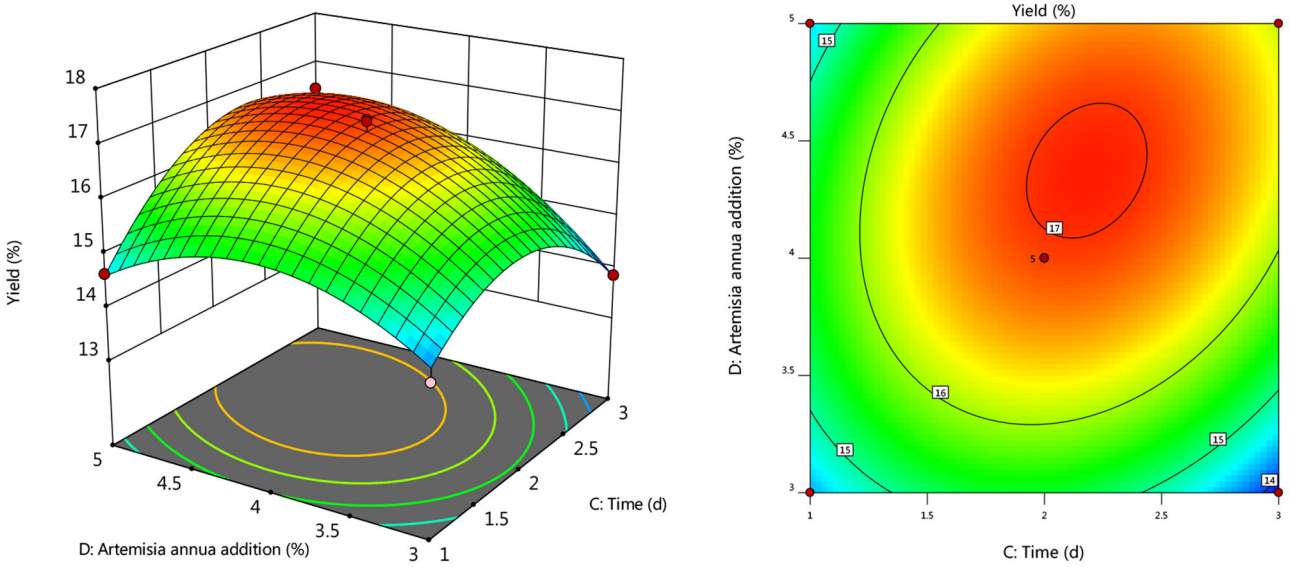

FIGURE 11 | Response plot of the interaction between time and *Artemisia annua* addition on yield.

TABLE 4 | Comparison of fermentation method and hot water method.

Method	Time (h)	Temperature (°C)	*Artemisia annua* addition (%)	Yield (%)
Fermentation	48	36	4	17.04
Hot-water	4	90	4	9.81

wave, and the yield was 14.78%. Enzymatic extraction is the use of protease to hydrolyze free protein in plants, resulting in loose plant structure and reduced binding between protein and raw materials, which is beneficial to polysaccharide extraction (38). The cost of this method is slightly higher than that of microbial fermentation, and the enzyme is easily inactivated. With the advantages of mildness, no pollution and good product quality, Shuai et al. (13) used *papain* method to extract polysaccharides from *Artemisia annua* with a yield of nearly 11%. The principle of microwave extraction is to use electromagnetic waves with a frequency between 300 MHz and 300 GHz in plants, causing the internal temperature of the plant to rise, increasing collision and friction to promote cell breakage and exudation of polysaccharides (39). This method is energy-saving, fast, and controllable, but Wei et al. (18) used microwaves to extract polysaccharides from *Artemisia annua*, and the yield was only 9.72%. The traditional hot water extraction method, although the structure is not easily damaged, has high energy consumption, low yield, large amount of extractant, and high cost (40).

Polysaccharide content is an important indicator of microbial fermentation, and the fermentation conditions of microorganisms directly affect the yield. When using *Aspergillus niger* to ferment *Ginkgo biloba*, Wang et al. (34) found that the amount of inoculum did not affect the development process, while the temperature would cause large fluctuations in enzyme activity, sugar content, and bacterial growth. Black spores could be observed after 120 h fermentation at 31°C, 96 h at 31°C and 72 h at 34°C, and secondary germination of *Aspergillus niger* after 96 h fermentation at 34°C, It's a question worth thinking about. Ding et al. (41) used *Aspergillus niger* to ferment *Artemisia annua* and chose to ferment it at 37°C for 5 d, and found that *Aspergillus niger* increased the content of *Artemisinin* and *Artemisinin B* the most among many bacterial groups. The reason can be speculated that *Aspergillus niger* carried out secondary germination, this study also showed that microbial fermentation has a good prospect in the extraction of active ingredients of *Artemisia annua* and provided a theoretical basis. Kamal et al. (42) used banana peel to improve protein production and found that the optimal extraction conditions were 31°C fermentation for 4 d, and the substrate concentration was 19.92%. Therefore, different purposes have different optimal fermentation conditions, and suitable fermentation conditions are very important.

CONCLUSIONS

Aspergillus niger can secrete a variety of extracellular enzymes such as lignocellulose hydrolase, acid protease, phytase, glucoamylase, β-glucanase, arabinofuranosidase, and xylanase (43). It is speculated that the extracellular enzymes secreted by *Aspergillus niger* in the fermented *Artemisia annua* have changed its structural properties, thus facilitating the release of polysaccharides. In addition, with the increase of fermentation time and enzyme production, enzymatic reaction occurs, *Artemisia annua* is fully dissolved and cells begin to die or degrade to obtain products. This research adopts fermentation technology, inoculates *Aspergillus niger*, ferments *Artemisia annua* polysaccharide, conducts response surface analysis on

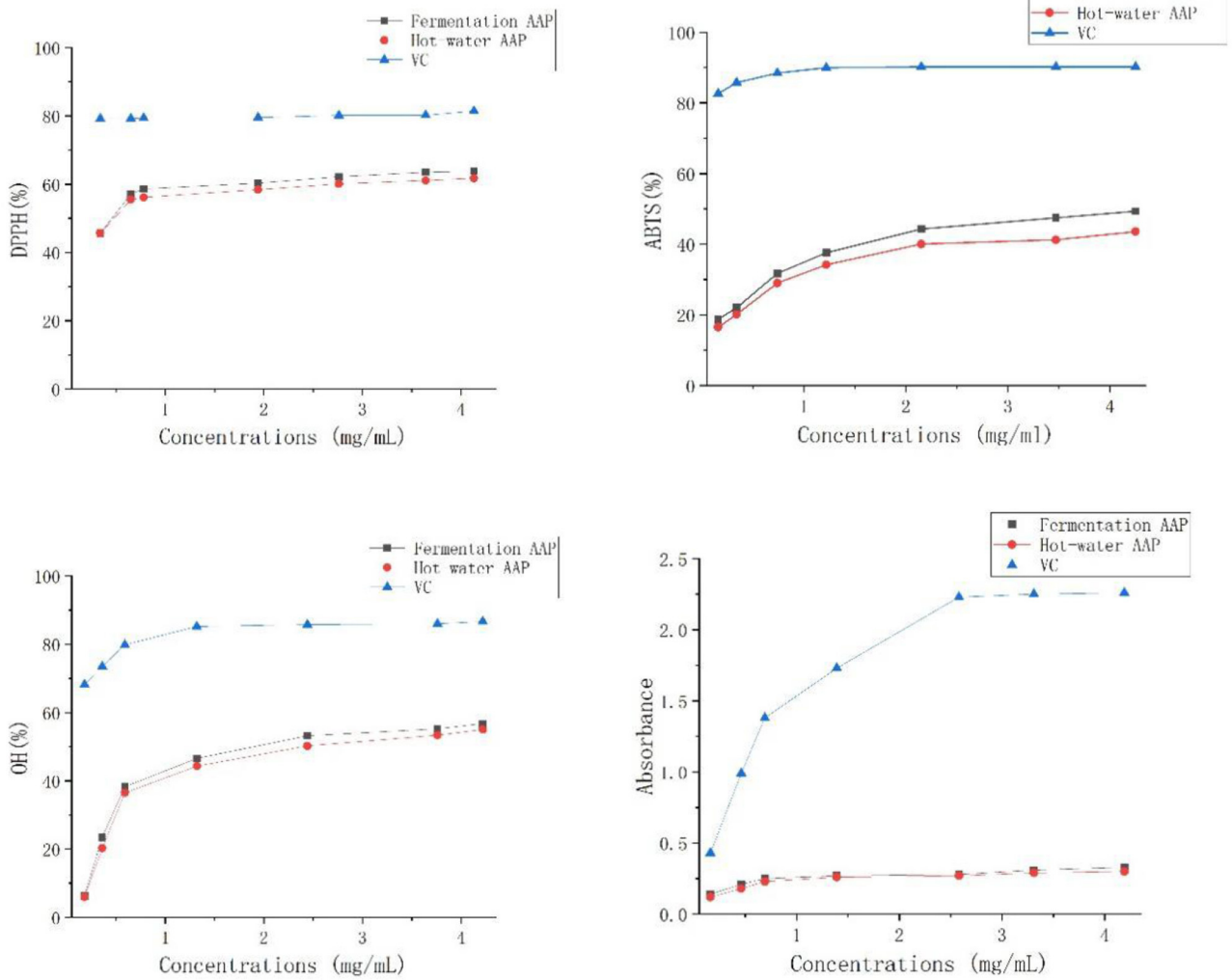

FIGURE 12 | Antioxidant activity assay.

the basis of single factor experiment, establishes regression model, and finally determines the optimal fermentation process: *Aspergillus niger* inoculation amount of 5%, temperature of 36°C, the shaking speed was 180 r/min, and the addition of *Artemisia annua* was 4% for 2 d. Under these conditions, the yield of *Artemisia annua* polysaccharide could reach 17.04%, which was not significantly different from the predicted value. The process parameters in this study are highly feasible and the model fits well, which can be used as a reference for the extraction of *Artemisia annua* polysaccharides in the future. According to the analysis of single-factor test and response surface test, the influence degree of each factor is addition amount of *Artemisia annua* > fermentation temperature > inoculation amount of *Aspergillus niger* > fermentation time > shaker rotation speed. Therefore, when using microbial fermentation to extract *Artemisia annua* polysaccharide, In the case of consistent addition of *Artemisia annua*, the temperature factor is given priority, which is beneficial to increase the yield. The yield of *Artemisia annua* polysaccharide extracted by the traditional hot water method was only 9.81%, but its antioxidant activity was almost the same as that of *Artemisia annua* polysaccharide extracted by the fermentation method, and both were weaker than ascorbic acid.

DATA AVAILABILITY STATEMENT

The original contributions presented in the study are included in the article/supplementary material, further inquiries can be directed to the corresponding author/s .

AUTHOR CONTRIBUTIONS

All authors listed have made a substantial, direct, and intellectual contribution to the work and approved it for publication.

FUNDING

This work was supported by Academic funding project of Anhui Provincial Department of Education for University Top-notch Talents (No. gxbjZD2021089) and Natural Science Research Foundation of the Department of Education of Anhui Province (Nos. KJ2020A0789 and KJ2021A1166).

REFERENCES

1. Hou C, Chen L, Yang L, Ji X. An insight into anti-inflammatory effects of natural polysaccharides. *Int J Biol Macromol.* (2020) 153:248–55. doi: 10.1016/j.ijbiomac.2020.02.315
2. Zhang Q, Jiang P, Qin L, Ruan Y. Progress in the study of polysaccharide function. *Guizhou Agri Sci.* (1998) 26:59–60.
3. Ji X, Hou C, Shi M, Yan Y, Liu Y. An insight into the research concerning Panax ginseng CA Meyer polysaccharides: a review. *Food Rev Int.* 2020:1–17. doi: 10.1080/87559129.2020.1771363
4. Ji X, Peng B, Ding H, Cui, B, Nie H, Yan Y. Purification, structure and biological activity of pumpkin polysaccharides: a review. *Food Rev Int.* 2021:1–13. doi: 10.1080/87559129.2021.1904973
5. Ji X, Hou C, Gao Y, Xue Y, Yan Y, Guo X. Metagenomic analysis of gut microbiota modulatory effects of jujube (Ziziphus jujuba Mill) polysaccharides in a colorectal cancer mouse model. *Food Funct.* (2020) 11:163–73. doi: 10.1039/C9FO02171J
6. Ji X, Cheng Y, Tian J, Zhang S, Jing Y, Shi M. Structural characterization of polysaccharide from jujube (*Ziziphus jujuba* Mill) fruit. *Chem Biol Technol Agric.* (2021) 8:1–7. doi: 10.1186/s40538-021-00255-2
7. Baraldi R, Isacchi B, Predieri S, Marconi G, Vincieri FF, Bilia AR. Distribution of artemisinin and bioactive flavonoids from *Artemisia annua L*. during plant growth. *Biochem Syst Ecol.* (2008) 36:340–8. doi: 10.1016/j.bse.2007.11.002
8. Das S. Artemisia annua (Qinghao): a pharmacological review. *Int J Pharm Sci Res.* (2012) 3:4573–7. doi: 10.13040/IJPSR.0975-8232.3(12).4573-77
9. Xu H, Wei Y, Wang Q, Zhang Y, Pu C. Clinical applications of artemisia annua and its dosage. *Jilin Chin Med.* (2020) 40:1509–12. doi: 10.13463/j.cnki.jlzyy.2020.11.030
10. Wang X, Xu Z, Jihua L. Optimization of the biotransformation fermentation medium of dihydroartemisinin. *Nat Prod Res.* (2013) 25:1690–5. doi: 10.16333/j.1001-6880.2013.12.022
11. Brisibe EA, Yannan S. Nutritional properties and antioxidant capacity of different tissues of *Artemisia annua*. Feed and Livestock. (2009) 115:1240–6.
12. Wang H, Xiao W, Hua H, Li N, Chen J. Advances in chemical constituents of artemisia annua. *Mod Med Clin.* (2011) 26:430–3. doi: 10.7501/j.issn.1674-5515
13. Shuai X, Chen J, Shi J, Huang Q, Wu L, Hu J. Preparation and *in vivo* anti-inflammatory effects of *Artemisia annua* polysaccharides. *J Southwest.* (2016) 38:102–6. doi: 10.13718/j.cnki.xdzk.2016.09.016
14. Yan L, Xiong C, Xu P, Zhu J, Yang Z, Ren H. Structural characterization and in vitro antitumor activity of A polysaccharide from *Artemisia annua L*. (Huang Huahao). *Carbohydr Polym.* (2019) 213:361–9. doi: 10.1016/j.carbpol.2019.02.081
15. Hou C, Yin M, Lan P, Wang H, Nie H, Ji X. Recent progress in the research of Angelica sinensis (Oliv) Diels polysaccharides: extraction, purification, structure and bioactivities. *Chem Biol Technol Agric.* (2021) 8:1–14. doi: 10.1186/s40538-021-00214-x
16. Zheng Q, Ren D, Yang N, Yang X. Optimization for ultrasound-assisted extraction of polysaccharides with chemical composition and antioxidant activity from the *Artemisia* sphaerocephala Krasch seeds. *Int J Biol Macromol.* (2016) 91:856–66. doi: 10.1016/j.ijbiomac.2016.06.042
17. Shuai X, Yang Y, Huang Q, Wu L, Jiang Z, Hu J. Process research on the extraction of *artemisia* polysaccharides by *papain* enzymatic method. *Jiangsu Agri Sci*. (2012) 40:273–5.
18. Wei Z, Zhao F, Zhang H. Optimization of microwave-assisted extraction process of Artemisia polysaccharides by response surface methodology. *North Hortic*. (2018) 16:155–9.
19. Song Y, Shi H, Fan M, Lu J, Bian C, Qiao X. The solidstate fermentation technology of Astragalus using Aspergillus application in laying hens. *Journal of Livestock Ecology.* (2021) 42:43–50. doi: 10.3969/j.issn.1673-1182.2021.04.007
20. Tao L, Wang H, Xu G, Yin J, Liang J, Guo K. Effect of fermentation of *Aspergillus niger* on the content of free berberine in Phellodendron chinensis. *J Chin Vet Med.* (2011) 13:41–3. doi: 10.3969/j.issn.1000-6354.2011.02.013
21. Liu C, Chen J, Yu C, Tao Y. Optimization of the solid fermentation conditions of the astragalus by response surface methodology. *Food Res Dev.* (2019) 40:184–8.
22. Zhang Q. Determination of polysaccharide content by phenol-sulfuric acid colorimetric method. *Food Infm Technol.* (2004) 11:56. doi: 10.3969/j.issn.1672-979X.2004.07.008
23. Dai X, Xiong Z, Luo L. Optimization of ultrasonic extraction of polysaccharides from *Artemisia* absinthium and its antioxidant properties by response surface methodology. *Food Sci.* (2011) 32:93–7.
24. Liu Y, Dong L, Luo C, Chen S, Xia F, Wang Z. Optimization of water-soluble polysaccharide production by Bacillus subtilis LY-05 fermentation of yucca and its antioxidant activity. *Food Ind Sci Technol.* (2022) 43:212–21. doi: 10.13386/j.issn1002-0306.2021060232
25. Li Y, Zhao T, Huang L, Zou T, Wu X. Optimization of total flavonoid extraction process and in vitro antioxidant activity of Rattlesnake [J] by response surface methodology. *Food Res Dev.* (2019) 49:79–84. doi: 10.12161/j.issn.1005-6521.2019.17.015
26. Jamróz E, Kulawik P, Krzyściak P, Talaga-Cwiertnia K, Juszczak L. Intelligent and active furcellaran-gelatin films containing green or pu-erh tea extracts: Characterization, antioxidant and antimicrobial potential. *Int J Biol Macromol.* (2019) 122:745–57. doi: 10.1016/j.ijbiomac.2018.11.008
27. Chen J, Chen J, Yuan S, Chen Z. Response surface optimization of ultrasound-assisted extraction process of cucumber peel polyphenols and its antioxidant activity. *Preserv Process.* (2021) 21:99–106. doi: 10.3969/j.issn.1009-6221.2021.04.016
28. Xie Y, Li P, Sui X, Fu D, Zhang X. Response surface optimization of the extraction process and antioxidant activity of fine leaf dulcimer. *Nat Prod Res Dev.* (2019) 31:475–81. doi: 10.16333/j.1001-6880.2019.3.017
29. Chen L, Huang G. Extraction, characterization and antioxidant activities of pumpkin polysaccharide. *Int J Biol Macromol.* (2018) 118:770–4. doi: 10.1016/j.ijbiomac.2018.06.148
30. Deng S, Ding D, Dai M, Xiang D. Advances in the pharmacological effects of plant polysaccharides. *J Tradit Chin Med.* (2006) 12:86–8. doi: 10.3969/j.issn.1672-951X.2006.09.043
31. Li S. Study on fermentation and enzymatic transformation of Poria polysaccharide process and its product activity. *Guizhou Univ*. (2018) 2018:89.
32. Gong G, Zhou H, Zhang X, Song S, An W. Study on microbial solid-state fermentation and compositional changes of sun-blue green maocha in Yunnan. *Tea Science.* (2019) 25:300–6. doi: 10.3969/j.issn.1000-369X.2005.04.011
33. Yan W, Wei L, Gen Y, Pei S. Advance in anti-fungus application of plant essential oil in food preservation. *J Agric Sci.* (2021) 35:1170. doi: 10.11869/j.issn.100-8551.2021.05.1170
34. Wang J, Cao F, Su E, Zhao L, Qin W. Improvement of animal feed additives of Ginkgo leaves through solid-state fermentation using *Aspergillus niger*. *Int J Biol Sci.* (2018) 14:736. doi: 10.7150/ijbs.24523
35. Hao J, Li D, Jing Y, Zhang L, Liu J, Ji Y. Solid-state fermentation of Aspergillus Niger to optimize extraction process of Isoliquiritigenin from Glycyrrhiza uralensis. *Evid Based Complement Altern Med.* (2020) 5:1–8. doi: 10.1155/2020/8927858
36. Zhang H, Liu L. Optimization of ultrasonic extraction of *Artemisia annua* Polysaccharide. *Food Res Dev.* (2006) 46–8. doi: 10.3969/j.issn.1005-6521.2006.05.018

37. Li C, Wang W, Zhang Y, Li J, Lao F. Research progress on extraction, separation and purification of polysaccharides from traditional Chinese medicine. *China Pharmacy.* (2016) 27:2700–3.
38. Meng Z, Zhu Y, Zhang H. Study on the extraction of jujube polysaccharide by *papain* enzymatic hydrolysis. *J Univ Sci Technol.* (2006) 34:49–50. doi: 10.3969/j.issn.1673-6060-B.2006.03.017
39. Hu Q, He Y, Wang F, Wu J, Ci Z, Chen L, et al. Microwave technology: a novel approach to the transformation of natural metabolites. *Chin Med.* (2021) 16:1–22. doi: 10.1186/s13020-021-00500-8
40. Hu B, Chen J, Wang G. Comparative study on extraction of Ganoderma lucidum polysaccharide by ultrasonic method and traditional hot water method. *Food Sci Technol.* (2007) 28:190–2. doi: 10.3969/j.issn.1002-0306.2007.02.053
41. Ding J, Su X, Yin X, Zhao L, Qin W. Microbial fermentation of *Artemisia annua l*eaves and leaf residues. *Biotechnology Bulletin.* (2021) 37:63. doi: 10.13560/j.cnki.biotech.bull.1985.2020-0493
42. Kamal MM, Ali MR, Shishir MRI, Saifullah M, Haque M, Mondal SC. Optimization of process parameters for improved production of biomass protein from *Aspergillus niger* using banana peel as a substrate. *Food Sci Biotechnol.* (2019) 28:1693–702. doi: 10.1007/s10068-019-00636-2
43. Shi C, He J, Yu J, Yu B, Mao X, Zheng P, et al. Physicochemical properties analysis and secretome of Aspergillus niger in fermented rapeseed meal. *PloS ONE.* (2016) 11:e0153230. doi: 10.1371/journal.pone.0153230

Conflict of Interest: The authors declare that the research was conducted in the absence of any commercial or financial relationships that could be construed as a potential conflict of interest.

Publisher's Note: All claims expressed in this article are solely those of the authors and do not necessarily represent those of their affiliated organizations, or those of the publisher, the editors and the reviewers. Any product that may be evaluated in this article, or claim that may be made by its manufacturer, is not guaranteed or endorsed by the publisher.

frontiers in Nutrition

ORIGINAL RESEARCH
published: 25 March 2022
doi: 10.3389/fnut.2022.835123

Diversity Analysis of Bacterial and Function Prediction in Hurunge From Mongolia

Wuyundalai Bao, Yuxing He and Wei Liu*

College of Food Science and Engineering, Inner Mongolia Agricultural University, Hohhot, China

With the continuous infiltration of industrialization and modern lifestyle into pastoral areas, the types and processing capacity of Hurunge are decreasing, and the beneficial microbial resources contained in it are gradually disappearing. The preservation and processing of Hurunge are very important for herdsmen to successfully produce high-quality koumiss in the second year. Therefore, in this study, 12 precious Hurunge samples collected from Bulgan Province, Ovorkhangay Province, Arkhangay Province, and Tov Province of Mongolia were sequenced based on the V3–V4 region of the 16S rRNA gene, and the bacterial diversity and function were predicted and analyzed. There were significant differences in the species and abundance of bacteria in Hurunge from different regions and different production methods ($p < 0.05$). Compared with the traditional fermentation methods, the OTU level of Hurunge fermented in the capsule was low, the *Acetobacter* content was high and the bacterial diversity was low. *Firmicutes* and *Lactobacillus* were the dominant phylum and genus of 12 samples, respectively. The sample QHA contained *Komagataeibacter* with the potential ability to produce bacterial nanocellulose, and the abundance of *Lactococcus* in the Tov Province (Z) was significantly higher than that in the other three regions. Functional prediction analysis showed that genes related to the metabolism of bacterial growth and reproduction, especially carbohydrate and amino acid metabolism, played a dominant role in microorganisms. In summary, it is of great significance to further explore the bacterial diversity of Hurunge for the future development and research of beneficial microbial resources, promotion, and protection of the traditional ethnic dairy products.

Keywords: high-throughput sequencing, Mongolia, Hurunge, bacterial diversity, functional prediction

OPEN ACCESS

Edited by:
Xiaolong Ji,
Zhengzhou University of Light Industry, China

Reviewed by:
Yingjian Lu,
Nanjing University of Finance and Economics, China
He Meng,
Shanghai Jiao Tong University, China
Qixiao Zhai,
Jiangnan University, China

****Correspondence:***
Wuyundalai Bao
wydl@imau.edu.cn

Specialty section:
This article was submitted to Food Chemistry, a section of the journal Frontiers in Nutrition

Received: *14 December 2021*
Accepted: *19 January 2022*
Published: *25 March 2022*

Citation:
Bao W, He Y and Liu W (2022) Diversity Analysis of Bacterial and Function Prediction in Hurunge From Mongolia. Front. Nutr. 9:835123. doi: 10.3389/fnut.2022.835123

INTRODUCTION

Traditional fermented koumiss (airag or chigee) is fresh horse milk without high-temperature sterilization in wooden buckets, porcelain cans, or animal skins (1), koumiss at room temperature for 1–3 days with natural microbial starter retained in the previous year or batch of koumiss, the whole process constantly stirs the fermented koumiss with wooden sticks and constantly adds fresh horse milk, in order to remove carbon dioxide and ensure uniform fermentation. Accelerate natural fermentation to eliminate the reproduction of pathogens (2). Koumiss is mainly fermented by microorganisms such as lactic acid bacteria and yeast (3), which can produce lactic acid, alcohol, and other small molecular flavor substances, and is rich in essential amino acids, trace elements, and various vitamins. Therefore, it has a unique flavor, texture, acidity,

and health benefits (4–6). For hundreds of years, koumiss has been regarded as not only a kind of food, but also a natural alternative medicine, so nomads invented "koumiss therapy," which combines traditional Mongolian medicine with koumiss used in the clinical treatment of intestinal indigestion, hypertension, tuberculosis, and other cases (7, 8). Therefore, koumiss is considered to be a complete diet, which is rich in nutrients. The nomads on the grasslands of Central Asia and Mongolia can persist in the nomadic lifestyle and cold grassland climate without the rich nutrients of koumiss. They constitute an important part of the daily diet of Mongolian herdsmen (9–11).

It has always been a Mongolian custom to use the starter to koumiss, the native starter used to make traditional fermented koumiss is called Hurunge. Since ancient times, the traditional method of fermenting koumiss is to use the skin made of cowhide to dry the fermented koumiss in the previous year and can continue to be used to ferment koumiss after putting fresh horse milk in the summer of the second year. Dried skins can well protect the activity of the starter. The Hurunge is fermented koumiss in the previous year into millet or raisins above 1 kg, put it into a clean bag sealed preservation, the next year fermented koumiss, add a certain amount of Hurunge in the fresh horse milk and continue to stir with sticks, you can complete the fermentation so that the fermented koumiss will maintain a good taste and quality. Studies have shown that Hurunge contains a complex microbial community, which strongly affects the final microbial community and the resulting quality of koumiss (12). However, with the development of science and technology, the brewing of koumiss has developed from traditional methods to commercial starter brewing. The traditional manual brewing method is gradually disappearing, resulting in the loss of a large number of excellent strains.

Mongolia belongs to the temperate continental steppe climate, with a significant temperature difference between day and night, its forage species and quantity are high-quality green, and it is rich in nutrients, so there is no doubt about the quality of fresh horse milk (13). Bulgan Province, Ovorkhangay Province, Arkhangay Province, and Tov Province are the main production areas of traditional koumiss. It is necessary to collect precious samples of Hurunge and analyze the bacterial diversity in this area because the rich bacteria play an important role in the quality and flavor of Hurunge, and play an important role in improving the quality of commercial starter fermented koumiss in the future. However, the traditional microbial culture methods are time-consuming and laborious, and some microorganisms cannot be isolated depending on the existing isolation methods, so it is easy to ignore the overall microbial diversity (14). Therefore, it is often limited to using traditional methods to analyze microbial diversity. In recent years, the rapid development of sequence technology, such as the second-generation sequencing platform Illumina-Miseq, provides a convenient method for the analysis of microbial components in various samples. It can fully cover the complex and low abundance of microbial communities in the samples and analyze the diversity of microbial communities at the genus and even species level (15).

In this study, samples of Hurunge from four regions of Mongolia were collected, and a high-throughput sequencing technique was used to predict the composition and function of the bacterial community. These data are not only of great significance to further study the mining of probiotics in Hurunge samples in Mongolia, but also have important prospects for the commercialization and industrial production of Koumiss.

MATERIALS AND METHODS

Collection of Samples

We collected 12 samples of Hurunge from town in four regions of Mongolia: Bulgan Province, Ovorkhangay Province, Arkhangay Province, and Tov Province. All of them were brewed by herdsmen through natural fermentation and were used for the fermentation of koumiss. Samples BEG, BEG1, and BEG2 were collected from Burgan Province (B), samples HHA, HHA1, and HHA2 (H) were collected from Ovorkhangay Province, samples QHA, QHA1, and QHA2 were collected from Arkhangay Province (Q), and samples ZY, ZY1, and ZY2 were collected from Tov Province (Z). These sampling sites cover most of the main producing areas of "Hurunge" in Mongolia, as shown in **Figure 1**. The samples BEG, HHA, QHA, and ZY are fermented "Hurunge" in animal skins, and the rest are made by the traditional fermentation process. At the same time, the production technology, fermentation environment, fermentation time, and storage conditions of "Hurunge" samples were recorded. The collected samples are stored in a sterile centrifugal tube and transferred to the laboratory in the shortest possible time for a foam box containing dry ice.

DNA Extraction and PCR Amplification

Microbial community genomic DNA was extracted from 12 samples using the E.Z.N.A.® soil DNA Kit (Omega Bio-tek, Norcross, GA, US) according to the manufacturer's instructions. The DNA extract was checked on 1% agarose gel, and DNA concentration and purity were determined with NanoDrop 2000 UV-vis spectrophotometer (Thermo Scientific, Wilmington, USA). The hypervariable region V3–V4 of the bacterial 16S rRNA gene was amplified with primer pairs 338F (5′-ACTCCTACGGGAGGCAGCAG-3′) and 806R (5′-GGACTACHVGGGTWTCTAAT-3′) by an ABI GeneAmp® 9700 PCR thermocycler (ABI, CA, USA). The PCR amplification of 16S rRNA gene was performed as follows: initial denaturation at 95°C for 3 min, followed by 27 cycles of denaturing at 95°C for 30 s, annealing at 55°C for 30 s and extension at 72°C for 45 s, and single extension at 72°C for 10 min, and end at 4°C. The PCR mixtures contain 5 × *TransStart* FastPfu buffer 4 μl, 2.5 mM dNTPs 2 μl, forward primer (5 μM) 0.8 μl, reverse primer (5 μM) 0.8 μl, *TransStart* FastPfu DNA Polymerase 0.4 μl, template DNA 10 ng, and finally ddH_2O up to 20 μl. PCR reactions were performed in triplicate. The PCR product was extracted from 2% agarose gel and purified using the AxyPrep DNA Gel Extraction Kit (Axygen Biosciences, Union City, CA, USA) according to manufacturer's instructions and quantified using Quantus™ Fluorometer (Promega, USA).

FIGURE 1 | Distribution of 12 Hurunge samples in Mongolia.

Illumina MiSeq Sequencing

Purified amplicons were pooled in equimolar and paired-end sequenced on an Illumina MiSeq PE300 platform/NovaSeq PE250 platform (Illumina, San Diego, USA) according to the standard protocols by Majorbio Bio-Pharm Technology Co. Ltd. (Shanghai, China). The raw reads were deposited into the NCBI Sequence Read Archive (SRA) database (Accession Number: PRJNA793521).

Processing of Sequencing Data

The raw 16S rRNA gene sequencing reads were demultiplexed, quality-filtered by fastp version 0.20.0 (16), and merged by FLASH version 1.2.7 (17). Operational taxonomic units (OTUs) with 97% similarity cutoff (18) were clustered using UPARSE version 7.1 (19), and chimeric sequences were identified and removed. The taxonomy of each OTU representative sequence was analyzed by RDP Classifier version 2.2 (20) against the 16S rRNA database (e.g., Silva v138) using a confidence threshold of 0.7.

Data Analysis

Mothur (v.1.30.2) software was used to calculate the Alpha diversity index of the flattened sample of OTU levels, such as Sobs, Chao1, Ace, Shannon, Simpson, and Coverage index. The Student's *t*-test method was used to test the significant difference between groups, and the R language tool was used to draw a dilution curve. The beta diversity distance matrix was calculated by Qiime software, and the Principal Coordinates Analysis (PCoA) diagram and relative abundance histogram of each sample gate (≥ 1%) and genus (≥ 1%) horizontal group were drawn by the R language (version3.3.1) tool. The prediction functional genomic analysis of the microbial community in the sample was carried out by using PICRUSt2 software, and the key functional gene modules of Pathwaylevel1, Pathwaylevel2, and Pathwaylevel3 metabolic pathway were selected from the KEGG functional module, and the R language tool was used to draw the relative abundance heat map of the functional module.

RESULTS

Sample Sequence Richness and Alpha-Diversity

A total of 577,699 high-quality sequences of bacteria were produced in 12 samples of Hurunge, with an average length of 447 bp, and the length of high-quality sequences was concentrated in 441–460 bp. After sequencing at a 97% similarity level, 141 OTUs were identified from 12 samples of Hurunge.

Alpha diversity can reflect the richness and diversity of the microbial community. Chao1 index, Ace index, Simpson index, and Shannon index are obtained by Alpha diversity analysis. Chao1 and Ace index are often used to estimate the total number and richness of species and are used to evaluate whether a sample has this species or not. The higher the index value, the more species, and species. Simpson and Shannon indexes are often used to quantitatively describe the biological diversity in a certain region, and more consideration is given to the evenness of species distribution. The smaller the Simpson index value is, the larger the Shannon index value is, indicating that the community diversity is higher. According to the data in **Table 1**, the total number of bacterial species in sample BEG1 is the most, while the number of BEG species is the least. The bacterial community diversity of sample ZY2 is the highest and that of BEG2 is the

TABLE 1 | Sequence information and diversity value of 12 Hurunge samples.

Areas	Sample-name	Sequences	Ace	Chao	Shannon	Simpson	Sobs	Coverage
B	BEG	37,312	16.45	15.50	0.37	0.84	14	0.9999
	BEG1	41,367	111.80	111.86	0.47	0.87	111	0.9999
	BEG2	37,076	33.45	36.00	0.27	0.90	31	0.9999
H	HHA	47,421	34.85	34.00	0.49	0.80	29	0.9999
	HHA1	57,819	47.37	45.60	0.61	0.79	45	0.9999
	HHA2	48,399	52.32	48.50	0.44	0.86	41	0.9998
Q	QHA	54,858	33.85	33.25	1.31	0.33	33	1.0000
	QHA1	57,213	59.40	56.43	0.63	0.79	50	0.9998
	QHA2	53,615	36.58	35.25	0.56	0.82	35	1.0000
Z	ZY	40,703	45.94	43.75	1.53	0.33	40	0.9999
	ZY1	40,155	49.59	49.20	1.65	0.36	45	0.9998
	ZY2	42,188	47.33	50.50	1.69	0.36	43	0.9999

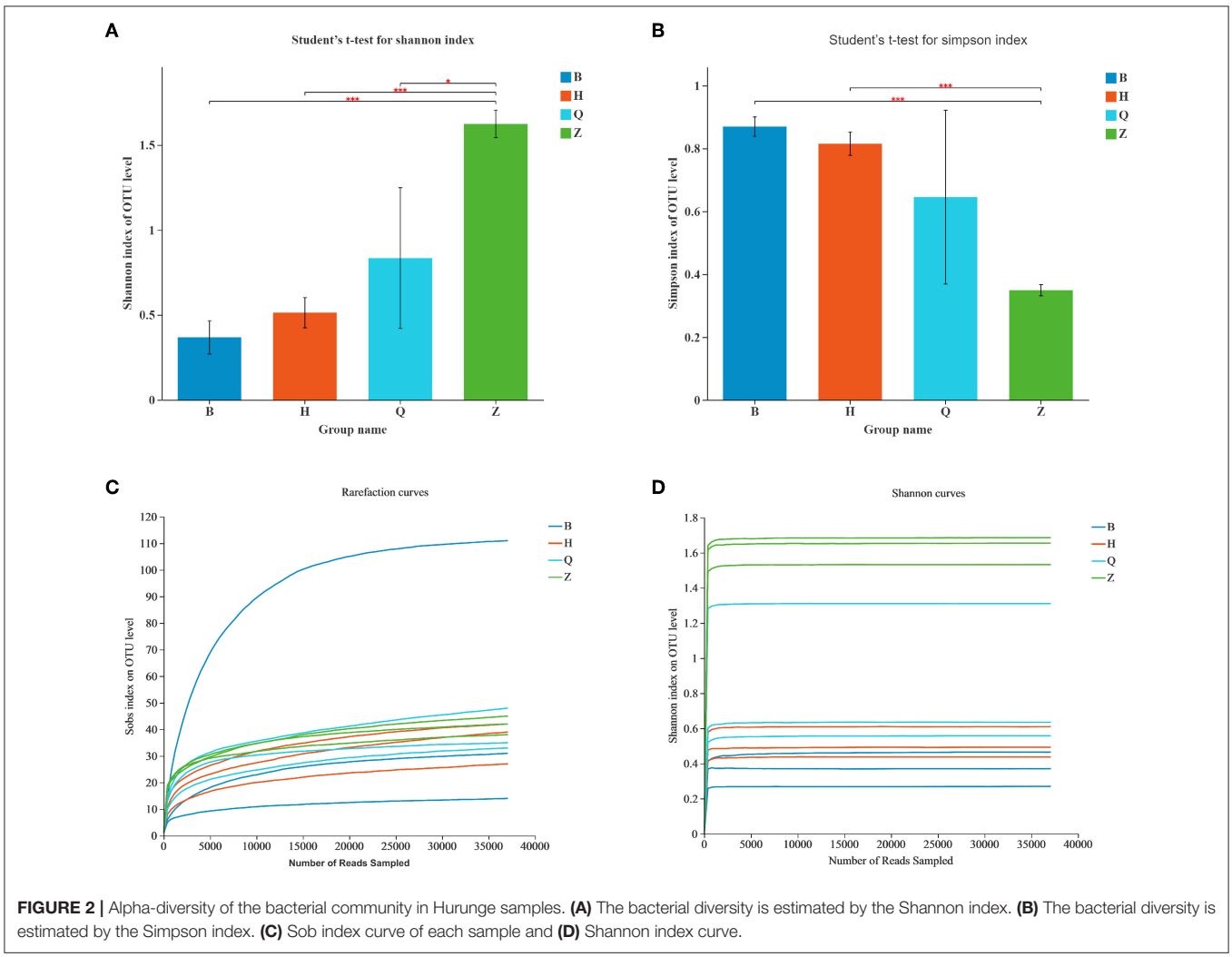

FIGURE 2 | Alpha-diversity of the bacterial community in Hurunge samples. **(A)** The bacterial diversity is estimated by the Shannon index. **(B)** The bacterial diversity is estimated by the Simpson index. **(C)** Sob index curve of each sample and **(D)** Shannon index curve.

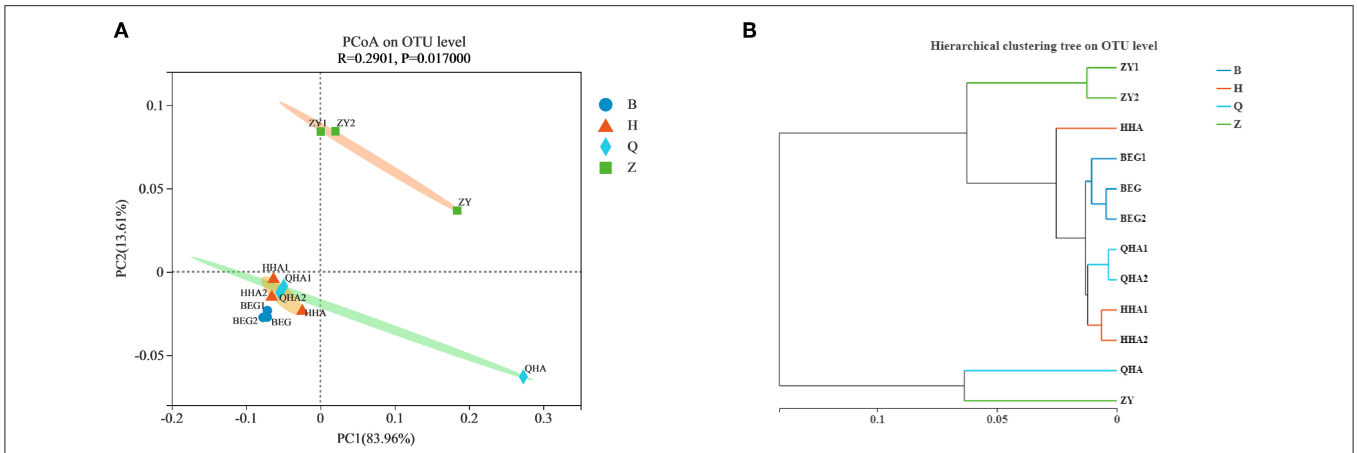

FIGURE 3 | (A) PCoA analysis and **(B)** sample level cluster analysis of the bacterial community in koumiss samples at OTU level.

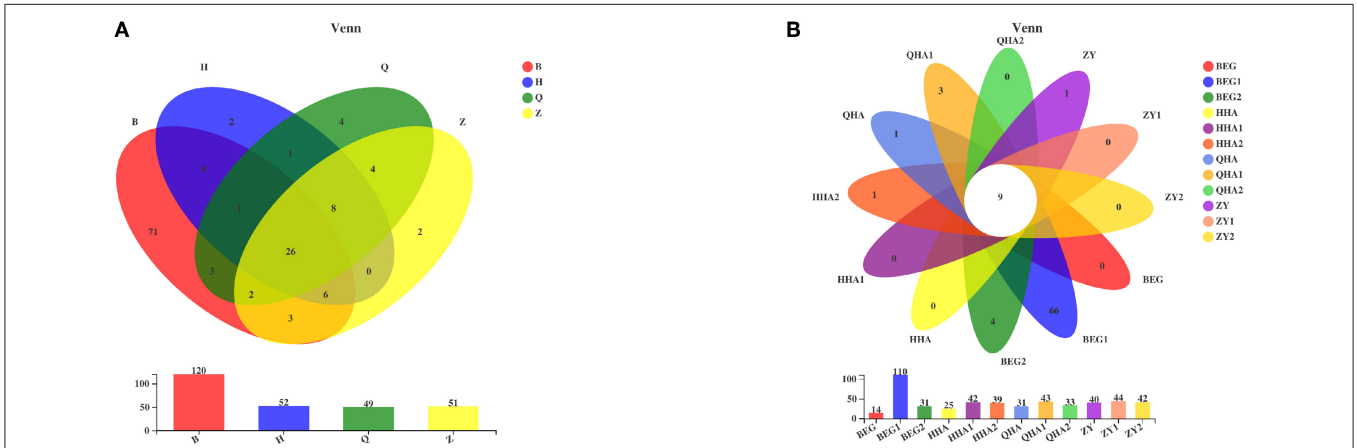

FIGURE 4 | Venn diagrams. **(A)** Venn diagram of OTU in 4 places of Mongolia is analyzed according to bacterial microbial diversity. **(B)** Venn diagram of OTU of each sample is analyzed according to bacterial microbial diversity.

lowest. In general, the bacterial diversity in the Z area is higher than that in other places, as shown in **Figures 2A,B**.

The dilution curve and aroma concentration curve were drawn according to the Sob index and Shannon index, and then the sequence quality and depth were evaluated. As shown in the Sob index curve in **Figure 2C**, the number of bacterial OTUs in the sample increased with the increase of sequencing depth. **Figure 2D** showed that the Shannon curve reached a stable platform, and the Good's coverage value was higher than 0.99, indicating that at the current sequence depth, diversity of the most bacteria in the sample was captured, enough to analyze most of the microflora (21). The current sequence quantity can meet the requirements of subsequent bioinformatics analysis.

Comparison of Bacterial Communities Among Groups

Although the original materials of 12 Hurunge samples were fresh horse milk and no commercial starter was added in the production process, the composition of the bacterial community of 12 Hurunge samples was different due to various reasons such as the production and preservation process, fermentation container, fermentation temperature, regional environment, and microbial species of milk source. Therefore, in order to explore the composition and difference of bacterial structure in different samples, the PCoA diagram of bacterial community principal coordinates is drawn based on weighted UniFrac to study the similarity or difference of sample community composition. It can be seen from **Figure 3A** that the three Hurunge samples from area Z are far away from other samples in the figure, indicating that the bacterial community structure and composition in area Z are significantly different from those in other areas ($P < 0.05$), while the other three areas are very close. The points represented by the samples in areas B, H, and Q are close in the spatial distribution distance and basically distributed in the same area. It shows that there is no significant difference in bacterial community composition of Hurunge samples from these three regions. However, sample QHA is far away from other samples and is alone in a region.

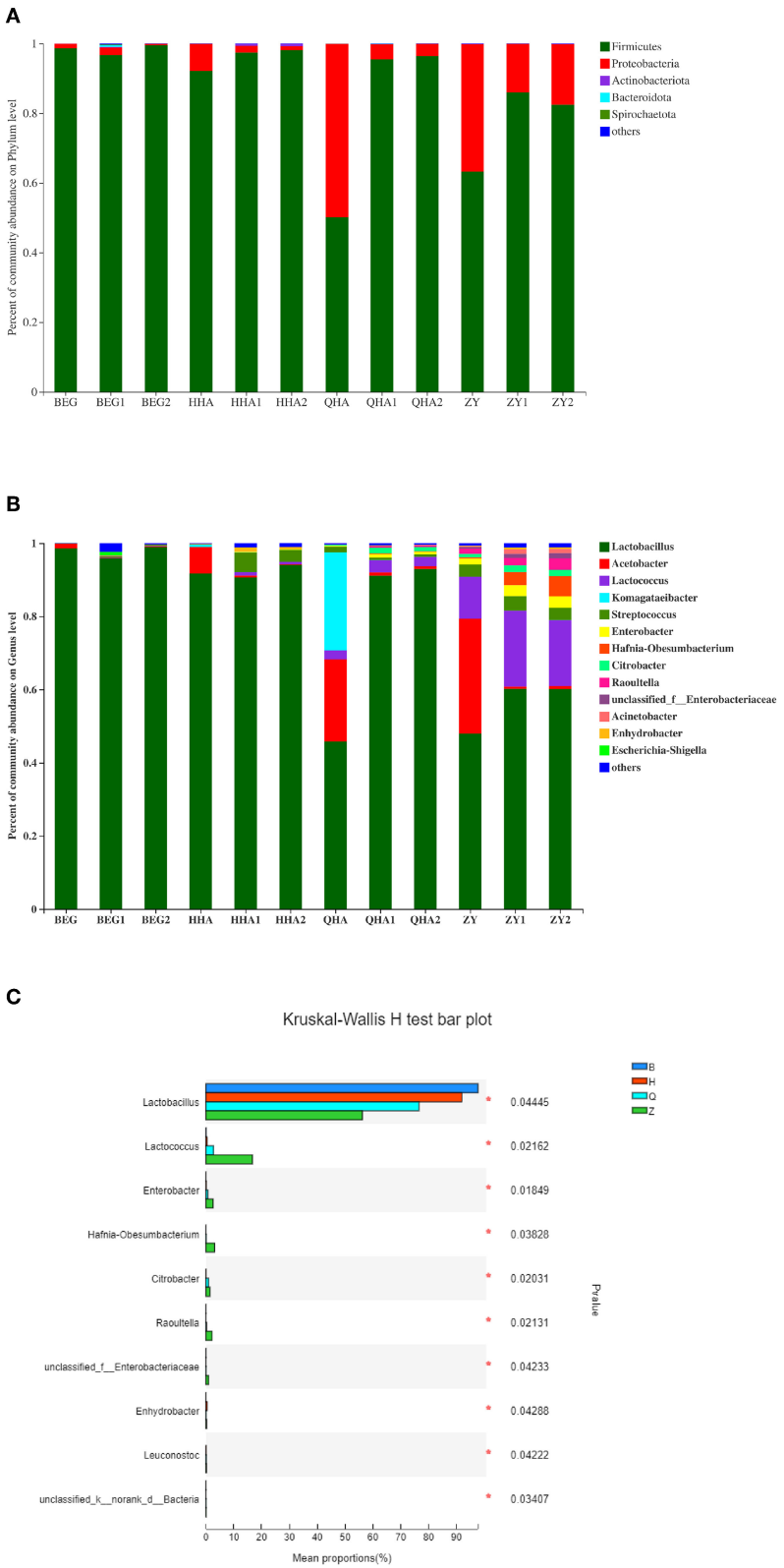

FIGURE 5 | Bacterial community structure of different Hurunge samples. **(A)** Phylum level and **(B)** Genus level. **(C)** Relative abundance at genus level with the significant difference among samples from different regions. The proportion of which is less than 1% is not listed.

Hurunge may have specific connections or differences in the microbial community structure due to differences in collection location, production habits, and containers. In order to further analyze the significance of the dominant microflora in Hurunge and the distribution of microorganisms in the collection site, the sample hierarchical cluster analysis of the distance matrix of bacterial community **Figure 3B** was carried out, which was consistent with the result of PCoA diagram. At the OTU level, the bacterial community could be divided into different groups, indicating that there were significant differences in bacterial species and richness with different geographical locations of the samples collected($p < 0.05$). The QHA samples and ZY samples in the bacterial community are grouped together, and the sample HHA is also in a single branch. The 3 samples are all from Hurunge fermented and preserved in animal skins. Therefore, it is inferred that the fermentation environment is similar and the microbial species contained in the samples are also similar.

Classification and Composition of Bacterial Communities

Venn diagram can reflect the situation of common and unique species among different groups. In this study, a Venn diagram was used to compare and analyze the bacteria in Hurunge samples at the OTU level. The results showed that there were significant differences among groups. At the OTU level, as shown in **Figure 4A**, 120, 52, 49, and 51 OTUs were obtained from the samples in regions B, H, Q, and Z, respectively, of which 26 OTUs were shared by Hurunge samples in 4 regions. The sample in region B had the highest OTU level, reaching 120, which may be related to its unique geographical environment. In addition, as shown in **Figure 4B**, 14, 25, 31, and 40 OTUs were detected in samples BEG, HHA, QHA, and ZY, respectively. These four were from Hurunge fermented and preserved in animal skins. Compared with the traditional fermentation method, the OTU level was lower, and only 9 OTUs of 12 samples were common.

Through 16S rRNA Gene Sequencing analysis, 12 samples of koumiss were identified with 17 phyla, 98 genera, and 120 species. The relative abundance of bacterial communities at the phylum and genus level is shown in **Figure 5A**. A total of 12 samples of Hurunge containing 5 main bacterial phyla (relative content > 1%), namely *Firmicutes*, *Proteobacteria*, *Actinobacteria*, *Bacteroidetes,* and *Spirochaetota*, which is consistent with the previous survey of bacterial diversity in koumiss (22). *Firmicutes* is the dominant bacteria in all samples, with the exception of QHA and ZY, the content of *Firmicutes* in other samples is more than 80%. The proportions of Firmicutes in samples QHA and ZY were 50.1 and 63.3%, respectively. Compared with other samples, Proteobacteria was the second dominant phylum.

As can be seen from **Figures 5B,C**, the main genera in the 4 regions of Mongolia are *Lactobacillus*, *Acetobacter*, *Lactococcus*, *Komagataeibacter*, *Streptococcus*, *Enterobacter*, *Hafnia-Obesumbacterium*, *Citrobacter*, *Raouitella*, *Acinetobacter*, *Escherichia-Shigella*, and other 11 genera with a relative content of more than 1%. The dominant genus is *Lactobacillus* (45.81–99.00%), which is consistent with the previous report on koumiss (23). There are more species of bacteria from Q and Z regions, and their bacterial composition is more complex. Compared with other areas, the Z region contains a certain abundance of *Lactococcus* (11.40–17.98%), which may be related to the climate and proximity to the city. There are significant differences in the relative abundance of bacterial genera in Hurunge from different regions. *Acetobacter* (0.08–22.41%) is the second dominant genus. The contents of BEG, HHA, QHA, and ZY fermented in the capsule are significantly higher than those in the traditional fermentation method. In the sample QHA, *komagataeibacter* exists uniquely, and the content is as high as 26.74%. This genus is a new genus isolated from *Acetobacter* in 2012 (24).

Functional Prediction of Bacterial Community

The KEGG PATHWAY analysis was used to predict the biological functions of bacteria in six areas: metabolism, genetic information processing, environmental information processing, cell processes, human diseases, and organism systems. As shown in **Figure 6A**, the abundance of metabolism-related genes is the highest in all samples, indicating that metabolism plays an important role in the microbial community and that the rapid growth of microorganisms is closely related to the abundance of metabolic genes.

The level 2 KEGG PATHWAY analysis is shown in **Figure 6B**. The color depth of each module in the functional heat map represents the different richness of each group of functional genes. Genes related to carbohydrate and amino acid metabolism exist and are highly rich in all populations, which highlights the biological significance of functions such as metabolism and rapid growth of microorganisms. The decomposition of carbohydrates usually acts as an energy source for the growth and development of microorganisms in the process of dairy fermentation (25), and amino acid catabolism is the core function of *bacteria*. Various bacteria play an important role in providing nutrition to other microorganisms in "Hurunge" by decomposing proteins into small molecules of amino acids (26). In addition, nucleotide metabolism, energy metabolism, cofactor and vitamin metabolism, and lipid metabolism pathway are also very rich in each group of samples. Especially in QHA and ZY samples, all the metabolic functions have a relatively high abundance. However, some genes related to human diseases, such as drug resistance, antibiotics, infectious diseases, cancer, and immune diseases, have been annotated. The existence of these genes might have adverse effects on human health.

The results of the grade 3 KEGG heat map, as shown in **Figure 6C,** show that the gene abundance of the metabolic pathway is the highest. The annotated results reveal the potential advantages of microorganisms in traditional fermented "Hurunge," which contain genes involved in a large number of metabolic processes, which are involved in important life pathways such as glucose metabolism and lipid metabolism. The abundance of genes such as biosynthesis of secondary metabolites, microbial metabolism in different environments, and biosynthesis of amino acids are at the forefront.

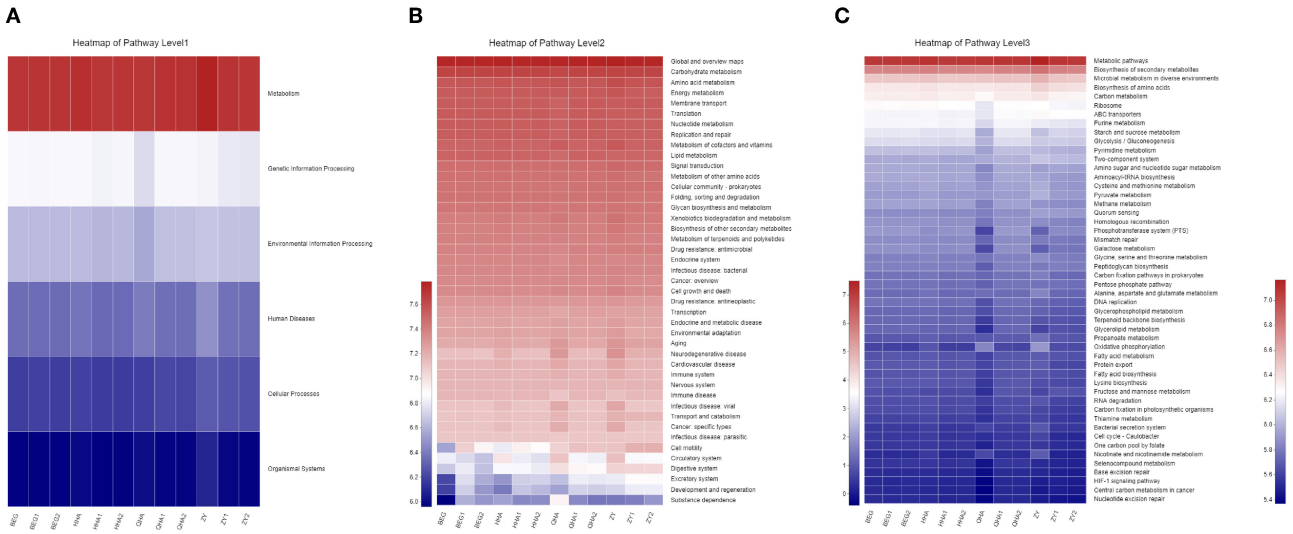

FIGURE 6 | Prediction of the bacterial community in different koumiss samples. **(A)** Overall KEGG gene function statistics (Level 1). **(B)** The heatmap of functional pathways (Level 2). **(C)** The heatmap of functional pathways (Level 3).

DISCUSSION

High-throughput sequencing has promoted significant progress in the understanding of microbial ecology. It is now widely used in many fields, from personalized medicine (27) to bioenergy (28). By sequencing the bacterial 16S rRNA gene, the community structure of microorganisms in the sample can be effectively revealed. However, so far, the microbial diversity of Hurunge samples in different regions of Mongolia has not been reported. Therefore, the bacterial diversity of 12 Hurunge samples collected from Bulgan Province, Ovorkhangay Province, Arkhangay Province, and Tov Province of Mongolia was studied by high-throughput sequencing of the 16Sr RNA gene. Hurunge is very important for brewing delicious koumiss in the coming year, and it is also the inheritance of the Mongolian working people to the excellent production technology of traditional koumiss. The regional environment, milking space environment, special fermentation mode, fermentation container, and temperature affect the richness and diversity of bacteria in Hurunge samples. Kamimura (29) showed that samples from different regions will have significant differences in bacterial flora structure due to different production environments. Samples QHA, ZY, HHA, and BEG are fermented in animal skins. The fermentation method is to put fresh horse milk in animal skins containing a small amount of fermented koumiss. In hot summer, it is usually hung on the horse's back. With the horses running, the horse milk in the skins is fully stirred to accelerate the fermentation of sour horse milk. The fermentation environment is a relatively closed small container sewn with animal skins. Therefore, compared with Hurunge made by traditional natural fermentation, the richness, and diversity of bacteria are low, but the microbial lineage contained in Hurunge in different regions is relatively stable.

PCoA and sample level cluster analysis showed the relationship between microbial diversity in the four regions and further emphasized that there were differences in microbial diversity among different regions, and they were related to geographical location. Vegetation in Mongolia ranges from the forest through grasslands to the sparse vegetation of the Gobi Desert from north to south, with steppe grasslands accounting for nearly 88% of the total land area (30). Area Z is located in the north of Mongolia, with precipitation decreasing from north to south, and water vapor mainly comes from the Arctic Ocean. Due to low temperature, less evaporation, and relatively humid climate, it should be a semi-humid area in climate zoning. It is found that relative humidity is the most important factor affecting the relative abundance of microbial communities (31). Region Z is relatively humid compared with regions B, H, and Q, so region Z is far away from the other 3 regions on the PCoA map. Another reason may be that area Z is located around the city, while areas B, H, and Q are located in sparsely populated primitive areas. Therefore, it is speculated that human production activities have a certain impact on the bacterial diversity in Hurunge, and the specific influencing factors need to be further studied. Burgan province is a well-known region of Mongolia rich in high-quality mare's milk, and the quality of its brewed koumiss is self-evident, and Hurunge in this region has the highest OTU. Therefore, it is inferred that the high-quality quality of koumiss in this region is closely related to the richness of microorganisms.

At the phylum level, *Firmicutes* is dominant in all 4 regions, followed by *Proteobacteria*, which is consistent with the results of Guo et al. (6) on the dominant bacteria in koumiss in Inner Mongolia. It may be that bacterial diversity is affected by geographical location, climatic conditions, environment, and animal feed (32); Hurunge's production methods also vary from region to region (33–35). For example, in Burgan Province, which is famous for its taste, they use the unique fermentation method invented by themselves to put Hurunge into the leather

bag containing animals and hang it on the horse's back in hot weather. That is, with the running of the horse, the temperature rises and the fermentation speeds up so that the quality of koumiss is delicious.

Lactic acid bacteria are the key bacteria in the fermentation process. The content of lactose in fresh mare's milk is high. Lactic acid bacteria can use the disaccharide in lactose for fermentation, hydrolyze protein and fat to a certain extent, help to improve the taste and aroma of fermented milk (36), and then facilitate human digestion and nutrient absorption. It is for this reason that patients with lactose intolerance can drink koumiss. It is also believed that the type of bacteria in the final fermentation product is related to its acid resistance. Generally speaking, the acid resistance of *Lactobacillus* is higher than that of *Lactococcus*, because *lactobacillus* has an unknown tolerance mechanism. The acidity of koumiss after fermentation will be very high, which might be one of the important reasons why lactobacillus is a dominant bacterium (37). This is also the reason why *lactobacillus* is the dominant genus and has a high abundance in all 4 regions. The interaction of microorganisms in the system forms the unique taste and texture of koumiss wine. The *Lactobacillus* content of fermented samples stored in animal skin bags is lower than that of ordinary fermentation methods, and the content of *Acetobacter* is higher. Because *Acetobacter* contains alcohol dehydrogenase, it can oxidize ethanol into acetic acid (38), so acetic acid bacteria can convert alcohol produced by yeast into acetic acid, and the acidity of koumiss will reach very high. Therefore, it is inferred that koumiss fermented in skin bags, the acidity is higher than that of traditional fermented koumiss.

In the sample QHA, a special bacterium *komagataeibacter* was found, which has a strong ability to produce bacterial nano cellulose. This substance has long-term application prospects in the fields of cosmetics, composite materials, and wound care (39). Khan, H isolated a *komagataeibacter xylinus* IITR DKH20 from rotten apples, improve the yield of bacterial nano cellulose by optimizing the culture medium (40); Top, B isolated a *komagataeibacter xylinus* S4 (41) from homemade wine vinegar; Gopu, G isolated a *komagataeibacter sacharivorans* strain BC1 from rotten green grapes (42). However, it has been reported that *komagataeibacter* was found and isolated from the safe traditional fermented koumiss, which shows that the bacteria of this genus have strong acid resistance, which provides a new research direction for the separation of bacteria producing nano bacterial cellulose in the future.

However, we found traces of foodborne pathogens in all four regions, such as *Enterbacter*, *Citrobacter*, and other pathogenic bacteria, which were not detected in previous studies (43). *Enterbacter* is a natural resident of the human and animal gastrointestinal tract. It also exists in vegetables, raw meat, milk, and cheese (44). Luoyizha et al. (45) found that *Enterobacter* in raw donkey milk does not pose a risk to human health and can be explored as a potential starter/food fermentation auxiliary culture. Therefore, it is speculated that the *Enterobacter* in the Hurunge sample may not cause harm to the human body. The existence of *Enterobacter* maybe because the koumiss is usually produced by the open natural fermentation process, and there may be bacterial pollution in the initial raw milk. Therefore, in the production process of traditional fermented koumiss, while improving the sanitary environment, we should gradually transition from traditional production to modern standardized production, which will help to reduce the pathogens in the environment. These results suggest that the structural differences of bacterial communities may be related to geographical location. In addition, since many bacteria have not been identified at the species level and a few have not been detected, it is possible to identify new bacteria in Hurunge, which will provide new ideas and directions for future research.

The KEGG database is a large knowledge base for systematically analyzing gene functions and connecting genomic information and functional information. The KEGG PATHWAY database includes various metabolic pathways, synthetic pathways, membrane transport, signal transmission, cell cycle, and disease-related pathways. In addition, it also collects various chemical molecules enzyme and enzymatic reactions (46). Through the functional prediction of the bacterial community, the potential risk of bacteria carrying pathogenic genes in samples can be further evaluated to ensure the edible safety of different dairy products. However, the metabolic function predicted by the KEGG PATHWAY in this study is the basic metabolic function of microorganisms, which has a certain error. It is necessary to further confirm the metabolism of each sample at the genome level through metagenomic sequencing (47).

CONCLUSION

With the increasing variety of portable and convenient foods and the continuous infiltration of modern lifestyle into pastoral areas, the types and processing capacity of Hurunge continue to decrease, and the microbial resources contained therein gradually disappear. Therefore, in this study, 12 precious Hurunge samples collected from four regions of Mongolia were used to analyze the diversity and predict the function of bacterial communities based on 16S rRNA. The results showed that the bacterial community structure and function of Hurunge were affected by the geographical sources and fermentation methods. Among the 12 Hurunge samples, the total number of bacterial species in sample BEG1 is the largest, and the diversity of the bacterial community in sample ZY2 is the highest. A total of 120 species in 98 genera and 17 phyla are identified, of which *Firmicutes* and *Lactobacillus* are the dominant phylum and genus, respectively, *Acetobacter* is the second dominant genus, and the sample QHA contains *komagataeibacter* with the potential ability to produce bacterial nano cellulose. Compared with traditional fermentation methods, Hurunge samples BEG, HHA, QHA, and ZY fermented by animal skin such as fermentation have lower OTU levels, higher *Acetobacter* content, and different bacterial diversity. The abundance of *Lactococcus* in the Z region is significantly higher than that in the other three regions. The KEGG function prediction analysis shows that new and old metabolism occupies a dominant position in all microorganisms, this is conducive to the rapid growth and reproduction of microorganisms. The high abundance of carbohydrate and amino acid catabolic genes are

closely related to the flavor, texture, and final product function of koumiss. The purpose of this study is to analyze the bacterial diversity of Hurunge collected from Mongolia, so as to lay a foundation for the isolation and identification of probiotics and the protection of microbial resources in Hurunge in the future. At the same time, it is also providing the necessary theoretical basis for the production of koumiss by Hurunge at the factory level, which is more conducive to the development of probiotics and carries forward traditional national dairy products.

DATA AVAILABILITY STATEMENT

The datasets presented in this study can be found in online repositories. The names of the repository/repositories and accession number(s) can be found below: SRA, PRJNA793521.

AUTHOR CONTRIBUTIONS

WB, YH, and WL designed the experiments and conducted most of the experiments. WB and YH wrote and edited the manuscript. WB and WL reviewed the manuscript. All authors read and approved the manuscript.

FUNDING

This study was supported by grants from the Transformation Program of Scientific and Technological Achievements of Inner Mongolia (2020CG0012), Intergovernmental Key Project for International Cooperation in Science, Technology and Innovation (2017YFE0108700), and Scientific Research Program of Colleges and Universities in the Inner Mongolia Autonomous Region (NJZY19054).

REFERENCES

1. Chen YJ, Aorigele C, Wang CJ, Hou WQ, Zheng YS, Simujide, H. Effects of antibacterial compound of *Saccharomyces cerevisiae* from koumiss on immune function and caecal microflora of mice challenged with pathogenic *Escherichia coli* O8. *Acta Vet Brno.* (2019) 88:233–41. doi: 10.2754/avb201988020233
2. Mo L, Yu J, Jin H, Hou Q, Yao C, Ren D, et al. Investigating the bacterial microbiota of traditional fermented dairy products using propidium monoazide with single-molecule real-time sequencing. *J Dairy Sci.* (2019) 102:3912–23. doi: 10.3168/jds.2018-15756
3. Gesudu Q, Zheng Y, Xi XX, Hou QC, Xu HY, Huang WQ, et al. Investigating bacterial population structure and dynamics in traditional koumiss from Inner Mongolia using single molecule real-time sequencing. *J Dairy Sci.* (2016) 99:7852–63. doi: 10.3168/jds.2016-11167
4. Li BH, Hui F, Yuan Z, Shang QX, Shuai G, Bao YS, et al. Untargeted fecal metabolomics revealed biochemical mechanisms of the blood lipid-lowering effect of koumiss treatment in patients with hyperlipidemia. *J Funct Foods.* (2021) 78:104355. doi: 10.1016/j.jff.2021.104355
5. Rakhmanova A, Wang T, Xing G, Ma LL, Hong Y, Lu Y, et al. Isolation and identification of microorganisms in Kazakhstan koumiss and their application in preparing cow-milk koumiss. *J Dairy Sci.* (2021) 104:151–66. doi: 10.3168/jds.2020-18527
6. Guo L, Ya M, Guo YS, Xu WL, Li CD, Sun JP, et al. Study of bacterial and fungal community structures in traditional koumiss from Inner Mongolia. *J Dairy Sci.* (2019) 102:1972–84. doi: 10.3168/jds.2018-15155
7. Meng YC, Chen XL, Sun ZH, Li YH, Chen DD, Fang S, et al. Exploring core microbiota responsible for the production of volatile flavor compounds during the traditional fermentation of koumiss. *Lwt-Food Sci Technol.* (2021) 135:110049. doi: 10.1016/j.lwt.2020.110049
8. AydemirAtasever M, Ozlu H, Istanbullugil FR, Atasever M. Determination of AFM(1) levels of mare's milk and koumiss produced in the highlands of the Kyrgyz Republic. *Kafkas Universitesi Veteriner Fakultesi Dergisi.* (2021) 27:37–42. doi: 10.9775/kvfd.2020.24703
9. Zhang M, Dang N, Ren DY, Zhao FY, Lv RR, Ma T, et al. Comparison of bacterial microbiota in raw mare's milk and koumiss using pacBio single molecule real-Time sequencing technology. *Front Microbiol.* (2020) 11:581610. doi: 10.3389/fmicb.2020.581610
10. Rong JJ, Zheng HF, Liu M, Hu X, Wang T, Zhang XW, et al. Probiotic and anti-inflammatory attributes of an isolate *Lactobacillus helveticus* NS8 from Mongolian fermented koumiss. *BMC Microbiol.* (2015) 15:196. doi: 10.1186/s12866-015-0525-2
11. Yusuf B, Gurkan U. Analysis of the kefir and koumiss microbiota with the focus on certain functional properties of selected lactic acid bacteria. *Mljekarstvo.* (2021) 71:112–23. doi: 10.15567/mljekarstvo.2021.0204
12. Shuangquan, B, Yu B, Miyamoto T. Microflora in traditional starter cultures for fermented milk, hurunge, from Inner Mongolia, China. *Anim Sci J.* (2006) 77:235–41. doi: 10.1111/j.1740-0929.2006.00343.x
13. Wang J, Cheng K, Liu Q, Zhu Junxiang, Ochir Altansukh, Davaasuren Davaadorj, et al. Land cover patterns in Mongolia and their spatiotemporal changes from 1990 to 2010. *Arabian J Geosci.* (2019) 12:778. doi: 10.1007/s12517-019-4893-z
14. Huang JQ, Zhang WJ, Fan R, Liu ZG, Huang T, Li JY, et al. Composition and functional diversity of fecal bacterial community of wild boar, commercial pig and domestic native pig as revealed by 16S rRNA gene sequencing. *Arch Microbiol.* (2020) 202:843–57. doi: 10.1007/s00203-019-01787-w
15. Cocolin L, Alessandria V, Dolci P, Gorra R, Rantsiou K. Culture independent methods to assess the diversity and dynamics of microbiota during food fermentation. *Int J Food Microbiol.* (2013) 167:29–43. doi: 10.1016/j.ijfoodmicro.2013.05.008
16. Chen SF, Zhou YQ, Chen YR, Gu J. fastp: an ultra-fast all-in-one FASTQ preprocessor. *Bioinformatics.* (2018) 34:884–90. doi: 10.1093/bioinformatics/bty560
17. Magoc T, Salzberg S L. FLASH: fast length adjustment of short reads to improve genome assemblies. *Bioinformatics.* (2011) 27:2957–63. doi: 10.1093/bioinformatics/btr507
18. Edgar R C. UPARSE: highly accurate OTU sequences from microbial amplicon reads. *Nat Methods.* (2013) 10:996–8. doi: 10.1038/nmeth.2604
19. Stackebrandt E, Goebel B M. Taxonomic note: a place for DNA-DNA reassociation and 16S rRNA sequence analysis in the present species definition in bacteriology. *Int J Syst Bacteriol.* (1994) 44:846–9. doi: 10.1099/00207713-44-4-846
20. Wang Q, Garrity GM, Tiedje JM, Cole J R. Naïve Bayesian classifier for rapid assignment of rRNA sequences into the new bacterial taxonomy. *Appl Environ Microbiol.* (2007) 73:5261–67. doi: 10.1128/AEM.00062-07
21. Amato KR, Yeoman CJ, Kent A, Righini N, Carbonero F, Estrada A, et al. Habitat degradation impacts black howler monkey (Alouattapigra) gastrointestinal microbiomes. *Isme Journal.* (2013) 7:1344–53. doi: 10.1038/ismej.2013.16
22. Wu Y, Li Y, Gesudu QM, Zhang JT, Sun ZH, Halatu H, et al. Bacterial composition and function during fermentation of Mongolia koumiss. *Food Sci Nutr.* (2021) 00:1–10. doi: 10.1002/fsn3.2377
23. Wurihan, Bao LS, Hasigaowa, Bao XP, Dai YJ, Jia S R. Bacterial community succession and metabolite changes during the fermentation of koumiss, a traditional Mongolian fermented beverage. *Int Dairy J.* (2019) 98:1–8. doi: 10.1016/j.idairyj.2019.06.013
24. Yamada Y, Yukphan P, Huong T LV, Muramatsu Y, Ochaikul D, Tanasupawat S et al. Description of *Komagataeibacter* gen. nov., with proposals of new combinations (Acetobacteraceae). *J Gen Appl Microbiol.* (2012) 58:397–404. doi: 10.2323/jgam.58.397

25. Rizo J, Guillen D, Farres A, Diaz-Ruiz G, Sanchez S, Wacher C, et al. Omics in traditional vegetable fermented foods and beverages. *Crit Rev Food Sci Nutr.* (2020) 60:791–809. doi: 10.1080/10408398.2018.1551189
26. Xiao YS, Huang T, Huang CL, Hardie J, Peng Z, Xie MY, et al. The microbial communities and flavour compounds of Jiangxi yancai, Sichuan paocai and Dongbeisuancai: three major types of traditional Chinese fermented vegetables. *Lwt-Food Sci Technol.* (2020) 121:108865. doi: 10.1016/j.lwt.2019.108865
27. Ilseung C, J B M. The human microbiome: at the interface of health and disease. *Nat Rev Genet.* (2012) 13:260–70. doi: 10.1038/nrg3182
28. Suen G, Scott JJ, Aylward FO, Adams SM, Tringe SG, Pinto-Tomas AA, et al. An insect herbivore microbiome with high plant biomass-degrading capacity. *PLoS Genet.* (2010) 6:e1001129. doi: 10.1371/journal.pgen.1001129
29. Kamimura BA, De Filippis F, Sant'ana AS, Ercolini D. Large-scale mapping of microbial diversity in artisanal Brazilian cheeses. *Food Microbiol.* (2019) 80:40–9. doi: 10.1016/j.fm.2018.12.014
30. Bao G, Tuya A, Bayarsaikhan S, Dorjsuren A, Mandakh U, BaoYH, et al. Variations and climate constraints of terrestrial net primary productivity over Mongolia. *Quatern Int.* (2020) 537:112–25. doi: 10.1016/j.quaint.2019.06.017
31. Chai QQ, Li Y, Li XL, Wu WB, Peng H, Jia R, et al. Assessment of variation in paddy microbial communities under different storage temperatures and relative humidity by Illumina sequencing analysis. *Food Res Int.* (2019) 126:1–10. doi: 10.1016/j.foodres.2019.108581
32. Watanabe K, Fujimoto J, Sasamoto M, Dugersuren J, Tumursuh T, Demberel S. Diversity of lactic acid bacteria and yeasts in Airag and Tarag, traditional fermented milk products of Mongolia. *World J Microbiol Biotechnol.* (2008) 24:1313–25. doi: 10.1007/s11274-007-9604-3
33. Devirgiliis C, Zinno P, Perozzi G. Update on antibiotic resistance in foodborne *Lactobacillus* and *Lactococcus* species. *Front Microbiol.* (2013) 4. doi: 10.3389/fmicb.2013.00301
34. Cavanagh D, Fitzgerald GF, Mcauliffe O. From field to fermentation: The origins of *Lactococcus lactis* and its domestication to the dairy environment. *Food Microbiol.* (2015) 47:45–61. doi: 10.1016/j.fm.2014.11.001
35. Zhong Z, Hou Q, Kwok L, Yu Z, Zheng Y, Sun Z, et al. Bacterial microbiota compositions of naturally fermented milk are shaped by both geographic origin and sample type. *J Dairy Sci.* (2016) 99:7832–41. doi: 10.3168/jds.2015-10825
36. Liang TT, Xie XQ, Zhang JM, Ding Y, Wu Q P. Bacterial community and composition of different traditional fermented dairy products in China, South Africa, and Sri Lanka by high-throughput sequencing of 16S rRNA genes. *Lwt-Food Sci Technol.* (2021) 144:111209. doi: 10.1016/j.lwt.2021.111209
37. Yao GQ, He QW, Zhang WY, Zhang HP, Sun T S. Single molecule, real-time sequencing technology improves the sensitivity for detecting bacteria in koumiss, a traditional fermented mare milk product. *Sci Bull.* (2020) 65:2065–67. doi: 10.1016/j.scib.2020.07.028
38. Tian L, Perot SJ, Hon SE, Zhou J, Lynd L R. Enhanced ethanol formation by Clostridium thermocellum via pyruvate decarboxylase. *Microb Cell Fact.* (2017) 16:171. doi: 10.1186/s12934-017-0783-9
39. Gupte Y, Kulkarni A, Raut B, Sarkar P, Choudhury R, Chawande A, et al. Characterization of nanocellulose production by strains of *Komagataeibacter* sp. isolated from organic waste and Kombucha. *Carbohyd Polym.* (2021) 266:118176. doi: 10.1016/j.carbpol.2021.118176
40. Khan H, Saroha V, Raghuvanshi S, Bharti AK, Dutt D. Valorization of fruit processing waste to produce high value-added bacterial nanocellulose by a novel strain *Komagataeibacterxylinus* IITR DKH20. *Carbohyd Polym.* (2021) 260:117807. doi: 10.1016/j.carbpol.2021.117807
41. Top B, Uguzdogan E, Dogan NM, Arslan S, Kabalay B. Production and characterization of bacterial cellulose from *KomagataeibacterXylinus* isolated from home-made turkish wine vinega. *Cell Chem Technol.* (2021) 55:243–54. doi: 10.35812/CelluloseChemTechnol.2021.55.24
42. Gopu G, Govindan S. Production of bacterial cellulose from *Komagataeibacter saccharivorans* strain BC1 isolated from rotten green grapes. *Prep BiochemBiotechnol.* (2018) 48:842–52. doi: 10.1080/10826068.2018.1513032
43. Yao GQ, Yu J, Hou QC, Hui WY, Liu WJ, Kwok LY, et al. A perspective study of koumiss microbiome by metagenomics analysis based on single-cell amplification technique. *Front Microbiol.* (2017) 8:165. doi: 10.3389/fmicb.2017.00165
44. Giraffa G. *Enterococci* from foods. *FEMS Microbiol Rev.* (2002) 26:163–71. doi: 10.1111/j.1574-6976.2002.tb00608.x
45. Luoyizha W, Wu XM, Zhang M, Guo XF, Li H, Liao X J. Compared analysis of microbial diversity in donkey milk from Xinjiang and Shandong of China through High-throughput sequencing. *Food Res Int.* (2020) 137:109684. doi: 10.1016/j.foodres.2020.109684
46. K CS, Mustafa A, Handan C, Otu H H. KEGG2Net: Deducing gene interaction networks and acyclic graphs from KEGG pathways. *EMBnet J.* (2021) 26:e949. doi: 10.14806/ej.26.0.949
47. Douglas GM, Maffei VJ, Zaneveld JR, Yurgel SN, Brown JR, Taylor CM, et al. PICRUSt2 for prediction of metagenome functions. *Nat Biotechnol.* (2020) 38:685–8. doi: 10.1038/s41587-020-0548-6

Conflict of Interest: The authors declare that the research was conducted in the absence of any commercial or financial relationships that could be construed as a potential conflict of interest.

frontiers | Frontiers in Nutrition

ORIGINAL RESEARCH
published: 14 April 2022
doi: 10.3389/fnut.2022.865991

Evaluation of Volatile Profile and *In Vitro* Antioxidant Activity of Fermented Green Tea Infusion With *Pleurotus sajor-caju* (Oyster Mushroom)

Wei-Ying Su[1†], *Shu-Yi Gao*[1†], *Si-Jia Zhan*[1], *Qi Wu*[1], *Gui-Mei Chen*[1], *Jin-Zhi Han*[1,2], *Xu-Cong Lv*[1,2*], *Ping-Fan Rao*[1] *and Li Ni*[1,2*]

[1] *Institute of Food Science and Technology, College of Biological Science and Engineering, Fuzhou University, Fuzhou, China,*
[2] *Food Nutrition and Health Research Center, School of Advanced Manufacturing, Fuzhou University, Fuzhou, China*

OPEN ACCESS

Edited by:
Xiudong Xia,
Jiangsu Academy of Agricultural Sciences (JAAS), China

Reviewed by:
Majid Mohammadhosseini,
Islamic Azad University, Iran
Charles Oluwaseun Adetunji,
Edo University, Nigeria

***Correspondence:**
Xu-Cong Lv
xucong1154@163.com
Li Ni
nili@fzu.edu.cn

[†] *These authors have contributed equally to this work and share first authorship*

Specialty section:
This article was submitted to Food Chemistry, a section of the journal Frontiers in Nutrition

Received: *30 January 2022*
Accepted: *14 March 2022*
Published: *14 April 2022*

Citation:
Su W-Y, Gao S-Y, Zhan S-J, Wu Q, Chen G-M, Han J-Z, Lv X-C, Rao P-F and Ni L (2022) Evaluation of Volatile Profile and In Vitro Antioxidant Activity of Fermented Green Tea Infusion With Pleurotus sajor-caju (Oyster Mushroom). Front. Nutr. 9:865991. doi: 10.3389/fnut.2022.865991

Green tea has distinct astringency, bitter taste, and typical green flavor because of its post-harvest treatment without withering and enzymatic oxidation. Microbial fermentation has been identified as a promising strategy that could give green tea infusion a special taste flavor. This might be linked to the metabolic transformation ability of microorganisms. In this study, starter culture of edible mushroom *Pleurotus sajor-caju* (oyster mushroom) was used for submerged fermentation of green tea infusion in order to improve its flavor and taste quality. The volatile profile determined by headspace solid-phase microextraction, coupled with gas chromatography mass spectrometry, showed that the contents of (*Z*)-2-penten-1-ol and methyl heptadienone in green tea infusion were decreased significantly by the fermentation with the basidiomycete *P. sajor-caju* ($p < 0.01$), which would alleviate the herbal and grass flavor of green tea infusion to a certain extent. Meanwhile, the contents of linalool and geraniol were increased 9.3 and 11.3 times, respectively, whereas methyl salicylate was newly produced after fermentation by *P. sajor-caju*, endowing the fermented tea infusion with a pleasant flower and fruit aroma. In addition, the polyphenol profile was determined using high-performance liquid chromatography equipped with ion trap mass spectrometry, and the results indicated that the contents of most polyphenols in green tea infusion decreased significantly after fermentation by *P. sajor-caju*. The reduction of catechins and anthocyanins in fermented green tea infusion alleviated the astringency and bitterness. Moreover, the antioxidant activity of fermented green tea infusion was obviously decreased, especially the DPPH-free radical-scavenging ability and the ferric-reducing power. However, it is noteworthy that the ABTS-free radical scavenging ability was improved compared with the unfermented one, indicating that the increased tea pigments and volatile metabolites (such as linalool and geraniol) after fermentation with *P. sajor-caju* may also contribute to the antioxidant capacity of fermented green tea infusion. Overall, the innovative approach driven by *P. sajor*-caju fermentation has achieved promising potential to manipulate the green tea flavor.

Keywords: antioxidant activity, green tea, *Pleurotus sajor-caju*, submerged fermentation, volatile components

INTRODUCTION

Green tea is very popular in most of Asia, especially in China and Japan, because it contains more bioactive compounds (e.g., polyphenols) than black tea, which makes it have even greater benefits (1). However, green tea usually has a distinct astringency and bitter taste, as well as a typical green flavor, mainly due to its post-harvest treatment without withering and enzymatic oxidation (2). A variety of catechins, especially epigallocatechin gallate (EGCG) and epigallocatechin (EGC), play a key role in the distinct astringency and bitterness of green tea drinks. It is urgent to carry out deep processing to develop more diversified products and expand the product's category and sales market of the green tea. Fermented foods are known for their good nutritional and health benefits. Microbial fermentation is a promising and effective strategy to improve low-grade green tea, and it not only gives green tea infusion a special taste and flavor, but also produces certain physiological effects to promote health. It has been reported so far that the microorganisms used for the fermentation of tea infusion mainly include *Lactobacillus* and *Acetobacter* in bacteria (3–5), yeasts and molds in fungi (6–9), and edible fungi (10, 11).

Edible fungi belong to the classification Eumycophyta. Most of them are Basidiomycotina, whereas a few are Ascomycotina (12). Basidiomycetes are considered to be a promising tool because they can synthesize natural flavor compounds and rich extracellular enzymes, and can be used to regulate the sensory properties of beverages and foods in the food industry. A lot of research evidence has shown that basidiomycetes can be used to develop alcoholic drinks and plant beverages. It was previously reported that wine, beer, and sake were fermented by using the characteristics of ethanol dehydrogenase produced by *Tricholoma matsutake* and *Pleurotus ostreatus*, and the fermented products have the physiological functions of preventing cancer and thrombosis (13). The two techniques of *Grifola frondosa*-fermented soybean milk and *Ganoderma lucidum*-fermented pumpkin juice can obviously improve the bad flavor of plant beverages produced by thermal processing. According to the inspiration of the above two techniques, it was found that basidiomycete fermentation can improve the flavor and taste of tea. In a previous study, fresh tea was used as a substrate to obtain a new type of fermented tea with a good flavor through solid-state fermentation of *G. frondosa* and *G. lucidum* (14). *Flammulina velutipes* was reported to produce the characteristic flavor compound 2-ethyl-3,5-dimethyl pyrazine, creating a nutty and chocolate-like floral odor impression after low-grade *Longjing* green tea fermentation (11). It was also reported that *Wolfiporia cocos* (Fu Ling) fermentation changed the characteristic green grass smell of green tea infusion into a strong fragrance of flower and jasmine flower, and significantly improved the flavor quality of green tea (10). Moreover, beverages fermented by basidiomycetes can have some functional activities, such as antibacterial, immune regulation, and antioxidant (15, 16). At the same time, the rich extracellular enzyme system of basidiomycetes will produce some unique flavors in beverage production (15, 17, 18).

As a typical basidiomycetes, *Pleurotus sajor-caju* (oyster mushroom) has high nutritional values, therapeutic properties, and a variety of environmental and biotechnological applications (19). The fruiting body and mycelium of *P. sajor-caju* are rich in vitamins and amino acids and other nutrients. Besides, it has been widely used as a traditional medicine because of its various bioactive properties, including antitumor, antioxidant, and antimicrobial properties (20, 21). It especially possesses a distinctive flavor, in which a series of aliphatic components such as 1-octen-3-ol and 3-octanone are the main flavor active components contributing to the "fungal flower" and "fruity taste" (22). Phenolic compounds are among several compounds that have been proved to have antioxidant effects on the scavenging-free radicals present in the body (23, 24). The most abundant phenolic compounds reported in edible mushrooms belong to the phenolic acid family. In addition, *P. sajor-caju* can use various by-products of the food industry as a growth matrix to secrete a variety of extracellular enzymes, including phenol oxidase, peroxidase, and glucosidase, which are closely related to the formation of flavor quality (25–29). However, the effects of the fermentation with *P. sajor-caju* on the volatile flavor composition and antioxidant activity of green tea infusion have not been investigated.

Headspace solid-phase microextraction technology (HS-SPME) was used to extract the volatile components in fermented tea infusion, and gas chromatography with mass spectrometry (GC-MS) was used to measure and compare the difference between volatile components in green tea infusion before and after fermentation with *P. sajor-caju*. In this study, the high-performance liquid chromatography with mass spectrometry (HPLC-MS) was used to compare the differences in polyphenols caused by fermentation processing. ABTS- and DPPH-free radical-scavenging abilities and the ferric-reducing antioxidant power were used to evaluate the *in vitro* antioxidant activity of green tea beverage produced by the fermentation with *P. sajor-caju*.

The aim of this study was to investigate the effects of *P. sajor-caju* fermentation on volatile profile and *in vitro* antioxidant activity, and to provide feasible technical support and innovative approaches for the deep processing of low-grade green tea. The results of the research play an important guiding role in the development of new green tea beverages in China and even in the world.

MATERIALS AND METHODS

Chemicals and Materials

P. sajor-caju CGMCC 5.593 strain was purchased from the China General Microbiological Culture Collection Center (CGMCC) and deposited at the Fuzhou University Institute of Food Science and Technology. Green tea (Fuyun No. 6) was purchased from the market. Potatoes were purchased from the local supermarkets. Agar powder, anhydrous glucose, soy peptone, yeast extract powder, vitamin B1, KH_2PO_4, $MgSO_4$, and NaCl were obtained from the Sinopharm Chemical Reagent Co., Ltd.

2-Octanol was purchased from the German Dr. Ehrensorfer company. All were analytically pure.

Preparation of Green Tea Infusion

Tea and boiling water were prepared according to the material ratio of 1:30 and leached in a water bath at 95°C for 15 min. The filtrate was divided into 50 ml/250 ml (filtrate volume/conical flask volume), pasteurized at 80°C for 30 min. The tea infusion was stored at −20°C until usage.

Culture of Strain

Liquid seed medium for *P. sajor-caju* CGMCC 5.593 contains 3% glucose (*w*/*v*), 4‰ yeast extract powder (*w*/*v*), 4‰ soy peptone (*w*/*v*), 1‰ KH_2PO_4 (*w*/*v*), 0.5‰ $MgSO_4$ (*w*/*v*), and 0.05‰ vitamin B1 (*w*/*v*). Distilled water was used as a solvent, boiled, divided into 50 ml/100 ml (filtrate volume/conical flask volume), and sterilized at 121°C for 20 min (27). Inoculation shovel was used to take a fungus block of approximately 0.5 × 0.5 cm^2 from the original strain *P. sajor-caju* CGMCC 5.593, which was maintained on potato dextroseagar (PDA) slants to the plate with about 20 ml PDA medium. The plate was cultured in a constant temperature incubator at 28°C until the mycelium covered the whole plate and was stored at 4°C. A hole punch with a diameter of 14 mm was used to take a block of mycelium from the plate and then added block to the liquid seed medium of *P. sajor-caju*. The medium was incubated on a rotary shaker (28°C, 200 rpm) for 6 days in darkness to get a sufficient amount of mycelium.

Fermentation of Tea Infusion

The fermentation process parameters of tea infusion referred to the methods described by Zhang et al. (12). In detail, *P. sajor-caju* mycelia were prepared from 30 ml pre-cultured seed fermentation broth and collected by centrifugation (4,000 rpm, 2,150 × *g*, 10 min, 20°C) and washed twice with sterile water. The collected *P. sajor-caju* mycelia were resuspended in sterilized tea infusion to obtain a stock culture at a concentration of 0.3 g/ml. The stock culture was then inoculated into an Erlenmeyer flask (250 ml) containing 50 ml tea infusion at a 10% inoculation volume. The fermentation was carried out at 28°C for 3 days under aerobic conditions on a rotary shaker (200 rpm) in the dark (28). During the fermentation, the detection solution of the samples obtained by means of centrifugation (4,000 rpm, 2,150 × *g*, 10 min, 4°C) was used for GC-MS analysis, sensory evaluation, and antioxidant activity determination.

Sensory Evaluation

The sensory evaluation method referred to previously has been described with minor modifications (30). Six odor qualities (herbal, green, floral, fruity, sweetish, and toasty) and three taste qualities (bitter, sweet, and astringent) were selected to describe the flavor of the tea infusion before and after fermentation. The unfermented and fermented tea infusions were preheated at 80°C and packed 15 ml in teacups (capacity, 20 ml; bottom diameter, 32 mm; top diameter, 45 mm). The detection solution was evaluated by the sensory panel (5 men and 7 women). They were invited to rate the given odor qualities of the unfermented and fermented tea infusion according to a five-level intensity scale, which ranged from 1 to 5 (1 = very weak, 2 = weak, 3 = medium intense, 4 = strong, and 5 = very intense). Finally, the sensory score was averaged and analyzed by *t*-test.

Headspace Solid-Phase Microextraction

The HS-SPME for the extraction of volatiles from the fermented tea infusion is a valuable technique that can effectively trap volatile compounds in various samples present on the surface of the synthetic organic fiber polymers (31, 32). For HS-SPME, divinylbenzene/carboxen/polydimethylsiloxane fiber (50/30 μm, 2 cm, SUPE- LCO, USA) in combination with a manual solid-phase microextraction injection handle were used. The fiber was aged by the gas chromatography inlet at 230°C for 30 min before use. Then, 2 g NaCl, 6 ml detection solution, and 10 μl 2-octanol at a concentration of 1 mg/l (as an internal standard) were added into a 15-ml screw-top headspace vial (33). The samples were preheated at 50°C for 10 min, followed by headspace extraction, at the same temperature for 30 min. Finally, the analytes were directly desorbed in GC-MS inlet at 230°C for 15 min.

Gas Chromatography Mass Spectrometer

Gas chromatography was carried out using an Agilent 7890-B chromatograph equipped with an Agilent 5977A quadrupole mass spectrometer. The column used was a polar 30 m × 0.25 mm i.d., 0.25 μm (HP-INVOWAX, USA). Helium (99.999%) was used at a constant flow rate of 1 ml/min as the carrier gas. According to the method of Wang et al. (34), the chromatographic heating procedure was as follows: the initial temperature was 40°C, held for 4 min; then, the temperature was raised to 230°C at 5°C/min and held for 3 min. The mass spectrometry conditions were as follows: electron ionization energy, 70 eV; ion source temperature, 230°C; quadrupole temperature, 150°C; scan mode, TIC; and scan range, *m*/*z* 33–550. The volatile peaks were identified by matching the National Institute of Standards and Technology 11 mass spectral database and the retention index (RI, determined by n-alkanes C7–C40). As it is difficult to collect all the standards of the identified volatile compounds, a semi-quantification with a single internal standard of 2-octanol was used in this study, as described by Liu et al. (35).

LC-MS Analysis

The samples in this experiment were taken from the fermented tea sample on the zeroth and third day of the blank group, as well as the tea infusion on the third day of fermentation. The sample was detected after passing through the 0.22 μm filter membrane. Referring to the methods described by Ana López-Cobo et al. (36), the HPLC system consisted of a C18 column (4.6 × 250 mm, 5 μm; Waters, Milford, MA). The mobile phase, consisting of 0.1% FA (v/v) in water (A) and 100% ACN (B), was used at a flow rate of 1 ml/min. The injection volume was 10 μl. B gradient program was set as follows: 0–4 min, from 10 to 15%; 4–5 min was linear gradient increased to 16%; 5–8 min, linear gradient increased to 18%; 8–12 min, linear gradient increased to 20%; 12–13 min, linear gradient increased to 22%; 13–14 min, increased to 25%; 14–16 min, gradient increased to 28%; 16–17 min, increased to 30%; 17–18 min, linear gradient increased to 31%; 17–18 min, linear gradient increased to 31%; 18–19 min,

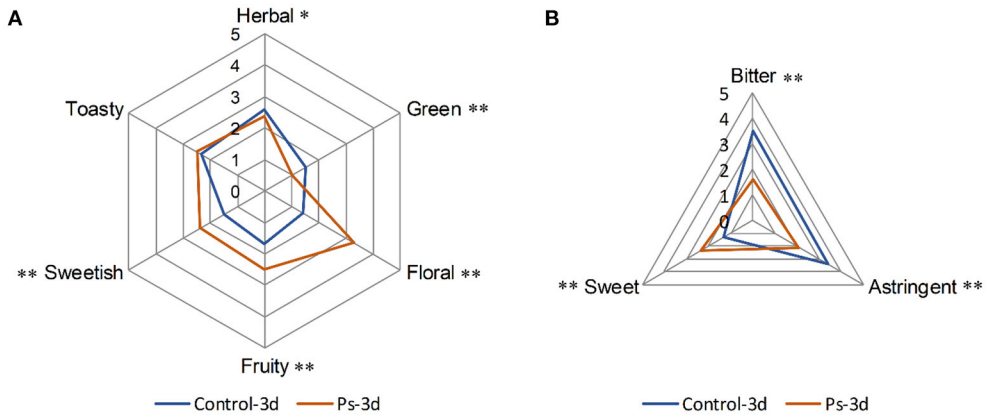

FIGURE 1 | Comparative flavor profile analysis of the aroma **(A)** and taste **(B)** in green tea infusion before and after fermentation by *Pleurotus sajor-caju* (Control-3d: unfermented green tea infusion; Ps-3d: green tea infusion fermentation for 3 days; *p value of before vs. after fermentation was lower than 0.05, **p value of before vs. after fermentation was lower than 0.01).

linear gradient increased to 32%; 19–24 min, linear gradient increased to 50%; 24–27 min, linear gradient increased to 75%; 27–36 min, linear gradient decreased to 10%; and 36–38 min, isocratic at 10%. Column temperature was set at 25°C, and the detection wavelength was 254 nm. The mass spectrometer was operated in negative modes with an electrospray ionization spray voltage of 4 kV, gas temperature of 210°C, gas flow of 8l/min, and full-scan range of 50–1,100 (m/z).

Determination of Antioxidant Activity

The antioxidant activity was carried out by three assays, namely, 2,2′-azino-bis-3-ethylbenzthiazoline-6-sulphonic acid (ABTS) free radical-scavenging rate, 2,2-diphenyl-1-picrylhydrazyl (DPPH) free radical-scavenging rate, and ferric iron-reducing antioxidant power (FRAP). ABTS-free radical-scavenging activity (7 mM in H_2O) contains 2.45 mM potassium persulfate. The tea sample (about 200 μl) was mixed with 800 μl ABTS-free radical solution for 6 min at 30°C, and the absorbance was determined at 734 nm. DPPH is a stable free radical molecule of red color. About 100 μl tea samples were mixed with 100 μl of DPPH (0.2 mM) in methanol, and after 30 min incubation at room temperature, the absorbance at 517 nm was read. The FRAP assay was performed with 100 μl tea sample, then 500 μl phosphate buffer (0.2 M, pH 6.6) and 500 μl 1% $K_3Fe(CN)_6$ was added and place in a water bath at 50°C for 20 min. After cooling, 500 μl of 10% trichloroacetic acid was added and allowed to stand at room temperature for 10 min. Then, 500 μl of the above reaction solution was taken, 500 μl deionized water and 100 μl 0.1% ferric chloride solution were added, and the absorbance at 517 nm was read. The detailed approaches of antioxidant activities have been described by Li et al. (37).

Statistical Analysis

The experimental data were expressed as a mean of three separate determinations using Excel. The significant changes between the groups were assessed by SPSS software (version 22.0, 1989, IBM, USA) with t-test and one-way ANOVA. Heatmap analysis, hierarchical clustering analysis (HCA), and principal component analysis (PCA) were done using R software (version 3.6.1).

RESULTS

Sensory Evaluation of Tea Infusion Before and After Fermentation

To compare the aroma and taste changes of tea infusion by fermentation of *P. sajor-caju*, a panel of 12 assessors evaluated the scent of each sample in the descriptors herbal, green, floral, fruity, sweetish, and toasty. Meanwhile, three flavor attributes, including bitter, sweet, and astringent, were evaluated in each sample. Till 3-day fermentation, the aroma and taste in green tea infusion varied in both its quality and intensity (**Figure 1**). The fermented tea infusion changed in a favorable direction that the floral, fruity, and sweetish scents significantly increased ($p < 0.01$) while the odors of herbal ($p < 0.05$) and green ($p < 0.01$) significantly decreased (**Figure 1A**). Additionally, fermented green tea displayed a significantly lower intensity ($p < 0.05$) of bitter and astringent attributes (**Figure 1B**).

Changes of Volatile Components in Tea Infusion After Fermentation

By applying HS-SPME/GC-MS, a total of 72 substances were identified in green tea infusion before and after fermentation, including 5 hydrocarbons, 23 alcohols, 8 aldehydes, 12 ketones, 6 esters, 8 acids, 6 benzenes, 1 pyrrole, and 3 pyrazines. As shown in the total ion flow diagram obtained by gas chromatography (**Figure 2**), the fermentation made little difference to the overall peak. However, there was a significant increase in the content of substances fermented by *P. sajor-caju*, mainly including (*Z*)-3-hexen-1-ol, linalool, citral, geraniol, and (*R*)-citronellol. These substances present floral and fruity fragrance, which are beneficial to enhance the flavor. Moreover, the heatmap analysis revealed that there was a remarkable difference between the unfermented and

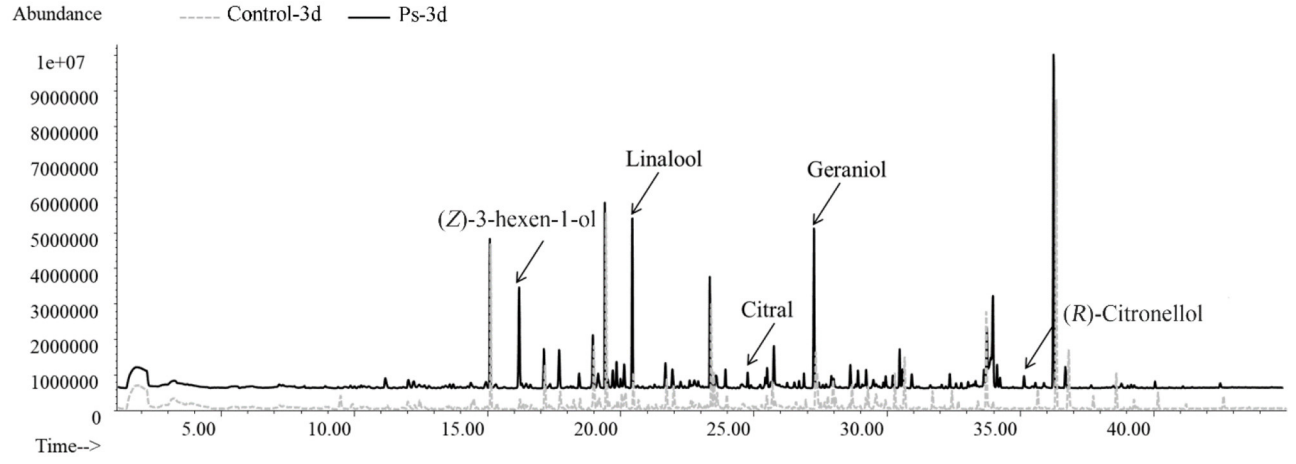

FIGURE 2 | Gas chromatography total ion chromatogram of volatile components in tea infusion before and after fermentation.

fermented groups for presenting two characterized clusters correspondingly (**Figure 3**). These volatile components can be further divided into three groups, namely, significantly higher experimental group (type 1), no significant difference (type 2), and significantly higher control group (type 3). Type 1 contained 28 substances, of which 12 chemicals were added, such as methylbenzoate, citral, (*R*)-citronellol, methyl salicylate, nerol, and dihydroactini-diolide. In addition, the amount of (*Z*)-3-hexen-1-ol, benzaldehyde, α-terpineol, linalool, geraniol, β-damascenone, and phenethyl alcohol increased greatly. Type 2 consisted of 12 substances, such as geranylacetone, *cis*-jasmone, and phenol. Type 3 comprised 32 substances with 12 chemicals disappearing after fermentation, including β-ionone, (*Z*)-2-penten-1-ol, methyl-heptadienone, hexanoic acid, 2-furanmethanol, and 1-hexanol. Furthermore, the contents of benzyl alcohol, 1-octanol, theapirane, indole, and other substances were significantly reduced after fermentation.

According to the odor characteristics of these volatile components, it could be roughly classified into seven categories, namely, herbal, green, floral, fruity, sweetish, toasty, and other. As shown in **Figure 3**, type 1 contained a large number of substances that presented floral and fruity odors as well as a few substances that presented sweetish and toasty flavors. The overall odor was rich, especially fruity and floral scents. Type 2 covered all categories sharing comparable proportions except fruit and sweetish odors. Compared with other substances, floral, fruity, and sweetish chemicals accounted for a much less percentage in type 3, which is attributed to a faint overall odor. Above all, our experiment found that the volatile flavor of green tea infusion could be significantly improved after the fermentation of *P. sajor-caju*.

Based on the concentrations of all volatile components in green tea infusion samples, HCA and PCA were further performed to clarify diversities among them, as shown in **Figure 4**. In HCA, the volatile components were clustered into two main groups, namely, tea infusion before fermentation and after fermentation. The hierarchical clustering dendrogram is shown in **Figure 4A**. The PCA score plot was further performed for the dynamic changes of volatile components during the fermentation process (**Figure 4B**). The variances of the first two major components were 67.05% and 26.31%, which collectively account for 93.36% of the total variability of volatile compounds. The data made the information of the volatile components in each tea sample clear. The PCA scatter plot demonstrated that tea infusion before fermentation had a similar volatile profile. Combining the results of their same cluster identified in HCA, it can be concluded that during the fermentation time the flavor of unfermented tea infusion slightly changed within 3 days. Remarkably, the fermentation processes had changed the profiles of tea infusion volatile greatly, which lead to a distinctive scatter of the sample. The volatile profile was mainly composed of (*Z*)-3-hexen-1-ol and linalool oxide after 1-day fermentation, whereas it turned to be linalool, geraniol, and methyl salicylate and other substances in a few days.

Significant Changes in Volatile Flavor Components After Fermentation

Significant analysis was performed to further clarify whether the changes of volatile components of the tea soup after fermentation were significant. A total of 54 volatile components of the experimental group showed significant difference compared with the control group after fermentation of 3 days. Among them, in the experimental group, 30 substances such as geraniol, linalool, (*R*)-citronellol, β-damascenone, methyl salicylate, and dihydroactinidiolide were increased remarkably ($p < 0.01$). They mainly had a floral aroma (e.g., linalool, geraniol and (*R*)-citronellol), fruity aroma (e.g., dihydroactinidiolide), and sweetish flavor (e.g., methyl salicylate). The higher the content, the richer the fragrance. In the control group, 24 components, including indole, hexanoic acid, nonanoic acid, hexadecane, and theaspirane, were at a significantly higher level. **Table 1** lists several vital volatiles in tea infusion before and after fermentation by *P. sajor-caju.*

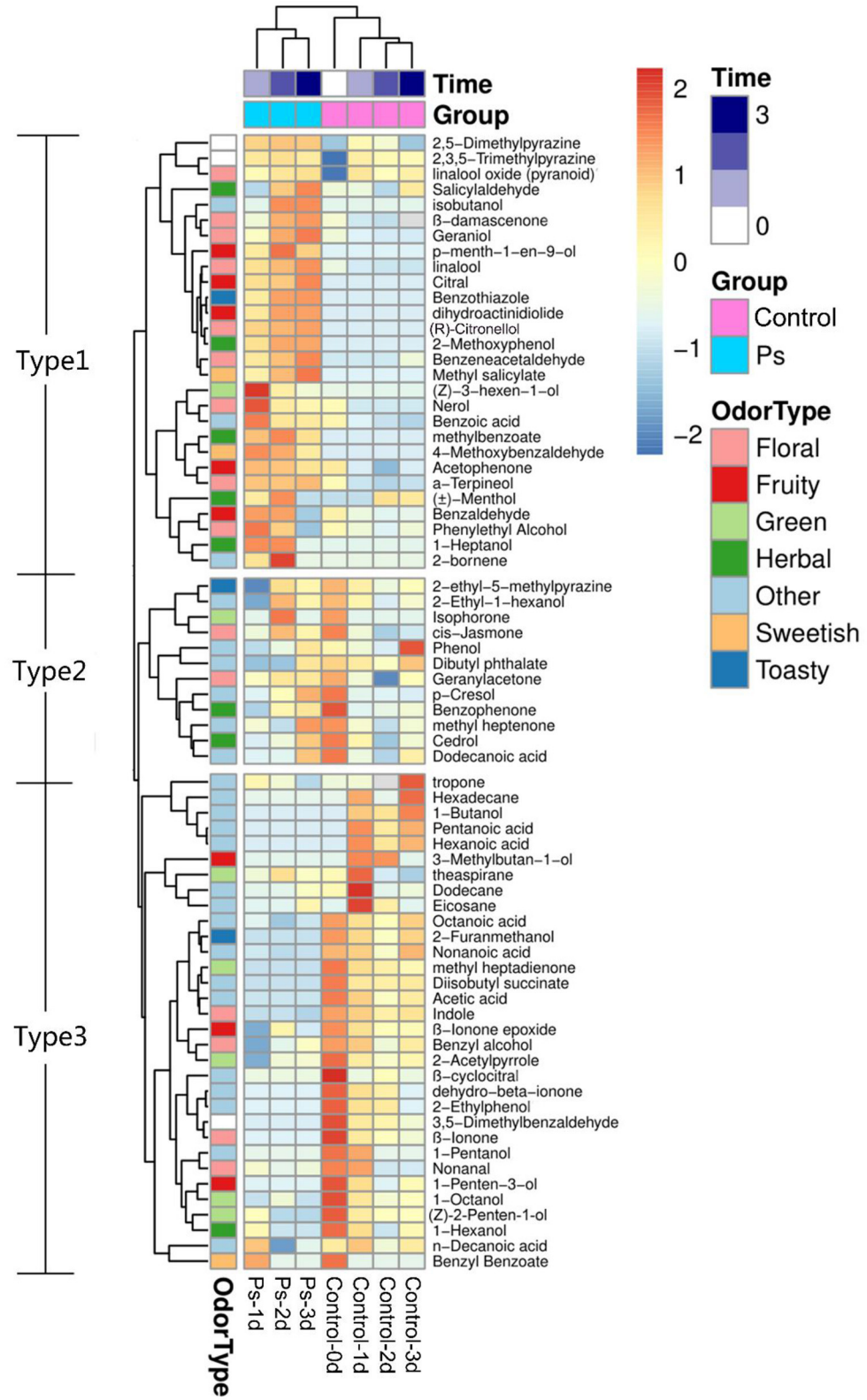

FIGURE 3 | Heatmap of volatile components of green tea infusion before and after fermentation (Control: unfermented green tea infusion; Ps: green tea infusion fermented by *Pleurotus sajor-caju;* time: from 1 to 3 days).

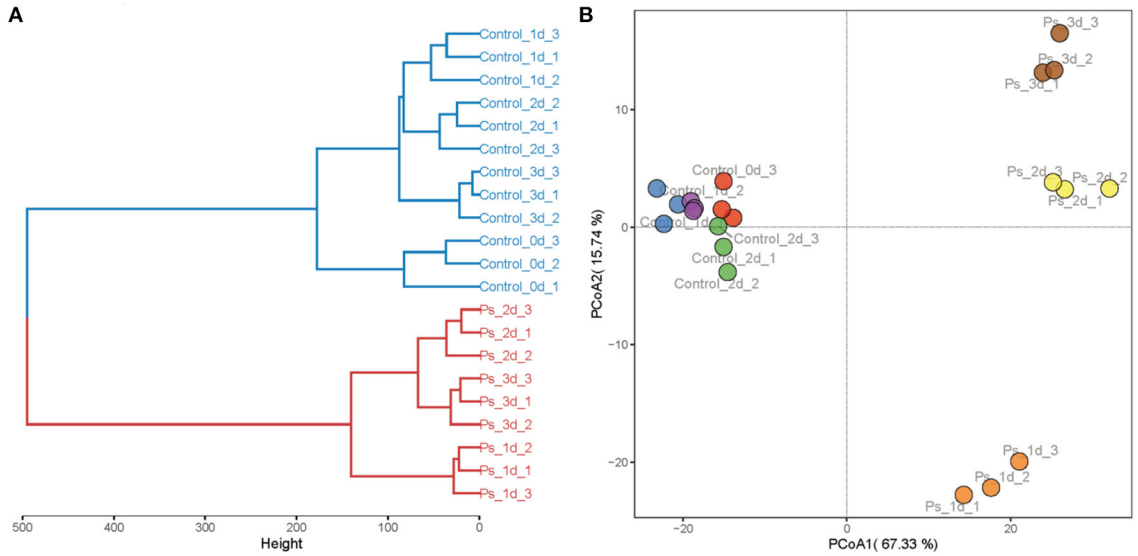

FIGURE 4 | Hierarchical clustering analysis **(A)** and principal component analysis **(B)** of the volatile compounds in tea infusion (Control: unfermented green tea infusion; Ps: green tea infusion fermented by *Pleurotus sajor-caju*; time: from 1 to 3 days).

TABLE 1 | Volatile flavor components that changed significantly after fermentation by *Pleurotus sajor-caju*[a].

No.	Compounds	Odor description	RI	Content (μg/L)	
				Control-3d	Ps-3d
1	Geraniol	Rose-like, citrus-like	1805	1.20 ± 0.11	12.38 ± 0.96**
2	Linalool	Floral, fruity	1535	0.75 ± 0.08	9.19 ± 0.57**
3	Benzeneacetaldehyde	Floral, honey, sweet, chocolate-like	1649	0.19 ± 0.01	0.92 ± 0.02**
4	Benzaldehyde	Fruity, nutty, woody	1518	0.30 ± 0.02	1.18 ± 0.13**
5	*β*-damascenone	Sweet, honey, apple-like, rose-like	1789	0.10 ± 0.01	0.43 ± 0.05**
6	(*Z*)-3-hexenol	Floral	1399	0.31 ± 0.02	1.75 ± 0.31**
7	(*R*)-Citronellol	Floral, sweet, rose, fruity citrus nuances	1774	n.d.	0.39 ± 0.04
8	Methyl salicylate	Fresh, faint gingery, grass and milky	1790	n.d.	2.72 ± 0.02
9	2,5-Dimethylpyrazine	Nutty, coffee, cocoa-like	1350	n.d.	0.49 ± 0.32
10	Methyl benzoate	Herb, lettuce, prune, violet	1638	n.d.	0.24 ± 0.01
11	Nerol	Lemon-like, floral	1785	n.d.	0.20 ± 0.04
12	Dihydroactinidiolide	Roasted, musk, coumarin	2163	n.d.	1.12 ± 0.04
13	*β*-Ionone	Woody, violet-like	1983	0.20 ± 0.04	n.d.
14	(*Z*)-2-penten-1-ol	Green	1352	0.61 ± 0.02	n.d.
15	methyl heptadienone	Green, slightly herbal	1581	0.23 ± 0.02	n.d.
16	Indole	Floral, animal-like	2132	1.12 ± 0.07	0.22 ± 0.13**
17	Nonanoic acid	Fatty, waxy-like, cheesy-like	2140	2.84 ± 0.09	1.00 ± 0.18**

*(A) Since the difference in volatile components is the most significant when fermenting for 3 days, the content in the figure is presented for 3 days. (B) Odor descriptions were from the literature (38–41), or from FEMA database. (C) [a]Data are expressed as mean ± SD (n = 3), **p value of before vs. after fermentation was <0.01.*

Changes of Antioxidant Activity in Tea Infusion Before and After Fermentation

The representative chromatograms before and after tea fermentation obtained from the LC-MS are demonstrated in **Figure 5**. A total of 21 peaks were measured. Compared with the control group, a total of 9 peaks decreased significantly after fermentation based on Mass and MassBank. We identified 15 compounds (**Table 2**), including 4 catechins (compounds 10, 11, 12, and 16), 1 anthocyanins (compound 7), 5 flavonols (compounds 5, 14, 15, 17, and 18), and 5 phenolic acids (compounds 1, 3, 4, 6, and 8). After fermentation, catechins and anthocyanins were noticeably reduced. In contrast, any differences cannot be seen in the level of flavonols (except for compound 5) and phenolic acids. ABTS-free radical-scavenging

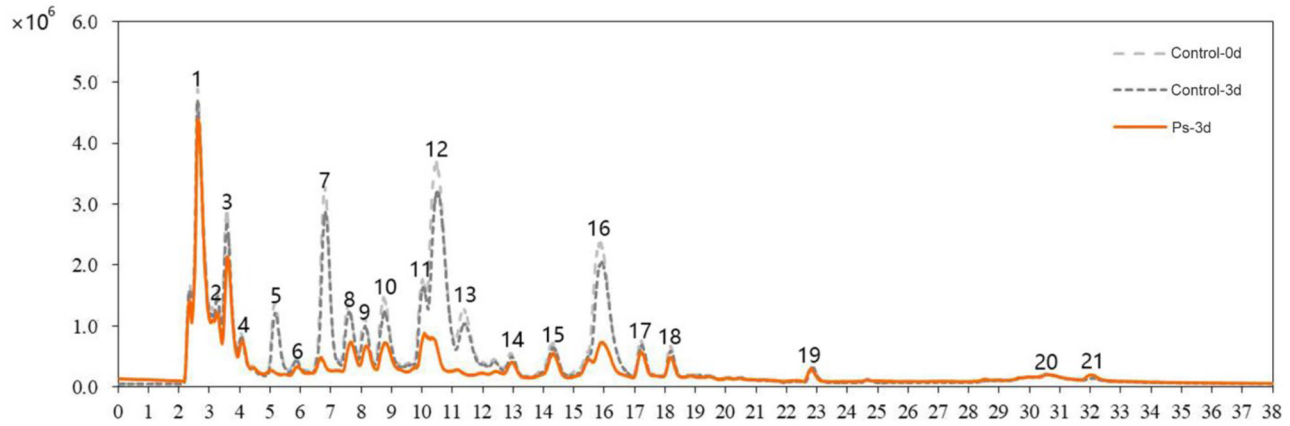

FIGURE 5 | TIC chromatogram of green tea infusion before and after fermentation.

TABLE 2 | LC-MS qualitative analysis of polyphenols and anthocyanins in green tea infusion before and after the fermentation by *P. sajor-caju*.

Peak No.	Tentative identification	Measured $[M-H]^-$(m/z)
1	Quinic acid	191.05
3	Theogallin	343.07
4	Gallic acid	169.01
5	Cyanidin-3,5-di-O-glucoside	611.16
6	Caffeoylquinic acid	353.08
7	2,3-(*E*)-3,4-(*E*)-Anthocyanin	306.07
8	*p*-Coumaroylquinic acid	337.10
10	Procyanidin B1	557.14
11	Epicatechin	289.07
12	Epigallocatechin gallate	458.08
14	Quercetin-hexosyl-hexosyl-deoxyhexoside	771.20
15	Rutin	609.15
16	Epicatechin gallate	442.09
17	Kaempferol-hexosyl-hexoside	593.15
18	Kaempferol-hexoside	447.09

rate, DPPH-free radical-scavenging rate, and ferric iron-reducing antioxidant power were used as indicators to measure the change of antioxidant activity before and after fermentation (**Figure 6**). Compared with the control group, the ABTS-free radical-scavenging activity in tea infusion fermented for 3 days was slightly increased (**Figure 6A**) and the calculated Vc equivalents were 11.26 mg/ml (IC_{50} = 0.05‰) and 14.65 mg/ml (IC_{50} = 0.08‰), respectively; the DPPH-free radical-scavenging activity after fermentation was significantly decreased (**Figure 6B**), and the calculated Vc equivalents were 20.49 mg/ml (IC_{50} = 0.34‰) and 12.08 mg/ml (IC_{50} = 0.50‰), respectively; the ferric ion-reducing power of the experimental group showed a downward trend (**Figure 6C**). Although the antioxidant activity was lost, it still maintained a high activity after the fermentation of *P. sajor-caju*.

DISCUSSION

The aroma profile of green tea infusion showed remarkable differences before and after fermentation. Herbal and green, as two original aromas of green tea, are stronger in the unfermented tea infusion. After fermentation, these two odors became much weaker mainly due to the reduction in green-like substances such as (Z)-2-penten-1-ol and methyl heptadienone. In fermented tea infusion, the floral and fruity aroma are enhanced significantly, especially the floral odor. From the results of **Figures 2**, **4**, it can be found that after fermentation of *P. sajor-caju*, linalool (orange, lemon, floral), geraniol (floral, rosy), β-damascenone (apple, rose), (R)-citronellol (floral, rose, citrus), nerol (sweet natural neroli citrus magnolia), citral (lemon sweet), benzaldehyde (sweet, cherry, almond), and phenethyl alcohol (floral, sweet, rosey) increased significantly. The above aromas are predominantly presented floral and fruity. Thereinto, methyl salicylate (sweet taste), displaying a sweetish odor, is a newly added ingredient after fermentation. The toasty odor has a slight variation during fermentation. This kind of odor is mostly derived from the caramel aroma of pyrazine and pyrrole (42), and the composition of such substances has no significant difference before and after fermentation, except for the newly formed 2,5-dimethylpyrazine during fermentation. In addition, analyzing changes in categories of volatile compound after fermentation revealed that aldehydes, esters, and benzene aromatic substances increased, acids and ketones decreased, and there was no significant difference in other types. The L-phenylalanine contained in green tea can be converted into benzene aromatic substances through the action of amino acid decarboxylase and aminotransferase (43). Edible fungi can produce extracellular enzymes such as laccase, lipoxygenase, and hydroperoxide lyase, which may peroxidize and degrade unsaturated fatty acids to form aldehydes (38), and acids will degrade as an immediate carbon source for fungal growth (12).

After fermentation of *P. sajor-caju*, components such as geraniol, linalool, benzaldehyde, β-damascone, and methyl salicylate were significantly increased, imparting floral, fruity,

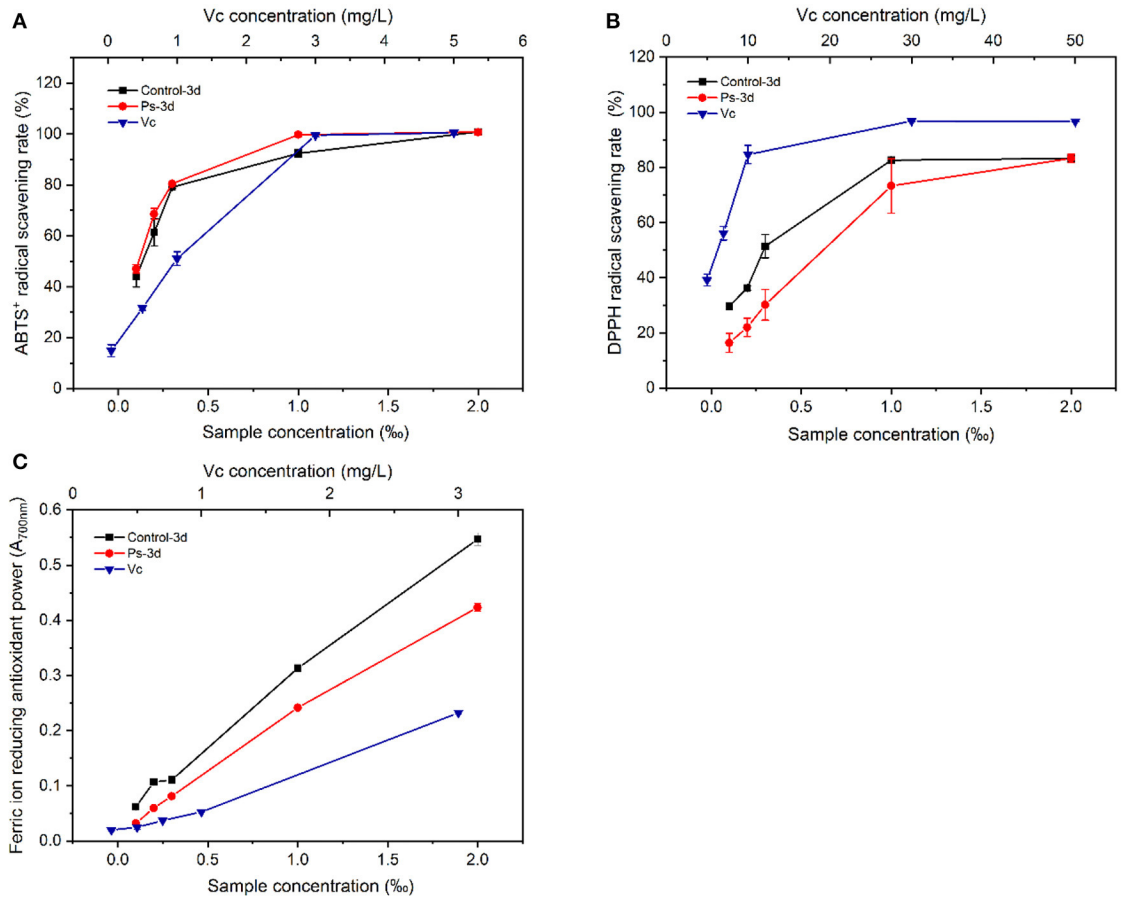

FIGURE 6 | Comparison of antioxidant activity between unfermented green tea infusion and the tea infusion fermented by *Pleurotus sajor-caju* [**(A)** ABTS; **(B)** DPPH; **(C)** FRAP; ferric ion-reducing antioxidant power].

honey-like scent, and have long been recognized as important contributors to the flavor and aroma of various kinds of tea. Among them, geraniol, linalool, and (*Z*)-3-hexen-o-l increased by 9.3, 11.3, and 4.6 times, respectively. Therefore, the strong floral, fruity, and sweetish scents in the after-fermentation infusion were largely improved, which was documented similar to the odor impression as sniffed in fermented green tea infusion (10, 44). Nevertheless, no detailed information regarding the biosynthesis of the odorants in *P. sajor-caju* has been reported so far. Geraniol can be obtained by decomposition of carotenoids; also, geraniol, linalool, and methyl salicylate can also be obtained by enzymatic hydrolysis of the corresponding glycosides. Studies have shown that an increase in linalool, geraniol, (*Z*)-3-hexen-1-ol, and methyl salicylate is related to the effect of β-glucosidase (30). Among the extracellular enzymes produced by *P. sajor-caju*, β-glucosidase activity is high (45–47), and similar results were observed in this study (**Supplementary Figure S1**). This shows that β-glucosidase can promote the accumulation of the above four substances. Benzaldehyde, as one of the characteristic volatiles of black tea, has an intense nutty scent. Its content increases significantly in the green tea infusion fermenting process, which can be formed by phenylalanine pathway and liberated from glycosidic precursors. Moreover, β-damassterone is a major aroma constituent in green tea, and its content is detected to increase significantly, which may be due to the enzymatic and nonenzymatic degradation of carotenoids, as well as liberation from glycosidic precursors. Further enzymatic cleavage of glycosides and the degradation of carotenoids by *P. sajor-caju* may be the reasons for the increase in β-damassterone concentration during fermentation. Nevertheless, the concentration of β-ionone, which is another kind of carotenoid cleavage product, decreased with fermentation. One reason could be the enzyme system of *P. sajor-caju* preferring the catabolic pathway of carotenoids toward β-damassterone rather than β-ionone. The production of β-damassterone consumes a large amount of β-carotene, which hinders the production of β-ionone (14, 42, 48). Another reason may be no β-ionone glycosides in the tea infusion after it was fermented by *P. sajor-caju*. β-Ionone was oxidized to dihydroactinidiolide by enzymes during fermentation. There

are two possible reasons for the formation of this secondary oxidation product, i.e., one is directly generated by secondary enzymatic oxidations from carotenoid precursors, and the other is due to the further oxidation of β-ionone, which may also be the reason for the disappearance of β-ionone after fermentation.

In particular, we also observed that (*R*)-citronellol, methyl salicylate, and 2,5-dimethylpyrazine were newly generated during fermentation. It was reported by Baebara et al. that (*R*)-citronellol could attenuate caffeine bitterness (49). It is worth noting that the (*R*)-citronellol that was newly formed in fermentation may have improved the flavor of tea infusion. 2,5-Dimethylpyrazine is derived from Maillard-type reactions, imparting an intensely roasted, nutty, cocoa-like, chocolate-like scent (35), which was newly formed in fermentation. Marina et al. first highlighted the contribution of vitamin B1 and sodium acetate to the formation of 2,5-dimethylpyrazine during the enokitake fermentation (11). However, further investigations on the formation mechanism of the 2,5-dimethylpyrazine in *P. sajor-caju* are warranted. Methyl salicylate is present only in teas with a fermentation degree of at least semi-fermented, and it cannot be detected in unfermented teas and lightly fermented teas (34), while green tea is unfermented tea without methyl salicylate. It means that methyl salicylate is produced by fermented tea infusion of *P. sajor-caju*. Indole is often accompanied by a spicy pungent odor in green tea, while low-concentration indole presents an aromatic odor. The indole in the experimental group shows a downward trend, which is more conducive to the presentation of a pleasant odor.

To clarify the causes of the abovementioned changes in antioxidant activity (**Figure 5** and **Table 2**), we carried out the LC-MS analysis on the tea infusion in the process of fermentation, and the results showed that a total of 21 peaks were obtained. Compared with the control group, nine peaks were significantly reduced after fermentation. Then, compared with the MassBank database (http://www.massbank.jp/Search) with *m*/*z*, it was found that catechins, including EC, EGCG, ECG, and procyanidin B1, were significantly reduced in the fermented tea infusion. Tea polyphenols with catechins as the key contributor of antioxidant activity are astringent, bitter, and water-soluble compounds. These substances not only reduce the antioxidant capacity of fermented tea but also lead to the decrease in bitterness and astringency of tea (10, 23). This is mainly due to the oxidation of polyphenol oxidase and peroxidase produced in the fermentation of *P. sajor-caju*. After the action of these two enzymes, catechin will be converted into catechin monoquinone, and these quinones or monomers of quinones and catechin will be coupled and polymerized to form catechin polymers, such as theaflavins, thearubins, and tan (50). In this study, it was observed that the activities of these two enzymes gradually increased during the fermentation ($p < 0.01$) (**Supplementary Figure S2**), and the color of the tea infusion deepened (**Supplementary Figure S3**), which also confirmed the occurrence of the oxidation process. Furthermore, we found that EGCG containing a pyrogallol-type B-ring declined the most during the fermentation, possibly due to the fact that fungal enzymes might prefer to degrade the pyrogallol-type B ring for degradation, which is similar to the study by Zhang et al. (10).

At present, many previous works indicated that anthocyanins exhibit a good antioxidant activity (51, 52). It is a glycoside derivative, and its reduction may be related to the role of glycosidase, which further reduces the resistance of antioxidant activity. Furthermore, glycoside precursors were found from several components identified, and their reduction is inseparable from the role of glycosidases. *P. sajor-caju* can produce glycosidases to decompose glycosides to release aromatic substances and enhance the sense quality of green tea. Compared with the control group, the ABTS-free radical-scavenging ability was improved to a certain extent after fermentation with the *P. sajor-caju*, and the DPPH-free radical-scavenging power as well as the ferric-reducing antioxidant power had less loss of antioxidant activity. From the results of LC-MS, it can be found that catechins and anthocyanins with antioxidant activity declined significantly, whereas the contents of theaflavins, thearubins (53–55), and volatile components such as linalool and geraniol (56–58), which also have an antioxidant activity, were increased. Based on the findings of this study, these substances may affect the antioxidant activity and need to be further investigated.

CONCLUSION

Green tea infusion usually has distinct astringency, bitter taste, and typical green flavor as a consequence of its post-harvest treatment without withering and enzymatic oxidation. In this study, the innovative approach driven by edible mushroom *P. sajor-caju* has achieved promising potential to manipulate the green tea flavor during the fermentation process. Herbal and grass odorants produced by green-like (*Z*)-2-penten-1-ol and methyl heptadienone were decreased significantly as a result of the fermentation with *P. sajor-caju* mycelium ($p < 0.01$). In contrast, the contents of linalool and geraniol infusion were increased 9.3 and 11.3 times, respectively, whereas methyl salicylate newly produced during this process augmented pleasant flower and fruit flavors. Moreover, polyphenol profile performed by HLPC-MS revealed that the contents of most polyphenols in green tea infusion declined markedly. Due to the noticeable reduction of catechins and anthocyanins in fermented green tea infusion, the astringency and bitterness were significantly improved. There was an obvious decrease in antioxidant activity, especially the DPPH-free radical-scavenging ability and the ferric-reducing power. It is noteworthy that the ABTS-free radical-scavenging ability of green tea infusion was improved by *P. sajor-caju* fermentation to a certain extent, indicating that the increased tea pigments and volatile metabolites after fermentation with *P. sajor-caju* may contribute to the antioxidant capacity of green tea infusion. Based on the findings of this study, further studies on the *in vivo*

antioxidant activity of flavor compounds in animal experiments are required.

DATA AVAILABILITY STATEMENT

The original contributions presented in the study are included in the article/**Supplementary Material**, further inquiries can be directed to the corresponding author/s.

AUTHOR CONTRIBUTIONS

W-YS: conceptualization, methodology, investigation, and writing—original draft. S-YG: validation, investigation, formal analysis, and writing—original draft. S-JZ: writing—original draft and visualization. QW: methodology and validation. G-MC, J-ZH, X-CL, and P-FR : validation, writing—review and editing and supervision. LN: methodology, validation, writing—review and editing, supervision, and project administration. All authors contributed to the article and approved the submitted version.

FUNDING

This study was financially supported by the National Natural Science Foundation of China, Science Foundation of Two Sides of Strait (No. U2005209).

SUPPLEMENTARY MATERIAL

The Supplementary Material for this article can be found online at: https://www.frontiersin.org/articles/10.3389/fnut.2022.865991/full#supplementary-material

REFERENCES

1. Zhao C, Tang G, Cao S, Xu X, Gan R, Liu Q et al. Phenolic profiles and antioxidant activities of 30 tea infusions from green, black, oolong, white, yellow and dark Teas. *Antioxidants.* (2019) 8:215–29. doi: 10.3390/antiox8070215
2. Han ZX, Rana MM, Liu GF, Gao MJ Li DX, Wu FG. et al. Green tea flavour determinants and their changes over manufacturing processes. *Food Chem.* (2016) 212:739–48. doi: 10.1016/j.foodchem.2016.06.049
3. Filippis FD, Troise AD, Vitaglione P, Ercolini D. Different temperatures select distinctive acetic acid bacteria species and promotes organic acids production during Kombucha tea fermentation. *Food Microbiol.* (2018) 73:11–6. doi: 10.1016/j.fm.2018.01.008
4. Zhao D, Shah NP. Antiradical and tea polyphenol-stabilizing ability of functional fermented soymilk–tea beverage. *Food Chem.* (2014) 158:262–9. doi: 10.1016/j.foodchem.2014.02.119
5. Marsh AJ, O'Sullivan O, Hill C, Ross RP, Cotter PD. Sequence-based analysis of the bacterial and fungal compositions of multiple kombucha (tea fungus) sample. *Food Microbiol.* (2014) 38:171–8. doi: 10.1016/j.fm.2013.09.003
6. Jiang C, Zeng Z, Huang Y, Zhang X. Chemical compositions of Pu'er tea fermented by Eurotium Cristatum and their lipid-lowering activity. *Food Sci Technol.* (2018) 98:204–11. doi: 10.1016/j.lwt.2018.08.007
7. Wang L, Luo Y, Wu Y, Liu Y, Wu Z. Fermentation and complex enzyme hydrolysis for improving the total soluble phenolic contents, flavonoid aglycones contents and bio-activities of guava leaves tea. *Food Chem.* (2018) 264:189–98. doi: 10.1016/j.foodchem.2018.05.035
8. Wang Y, Zhang M, Zhang Z, Lu H, Gao X, Yue P. High-theabrownins instant dark tea product by *Aspergillus niger* via submerged fermentation α-glucosidase and pancreatic lipase inhibition and antioxidant activity. *J Sci Food Agric.* (2017) 97:5100–6. doi: 10.1002/jsfa.8387
9. Sun T, Li J, Chen C. Effects of blending wheatgrass juice on enhancing phenolic compounds and antioxidant activities of traditional kombucha beverage. *J food Drug Anal.* (2015) 23:709–18. doi: 10.1016/j.jfda.2015.01.009
10. Rigling M, Liu Z, Hofele M, Prozmann J, Zhang C, Ni L et al. Aroma and catechin profile and in vitro antioxidant activity of green tea infusion as affected by submerged fermentation with Wolfiporia cocos (Fu Ling). *Food Chemistry.* (2021) 361:130065. doi: 10.1016/j.foodchem.2021.130065
11. Rigling M, Yadav M, Yagishita M, Nedele AK, Sun J. Biosynthesis of pleasant aroma by enokitake (*Flammulina velutipes*) with a potential use in a novel tea drink. *LWT Food Sci Technol.* (2021) 140:110646. doi: 10.1016/j.lwt.2020.110646
12. Zhang Y, Fraatz MA, Horlamus F, Quitmann H, Zorn H. Identification of potent odorants in a novel nonalcoholic beverage produced by fermentation of *Wort* with *Shiitake* (*Lentinula edodes*). *J Agric Food Chem.* (2014) 62:4195–203. doi: 10.1021/jf5005463
13. Okamura-Matsui T, Tomoda T, Fukuda S, Ohsugi M. Discovery of alcohol dehydrogenase from mushrooms and application to alcoholic beverages. *J Mol Catal B Enzym.* (2003) 23:133–44. doi: 10.1016/S1381-1177(03)00079-1
14. Bai W, Guo X, Ma L, Guo L, Lin J. Chemical composition and sensory evaluation of fermented tea with medicinal mushrooms. *J Microbiol.* (2013) 53:70–6. doi: 10.1007/s12088-012-0345-0
15. Marzban F, Azizi G, Afraei S, Sedaghat R, Seyedzadeh MH, Razavi A et al. Kombucha tea ameliorates experimental autoimmune encephalomyelitis in mouse model of multiple sclerosis. *Food Agric Immunol.* (2015) 26:782–93. doi: 10.1080/09540105.2015.1036353
16. Yu K, Lee J. The pharmacological activity of coffee fermented using *Monascus purpureus* mycelium solid-state culture depends on the cultivation area and green coffees variety. *Korean J Food Sci Technol.* (2014) 46:79–86. doi: 10.9721/KJFST.2014.46.1.79
17. Yang Z, Baldermann S, Watanabe N. Recent studies of the volatile compounds in tea. *Food Res Int.* (2013) 53:585–99. doi: 10.1016/j.foodres.2013.02.011
18. Zhang Y, Fraatz MA, Müller J, Schmitz H, Birk F, Schrenk D et al. Aroma characterization and safety assessment of a beverage fermented by *Trametes versicolor*. *J Agri Food Chem.* (2015) 63:6915–21. doi: 10.1021/acs.jafc.5b02167
19. Finimundy TC, Barros L, Ricardo CC, Maria JA, Miguel AP, Rui MV, et al. Multifunctions of *Pleurotus sajor-caju* (Fr) Singer: a highly nutritious food and a source for bioactive compounds. *Food Chemistry.* (2018) 245:150–8. doi: 10.1016/j.foodchem.2017.10.088
20. Mohammadhosseini M, Venditti A. Akbarzadeh A. Toxin reviews the genus perovskia kar: ethnobotany, chemotaxonomy and phytochemistry: a review The genus Perovskia Kar: ethnobotany, chemotaxonomy and phytochemistry: a review. *Toxin Rev.* (2019) 40:484–505. doi: 10.1080/15569543.2019.1691013
21. David S, Blaise B, Bruce CV, Campbell MBBS, Jeffrey S, Carpenter MD. Multisociety consensus quality improvement revised consensus statement for endovascular therapy of acute ischemic stroke. *Int J Stroke.* (2018) 13:612–32. doi: 10.1177/1747493018778713
22. Usami A, Nakaya S, Nakahashi H, Miyazawa M. Chemical composition and aroma evaluation of volatile oils from edible mushrooms (*Pleurotus salmoneostramineus and Pleurotus sajor-caju*). *J Oleo Sci.* (2014) 63:1323–32. doi: 10.5650/jos.ess14147
23. Liu Z, Marieke ME, Bruijna WJ, Vincken JP, A. comparison of the phenolic composition of old and young tea leaves__reveals a decrease in flavanols and phenolic acids and an increase in flavonols upon tea leaf maturation. *J Food Compos Anal.* (2020) 86:1–9. doi: 10.1016/j.jfca.2019.103385
24. Liu ZB, Chen Q, Zhang C, Ni L. Comparative study of the anti-obesity and gut microbiota modulation effects of green tea phenolics and their oxidation products in high-fat-induced obese mice. *Food Chem.* (2022) 367:130735. doi: 10.1016/j.foodchem.2021.130735
25. Fang X, Dong Y, Xie Y, Wang L, Wang J, Liu Y et al. Effects of β-glucosidase and α-rhamnosidase on the contents of flavonoids, ginkgolides,

and aroma components in ginkgo tea drink. *Molecules.* (2019) 24:2009. doi: 10.3390/molecules24102009
26. Ozturk B, Seyhan F, Ozdemir IS, Karadeniz B, Bahar B, Ertas E et al. Change of enzyme activity and quality during the processing of Turkish green tea. *LWT Food Sci Technol.* (2016) 65:318–24. doi: 10.1016/j.lwt.2015.07.068
27. Quevedo-Hidalgo B, Narvaéz-Rincón PC, Pedroza-Rodríguez AM, Velásquez-Lozano ME. Degradation of *Chrysanthemum* (*Dendranthema grandiflora*) wastes by *Pleurotus ostreatus* for the production of reducing sugars. *Biotechnol Bioprocess Eng.* (2012) 17:1103–12. doi: 10.1007/s12257-012-0227-7
28. Sánchez C. Cultivation of *Pleurotus ostreatus* and other edible mushrooms. *Appl Microbiol Biotechnol.* (2010) 85:1321–37. doi: 10.1007/s00253-009-2343-7
29. Zhang S, Yang C, Idehen E, Shi L, Lv L, Sang S. Novel theaflavin type chlorogenic acid derivatives identified in black tea. *J Agric Food Chem.* (2018) 66:3402–7. doi: 10.1021/acs.jafc.7b06044
30. Zhu YB, Zhang ZZ, Yang YF, Du XP, Chen F, Ni H. Analysis of the aroma change of instant green tea induced by the treatment with enzymes from *Aspergillus niger* prepared by using tea stalk and potato dextrose medium. *Flavour Fragr J.* (2017) 32:451460. doi: 10.1002/ffj.3402
31. Mohammadhosseini M, Akbarzadeh A, Flamini G. Profiling of compositions of essential oils and volatiles of salvia limbata using traditional and advanced techniques and evaluation for biological activities of their extracts. *Chem Biodivers.* (2017) 14:1–19. doi: 10.1002/cbdv.201600361
32. Mohammadhosseini M. Chemical composition of the volatile fractions from flowers, leaves and stems of salvia mirzayanii by HS-SPME-GC-MS. *J Essent Oil Bearing Plants.* (2015) 18:464–76. doi: 10.1080/0972060X.2014.100118
33. Wang C, He L, Chen F, Zhang C, Zhang W, Liu Z et al. Volatile aroma components of Wuyi Rock tea and their release pattern under multiple times of boiling water infusing. *J Chin Inst Food Sci Technol.* (2018) 18:309–18. doi: 10.16429/j.1009-7848.2018.12.038
34. Wang L, Lee J, Chung J, Baik J, So S, Park S. Discrimination of teas with different degrees of fermentation by SPME–GC analysis of the characteristic volatile flavour compounds. *Food Chem.* (2008) 109:196–206. doi: 10.1016/j.foodchem.2007.12.054
35. Liu Z, Chen F, Sun J, Ni L. Dynamic changes of volatile and phenolic components during the whole manufacturing process of Wuyi Rock tea (Rougui). *Food Chem.* (2022) 367:130624. doi: 10.1016/j.foodchem.2021.130624
36. López-Cobo A, Gómez-Caravaca AM. Švarc-Gajic' J, Antonio Segura-Carretero. Determination of phenolic compounds and antioxidant activity of a Mediterranean plant: the case of *Satureja montana* subsp kitaibelii. *J Funct Foods.* (2015) 18:1167–78. doi: 10.1016/j.jff.2014.10.023
37. Li Z, Xue Y, Li M, Guo Q, Sang Y, Wang C. et al. The antioxidation of different fractions of dill (*Anethum graveolens*) and their influences on cytokines in macrophages RAW2647. *J Oleo Sci.* (2018) 67:1535–41. doi: 10.5650/jos.ess18134
38. Noordermeer MA, Veldink GA, Vliegenthart JFG. Fatty Acid Hydroperoxide Lyase: A plant cytochrome P450 enzyme involved in wound healing and pest resistance. *Chembiochem.* (2001) 2:494–504. doi: 10.1002/1439-7633(20010803)2:7/8<494::AID-CBIC494>3.0.CO;2-1
39. Liao X, Yana J, Wang B, Meng Q, Zhang L, Tong H. Identification of key odorants responsible for cooked corn-like aroma of green teas made by tea cultivar '*Zhonghuang 1*'. *Food Res Int.* (2020) 136:109355. doi: 10.1016/j.foodres.2020.109355
40. Flaig M, Sally Q. Guo w, Yang X, Schieberle P. Characterization of the key odorants in a high-grade chinese green tea beverage (Camellia sinensis; Jingshan cha) by means of the sensomics approach and elucidation of odorant changes in tea leaves caused by the tea manufacturing process *J Agri Food Chem.* (2020) 68:5168–79. doi: 10.1021/acs.jafc.0c01300
41. Joshi B, Gulati A. Fractionation and identification of minor and aroma-active constituents in Kangra orthodox black tea. *Food Chem.* (2015) 167:290–8. doi: 10.1016/j.foodchem.2014.06.112
42. Lewinsohn E, Sitrit Y, Bar E, Azulay Y, Meir A, Zamir D et al. Carotenoid pigmentation affects the volatile composition of tomato and watermelon fruits, as revealed by comparative genetic analyses. *J Agric Food Chem.* (2005) 53:3142–8. doi: 10.1021/jf047927t
43. Hirata H, Ohnishi T, Ishida H, Tomida K, Sakai M, Hara M et al. Functional characterization of aromatic amino acid aminotransferase involved in 2-phenylethanol biosynthesis in isolated rose petal protoplasts. *J Plant Physiol.* (2012) 169:444–51. doi: 10.1016/j.jplph.2011.12.005
44. Zheng X, Li Q, Xiang L, Liang Y. Recent advances in volatiles of teas. *Molecules.* (2016) 21:130624. doi: 10.3390/molecules21030338
45. Khalil MI, Hoque MM, Basunia MA, Alam N, Khan MA. Production of cellulase by *Pleurotus ostreatus* and *Pleurotus sajor-caju* in solid state fermentation of lignocellulosic biomass. *Turk J Agric Forestry.* (2011) 35:333–41. doi: 10.3906/tar-1002-684
46. Nakajima VM, Soares FEDF, Queiroz JHD. Screening and decolorizing potential of enzymes from spent mushroom composts of six different mushrooms. *Biocatalysis Agricult Botechnol.* (2018) 13:58–61. doi: 10.1016/j.bcab.2017.11.011
47. Valášková V, Baldrian P. Estimation of bound and free fractions of lignocellulose-degrading enzymes of wood-rotting fungi *Pleurotus ostreatus*, *Trametes versicolor* and *Piptoporus betulinus*. *Res Microbiol.* (2006) 152:119–24. doi: 10.1016/j.resmic.2005.06.004
48. Song L, Ma Q, Zou Z, Sun K, Yao Y, Tao J et al. Molecular link between leaf coloration and gene expression of flavonoid and carotenoid biosynthesis in *Camellia sinensis* Cultivar 'Huangjinya'. *Front Plant Sci.* (2017) 8:803. doi: 10.3389/fpls.2017.00803
49. Suess B, Brockhoff A, Meyerhof W, Hofmann T. The odorant (*R*)-Citronellal attenuates caffeine bitterness by Inhibiting the Bitter Receptors TAS2R43 and TAS2R46. *J Agric Food Chem.* (2018) 66:2301–11. doi: 10.1021/acs.jafc.6b03554
50. Li S, Lo C, Pan M, Lai C, Ho C. Black tea: chemical analysis and stability. *Food Funct.* (2013) 4:10–8. doi: 10.1039/c2fo30093a
51. Koh J, Xu Z, Wicker L. Blueberry pectin and increased anthocyanins stability under in vitro digestion. *Food Chem.* (2020) 302:125343. doi: 10.1016/j.foodchem.2019.125343
52. Wu Y, Zhou Q, Chen X, Li X, Wang Y, Zhang J. Comparison and screening of bioactive phenolic compounds in different blueberry cultivars Evaluation of antioxidation and α-glucosidase inhibition effect. *Food Res Int.* (2017) 100:312–24. doi: 10.1016/j.foodres.2017.07.004
53. Kusano R, Matsuo Y, Saito Y, Tanaka T. Oxidation mechanism of black tea pigment theaflavin by peroxidase. *Tetrahedron Lett.* (2015) 56:5099–102. doi: 10.1016/j.tetlet.2015.07.037
54. Luczaj W, Skrzydlewska E. Antioxidative properties of black tea. *Prevent Med.* (2005) 40:910–8. doi: 10.1016/j.ypmed.2004.10.014
55. Yang Z, Tu Y, Xia H, Jie G, Chen X, He P. Suppression of free-radicals and protection against H[[sb]]2[[/s]]O[[sb]]2[[/s]]-induced oxidative damage in HPF-1 cell by oxidized phenolic compounds present in black tea. *Food Chem.* (2007) 105:1349–56. doi: 10.1016/j.foodchem.2007.05.006
56. Lee S, Umano K, Shibamoto T. Lee K. Identification of volatile components in basil (*Ocimum basilicum* L)__and thyme leaves (*Thymus vulgaris* L) and their antioxidant properties. *Food Chem.* (2005) 91:131–7. doi: 10.1016/j.foodchem.2004.05.056
57. Li Y, Kawasaki Y, Tomita I, Kawai K. Antioxidant properties of green tea aroma in mice. *J Clin Biochem Nutr.* (2017) 61:14–7. doi: 10.3164/jcbn.1680
58. Wang T, Xi M, Guo Q, Wang L. Shen Z. Chemical components and antioxidant activity of volatile oil of a Compositae tea (*Coreopsis tinctoria Nutt*) from Mt Kunlun. *Indus Crops Prod.* (2015) 67:318–24. doi: 10.1016/j.indcrop.2015.01.043

Conflict of Interest: The authors declare that the research was conducted in the absence of any commercial or financial relationships that could be construed as a potential conflict of interest.

Publisher's Note: All claims expressed in this article are solely those of the authors and do not necessarily represent those of their affiliated organizations, or those of the publisher, the editors and the reviewers. Any product that may be evaluated in

this article, or claim that may be made by its manufacturer, is not guaranteed or endorsed by the publisher.

frontiers | Frontiers in Nutrition

ORIGINAL RESEARCH
published: 12 May 2022
doi: 10.3389/fnut.2022.899421

The Methanol Extract of *Polygonatum odoratum* Ameliorates Colitis by Improving Intestinal Short-Chain Fatty Acids and Gas Production to Regulate Microbiota Dysbiosis in Mice

Xuewei Ye[1,2†], Xionge Pi[3†], Wenxin Zheng[2†], Yingxin Cen[2], Jiahui Ni[2], Langyu Xu[2], Kefei Wu[2], Wei Liu[3] and Lanjuan Li[1*]*

[1] State Key Laboratory for Diagnosis and Treatment of Infectious Diseases, Collaborative Innovation Center for Diagnosis and Treatment of Infectious Diseases, Zhejiang University, Hangzhou, China, [2] Key Laboratory of Pollution Exposure and Health Intervention of Zhejiang Province, Department of Basic Medical Sciences, Shulan International Medical College, Zhejiang Shuren University, Hangzhou, China, [3] Institute of Plant Protection and Microbiology, Zhejiang Academy of Agricultural Sciences, Hangzhou, China

The potential impacts of methanol extract from *Polygonatum odoratum* on (YZM) colonic histopathology, gut gas production, short-chain fatty acids (SCFAs), and intestinal microbiota composition were evaluated with dextran sulfate sodium (DSS)-induced colitis mice in this study. These results indicated that YZM increased colon length and ameliorated colonic histopathology in DSS-induced colitis mice. Moreover, YZM administration reversed intestinal microbiota compositions leading to the inhibition of H_2S-related bacteria (e.g., *Desulfovibrionaceae*) and the lower level of H_2S and higher contents of SCFA-related bacteria (e.g., *Muribaculaceae*). Taken together, the effects of methanol extract from *Polygonatum odoratum* are studied to provide new enlightenment and clues for its application as a functional food and clinical drug. Our study first revealed the relationship between intestinal gas production and key bacteria in ulcerative colitis.

Keywords: ***Polygonatum odoratum*, DSS-induced colitis mice, gas production, SCFAs, microbiota**

OPEN ACCESS

Edited by:
Xiaolong Ji,
Zhengzhou University of Light Industry, China

Reviewed by:
Hongshun Yang,
National University of Singapore, Singapore
Syed Shams Ul Hassan,
Shanghai Jiao Tong University, China
Xiufang Hu,
Zhejiang Sci-Tech University, China

****Correspondence:***
Wei Liu
biolwei@sina.com
Lanjuan Li
ljli@zju.edu.cn

† These authors have contributed equally to this work

Specialty section:
This article was submitted to Food Chemistry, a section of the journal Frontiers in Nutrition

Received: *18 March 2022*
Accepted: *12 April 2022*
Published: *12 May 2022*

Citation:
Ye X, Pi X, Zheng W, Cen Y, Ni J, Xu L, Wu K, Liu W and Li L (2022) The Methanol Extract of Polygonatum odoratum Ameliorates Colitis by Improving Intestinal Short-Chain Fatty Acids and Gas Production to Regulate Microbiota Dysbiosis in Mice. Front. Nutr. 9:899421. doi: 10.3389/fnut.2022.899421

INTRODUCTION

Inflammatory bowel disease (IBD) is a relapsing non-specificity inflammatory condition that results from a chronic disorder of the gastrointestinal mucosa immunity system, including Ulcerative colitis (UC) and Crohn's disease (CD) (1). Recent investigations indicate that the prevalence rate of IBD has also increased sharply, especially among younger people. Typical clinical manifestations of IBD include abdominalgia, enterorrhagia, hematochezia weight loss, and recurrence due to inflammatory cell infiltration. Some studies have found that the causes of UC include pathogenic microorganism infection, genetic susceptibility, intestinal microbiome imbalance, and intestinal mucosal barrier defect. However, at present, the pathological mechanism is not clear. The current clinical treatments (sulfasalazine and mesalazine) are mainly to relieve the symptoms of the disease

but accompany adverse impacts (2). Thus, developing a safe and high efficacy treatment to remiss IBD is urgently required.

The intestinal mucosal barrier prevents disease-causing substances and bacteria from entering the bloodstream. The microbial barrier composed of a large number of microbial colonies is crucial in the development of IBD. Extensive research has suggested that changes in colon microflora composition caused by an abnormal increase in pathogenetic bacteria or deficiency of probiotics are associated with IBD. Accompanied by intestinal microbiota disturbance, the alteration of metabolites such as short-chain fatty acids (SCFAs) and gas affect colitis's progression, which is intimately related to colon cancer (3). Although the exact mechanisms related to microorganisms remain to be elucidated, emerging evidence suggests that various natural substances contribute significantly to the improvement of IBD by regulating gut microbiota (4).

Dietary intake is closely associated with the pathogenesis and prevention of IBD without adverse influence (5). The interaction between dietary nutrients and intestinal immunity is very complex, referring to the immune response and the regulation of intestinal microflora composition (6). Ingested natural nutrients can accumulate and interact with intestinal microbiota (7, 8). As the sole input resource for intestinal microbiota, dietary intake has a significant impact on the intestinal microbiome composition (9, 10). Therefore, natural nutrients, which are characterized by low toxicity, multiple components, and targets, play an important role in potentially maintaining microbial homeostasis in patients with IBD with long-term use.

Polygonatum odoratum (Mill.) Druce (YZ) is a perennial herbaceous plant in the Liliaceae family that is widespread in East Asia and Europe. The root of YZ is a sweet and light food, and it is also traditional Chinese medicine that can relieve intestinal problems (11). YZ contains a variety of active substances, namely, flavonoids, terpenoids, phenols, coumarin alkaloids, and organic acids (12). Flavonoids, as an antioxidant, can delay aging, inhibit viral activity, inhibit bacterial reproduction, prevent cancer, and enhance the immune system. In addition, flavonoids are considered a functional factor in healthy foods. Resveratrol, a polyphenol, has a protective effect on acute or chronic colitis in different models, downregulating inflammatory biomarkers and reducing clinical symptoms (13).

Methanol extract of *Polygonatum odoratum* (YZM) was prepared to elucidate its protective effect on UC and further explore its related mechanism in our research. We assessed the impacts of YZM on body weight, colon length, colon lesion degree, intestinal microbiota composition, and metabolites of DSS-induced colitis mice. Our investigation provides insights into the influence of YZM on colitis related to the interactions of microbiota and metabolites. This evidence could support the new therapeutic and preventive avenues for IBD.

MATERIALS AND METHODS

Preparation of the YZM

Polygonatum odoratum was derived from Bozhou Zhongyitang Traditional Chinese Medicine Sales Co., Ltd. The crushed medicinal materials were extracted with methanol at room temperature and repeated three times. The extracts were concentrated and named YZM (yield 20%), the methanol extract from *Polygonatum odoratum*. YZM was dried under vacuum conditions (decompress distillation and vacuum desiccation) for biological tests and stored at 4°C.

Compositions Analysis of YZM

Orbitrap MS (Thermo Fisher Scientific, United States) with the ACQUITY UPLC® HSS T3 (150 mm × 2.1 mm, 1.8 μm, Waters) column was applied for UHPLC-MS analyses. The mobile phase flow rate was 0.25 ml/min; solvent A was composed of 0.1% formic acid in the water, and solvent B was composed of 0.1% formic acid in acetonitrile. The elution condition was as follows: 2% B for 1 min, 2–50% B for 8 min, 50–98% B for 4 min, 98% B for 1.5 min, 98–2% B for 1.5 min, and 2% B for 6 min. The electrospray ionization mass spectrometry (ESI-MS) setting was as follows: positive mode (3.5 kV), negative mode (−2.5 kV), auxiliary gas at 30 units, capillary temperature at 325°C (14, 15). The mass spectra were scanned at a resolution of 60,000 from 100 to 1,000 m/z.

Design of Experiments

Male BABL/c mice (6–8 week old, specific pathogen-free grade, 20 ± 2 g, n = 30) were purchased from the Zhejiang Academy of Medical Science and raised at the Zhejiang Academy of Agricultural Sciences. Mice were subjected to an artificial LED light cycle (12-h light/12-h dark) and ambient temperature (24–26°C) indoors. Mice were free to intake standard food and water for 2 weeks under laboratory conditions. The mice were randomly divided into five groups: a control group treated with phosphate-buffered saline (PBS), a model group treated with PBS, a positive control group treated with salicylazosulfapyridine (SASP, 50 mg/kg), a YZM-L group treated with a low concentration of YZM (YZM-L, 200 mg/kg), and a YZM-H group treated with a high concentration of YZM (YZM-H, 400 mg/kg). All drugs were administered by intragastric administration. The control group supplied sterile water. The other groups were supplied with 3% DSS solution for 8 days to induce colitis. All mice were sacrificed on day 9.

Evaluation of Disease Activity Index Score

The disease activity index (DAI) score is a common index to assess the colitis severity of mice. All mice were evaluated for weight loss, stool character, and fecal occult blood. The

TABLE 1 | Criteria for DAI.

DAI score	Weight loss	Dropping consistency	Occult/blood bleeding
0	None	Normal	Normal
1	1–5		
2	5–10	Loose droppings	Occult blood positive
3	10–20		
4	>20	Diarrhea	Blood bleeding

average of these scores was assigned according to DAI criteria (**Table 1**) (5).

Evaluation of Colonic Pathological Changes

Fresh colon tissues were fixed in 4% buffered paraformaldehyde for 48 h and then embedded in paraffin. After stained with hematoxylin–eosin (H&E), photomicrographs were obtained using a microscope for histological examination and histopathological score (**Table 2**) on 4-μm-thick sections (16).

Fermentation With Mice Fecal

Fresh fecal samples (0.24 g) were homogenized with 2.4 ml of 0.1 M PBS (pH 7.0). After filtration by 300 mesh filter sieves, the supernatants were transferred into modified medium (17). The recipe for 1 L was as follows: starch, 8 g; yeast extract 4.5 g; tryptone, 6 g; L-cysteine hydrochloride, 0.8 g; bile salt, 0.4 g; hemin, 0.05 g; NaCl, 4.5 g; $MgCl_2 \cdot 6H_2O$, 0.45 g; $CaCl_2 \cdot 6H_2O$,0.2 g; KCl, 2.5 g; KH_2PO_4, 0.4 g; 1 ml of Tween-80 and 2 ml of a solution of trace elements (g/L, $MgSO_4 \cdot 7H_2O$, 3.0; $MnCl_2 \cdot 4H_2O$, 0.32; $FeSO_4 \cdot 7H_2O$, 0.1; $CoSO_4 \cdot 7H_2O$, 0.18;

TABLE 2 | Histological scoring system.

Histological score	Degree of inflammation	Infiltration of inflammatory cells	Degree of damage to the crypt	Crypt abscesses	Degree of submucosal edema	Reduction of goblet cells	Degree of epithelial hyperplasia
0	Normal	Normal	Normal	Normal	Normal	Normal	Normal
1	Mucosa	Unifocal	Basal 1/3 of crypt	Unifocal	Unifocal	Unifocal	Unifocal
2	Submucosa	Multifocal	Basal 2/3 of crypt	Multifocal	Multifocal	Multifocal	Multifocal
3	Muscular	Suffuse	Entire crypt		Suffuse	Suffuse	Suffuse
4	Serous		Damage to the crypt and ulceration				

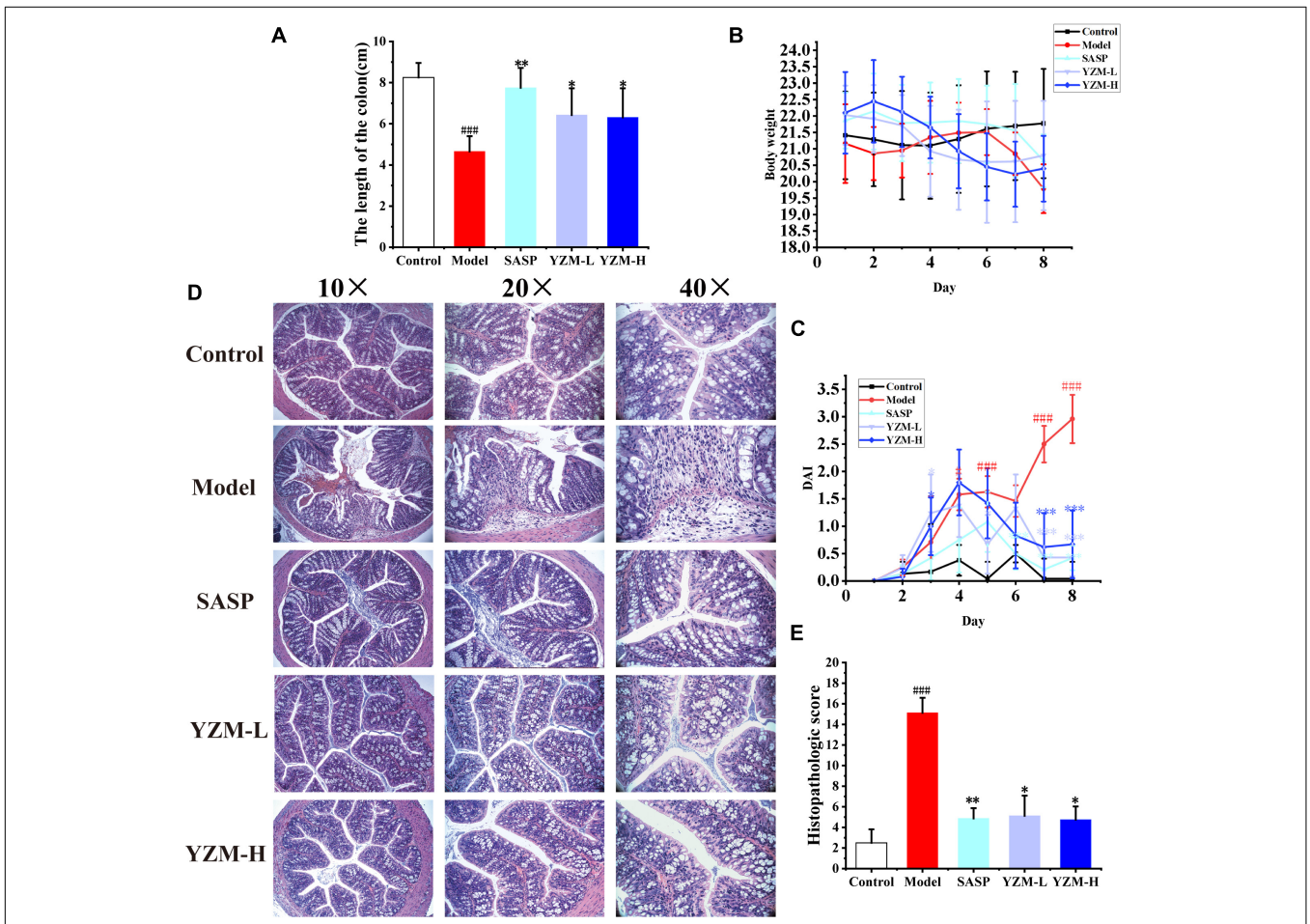

FIGURE 1 | The effect of YZM on colitis mice. **(A)** Analysis of colon length. **(B)** Body weight changes. **(C)** DAI changes. **(D)** Representative images of colon sections. **(E)** Histological score. $^{###}p < 0.001$ vs. control, $^{**}p < 0.01$ vs. model, $^{*}p < 0.05$ vs. model.

$CaCl_2 \cdot 2H_2O$, 0.1; $ZnSO_4 \cdot 7H_2O$, 0.18; $CuSO_4 \cdot 5H_2O$, 0.01; and $NiCl_2 \cdot 6H_2O$, 0.092).

Gas Production

The gas detector measured gas composition after fermentation. Carbon dioxide (CO_2), hydrogen (H_2), methane (CH_4), hydrogen sulfide (H_2S), and ammonia (NH_3) were measured simultaneously after being incubated at 37°C for 24 h (17).

Analysis of Short-Chain Fatty Acids

Gas chromatography (Shimadzu, Japan) with DB-FFAP column (0.32 mm × 30 m × 0.5 μm, Agilent Technologies, United States) was used to quantify the SCFAs. The operation condition was as follows: the flow rate of nitrogen carrier gas: 19.0 ml/min; split ratio: 1:10, the temperature of both detector and injection port: 250°C. Crotonic acid was used as an internal standard (17).

The Intestinal Microbiota Analysis

After the fecal sample's DNA was extracted, and the V3-V4 fragment of the bacterial 16S rDNA gene was amplified with primers (341F/805R). Agilent 2100 Bioanalyzer (Agilent, United States) evaluated the amplicon library. Then, sequencing was performed on the NovaSeq PE250 platform. According to the specific barcode of the sample, the paired-end data were overlapped using the FLASH (v1.2.11). The feature table and sequence, obtained with DADA2 (Divisive Amplicon Denoising Algorithm), were analyzed using QIIME tools (18). Alpha diversity was estimated with the Observed OTUs, Chao 1, Simpson, and Shannon index. Beta diversity was assessed by the Bray–Curtis distance and presented by principal coordinate analysis (PCA) and non-metric multidimensional scaling (NMDS). The differences between groups in taxonomic composition taxa were analyzed using the linear discriminant analysis (LDA) effect size (LEfSe) analysis, and LDA scores > 4 were defined as discriminative taxa. R package (v3.5.2) was utilized to draw diagrams.

Statistical Analysis

Data were reported as means ± SD (n = 6). SPSS 16.0 was conducted to statistically analyze the obtained data. The t-test for unpaired results was used to evaluate differences between two groups. P-value < 0.05 was considered statistically significant. $^{###}p < 0.001$ vs. control, $^{##}p < 0.01$ vs. control, $^{#}p < 0.05$ vs. control; $^{***}p < 0.001$ vs. model, $^{**}p < 0.01$ vs. model, $^{*}p < 0.05$ vs. model.

RESULTS

Identification of Active Components of YZM

A total of fifty-five active compounds were identified through UHPLC-QE-MS, which belonged to the following chemical classes: flavonoids (14), coumarins (8), organic acids (7), phenols (6), terpenoids (4), alkaloids (3), and lactones (3), such as resveratrol, oxyresveratrol, (R)-oxypeucedanin, phloroglucinol, atractylenolide II, neocnidilide maltol, kaempferol, fisetin, isomeranzin, and allocryptopine. The identified active chemical compounds, retention time, experimental mass with positive/negative mode, formula, and class are presented in **Supplementary Table 1**.

YZM Improved the Pathological States of Colitis Mice

Compared to the control group, the model group and drug intervention groups induced with DSS showed significant weight loss, shorter colon length, and decreased stool consistency (**Figure 1** and **Supplementary Figure 1**). The colon length decreased by approximately 43.52, 6.06, 22.06, and 23.52% in the model group, SASP group, YZM-L group, and YZM-H group (**Figure 1A**). The weight loss of YZM-treated mice was recovered from days 5 to 8 (**Figure 1B**). Furthermore, the DAI scores in the SASP and YZM groups were improved (**Figure 1C**).

The structure of the control group was well structured with no damage to the crypt, without prominent inflammatory infiltration. The mucous membrane of the model group was widely absent, and situations of erosion, hyperemia, and edema were observed. Obvious inflammation with considerable lymphocytes infiltrated and gathered between the basal layer and mucosal muscle in the model group. There was edema in the submucosa, and a large number of goblet cells disappeared, showing classic inflammatory changes, and the damaged area of the colon accounted for more than 50% of the entire colon (**Figure 1D**). The histopathological score of the model group was significantly higher than other groups. Compared with the model group, mucosal inflammatory cell infiltration, erosion, and edema in YZM groups (**Figure 1E**) were improved significantly.

YZM Restores the Gut Microbiota and Metabolites

YZM Influenced Gas Production in Fermentation

Intestinal gases produced by the microbiota could take a series of impacts on intestine homeostasis. Gas pressure and composition (CO_2, followed by H_2, H_2S, CH_4, and NH_3) were detected as the indicators of fermentation rate. The pressure increased with the increasing YZM dose (**Figure 2A**), suggesting that YZM stimulated the gas production from bacteria. In **Figure 2B**, CH_4 production of YZM-L was lower than in other groups but increased with the increasing concentration of YZM. The production of NH_3 and H_2S was inhibited in YZM-L and YZM-H groups (**Figures 2C,D**). In addition, H_2 production was inhibited in the YZM-H group (**Figure 2E**). Since CO_2 is the main component of intestinal gas, it shows a similar trend to gas pressure (**Figure 2F**).

YZM Restored the Production of Short-Chain Fatty Acids

Short-chain fatty acids play crucial roles in human microorganism–host interaction and the pathogenetic mechanism of colitis. In fecal samples, we measured the SCFA (acetic, propionic, isobutyric, butyric, valeric acids, and

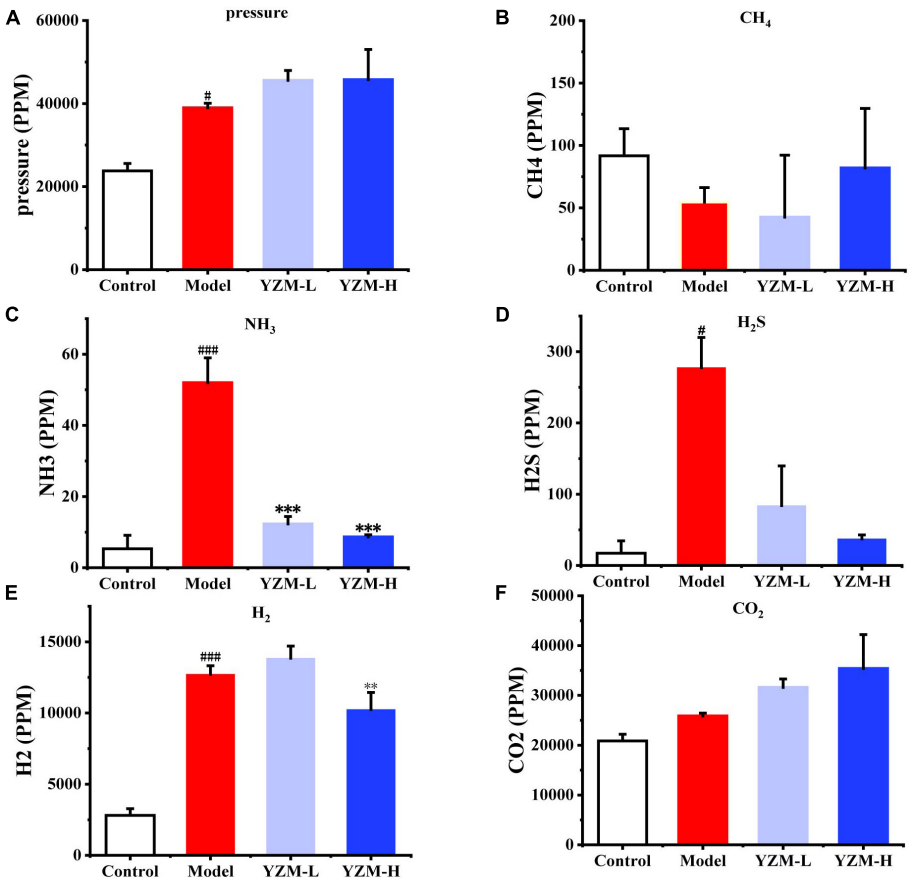

FIGURE 2 | Gas produced by intestinal microbiota. **(A)** The pressure after fermentation. **(B–F)** The abundance of CH_4, NH_3, H_2S, H_2, and CO_2, respectively. $^{###}p < 0.001$ vs control, $^{#}p < 0.05$ vs control; $^{***}p < 0.001$ vs model, $^{**}p < 0.01$ vs model.

isovaleric) level. Compared with the control group, the model group mice showed decreased contents of SCFAs (**Figure 3**). YZM treatment particularly increased the concentrations of acetic and propionic acids (**Figures 3A,B**). The contents of other measured SCFAs displayed similar increasing trends, whereas the changes were not significant in YZM-treated groups (**Figures 3C–F**).

YZM Modulated Intestinal Microbiome Composition

The observed species, Chao 1, Shannon index, and Simpson index of the samples were chosen to represent the alpha diversity of the microbes in the samples (**Table 3**) (19). These indices of YZM groups were higher than that of the model. However, these effects were not significant. These results indicated that the sum of bacterial species in the faces sample of YZM groups was higher than that in the sample of the model, to a certain extent. The microbiota alpha's diversity in the model group was repressed, which was reversed by YZM treatment (**Figures 4A,B**). It was largely improved in observed OTUs and Chao1 indices after the treatment of YZM-H.

Principal coordinate analysis and non-metric multidimensional scaling (NMDS) showed that an apparent clustering division between the control group and model group revealed various differential OTUs (**Figures 4C,D**). Meanwhile, the community structures of the YZM-L group (PCA) and YZM-H (NMDS) were tended to the control group. These results implied that YZM treatment significantly promotes microbial richness.

According to the differences in composition at the phylum level, *Campylobacterota* and *Desulfobacterota* displayed a higher abundance in the model group and a lower abundance of *Actinobacteriota* (**Figure 5A**). The relative abundance of these three taxonomic microbiotas was corrected in SASP and YZM groups (**Figures 5B–D**). The abundance of *Ruminococcus* increased, whereas *Muribaculaceae_unclassified* and *Alloprevotella* decreased in the model group at the genus level (**Figure 5E**). However, YZM-L, YZM-H, and SASP significantly reversed the intestinal bacterial composition (**Figures 5F–H**). This reflected that YZM administration could change the intestinal flora of colitis mice to adjust them to be a healthy biological barrier.

Consistent with other results, linear discriminant analysis effect size (LEfSe) was conducted to identify the differences in the dominant communities (**Figures 6A,B**). *Campylobacteria* was the key bacteria associated with intestinal microbiota disorder in the model group (LDA = 4.14, $p = 0.003$). The

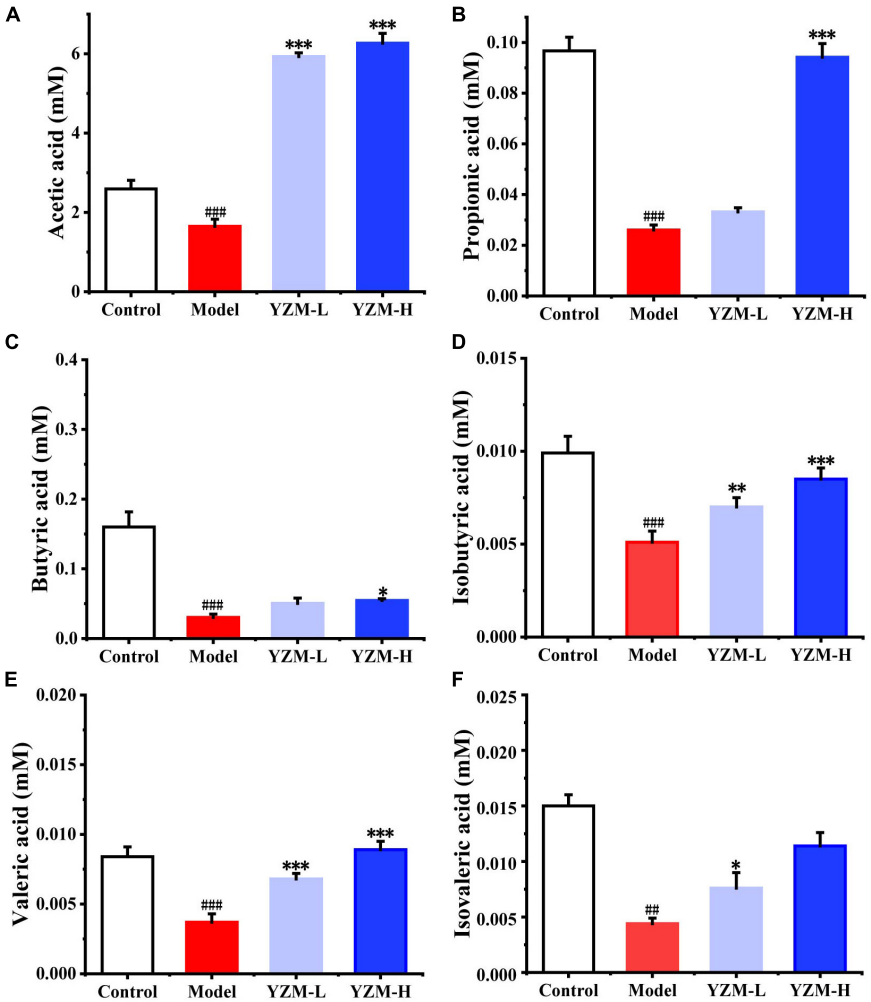

FIGURE 3 | SCFAs produced by intestinal microbiota. **(A–F)** Represents SCFAs amount as acetic acid, propionic acid, butyric acid, isobutyric acid, valeric acid, Isovaleric acid. $^{###}p < 0.001$ vs control, $^{#}p < 0.05$ vs control; $^{***}p < 0.001$ vs model, $^{**}p < 0.01$ vs model, $^{*}p < 0.05$ vs model.

TABLE 3 | Effects of YZM on overall structural modulation of gut microbiota.

	Control	Model	SASP	YZM_L	YZM_H
Observed OTUs	624.50 ± 103.27	505.17 ± 141.76	424.00 ± 142.15	569.83 ± 160.10	609.80 ± 73.15
Shannon	6.77 ± 0.59	6.42 ± 0.32	5.61 ± 0.28*	6.39 ± 0.76	6.59 ± 0.27
Simpson	0.97 ± 0.01	0.96 ± 0.01	0.94 ± 0.01**	0.96 ± 0.02	0.97 ± 0.01
Chao1	632.96 ± 105.22	509.10 ± 145.26	428.15 ± 145.07	572.49 ± 159.29	612.96 ± 74.63

** Indicates significant difference (**p < 0.01 vs. model, *p < 0.05 vs. model).*

strain dramatically decreased once YZM and SASP intervened (**Figure 5B**). In the YZM-H group, *Muribaculaceae_unclassified* at genus level exhibited comparative enrichment (LDA = 5.27, $p = 0.001$). Pearson correlation analysis assessed relationships among intestinal microbiota, microbiota-derived metabolites, and gas production (**Figure 6C**). Potential pathogens, such as *Clostridiales,* were highly correlated with risk factors (high DAI score, HE score, H_2S, and NH_3), whereas beneficial bacteria, including *Prevotellaceae NK3B31*, were negatively associated with these hazard factors.

DISCUSSION

Polygonatum odoratum (Mill.) Druce (YZ) has been widely used as a food source and traditional medicine (20). It has been used to remedy various inflammatory diseases, such as flu virus, diabetes, obesity, and antitumor (21). We identified 46 compounds in YZM, flavonoids, coumarins, alkaloids, terpenoids, phenols, organic acids, and lactones, such as resveratrol. Studies show that resveratrol exerts anti-inflammatory effects within intestinal cells and prevents the onset of DSS-induced colitis (22–24).

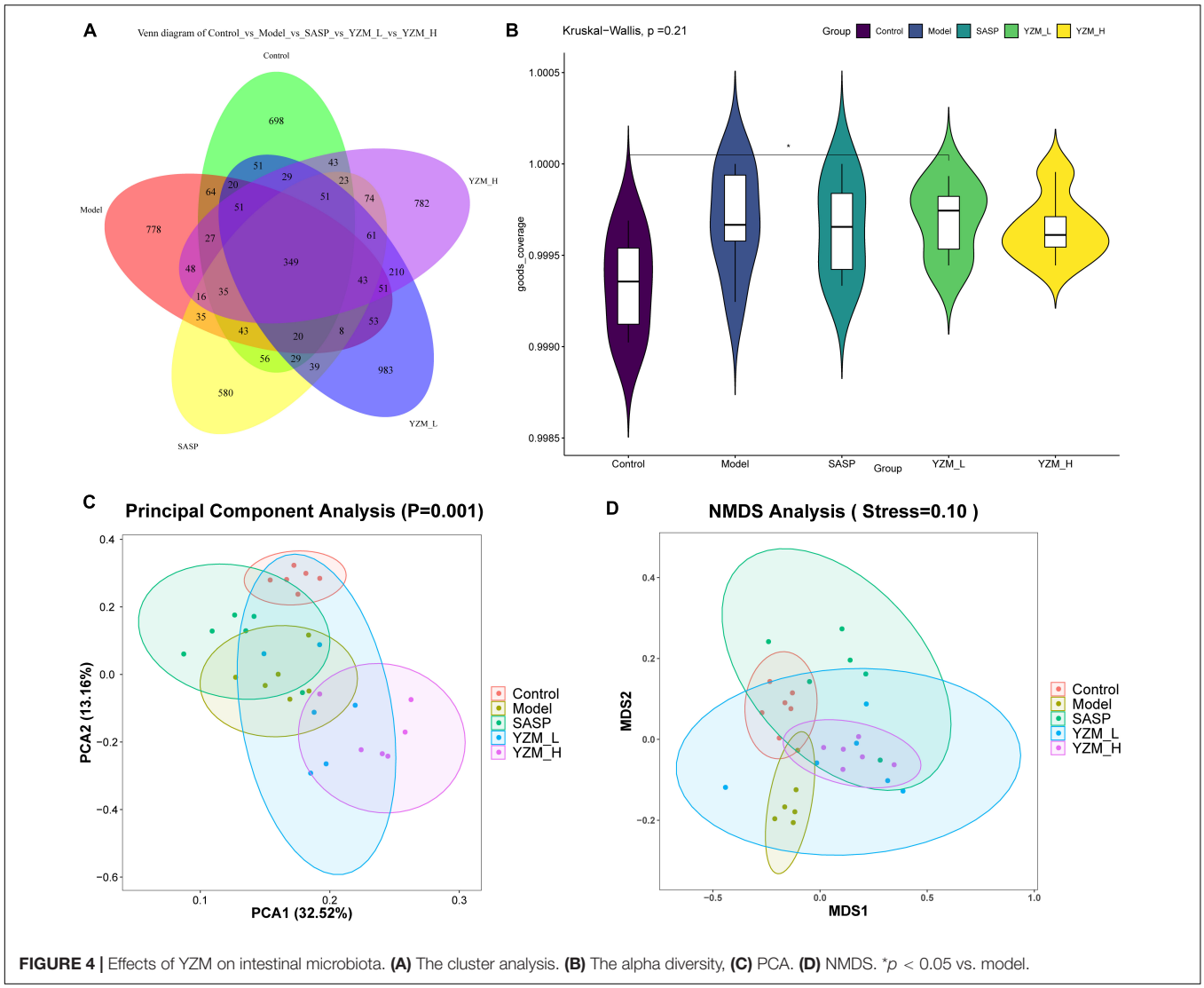

FIGURE 4 | Effects of YZM on intestinal microbiota. **(A)** The cluster analysis. **(B)** The alpha diversity, **(C)** PCA. **(D)** NMDS. *$p < 0.05$ vs. model.

Furthermore, human clinical trials of resveratrol indicated that it improves the quality of life in patients with IBD by lowering inflammation and oxidative stress (25). Increasing evidence demonstrates that flavonoids play a critical role against IBD by modulating the gut microbiota and the metabolites (13, 26). Further studies provided an adequate theoretical basis for the anti-IBD effect of YZM. It is the first time demonstrating that *Polygonatum odoratum* could be a potential treatment for colitis. Our present results suggested that YZM, the methanol extract from *Polygonatum odoratum*, could remarkably improve colon shortening, body weight reduction, and decreased DAI score in colitis mice. H&E staining indicated that the intestinal tissue of the YZM group was similar to the control group. YZM could improve the integrity of the intestinal epithelium layer and prevent mucosal damage in DSS-induced mice. Our study lays the groundwork for developing the *Polygonatum odoratum*, a new treat from nature food and traditional Chinese medicine. In addition, an in-depth research is being developed in our laboratory.

Subsequently, we demonstrated that YZM efficiently influenced gut gas production, SCFAs synthesis, and gut microbiota composition.

The gases generated from the gut are becoming increasingly intrigued. Various gases, including H_2, CH_4, CO_2, H_2S, and NH_3, work as the modulator of human health. In the gut, these gases are generated via the metabolic actions of resident microbiota in the colon. CO_2 is the main product of gut microbiota and is rapidly excreted via breath, whereas it is a noble gas with volume-related mechanical stimuli (27). H_2 is the major gas marker of carbohydrate fermentation, which is used to diagnose poor carbohydrate absorption. Studies are highlighting emerging links between H_2 and *Ruminococcus* spp., but it is still inconclusive (28, 29). CH_4 is generated from the metabolism of CO_2 and H_2 by archaea in the colon. The value of the CH_4 profile in the breathing is more controversial than for H_2 in clinical diagnostic tests (29). H_2S is produced during the fermentation of proteins and has toxic impacts at high concentrations in human tissues (29). A high concentration of NH_3 is a precipitating factor causing

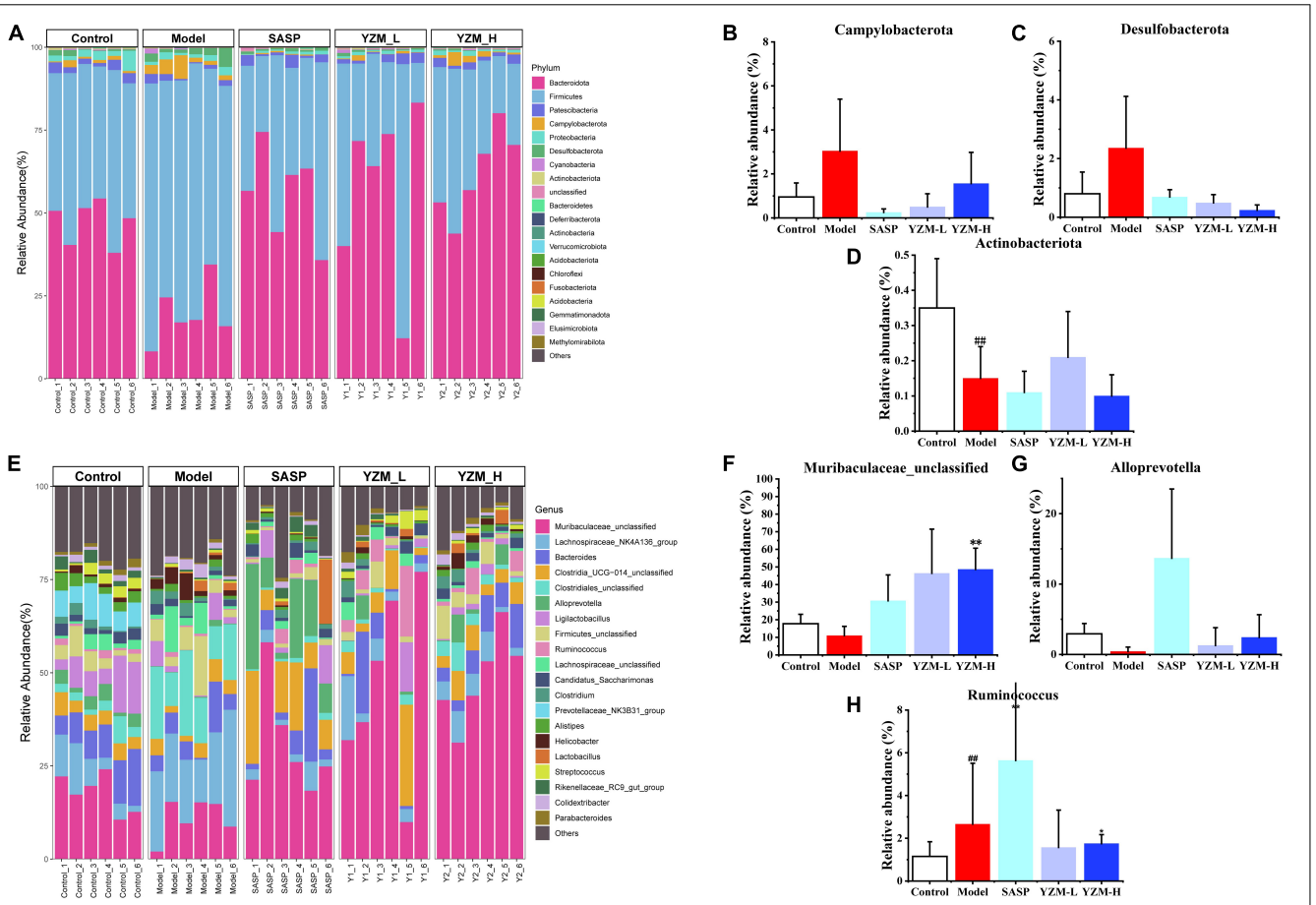

FIGURE 5 | Impacts of YZM at *phylum* and *genus* level. **(A)** The proportion of intestinal microbiota at *phylum* level **(B–D)**. Relative abundance of *Campylobacterota*, *Desulfobacterota*, *Actinobacteriota*. **(E)** The proportion of intestinal microbiota at *genus* level. **(F–H)** Relative abundance of *Muribaculaceae unclassified*, *Alloprevotella*, *Ruminococcus*. $^{\#\#}p < 0.01$ vs. control; $^{**}p < 0.01$ vs. model, $^{*}p < 0.05$ vs. model.

hepatic encephalopathy. After fermentation, the production of H_2S and NH_3 was inhibited considerably. The production of H_2S and NH_3 was significantly inhibited in YZM groups; this may be because YZM inhibited the gas-producing bacteria or modulated the microbiome composition, which inhibited the H_2S and NH_3 production in samples. An increase in the *Desulfobacterota* phylum has been associated with rising toxins production and bacterial genes attached to virulence agents (30). Interestingly, *Desulfobacterota* phylum's abundance was dramatically decreased in YZM-treated compared with the model group. It is similar to H_2S production. YZM may contribute to the decrease of H_2S by reducing the abundance of bacteria that produce H_2S.

Polygonatum odoratum on recovered the production of SCFAs in colitis mice. SCFAs are the main metabolites produced by gut microbiome fermentation and have anti-inflammatory properties and immunomodulatory effects. For the reasons mentioned above, SCFAs are critical in maintaining colon health. Studies showed that low concentrations of SCFAs were observed in colitis mice (31). In this study, the contents of measured SCFAs in model mice showed a decrease compared to control group mice. On the other hand, the high dose of YZM administration dramatically increased valeric and acetic acids. Our results suggested that YZM reversed the abundance of beneficial symbiotic and SCFA-related bacteria, such as *Muribaculaceae* (32), *Ruminococcus* (33), and *Alloprevotella* (34). The changes in SCFA-related bacteria caused by YZM might contribute to and restore SCFAs and ameliorate DSS-induced colitis.

Dextran sulfate sodium-treated mice were usually associated with the changes in the gut microbial composition as the increase in the pernicious microbe and the decrease in beneficial microorganisms (3). Our results indicated a large shift in the microbial community and changes in abundance or dominance of microbial groups under YZM treatments. *Campylobacter jejuni* disorder the protective toll-like receptor 9 (TLR9) signaling in intestinal epithelial cells and aggravated colitis in mice treated with DSS (35). *Desulfobacterota*, as a toxin bacteria, can accelerate the generation of inflammatory factors and exacerbations of colitis (30). YZM observably restored the microbiota composition by modulating phylum *Campylobacterota*, *Desulfobacterota,* and *Actinobacteriota* in DSS-treated mice. The results suggest that the *Actinobacteria* changed with YZM administration compared to the model

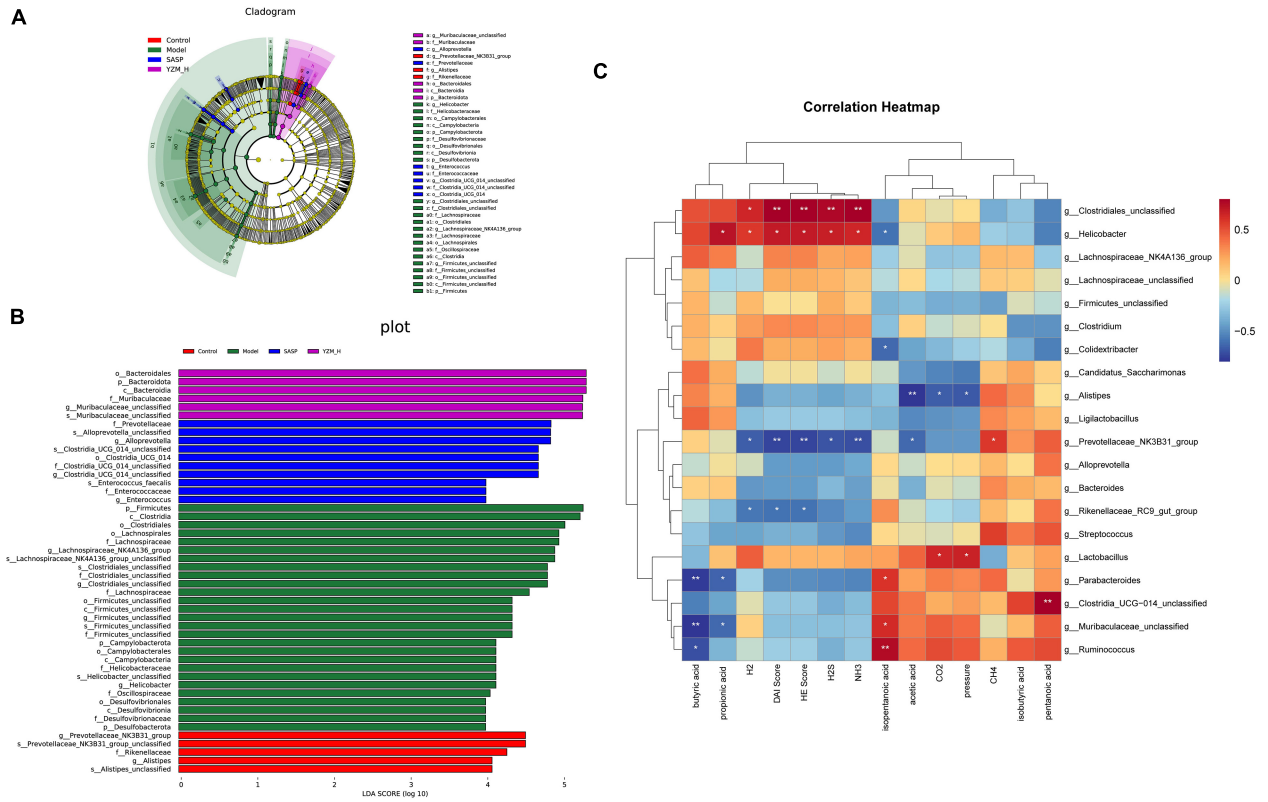

FIGURE 6 | LEfSe analysis and correlation analysis. **(A)** LEfSe analysis. **(B)** LDA scores (LDA) >4, $p < 0.05$. **(C)** Heatmap of Pearson correlation analysis, Red-white-blue color: positive correlation-no correlation-negative correlation. $^{**}p < 0.01$, $^{*}p < 0.05$.

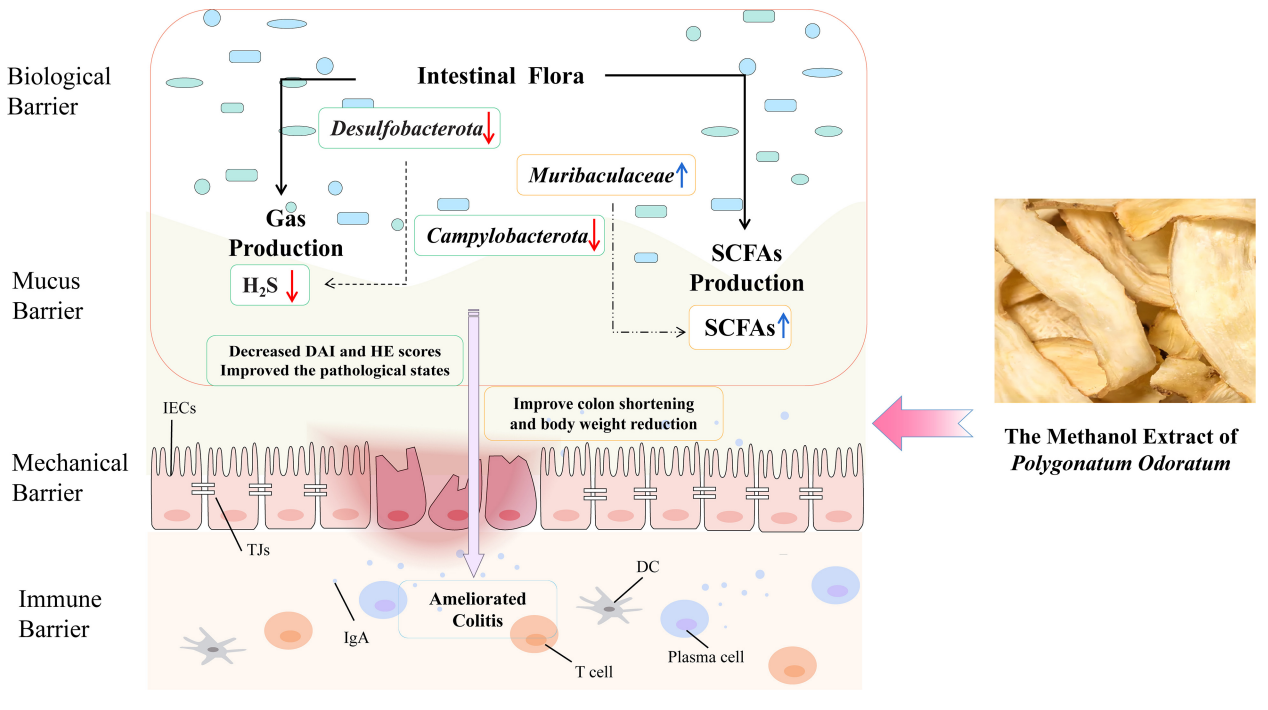

FIGURE 7 | Schematic of YZM alleviating colitis.

group (36, 37). Similarly, *Actinobacteria* was raised sharply after the colitis-associated colon cancer mice were replenished with probiotics. Meanwhile, *Muribaculaceae* was related to SCFAs to tolerate immunity stimulation (38). YZM also could increase the abundance of *Muribaculaceae*. *Clostridiales* contributed to the enhanced colitis severity in chronic colitis observed in mice, and in our experiment (39), it also can increase the production of harmful gases (H_2S and NH_3). *Prevotellaceae* of the gut can degrade polysaccharides and high carbohydrates and benefit the disease status (40, 41). It is similar to our results, which could reverse the production of harmful gases. Altogether, we had shown that YZM evidently could alleviate colitis via reversed intestinal microbiota disorder in colitis mice.

Taken together, we found that *Polygonatum odoratum* might be a multi-targeted resource as food and medicine, for protecting against IBD (**Figure 7**). YZM ameliorates colonic pathological damage to relieve inflammation injure. Moreover, YZM has a modulation affection on the gut microbiome community to decrease the maleficent bacteria associated with gas production (H_2S and NH_3). On the other hand, it improved the intestinal microbiota's composition and metabolites (such as SCFAs) to benefit the gut.

In summary, the methanol extract of *Polygonatum odoratum* (YZM), a plant resource used in food and medicine, was confirmed to alleviate mice colitis and is considered a novel intestinal microecological modifier with bright development prospects. The complex mechanism of YZM regulatory modulation of the intestinal immune response through microbiota needs further study.

DATA AVAILABILITY STATEMENT

The original contributions presented in the study are included in the article/**Supplementary Material**, further inquiries can be directed to the corresponding authors. All consensus sequence data of mice were submitted to the National Center for Biotechnology Information Short Read Archive under accession no. PRJNA817426.

ETHICS STATEMENT

The animal study was reviewed and approved by the Ethics Committee of Zhejiang Academy of Agricultural Sciences (No. 2021ZAASLA82). Written informed consent was obtained from the owners for the participation of their animals in this study.

AUTHOR CONTRIBUTIONS

LL, XY, and WL contributed to the study design. XY, XP, WZ, YC, and JN conducted animal experiments. KW and LX analyzed the samples and data. All authors contributed to the article, read, and approved the submitted version.

FUNDING

This work was supported by the National Key Research and Development Program of China (2018YFC2000500), start-up funds from Zhejiang Shuren University (2018R006), National Innovation and Entrepreneurship Program for College Students (202011842025), Zhejiang Public Welfare Project (LGN22C030008), and Hangzhou Agricultural and Society Development Project (202004A20).

SUPPLEMENTARY MATERIAL

The Supplementary Material for this article can be found online at: https://www.frontiersin.org/articles/10.3389/fnut.2022.899421/full#supplementary-material

REFERENCES

1. Zhu X, Yang Y, Gao W, Jiang B, Shi L. Capparis spinosa alleviates DSS-Induced ulcerative Colitis via regulation of the gut microbiota and oxidative stress. *Evid Based Complement Alternat Med.* (2021) 2021:1227876. doi: 10.1155/2021/1227876
2. McGuckin MA, Eri R, Simms LA, Florin TH, Radford-Smith G. Intestinal barrier dysfunction in inflammatory bowel diseases. *Inflamm Bowel Dis.* (2009) 15:100–13. doi: 10.1002/ibd.20539
3. Nishida A, Inoue R, Inatomi O, Bamba S, Naito Y, Andoh A. Gut microbiota in the pathogenesis of inflammatory bowel disease. *Clin J Gastroenterol.* (2018) 11:1–10. doi: 10.1007/s12328-017-0813-5
4. Zuo T, Ng SC. The gut microbiota in the pathogenesis and therapeutics of inflammatory bowel disease. *Front Microbiol.* (2018) 9:2247. doi: 10.3389/fmicb.2018.02247
5. Li F, Han Y, Cai X, Gu M, Sun J, Qi C, et al. Dietary resveratrol attenuated colitis and modulated gut microbiota in dextran sulfate sodium-treated mice. *Food Funct.* (2020) 11:1063–73. doi: 10.1039/c9fo01519a
6. Ji XL, Guo JH, Ding DQ, Gao J, Hao LR, Guo XD, et al. Structural characterization and antioxidant activity of a novel high-molecular-weight polysaccharide from Ziziphus Jujuba cv. Muzao. *J Food Meas Charact.* [Preprint]. (2022):doi: 10.1007/s11694-022-01288-3
7. Ji XL, Hou CY, Gao YG, Xue YQ, Yan YZ, Guo XD. Metagenomic analysis of gut microbiota modulatory effects of jujube (Ziziphus jujuba Mill.) polysaccharides in a colorectal cancer mouse model. *Food Funct.* (2020) 11:163–73. doi: 10.1039/c9fo02171j
8. Memariani Z, Abbas SQ, Ul Hassan SS, Ahmadi A, Chabra A. Naringin and naringenin as anticancer agents and adjuvants in cancer combination therapy: efficacy and molecular mechanisms of action, a comprehensive narrative review. *Pharmacol Res.* (2021) 171:105264. doi: 10.1016/j.phrs.2020.105264
9. Ji XL, Hou CY, Shi MM, Yan YZ, Liu YQ. An insight into the research concerningpanax ginsengC. A. meyer polysaccharides: a Review. *Food Rev Int.* (2020) 2020:1771363. doi: 10.1080/87559129.2020.1771363
10. Bauer C, Duewell P, Mayer C, Lehr HA, Fitzgerald KA, Dauer M, et al. Colitis induced in mice with dextran sulfate sodium (DSS) is mediated by the NLRP3 inflammasome. *Gut.* (2010) 59:1192–9. doi: 10.1136/gut.2009.197822
11. Zhou D, Feng Y, Li W, Liu B, Liu X, Sun L, et al. Cytotoxic steroidal glycosides from Polygonatum odoratum (Mill.) Druce. *Phytochemistry.* (2021) 191:112906. doi: 10.1016/j.phytochem.2021.112906
12. Pang X, Zhao JY, Wang YJ, Zheng W, Zhang J, Chen XJ, et al. Steroidal glycosides, homoisoflavanones and cinnamic acid derivatives from Polygonatum odoratum and their inhibitory effects against influenza A virus. *Fitoterapia.* (2020) 146:104689. doi: 10.1016/j.fitote.2020.104689

13. Wu T, Wang X, Xiong H, Deng Z, Peng X, Xiao L, et al. Bioactives and their metabolites from Tetrastigma hemsleyanum leaves ameliorate DSS-induced colitis via protecting the intestinal barrier, mitigating oxidative stress and regulating the gut microbiota. *Food Funct.* (2021) 12:11760–76. doi: 10.1039/d1fo02588k
14. Abdelhafez OH, Othman EM, Fahim JR, Desoukey SY, Pimentel-Elardo SM, Nodwell JR, et al. Metabolomics analysis and biological investigation of three Malvaceae plants. *Phytochem Anal.* (2020) 31:204–14. doi: 10.1002/pca.2883
15. Liu Q, Chen L, Laserna AKC, He Y, Feng X, Yang HS. Synergistic action of electrolyzed water and mild heat for enhanced microbial inactivation of *Escherichia coli* O157:H7 revealed by metabolomics analysis. *Food Control.* (2020) 110:107026. doi: 10.1016/j.foodcont.2019.107026
16. Li D, Feng Y, Tian M, Ji J, Hu X, Chen F. Gut microbiota-derived inosine from dietary barley leaf supplementation attenuates colitis through PPARgamma signaling activation. *Microbiome.* (2021) 9:83. doi: 10.1186/s40168-021-01028-7
17. Liu W, Li Z, Yang K, Sun P, Cai M. Effect of nanoemulsion loading finger citron (Citrus medica L. var. Sarcodactylis) essential oil on human gut microbiota. *J Funct Foods.* (2021) 77:104336. doi: 10.1016/j.jff.2020.104336
18. Logue JB, Stedmon CA, Kellerman AM, Nielsen NJ, Andersson AF, Laudon H, et al. Experimental insights into the importance of aquatic bacterial community composition to the degradation of dissolved organic matter. *ISME J.* (2016) 10:533–45. doi: 10.1038/ismej.2015.131
19. Zhao X, Chen L, Wongmaneepratip W, He Y, Zhao L, Yang HS. Effect of vacuum impregnated fish gelatin and grape seed extract on moisture state, microbiota composition, and quality of chilled seabass fillets. *Food Chem.* (2021) 354:129581. doi: 10.1016/j.foodchem.2021.129581
20. Wang Y, Fei Y, Liu L, Xiao Y, Pang Y, Kang J, et al. Polygonatum odoratum polysaccharides modulate gut microbiota and mitigate experimentally induced obesity in rats. *Int J Mol Sci.* (2018) 19:19113587. doi: 10.3390/ijms19113587
21. Shu XS, Lv JH, Tao J, Li GM, Li HD, Ma N. Antihyperglycemic effects of total flavonoids from Polygonatum odoratum in STZ and alloxan-induced diabetic rats. *J Ethnopharmacol.* (2009) 124:539–43. doi: 10.1016/j.jep.2009.05.006
22. Nunes S, Danesi F, Del Rio D, Silva P. Resveratrol and inflammatory bowel disease: the evidence so far. *Nutr Res Rev.* (2018) 31:85–97. doi: 10.1017/S095442241700021X
23. Serra D, Almeida LM, Dinis TC. Anti-inflammatory protection afforded by cyanidin-3-glucoside and resveratrol in human intestinal cells via Nrf2 and PPAR-gamma: comparison with 5-aminosalicylic acid. *Chem Biol Interact.* (2016) 260:102–9. doi: 10.1016/j.cbi.2016.11.003
24. Wagnerova A, Babickova J, Liptak R, Vlkova B, Celec P, Gardlik R. Sex Differences in the Effect of Resveratrol on DSS-Induced Colitis in Mice. *Gastroenterol Res Pract.* (2017) 2017:8051870. doi: 10.1155/2017/8051870
25. Samsamikor M, Daryani NE, Asl PR, Hekmatdoost A. Resveratrol supplementation and oxidative/anti-oxidative status in patients with ulcerative colitis: a randomized, double-blind, placebo-controlled pilot study. *Arch Med Res.* (2016) 47:304–9. doi: 10.1016/j.arcmed.2016.07.003
26. Zhang J, Xu X, Li N, Cao L, Sun Y, Wang J, et al. Licoflavone B, an isoprene flavonoid derived from licorice residue, relieves dextran sodium sulfate-induced ulcerative colitis by rebuilding the gut barrier and regulating intestinal microflora. *Eur J Pharmacol.* (2022) 916:174730. doi: 10.1016/j.ejphar.2021.174730
27. Modak A. Breath tests with (13)C substrates. *J Breath Res.* (2009) 3:040201. doi: 10.1088/1752-7155/3/4/040201
28. Simmering R, Taras D, Schwiertz A, Le Blay G, Gruhl B, Lawson PA, et al. Ruminococcus luti sp. nov., isolated from a human faecal sample. *Syst Appl Microbiol.* (2002) 25:189–93. doi: 10.1078/0723-2020-00112
29. Chatterjee S, Park S, Low K, Kong Y, Pimentel M. The degree of breath methane production in IBS correlates with the severity of constipation. *Am J Gastroenterol.* (2007) 102:837–41. doi: 10.1111/j.1572-0241.2007.01072.x
30. Goldstein EJ, Citron DM, Peraino VA, Cross SA. Desulfovibrio desulfuricans bacteremia and review of human Desulfovibrio infections. *J Clin Microbiol.* (2003) 41:2752–4. doi: 10.1128/JCM.41.6.2752-2754.2003
31. Zhao Y, Luan H, Gao H, Wu X, Zhang Y, Li R. Gegen Qinlian decoction maintains colonic mucosal homeostasis in acute/chronic ulcerative colitis via bidirectionally modulating dysregulated Notch signaling. *Phytomedicine.* (2020) 68:153182. doi: 10.1016/j.phymed.2020.153182
32. Zhao L, Zhang F, Ding X, Wu G, Lam YY, Wang X, et al. Gut bacteria selectively promoted by dietary fibers alleviate type 2 diabetes. *Science.* (2018) 359:1151–6. doi: 10.1126/science.aao5774
33. Mottawea W, Chiang CK, Muhlbauer M, Starr AE, Butcher J, Abujamel T, et al. Altered intestinal microbiota-host mitochondria crosstalk in new onset Crohn's disease. *Nat Commun.* (2016) 7:13419. doi: 10.1038/ncomms13419
34. Ren Y, Geng Y, Du Y, Li W, Lu ZM, Xu HY, et al. Polysaccharide of Hericium erinaceus attenuates colitis in C57BL/6 mice via regulation of oxidative stress, inflammation-related signaling pathways and modulating the composition of the gut microbiota. *J Nutr Biochem.* (2018) 57:67–76. doi: 10.1016/j.jnutbio.2018.03.005
35. O'Hara JR, Feener TD, Fischer CD, Buret AG. Campylobacter jejuni disrupts protective Toll-like receptor 9 signaling in colonic epithelial cells and increases the severity of dextran sulfate sodium-induced colitis in mice. *Infect Immun.* (2012) 80:1563–71. doi: 10.1128/IAI.06066-11
36. He Y, Xie Z, Xu Y, Zhao X, Zhao L, Yang H. Preservative effect of slightly acid electrolysed water ice generated by the developed sanitising unit on shrimp (Penaeus vannamei). *Food Control.* (2022) 136:108876. doi: 10.1016/j.foodcont.2022.108876
37. Mendes MCS, Paulino DSM, Brambilla SR, Camargo JA, Persinoti GF, Carvalheira JBC. Microbiota modification by probiotic supplementation reduces colitis associated colon cancer in mice. *World J Gastroentero.* (2018) 24:1995–2008. doi: 10.3748/wjg.v24.i18.1995
38. Biggs MB, Medlock GL, Moutinho TJ, Lees HJ, Swann JR, Kolling GL, et al. Systems-level metabolism of the altered Schaedler flora, a complete gut microbiota. *ISME J.* (2017) 11:426–38. doi: 10.1038/ismej.2016.130
39. Liu XY, He SW, Li QY, Mu X, Hu G, Dong H. Comparison of the gut microbiota between pulsatilla decoction and levofloxacin hydrochloride therapy on *Escherichia coli* infection. *Front Cell Infect Mi.* (2020) 10:319. doi: 10.3389/fcimb.2020.00319
40. Gu CH, Suleria HAR, Dunshea FR, Howell K. Dietary lipids influence bioaccessibility of polyphenols from black carrots and affect microbial diversity under simulated gastrointestinal digestion. *Antioxidants Basel.* (2020) 9:9080762. doi: 10.3390/antiox9080762
41. Ferrario C, Statello R, Carnevali L, Mancabelli L, Milani C, Mangifesta M, et al. How to feed the mammalian gut microbiota: bacterial and metabolic modulation by dietary fibers. *Front Microbiol.* (2017) 8:1749. doi: 10.3389/fmicb.2017.01749

Conflict of Interest: The authors declare that the research was conducted in the absence of any commercial or financial relationships that could be construed as a potential conflict of interest.

Publisher's Note: All claims expressed in this article are solely those of the authors and do not necessarily represent those of their affiliated organizations, or those of the publisher, the editors and the reviewers. Any product that may be evaluated in this article, or claim that may be made by its manufacturer, is not guaranteed or endorsed by the publisher.

frontiers | Frontiers in Nutrition

ORIGINAL RESEARCH
published: 13 June 2022
doi: 10.3389/fnut.2022.926637

Dynamic Changes in Microbial Communities and Physicochemical Characteristics During Fermentation of Non-post Fermented Shuidouchi

Yuyong Chen[1,2], *Feng Qin*[2] *and Mingsheng Dong*[1]*

[1] College of Food Science and Technology, Nanjing Agricultural University, Nanjing, China, [2] Jiangsu Agri-Animal Husbandry Vocational College, Taizhou, China

Non-post fermented Shuidouchi is a Chinese spontaneously fermented soybean food with multifunctionality in human health. The functionality and safety of this plant-based food will be affected by the microorganisms during fermentation. In this study, microbial diversity was investigated using culture-dependent and culture-independent methods. The functional metabolites such as polyamines and alkylpyrazines were also determined at different time points during fermentation. We found that *Bacillus* was the most dominant microbe throughout the fermentation process, while the temperature was the most important influencing factor. During fermentation, the microbial diversity increased at a moderate temperature and decreased at a high temperature (52°C). High temperature caused the prosperity of the spore-producing bacteria such as *Bacillus* (more than 90% relative abundance in bacteria) and *Aneurinibacillus* (2% or so relative abundance in bacteria), and the inhibition of fungi. Furthermore, it was found by correlation analysis that the relative abundances of *Bacillus* and *Aneurinibacillus* were positively correlated with the relative content of amino acid metabolism pathway and the content of most alkylpyrazines and biogenic amines. Meanwhile, the relative abundances of many non-dominant bacteria were negatively correlated with the content of biogenic amines and positively correlated with the relative content of carbohydrate metabolism pathway. These effects were helpful to control the biogenic amine contents under the safety limits, increasing the alkylpyrazine type and product functionality. A two-stage temperature control strategy—a moderate temperature (35–42°C) first, then a high temperature (52°C)—was concluded from the spontaneous fermentation of non-post fermented Shuidouchi. This strategy could improve the safety of product by inhibiting or sterilizing the thermolabile microbes. The non-post fermented Shuidouchi product is rich in functional compounds such as polyamines and alkylpyrazines.

Keywords: non-post fermented Shuidouchi, microbial diversity, biogenic amines, alkylpyrazines, metabolism pathway, functional compounds

OPEN ACCESS

Edited by:
Xiaolong Ji,
Zhengzhou University of Light Industry, China

Reviewed by:
Qingli Dong,
University of Shanghai for Science and Technology, China
Rina Wu,
Shenyang Agricultural University, China

***Correspondence:**
Mingsheng Dong
dongms@njau.edu.cn

Specialty section:
This article was submitted to Food Chemistry, a section of the journal Frontiers in Nutrition

Received: *22 April 2022*
Accepted: *23 May 2022*
Published: *13 June 2022*

Citation:
Chen Y, Qin F and Dong M (2022) Dynamic Changes in Microbial Communities and Physicochemical Characteristics During Fermentation of Non-post Fermented Shuidouchi. Front. Nutr. 9:926637. doi: 10.3389/fnut.2022.926637

INTRODUCTION

Shuidouchi is a traditional fermented soybean product widely distributed in China (1). Previous research found that Shuidouchi is highly digestible and absorbable (2), and is rich in nutritional and functional compounds such as proteins, peptides, and active isoflavones (3, 4). Though the process may vary among different regions, there are two main types of traditional spontaneously fermented Shuidouchi. The first type involves fermenting boiled or steamed soybeans until it becomes the finished product, commonly known as mucous sauce beans or stinky Douchi, using insulation, starting with a warm temperature. The second type involves further fermenting the previous product for a ripening period after adding the boiled soybean soup and condiments such as spices and salt, without the use of insulation (3). The first type of product in this article was denoted as non-post fermented Shuidouchi, similar to Natto, with a mucous appearance and a shorter production cycle compared to the second type of product. Shuidouchi offers many health benefits, such as gastric injury prevention (4), as well as anti-oxidation (5), *in vitro* anticancer, and antimutagenic effects (6). Because non-post fermented Shuidouchi has shown vascular protective and anti-hypertension functionality (7, 8), as well as a high activity of fibrinolytic enzymes (9), with lower salt content, a shorter processing cycle, and a lower cost, it has attracted increasing attention from researchers and enterprises.

Although the fermentation process of non-post fermentation Shuidouchi is relatively short (48–72 h), various microorganisms secrete a variety of enzymes in the product that will promote the hydrolysis of soybeans and the generation of various metabolites, resulting in the appearance of a brown mucous, a Douchi smell, and a spontaneous increase in temperature. Previous research has focused on comparative studies of bacterial diversity in the initial and final stages of Shuidouchi (10) and the microbial diversity of products from different regions (11). However, there is still a lack of detailed research on the relationship of microbes and functional metabolites during the fermentation of non-post fermented Shuidouchi. Recently, the high-throughput nucleotide sequencing technique was applied to analyze the microbial diversity in many foods, as it can identify unculturable microbes (11–14). However, the culture-dependent method should also be used to investigate the microbial ecology for more accurate results. A variety of physiologically active substances such as biogenic amines (BAs) were found to generate during the fermentation of non-post fermented Shuidouchi, among which polyamines were found to exhibit protective effects against chronic diseases (15, 16). In recent years, studies have found that the content of certain BAs reached or approached harmful levels in commercial Natto and Shuidouchi products. Certain *Bacillus subtilis* strains in Natto were found to accumulate high concentrations of β-phenylethylamine and tyramine, which could cause food safety problems; thus, BAs must be monitored during fermentation (16, 17). In addition, other physiologically active substances such as alkylpyrazines were also found in fermented soybean products. Among the alkylpyrazines, 2,3,5,6-tetramethylpyrazine (tetramethylpyrazine) has been shown to promote human cardiovascular and cerebrovascular health (18–20), increase immune organ indices and natural immunoglobulins (21), relieve symptoms of animal experimental autoimmune myasthenia gravis (22), and protect against acute alcoholic liver injury (23). Tetramethylpyrazine has also been found in mold type Douchi (24, 25). These metabolites were shown to be related to the population changes and physiological metabolic pathways of microbes during fermentation. However, the correlation between microbes and alkylpyrazines in Douchi (including non-post fermented Shuidouchi) remains unknown. Thus, an investigation into the relationship of functional compounds and microbial metabolism pathways in Douchi is needed.

This research explored the microbial community structure of non-post fermented Shuidouchi, and its associations with both the functional metabolites and microbial metabolism pathways, to provide information for optimizing the safe and functional qualities of this product.

MATERIALS AND METHODS

Chemicals and Materials

The study material consisted of yellow soybeans [*Glycine max* (Linn.) Merr.], which were purchased from a market in Yantai city, Shandong province, China.

BAs or amine hydrochlorides, such as histamine (HIS), β-phenylethylamine (PHE), Tryptamine (TRP), cadaverine dihydrochloride (CAD), putrescine dihydrochloride (PUT), tyramine hydrochloride (TYR), spermine (SPM), and spermidine (SPD), were purchased from Shanghai Yuanye Bio-Technology Co., Ltd. (Shanghai, China), with purities of ≥ 98%.

Acetone and acetonitrile were of HPLC grade, while the other chemicals were analytically pure. All chemicals were purchased from Sinopharm Group Co., Ltd. (Beijing, China), and the plate count agar (PCA, CM101), De Man Rogosa Sharpe agar (MRSA, CM188), Manitol salt agar (MSA, CP813), brain heart infusion agar (BHIA, CM918), potato dextrose agar (PDA, CM123, and yeast extract glucose chloramphenicol agar (YGC, CM840) were purchased from Land Bridge Technology Co., Ltd. (Beijing, China). Bacterial and yeast genome extraction kits and lyticase were purchased from Tiangen Biotech Co., Ltd. (Beijing, China), and the 2 × Taq master mix (P111-03) was purchased from Vazyme Biotech Co., Ltd. (Nanjing, China).

Non-post Fermented Shuidouchi Fermentation and Sampling

The spontaneous fermentation steps for non-post fermented Shuidouchi were similar to the methods described by Chen et al. and were as follows (**Figure 1**): (1) the soybeans were selected; (2) the impurities were removed and the soybeans were washed twice; (3) the soybeans were soaked in water overnight; (4) then the soybeans were cleaned and boiled; (5) corn bracts were washed together with the bamboo basket after trimming and moderately dried on a hot pot cover; (6) the soybeans were kept hot or warm with the remaining heat from the clay oven overnight to turn them from yellow to yellow-red; (7) the corn bracts were spread on the bottom of a bamboo

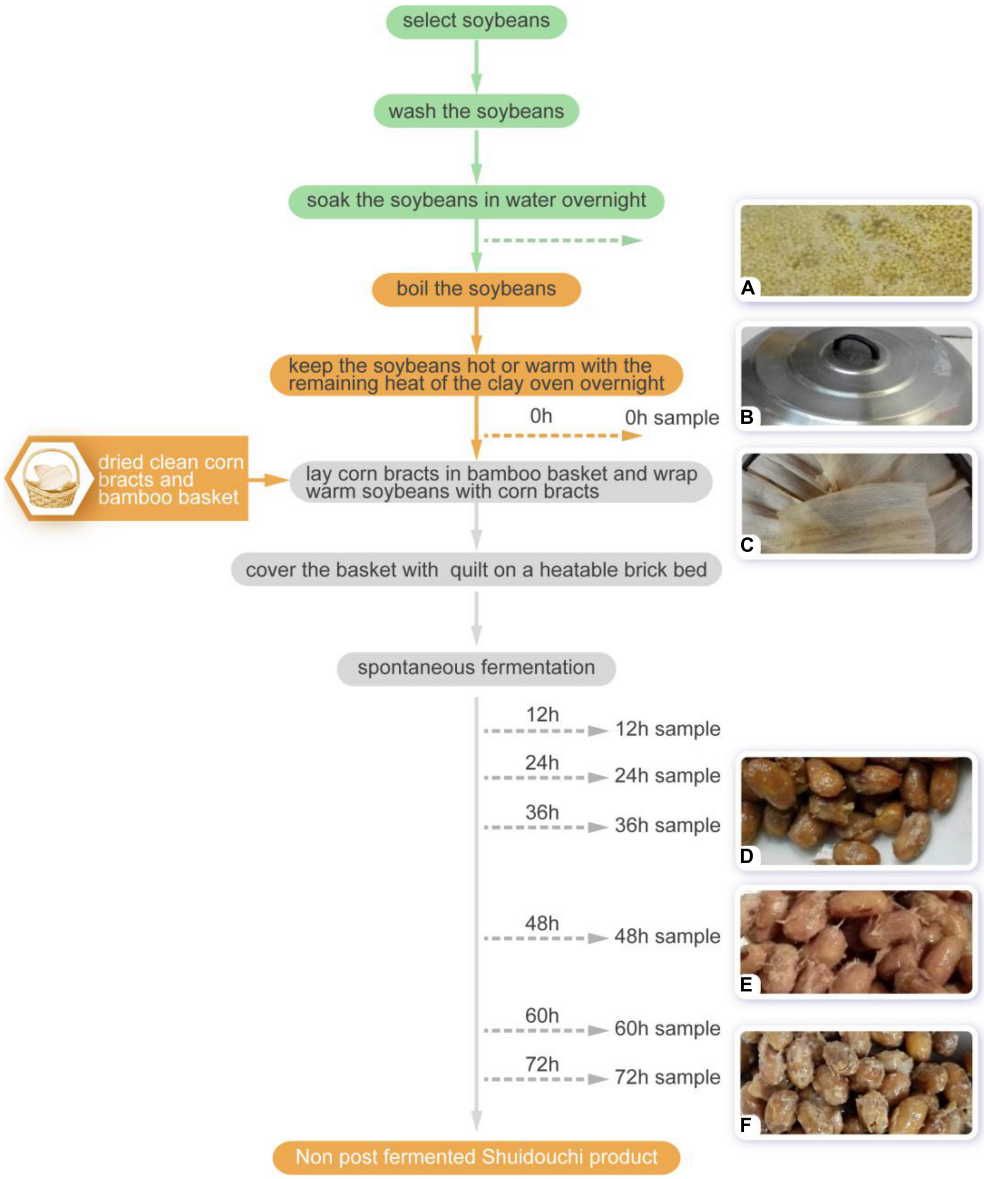

FIGURE 1 | The non-post fermented Shuidouchi process and sampling time points. **(A)** Boiled soybeans; **(B)** the soybeans were kept warm with the lid covered; **(C)** the soybeans were wrapped in corn husks; **(D)** mucus appeared at 36 h; **(E)** ropy appearance of the product 48 h; **(F)** 72-h product.

basket and the warm (35–42°C) cooked soybeans were scooped into the basket, where the soybeans were wrapped with corn bracts and the basket was covered with cotton clothes and a quilt on a Kang (a heatable brick bed) to adjust the soybean temperature to slightly lower than body temperature, and to start the spontaneous fermentation process; and (8) fermentation was maintained (generally for 2–3 days) until the soybeans could be removed from the mucus filaments, which were soft with a Douchi aroma (9).

Samples were collected after 0, 12, 24, 36, 48, 60, and 72 h of fermentation. About 400 g soybeans were taken out from different positions of soybean pile, mixed thoroughly and split into two parts by sterile operation. All samples were packed in sterilized containers, transported to the laboratory at −10°C, and stored at −70°C.

Sensory Evaluation and Determination of the Temperature and pH Value

Before sampling, the core temperature of the Shuidouchi was detected by a sterilized thermometer and recorded. Then, sensory evaluation was carried out after sampling, which was described according to the Chinese standard of Natto (26). The sensory features such as color, flavor, and texture were recorded in time. The pH values of the soybean surface materials in the sample were determined using a pH meter (Mettler EL20, Switzerland) according to the standard method (27, 28).

Enumeration of Bacteria and Fungi

Enumeration was performed according to the colony counting method using the gradient dilution spread-plate technique, similar to the procedure described by Chen et al. (9). PCA and MRSA plates were used to enumerate the bacteria at 37°C under micro aerobic or anaerobic conditions. The MSA plates were incubated micro-aerobically at 37°C to count the NaCl tolerant bacteria. In this process, BHIA, basal medium agar (BMA) (consisting of 5.0 g of yeast extract, 5.0 g of tryptone, 1.0 g of KH_2PO_4, 0.4 g of $MgCl_2{\cdot}6H_20$, 1.0 g of NH_4Cl, 5.0 mg of $FeSO_4{\cdot}7H_2O$, 1.0 g of glucose, 25 mL of a mineral solution, 1 mL of Tween 80, 16 g of agar for 1 L of the medium, where the pH was adjusted to 7.0 with 10 M KOH) (29), and CESP agar (CESPA) (15 g of casitone, 5 g of yeast extract, 3 g of soytone, 2 g of peptone, 0.015 g of $MgSO_4$, 0.007 g of $FeCl_3$, 0.002 g of $MnCl_2$, 20 g of agar for 1 L medium, at a pH of 7.2) (30) plates were cultured aerobically at 50°C to count the thermophilic bacteria. The PDA plates and YGC plates, which were used to count the fungi, were cultured aerobically at 28°C. Micro-aerobic conditions were achieved by sealing the Petri dishes in a plastic bag. The plates were generally incubated for 2–3 days, while the plates without the appearance of colonies were incubated and observed for 5 days.

DNA Extraction, PCR Amplification, and High-Throughput Nucleotide Sequencing

For bacterial total genome DNA extraction, we obtained 20 g of the Shuidouchi sample and added 180 mL of the sterile physiological saline (40 g of 0 h sample and 160 mL of sterile physiological saline) in a sterile conical flask with a cover, which was shaken at 4°C for 30 min. The solution was then centrifuged for 15 min at 4°C and 2,000 g, and the supernatant was centrifuged for 20 min at 4°C and 12,000 g. Then, the supernatant was discarded, and the precipitate was placed into a sterile 1.5 mL EP tube to extract the DNA with a bacterial genome extraction kit (31). During fungal genome extraction, the same method was used; however, during the second centrifugation, the supernatant of the first centrifugation was centrifuged for 20 min at 14,000 g. The fungal precipitate was treated with lyticase, and then extracted with the yeast genome extraction kit (32).

Regions V3 to V4 of the 16S rDNA were amplified using primers (341F, 5′-(CCCTACACGACGCTCTTCCGATCTG) (barcode) CCTACGGGNGGCWGCAG-3′, 805R, 5′-(GACTGGAGTTCCTTGGCACCCGAGAATTCCA) (barcode) GACTACHVGGGTATCTAATCC-3′) with the barcode. The fungal internal transcribed spacer (ITS) regions ITS1-ITS2 were amplified using primers (ITS1F, 5′- (CCCTACACGACGCTCTTCCGATCTN) (barcode) CTTGGTCATTTAGAGGAAGTAA-3′, ITS2R, 5′-(GTGACTGGAGTTCCTTGGCACCCGAGAATTCCA) (barcode) GCTGCGTTCTTCATCGATGC-3′). Amplification was performed in a reaction volume of 30 μL containing 15 μL of 2 × Taq master mix, with 1 μL of each primer (10 μM), 10–20 ng of the DNA and dd-H_2O samples, according to the following procedures. Initialization was conducted at 94°C for 3 min, with 5 cycles of 30 s at 94°C, 20 s at 45°C, and 30 s at 65°C. Then, 20 cycles consisting of 20 s at 94°C, 20 s at 55°C, and 30 s at 72°C, with an extension step for 5 min at 72°C, were undertaken. The PCR products were stored at 10°C before the second round of PCR.

Illumina bridge PCR compatible primers were introduced into the second round of PCR, where the reaction was performed in a 30 μL mixture containing 15 μL of 2 × Taq master mix, 1 μL of primer F (10 μM), 1 μL of primer R (10 μM), 20 ng of the last round of the PCR and dd-H_2O products, using the following procedures. Initialization was conducted at 95°C for 3 min, with 5 cycles of 20 s at 94°C, 20 s at 55°C, and 30 s at 72°C. Then, an extension step at 72°C was conducted for 5 min, and cooled down to 10°C. The PCR products were purified by MagicPure size selection DNA beads (TransGen Biotech, Beijing, China), and pooled in equimolar and then paired-end sequenced on an Illumina MiSeq PE300 platform (Illumina, San Diego, United States), according to the standard protocols by Sangon Biotech Co., Ltd. (Shanghai, China).

Bioinformatics Data Processing and Analysis

Operational taxonomic units (OTUs) were clustered with a 97% similarity cutoff using Usearch (version5.2.236),[1] while the chimeric sequences were identified and removed using UCHIME (version 4.2.40).[2] The taxonomy of each 16S rRNA and ITS rRNA gene sequence was analyzed by an RDP Classifier algorithm[3] against the RDP,[4] Silva bacterial[5] and Unite fungal databases,[6] using a confidence threshold of 0.8. α- and β-diversity, as analyzed by R and Mothur software.[7] Principle coordinate analysis (PCoA) was carried out on the Unifrac metric with the vegan (version 2.0-10) package of the R language. The relationships between the bacterial or fungal communities of samples and environmental factors (pH, temperature, bioamine, 2,3-butanediol and tetramethylpyrazine) were explored by canonical correspondence analysis (CCA) using the vegan (version 2.0-10) package of the R language. The correlation between microbes and physical or chemical characteristics was evaluated by Pearson correlation analysis. The Kyoto Encyclopedia of Genes and Genomes (KEGG) pathway information was obtained by the Phylogenetic Investigation of Communities by Reconstruction of Unobserved States (PICRUSt) software (33).

Determination of Biogenic Amines in the Samples

BA determination was performed according to the methods described in the national standards in China (34).

According to Han's method, 5 g of each ground sample was placed into 50 mL capped centrifuge tubes, with 20 mL perchloric

[1]http://drive5.com/usearch

[2]http://drive5.com/usearch/manual/uchime_algo.html

[3]http://rdp.cme.msu.edu

[4]http://rdp.cme.msu.edu/misc/resources.jsp

[5]http://www.arb-silva.de

[6]http://unite.ut.ee/index.php

[7]https://mothur.org

acid solution (0.4 mol/L) added, before mixing and shaking for 30 min. Each mixture was centrifuged at 7,000 rpm for 6 min at 4°C, and the supernatant was collected. Then the precipitate was extracted according to the above methods. The supernatant was extracted twice and then combined to fill 50 mL with perchloric acid solution. Then, 1 mL of the mixed solution was obtained for derivatization (17).

Next, 1 mL of each extracted sample or standard BA solution was homogeneously mixed with 200 μL of 2 M NaOH solution, 300 μL of saturated $NaHCO_3$ solution and then 1 mL of dansyl chloride solution (10 mg/mL in acetone) in a 5 mL centrifuge tube. The homogenized mixture was incubated in a water bath at 60°C for 30 min, protected from light, and sufficiently shaken every 15 min. Then, 100 μL of 25% ammonia solution was added into the mixture and blended to stop the reaction. After 30 min, the reaction solution was blended with 700 μL of acetonitrile. The final solution was filtered through a 0.22-μm filter, and the filtrate was maintained at 4°C for HPLC inspection (17).

Quantitative analysis of the BAs was carried out using an HPLC (1260 Infinity, Agilent, United States) with a UV detector and acid resistant liquid chromatography column (ZORBAX SB-Aq 4.6 × 250 mm, 5 μm, Agilent, United States). The mobile phase solvent A was dd-H_2O, while solvent B was acetonitrile. The gradient elution program followed the ratio of A:B, with 100:0 at 0 min, which decreased gradually to 30:100 at 5 min and 0:100 at 16 min, and then increased to 35:65 at 18 min and maintained at 35:65 until 30 min. The flow velocity of the previous 5 min was 5 mL/min, and then adjusted to 0.8 mL/min. The temperature of the column was 30°C, with 20 μL of injected sample and a UV detection wavelength of 254 nm.

2,3-Butanediol, Acetoin and Alkylpyrazine Determination

The solid phase microextraction method (SPME) was used to analyze 2,3-butanediol, acetoin, and alkylpyrazine according to the methods described by Zhang et al. (24), with minimal modifications. First, 3 g of the sample was put into a 15 mL headspace vial, equilibrated for 10 min at 60°C. Then the volatile components were extracted using a 50/30 μm divinylbenzene/carboxen/polydimethylsiloxane (DVB/CAR/PDMS, Supelco, Bellefonte, PA, United States) fiber for 30 min at 60°C, which was conditioned in a GC injector port at 250°C for 2 h prior to use. After extraction, the volatiles that adsorbed on the SPME fibers were thermally desorbed at 230°C in the injection port of an Agilent 7890B gas chromatography system (Agilent Technologies, United States) coupled to an Agilent 5977A quadrupole inert mass selective detector by holding it in splitless mode for 3 min. An Hp-5 fused silica capillary column (30 m × 0.32 mm I.D. × 0.25 μm film thickness) with helium flow at 1.2 mL/min was used to separate the volatile components. The GC condition consisted: the injector at 230°C, initial column temperature of 20°C for 5 min, which was increased to 30°C at a rate of 2°C/min, maintained at 30°C for 3 min, further increased to 150°C at a rate of 3°C/min, then increased to 250°C at a rate of 10°C/min and maintained at 250°C for 10 min. The MS condition was: 250°C of transfer line, 230°C of electron ionization (70 eV), where the temperature of the quadrupole mass analyzer was 150°C, and at full scanning mode (35–550 m/z). The compounds were determined by comparing with the NIST 14.L database. The relative content of 2,3-butanediol, acetoin and alkylpyrazine was quantified by area normalization.

Statistical Analysis

The relationships between the relative abundance of microbial communities and the chemical/physical characteristics were analyzed using R language (V 4.1.2), by calculating the Pearson correlation coefficient. Duncan multiple comparison of the data was provided by mean comparisons using one-way variance analysis using IBM SPSS Statistics 26 with a level of significance of $p < 0.05$ when the variances were homogeneous. When the variances were not homogeneous, Games-Howell comparison was used.

RESULTS

Changes in Temperature, pH Value, Sensory Characteristics, and Microbial Growth

During fermentation of the non-post fermented Shuidouchi, the temperature increased spontaneously (**Table 1**). In the early 12 h, the temperature increased slowly and the soybeans were maintained in a warm state, while the temperature increased sharply to 52°C between 12 and 24 h during the initial fermentation stage and remained as high as approximately 51°C during fermentation metaphase. In the next fermentation phase (anaphase), the temperature decreased slowly but was still maintained at a high level, and the pH of the soybeans increased significantly after 12 h. The increase in temperature also brought about changes in the sensory characteristics. During the moderate temperature fermentation stage (0–24 h), a sour and mellow aroma arose from the fermented soybeans at 12 h, accompanied by the growth of mesophilic bacteria, yeast, and mold (8.10, 4.09, and 2.78 log CFU/g) (**Table 2**, 12 h). Then, the high temperatures throughout the metaphase and anaphase of fermentation also brought about a dark color of the soybeans (**Table 1** and **Figure 1**), mucus filaments, and a Douchi flavor (**Table 1**). After 72 h of fermentation, the pH value reached 8.10, and the taste of the product would be more bitter if the fermentation was not terminated. Thus, the optimal fermentation time was 48–72 h.

According to the colony counting results, we found that there were low counts of mesophilic bacteria at the starting point (**Table 2**, 0 h) of fermentation; however, there were fewer thermoduric bacteria, yeast, and molds with counts below the detection limit. In the first 12 h of fermentation, due to the appropriate temperature and pH, the mesophilic bacterial counts were as high as 10–100 times those of the thermoduric bacterial counts. After 12 h, the thermoduric bacteria gradually increased. At 24 h, the thermoduric bacterial counts increased to the same level as the mesophilic bacteria, and then gradually surpassed the

TABLE 1 | Changes in the pH value, temperature, and sensory characteristics of the non-post fermented Shuidouchi during fermentation.

Characteristic	Fermentation time/hours						
	Initial stage			Metaphase		Anaphase	
	0	12	24	36	48	60	72
Temperature/°C	41.93 ± 0.06^{d}	42.33 ± 0.58^{d}	52.17 ± 0.76^{a}	51.87 ± 0.23^{a}	50.67 ± 0.58^{ab}	47.50 ± 0.87^{bc}	44.67 ± 0.58^{cd}
pH	6.30 ± 0.02^{f}	6.36 ± 0.01^{f}	6.48 ± 0.01^{e}	7.43 ± 0.01^{d}	7.79 ± 0.00^{c}	7.85 ± 0.01^{b}	8.10 ± 0.01^{a}
Color	Yellow with red	Yellow with red	Yellow with red	Brownish orange	Brownish orange	Brownish orange	Light brown
Flavor	Cooked soybean flavor	Sour and mellow	Slight Douchi flavor	Douchi flavor	Strong Douchi flavor	Strong Douchi flavor	Strong Douchi flavor
Texture	Soft, without mucus	Soft, without mucus	Soft, short mucus filaments	Soft, long mucus filaments	Softer, a lot of mucus and long mucus filaments	Softer, a lot of mucus and long mucus filaments	Softer, the mucus thickened and filaments decreased

Trials were conducted in triplicate. $^{a-f}$Values in the columns with different lowercase letters were considered significantly different ($p < 0.05$).

TABLE 2 | Evolution of microbial population in the non-post fermented Shuidouchi during fermentation (unit was log CFU/g).

Culture medium	Culture conditions	Fermentation time/hours						
		Initial stage			Metaphase		Anaphase	
		0	12	24	36	48	60	72
Bacteria								
PCA	37°C, micro aerobic	2.91	8.10	8.10	8.13	8.20	8.40	8.58
	37°C, anaerobic	2.30	8.09	7.84	7.97	8.11	8.02	8.48
MRSA	37°C, micro aerobic	2.00	7.47	8.00	6.72	6.81	7.08	6.78
	37°C, anaerobic	2.00	7.62	8.09	6.46	7.43	7.21	8.28
MSA	37°C, micro aerobic	<2.00	6.30	7.28	6.60	7.45	7.45	8.30
BHIA	50°C, aerobic	<2.00	6.66	8.26	8.78	9.58	10.30	10.66
BMA	50°C, aerobic	<2.00	4.90	8.30	9.28	9.53	10.28	9.90
CESPA	50°C, aerobic	<2.00	5.72	8.48	9.11	9.00	9.00	9.38
Yeast								
PDA	28°C, aerobic	<1.70	4.03	<3.00	<2.00	<2.00	<2.00	2.86
YGC	28°C, aerobic	<1.70	4.09	<3.00	-	-	-	-
Mold								
PDA	28°C, aerobic	<1.70	2.78	<3.00	<2.00	<2.00	<2.00	<2.00
YGC	28°C, aerobic	<1.70	2.66	<3.00	-	-	-	

"-", undo.

mesophilic bacteria. At the end of fermentation, the thermoduric bacterial counts reached 10–100 times those of the mesophilic bacteria. The fungi were detected only 12 h in the initial stage of fermentation, indicating that the yeast and mold grew at a moderate temperature, though the yeast counts were slightly higher. The bacteria were the most dominant, and the yeast also occupied a certain position; however, the mold was inhibited. The high temperatures during metaphase and anaphase of fermentation reduced the counts of yeast and mold below the detection limit (< 2 log CFU/g). However, the temperature drop (45°C) at the end of fermentation allowed the yeast to recover and proliferate, and the mold was not detected under the combined effect of high temperature and pH. We concluded that the bacteria occupied the most dominant position during the fermentation of non-post fermented Shuidouchi, and the fungi only proliferated during the early and end stages without a dominant position throughout the fermentation process, while the products were dominated by the thermoduric bacteria.

Microbial Diversity of the Non-post Fermented Shuidouchi

Alpha Diversity of the Fermentation Samples

In this study, 335,947 bacterial and 295,019 fungal high-quality reads were obtained from the non-post fermented Shuidouchi samples (**Table 3**), where the average of the bacterial and fungal reads in the samples were 47,992 and 42,145, respectively. In addition, the Good's coverages of all samples were more than 0.998 (**Table 3**) with a similarity level of 97%, proving an effective cover for the microbial species. Furthermore, 592 OTUs were obtained from the bacterial reads, which were clustered into 15 phyla and 119 genera, and 2,809 OTUs were obtained from

TABLE 3 | Sequence number and alpha diversity indices of bacterial and fungal community of the non-post fermented Shuidouchi samples.

Sample	16S rDNA gene				ITS rDNA gene			
	Sequence number	Shannon	Chao1	Coverage	Sequence number	Shannon	Chao1	Coverage
0 h	61,606	0.20	131.85	0.999	40,978	4.98	966.65	0.998
12 h	42,239	1.70	222.03	0.999	39,782	5.13	906.15	0.998
24 h	53,141	2.14	264.50	0.999	39,895	5.14	974.67	0.998
36 h	46,327	1.73	341.06	0.998	50,440	5.14	1050.55	0.998
48 h	26,926	1.24	202.96	0.998	32,319	5.01	891.06	0.998
60 h	50,228	1.14	222.75	0.999	55,840	1.60	772.94	0.998
72 h	55,480	1.13	282.77	0.999	35,765	5.16	892.13	0.998

fungal reads belonging to 15 phyla and 377 genera. Indices of alpha diversity such as Chao1, Shannon, and Good's coverage (Coverage) are also listed in **Table 3**. The bacterial Shannon index increased first and then gradually decreased, and was the highest at a time point of 12 h. During fermentation, the bacterial Shannon index gradually decreased with increasing temperature and pH (**Tables 1**, **3**), and the fungal Shannon index was greater than the bacteria. During fermentation, the fungal Shannon index increased slightly after 12 h of fermentation and remained stable; however, with increasing temperature and pH, it decreased sharply after 60 h of fermentation. It increased again after 72 h at the end of fermentation with decreasing temperature (**Tables 1**, **3**).

Venn Diagrams of Bacteria and Fungi in Samples

As shown by the Venn diagram in **Figure 2A**, a total of 592 bacterial OTUs were detected in all samples, and 13 shared OTUs were found. The number of unique OTUs in the 0, 12, 24, and 36 h samples was larger than in the 48, 60, and 72 h samples. The common OTUs were allocated to *Bacillus* (30.77%), *Acinetobacter* (23.08%), *Pantoea* (15.38%), *Enterococcus* (7.69%), *Lactococcus* (7.69%), *Citrobacter* (7.69), and *Klebsiella* (7.69%) in the genus level.

As shown in **Figure 2B**, 2,809 fungal OTUs were observed in the diagram, which was significantly more than the bacterial counterpart. Thus, 141 common OTUs were allocated to unclassified (20.57%), unclassified Fungi (6.38%), *Aspergillus* (4.26%), *Mortierella* (3.55%), *Tomentella* (2.84%), unclassified *Sordariomycetes* (2.84%), *Lactarius*, *Sarocladium*, unclassified *Ascomycota*, unclassified *Lasiosphaeriaceae* (each of the former 4 genera 2.13%), *Alternaria*, *Candida*, *Fusarium*, unclassified *Hypocreales*, unclassified *Pleosporales*, unclassified *Rozellomycota*, unclassified *Sordariales*, *Verticillium* (each of the former 8 genera 1.42%), and other 56 genera (each 0.71%) in the genus level. The number of unique OTUs in each sample was 225, 211, 249, 287, 199, 169, and 204 for 0, 12, 24, 36, 48, 60, and 72 h, respectively.

These results suggested that a higher fermentation temperature coupled with a higher pH reduced the number of unique microbes and microbial diversity of the samples in the second half of fermentation.

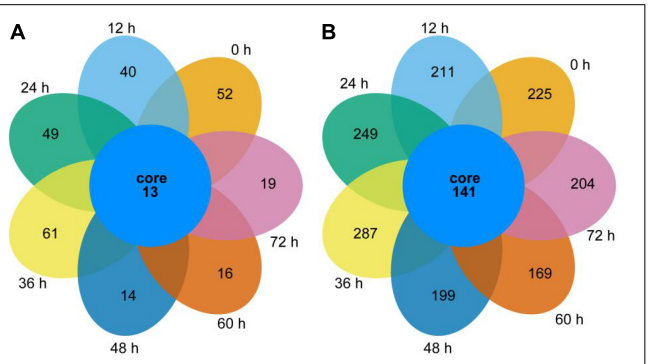

FIGURE 2 | Bacterial and fungal Venn diagrams of the non-post fermented Shuidouchi. **(A)** Venn diagrams of the bacterial OTUs, **(B)** Venn diagrams of the fungal OTUs.

Changes in the Microbial Communities of the Non-post Fermented Shuidouchi

The changes in bacterial community composition are shown in **Figures 3A,C**. We observed the lowest level of richness and evenness at the starting point of fermentation (0 h), and the evenness increased at 12 and 24 h in the initial stage and decreased in the metaphase and anaphase stages (36, 48, 60, and 72 h). At a time point of 12 h, the number of genus types, and the relative abundance of genera in the orders of *Enterobacterales* and *Pseudomonadales* were high, mainly including *Klebsiella*, *Citrobacter*, *Acinetobacter*, *Pantoea*, *Cronobacter*, *Escherichia/Shigella,* and *Pseudomonas*. In the metaphase stage of fermentation, only *Klebsiella*, *Citrobacter,* and *Acinetobacter* remained with their relative abundance, which continued to decrease, and only *Klebsiella* remained with a low relative abundance (about 1%) at the end of fermentation (72 h). The reason for this phenomenon was that the moderate temperature during the initial stage was suitable for the growth of most types of bacteria, while the temperature after 12 h continued to remain at approximately 50°C and the pH gradually increased to 8.1 (**Table 1**), reaching the growth limit of most bacteria. *Lactococcus* increased during the initial stage of fermentation; however, it maintained a low relative abundance level of about 5% in the metaphase and anaphase stages. The relative abundance of *Aneurinibacillus* increased gradually to 2% or so in the metaphase and anaphase stages. Meanwhile, *Bacillus* had the highest abundance in all bacterial sequences, where the relative abundance was the highest in all samples and gradually increased

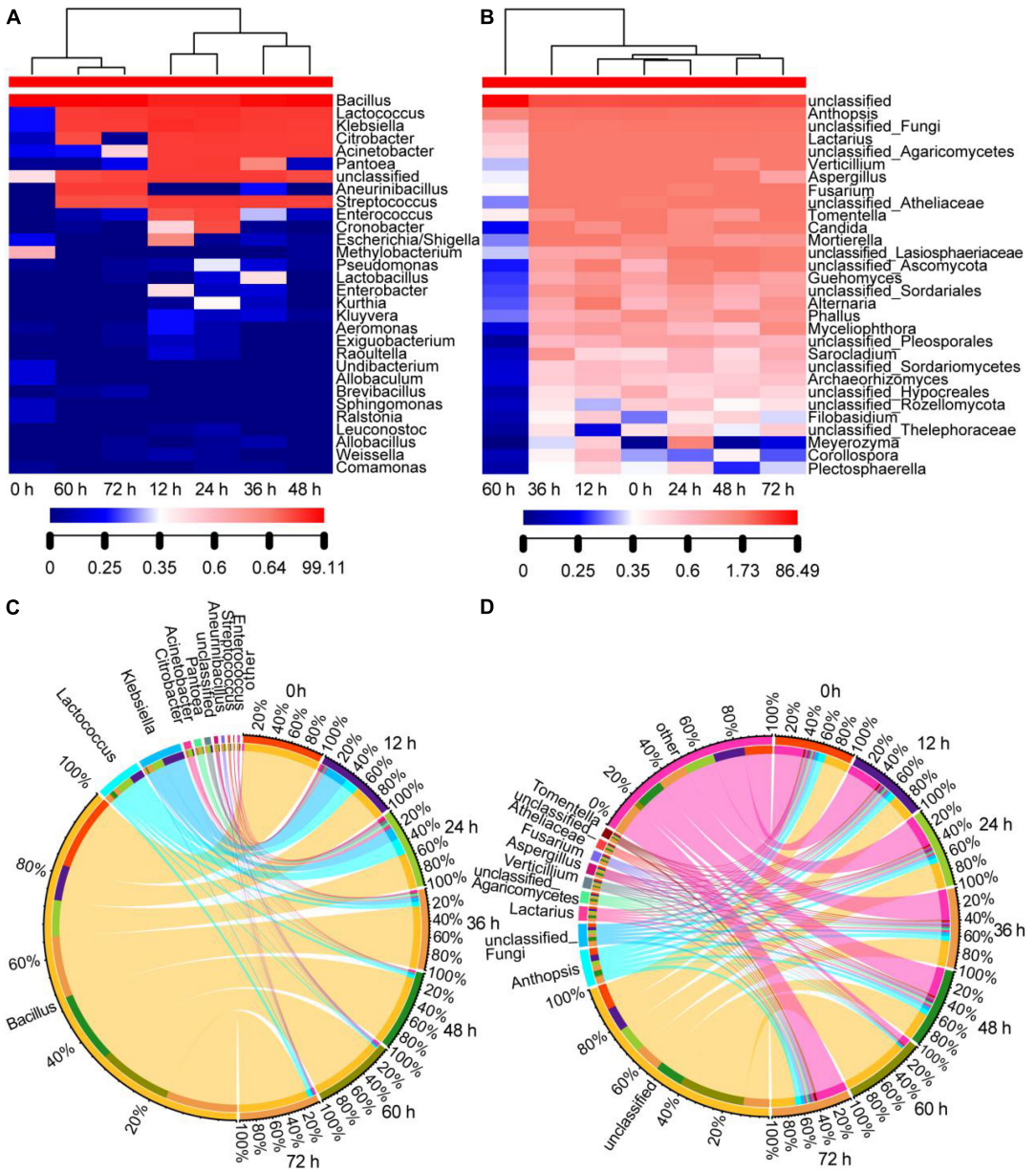

FIGURE 3 | Genera distribution of the bacterial and fungal communities in the non-post fermented Shuidouchi: **(A)** Bacterial community heatmap (top 30 genera); **(B)** fungal community heatmap (top 30 genera), where the number indicates the value of the genus relative abundance; **(C)** the Circos of the bacterial genera distribution in the samples; **(D)** the Circos of the fungal genera distribution in the samples, where the relative abundance of the genera is represented by the relative tick on the outer circle, and the relative abundance of the genera is represented by the thickness of the colorful ribbons.

to more than 90% during fermentation, and it was the most dominant bacterial genus throughout fermentation. The high temperature and pH reduced the bacterial diversity of the samples, resulting in clustering of the samples during anaphase and in the 0 h sample (**Figure 3A**).

The fungal heatmap (**Figure 3B**) showed that the diversity of fungi was much higher than the bacteria, and the evenness and richness of the fungi remained constant during fermentation compared to the bacterial community, except for the 60-h sample, which decreased due to the high temperature (50°C) and high pH (7.85) effect for 12 h. However, the richness and evenness of the fungal community returned when the temperature dropped to 45°C (72 h sample). The top 10 genera of classified fungi, arranged in the order of relative abundance from high to low, consisted of *Anthopsis*, unclassified Fungi, *Lactarius*, unclassified *Agaricomycetes*, *Verticillium*, *Aspergillus*, *Fusarium*, unclassified *Atheliaceae*, *Tomentella*, and *Candida*. However, the relative abundance of each genus in these classified fungi was lower than 10%, and 352 genera of all 372 classified genera had a relative abundance that was lower than 1%. The relative abundance

of the top 10 genera in the different samples was similar (**Figure 3D**). These phenomena indicated that the fungi were not prosperous, as the fermentation temperature was higher than their growth limits.

Principal Coordinate Analysis

As shown by the bacterial PCoA (**Figure 4A**), the samples were regularly clustered based on the evolutionary distance (weighted Unifrac distance) of the bacterial OTUs, where the 12 and 24 h samples were clustered, while the 36, 48, 60, and 72 h samples were also grouped, and the 0 h sample was far away from the samples of the other time points. The results showed that the number and abundance of the bacterial genera were nearly the same at 12 and 24 h; however, this changed greatly after 24 h during fermentation. The number and abundance of the bacterial genera in the latter half of fermentation (48, 60, and 72 h) were similar. The clustering results shown in **Figure 4A** were consistent with the changes in the fermentation temperature and pH (**Table 1**), because the 0 h sample had the lowest temperature while the samples at the other time points had higher temperatures, and the pH increased sharply during fermentation from 24 to 72 h, which changed the evolutionary distance of the fermentation samples.

Meanwhile, the number and abundance of the fungal genera in the different samples were similar, because the distances between the samples were far shorter in **Figure 4B** than in **Figure 4A**. That indicated that the fungi did not flourish because of an unsuitable temperature and pH (**Figure 4B**, Section "Changes in Temperature, pH Value, Sensory Characteristics, and Microbial Growth").

Chemical Analysis of the Non-post Fermented Shuidouchi

The concentrations of each biogenic amine were lower than 50 μg/g (**Table 4**). We also found that TRP increased sharply at the end of fermentation, while PHE increased slowly from 36 to 72 h. PUT was found in the cooked soybeans, which increased rapidly during the initial stage of fermentation (24 h), and then decreased slowly. CAD gradually increased in the metaphase and anaphase stages of fermentation, and HIS appeared in the metaphase stage of fermentation (36 h) and then decreased gradually. TYR appeared at a very low concentration at 24 h, and then was maintained at a low level. In addition, SPD was originally at a high level in the cooked soybeans, and increased slightly during fermentation, while SPM was found in a small amount in the cooked soybeans and increased significantly from the metaphase stage (36 h); however, the concentration was not high. Total biogenic amine content (total concentration of 8 biogenic amines) increased significantly with time.

Pearson correlation (r) analysis of the biogenic amines is shown in **Table 5**, where the r value between HIS and bioamine (total biogenic amines) was close to 0. The other seven biogenic amines had a positive correlation with bioamine; thus, bioamine could be used as an important monitoring index. Similarly, the correlation between the histamine and fermentation time was low, while the r values between the other seven biogenic amines, bioamine, and time showed a significantly positive correlation.

The alkylpyrazines and related compounds (2,3-butanediol and acetoin) were identified and are listed in **Table 6**. No alkylpyrazine content was found before 12 h, and minimal alkylpyrazine content appeared at 24 h during fermentation. Between 36 and 72 h, alkylpyrazine was always the main volatile compound in the product (relative content of more than 20%), where the highest was tetramethylpyrazine, followed by trimethylpyrazine, 2,5-dimethylpyrazine (2,5-DMP), 2-ethyl-3,5,6-trimethylpyrazine (3,5,6-ETMP), and 2-ethyl-3,6-dimethylpyrazine (3,6-EDMP). Tetramethylpyrazine is also named ligustrazine (2,3,5,6-tetramethylpyrazine), which could be used as a promising remedy for cardiovascular diseases (35). The high relative content of tetramethylpyrazine during fermentation (36–72 h) of the non-post fermented Shuidouchi indicated that this product offered cardiovascular and cerebrovascular health care properties after 36 h of fermentation.

Correlation of Microbiota and Influence Factors in Non-post Fermented Shuidouchi

As shown in **Figures 4C,D**, the arrows of temperature were longer than other arrows, indicating the temperature was the most significant influential factor toward the changes in bacterial and fungal communities. The angle between the temperature and BA was acute, as it indicated a positive correlation between the temperature and total biogenic amine concentration. We observed weak positive correlations between the temperature and pH, tetramethylpyrazine, or 2,3-butanediol (**Figure 4C**); however, 2,3-butanediol was negatively correlated with tetramethylpyrazine, pH, and BA because the intersection angles of the arrows were obtuse (**Figures 4C,D**).

In CCA figures, the closer the projection point of the sample (or community structure, OTU) is to the arrow, the greater the impact of the environmental factor on the sample (or community structure, OTU). For the bacterial CCA diagram (**Figure 4C**), we found that temperature had a significant impact on the bacterial communities in the 24- and 36-h samples, where 2,3-butanediol had a significant effect on the bacterial communities in the 12- and 24-h samples. In addition, tetramethylpyrazine, pH, and BA had great effects on the bacterial communities of the fermentation samples at 0, 60, 72, and 48 h, while the 12- and 24-h samples had the highest relative abundance of bacterial flora on the genus level.

The temperature in the CCA diagram of the fungi (**Figure 4D**) had a significant impact on the fungal community in the 24- and 60-h samples, while the tetramethylpyrazine and pH had the greatest effects on the fungal community in the sample fermented for 60 h. The relative abundance of fungal flora in the 12-, 24-, and 60-h samples was higher than in the other samples.

Pearson Correlation Between the Microbes and Chemicals in the Non-post Fermented Shuidouchi

The chemical characteristics, temperature, and pH were used to analyze their Pearson correlation with the bacterial and fungal abundance (top 20 genera) in the non-post fermented

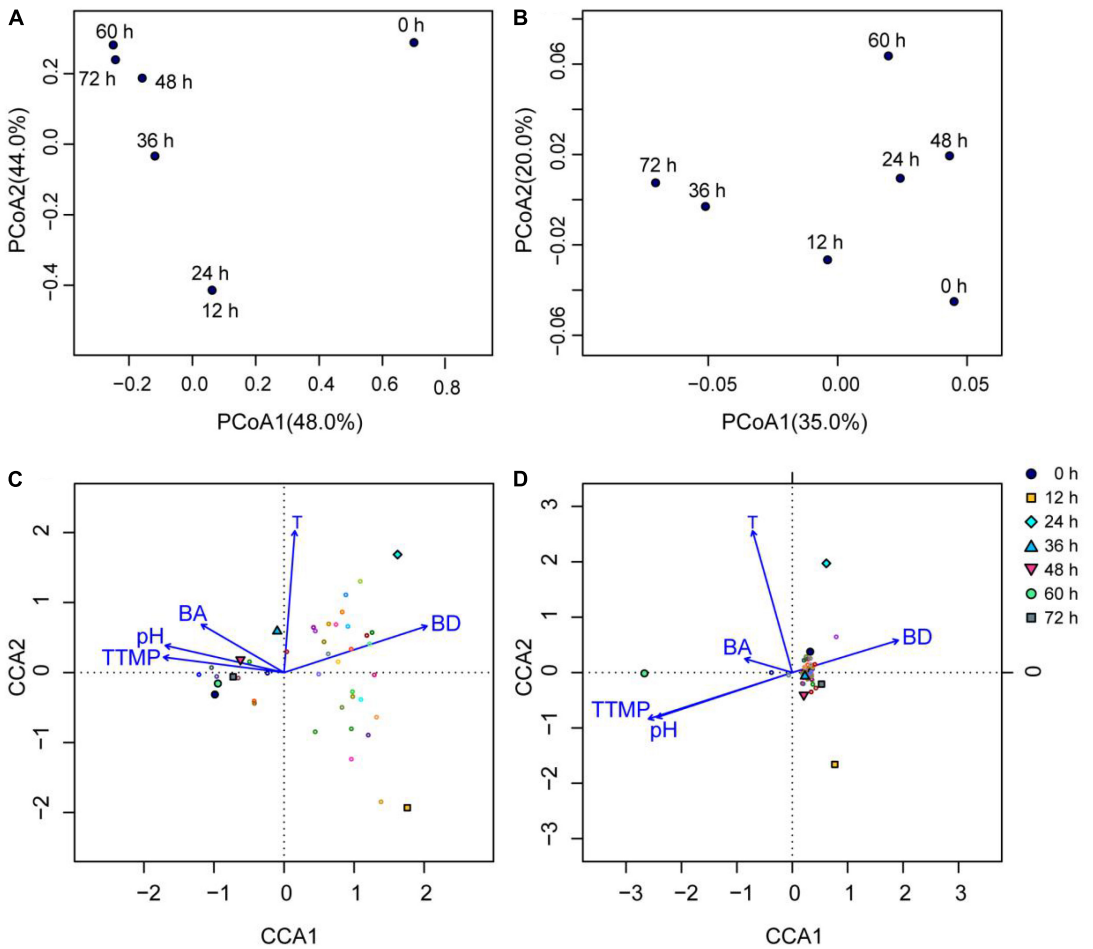

FIGURE 4 | Bacterial and fungal principle coordinate analysis (PCoA) based on the weighted Unifrac distance at the OTU level, and CCA analysis based on the genus level (top 20 genera) in the non-post fermented Shuidouchi: **(A)** bacterial PCoA; **(B)** fungal PCoA; **(C)** the CCA of the bacterial communities in the samples; **(D)** CCA of the fungal communities in the samples, where T, temperature; BA, total biogenic amines concentration; BD, 2,3-butanediol.

TABLE 4 | Changes in the biogenic amine concentration in the non-post fermented Shuidouchi.

Biogenic amine	0 h	12 h	24 h	36 h	48 h	60 h	72 h
TRP (μg/g)	0^{b}	0.44 ± 0.76^{b}	0^{b}	0^{b}	2.09 ± 3.62^{b}	0^{b}	22.54 ± 14.09^{a}
PHE (μg/g)	0^{b}	0^{b}	0^{b}	1.88 ± 0.02^{b}	1.06 ± 0.63^{b}	1.80 ± 0.02^{b}	8.44 ± 7.04^{a}
PUT (μg/g)	4.93 ± 0.91^{d}	5.38 ± 0.03^{d}	19.01 ± 0.19^{a}	12.53 ± 0.30^{bc}	13.28 ± 1.13^{b}	12.19 ± 0.64^{bc}	11.42 ± 0.54^{c}
CAD (μg/g)	0.91 ± 0.10^{d}	2.28 ± 0.06^{cd}	3.57 ± 0.28^{c}	6.40 ± 0.23^{b}	7.23 ± 0.19^{b}	9.65 ± 0.06^{a}	11.08 ± 3.52^{a}
HIS (μg/g)	0^{c}	0^{c}	0^{c}	2.74 ± 0.30^{a}	1.51 ± 1.31^{b}	0^{c}	0.73 ± 1.26^{bc}
TYR (μg/g)	0^{d}	0^{d}	0.55 ± 0.01^{d}	3.34 ± 0.01^{b}	1.41 ± 0.02^{c}	4.81 ± 0.02^{a}	2.68 ± 1.08^{b}
SPD (μg/g)	8.37 ± 0.01^{bc}	7.03 ± 0.01^{bc}	6.52 ± 0.01^{c}	8.84 ± 0.01^{b}	8.10 ± 0.01^{bc}	7.58 ± 0.01^{bc}	11.55 ± 2.99^{a}
SPM (μg/g)	3.93 ± 0.03^{c}	2.60 ± 0.27^{c}	3.15 ± 0.02^{c}	6.52 ± 0.01^{b}	5.03 ± 0.01^{bc}	9.23 ± 0.02^{a}	9.16 ± 3.59^{a}
Total biogenic amines (μg/g)	18.14 ± 0.81^{c}	17.73 ± 1.07^{c}	32.80 ± 0.35^{bc}	42.25 ± 0.85^{b}	39.72 ± 2.47^{b}	45.26 ± 0.60^{b}	77.60 ± 30.45^{a}

Trials were conducted in triplicate. $^{a-d}$*Values in the columns with different lowercase letters were considered significantly different ($p < 0.05$).*

Shuidouchi (**Figure 5**). As shown in **Figure 5A**, there were 27 positive correlations between 20 bacterial genera and the above characteristics at a significance level of $P < 0.1$, while 40 negative correlations were found at the same significance level. Thirteen significant positive correlations were found between the bacterial genera and characteristics, while a significant negative correlation ($P < 0.05$) was found. No bacterial genus was correlated with TRP, PHE, total biogenic amines, trimethylpyrazine, and pH. Among the 13 significant positive correlations, *Lactobacillus* and Acetoin were the strongest ($r = 0.959$, $P < 0.001$), followed by *Acinetobacter* and 2,3-butanediol ($r = 0.90$, $P < 0.01$), *Aneurinibacillus* and SPM

TABLE 5 | Pearson correlation coefficients of the biogenic amine index during fermentation of the non-post fermented Shuidouchi.

	TRP	PHE	PUT	CAD	HIS	TYR	SPD	SPM	Bioamine	Time
TRP	1.000	0.940**	–0.007	0.654**	–0.122	0.253	0.901**	0.634**	0.873**	0.548**
PHE	0.940**	1.000	0.051	0.762**	–0.099	0.463*	0.930**	0.783**	0.929**	0.605**
PUT	–0.007	0.051	1.000	0.355	0.183	0.292	–0.136	0.137	0.324	0.432
CAD	0.654**	0.762**	0.355	1.000	0.148	0.827**	0.645**	0.915**	0.911**	0.950**
HIS	–0.122	–0.099	0.183	0.148	1.000	0.234	0.079	0.042	0.083	0.232
TYR	0.253	0.463*	0.292	0.827**	0.234	1.000	0.376	0.884**	0.637**	0.761**
SPD	0.901**	0.930**	–0.136	0.645**	0.079	0.376	1.000	0.720**	0.840**	0.490*
SPM	0.634**	0.783**	0.137	0.915**	0.042	0.884**	0.720**	1.000	0.860**	0.797**
Bioamine	0.873**	0.929**	0.324	0.911**	0.083	0.637**	0.840**	0.860**	1.000	0.817**
Time	0.548**	0.605**	0.432	0.950**	0.232	0.761**	0.490*	0.797**	0.817**	1.000

*Bioamine, total biogenic amines; *P < 0.05, **P < 0.01.*

TABLE 6 | Changes in 2,3-butanediol, acetoin, and alkylpyrazine in the non-post fermented Shuidouchi.

Compounds	Relative content (%)						
	0 h	12 h	24 h	36 h	48 h	60 h	72 h
BD	0	1.67	**2.03**	2.36	0.82	0.30	0
Acetoin	0	0	0	2.55	0	0	0.01
2,5-DMP	0	0	**0.12**	**9.07**	**15.97**	**9.76**	**8.34**
3,6-EDMP	0	0	0	**0.81**	**1.15**	**0.84**	**0.67**
TTMP	0	0	**0.04**	**16.17**	**13.99**	**23.28**	**28.99**
3,5,6-ETMP	0	0	0	**0.89**	**1.36**	**2.00**	**2.02**
TMP	0	0	0	0	0	0	**9.58**

In this work, the following definitions were used: BD, 2,3-butanediol; 2,5-DMP, 2,5-dimethylpyrazine; 3,6-EDMP, 2-ethyl-3,6-dimethylpyrazine; TTMP, tetramethylpyrazine; 3,5,6-ETMP, 2-ethyl-3,5,6-trimethylpyrazine; TMP, trimethylpyrazine. The matching degree between the compounds corresponding to the bold black number and the NIST 14.L library was greater than or equal to 80%, while the matching degree of the corresponding compounds with the red numbers was 50–80%.

(r = 0.85, $P < 0.01$). The others included *Pseudomonas*, *Kurthia,* and PUT (rp = 0.67, rk = 0.71), with *Aneurinibacillus* and CAD (r = 0.74), *Lactobacillus* and HIS (r = 0.77), *Aneurinibacillus* and TYR (r = 0.79), *Citrobacter*, *Streptococcus*, *Kluyvera*, unclassified, and 2,3-butanediol (rc = 0.76, rs = 0.84, rk = 0.85, ru = 0.86), *Aneurinibacillus* and 3,5,6-ETMP (r = 0.79) showing weaker positive correlations ($P < 0.05$). *Aeromonas* was negatively correlated with 3,6-EDMP (r = –0.69, $P < 0.05$). As the highest abundance genus (**Figure 3A**), *Bacillus* was positively correlated with many chemical characteristics, such as SPD (r = 0.57, P = 0.09), SPM (r = 0.64, P = 0.06), 2,5-DMP (r = 0.57, P = 0.09), 3,6-EDMP (r = 0.58, P = 0.09), 3,5,6-ETMP (r = 0.61, P = 0.07), and tetramethylpyrazine (r = 0.58, P = 0.17), which indicated a positive correlation between *Bacillus* and the functionality of non-post fermented Shuidouchi.

As shown in **Figure 5B**, there were eight positive correlations between fungal genera and the chemical characteristics at a significance level of $P < 0.1$, while 33 negative correlations were found at the same significance. Four significant positive correlations were found between fungal genera and the assessed characteristics, while 14 significant negative correlations ($P < 0.05$) were found. No fungal genus was found to be correlated with PUT, total biogenic amines, 2,3-butanediol, 2,5-DMP, 3,6-EDMP, pH and temperature. Among the four significant positive correlations ($P < 0.05$), three positive correlations were found between *Tomentella* and TRP (r = 0.81), SPD (r = 0.71), trimethylpyrazine (r = 0.81), while one positive correlation was between unclassified and TYR (r = 0.72). Among the 14 significant negative correlations, unclassified *Pleosporales* and TYR showed the strongest correlation (r = –0.85, $P < 0.01$), while the others including *Anthopsis*, *Lactarius*, *Aspergillus*, *Mortierella*, *Guehomyces*, *Phallus,* and TYR (ra = –0.80, rl = –0.75, ra = –0.75, rm = –0.73, rg = –0.83, rp = –0.74), *Lactarius*, *Aspergillus*, *Mortierella*, *Guehomyces*, unclassified *Pleosporales* and SPM (rl = –0.69, ra = –0.80, rm = –0.70, rg = –0.75, ru = –0.71), *Aspergillus*, *Mortierella* and 3,5,6-ETMP (ra = –0.70, rm = –0.69) showed weaker positive correlations ($P < 0.05$). We found from the Pearson correlation heat map that many fungi were negatively correlated with TYR and SPM, indicating that the fungi could reduce the concentration of biogenic amines and improve the safety of the product.

Analysis of Phylogenetic Investigation of Communities by Reconstruction of Unobserved States Functional Annotation

The KEGG functional annotation of the bacterial community is shown in **Table 7**. Seven primary functions were annotated during fermentation. The most abundant primary function was metabolism, which accounted for more than 30% of the reads in the samples. In addition, 39 KEGG pathways

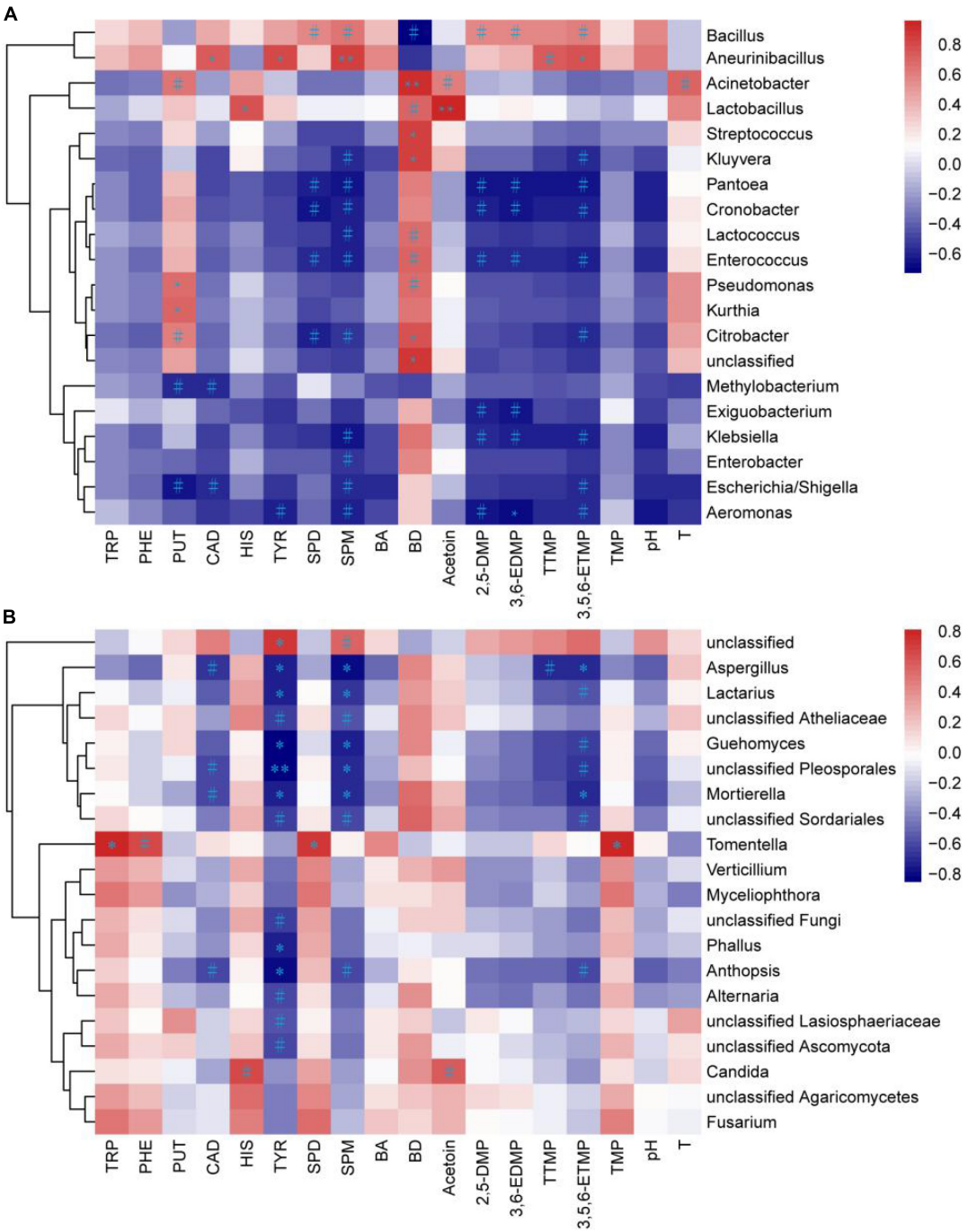

FIGURE 5 | Heatmap of the correlations between the microbiota and chemical characteristics in the non-post fermented Shuidouchi samples. The Pearson correlation coefficient r in the bacterial **(A)** and fungal **(B)** communities ranged from –1 to 1; positive correlation was $r > 0$, and the negative correlation was $r < 0$, where #represents $p < 0.1$, *represents $p < 0.05$ and **represents $p < 0.01$, and T, temperature; BA, total biogenic amine concentration; BD, 2,3-butanediol.

were annotated at level 2, including membrane transport, carbohydrate metabolism, amino acid metabolism, replication and repair, cellular processes, and signaling, poorly characterized, energy metabolism, metabolism of the cofactors and vitamins, translation, lipid metabolism, cell motility, metabolism, nucleotide metabolism, transcription, xenobiotic biodegradation, and metabolism, genetic information processing, enzyme families, signal transduction, folding, sorting and degradation, metabolism of terpenoids and polyketides, and the others (< 2%) were arranged in descending order of percentage. As shown in **Table 7**, the relative abundance of membrane transport, poorly characterized, metabolism, signal transduction, glycan

biosynthesis and metabolism, biosynthesis of the other secondary metabolites, and infectious diseases decreased gradually. The relative abundance of amino acid metabolism, replication and repair, energy metabolism, metabolism of cofactors and vitamins, translation, lipid metabolism, cell motility, nucleotide metabolism, metabolism of terpenoids and polyketides, cell growth and death, endocrine system, transport and catabolism, neurodegenerative diseases, and environmental adaptation increased step by step. However, the relative abundances of other second level metabolic pathways were relatively stable.

The Pearson correlations between the relative abundances of the top 20 bacterial genera and the percentages of the 39 KEGG second level function pathways are shown in **Figure 6**. More than half of the correlations were significant, where the number of negative correlation coefficients was slightly more than the positive correlation coefficients. Among the top 20 bacteria, *Bacillus*, *Aneurinibacillus*, and *Methylobacterium* were positively correlated with amino acid metabolism, the metabolism of other amino acids, lipid metabolism, and the energy metabolism, while the other bacteria were positively correlated with carbohydrate metabolism, glycan biosynthesis and metabolism, biosynthesis of the other secondary metabolites, and metabolism. As the most dominant genus, *Bacillus* had complementary metabolic pathways with the other genera, as shown in **Figure 6**. The functional pathway analysis results indicated that the thermoduric and thermophilic bacteria such as *Bacillus* and *Aneurinibacillus* continued to reproduce at higher temperatures, which further caused the temperature of the product to increase to the limit value by the energy metabolism pathway. Meanwhile, the low abundance of bacterial genera decreased in the metaphase and anaphase stages of fermentation due to the high temperatures. They were prosperous in the initial stage of fermentation at moderate temperatures (**Figure 3C**), which was conducive to the formation of functional products by bringing about numerous metabolites into the product through the functional pathways of carbohydrate metabolism, glycan biosynthesis and metabolism, and the biosynthesis of other secondary metabolites (**Figure 6**).

DISCUSSION

Considering the bacterial communities in this research, we found that *Bacillus* was the most dominant bacterial genus in the fermentation process of the non-post fermented Shuidouchi, according to Illumina Miseq sequencing, and *Lactococcus* maintained a certain proportion in the different periods. *Klebsiella* was also found; however, it gradually decreased to low abundance in the metaphase and anaphase stages of fermentation. During the second half of fermentation (48–72 h), the diversity and relative abundance of the bacterial flora remained relatively steady, and the number of dominant bacterial genera decreased; however, the spore producing bacteria showed a diversified trend. In addition to *Bacillus*, *Aneurinibacillus* with a low relative abundance also appeared in the second half of fermentation. These results were similar to other studies on Shuidouchi. Chen et al. found that *Bacillus*, *Bacteroides*, and *Lactobacillus* were the main genera in Shuidouchi with post-fermentation from the different regions in China (9). Wang et al. found that the dominant bacteria were *Bacillus*, *Staphylococcus*, *Enterococcus*, *Proteus*, *Brevibacillus*, *Providencia*, *Weissella,* and *Ureibacillus* in wet and dry Enshi Douchi, and *Aneurinibacillus* also appeared in certain samples (36). The dominant bacteria in bacterial Douchi from Gansu province in China were *Bacillus* and *Ignatzschineria*, and *Aneurinibacillus* was also found in some samples (11). Further analysis of the bacterial community in Shuidouchi showed that the dominant bacteria were *Caldibacillus thermoamylovorans*, *Bacillus smithii*, *Bacillus licheniformis,* and *Bacillus subtilis*. Some harmful bacteria were also found, including *Proteus mirabilis*, *Serratia marcescens*, *Alcaligenes faecalis*, *Bacillus cereus*, which came from the condiments, such as spices, salt in Shuidouchi with post fermentation. The Shuidouchi with post-fermentation needs adding unsterilized condiments before post-fermentation at a room temperature. The harmful bacteria might enter the product with the unsterilized condiments, and the moderate temperature also accelerates the growth of these bacteria (10, 37, 38). The non-post fermented Shuidouchi in this research also contained *C. thermoamylovorans*, *B. licheniformis*, and *B. subtilis*, which was identified by the PCR-DGGE method and identification of the pure isolated cultures, while *Caldibacillus thermolactis* and *Ureibacillus thermosphaericus* were only detected by PCR-DGGE (data not shown); however, not by high-throughput sequencing in this research, which was possibly caused by different PCR methods (PCR-DGGE inspected the V6-V8 region of bacterial 16 S rDNA, while the bacterial high-throughput sequencing in this research inspected the V3-V4 region of 16 S rDNA). As a conclusion of this research and relative articles, the main bacterial genera in non-post fermented Shuidouchi were *Bacillus*, *Caldibacillus*, *Ureibacillus,* and *Aneurinibacillus*. The temperature had the greatest impact on the diversity of the bacterial flora in the non-post fermented Shuidouchi on the genus level (**Figure 4C**). At a moderate temperature in the initial stage of fermentation, the richness and evenness of the bacterial community increased; however, at a high temperature in the metaphase and anaphase stages of fermentation, only *Bacillus* grew normally, which reduced the richness and evenness of the bacterial communities in the samples (**Figures 3A,C**). *Bacillus* showed high levels of protease (39) and amino acid metabolism functionality (**Figure 6**) at high temperatures (45–50°C), which caused the pH to increase (**Figure 5A** and **Table 1**), reaching the growth limit of a variety of bacteria (**Table 1**). This further consolidated the absolute dominant position of the spore producing bacteria and promoted the diversification of spore producing bacteria.

The fungi in non-post fermented Shuidouchi during fermentation were much more diversified than the bacteria (**Figure 2**), and the richness and evenness of the fungal communities in the samples remained relatively constant compared to the bacterial communities (**Figures 3B,D**). We observed hundreds of fungal genera in the samples, such as unclassified, *Anthopsis*, unclassified fungi, *Lactarius*, unclassified *Agaricomycetes*, *Verticillium*, *Aspergillus*, *Fusarium*, unclassified *Atheliaceae*, *Tomentella*, and *Candida*. When the temperature

TABLE 7 | The KEGG functional annotation of bacterial 16S rDNA in the non-post fermented Shuidouchi.

KEGG pathways	Percentage composition in samples (%)						
	0 h	12 h	24 h	36 h	48 h	60 h	72 h
Cellular processes; cell growth and death	0.40	0.24	0.27	0.31	0.36	0.38	0.37
Cellular processes; cell motility	3.55	0.89	1.19	2.11	3.11	3.66	3.30
Cellular processes; transport and catabolism	0.27	0.16	0.17	0.21	0.25	0.27	0.26
Environmental information processing; membrane transport	11.61	18.92	18.00	15.88	13.43	12.87	13.38
Environmental information processing; signal transduction	2.36	2.45	2.39	2.30	2.15	2.05	2.05
Environmental information processing; signaling molecules and interaction	0.21	0.15	0.16	0.16	0.18	0.17	0.18
Genetic information processing; folding, sorting and degradation	2.14	1.96	1.99	2.02	2.03	2.00	1.99
Genetic information processing; replication and repair	7.26	5.46	5.80	6.27	6.96	7.13	7.04
Genetic information processing; transcription	3.10	3.31	3.24	3.22	3.17	3.21	3.21
Genetic information processing; translation	4.16	3.24	3.46	3.72	4.11	4.18	4.17
Human diseases; cancers	0.12	0.08	0.09	0.09	0.09	0.08	0.08
Human diseases; cardiovascular diseases	0.00[a]	0.00	0.00	0.00	0.00	0.00	0.00
Human diseases; immune system diseases	0.03	0.04	0.04	0.04	0.04	0.03	0.04
Human diseases; infectious diseases	0.28	0.51	0.50	0.42	0.35	0.32	0.34
Human diseases; metabolic diseases	0.06	0.06	0.06	0.06	0.07	0.07	0.07
Human diseases; neurodegenerative diseases	0.27	0.19	0.19	0.22	0.24	0.25	0.24
Metabolism; amino acid metabolism	10.56	8.79	8.91	9.47	10.13	10.36	10.19
Metabolism; biosynthesis of other secondary metabolites	0.61	0.79	0.77	0.70	0.64	0.60	0.63
Metabolism; carbohydrate metabolism	9.98	11.52	11.31	11.02	10.56	10.50	10.63
Metabolism; energy metabolism	4.91	4.63	4.65	4.85	5.04	5.24	5.16
Metabolism; enzyme families	2.52	2.02	2.03	2.07	2.11	2.01	2.00
Metabolism; glycan biosynthesis and metabolism	1.02	1.94	1.91	1.60	1.23	1.06	1.17
Metabolism; lipid metabolism	3.97	2.88	2.99	3.32	3.62	3.69	3.60
Metabolism; metabolism of cofactors and vitamins	3.90	3.82	3.82	4.01	4.20	4.43	4.36
Metabolism; metabolism of other amino acids	1.82	1.75	1.77	1.80	1.81	1.82	1.82
Metabolism; metabolism of terpenoids and polyketides	2.05	1.55	1.60	1.72	1.87	1.87	1.84
Metabolism; nucleotide metabolism	3.32	2.77	2.91	3.04	3.27	3.31	3.30
Metabolism; xenobiotics biodegradation and metabolism	3.28	2.84	2.86	2.90	2.94	2.79	2.81
Organismal systems; circulatory system	0.00[b]	0.00	0.00	0.00[c]	0.00	0.00	0.00
Organismal systems; digestive system	0.06	0.04	0.04	0.05	0.06	0.06	0.06
Organismal systems; endocrine system	0.30	0.16	0.18	0.23	0.29	0.32	0.30
Organismal systems; environmental adaptation	0.15	0.09	0.10	0.11	0.13	0.13	0.13
Organismal systems; excretory system	0.03	0.05	0.04	0.04	0.03	0.03	0.03
Organismal systems; immune system	0.06	0.04	0.04	0.04	0.03	0.02	0.02
Organismal systems; nervous system	0.06	0.05	0.05	0.06	0.06	0.06	0.06
Unclassified; cellular processes and signaling	5.90	5.33	5.24	5.42	5.52	5.57	5.46
Unclassified; genetic information processing	2.04	2.44	2.52	2.37	2.32	2.28	2.37
Unclassified; metabolism	2.47	3.46	3.34	2.94	2.55	2.31	2.45
Unclassified; poorly characterized	5.15	5.40	5.40	5.23	5.03	4.86	4.92

[a]0.0004, [b]0.0007, [c]0.0002.

was suitable, the fungi were prosperous and formed a mold type Douchi, which was the reason why so many types of Douchi in China were found to be mold type (24). However, in this non-post fermented Shuidouchi, the high temperatures suppressed fungal activity and prevented germination of the yeast cells, reproductive hyphae, spores and dormant hyphae, which caused a high diversity and evenness of the fungi in the different fermentation stages. As a result, the counts of culturable fungi were very low during fermentation (**Table 2**), among which the counts of yeast were lower than post fermented Shuidouchi due to non-post fermentation (9). The temperature was the environmental factor that had the greatest impact on the fungal communities of the non-post fermented Shuidouchi samples (**Figure 4D**), while high temperatures inhibited the growth of fungi. Consequently, the microbes in the non-post fermented Shuidouchi samples were mainly bacteria, and fungi only occupied a certain proportion when the temperatures at the beginning and end of fermentation were close to the appropriate temperature (**Table 2**). *Bacillus* potentially caused a pH increase in the product, which also inhibited the growth of fungi. Moreover, the volatiles generated by *Bacillus* could inhibit fungi such as *Botrytis cinerea* and *Phaeomoniella*

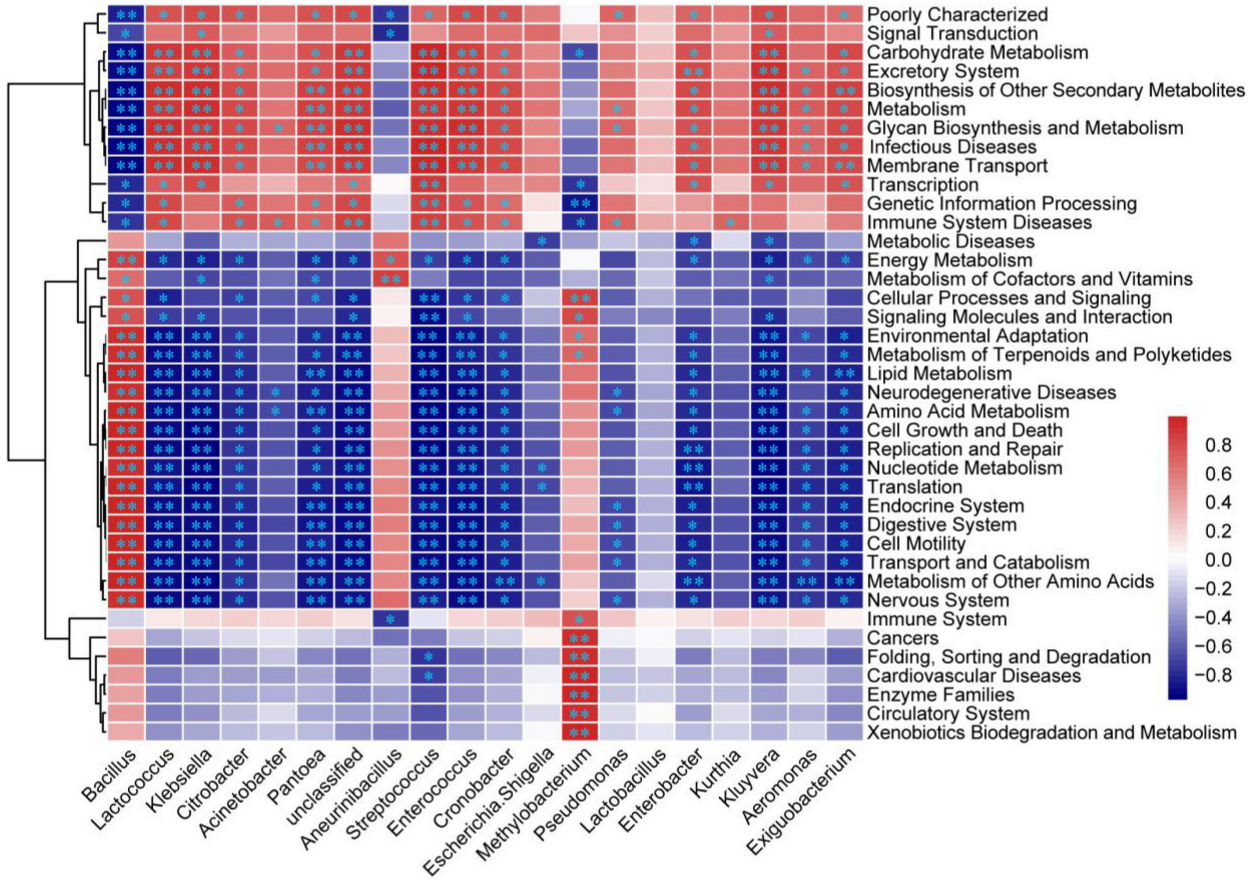

FIGURE 6 | Heatmap of correlations between the bacteria and KEGG function pathways in the non-post fermented Shuidouchi. The Pearson correlation coefficient r between the bacteria and function pathway ranged from –1 to 1, where the positive correlation was $r > 0$, and the negative correlation was $r < 0$. *Represents $p < 0.05$ and **represents $p < 0.01$.

chlamydospora by the function of alkylpyrazines (40, 41). *Bacillus* could also produce lipopeptide antibiotic iturin A, inhibiting fungi such as *Fusarium oxysporum* and *Rhizoctonia solani* (42). The former four conditions in the non-post fermented Shuidouchi formed a superimposed inhibitory effect on the fungi, especially on the molds.

Food born biogenic amines contain nitrogenous chemicals that originate from amino acids from microbial decarboxylation, and eight biogenic amines are often found. Some of these include polyamines such as PUT, SPM, and SPD, especially SPD, which have been found to exhibit protective effects against chronic diseases, such as metabolic disease, heart disease, neurodegeneration, and cancer (15, 16). PUT, SPM, and SPD were originally in cooked soybeans, and their quantities in non-post fermented Shuidouchi increased significantly to 11.42, 9.16, and 11.55 μg/g (**Table 4**), respectively. This would enhance the health protection functionality of the product, compared to cooked soybeans. The quantities of PUT, SPM, and SPD in this product were lower than Shuidouchi (12.21, 39.00, and 24.72 μg/g, respectively) and Natto (7.98, 45.48, and 339.70 μg/g, respectively). This led to a quantity of total biogenic amines that was far below the safety limit of 1,000 μg/g (16). The content of TRP in this product was 22.54 μg/g, which was nearly the same level as Shuidouchi and Natto, while the content of CAD was 22.54 μg/g, similar to Natto, but higher than Shuidouchi. PHE, HIS, and TYR were recognized as the toxic biogenic amines, monitored as safety indicators in foods. The content of PHE in this product was 8.44 μg/g, which was higher than Shuidouchi, but lower than the limit concentration of 30 μg/g. In this research, the maximum content of HIS and average content of TYR were 2.18 and 2.68 μg/g, respectively, lower than certain Natto and Shuidouchi products and far below the limit concentration (9, 16, 43, 44). *Bacillus* and *Aneurinibacillus* were positively correlated with a variety of bioamines (**Figure 5A**), mainly because these bacteria had strong amino acid metabolic functionality, secreting a large amount of protease (**Figure 6**). Some studies have found that *Bacillus subtilis* produced a large amount of toxic bioamines (15), while the content of biogenic amines did not exceed the safety limits in this study. This was most likely because many low abundance bacteria could efficiently use carbohydrate metabolism to produce various intermediate metabolites (**Figure 6**), which reacted with bioamines at high temperatures in the metaphase and anaphase stages of fermentation, reducing the concentration of bioamines

via the Maillard reaction phenomena, such as Douchi browning. This improved the safety of the product. At the same time, polyamine quantity significantly increased during fermentation, resulting in greatly improved product functionality.

Alkylpyrazines are considered important flavor compounds and potential pharmacophores. Many bacteria can produce alkylpyrazines, such as *B. subtilis*, *B. licheniformis*, *Corynebacterium glutamicum*, *Paenibacillus polymyxa*, and *Serratia marcescens* (20–23, 45–47). *C. glutamicum* was also shown to produce a large amount of tetramethylpyrazine, trimethylpyrazine, 2, 3-dimethylpyrazine, 2-ethyl-3,6-dimethylpyrazine and a small amount of 2,5-dimethylpyrazine (45). In addition, *B. subtilis* was also shown to produce the above alkylpyrazines except for 2, 3-dimethylpyrazine (19). In our product, the same alkylpyrazines as *B. subtilis* were produced, in addition to 2, 3-dimethylpyrazine. *B. subtilis* was the dominant bacteria during the fermentation of non-post fermented Shuidouchi, and *Corynebacterium callunae* was found at a concentration of 7 log (CFU/g) only at 24 h during fermentation (data not shown). This indicated that *Corynebacterium* sp. could also benefit the production of 2, 3-dimethylpyrazine in this product, even as a small portion of bacteria. Tetramethylpyrazine, trimethylpyrazine, and 2, 5-DMP were the dominant alkylpyrazines, which correlated with the dominant bacteria such as *B. subtilis* and *B. licheniformis* in the non-post fermented Shuidouchi. The synthesis mechanisms of alkylpyrazines are proposed in **Figure 7**, according to the conclusions of Zhang et al. (46, 47). As the dominant bacteria, the species of *Bacillus* were positively correlated with amino acid metabolism and the metabolism of other amino acids (**Figure 6**), which included the dehydrogen reaction of amino acids such as L-threonine. This could be transformed to L-2-amino-acetoacetate by L-threonine-3-dehydrogenase, and further to aminoacetone by spontaneous reaction. Two molecules of aminoacetone could be combined to 3, 6-dihydro-2,5-DMP, transforming into 2,5-DMP spontaneously. Many bacteria were significantly correlated with carbohydrate metabolism, as well as glycan biosynthesis and the metabolism pathway, which caused the hydrolysis of polysaccharides and the formation of acetoin by the EM pathway (**Figures 6**, **7**). Thus, acetoin reacted with ammonia or ammonium (originating from amino acid metabolism) to form α-hydroxyimine, and further 2-amino-3-butanone spontaneously. Two molecules of 2-amino-3-butanone could condense to 2,5-dihydro-TTMP, transforming to tetramethylpyrazine spontaneously. This chemical reaction would then be accelerated by higher temperatures (20); thus, tetramethylpyrazine accumulated quickly during high temperature fermentation (**Table 6**), improving the health protection functionality of the product. The initial stage of fermentation was also important because of its moderate temperature, which was suitable for the growth of most types of bacteria and the accumulation of fermentable sugar, accelerating the formation of acetoin by the carbohydrate metabolism pathway (**Figure 6**). Acetoin could enter the environment outside the bacterial cells, reacting with ammonia or ammonium to form 2-amino-3-butanone, and 2-amino-3-butanone and aminoacetone could form 3,6-dihydro-TMP, transforming into trimethylpyrazine spontaneously (**Figure 7**). Tetramethylpyrazine, 2,5-DMP, and trimethylpyrazine were the alkylpyrazines with the highest content in the non-post fermented Shuidouchi, while 2-ethyl-3,6-dimethylpyrazine and 2-ethyl-3,5,6-trimethylpyrazine had less content (**Table 6**). This was attributed to the excessive amount of ammonium ions that were produced by *Bacillus* through amino acid metabolism, caused the pH to increase (**Table 1**), and bacterial cells had to convert pyruvate into acetoin to more effectively consume the ammonium, while the efficiency of the 2,3-pentanedione pathway was too low because one ammonium ion consumed two pyruvate molecules (**Figure 7**). The successive inoculation of *Pichia kudriavzevii*, *Rhizopus* sp., and *B. licheniformis* increased the production of tetramethylpyrazine in the Chinese liquor. Thus, lowering the temperature of initial fermentation could be adopted as a method to facilitate the growth of more fungi, potentially increasing tetramethylpyrazine production due to the high hydrolase activity of the fungi for the polysaccharides (48).

The processing of non-post fermented Shuidouchi is a heat preservation process (Section "Non-post Fermented Shuidouchi Fermentation and Sampling"). It first involves a two-stage temperature control strategy [moderate temperature (35–42°C) before a high-temperature (52°C) stage], which could be observed from spontaneous fermentation. Before a timepoint of 24 h of fermentation (initial stage of fermentation), the temperature increased slowly (**Table 1**), and the bacterial community structures were consequently similar between 12 and 24 h (**Figure 4A**). The genera of *Bacillus*, *Lactococcus*, *Klebsiella*, *Citrobacter*, *Acinetobacter*, and *Pantoea* were more than 1% of the relative abundance in the initial stage with moderate temperature (**Table 1** and **Figure 3A**). However, the temperature remained high (45–52°C) after a timepoint of 24 h (**Table 1**). The high temperature caused the relative abundance of *Bacillus* and *Aneurinibacillus* to increase, accompany with increasing pH value (**Table 1** and **Figure 3A**). The genera of *Bacillus*, *Lactococcus*, *Klebsiella,* and *Aneurinibacillus* remained more than 1% of the relative abundance after a timepoint of 24 h of fermentation (**Figure 3A**). These changes in the bacterial community structure caused the changes in bacterial metabolic pathways at the two main temperature stages. Before a timepoint of 24 h during fermentation, the percentage composition of carbohydrate metabolism was higher than at the stage after a timepoint of 24 h (**Table 7**). However, the percentage compositions of amino acid metabolism, other amino acids metabolism, and lipid metabolism were higher after a timepoint of 24 h during fermentation (**Table 7**). Combined with high temperature, these changes in metabolisms caused the accumulations of the functional metabolites such as alkylpyrazines and polyamines, as discussed previously. Metagenomic (49) and metatranscriptomic (50) analyses should be adopted in further research, for a more comprehensive and in-depth understanding of the fermentation process. Some researchers had used functional microbe to increase the antioxidant activity of fermented soybeans by solid-state fermentation (51). We have isolated the cultured microbes in non-post fermented Shuidouchi, and the functional microbes will be screened to increase the multifunctionality of the product.

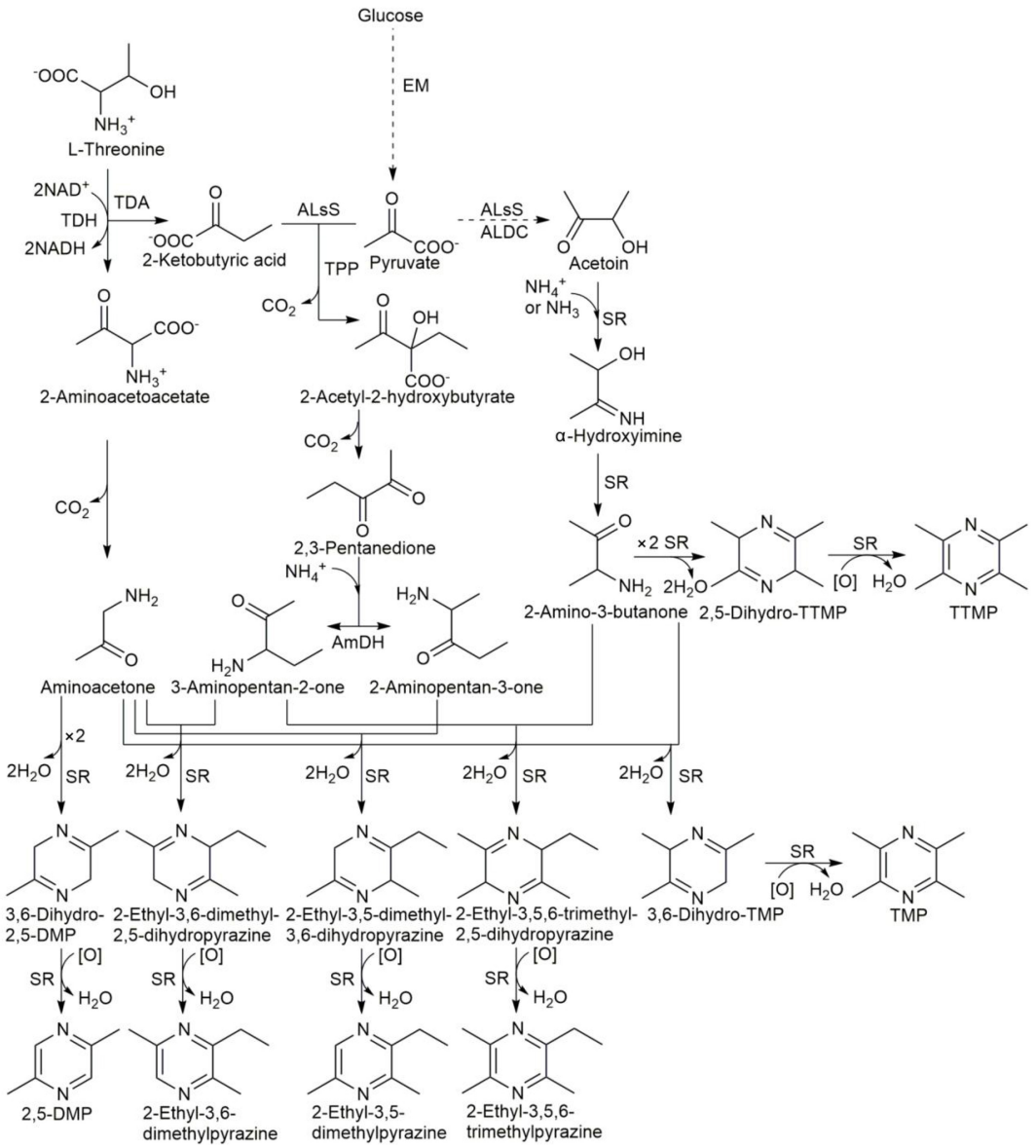

FIGURE 7 | Synthesis pathways of alkylpyrazines in *B. subtilis*. EM, Embden-Meyerhof pathway; ALsS, acetolactate synthase; ALDC, α-acetolactate decarboxylase; TDH, L-threonine-3-dehydrogenase; TDA, threonine deaminase; AmDH, amine dehydrogenase; SR, spontaneous reaction under standard pressure and moderate or high temperature. The pathways were proposed by Zhang et al. (46, 47).

In conclusion, non-post fermented Shuidouchi was confirmed as bacterial type Douchi due to the high counts of bacteria and very low counts of fungi, as determined during fermentation. The bacterial genus *Bacillus* was the most dominant microbe throughout the fermentation process, and high counts of species such as *B. subtillus* could improve the probiotic functionality of this product. The temperature was the most important influential factor for the microbial diversity of the samples, and the succession of microbial communities brought about changes in the characteristic metabolites. Furthermore, a two-stage temperature control strategy [moderate temperature (35–42°C) at first, then at a high temperature (52°C)] could be summarized from this spontaneous fermentation. This strategy could control the concentration of biogenic amines within the safety limit, and significantly increase the concentration of polyamines such as SPD, which offer multiple protective health effects. This strategy could also increase the types and concentrations of alkylpyrazines, especially tetramethylpyrazine, which has shown a functional effect on human cardiovascular and cerebrovascular health. This two-stage temperature control strategy could be applied to the industrial production of non-post fermented Shuidouchi to accelerate the function of fermented soybeans. Meanwhile, this strategy was low cost and could be widely popularized in households

everywhere, offering a worldwide solution to human hunger and nutrition issues.

DATA AVAILABILITY STATEMENT

The datasets presented in this study can be found in online repositories. The names of the repository/repositories and accession number(s) can be found below: BioProject: PRJNA830651; PRJNA830678; https://www.ncbi.nlm.nih.gov/.

AUTHOR CONTRIBUTIONS

YC and FQ designed and conducted this research, performed the experiments, and completed the manuscript. MD acquired funding, designed the experimental scheme, supervised the experiments, and revised the manuscript. All authors contributed to the article and approved the submitted version.

FUNDING

This research was funded by the Jiangsu Agriculture Science and Technology Innovation Fund [Grant No. CX (21)2003], Taizhou Science and Technology Support Social Development Plan (guiding) Project (2015 No. 49 "Research on Rapid Detection Technology of Dominant Bacteria during Fermentation of Shuidouchi"), and Scientific Research Project of Jiangsu Agri-animal Husbandry Vocational College (YB1207).

ACKNOWLEDGMENTS

We would like to thank Ms. Zhan at the Jiangsu Agri-animal Husbandry Vocational College for her guidance in operating the HPLC and GC-MS. We would also like to thank LetPub (www.letpub.com) for its linguistic assistance during the preparation of this manuscript.

REFERENCES

1. Jamet JP, Chaumet JM. Soybean in China: adaptating to the liberalization. *OCL.* (2016) 23:D604. doi: 10.1051/ocl/2016044
2. Kiers JL, Van Laeken AEA, Rombouts FM, Nout MJR. *In vitro* digestibility of *Bacillus* fermented soya bean. *Int J Food Microbiol.* (2000) 60:163–9. doi: 10.1016/S0168-1605(00)00308-1
3. Liang Y, Zhang L, Gao F, Zhang X, Li X, Zhang H, et al. Research progress on production technology and physiological active components of Shuidouchi. *South Chin Agric.* (2017) 11:36–8. doi: 10.19415/j.cnki.1673-890x.2017.34.009
4. Suo H, Feng X, Zhu K, Wang C, Zhao X, Kan J. Shuidouchi (fermented soybean) fermented in different vessels attenuates HCl/ethanol-induced gastric mucosal injury. *Molecules.* (2015) 20:19748–63. doi: 10.3390/molecules201119654
5. Feng X, Zhao X. Comparison of the antioxidant activities of ethanol extracts from Shuidouchi samples fermented using different vessels. *Mod Food Sci Tech.* (2016) 32:151–6. doi: 10.13982/j.mfst.1673-9078.2016.7.024
6. Zhao X, Song JL, Wang Q, Qian Y, Li GJ, Pang L. Comparisons of Shuidouchi, Natto, and Cheonggukjang in their physicochemical properties, and antimutagenic and anticancer effects. *FOOD Sci Biotechnol.* (2013) 22:1077–84. doi: 10.1007/s10068-013-0186-6
7. Okamoto A, Hanagata H, Kawamura Y, Yanagida F. Anti-hypertensive substances in fermented soybean, natto. *Plant Food Hum Nutr.* (1995) 47:39–47. doi: 10.1007/BF01088165
8. Suzuki Y, Kondo K, Matsumoto Y, Zhao BQ, Otsuguro K, Maeda T, et al. Dietary supplementation of fermented soybean, natto, suppresses intimal thickening and modulates the lysis of mural thrombi after endothelial injury in rat femoral artery. *Life Sci.* (2003) 73:1289–98. doi: 10.1016/S0024-3205(03)00426-0
9. Chen YH, Liu XW, Huang JL, Baloch S, Xu X, Pei XF. Microbial diversity and chemical analysis of Shuidouchi, traditional Chinese fermented soybean. *Food Res Int.* (2019) 116:1289–97. doi: 10.1016/j.foodres.2018.10.018
10. Deng GW, Liu Y, Li P, Liao LY, Yin HL, Jiang LW, et al. Analysis of bacterial diversity in guizhou water-Douchi based on Illumina MiSeq high-throughput sequencing technology. *Food Sci.* (2021) 42:61–6. doi: 10.7506/spkx1002-6630-20200902-017
11. Zhang WB, Luo QQ, Zhu Y, Ma J, Cao L, Yang M, et al. Microbial diversity in two traditional bacterial douchi from Gansu province in northwest China using Illumina sequencing. *PLoS One.* (2018) 13:e0194876. doi: 10.1371/journal.pone.0194876
12. Yang S, Shan CS, Xu YQ, Jin L, Chen ZG. Dissimilarity in sensory attributes, shelf life and spoilage bacterial and fungal microbiota of industrial-scale wet starch noodles induced by different preservatives and temperature. *Food Res Int.* (2021) 140:109980. doi: 10.1016/j.foodres.2020.109980
13. Zhang PW, Li H, Zhao WP, Xiong K, Wen H, Yang HL, et al. Dynamic analysis of physicochemical characteristics and microbial communities of *Aspergillus*-type douchi during fermentation. *Food Res Int.* (2022) 153:110932. doi: 10.1016/j.foodres.2021.110932
14. Wu JR, Tian T, Liu YM, Shi YX, Tao DB, Wu RN, et al. The dynamic changes of chemical components and microbiota during the natural fermentation process in Da-Jiang, a Chinese popular traditional fermented condiment. *Food Res Int.* (2018) 112:457–67. doi: 10.1016/j.foodres.2018.06.021
15. Madeo F, Eisenberg T, Pietrocola F, Kroemer G. Spermidine in health and disease. *Science.* (2018) 359:410–21. doi: 10.1126/science.aan2788
16. Kim B, Byun BY, Mah JH. Biogenic amine formation and bacterial contribution in Natto products. *Food Chem.* (2012) 135:2005–11. doi: 10.1016/j.foodchem.2012.06.091
17. Han Z, Luo XX, Yang CY, Wu YJ. Dynamic changes of biogenic amines content in Douchi. *Chin Brew.* (2016) 35:60–4. doi: 10.11882/j.issn.0254-5071.2016.05.013
18. Larroche C, Besson I, Gros JB. High pyrazine production by *Bacillus subtilis* in solid substrate fermentation on ground soybeans. *Process Biochem.* (1999) 34:667–74. doi: 10.1016/S0032-9592(98)00141-1
19. Owens JD, Allagheny N, Kippinga G, Ames JM. Formation of volatile compounds during *Bacillus subtilis* fermentation of soya beans. *J Sci Food Agric.* (1997) 74:132–40. doi: 10.1002/(SICI)1097-0010(199705)74:13.0.CO;2-8
20. Xiao ZJ, Hou XY, Lyu X, Xi LJ, Zhao JY. Accelerated green process of tetramethylpyrazine production from glucose and diammonium phosphate. *Biotechnol Biofuels.* (2014) 7:106. doi: 10.1186/1754-6834-7-106
21. Zheng JP, Liu N, Bai XR, Zhang FK. Effect of tetramethylpyrazine on Listeria monocytogenes infection and innate immunity of rex rabbits. *Chin Anial Husbandry Vete Med.* (2020) 47:1531–8. doi: 10.16431/j.cnki.1671-7236.2020.05.028
22. Ren YG, Zhang BC, Jia DP, Hu K. Tetramethylpyrazine attenuates experimental autoimmune myasthenia gravis in rats *via* regulating related cytokines and antibodies. *Chin J Cell Mol Immunol.* (2016) 32:1471–4. doi: 10.13423/j.cnki.cjcmi.007944
23. Sun XS, Tian JR, Cui GY. The Protective Effects of trimethylpyrazine and tetramethylpyrazine on acute alcoholic liver injury in mice. *Acta Nutr Sin.* (2013) 35:480–3. doi: 10.13325/j.cnki.acta.nutr.sin.2013.05.017
24. Zhang Y, Zeng T, Wang HW, Song JJ, Suo HY. Correlation between the quality and microbial community of natural-type and artificial-type Yongchuan Douchi. *LWT - Food Sci Tech.* (2021) 140:110788. doi: 10.1016/j.lwt.2020.110788

25. Chen Y, Li P, Liao LY, Qin YY, Jiang LW, Liu Y. Characteristic fingerprints and volatile flavor compound variations in Liuyang Douchi during fermentation *via* HS-GC-IMS and HS-SPME-GC-MS. *Food Chem.* (2021) 361:130055. doi: 10.1016/j.foodchem.2021.130055
26. SB/T 10528-2009. *Code of Internal Commerce Industry Standard of China*. Beijing: Quality and Standards Publishing & Media Co., Ltd. (2009).
27. GB 5009.237-2016. *Code of National Food Safety Standard of China. Determination of pH Value of Food*. Beijing: Quality and Standards Publishing & Media Co., Ltd. (2016).
28. GB 10468-1989. *Code of National Standard of China. Fruit and Vegetable Products – Determination of pH*. Beijing: Quality and Standards Publishing & Media Co., Ltd. (1989).
29. Combet-Blanc Y, Ollivier B, Streicher C, Patel BKC, Dwivedi PP, Pot B, et al. *Bacillus thermoamylovorans* sp. nov., a moderately thermophilic and amylolytic bacterium. *Int J Syst Bacteriol.* (1995) 45:9–16. doi: 10.1099/00207713-45-1-9
30. Grazia Fortina M, Pukall R, Schumann P, Mora D, Parini C, Manachini PL, et al. *Ureibacillus* gen. nov., a new genus to accommodate *Bacillus thermosphaericus* (Andersson et al. 1995), emendation of *Ureibacillus thermosphaericus* and description of *Ureibacillus terrenus* sp. nov. *Int J Syst Evol Microbiol.* (2001) 51:447–55. doi: 10.1099/00207713-51-2-447
31. Xu WY, Liu F, Zhu EJ, Wang DY, Zhu YZ, Zhang MH, et al. Growth of *Enterococcus faecalis* R-612-Z1 in water-boiled salted ducks under different storage conditions. *Jiangsu J Agric Sci*. (2013) 29:178–83.
32. Greppi A, Rantisou K, Padonou W, Hounhouigan J, Jespersen L, Jakobsen M, et al. Yeast dynamics during spontaneous fermentation of mawè and tchoukoutou, two traditional products from Benin. *Int J Food Microbiol.* (2013) 165:200–7. doi: 10.1016/j.ijfoodmicro.2013.05.004
33. Langille MG, Zaneveld J, Caporaso JG, McDonald D, Knights D, Reyes JA, et al. Predictive functional profiling of microbial communities using 16S rRNA marker gene sequences. *Nat Biotechnol.* (2013) 31:814–21. doi: 10.1038/nbt.2676
34. GB 5009.208-2016. *Code of National Food Safety Standards of China. Determination of Biogenic Amine of Food*. Beijing: Quality and Standards Publishing & Media Co., Ltd. (2016).
35. Xu YQ, Jiang YF, Li XT, Sun BG, Teng C, Yang R, et al. Systematic characterization of the metabolism of acetoin and its derivative ligustrazine in *Bacillus subtilis* under micro-oxygen conditions. *J Agric Food Chem.* (2018) 66:3179–87. doi: 10.1021/acs.jafc.8b00113
36. Wang YR, Xiang FS, Zhang ZD, Hou QC, Guo Z. Characterization of bacterial community and flavor differences of different types of Douchi. *Food Sci Nutr.* (2021) 9:3460–9. doi: 10.1002/fsn3.2280
37. Ma SC, Cheng C, Tian C, Chen Y, Mo KJ, Wang XP. Analysis of bacterial diversity in enshi prefecture sojae semen praeparatum based on high-throughput sequencing technology. *Food Sci.* (2022) 43. doi: 10.7506/spkx1002-6630-20211028-305
38. Huang XR, Guo Y, Li ZJ, Zeng JX, Wu YJ. Study on dynamic monitoring of bacterial flora of naturally fermented soya beans. *Chin Condiment* (2020) 45:103–6. doi: 10.3969/j.issn.1000-9973.2020.06.022
39. Pant G, Prakash A, Pavani JVP, Bera S, Deviram GVNS, Kumar A, et al. Production, optimization and partial purification of protease from *Bacillus subtilis*. *J Taibah Univ Sci* (2015) 9:50–5. doi: 10.1016/j.jtusci.2014.04.010
40. Chen H, Xiao X, Wang J, Wu L, Zheng ZM, Yu ZL. Antagonistic effects of volatiles generated by *Bacillus subtilis* on spore germination and hyphal growth of the plant pathogen *Botrytis cinerea*. *Biotechnol Lett* (2008) 30:919–23. doi: 10.1007/s10529-007-9626-9
41. Haidar R, Roudet J, Bonnard O, Dufour MC, Corio-Costet MF, Fert M, et al. Screening and modes of action of antagonistic bacteria to control the fungal pathogen *Phaeomoniella chlamydospora* involved in grapevine trunk diseases. *Microbiol Res.* (2016) 192:172–84. doi: 10.1016/j.micres.2016.07.003
42. Murata D, Sawano S, Ohike T, Okanami M, Ano T. Isolation of antifungal bacteria from Japanese fermented soybeans, natto. *J Environ Sci.* (2013) 25:S127–31. doi: 10.1016/S1001-0742(14)60641-0
43. Li DW, Li DD, Liang JJ, Shi RQ, Ma YL. Determination of biogenic amines in commercially sufu by high performance liquid chromatography. *Food R D.* (2018) 39:120–4. doi: 10.3969/j.issn.1005-6521.2018.16.022
44. Hu P, Suo HY, Kan JQ, Chen GJ, Hu GZ. Biogenic amine content of traditionally fermented Douchi. *Food Sci.* (2013) 34:108–12. doi: 10.7506/spkx1002-6630-201320021
45. Dickschat JS, Wickel S, Bolten CJ, Nawrath T, Schulz S, Wittmann C. Pyrazine biosynthesis in *Corynebacterium glutamicum*. *Eur J Org Chem.* (2010) 2010:2687–95. doi: 10.1002/ejoc.201000155
46. Zhang LJ, Cao YL, Tong JN, Xu Y. An alkylpyrazine synthetis mechanism involving L-threonine-3-dehydrogenase describes the production of 2,5-dimethylpyrazine and 2,3,5-trimethylpyrazine by *Bacillus subtilis*. *Appl Environ Microbiol.* (2019) 85:e1807–19. doi: 10.1128/AEM.01807-19
47. Zhang HZ, Zhang LJ, Yu XW, Xu Y. The biosynthesis mechanism involving 2, 3-pentanedione and aminoacetone describes the production of 2-Ethyl-3, 5-dimethylpyrazine and 2-Ethyl-3, 6-dimethylpyrazine by *Bacillus subtilis*. *J Agric Food Chem*. (2020) 68:3558–67. doi: 10.1021/acs.jafc.9b07809
48. Wu QD, Wu MH, Shen Y, Wang X, Luo AM. Increasing tetramethylpyrazine content in baijiu by co-fermentation of *Bacillus licheniformis*, *Pichia kudriavzevii* and *Rhizopus* starter. *Liquor Making Sci Tech.* (2021) 42:17–21. doi: 10.13746/j.njkj.2020258
49. Ji XL, Hou CY, Gao YG, Xue YQ, Yan YZ, Guo XD. Metagenomic analysis of gut microbiota modulatory effects of jujube (*Ziziphus jujuba* Mill.) polysaccharides in a colorectal cancer mouse model. *Food Funct.* (2020) 11:163–73. doi: 10.1039/c9fo02171j
50. An FY, Li M, Zhao Y, Zhang Y, Mu DL, Hu XY, et al. Metatranscriptome-based investigation of flavor-producing core microbiota in different fermentation stages of dajiang, a traditional fermented soybean paste of Northeast China. *Food Chem.* (2021) 343:128509. doi: 10.1016/j.foodchem.2020.128509
51. Chen YL, Wang YL, Chen JX, Tang H, Wang CH, Li ZJ, et al. Bioprocessing of soybeans (*Glycine max* L.) by solid-state fermentation with *Eurotium cristatum* YL-1 improves total phenolic content, isoflavone aglycones, and antioxidant activity. *RSC Adv.* (2020) 10:16928–41. doi: 10.1039/c9ra10344a

Conflict of Interest: The authors declare that the research was conducted in the absence of any commercial or financial relationships that could be construed as a potential conflict of interest.

Publisher's Note: All claims expressed in this article are solely those of the authors and do not necessarily represent those of their affiliated organizations, or those of the publisher, the editors and the reviewers. Any product that may be evaluated in this article, or claim that may be made by its manufacturer, is not guaranteed or endorsed by the publisher.

frontiers | Frontiers in Nutrition

ORIGINAL RESEARCH
published: 17 June 2022
doi: 10.3389/fnut.2022.918240

Carotenoid Biosynthesis: Genome-Wide Profiling, Pathway Identification in *Rhodotorula glutinis* X-20, and High-Level Production

Shaobo Bo, Xiaoxia Ni, Jintang Guo, Zhengyang Liu, Xiaoya Wang, Yue Sheng, Genlin Zhang and Jinfeng Yang**

Key Laboratory for Green Processing of Chemical Engineering of Xinjiang Bingtuan, School of Chemistry and Chemical Engineering, Shihezi University, Shihezi, China

OPEN ACCESS

Edited by:
Xiaolong Ji,
Zhengzhou University of Light Industry, China

Reviewed by:
Aamir Rasool,
University of Balochistan, Pakistan
Lihu Wang,
Hebei University of Engineering, China
Zhu Qiao,
Huanghuai University, China

***Correspondence:**
Genlin Zhang
zhgl_food@sina.com
Jinfeng Yang
yangjinfeng@shzu.edu.cn

Specialty section:
This article was submitted to Food Chemistry, a section of the journal Frontiers in Nutrition

Received: *12 April 2022*
Accepted: *13 May 2022*
Published: *17 June 2022*

Citation:
Bo S, Ni X, Guo J, Liu Z, Wang X, Sheng Y, Zhang G and Yang J (2022) Carotenoid Biosynthesis: Genome-Wide Profiling, Pathway Identification in Rhodotorula glutinis X-20, and High-Level Production. Front. Nutr. 9:918240. doi: 10.3389/fnut.2022.918240

Rhodotorula glutinis, as a member of the family *Sporidiobolaceae*, is of great value in the field of biotechnology. However, the evolutionary relationship of *R. glutinis* X-20 with *Rhodosporidiobolus*, *Sporobolomyces*, and *Rhodotorula* are not well understood, and its metabolic pathways such as carotenoid biosynthesis are not well resolved. Here, genome sequencing and comparative genome techniques were employed to improve the understanding of *R. glutinis* X-20. Phytoene desaturase (crtI) and 15-cis-phytoene synthase/lycopene beta-cyclase (crtYB), key enzymes in carotenoid pathway from *R. glutinis* X-20 were more efficiently expressed in *S. cerevisiae* INVSc1 than in *S. cerevisiae* CEN.PK2-1C. High yielding engineered strains were obtained by using synthetic biology technology constructing carotenoid pathway in *S. cerevisiae* and optimizing the precursor supply after fed-batch fermentation with palmitic acid supplementation. Genome sequencing analysis and metabolite identification has enhanced the understanding of evolutionary relationships and metabolic pathways in *R. glutinis* X-20, while heterologous construction of carotenoid pathway has facilitated its industrial application.

Keywords: genomic analysis, comparative genomes, *R. glutinis*, carotenoid pathway, heterologous expression

HIGHLIGHTS

- High quality of genome map of *R. glutinis* X-20 was assembled.
- Carotenoid pathway and new enzymes were identified by comparative genome.
- High level of carotenoids was produced in *S. cerevisiae* expressing crtI and crtYB.

INTRODUCTION

Wet oleaginous yeast has been widely studied because of its great application value in bioenergy (1). *Rhodotorula glutins* is a kind of typical wet oleaginous yeast, which is widely found in the ecological environment. Most of them live in the soil and the sea, but a small number grow by adhering to plants or symbiosing with other organisms (2). *Rhodotorula glutinis* can convert low-cost carbohydrates into lipids (3). The proportion of lipids in cells dry mass can reach 70%, mainly

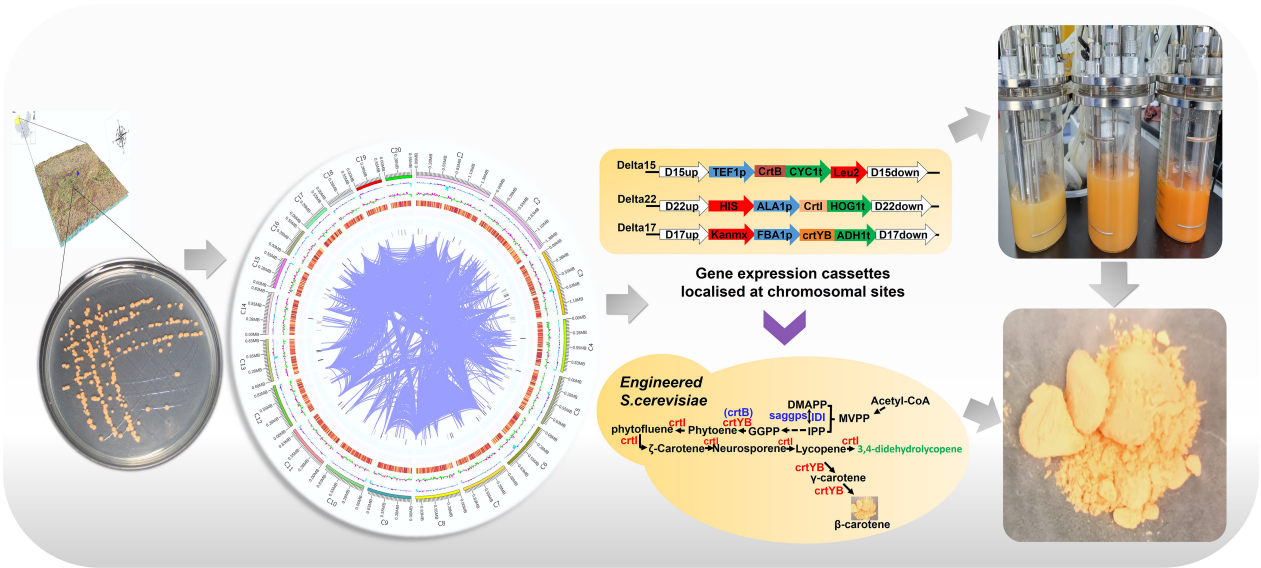

GRAPHICAL ABSTRACT

including monounsaturated fatty acids (C18:1), saturated fatty acids (C16:0) and polyunsaturated fatty acids (C18:2) (4, 5). Carotenoids are another important product from *R. glutinis*. For example, *R. glutinis* from the beer wastewater with high concentration of sugar (24.34 $g{\cdot}L^{-1}$ maltose and 5.77 $g{\cdot}L^{-1}$ glucose) produced 1.2 $mg{\cdot}L^{-1}$ β-carotene (6). Because of synthesized carotenoids with different type or content, *R. glutinis* will show different color, including pink, red, or light red (7). β-Carotene, β-cryptoxanthin, torulene, and torularhodin can be produced by *R. glutinis* (8). And also, *R. glutinis* can produce some important industrial enzymes, such as phenylalanine ammonia lyase (PAL), a key enzyme in the phenylalanine pathway for the removal of ammonia from phenylalanine to produce trans-cinnamic acid (9). In addition, *R. glutinis* can achieve the purpose of improving the soil environment by adsorbing heavy metal elements (10). Even, we have screened a selenium-rich *R. glutinis* that is beneficial to the human body after converting inorganic selenate to organic selenic acid (11). Because *R. glutinis* can be cultivated from low-value raw materials and can create industrialized products through high-efficiency transformation processes, increasing researches are focusing on analyzing the reasons for its multiple applications by mining and verifying the genomic information (12, 13). The genomic data of *R. glutinis* ATCC 204091 is thought to be the first genome sequencing analysis of *R. glutinis* (14). The whole genome sequencing of *R. glutinis* WP1 was considered to be the earliest sequencing analysis to study the mechanism of mutual aid in plants by endophytic yeast (15). Through whole-genome sequencing of *R. toruloides,* lipid pathway was systematically analyzed and 150 genes that affect lipid accumulation were identified (16). Whole-genome Sequencing of *Rhodotorula* sp. CCFEE 5036 originated from Antarctica showed that a large number of genes in the metabolic pathway were positively evolved by the extreme cold environment, providing insights into the diversity of strains inhabiting polar regions (17). The omics studies of *R. mucilaginosa* revealed a positive feedback on carotenoid metabolic pathways (18). The use of genomics to investigate the function of *Rhodotorula* is a highly effective strategy.

Previously, *R. glutinis* X-20 was screened from a selenium-enriched soil on the northern slopes of the Tianshan Mountains in Xinjiang Province, China, showing a high selenium-enriched capacity with 5,349.6 $\mu g{\cdot}g^{-1}$ DWC (11). And also, it can generate large levels of β-carotene and lipids. However, the evolutionary relationship of *R. glutinis* X-20 with other *Rhodotorula* in the *Sporidiobolaceae* family is unknown. The metabolic pathways such as lipids, terpenoid biosynthesis are not well understood (19). Therefore, to reveal the evolutionary relationship of *R. glutinis* X-20 and explore its application potential in product production such as carotenoid and lipid, the whole genome was sequenced in this study. Comparative genomic analysis was then carried out to analyze the protein-coding genes of *R. glutinis* X-20. As an application case of mined functional genes from *R. glutinis* X-20, carotenoid biosynthesis pathway was heterologously expressed in *S. cerevisiae,* and carotenoid production was optimized by fermentation engineering.

MATERIALS AND METHODS

Strain and Growth Conditions

Rhodotorula glutinis X-20 (CCTCC M2017225) was isolated from Shawan County (85.56E, 44.29N) on the northern slope of the Tianshan Mountains in Xinjiang, China and was preserved in the China Center for Type Culture Collection. *Rhodotorula glutinis* X-20 was incubated in conical flasks containing 100/250 mL of YPD medium (yeast extract: 10 $g{\cdot}L^{-1}$, peptone: 20 $g{\cdot}L^{-1}$, glucose: 20 $g{\cdot}L^{-1}$). Incubation was carried out at 30°C and 200 rpm. After

96 h cultivation, cells were centrifuged (8,000 × g, 4°C, 5 mins), frozen in liquid nitrogen for future experiments. **Table 1** lists the additional strains utilized in this investigation. All strains were grown in YPD medium when necessary additional 10 $mg{\cdot}L^{-1}$ G418 was added. The biomass was measured using a UV spectrophotometer (UV-2600, Suzhou, Shimadzu Instruments Co., Ltd.) at 600 nm.

Genomic DNA Extraction and Sequencing

The DNA of *R. glutinis* X-20 was extracted according to the report by Lim et al. (23). DNA quality was checked by agarose gel electrophoresis and quantified using a Qubit® 2.0 fluorometer (Thermo Fisher Scientific, Waltham, MA, United States). The whole genome of *R. glutinis* X-20 was sequenced at Beijing Novogene Bioinformatics Technology Co., Ltd. using the PacBio Sequel platform and the Illumina NovaSeq PE150 according to the manufacturer's protocols.

Genome Assembly, Prediction, and Functional Annotation

The genome was assembled using the SMRT Link v5.0.1 program. To get clean data, low quality reads (less than 500 bp) were filtered away to assure the correctness of the future analytical results. SMRT was used to fix errors, which were then combined to produce preliminary findings. The first assembly findings were compared and reviewed by comparing the reads to the assembled genome sequence in order to measure the GC content and depth of coverage of the reads in order to acquire a complete genome.

The coding genes were predicted using the program August (default parameters). RepeatMasker software (Version open-4.0.5) was used to predict repetitive elements (24). To predict gene models, RNA-seq data were aligned to the genome using the hisat2 program (25). Transcripts were reconstructed using stringtie software (version: 2.0.4), the new genes were identified in RNA-seq though not in the genome (26). The software rRNAmmer was used for rRNA prediction (27). tRNA was predicted by the Ascan-SE software (28). For sRNAs, the Rfam database was annotated first, then the final sRNA was discovered using the cmsearch program. Protein sequences of the predicted genes match from DIAMOND software (default parameters set to e-value $\leq 1e^{-5}$) and the highest score results (default identity $\geq$ 40%, coverage $\geq$ 40%) were selected for annotation (29). The functional annotation of predicted genes was performed using a variety of public databases, including Gene Ontology (GO), Kyoto Encyclopedia of Genes and Genomes (KEGG), Cluster of Orthologous Groups of Proteins (COG), Non-Redundant Protein Database (Nr), Transporter Classification Database (TCDB), Protein Families (Pfam), Swiss-Prot, and Carbohydrate-Active enZYmes Database (CAEZY). Secretory proteins were predicted by SignalP. Secondary metabolites were predicted using the antiSMASH program. Multiple enzymes of the cytochrome P450 family can be predicted according to the FCPD database.

RNA Extraction and Transcriptome Sequencing

The Spin Column Fungal Total RNA Purification Kit (Sangon Biotech, Shanghai, China) was used to extract total RNA as directed by the manufacturer. RNA integrity was tested using Q-sep1 (Bioptic, New Taipei City, Taiwan China) and agarose gel electrophoresis (RNase-free). Qualified samples were subjected to DNase I digestion, followed by mRNA isolation using oligo (dT) magnetic beads, mRNA fragmentation and cDNA synthesis. "A" was added to the 3′ end of the cDNA fragment, a library adapter was attached and PCR was performed to bring up the Hybrid library. The cDNA libraries were assigned using an Illumina HiSeqTM2000 sequencer (Illumina, United States) and the raw image data files were converted to raw sequenced reads (Sequenced Reads) through Base Calling. The resulting Fastaq format files were quality controlled using the FASTQC program (version 0.11.). Clean data were obtained by cu-T adapter (version 1.11) to delete the 5′ end primer sequence and remove mismatched sequences (30). The sequence information on the comparison was obtained through the stringtie software (version: 2.0.4) to obtain the reconstructed transcript (26). To standardize the valid data, the feature Counts software (version: v1.6.0) was used to count the number of falls on the genome (31). The standardized method used in this case was FPKM (32). ANNOVAR (default parameters) software was used to annotate SNP and Indel sites. Quantitative Real-time PCR was used to assess gene expression levels. The reference gene was TUB1 and $2^{-D\Delta CT}$ method was utilized to normalize the expression

TABLE 1 | Strain types.

Strain	Description	Source/References
Saccharomyces cerevisiae INVSc1	MATa/MAT a his341 leu2 trp1-289 ura3-52	Blazic et al. (20)
Saccharomyces cerevisiae CEN.PK2-1C	MATa; ura3-52; trp1-2 89; Leu2-3,112; his3 D 1; MAL2-8C; SUC2	Paramasivan et al. (21)
W8	MVA pathway enhancement	Li et al. (22)
Sc. CEN (B1)	*Saccharomyces cerevisiae* CEN.PK2-1C phenotype; Delta15-crtB; Delta 22-crtI	This study
Sc. INV (B2)	*Saccharomyces cerevisiae* INVSc1 phenotype; Delta 15-crtB; Delta 22-crtI	This study
Sc. CEN (B3)	*Saccharomyces cerevisiae* CEN.PK2-1C phenotype; Delta 17-crtYB; Delta 22-crtI	This study
Sc. INV (B4)	*Saccharomyces cerevisiae* INVSc1 phenotype; Delta 17-crtYB; Delta 22-crtI	This study
Sc. CEN (B5)	W8 phenotype; Delta 22-crtI	This study
Sc. CEN (B6)	W8 phenotype; Delta 17-crtYB	This study
Sc. CEN (B7)	W8 phenotype; Delta 17-crtYB; Delta 22-crtI	This study

level. The One-way ANOVA method was used to do statistical analysis on all data.

Phylogenetic Trees and the Genome Collinearity Block Analysis

The 18S rDNA sequence of *R. glutinis* X-20 was compared to other similar species in the order *Sporidiobolales* for phylogenetic analysis. The NCBI nucleotide database was used to generate all 18S rDNA sequences. MEGA 7.0 is being used to process all 18S rDNA sequences, with Clustalw (the default setting) employed for multiple sequence alignment (33). The derived glutamic acid sequencing of *R. glutinis* X-20 and closely related species were used to construct a neighbor-joining phylogenic tree. Bootstrap sampling was used with 1,000 replicates. Analysis of covariance between genomic sequences of *Rhodotorula* species was conducted out by the MCScanX (jcvi 1.1.19) program with default parameters (34).

Comparative Genomic Analysis and Ka/Ks Calculation

Genomic data for *R. graminis* WP1, *R. taiwanensis*, and *R. toruloides* NP11 were downloaded from the NCBI database. Cluster analysis of gene families was carried out using OrthoFinder 2.5.4. AgBase-GOanna database was used for GO annotation with default parameters. Statistical annotation results were then plotted using the R language ggolot2 package. As the NG model, the Ka/Ks Calculator 2.0 model was used to estimate Ka/Ks values for each single copy gene trio.

Cloning and Functional Analysis of Target Genes

The Primer 5 software was used to design primers for the crtI (GenBank Accession: OL518983) and crtYB (GenBank Accession: OL518982) genes derived from *R. glutinis* X-20. Conserved domain analysis was performed by CD-search[1] on NCBI website. Secondary structure analysis was performed using Secondary Structure Prediction Server, while molecular masses and theoretical isoelectric points were also performed using Expasy for preliminary prediction of function. The gene expression cassettes crtI and crtYB were constructed to further validate their expression in *S. cerevisiae*.

Production of Carotenoids in *Saccharomyces cerevisiae* by Expressing crtI and crtYB

The genes of crtI and crtYB were amplified from the cDNA of *R. glutinis* X-20. The crtB (GenBank Accession: KC954270.1) originated from *Erwinia* was chemically synthesized. The promoters (FBA1p, ALA1p, and TEF1p) and terminators (ADH1t, HOG1t, and CYC1t) were amplified from *S. cerevisiae* genome. The gene expression cassettes TEF1p-crtB-CYC1t, ALA1p-crtI-HOG1t, and FBA1p-crtYB-ADH1t were constructed by OE-PCR. The crtB, crtI, and crtI gene expression cassettes were co-transferred into *S. cerevisiae* by the lithium acetate method (35). Positive strains were obtained by colony PCR and sequencing. The engineered strain was fermented in culture medium at 200 rpm and 25°C to produce carotenoids.

Extraction and Identification of Metabolites

For the analysis of metabolites, approximately 60 mg of cells were obtained by centrifuging (8,000 × g, 4°C, 10 mins). Then, 500 μL of methanol (−20°C) and 500 μL of H_2O (4°C) were added into a 2 mL tube containing cells. After vortexing for 30 s, 100 mg of glass beads were added, and immersed in liquid nitrogen for 5 mins. Samples were agitated in a grinder at 55 Hz for 2 mins and centrifuged (8,000 × g, 4°C, 10 mins). The supernatant was extracted, concentrated, and dried. To acquire prepared samples for LC-MS, the sample was dissolved by 300 μL of 2-chlorophenylalanine (4 ppm) methanol aqueous solution (1:1, 4°C) and the supernatant was aspirated and filtered through 0.22 μm filter membrane. For HPLC-MS analysis, an ACQUITY UPLC® HSS T3 (150 × 2.1 mm, 1.8 μm, Waters) column with an electrospray ionization source (ESI-MSn) was used to separate and identify the metabolites of extracts, as determined by Monnerat et al. (36). Lycopene and β-carotene were determined according to the report by Li et al. (37).

Statistics and Analysis

The experimental data were replicated three times and the data are presented as the average of three independent experimental samples with mean ± SD (n = 3). To evaluate if there was a statistically significant difference between the group data, the One-way ANOVA method was utilized.

RESULTS

Assembly Features of *Rhodotorula glutinis* X-20

The whole genome shotgun strategy of *R. glutinis* X-20 was carried out utilizing a PacBio Sequel system with a single molecule real time (SMRT) sequencer and an Illumina NovaSeq PE150 system. In total, 2.95 Gb of polymerase reads were generated. To calculate the genome size of *R. glutinis* X-20, we computed the overall 15-mer number to be 650,302,860 bp and the k-mer depth to be 28.27 Mb. The estimated genome size of *R. glutinis* X-20 was calculated to be 23 Mb using formula for 15-mer depth frequency distribution. Based on the genome information of proximate yeast, according to the genome size of about 20 M, the depth of this sequencing was probably more than 100× (38). The assembled genomic sequences were merged with the expected coding gene findings, and the sample genomes were displayed using Circos software (39). As shown in **Figure 1**, the genome of *R. glutinis* X-20 was finally assembled by organizing the contigs larger than 500 kb from longest to smallest, corresponding to 20 contigs in order, the longest scaffold is 1,634,659 bp, N50 length is 913,949 bp, GC content is 68.21%, and the sum of Contig Lengths is 21,850,050 bp,

[1]https://www.ncbi.nlm.nih.gov/cdd/

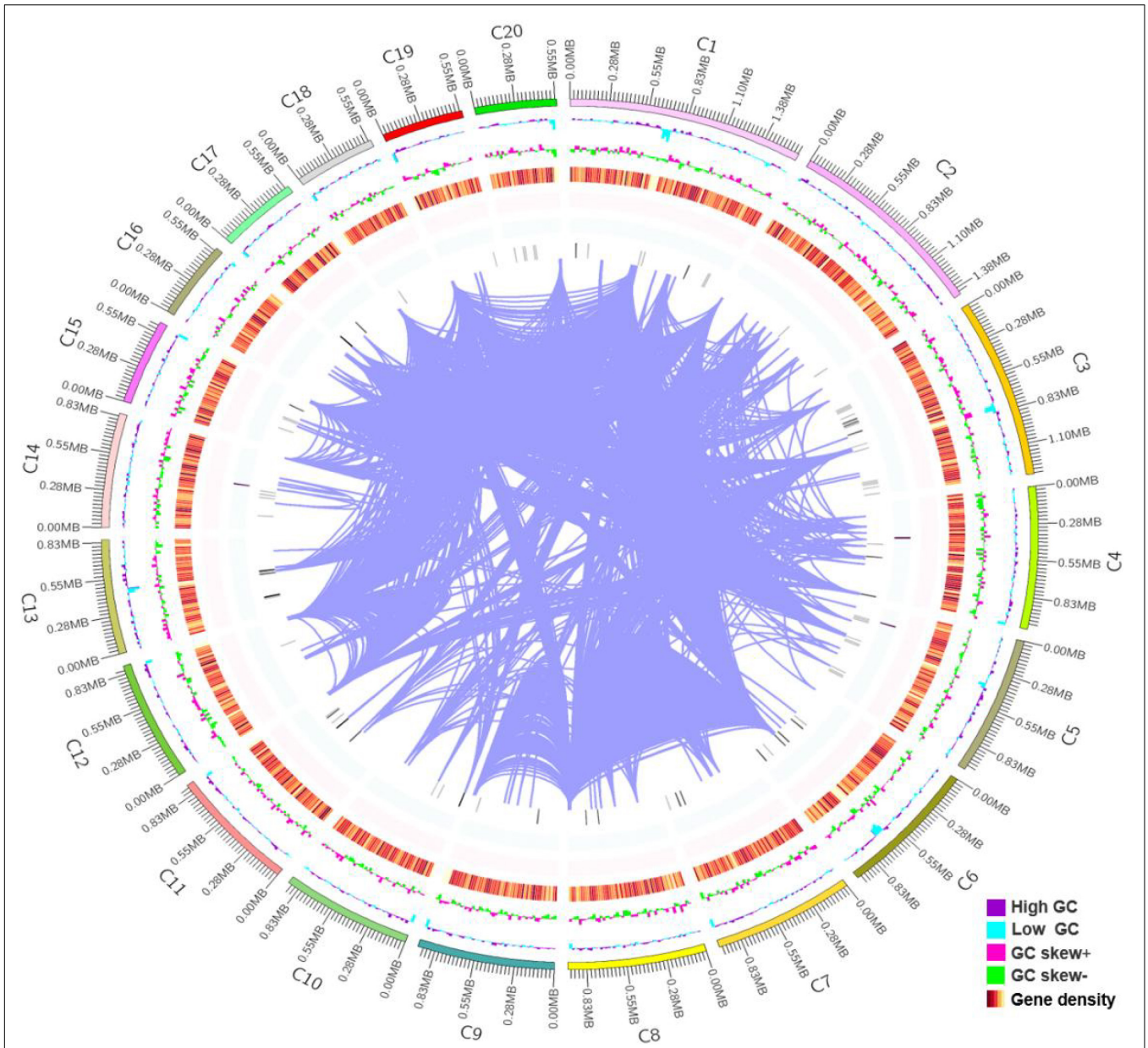

FIGURE 1 | Genomic features of *Rhodotorula glutinis* X-20. The 21.6 Mb genome of *R. glutinis* X-20 contains 20 scaffolds (the longest length scaffold of 1,634,659 bp, a N50 length of 913,949 bp, sum of Contig Lengths of 21,850,050 bp, GC content of 68.21%). The *R. glutinis* X-20 genome encodes 6,892 predicted proteins and 157 transfer RNAs (tRNAs), which are validated by RNA-seq. From the outer circle to the inner, it represents the length of scaffolds, GC content is higher than the average (purple), GC content is lower than the average (blue), GC skew curve (Pink: positive GC skew; Green: negative GC skew) and the gene density of coding genes, rRNA, snRNA, tRNA (gradient color), the darker the color, the greater the gene density in the window and chromosome duplication, respectively.

with a size of 21.6 Mb. A total of 6892 genes were projected from scratch by Augustus software, with an average length of 1,813 bp and an average GC content of 69.59%, representing 55.0% of the whole genome sequence. Tandem repeat sequences can be obtained by genome sequencing as an indicator of species genetic characteristics and evolutionary relationships. TRF (Tandem Repeats Finder, Version 4.07b) (40) detected 6,617 tandem repeats (TR), including 4,555 minisatellite DNA and 1,255 microsatellite DNA, accounting for 4.56% of the genomic sequence. The integrity of gene assembly was assessed by BUSCOs (41). The integrity assessment of BUSCOs discovered that the assembled genome comprised 735 intact BUSCOs (97.0%), 733 in single-copy, and 2 in duplicated form. The RNA-seq results revealed that 6,822 (98.98%) of the genes predicted for the *R. glutinis* X-20 genome regions were expressed, and 441 new genes were identified. These findings revealed that the assembled genome included a sizable proportion of the entire number of genes. The BUSCOs calibrations and transcript sequencing

both demonstrated that our present genomic assemble was of good quality.

Functional Annotation

The predicted gene protein sequences were compared to each functional database using DIAMOND (E-value $< 1e^{-5}$). First, annotation using Nr database indicated that 6,547 (94.99%) of the 6,892 predicted genes have been annotated on 29 different species. Based on the distribution of the number of annotations, the top three strains were *Rhodotorula graminis* (5,379, 82%), *Rhodotorula toruloides* (899, 13.7%), and *Rhodotorula taiwanensis* (104, 1.58%). According to the KEGG, GO, TCDB, Swissport, and Pfam databases, 3,584 (52.00%), 4,558 (66.13%), 248 (3.6%), 1,917 (29.28%), and 4,558 (69.62%) genes could be annotated. Furthermore, the antiSMASH software, which analyzes secondary metabolites, identified 70 genes that express six clusters (three terpene, one NRPS, and two others). To study the metabolic pathways of gene products and compounds, a total of 3,584 genes were effectively mapped to 354 KEGG pathways (**Supplementary Figure 1**). Furthermore, 4,558 genes were predicted to classify into three Gene Ontology (GO) categories (**Supplementary Figure 2**). Cellular processes and metabolic processes accounted for 28.25 and 26.13%, respectively. Porters (uniporters symporters antiporters) (92, 37.09%), P–P-bond-hydrolysis-driven transporters (65, 26.21%), and Oxidoreduction-driven transporters (29, 11.69%) were the top three membrane transport proteins studied from the 248 genes identified in the TCDB database. These indicate that its transport proteins pathway has been strengthened.

Analysis of Phylogenetic and Syntenic Relationships

The relationship of *R. glutinis* X-20 to other red yeast species was investigated by constructing phylogenetic trees from three directly homologous *Sporobolomyces* families (*Rhodosporidiobolus*, *Rhodotorula*, and *Sporobolomyces*). The 18sDNA sequence of *R. glutinis* X-20 was compared with the 18s rDNA sequences of other strains (data from the NCBI nucleotide database). As shown in **Figure 2**, the evolutionary tree demonstrated that *R. glutinis* X-20 is more closely related to *R. graminis*, *R. graminis* WP1, and *R. diobovata* than other species, supporting the annotated results in the Nr database. The genome collinearity blocks of *R. glutinis* X-20 and its two accessible *R. graminis* WP1 and *R. diobovata* genomes were examined using phylogenetic tree results and genome sequences from the NCBI website. As shown in **Figure 3**, there are 38 blocks (6,343 synthetic gene pairs) between the *R. glutinis* X-20 genome and the *R. graminis* WP1 genome sequence. The number of genes was 92.03% for *R. glutinis* X-20 and 89.79% for *R. graminis* WP1. Between the *R. glutinis* X-20 genome and the *R. diobovata* genome sequence, there are 350 blocks (6,086 synthetic gene pairs). The number of genes in *R. glutinis* X-20 and *R. diobovata* was 88.31 and 79.36%. The complete length of collinearity blocks accounted for 20.26% of the genome length of *R. glutinis* WP1 and 63.70% of the genome length of *R. diobovata*, in both. These findings imply that the *R. glutinis* X-20 genome is more closely in linked to the *R. graminis* WP1 genome than the *R. diobovata* genome, and that the *R. glutinis* X-20 genome is better annotated.

Protein Families and Comparative Genomes

For the 6892 protein-coding genes predicted in *R. glutinis* X-20, the top three predicted *Rhodotorula* strains in the NR database, *R. graminis* WP1, *R. taiwanensis*, and *R. toruloides* NP11, were selected for functional gene analysis of homologous strains. The protein sequences of four *Rhodotorula* were analyzed by cluster the data of gene families separately using OrthoFinder 2.5.4 (default parameters). By cluster analysis, 6951 protein cluster families (6235 cluster of *R. glutinis* X-20, 6244 cluster of *R. graminis* WP1, 5922 cluster of *R. taiwanensis,* and 6439 cluster of *R. toruloides* NP11) and 4486 shared_cluster (1183 shared_cluster of *R. glutinis* X-20, 1196 shared_cluster of *R. graminis* WP1, 828 shared_cluster of *R. taiwanensis,* and 1279 shared_cluster of *R. toruloides* NP11) were identified, while 694 common_cluster families and 4344 single_cluster gene families were identified (**Figure 4A**). 14 Uniq clusterN (38 genes), 10 Uniq clusterN (21 genes), 56 Uniq clusterN (235 genes), and 122 Uniq clusterN (516 genes) protein families are Uniq clusterN (Uniq geneN) in *R. glutinis* X-20, *R. graminis* WP1, *R. taiwanensis,* and *R. toruloides* NP11, respectively. In addition, in order to understand the functional categorization of Uniq geneN in *R. glutinis* X-20, specific genes in each of the four red yeast species were subjected to GO analysis. As shown in **Figure 4B**, 46.14% of the cellular component, 39.01% of the biological process and 14.85% of the molecular function were identified in *R. glutinis* X-20. *R. glutinis* X-20 functional distribution is more oriented toward cellular component. 10, 18, and 7 GO terms in Uniq_geneN of *R. glutinis* X-20 were significantly enriched in three categories of biological processes (BP), molecular functions (MF), and cellular components (CC), respectively (**Figure 4C**). According the results, Uniq geneN and transmembrane function were related, including MF: sigma factor activity (GO:0016987), structural molecule activity (GO: 0005198), carbonate dehydratase activity (GO:0004089), cysteine-type endopeptidase activity (GO:0004197), cation transmembrane transporter activity (GO:0008324); CC: viral capsid (GO:0019028), intracellular (GO:0005622), periplasmic space (GO:0042597); BP: DNA integration (GO:0015074), regulation of mitotic metaphase/anaphase transition (GO:0030071). Finally, Uniq geneN was counted through the KEGG database. The KEGG pathway that shows to be enriched in *R. glutinis* X-20 Uniq geneN comprises primarily nitrogen metabolism (ko00910), viral carcinogenesis (ko05203), transcriptional misregulation in cancers (ko05202), alcoholism (ko05034), systemic lupus erythematosus (ko05322) (**Figure 4D**). This shows that *R. glutinis* X-20 may be pathogenic as well. The assessment of Ka/Ks for single-copy orthologous genes is generally accepted as an indicator of selection pressure during biological evolution. The 4344 single-copy cluster family between *R. glutinis* X-20 and three of his related strains was used as a proxy to calculate the Ka/Ks ratio in order to investigate the evolution of the target strains. The substitution rate (Ka/Ks)

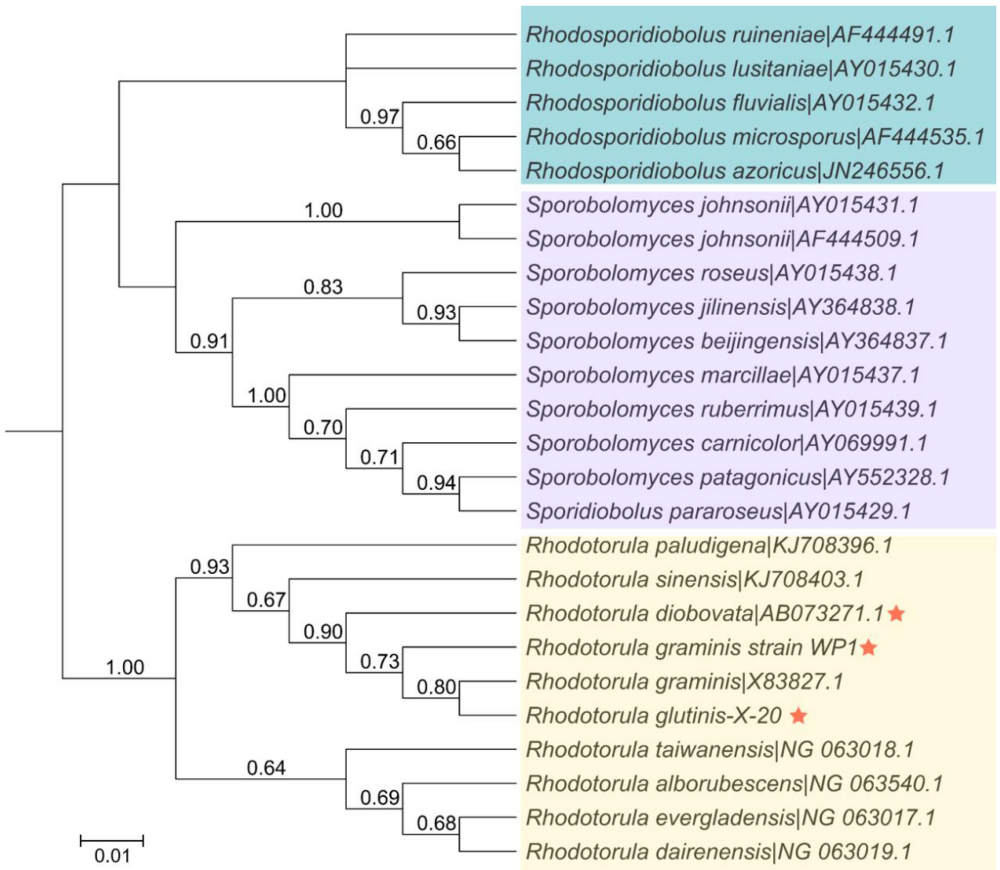

FIGURE 2 | Phylogenetic and evolutionary analysis between 25 strains of red yeasts of the order *Sporidiobolales*. The phylogenetic tree was built in MEGA 7.0 using an alignment of the 18S rDNA sequences, the Neighbor-joining technique, and a Bootstrap analysis of 1,000 iterations. An asterisk denotes the strain *R. glutinis* X-20 and its closely related species. The bootstrap value is shown by the number at each branch of the phylogenetic tree (1,000 replicates). Shades of blue, purple, and yellow represent the various clusters of *Rhodosporidiobolus*, *Sporobolomyces*, and *Rhodotorula* isolates, respectively.

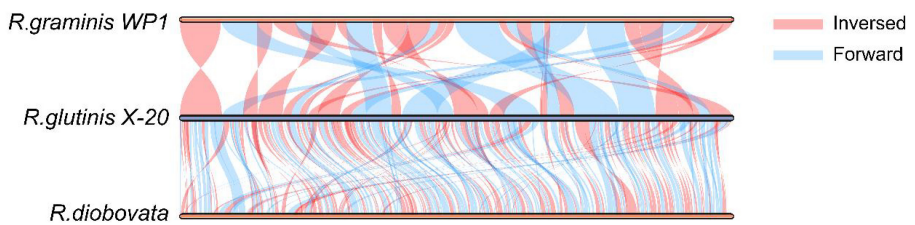

FIGURE 3 | Analysis of the genome collinearity blocks between *R. glutinis* X-20 genes with its two close related species. MCScanX was used to conduct pair-wise alignments of *R. glutinis* X-20, *R. graminis* WP1, and *R. diobovata* complete genome sequences. In three genomes, blue lines represent Forward collinear blocks and pink bars represent Inversed collinear blocks.

for each orthologous gene was calculated using the NG model. There were three pairs with Ka/Ks values greater than 1.0 (strong positive selection), 114 pairs with Ka/Ks values between 0.5 and 1.0 (positive selection), 3,204 pairs with Ka/Ks values between 0.1 and 0.5 (weak positive selection), and 1,015 pairs with Ka/Ks values less than 0.1 (purifying selection). Only three gene pairs with Ka/Ks $>$ 1 in *R. glutinis* X-20 were significant, suggesting that the most of genes were preserved by a sequence of purifying natural selections. By KEGG and GO annotation of purifying selected genes (Ka/Ks $>$ 0.1), *R. glutinis* X-20 is believed to have a strong evolutionary tendency in metabolite biosynthesis as well as cell division function (**Supplementary Figures 3, 4**).

Metabolites Identification in *Rhodotorula glutinis* X-20

To further analyze the function of the *R. glutinis* X-20 strain from a metabolite point of view, metabolites in samples obtained after

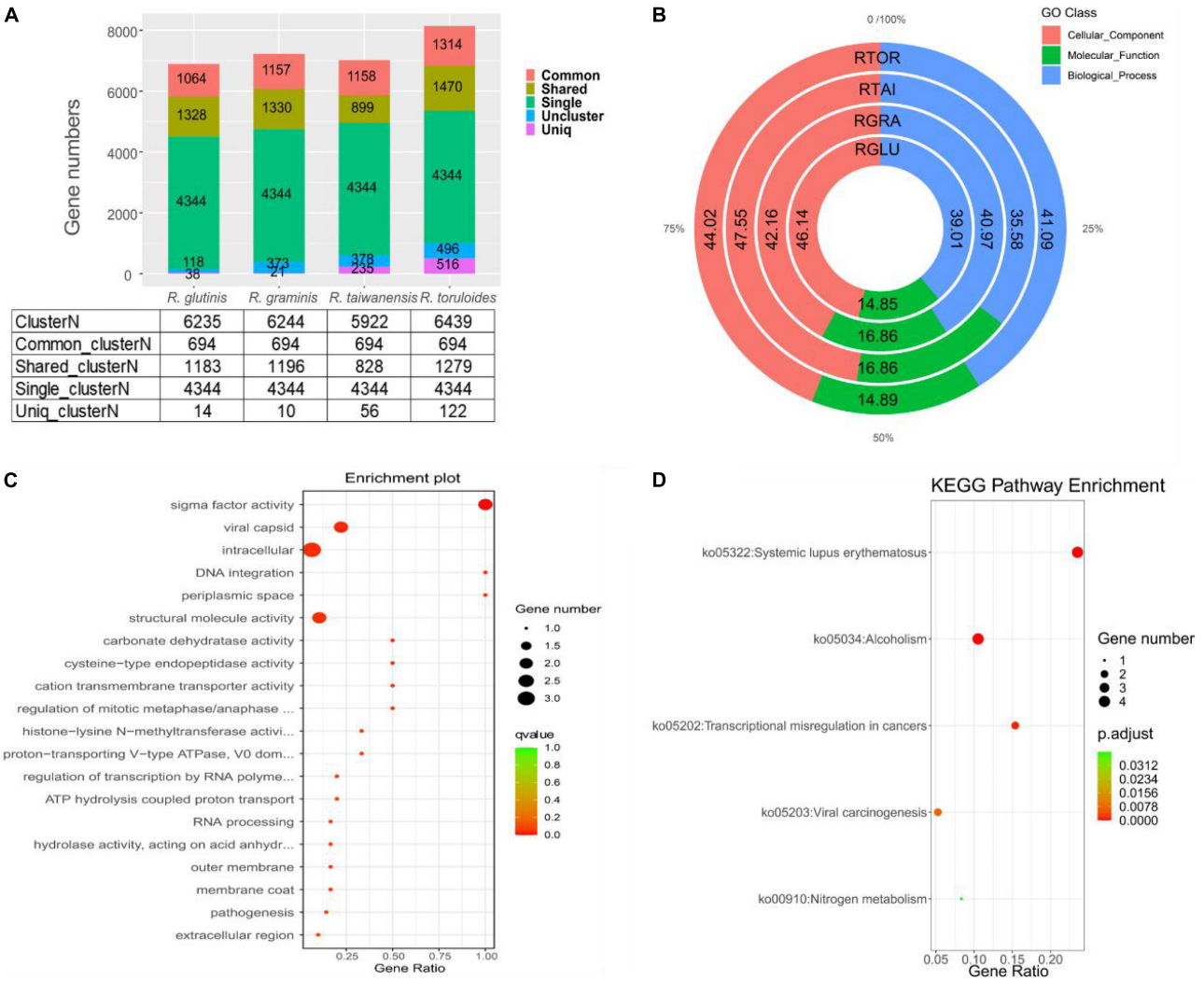

FIGURE 4 | *Rhodotorula glutinis* X-20 and closely related *Rhodotorula* strains such as *R. graminis* WP1, *R. taiwanensis*, and *R. toruloides* NP11 were used for comparative genomic analysis. **(A)** Gene family analysis on four red yeast strains. **(B)** The relative proportions (%) of Uniq geneN enrichment in four red yeast species in GO categories. **(C)** Top 20 enriched GO annotations of these species-specific genes in *R. glutinis* X-20 whole genome. **(D)** Enrichment of the Uniq gene N in *R. glutinis* X-20 by the KEGG pathway. The rich factor is the ratio of the number of enriched genes to the total number of genes in a given pathway. The Q-value is derived from the p-value after multi-test correction. Q-values vary from 0 to 1, with the closer to 0 indicating greater enrichment.

120 h of growth were analyzed using HPLC-MS for qualitative and quantitative characterization (42). In total, 654 species were detected by scanning in data-dependent MS/MS mode, mainly including 171 amino acid, 65 carbohydrate, 32 cofactors and vitamins, 124 lipid, 44 nucleotide, 4 peptide, and 214 others (**Table 2**). The important lipids were identified, including 40.14% fatty acyl, and 8.45% prenol lipids. This suggests that *R. glutinis* X-20 is a typical lipid-producing yeast strain, producing mainly fatty acyl and prenol lipids (**Table 3**). Further analysis of lipids found several more important compounds such as linolenate, methyl palmitate, β-carotene, and L-phenylalanine (**Supplementary Table 4**). Linoleic and methyl palmitate, the main lipid compounds produced by *R. glutinis* have a positive impact on softening blood vessels and lowering blood pressure in humans. β-carotene and L-phenylalanine are two of the most widely studied substances in *R. glutinis*, with considerable industrial applications.

Validation of Putative Phytoene Desaturase and Putative 15-Cis-Phytoene Synthase/Lycopene Beta-Cyclase

On the basis of whole genome sequencing, nucleotide primers crtI-F and crtI-R were constructed, as well as crtYB-F and crtYB-R, to clone the putative phytoene desaturase gene (crtI) and the putative 15-cis-phytoene synthase/lycopene beta-cyclase gene (crtYB) from *R. glutinis* X-20 (**Supplementary Table 1**). The CDS region encoding the crtI sequence is composed of a full-length ORF region and six shorter ORF sections,

TABLE 2 | Identified metabolites using HPLC-MS profiling in *Rhodotorula glutinis* X-20.

Metabolites	Positive	Negative	Percentage (%)
Amino acid	113	58	26.14
Carbohydrate	29	36	9.94
Cofactors and Vitamins	21	11	4.89
Lipid	83	41	18.96
Nucleotide	30	14	6.73
Peptide	2	2	0.61
Others	170	44	32.72
Total	448	206	100

1,644 bp long (containing 547 amino acids) (**Supplementary Table 2**). Molecular weight, Isoelectric point, Domain, Protein Family, Secondary structure of crtI and crtYB genes were statistics (**Table 4**).

Expression of crtI and crtYB in *Saccharomyces cerevisiae*

To detect the putative phytoene desaturase (crtI) in *R. glutinis* X-20, the gene of phytoene synthase (crtB) from *Erwinia* (GenBank Accession: KC954270.1) was cloned to provide the necessary supply of precursors. The gene expression cassettes TEF1p-crtB-CYC1t and ALA1p-crtI-HOG1t were first homologously transferred to wild *S. cerevisiae* chromosomes Delta 15 and Delta 22, respectively (**Figure 5A**). The shake flask fermentation revealed that the strains with the properly modified gene expression cassette changed color from white to pink, whereas the control showed no color change (**Figure 5C**). HPLC analysis showed that the accumulated carotenoids in the hybrid strains containing TEF1p-crtB-CYC1t and ALA1p-crtI-HOG1t were identical with the standard lycopene, showing that the crtI gene functions as a multi-step phytoene desaturase (**Supplementary Figure 7**). In addition, to test the effect of different chassis hosts on the products, crtI and crtB were inserted into *S. cerevisiae* CEN.PK2-1C (*Sc*. CEN) and *S. cerevisiae* INVSc1 (*Sc*. INV) to construct strains *Sc*. CEN (B1) and *Sc*. INV (B2), respectively (**Figure 5B**).

To assay the activity of the putative 15-cis-phytoene synthase/lycopene beta-cyclase (crtYB) from *R. glutinis* X-20, the gene expression cassettes FBA1p-crtYB-ADH1t and ALA1p-crtI-HOG1t were similarly constructed into Delta 17 and Delta 22, respectively, on the chromosome of wild *S. cerevisiae* (**Figure 5A**). The fermented strains show a change from white to yellow in the transformed strains and no change in the control (**Figure 5C**). HPLC analysis showed that the accumulated carotenoids in the hybrid strains containing gene expression cassettes ALA1p-crtI-HOG1t and FBA1p-crtYB-ADH1t were identical with the standard β-carotene, showing that the crtYB gene functions as 15-cis-phytoene synthase/lycopene beta-cyclase (**Supplementary Figure 7**). Meanwhile, crtYB and crtI were co-introduced into the different chassis hosts *S. cerevisiae* CEN.PK2-1C and *S. cerevisiae* INVSc1 to construct strains *Sc*. CEN (B3) and *Sc*. INV (B4) (**Figure 5B**).

TABLE 3 | Identified lipids using HPLC-MS profiling in *Rhodotorula glutinis* X-20.

Lipids	Positive	Negative	Percentage (%)
Azacyclic compounds	1	1	1.40
Benzene and substituted derivatives	1	–	0.70
Carboxylic acids and derivatives	5	1	4.22
Fatty Acyls	37	20	40.14
Flavonoids	4	1	3.52
Glycerophospholipids	2	1	2.11
Hydroxy acids and derivatives	1	1	1.40
Isoflavonoids	–	1	0.70
Keto acids and derivatives	2	–	1.40
Organic oxides	–	1	0.70
Organic phosphoric acids and derivatives	–	1	0.70
Organonitrogen compounds	–	3	2.11
Organooxygen compounds	1	1	1.40
Oxanes	1	–	0.70
Polycyclic hydrocarbons	3	–	2.11
Prenol lipids	11	1	8.45
Pyrans	1	–	0.70
Pyrimidine nucleotides	1	–	0.70
Steroids and steroid derivatives	6	5	7.74
Stilbenes	1	–	0.70
Unsaturated hydrocarbons	1	–	0.70
Others	22	3	17.60
Total	101	41	100

TABLE 4 | Functional analysis of crtI and crtYB.

Type	crtI	crtYB
Sequence length	1,644 bp (547 amino acid)	1,776 bp (591 amino acid)
Molecular weight	60.84 kDa	65.39 kDa
Isoelectric point	7.35	6.3
Domain	crtI	CarR; Isoprenoid biosynthesis enzyme
Protein Family	crtI subfamily member	cl11889 super family; Isoprenoid BiosynC1 super family
Secondary structure	(H): 75.5%, (E): 64.6%, (T): 11.1%	(H): 76.6%, (E): 45.7%, (T): 10.5%

The qPCR showed the effective transcription of crtI, crtB genes in *Sc*. CEN(B1), *Sc*. INV (B2), and crtI, crtYB genes in *Sc*. CEN (B3), *Sc*. INV (B4). Besides, compared to *Sc*. CEN(B3), mRNA levels of both crtI and crtYB genes were boosted in strain *Sc*. INV(B4), and compared to mRNA levels of crtB in *Sc*. CEN(B1) and *Sc*. INV(B2), mRNA levels of crtYB genes in *Sc*. CEN(B3) and *Sc*. INV(B4) were increased 1.87- and 4.12-fold (**Figure 6A**).

This effect was more pronounced when crtI and crtYB were co-expressed. These results indicated that the crtI, crtYB genes were fully functional in *S. cerevisiae,* and the mRNA level of the crtYB gene in *S. cerevisiae* was increased compared to the

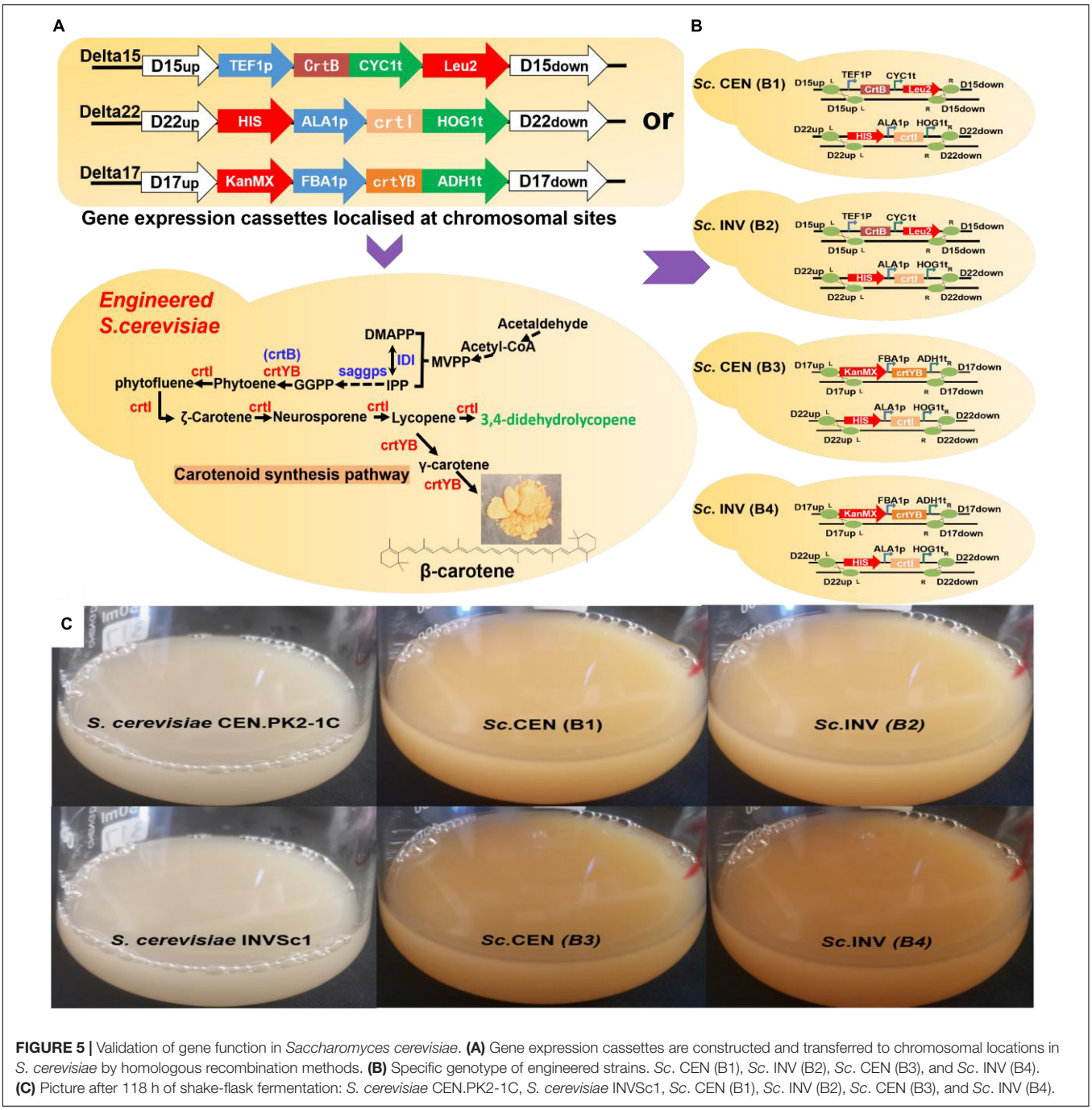

FIGURE 5 | Validation of gene function in *Saccharomyces cerevisiae*. **(A)** Gene expression cassettes are constructed and transferred to chromosomal locations in *S. cerevisiae* by homologous recombination methods. **(B)** Specific genotype of engineered strains. *Sc*. CEN (B1), *Sc*. INV (B2), *Sc*. CEN (B3), and *Sc*. INV (B4). **(C)** Picture after 118 h of shake-flask fermentation: *S. cerevisiae* CEN.PK2-1C, *S. cerevisiae* INVSc1, *Sc*. CEN (B1), *Sc*. INV (B2), *Sc*. CEN (B3), and *Sc*. INV (B4).

mRNA level of crtB in *S. cerevisiae*. After 118 h of shake-flask fermentation, HPLC analysis were used to determine the products (**Figure 6B**). HPLC analysis showed that the engineered strain *Sc*. CEN (B2), constructed with *S. cerevisiae* CEN.PK2-1C as the chassis host, produced lycopene at a titer of 0.74 $mg{\cdot}L^{-1}$ (0.36 $mg{\cdot}g^{-1}$ DCW) and the engineered strain *Sc*. INV (B1), constructed with *S. cerevisiae* INVSc1 as the chassis host, produced lycopene at a titer of 0.41 $mg{\cdot}L^{-1}$ (0.17 $mg{\cdot}g^{-1}$ DCW). In comparison, *Sc*. CEN (B2) was 1.8 folds higher in titer than *Sc*. INV (B1). Similarly, when the engineered strain *Sc*. CEN (B3), constructed with *S. cerevisiae* CEN.PK2-1C as the chassis host, produced β-carotene at a titer of 0.18 $mg{\cdot}L^{-1}$ (0.18 $mg{\cdot}g^{-1}$ DCW), the engineered strain *Sc*. INV (B4), constructed with *S. cerevisiae* INVSc1 as the chassis host, produced β-carotene at a titer of 1.59 $mg{\cdot}L^{-1}$ (0.63 $mg{\cdot}g^{-1}$ DCW). The 8.8-fold increase in the titer of *Sc*. INV (B4) suggests that *S. cerevisiae* INVSc1 is better suited as a chassis host for crtI and crtYB gene expression. This finding is consistent with prior findings by Westfall et al. such as the production of artemisinin by *S. cerevisiae* (43).

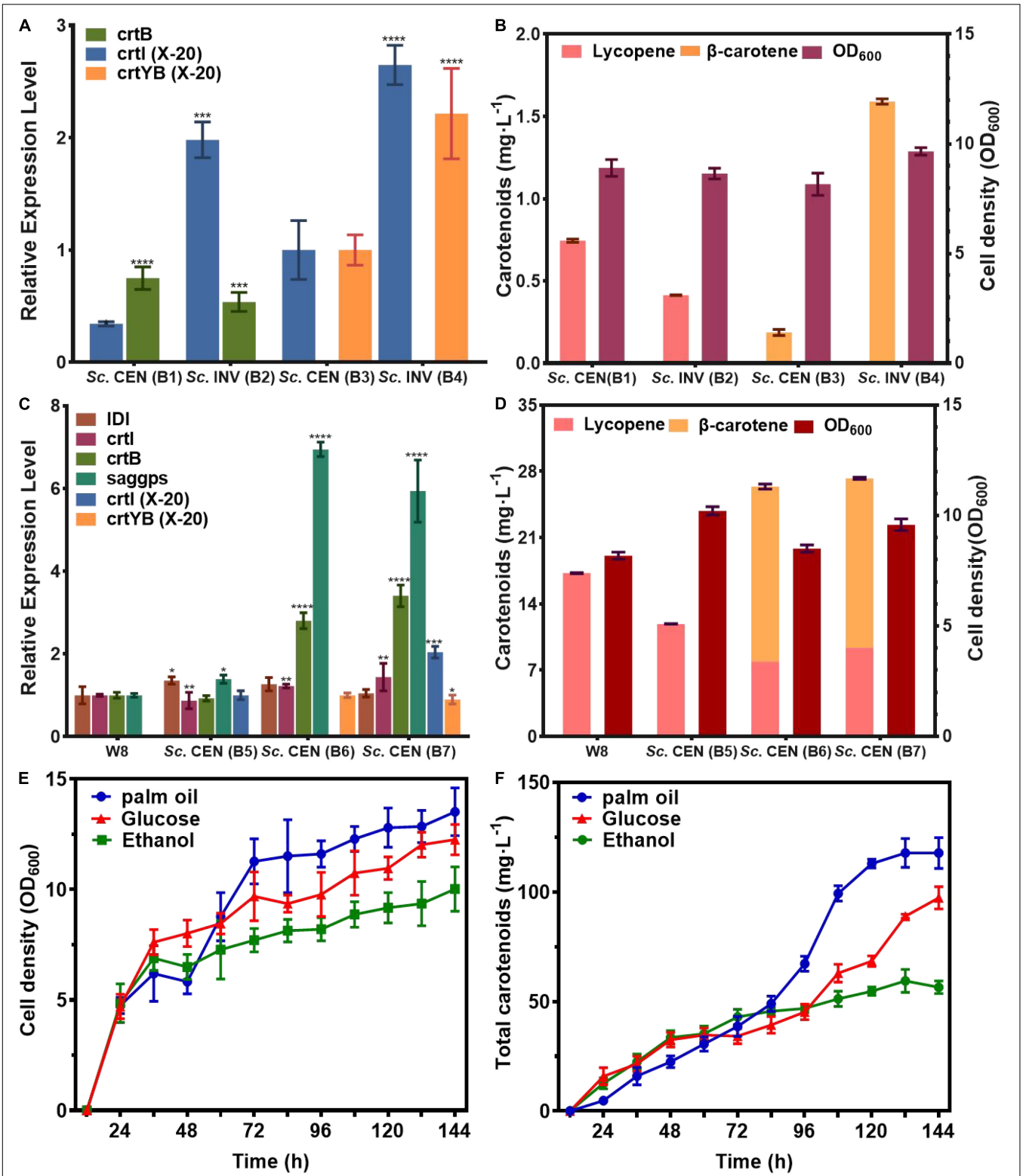

FIGURE 6 | Efficient expression and fermentation optimization of engineered strains. Validation of genetically functional engineered strains for **(A)** mRNA expression levels, **(B)** metabolite production. Optimization of **(C)** mRNA expression levels of genes of interest in the upstream pathway for engineered strains with **(D)** metabolite production. **(E)** Cell growth density of *Sc*. CEN (B7) strain, **(F)** total carotenoids production of *Sc*. CEN (B7) strain (relative mRNA levels were calculated from the mRNA of the reference gene TUB1, data shown as the mean of three independent experiments, error expressed as ±SD). Significant differences between groups were calculated by one-way ANOVA (****$p < 0.001$, ***$p < 0.01$).

Carotenoids Production in *Saccharomyces cerevisiae* by Expressing crtI and crtYB

The rate-limiting step in carotenoid biosynthesis is the mevalonate pathway, and GGPP is the key rate-limiting enzyme (44). To further clarify the expression effect of genes from *R. glutinis* X-20, the mevalonate pathway in *S. cerevisiae* was fortified for further functional analysis of crtI and crtYB. crtI, crtYB or crtI-crtYB were transferred to previously constructed mevalonate pathway optimized the engineered strain W8 (22), produced *Sc*. CEN (B5), *Sc*. CEN (B6), and *Sc*. CEN (B7). The results of qPCR showed the effective transcription of the crtI and crtYB in engineered yeasts (**Figure 6C**). Significant transcription of the crtI gene in *Sc.* CEN (B5), the rate-limiting enzyme IDI of the MVA pathway, and saggps of the carotenoid synthesis pathway both were up-regulated in *Sc*. CEN (B5) compared to the control engineered strain W8 (**Figure 6C**). The control strain W8 produced 17.25 mg·L^{-1} (2.78 mg·g^{-1} DCW), but the lycopene production of strain *Sc*. CEN (B5) was reduced to 11.89 mg·L^{-1} (1.99 mg·g^{-1} DCW) (**Figure 6D**). This may be due to further conversion of the crtI gene to 3,4-didehydrolycopene, causing further expression of the upstream rate-limiting enzyme and at the same time consumption of lycopene (45). In the *Sc*. CEN (B6) strain, IDI, saggps, crtB and crtI were also found up-regulated with 1. 26-, 6. 94-, 2. 8-, and 1.22-fold, respectively, probably caused by dragging *via* overexpression of the crtYB gene (**Figure 6C**). *Sc*. CEN (B6) produced 7.91 mg·L^{-1} (1.25 mg·g^{-1} DCW) lycopene and 18.48 mg·L^{-1} (2.92 mg·L^{-1} DCW) β-carotene, a 0.66-fold decrease in lycopene production compared to *Sc*. CEN (B5), which newly accumulated high concentrations of β-carotene (**Figure 6D**). Furthermore, strain *Sc*. CEN (B7) including crtI and crtYB showed a 5.93-fold upregulation of saggps, a 1.44-fold upregulation of crtI and a 3.4-fold upregulation of crtB compared to the control engineered W8 strain (**Figure 6C**). Expression of crtI and crtYB resulted in a 0.78-fold decrease in lycopene 9.37 mg·L^{-1} (1.47 mg·L^{-1} DCW) compared to *Sc.* CEN (B5), but production 17.89 mg·L^{-1} (2.80 mg·L^{-1} DCW) of β-carotene (**Figure 6D**). These results indicated that crtI and crtYB can be efficiently expressed in *S. cerevisiae*.

In order to obtain high levels of carotenoid production, the *Sc*. CEN (B7) strain was used in 1L bioreactors (TJ-Mini Box, Parallel-Bioreactor, Shanghai) for carotenoid fermentation. The initial glucose was 20 and 2 g·L^{-1} palmitic acid, 2 g·L^{-1} glucose, and 2 g·L^{-1} ethanol was added after 24 h of fermentation. Sodium hydroxide/sulfuric acid was used to maintain pH at 6.0 during fermentation. The addition of palmitic acid well increased the cell growth (46). Supplementing palmitic acid resulted in a faster cell growth 48–72 h compared to the addition of glucose or ethanol (**Figure 6E**). Total carotenoids (β-carotene, lycopene) production gradually increased throughout the fermentation, with glucose and ethanol titers of 97.29 and 64.97 mg·L^{-1}, respectively, and 117.78 mg·L^{-1} under palmitic acid conditions (**Figure 6F**). With the addition of palmitic acid, the titers of lycopene and β-carotene were 53.55 and 64.23 mg·L^{-1}, respectively, with a 5.75- and 3.59-fold rise in supplementary fermentation, respectively.

DISCUSSION

The functional genes of *R. glutinis*, an oil-producing yeast, are used to produce a range of metabolites. Researchers are increasingly considering *R. glutinis* as a potential strain for industrial applications (47). Unfortunately, several *R. glutinis* have been described in the literature for the commercial production of lipids and carotenoids, but there are few validation studies on their molecular biology and functional genes. As a result, genomic analysis enables more in-depth research of its function. Furthermore, it is valuable that the engineered strains are used and perfectly expressed by key functional genes.

The functional resolution of the *R. glutinis* X-20 genome and metabolite assay showed a substantial number of lipid metabolism genes, as well as a number of other relevant genes. The results of the whole genome assembly were classified according to their valuable functional genes and a phylogenetic tree was performed to analyse their evolutionary position in the family. *R. graminis* WP1 and *R. diobovata* were identified as strains with the highest affinity, and analysis of genome collinearity blocks revealed that *R. glutinis* X-20 was better assembled. Three direct homologous *Rhodotorula* families were selected for comparative genomic analysis to better investigate its gene function. The gene function of *R. glutinis* X-20 was shown to be prominently distributed in functions related to transmembrane transport. According to the KEGG annotation, *R. glutinis* X-20 has a number of disease-causing genes that are consistent with those revealed for Wirth et al. (2). Though Ka/Ks analysis, *R. glutinis* X-20 has a strong evolutionary tendency in metabolite biosynthesis as well as in cell division functions.

Rhodotorula glutinis is a lipid-producing strain which can synthesize a wide range of lipids in the body (48). *Rhodotorula glutinis* synthesizes acylglycerols, fatty acids, phospholipids and sterols in general, which are essential for cellular life (49). The typical method involves overexpression of important enzymes, suppression of competing pathways, and strain adjustment of the transcription pathway of the relevant genes (48). Comparison with the gene annotation results identified a number of functionally significant genes. Such as GPD1, FAS1, ACACa, ACOX3, TGL2, MGLL, and PDAT. As a case, a valuable phenylalanine ammonia lyase (PAL) was also identified, which has been used as an enzyme-based biopharmaceutical therapy for the treatment of phenylketonuria (PKU) (50). A number of genes associated with fatty acid synthesis were identified, as these lipases were closely related to lipid metabolism (51). With the further exacerbation of energy crisis in the face of both global epidemics and economic pressures, biofuels production by *R. glutinis* maybe more advantageous as the third generation than first and second generation biofuels (52). Therefore, it is of great significance to study the lipid metabolism of *R. glutinis* X-20.

When metabolites were analyzed by HPLC-MS, a variety of carotenoid species, including canthaxanthin, astaxanthin, and β-carotene were identified. The crtI and crtYB genes are associated with the formation of β-carotene. This was consistent with the production of β-carotene by *R. glutinis* ATCC 15125 reported by Braunwald et al. (53). As the most important carotenoid in *R. glutinis*, β-carotene is unique in that it acts as a precursor to

vitamin A, which is converted to vitamin A in the body after consumption and is used in the treatment of night blindness, skin diseases, bronchitis, and chronic pharyngitis (54, 55). However, the construction of engineered strains for efficient carotenoid synthesis is still lacking, especially with *R. glutinis* as the original host. In order to achieve commercial application of β-carotene, it is essential to obtain efficient *R. glutinis* strains, but there are not strains of *R. glutinis* for industrial application so far. The main reasons for this are the high cost of the culture medium, the complexity of the operation and the low yield per unit volume of the culture vessel, among other disadvantages that make it unsuitable for industrial production (56). Furthermore, *Rhodotorula* has previously been reported to cause fungemia associated with central venous catheter (CVC) use, which may be the reason why this strain is not suitable for direct use as an industrial strain. The use of synthetic biology approaches could therefore enable us to establish a strain with high β-carotene production by heterologously expressing the relevant genes in a safe and healthy strain. Due to its depth of research and safety, *S. cerevisiae* is widely used as a gene expression host (57). Thus, the crtI and crtYB key genes in *R. glutinis* X-20 were cloned and constructed onto chromosomes in *S. cerevisiae*. As shown in **Figure 6**, crtI can synthesize lycopene, and the crtYB is bifunctional which can synthesizes phytoene and β-carotene. This was consistent with what was previously reported by Li et al. (58). In addition, in comparison to crtB, crtI, and crtYB were more highly expressed in *S. cerevisiae* INVSc1. This indicated that the genetic background has an influence on the expression of the target enzymes (59). Co-expression of crtI and crtYB in *S. cerevisiae* INVSc1 produced 1.59 $mg{\cdot}L^{-1}$ (0.63 $mg{\cdot}L^{-1}$ DCW) of β-carotene. Compared with the previous results that transferred crtE, crtYB, and crtI from *Phaffia rhodozyma* into *S. cerevisiae* to produce 258.8 $\mu g{\cdot}g^{-1}$ DWC (60), the yield of co-expressed crtI and crtYB was increased by 2.45-fold.

To explore the application potential of crtI and crtYB, they were transferred into strain W8, in which the mevalonate pathway had been strengthened (22, 44). When the crtI gene was introduced alone, the rate-limiting enzyme of the upstream MVA pathway was up-regulated 1.39-fold, but the *Sc.* CEN (B5) strain produced 0.31-fold less lycopene. This suggests that crtI possesses a further conversion to 3,4-didehydrolycopene, leading to further expression of the upstream rate-limiting enzyme and concomitant depletion of lycopene. When the crtYB gene was introduced alone, HPLC showed that *Sc.* CEN (B6) produced 7.91 $mg{\cdot}L^{-1}$ (1.24 $mg{\cdot}g^{-1}$ DCW) of lycopene and 18.48 $mg{\cdot}L^{-1}$ (2.92 $mg{\cdot}g^{-1}$ DCW) of β-carotene compared to W8, when the transcript levels of the key upstream rate-limiting enzyme saggps were up-regulated by 6.94-fold. This was consistent with Rathod et al. who showed that the introduction of crtYB (phytone-β-carotene) from the red yeast *Xanthophyllomyces dendrorhous* into *Chlamydomonas reinhardtii* to overexpress lycopene synthase, this was consistent with the production of β-carotene (22.8 $mg{\cdot}L^{-1}$) and lutein (8.9 $mg{\cdot}L^{-1}$), suggesting that Sc. CEN(B6) itself can consume some precursors to produce β-carotene (61). When crtI and crtYB were co-expressed, 9.37 $mg{\cdot}L^{-1}$ (1.47 $mg{\cdot}L^{-1}$ DCW) lycopene and 17.89 β-carotene $mg{\cdot}L^{-1}$ (2.80 $mg{\cdot}L^{-1}$ DCW) were produced in *Sc.* CEN (B6). Lycopene rose 0.18-fold and β-carotene remained essentially unchanged, indicating that the crtYB gene had reached its highest level of expression. This further validated the importance of rate-limiting enzymes for product synthesis (62). Additionally, fermentation technology is an important means to improve the product synthesis. Among palmitic acid, glucose, and ethanol supplement, it was discovered that palmitic acid contributed to both cell growth and product synthesis. The addition of palmitic acid resulted in a considerable advantage in cell development after 72 h, with a rapid increase in carotenoid synthesis from 38.66 to 117.78 $mg{\cdot}L^{-1}$, an approximate 2-fold increase. Palmitic acid was found in most agricultural waste and was less expensive and easier to obtain than glucose, which can be repurposed as a source of carbon to produce a more valuable product.

In summary, a systematic study of the whole genome sequencing of *R. glutinis* X-20, metabolite identification, carotenoid synthesis pathway and its functional validation. The crtI and crtYB genes, obtained by genome sequencing annotation, were verified to indeed function as carotenoid synthesizers. Heterologous constructs in *S. cerevisiae* are an effective solution strategy to validate this class of organisms, and optimization of the precursor pathway and improvement of fermentation conditions facilitate further enhanced expression of gene function. This work has the potential to form the basis for studying the function of different genes in *Rhodotorula* and to guide the selection of host cells and fermentation mechanisms.

DATA AVAILABILITY STATEMENT

The datasets presented in this study can be found in online repositories. The names of the repository/repositories and accession number(s) can be found in the article/ **Supplementary Material**.

AUTHOR CONTRIBUTIONS

SB designed and performed the experiments and data analysis. JG and XW contributed the bioinformatic analysis and other support. XN performed the sequencing library construction. ZL and YS supervised the writing of the manuscript throughout. GZ and JY revised the manuscript. All authors read and approved the final manuscript.

FUNDING

This work was supported by the National Natural Science Foundation of China (grant number: 22178226), Research Project of XPCC (grant number: 2020AB026), and Research Project of Youth Science and Technology Innovation Leader of XPCC (grant number: 2017CB007).

SUPPLEMENTARY MATERIAL

The Supplementary Material for this article can be found online at: https://www.frontiersin.org/articles/10.3389/fnut.2022.918240/full#supplementary-material

REFERENCES

1. Kruger JS, Cleveland NS, Yeap RY, Dong T, Ramirez KJ, Nagle NJ, et al. Recovery of fuel-precursor lipids from oleaginous yeast. *ACS Sustain Chem Eng.* (2018) 6:2921–31.
2. Wirth F, Goldani LZ. Epidemiology of *Rhodotorula*: an emerging pathogen. *Interdiscip Perspect Infect Dis.* (2012) 2012:465717.
3. Gong G, Liu L, Zhang X, Tan T. Multi-omics metabolism analysis on irradiation-induced oxidative stress to *Rhodotorula glutinis*. *Appl Microbiol Biotechnol.* (2019) 103:361–74.
4. Maza DD, Vinarta SC, Su Y, Guillamon JM, Aybar MJ. Growth and lipid production of *Rhodotorula glutinis* R4, in comparison to other oleaginous yeasts. *J Biotechnol.* (2020) 310:21–31. doi: 10.1016/j.jbiotec.2020.01.012
5. Ratledge C, Cohen Z. Microbial and algal oils: do they have a future for biodiesel or as commodity oils? *Lipid Technol.* (2008) 20:155–60.
6. Schneider T, Graeff-Hönninger S, French WT, Hernandez R, Merkt N, Claupein W, et al. Lipid and carotenoid production by oleaginous red yeast *Rhodotorula glutinis* cultivated on brewery effluents. *Energy.* (2013) 61:34–43.
7. Frengova G, Simova E, Pavlova K, Beshkova D, Grigorova D. Formation of carotenoids by *Rhodotorula glutinis* in whey ultrafiltrate. *Biotechnol Bioeng.* (1994) 44:888–94. doi: 10.1002/bit.260440804
8. Parasar DP, Ramakrishnan E, Kabilan S, Kotoky J, Sarma HK. Characterization of beta-cryptoxanthin and Other carotenoid derivatives from *Rhodotorula* taiwanensis, a novel yeast isolated from traditional starter culture of Assam. *Chem Biodivers.* (2020) 17:e2000198. doi: 10.1002/cbdv.202000198
9. Xue F, Liu Z, Yu Y, Wu Y, Jin Y, Yang M, et al. Codon-optimized *Rhodotorula glutinis* PAL expressed in *Escherichia coli* with enhanced activities. *Front Bioeng Biotechnol.* (2020) 8:610506. doi: 10.3389/fbioe.2020.610506
10. White C, Sayer JA, Gadd GM. Microbial solubilization and immobilization of toxic metals: key biogeochemical processes for treatment of contamination. *FEMS Microbiol Rev.* (1997) 20:503–16. doi: 10.1111/j.1574-6976.1997.tb00333.x
11. Wang T, Lou X, Zhang G, Dang Y. Improvement of selenium enrichment in *Rhodotorula glutinis* X-20 through combining process optimization and selenium transport. *Bioengineered.* (2019) 10:335–44. doi: 10.1080/21655979.2019.1644853
12. Saenge C, Cheirsilp B, Suksaroge TT, Bourtoom T. Efficient concomitant production of lipids and carotenoids by oleaginous red yeast *Rhodotorula glutinis* cultured in palm oil mill effluent and application of lipids for biodiesel production. *Biotechnol Bioprocess Eng.* (2011) 16:23–33.
13. Escobar-Zepeda A, Vera-Ponce de León A, Sanchez-Flores A. The road to metagenomics: from microbiology to DNA sequencing technologies and bioinformatics. *Front Genet.* (2015) 6:348. doi: 10.3389/fgene.2015.00348
14. Paul D, Magbanua Z, Arick M, French T, Bridges SM, Burgess SC, et al. Genome sequence of the oleaginous yeast *Rhodotorula glutinis* ATCC 204091. *Genome Announc.* (2014) 2:e46–14. doi: 10.1128/genomeA.00046-14
15. Firrincieli A, Otillar R, Salamov A, Schmutz J, Khan Z, Redman RS, et al. Genome sequence of the plant growth promoting endophytic yeast *Rhodotorula* graminis WP1. *Front Microbiol.* (2015) 6:978. doi: 10.3389/fmicb.2015.00978
16. Coradetti ST, Pinel D, Geiselman GM, Ito M, Mondo SJ, Reilly MC, et al. Functional genomics of lipid metabolism in the oleaginous yeast *Rhodosporidium toruloides*. *eLife.* (2018) 7:e32110. doi: 10.7554/eLife.32110
17. Coleine C, Masonjones S, Onofri S, Selbmann L, Stajich JE. Draft genome sequence of the Yeast *Rhodotorula* sp. strain CCFEE 5036, isolated from McMurdo Dry Valleys, Antarctica. *Microbiol Resour Announce.* (2020) 9:e00020–20. doi: 10.1128/MRA.00020-20
18. Wang Z, Zhang Y, Jiang L, Qiu J, Gao Y, Gu T, et al. Responses of *Rhodotorula mucilaginosa* under Pb(II) stress: carotenoid production and budding. *Environ Microbiol.* (2022) 24:678–88. doi: 10.1111/1462-2920.15603
19. Ma Y, Yuan L, Wu B, Li X, Chen S, Lu S. Genome-wide identification and characterization of novel genes involved in terpenoid biosynthesis in *Salvia miltiorrhiza*. *J Exp Bot.* (2012) 63:2809–23. doi: 10.1093/jxb/err466
20. Blazic M, Balaz AM, Tadic V, Draganic B, Ostafe R, Fischer R, et al. Protein engineering of cellobiose dehydrogenase from *Phanerochaete Chrysosporium* in yeast *Saccharomyces cerevisiae* InvSc1 for increased activity and stability. *Biochem Eng J.* (2019) 146:179–85.
21. Paramasivan K, Rajagopal K, Mutturi S. Studies on Squalene biosynthesis and the standardization of its extraction methodology from *Saccharomyces cerevisiae*. *Appl Biochem Biotechnol.* (2019) 187:691–707.
22. Li X, Wang Z, Zhang G, Yi L. Improving lycopene production in *Saccharomyces cerevisiae* through optimizing pathway and chassis metabolism. *Chem Eng Sci.* (2019) 193:364–9.
23. Lim HJ, Lee EH, Yoon Y, Chua B, Son A. Portable lysis apparatus for rapid single-step DNA extraction of *Bacillus subtilis*. *J Appl Microbiol.* (2016) 120:379–87. doi: 10.1111/jam.13011
24. Saha S, Bridges S, Magbanua ZV, Peterson DG. Empirical comparison of ab initio repeat finding programs. *Nucleic Acids Res.* (2008) 36:2284–94. doi: 10.1093/nar/gkn064
25. Kim D, Langmead B, Salzberg SL. HISAT: a fast spliced aligner with low memory requirements. *Nat Methods.* (2015) 12:357–60. doi: 10.1038/nmeth.3317
26. Pertea M, Pertea GM, Antonescu CM, Chang T-C, Mendell JT, Salzberg SL. StringTie enables improved reconstruction of a transcriptome from RNA-seq reads. *Nat Biotechnol.* (2015) 33:290–5. doi: 10.1038/nbt.3122
27. Lagesen K, Hallin P, Rødland EA, Stærfeldt H-H, Rognes T, Ussery DW. RNAmmer: consistent and rapid annotation of ribosomal RNA genes. *Nucleic Acids Res.* (2007) 35:3100–8. doi: 10.1093/nar/gkm160
28. Lowe TM, Eddy SR. tRNAscan-SE: a program for improved detection of transfer RNA genes in genomic sequence. *Nucleic Acids Res.* (1997) 25:955–64. doi: 10.1093/nar/25.5.955
29. Nawrocki EP, Kolbe DL, Eddy SR. Infernal 1.0: inference of RNA alignments. *Bioinformatics.* (2009) 25:1335–7. doi: 10.1093/bioinformatics/btp157
30. Thrash A, Arick M, Peterson DG. Quack: a quality assurance tool for high throughput sequence data. *Anal Biochem.* (2018) 548:38–43. doi: 10.1016/j.ab.2018.01.028
31. Liao Y, Smyth GK, Shi W. featureCounts: an efficient general purpose program for assigning sequence reads to genomic features. *Bioinformatics.* (2014) 30:923–30. doi: 10.1093/bioinformatics/btt656
32. Mortazavi A, Williams BA, McCue K, Schaeffer L, Wold B. Mapping and quantifying mammalian transcriptomes by RNA-Seq. *Nat Methods.* (2008) 5:621–8. doi: 10.1038/nmeth.1226
33. Kumar S, Stecher G, Tamura K. MEGA7: molecular evolutionary genetics analysis Version 7.0 for bigger datasets. *Mol Biol Evol.* (2016) 33:1870–4. doi: 10.1093/molbev/msw054
34. Wang Y, Tang H, Debarry JD, Tan X, Li J, Wang X, et al. MCScanX: a toolkit for detection and evolutionary analysis of gene synteny and collinearity. *Nucleic Acids Res.* (2012) 40:e49–49. doi: 10.1093/nar/gkr1293
35. Shao Z, Zhao H, Zhao H. DNA assembler, an *in vivo* genetic method for rapid construction of biochemical pathways. *Nucleic Acids Res.* (2008) 37:e16–16. doi: 10.1093/nar/gkn991
36. Monnerat G, Seara FAC, Evaristo JAM, Carneiro G, Evaristo GPC, Domont G, et al. Aging-related compensated hypogonadism: role of metabolomic analysis in physiopathological and therapeutic evaluation. *J Steroid Biochem Mol Biol.* (2018) 183:39–50. doi: 10.1016/j.jsbmb.2018.05.005
37. Li C, Li B, Zhang N, Wang Q, Wang W, Zou H. Comparative transcriptome analysis revealed the improved β-carotene production in *Sporidiobolus* pararoseus yellow mutant MuY9. *J Gen Appl Microbiol.* (2019) 65:121–8.
38. Sims D, Sudbery I, Ilott NE, Heger A, Ponting CP. Sequencing depth and coverage: key considerations in genomic analyses. *Nat Rev Genet.* (2014) 15:121–32. doi: 10.1038/nrg3642
39. Krzywinski M, Schein J, Birol I, Connors J, Gascoyne R, Horsman D, et al. Circos: an information aesthetic for comparative genomics. *Genome Res.* (2009) 19:1639–45. doi: 10.1101/gr.092759.109
40. Benson G. Tandem repeats finder: a program to analyze DNA sequences. *Nucleic Acids Res.* (1999) 27:573–80. doi: 10.1093/nar/27.2.573
41. Waterhouse RM, Seppey M, Simão FA, Manni M, Ioannidis P, Klioutchnikov G, et al. BUSCO applications from quality assessments to gene prediction and Phylogenomics. *Mol Biol Evol.* (2018) 35:543–8. doi: 10.1093/molbev/msx319
42. Ji X, Cheng Y, Tian J, Zhang S, Jing Y, Shi M. Structural characterization of polysaccharide from jujube (*Ziziphus jujuba* Mill.) fruit. *Chem Biol Technol Agric.* (2021) 8:54.
43. Westfall PJ, Pitera DJ, Lenihan JR, Eng D, Woolard FX, Regentin R, et al. Production of amorphadiene in yeast, and its conversion to

dihydroartemisinic acid, precursor to the antimalarial agent artemisinin. *Proc Natl Acad Sci USA*. (2012) 109:E111–8. doi: 10.1073/pnas.1110740109
44. Xie W, Liu M, Lv X, Lu W, Gu J, Yu H. Construction of a controllable β-carotene biosynthetic pathway by decentralized assembly strategy in *Saccharomyces cerevisiae*. *Biotechnol Bioeng.* (2014) 111:125–33. doi: 10.1002/bit.25002
45. Hausmann A, Sandmann G. A Single Five-Step Desaturase Is Involved in the Carotenoid Biosynthesis Pathway to β-Carotene and Torulene in Neurospora crassa. *Fungal Genet Biol.* (2000) 30:147–53. doi: 10.1006/fgbi.2000.1212
46. Yen H-W, Palanisamy G, Su G-C. The influences of supplemental vegetable oils on the growth and β-carotene accumulation of oleaginous Yeast-*Rhodotorula glutinis*. *Biotechnol Bioprocess Eng.* (2019) 24:522–8.
47. Kot AM, Blazejak S, Kurcz A, Gientka I, Kieliszek M. *Rhodotorula glutinis*-potential source of lipids, carotenoids, and enzymes for use in industries. *Appl Microbiol Biotechnol.* (2016) 100:6103–17. doi: 10.1007/s00253-016-7611-8
48. Liang MH, Jiang JG. Advancing oleaginous microorganisms to produce lipid *via* metabolic engineering technology. *Prog Lipid Res.* (2013) 52:395–408. doi: 10.1016/j.plipres.2013.05.002
49. Ghazani SM, Marangoni AG. Microbial lipids for foods. *Trends Food Sci Technol.* (2022) 119:593–607.
50. Kawatra A, Dhankhar R, Mohanty A, Gulati P. Biomedical applications of microbial phenylalanine ammonia lyase: current status and future prospects. *Biochimie.* (2020) 177:142–52. doi: 10.1016/j.biochi.2020.08.009
51. Maharana AK, Singh SM. A cold and organic solvent tolerant lipase produced by Antarctic strain *Rhodotorula* sp. Y-23. *J Basic Microbiol.* (2018) 58:331–42. doi: 10.1002/jobm.201700638
52. Procentese A, Raganati F, Olivieri G, Russo ME, de la Feld M, Marzocchella A. Renewable feedstocks for biobutanol production by fermentation. *New Biotechnol.* (2017) 39:135–40. doi: 10.1016/j.nbt.2016.10.010
53. Braunwald T, Schwemmlein L, Graeff-Honninger S, French WT, Hernandez R, Holmes WE, et al. Effect of different C/N ratios on carotenoid and lipid production by *Rhodotorula glutinis*. *Appl Microbiol Biotechnol.* (2013) 97:6581–8. doi: 10.1007/s00253-013-5005-8
54. Hessel S, Eichinger A, Isken A, Amengual J, Hunzelmann S, Hoeller U, et al. CMO1 deficiency abolishes Vitamin A production from β-carotene and alters lipid metabolism in mice. *J Biol Chem.* (2007) 282:33553–61. doi: 10.1074/jbc.M706763200
55. Husseiny SM, Abdelhafez AA, Ali AA-A, Sand HM. Optimization of β-carotene production from *Rhodotorula glutinis* ATCC 4054 growing on agro-industrial substrate using plackett–burman design. *Proc Natl Acad Sci India Sect B Biol Sci.* (2017) 88:1637–46.
56. Timson DJ. The roles and applications of chaotropes and kosmotropes in industrial fermentation processes. *World J Microbiol Biotechnol.* (2020) 36:89. doi: 10.1007/s11274-020-02865-8
57. Yuan J, Ching CB. Combinatorial assembly of large biochemical pathways into yeast chromosomes for improved production of value-added compounds. *ACS Synth Biol.* (2015) 4:23–31. doi: 10.1021/sb500079f
58. Li C, Zhang N, Song J, Wei N, Li B, Zou H, et al. A single desaturase gene from red yeast *Sporidiobolus* pararoseus is responsible for both four- and five-step dehydrogenation of phytoene. *Gene.* (2016) 590:169–76. doi: 10.1016/j.gene.2016.06.042
59. Li Q, Sun Z, Li J, Zhang Y. Enhancing beta-carotene production in *Saccharomyces cerevisiae* by metabolic engineering. *FEMS Microbiol Lett.* (2013) 345:94–101.
60. Shi F, Zhan W, Li Y, Wang X. Temperature influences β-carotene production in recombinant *Saccharomyces cerevisiae* expressing carotenogenic genes from Phaffia rhodozyma. *World J Microbiol Biotechnol.* (2014) 30:125–33. doi: 10.1007/s11274-013-1428-8
61. Rathod JP, Vira C, Lali AM, Prakash G. Metabolic engineering of *Chlamydomonas reinhardtii* for enhanced β-Carotene and lutein production. *Appl Biochem Biotechnol.* (2020) 190:1457–69.
62. Song T-Q, Ding M-Z, Zhai F, Liu D, Liu H, Xiao W-H, et al. Engineering *Saccharomyces cerevisiae* for geranylgeraniol overproduction by combinatorial design. *Sci Rep*. (2017) 7:14991. doi: 10.1038/s41598-017-15005-4

Conflict of Interest: The authors declare that the research was conducted in the absence of any commercial or financial relationships that could be construed as a potential conflict of interest.

Publisher's Note: All claims expressed in this article are solely those of the authors and do not necessarily represent those of their affiliated organizations, or those of the publisher, the editors and the reviewers. Any product that may be evaluated in this article, or claim that may be made by its manufacturer, is not guaranteed or endorsed by the publisher.

frontiers | Frontiers in Nutrition

ORIGINAL RESEARCH
published: 11 July 2022
doi: 10.3389/fnut.2022.933193

From Function to Metabolome: Metabolomic Analysis Reveals the Effect of Probiotic Fermentation on the Chemical Compositions and Biological Activities of *Perilla frutescens* Leaves

Zhenxing Wang[1,2,3], Ximeng Jin[2], Xuechun Zhang[2], Xing Xie[3], Zongcai Tu[3] and Xiahong He[1,4]**

[1] Key Laboratory for Forest Resources Conservation and Utilization in the Southwest Mountains of China, Ministry of Education, Southwest Forestry University, Kunming, China, [2] College of Life Sciences, Southwest Forestry University, Kunming, China, [3] National R&D Center for Freshwater Fish Processing, College of Health, Jiangxi Normal University, Nanchang, China, [4] College of Horticulture and Landscape, Southwest Forestry University, Kunming, China

OPEN ACCESS

Edited by:
Yu Xiao,
Hunan Agricultural University, China

Reviewed by:
Gong Chen,
Wuhan Institute of Technology, China
Qiang Yu,
Nanchang University, China

***Correspondence:**
Zongcai Tu
tuzc_mail@aliyun.com
Xiahong He
hexiahong@hotmail.com

Specialty section:
This article was submitted to Food Chemistry, a section of the journal Frontiers in Nutrition

Received: *30 April 2022*
Accepted: *20 June 2022*
Published: *11 July 2022*

Citation:
Wang Z, Jin X, Zhang X, Xie X, Tu Z and He X (2022) From Function to Metabolome: Metabolomic Analysis Reveals the Effect of Probiotic Fermentation on the Chemical Compositions and Biological Activities of Perilla frutescens Leaves. Front. Nutr. 9:933193. doi: 10.3389/fnut.2022.933193

This study aimed to investigate the impact of probiotic fermentation on the active components and functions of *Perilla frutescens* leaves (PFL). PFL was fermented for 7 days using six probiotics (*Lactobacillus Plantarum* SWFU D16, *Lactobacillus Plantarum* ATCC 8014, *Lactobacillus Rhamnosus* ATCC 53013, *Streptococcus Thermophilus* CICC 6038, *Lactobacillus Casei* ATCC 334, and *Lactobacillus Bulgaricus* CICC 6045). The total phenol and flavonoid contents, antioxidant abilities, as well as α-glucosidase and acetylcholinesterase inhibition abilities of PFL during the fermentation process were evaluated, and its bioactive compounds were further quantified by high-performance liquid chromatography (HPLC). Finally, non-targeted ultra-HPLC–tandem mass spectroscopy was used to identify the metabolites affected by fermentation and explore the possible mechanisms of the action of fermentation. The results showed that most of the active component contents and functional activities of PFL exhibited that it first increased and then decreased, and different probiotics had clearly distinguishable effects from each other, of which fermentation with ATCC 53013 for 1 day showed the highest enhancement effect. The same trend was also confirmed by the result of the changes in the contents of 12 phenolic acids and flavonoids by HPLC analysis. Further metabolomic analysis revealed significant metabolite changes under the best fermentation condition, which involved primarily the generation of fatty acids and their conjugates, flavonoids. A total of 574 and 387 metabolites were identified in positive ion and negative ion modes, respectively. Results of Spearman's analysis indicated that some primary metabolites and secondary metabolites such as flavonoids, phenols, and fatty acids might play an important role in the functional activity of PFL. Differential metabolites were subjected to the KEGG database and 97 metabolites pathways were obtained, of which biosyntheses of unsaturated fatty acids, flavonoid, and isoflavonoid

were the most enriched pathways. The above results revealed the potential reason for the differences in metabolic and functional levels of PFL after fermentation. This study could provide a scientific basis for the further study of PFL, as well as novel insights into the action mechanism of probiotic fermentation on the chemical composition and biological activity of food/drug.

Keywords: *Perilla frutescens* leaves, fermentation, phytochemical composition, biological activity, metabolomics

INTRODUCTION

Fermentation is one of the classic methods of food processing. Under the effects of microorganisms, food components are transformed and degraded, resulting in a variety of secondary metabolites, which in turn have positive impacts on food quality, such as flavor, taste, nutritional value, functional properties, and shelf-life (1).

Due to the complexity of the food system, these quality characteristic changes in food and its underlying mechanisms during fermentation have been an important research focus. In recent years, metabolomics, including liquid chromatography-tandem mass spectrometry (LC-MS/MS), gas chromatography-tandem mass spectrometry (GC-MS/MS), and nuclear magnetic resonance (NMR), has been widely used in investigating the chemical composition and metabolite contents of food products (2). They provide fast and sensitive methods for the identification and quantification of the small molecules produced in food processing, which could be used to well explain the changes in product, flavor, and nutrition during the fermentation process (3, 4). However, in-depth studies on metabolite changes in fermented food and their association with functional activities are still lacking.

Perilla frutescens (L.) Britt. is a traditional food and medicinal plant and is widely cultivated and distributed in many East Asian countries (5). As its primary edible relevant part, the *perilla frutescens* leaf (PFL) is widely used for fresh vegetables, condiments, and kimchi. In addition, its medicinal properties have been proven in traditional medicine for centuries, such as diuresis, antitussive, detoxification, diaphoretic, etc. (6, 7). Modern pharmacological research has revealed that PFL exerts diverse effects on chronic diseases related to oxidative stress, such as diabetes, cancer, inflammatory, hypertension, Alzheimer's disease, etc. (8–11). Literature and our previous work (12, 13) indicated that PFL possessed excellent biological activities including antioxidant, anticancer, antibacterial, and anti-inflammatory activity, which was associated with their abundant active ingredients (e.g., phenolics and flavonoids) (14, 15). PFL has been considered to be an excellent raw material for fermented foods. Research shows that the nutritional value and biomedical benefits of *Perilla frutescens* seeds are enhanced by fermentation, although there are only a few studies on PFL fermentation, and the dynamic changes of its active components and functional activities in the fermentation process are not clear (16).

In this study, we employed six different probiotics to ferment PFL. The differences and variations in the chemical composition and functional activities of the fermented *perilla frutescens* leaf (FPFL) were evaluated by spectrophotometry and high-performance liquid chromatography (HPLC) methods, thus selecting the best performing strain and elucidating the dynamic changes of the ingredients and activities during the fermentation process. Then we characterized the metabolic transition before and after fermentation using mass spectrometry-based metabolomics. By combining mass-spectrometry metabolomics with the above *in vitro* study, the main compounds related to the functional activities of PFL were obtained. Finally, KEGG pathway enrichment analysis of the differential metabolites was performed to investigate the possible action mechanism of probiotic fermentation on PFL. We expect that our results could provide a novel insight into the biotransformation of the active components in natural products/foods and the scientific basis for the further development and utilization of *Perilla frutescens*.

MATERIALS AND METHODS

Chemicals and Reagents

Lactobacillus Plantarum SWFU D16 was isolated from Yunnan goat milk cake, a Chinese traditional fermented food in our Laboratory. *Lactobacillus Plantarum* ATCC 8014, *Lactobacillus Bulgaricus* CICC 6045, *Lactobacillus Casei* ATCC 334, and *Streptococcus Thermophilus* CICC 6038 were purchased from the Guangdong Microbial Culture Collection Center (GDMCC), and *Lactobacillus Rhamnosus* ATCC 53013 was purchased from the American Type Culture Collection (ATCC).

Folin–Ciocalteu reagent, gallic acid, rutin, 2,2-diphenyl-1-picrylhydrazyl radical (DPPH), 2,2'-azinobis (3-ethylbenzothiazoline-6-sulfonic acid) diammonium salt (ABTS), 2,4,6-tri (2-pyridyl)-1,3,5-triazine (TPTZ), iron chloride ($FeCl_3 6H_2O$), p-Nitrophenol α-D-glycopyranoside (pNPG), acetylthiocholine iodide (ATCI), 5,5'-Dithiobis-(2-nitrobenzoic acid) (DTNB), and other chemicals were purchased from Aladdin (Shanghai, China). Chromatographic acetonitrile was purchased from Merck (Darmstadt, Germany). α-Glucosidase (G5003), and acetylcholinesterase (AChE, C3389) were purchased from Sigma-Aldrich (St. Louis, United States). Syringic acid, (+)-catechin, rosmarinic acid, chlorogenic acid, and other standards were purchased from Yuanye Bio-Technology (Shanghai, China).

Material Preparation and Fermentation

Mature PFL were purchased from Meizhou city, Guangdong province, China. After drying at 50 °C (Thermostatic blast drying, DHG Series, Shanghai, China), samples were pulverized and sifted through a 40-mesh sieve, then mixed with distilled water in a 1:25 ratio (mass/volume) in a conical flask, and

autoclaved at 121°C for 15 min. When cooled to room temperature, 10 mL of probiotics (1.5×10^7 CFU) were added and incubated at 37°C for 7 days. For consistency, each probiotic was from the same culture bottle. In parallel, 2 g glucose and 2 g skimmed milk powder were added as the carbon and nitrogen source (CN) controls, respectively. During the fermentation, fermented *Perilla frutescens* leaves (FPFL) were sampled daily and frozen at -18°C pending determination.

pH Values

The pH was measured by directly placing a pH electrode of the pH meter (Hanna Instrument, Ann Arbor, Michigan, United States) into samples at room temperature.

Total Phenolic and Flavonoid Content

Total phenolic content (TPC) was quantified by the Folin–Ciocalteau method with some modifications (17). Briefly, 40 μL of properly diluted sample was mixed with 20 μL of Folin–Ciocalteau reagent (0.5 M) in a 96-well microplate and incubated for 5 min. Next, 160 μL of Na_2CO_3 (7.5%, w/v) was added to the mixtures. The reaction was then kept in the dark for 30 min at room temperature, after which the absorbance was measured at 765 nm. As for the standard, gallic acid was used, and the data were provided as milligram gallic acid equivalent (mg GAE/g sample). For easier comparison, the final TPC results were expressed as the relative content (%) compared with the equivalent value of FPFL at the 0 days, and the starting TPC was 100%.

Total flavonoid content (TFC) was measured by the aluminum nitrate colorimetric method (18). A total of 20 μL of $NaNO_2$ (3%, w/v) was mixed with 40 μl of a properly diluted sample. After 6 min of reaction, 20 μL of Al $(NO_3)_3$ (6%, w/v) was added after 6 min of incubation, and the mixture was incubated for another 6 min. Subsequently, 140 μL of NaOH (4%, w/v) and 60 μL of 70% methanol were added. The mixture solution stood for 15 min and the absorbance was measured at 510 nm. Rutin was used as a standard, and the data were calculated as milligram rutin equivalent per gram of sample (g RE/g sample). Similarly, the TFC was also expressed as a relative content (%).

Antioxidant Assays

The abilities to scavenge DPPH and ABTS radicals were estimated by following the methods of Dong (19) and Wang (12) with slight modifications. Briefly, samples (100 μL) and 100 μL of DPPH (0.15 mM) were added to the 96-well microplate. The mixture was shaken thoroughly and then kept for 30 min in the dark at room temperature. Subsequently, the absorbance was measured at 517 nm. In the ABTS assay, 50 μL of samples were added to 200 μL of $ABTS^{\cdot+}$ freshly prepared working solution in a 96-well microplate and incubated for 6 min in the dark, and then the absorbance was measured at 734 nm. The sodium phosphate buffer (pH 6.9) was used instead of the DPPH or $ABTS^{\cdot+}$ solution as the control, and sodium phosphate buffer instead of the sample was used as the blank. The percentage of scavenging was calculated following Formula (1). The radical scavenging abilities of DPPH and ABTS were expressed as a relative percentage (%) compared with the scavenging rate of FPFL on the 0th day.

$$Scavenging\ rate\ (\%) = \left(1 - \frac{A_{sample} - A_{control}}{A_{blank}}\right) \times 100 \quad (1)$$

The ferric reducing antioxidant power (FRAP) was quantified by the reported method (20). The FRAP solution was prepared with 1 ml of TPTZ (7 mM), 1 mL of $FeCl_3$ (20 mM), and 10 mL of acetate buffer (pH 3.6). Properly diluted samples (50 μL) were mixed with 200 μL of freshly prepared FRAP working solution in a 96-well microplate. After incubation in darkness for 10 min at 37°C, the absorbance was measured at 593 nm. The sodium phosphate buffer (pH 6.9) was used instead of the FRAP solution as the control, $FeSO_4$ was used as the standard, and the data were calculated as milligram of $FeSO_4$ equivalent per gram of sample (g $FeSO_4$/g sample). FRAP was expressed as the relative percentage (%) compared with the equivalent value of FPFL at the 0 days.

α-Glucosidase Inhibition Ability

The α-glucosidase inhibition ability was determined according to the previous method (21). Briefly, 50 μL of the samples were added to 50 μL of 0.1 U/mL α-glucosidase solutions and mixed in a 96-well plate. After incubation at 37°C for 10 min, a 50 μL of 5 mM pNPG solution was added and reacted for 15 min at 37°C. Finally, 100 μL of Na_2CO_3 (0.2 M) was added to terminate the reaction and the absorbance was determined at 405 nm. The sodium phosphate buffer (pH 6.9) was used instead of the α-glucosidase solution as control, and sodium phosphate buffer instead of the sample was used as the blank. The percentage of inhibition was calculated following Formula (1). The results were expressed as the relative percentage (%) compared with the inhibition rate of FPFL on the 0th day.

Acetylcholinesterase Inhibition Ability

The acetylcholinesterase (AChE) inhibition ability was assessed using a colorimetric method (22). Initially, 50 μL of samples, 15 μL of ATCI (15 mM), and 75 μL of DTNB (3 μM) were mixed in a 96-well plate and incubated for 10 min at 30°C. Then 20 μL of 0.1 U/mL AChE and 50 μL of sodium phosphate buffer (pH 8.0) were added and shaken for 10 s. Followed by exposure to blocking light for 30 min at room temperature, the absorbance was measured at 410 nm by using a microplate reader. The sodium phosphate buffer (pH 6.9) was used instead of the AChE solution as the control, and sodium phosphate buffer instead of the sample was used as the blank. The percentage of inhibition was calculated following Formula (1). The results were expressed as the relative percentage (%) compared with the inhibition rate of FPFL on the 0th day.

High-Performance Liquid Chromatography-DAD Analysis

HPLC-DAD analysis was performed by an HPLC 1260 (Agilent Technologies, CA, United States) equipped with a degasser, quaternary pump solvent delivery, thermo-stated column compartment, and a diode array detector. Samples were

filtered through 0.22-μm nylon syringe filters for HPLC analysis. The C18 reversed-phase analytical column (250 mm × 4.6 mm, 5 μm, Greenherbs Science and Technology, Beijing, China) was maintained at 25°C, with 0.1% formic acid (A) and acetonitrile (B) as the mobile phase with a flow rate of 0.8 mL/min. The gradient elution conditions of the mobile phase B were: 0–12 min, 2–8%; 12–15 min, 8–13%; 15–30 min, 13–18%; 30–50 min, 18–30%; 50–60 min, 30–50%; 60–70 min, 50–70%; 70–80 min, 70–90%; 80–85 min, 90–100%; 85–90 min, 100–2%. The DAD was set in four wavelengths: 280 nm for identification of gallic acid, (+)-catechin, epicatechin, rosmarinic acid, baicalin, luteolin, apigenin, hesperetin, and baicalein; 310 nm for chlorogenic acid; 340 nm for ferulic acid; and 360 nm for rutin. Finally, compounds were identified and quantified by comparison with the retention times and peak areas from standards, and information on these compounds is listed in **Table 1**.

Metabolomics Analysis

The metabolomics analysis was performed by Shanghai Applied Protein Technology Co. Ltd. An appropriate sample was added to precooled methanol/acetonitrile/aqueous solution (2:2:1, V/V) and vortex-mixed. After the ultrasound for 30 min at 4°C, the mixed sample was kept at -20°C for 10 min and then centrifuged (14,000 g, 4°C) for 20 min. The supernatant was vacuum-dried and redissolved in 100 μL acetonitrile solution (acetonitrile: water = 1:1, V/V), and then centrifuged again at 14,000 g for 15 min at 4 °C. Finally, the supernatant was eventually used for mass spectrometry (MS) analysis.

The samples were separated by an ultra-high performance liquid chromatography (UHPLC) system (Agilent, Santa Clara, United States) with a C18 column (1.7 μm, 2.1 mm × 100 mm). The sample was injected using an autosampler and the injection volume was 2 μL. The flow rate was 0.40 mL/min and the column temperature was 40°C. The mobile phase comprised of eluent A (water with 25 mM ammonium acetate and 0.5% formic acid) and eluent B (methanol). The gradient elution program was set as follows: 0–0.5 min, 5% B; 0.5–10 min, 5–100% B; 10–12 min, 100% B; 12.0–12.1 min, 100–5% B; and a final 12.1–16 min, 5% B.

TABLE 1 | List of compounds identified by HPLC.

Number	Retention time (min)	Name	Detection wavelength (nm)
1	9.99	Gallic acid	280
2	16.78	(+)-Catechin	280
3	22.4	Chlorogenic acid	310
4	23.46	Epicatechin	280
5	26.936	Rutin	360
6	29.743	Ferulic acid	340
7	39.83	Rosmarinic acid	280
8	43.86	Baicalin	280
9	46.442	Luteolin	280
10	56.102	Apigenin	280
11	56.87	Hesperetin	280
12	62.4	Baicalein	280

MS/MS was conducted in both positive and negative ion modes using electrospray ionization (ESI) on AB Triple TOF 6600 (AB Sciex, United States). The ESI source condition was set as follows: Ion Source Gas1 (60 psi), Ion Source Gas2 (60 psi), Curtain gas (30 psi), Source temperature (600°C), Ion Sapary Voltage Floating (± 5,500 V), TOF MS scan m/z range (60–1,000 Da), Declustering potential (± 60 V), and Collision energy (35 ± 15 eV). The information-dependent acquisition (IDA) conditions were: exclude isotopes within 4 Da, and candidate ions to monitor per cycle was 10. All samples were injected in sequence. The quality control (QC) samples were pooled samples prepared from mixed aliquots of equal volume from all samples to validate system stability and repeatability.

Statistical Analyses

All experiments were done in triplicate and expressed as mean ± standard deviation. The SPSS 22 software package was used to perform a one-way ANOVA for the determination of statistical significance. Principal component analysis (PCA), Spearmen correlation, volcano plots, heatmap, and associated network diagram were generated with R software (version 4.0.6). Significantly regulated metabolites between groups were determined by $Log_2FC \geq 1.5$, $p < 0.05$.

RESULTS

pH Values

The variation in pH values of the fermentation broth reflects the degree of fermentation (23). **Table 2** indicated that the pH values presented a dramatic decrease in the early stage, after which the trend became flat. There was a significant difference after a 1-day fermentation for each group when compared to the unfermented sample ($p < 0.05$). Among them, ATCC 53013 and CICC 6038 decreased faster than other probiotics from the third day ($p < 0.05$), which implied they exhibited the strongest fermentation properties. Overall, the CN control groups also showed similar trends to the experimental groups, but finally decreased to a greater extent. This indicated that the addition of CN sources might also contribute to increasing the extent of fermentation.

Total Phenolic and Flavonoid Content

From **Table 2**, the TPC and TFC of FPFL behaved in a general trend of increasing first and then decreasing for almost all probiotics besides SWFU-D16, while the turning points were pooled from days 1–3. Overall, we observed substantial decreases in TPC and TFC after fermentation ($p < 0.05$). Similarly, each of the corresponding CN control groups displayed a significantly higher reduction than that of the probiotic group ($p < 0.05$). Although final losses were significant for TPC and TFC, a significant improvement was observed in short-term fermentation (1–3 days), which was consistent with the previously reported literature (24, 25). Among them, the maximum TPC increase was observed in CICC 6038 (146.27% at 1 day), while the largest TFC increase was found for ATCC 53013 (152.38% at 2 days). A possible reason for the increase of

TABLE 2 | Change in the pH, TPC, and TFC of FEPL during different fermentation stages for different probiotics.

	Probiotics	Days							
		0	1	2	3	4	5	6	7
pH	SWFU D16	5.43 ± 0.01^{a}	4.31 ± 0.01^{b}	4.22 ± 0.01^{b}	4.32 ± 0.23^{b}	4.17 ± 0.01^{b}	4.24 ± 0.03^{b}	4.22 ± 0.03^{b}	4.22 ± 0.02^{b}
	SWFU D16 + CN	5.63 ± 0.02^{a}	3.90 ± 0.01^{b}	3.68 ± 0.01^{c}	3.55 ± 0.01^{d}	3.50 ± 0.02^{e}	3.44 ± 0.01^{f}	3.40 ± 0.02^{g}	3.41 ± 0.03^{g}
	ATCC 8014	5.92 ± 0.02^{a}	5.44 ± 0.02^{b}	4.67 ± 0.01^{c}	4.31 ± 0.01^{d}	4.15 ± 0.03^{e}	3.93 ± 0.03^{f}	3.81 ± 0.01^{g}	3.77 ± 0.02^{h}
	ATCC 8014 + CN	5.77 ± 0.12^{a}	5.48 ± 0.03^{b}	4.80 ± 0.27^{c}	4.52 ± 0.08^{d}	4.45 ± 0.01^{e}	4.43 ± 0.02^{e}	4.45 ± 0.02^{e}	4.46 ± 0.02^{e}
	ATCC 53013	5.49 ± 0.03^{b}	5.53 ± 0.01^{a}	5.44 ± 0.01^{c}	$4.48 \pm 0.01^{d,e}$	4.45 ± 0.01^{f}	$4.45 \pm 0.03^{e,f}$	$4.46 \pm 0.01^{e,f}$	4.50 ± 0.01^{d}
	ATCC 53013 + CN	5.71 ± 0.02^{a}	5.70 ± 0.01^{a}	5.40 ± 0.01^{b}	3.76 ± 0.02^{c}	3.59 ± 0.01^{d}	3.45 ± 0.02^{e}	3.40 ± 0.01^{f}	3.33 ± 0.01^{g}
	CICC 6038	5.70 ± 0.03^{a}	5.58 ± 0.02^{b}	5.50 ± 0.02^{c}	5.62 ± 0.01^{b}	4.48 ± 0.07^{e}	4.55 ± 0.02^{d}	4.55 ± 0.01^{d}	4.56 ± 0.01^{d}
	CICC 6038 + CN	5.71 ± 0.03^{a}	5.65 ± 0.03^{a}	5.71 ± 0.01^{a}	5.29 ± 0.01^{b}	3.83 ± 0.02^{c}	3.49 ± 0.13^{d}	3.48 ± 0.02^{d}	3.49 ± 0.01^{d}
	ATCC 334	5.67 ± 0.02^{c}	5.73 ± 0.01^{b}	5.75 ± 0.01^{a}	5.37 ± 0.01^{d}	4.74 ± 0.01^{e}	4.66 ± 0.01^{g}	4.69 ± 0.01^{f}	4.67 ± 0.01^{g}
	ATCC 334 + CN	5.68 ± 0.04^{a}	5.80 ± 0.02^{b}	4.47 ± 0.02^{c}	3.78 ± 0.01^{d}	3.60 ± 0.02^{e}	3.53 ± 0.01^{f}	3.43 ± 0.04^{g}	3.42 ± 0.02^{g}
	CICC 6045	5.69 ± 0.02^{d}	5.65 ± 0.01^{e}	$5.71 \pm 0.03^{c,d}$	5.77 ± 0.02^{a}	$5.73 \pm 0.01^{b,c}$	$5.72 \pm 0.03^{c,d}$	$5.73 \pm 0.00^{b,c}$	$5.76 \pm 0.01^{a,b}$
	CICC 6045 + CN	5.62 ± 0.01^{c}	5.70 ± 0.01^{b}	5.73 ± 0.01^{a}	3.95 ± 0.01^{d}	3.80 ± 0.02^{e}	3.50 ± 0.01^{f}	3.42 ± 0.01^{g}	3.37 ± 0.01^{h}
TPC (%)	SWFU D16	100.00 ± 1.11^{a}	94.12 ± 3.53^{b}	87.77 ± 1.39^{c}	$91.68 \pm 3.40^{b,c}$	66.63 ± 2.45^{e}	69.04 ± 3.12^{e}	76.90 ± 1.73^{d}	53.10 ± 1.38^{f}
	SWFU D16 + CN	100.22 ± 2.22^{a}	95.72 ± 1.85^{a}	80.87 ± 1.44^{b}	66.56 ± 3.83^{c}	65.49 ± 3.56^{c}	58.25 ± 3.12^{d}	44.54 ± 1.73^{e}	39.56 ± 1.72^{e}
	ATCC 8014	$100.00 \pm 0.49^{b,c}$	78.60 ± 2.64^{d}	85.24 ± 5.05^{d}	113.07 ± 5.19^{a}	$100.16 \pm 3.46^{b,c}$	96.71 ± 6.03^{c}	$107.23 \pm 7.25^{a,b}$	57.63 ± 1.25^{e}
	ATCC 8014 + CN	$100.00 \pm 5.45^{b,c}$	110.34 ± 1.96^{a}	84.58 ± 2.87^{d}	89.35 ± 4.86^{d}	$101.78 \pm 8.59^{a,b}$	51.00 ± 1.19^{e}	$92.45 \pm 0.83^{c,d}$	86.07 ± 2.67^{d}
	ATCC 53013	$100.00 \pm 1.61^{a,b}$	$95.64 \pm 5.50^{a,b}$	105.44 ± 9.35^{a}	$99.90 \pm 3.87^{a,b}$	$85.07 \pm 5.85^{c,d}$	$82.84 \pm 2.44^{c,d}$	78.04 ± 3.28^{d}	$91.25 \pm 4.22^{b,c}$
	ATCC 53013 + CN	100.00 ± 4.60^{a}	105.48 ± 1.53^{a}	91.06 ± 5.56^{b}	70.17 ± 3.48^{c}	68.77 ± 0.84^{c}	70.11 ± 2.21^{c}	60.60 ± 1.48^{d}	69.89 ± 1.85^{c}
	CICC 6038	100.00 ± 2.40^{c}	146.27 ± 8.70^{a}	105.63 ± 4.34^{c}	115.75 ± 2.47^{b}	91.18 ± 3.72^{d}	57.53 ± 3.85^{e}	57.39 ± 1.05^{e}	64.02 ± 1.83^{e}
	CICC 6038 + CN	100.00 ± 2.53^{c}	126.83 ± 2.46^{b}	132.78 ± 2.94^{a}	99.63 ± 2.48^{c}	98.07 ± 3.88^{c}	83.25 ± 3.30^{d}	83.46 ± 1.18^{d}	76.39 ± 1.46^{e}
	ATCC 334	$100.00 \pm 8.24^{c,d}$	$97.47 \pm 0.64^{c,d}$	90.47 ± 9.17^{d}	118.97 ± 4.89^{a}	64.78 ± 5.04^{f}	$113.83 \pm 1.35^{a,b}$	$105.90 \pm 1.77^{b,c}$	102.32 ± 5.50^{c}
	ATCC 334 + CN	100.00 ± 1.86^{a}	96.75 ± 2.99^{a}	68.85 ± 2.57^{b}	41.77 ± 2.92^{f}	53.82 ± 2.55^{d}	49.04 ± 0.99^{e}	61.65 ± 1.05^{c}	63.16 ± 1.78^{c}
	CICC 6045	$100.00 \pm 4.88^{a,b,d}$	$93.78 \pm 4.94^{b,c}$	$99.27 \pm 0.34^{a,b}$	$91.80 \pm 2.46^{c,d}$	87.14 ± 3.95^{d}	$95.03 \pm 4.60^{b,c}$	49.42 ± 1.81^{e}	105.72 ± 0.65^{a}
	CICC 6045 + CN	100.00 ± 0.98^{a}	66.01 ± 3.97^{d}	60.39 ± 3.18^{e}	81.80 ± 1.01^{b}	75.00 ± 0.73^{c}	$43.47 \pm 1.34^{f,g}$	41.16 ± 1.34^{g}	45.61 ± 0.63^{f}
TFC (%)	SWFU D16	100.00 ± 2.93^{a}	73.27 ± 1.91^{b}	65.34 ± 4.09^{c}	71.30 ± 3.83^{b}	50.84 ± 2.02^{d}	48.04 ± 3.39^{d}	60.88 ± 1.58^{c}	16.39 ± 1.53^{e}
	SWFU D16 + CN	100.00 ± 2.93^{a}	75.14 ± 9.09^{b}	68.95 ± 7.26^{b}	49.33 ± 3.93^{c}	36.43 ± 3.63^{d}	$35.45 \pm 2.65^{d,e}$	$26.01 \pm 3.66^{e,f}$	17.19 ± 0.21^{f}
	ATCC 8014	$100.00 \pm 10.75^{c,d}$	89.17 ± 6.30^{d}	144.86 ± 4.99^{a}	$130.39 \pm 17.41^{a,b}$	$101.89 \pm 6.03^{c,d}$	$100.68 \pm 7.39^{c,d}$	$116.90 \pm 3.14^{b,c}$	44.51 ± 6.26^{e}
	ATCC 8014 + CN	100.00 ± 2.80^{a}	97.78 ± 4.95^{a}	72.36 ± 5.77^{b}	53.45 ± 5.33^{c}	52.00 ± 3.89^{c}	3.14 ± 0.45^{e}	30.52 ± 3.78^{d}	25.22 ± 0.31^{d}
	ATCC 53013	100.00 ± 4.45^{c}	152.38 ± 4.75^{a}	150.00 ± 6.20^{a}	131.87 ± 10.76^{b}	50.00 ± 2.23^{d}	112.51 ± 10.26^{c}	107.35 ± 13.92^{c}	110.61 ± 4.17^{c}
	ATCC 53013 + CN	$100.00 \pm 2.78^{a,b}$	107.39 ± 13.99^{a}	93.22 ± 9.81^{b}	34.84 ± 6.11^{c}	$23.74 \pm 3.99^{c,d}$	15.01 ± 1.20^{d}	20.09 ± 2.81^{d}	16.82 ± 1.79^{d}
	CICC 6038	$100.00 \pm 9.54^{b,c}$	126.57 ± 2.72^{a}	138.09 ± 8.69^{a}	126.63 ± 8.37^{a}	$85.75 \pm 13.71^{c,d}$	70.06 ± 2.30^{d}	$90.23 \pm 3.87^{b,c}$	102.35 ± 7.72^{b}
	CICC 6038 + CN	100.00 ± 10.84^{b}	122.15 ± 3.24^{a}	137.68 ± 5.45^{a}	81.18 ± 17.03^{c}	50.32 ± 3.95^{d}	18.33 ± 0.81^{e}	17.61 ± 2.60^{e}	17.50 ± 1.52^{e}
	ATCC 334	100.00 ± 0.62^{a}	95.20 ± 2.91^{a}	66.84 ± 2.15^{c}	83.48 ± 4.40^{b}	34.27 ± 1.84^{d}	84.50 ± 5.24^{b}	83.11 ± 1.88^{b}	70.27 ± 5.09^{c}
	ATCC 334 + CN	100.00 ± 13.73^{a}	93.23 ± 5.36^{a}	51.26 ± 6.77^{b}	6.47 ± 1.71^{c}	17.66 ± 1.55^{c}	10.28 ± 1.79^{c}	12.04 ± 0.88^{c}	13.33 ± 0.82^{c}
	CICC 6045	100.00 ± 4.62^{a}	$85.17 \pm 6.87^{b,c}$	88.43 ± 4.85^{b}	$75.98 \pm 4.20^{c,d}$	102.78 ± 3.18^{a}	63.01 ± 4.35^{e}	37.58 ± 4.11^{f}	$69.80 \pm 5.73^{d,e}$
	CICC 6045 + CN	100.00 ± 6.39^{a}	86.42 ± 4.36^{b}	95.15 ± 0.43^{a}	86.76 ± 1.96^{b}	99.88 ± 2.12^{a}	19.45 ± 1.43^{c}	16.70 ± 2.40^{c}	17.15 ± 1.81^{c}

Different lower-case letters in the same row indicate significant differences at $p < 0.05$.

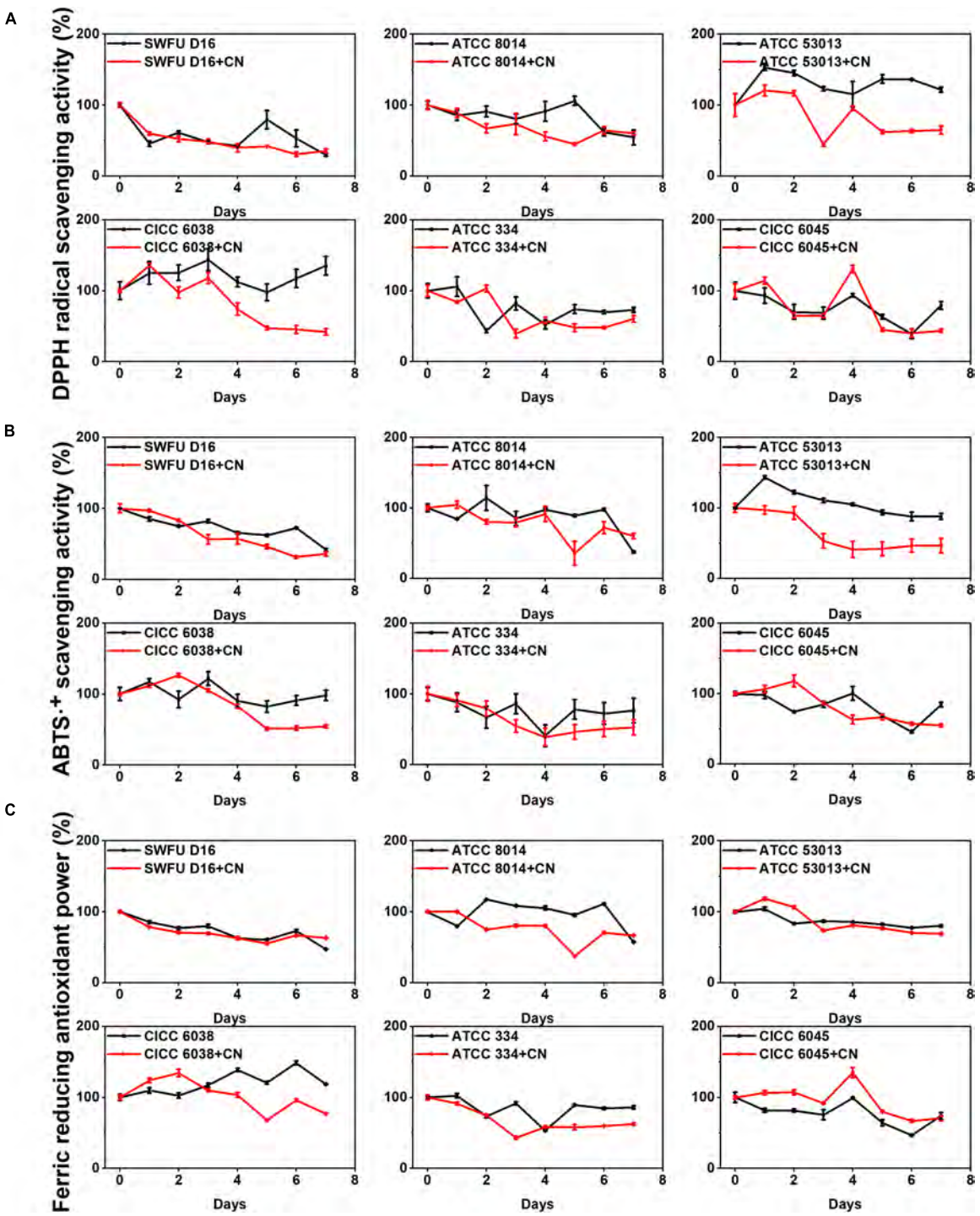

FIGURE 1 | Changes in the antioxidant abilities of FPFL during the fermentation process for different probiotics. **(A)** DPPH· scavenging ability. **(B)** ABTS·+ scavenging ability. **(C)** FRAP. Asterisks (*) represent the significant difference when comparing the unfermented sample (0 days) ($p < 0.05$*), the samples from the same group are represented by the same color.

TPC and TFC in the early fermentation stage was the vigorous growth of microorganisms, and their high metabolic activities consumed the components in PFL, such as starch, protein, pectin, etc., which led to the release of phenolics and flavonoids (26). With the continuation of the fermentation process, the substances in PFL were utilized, degraded, and transformed by microorganisms, which is the cause of the decrease in TPC and TFC (27).

Antioxidant Abilities

The antioxidant ability of the sample depends on the presence of various compounds with different action mechanisms. In this study, three methods were performed to evaluate the antioxidant effects of FPFL, including DPPH, ABTS radical scavenging abilities, and FRAP. Of these, DPPH and ABTS radical scavenging assays utilize hydrogen atom transfer and single electron transfer reaction mechanisms, while the FRAP assay takes up the single electron transfer method (28, 29).

From **Figure 1**, all the three antioxidant abilities were decreased after 7 days of fermentation ($p < 0.05$), and this decrease was more pronounced in the CN control groups. During short-term fermentation time, the antioxidant abilities were substantially improved for ATCC 53013, CICC 6038, and ATCC 8014 ($p < 0.05$), regardless of whether they were in the CN control groups or the unfermented samples. Similar to TPC and TFC, the time points with the highest antioxidant ability were focused primarily on the first 1–3 days. For DPPH and ABTS radical scavenging ability, the highest increase was noted for ATCC 53013 at 1 day (153.03 and 143.26%), while for FRAP, it was 148.63% (CICC 6038 at 6 days). It was also observed that FRAP was always high from the beginning of fermentation to the end of fermentation (1–7 days), which was different from DPPH and ABTS radical scavenging abilities, and this also illustrated the different antioxidant mechanisms between them. Overall, FPFL demonstrated excellent antioxidant abilities after short-term fermentation, of which CICC 6038 and ATCC 53013 had the strongest boosting effects, which was consistent with a previous study reported by Ru et al. (30).

A previous study reported that short-term fermentation could release bound phenols in plants, which in turn increased the TPC and TFC, and improved the antioxidant ability (31). To elucidate the similarities and differences between TPC, TFC, antioxidant ability, and the other variables more clearly, the correlation analysis and principal component analysis (PCA) were further performed and are displayed in **Figure 2** in the form of the correlation heatmap, correlation network, and PCA graph, respectively. The high and significant correlation coefficients indicated higher correlations between TPC/TFC and different antioxidant abilities, which had also been proved by the cluster distances, the intersection networks, and the relative distance in 2D principal-component space. This implicated phenolics and flavonoids, especially, phenolics were the main factors contributing to antioxidant ability, which also explained the similar changing trends among TPC/TFC and antioxidant abilities.

α-Glucosidase Inhibition Ability

α-Glucosidase is an essential target for type II diabetes. Inhibition of α-glucosidase can delay carbohydrate digestion and glucose absorption, which in turn leads to reducing postprandial blood glucose levels, and ultimately improves mitigation of diabetes and its complications (32). From **Figure 3A**, most of the probiotics could enhance the α-glucosidase inhibition ability of FPFL during the first 1–3 days ($p < 0.05$). Among them, ATCC 53013 showed the highest level of increase after fermentation for 1 day, 194.14% as large as the unfermented sample, and maintained at a high level (> 122%) over the following 3 days. Followed by ATCC 8014 (126.61% at the 2 days), in brief, these two strains were significantly better compared to their corresponding CN control groups. The reason may be that the addition of CN could facilitate PFL fermentation, which results in a higher degree of conversion and degradation of the active ingredients in FPFL, which in turn, reduces its α-glucosidase inhibition ability. However, the CN control groups of ATCC 334 and CICC 6045 presented better α-glucosidase inhibition ability than without CN samples, likely because different probiotics had different lactic fermentation, acid tolerance, and CN source utilization abilities (33). The proper amount of CN addition can make the bioactive ingredients of fermentation substrate release most, which in turn gives a stronger α-glucosidase inhibition ability. For example, *L. bulgaricus*, *L. casei*, *L. fermentum*, *L. delbrueckii,* and *L. lactis* showed different lactic acid yields under the same CN conditions, while lactic acid yields instead decreased at higher concentrations of carbon source for *L. casei* (34, 35). In addition, *Bacillus licheniformis* is a non-lactic acid bacteria regarded as a probiotic. It was found that high CN source concentration stimulated the cell growth of *B. licheniformis* but reduced its trypsin activity, while the opposite result was observed with low concentrations (36). From significant but lower correlations, and the long distances in the PCA graph (**Figure 2**), while the α-glucosidase inhibition ability was significantly influenced by TPC, TFC, and other antioxidant material, it was not determined entirely by them. Overall, the α-glucosidase inhibition ability of FPFL was decided by the integrated effect of various bioactive ingredients, and ATCC 53013 proved to be an excellent probiotic tool to increase the α-glucosidase inhibition ability (30).

Acetylcholinesterase Inhibition Ability

Up to today, acetylcholinesterase (AChE) is an attractive target for the treatment of Alzheimer's disease, and acetylcholinesterase inhibitors represent the major approved drugs to treat this neurodegenerative disease (37). With the advantage of being safe, cost-effective, and efficacious, natural food or medicinal plants are considered novel strategies for the prevention and treatment of Alzheimer's disease. Gratifyingly, almost all the samples presented a certain inhibition activity against AChE, and all six probiotics could enhance the AChE inhibition ability of FPFL after fermentation (**Figure 3B**), which is consistent with the conclusion of Li (38). Of these, after fermentation for 1 day, ATCC 53013 and CICC 6038 showed the strongest upregulation with the maximum value of 140.48 and 153.39%, respectively. Surprisingly, most of the CN control groups showed stronger AChE inhibition ability except SWFU D16. The reason could be that SWFU D16 was isolated from goat milk cake, which was not fit for PFL fermentation, and there was no obvious effect of CN-addition. Considering that the addition of CN had a greater degree of conversion and degradation for FPFL, we supposed that these new products were more likely to have a role in the inhibition of AChE. The correlation analysis and PCA analysis further validated our results that AChE inhibition ability was also weakly correlated with TPC/TFC, antioxidant abilities,

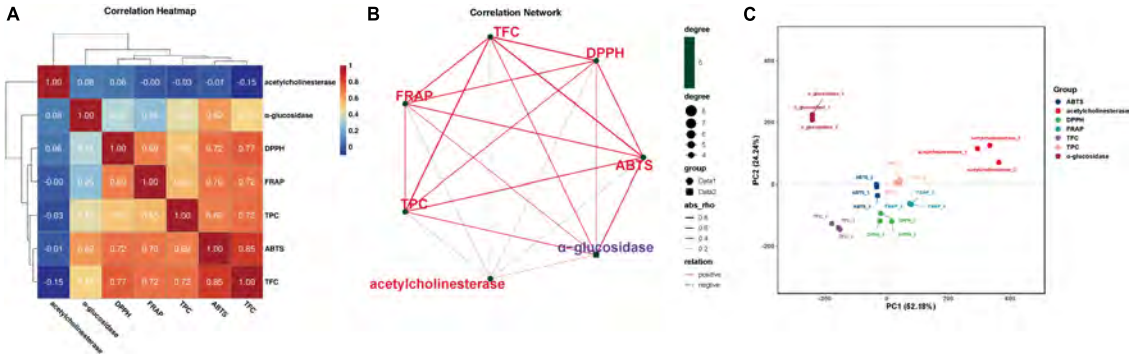

FIGURE 2 | Associations among different indicators. **(A)** Correlation heatmap. **(B)** Correlation network. **(C)** Principal component analysis. TPC, total phenolic content; TFC, total flavonoid content; DPPH, DPPH·scavenging activity; ABTS, ABTS·+ scavenging ability; FRAP, ferric reducing antioxidant power; α-glucosidase, α-glucosidase inhibition ability; AChE, acetylcholinesterase inhibition ability.

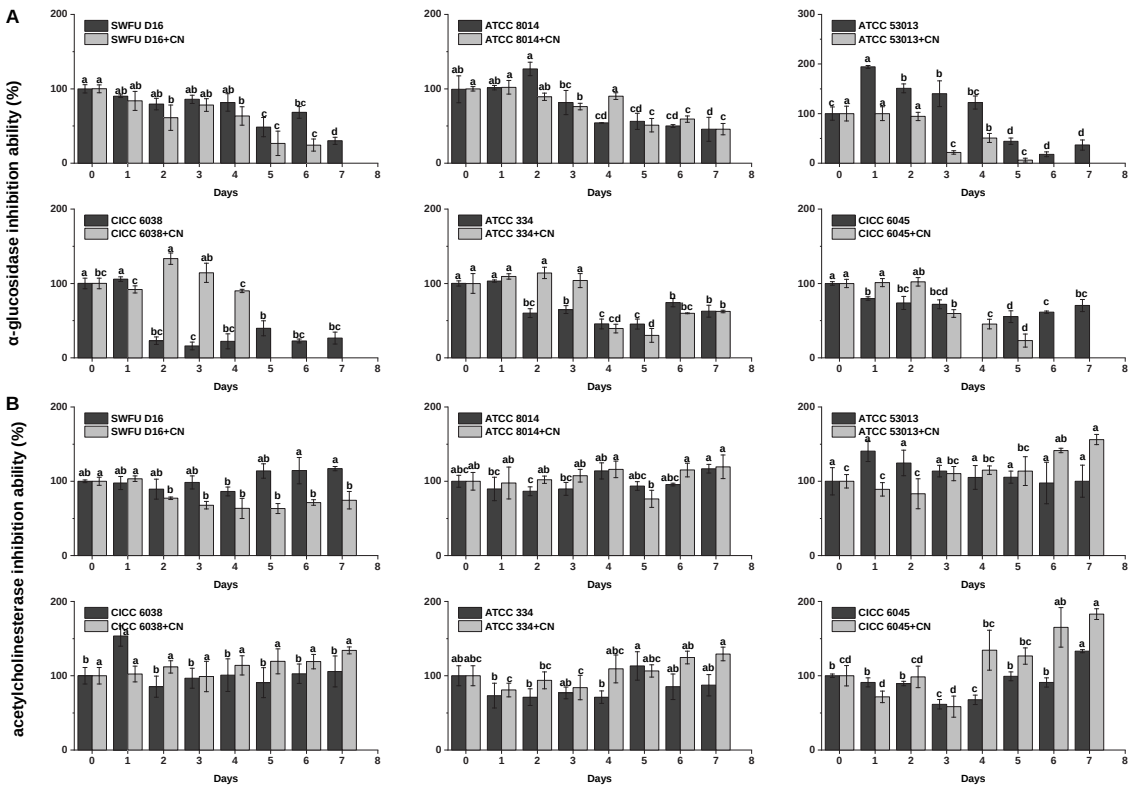

FIGURE 3 | The enzymes' inhibition abilities of the FPFL during the fermentation process for different probiotics. **(A)** α-glucosidase inhibition ability. **(B)** Acetylcholinesterase inhibition ability. Mean ± standard deviation, (n = 3). Bars with different letters indicate a significant difference ($p < 0.05$).

and α-glucosidase inhibition ability, and falls away from them on the PCA plot.

High-Performance Liquid Chromatography Analysis Results

To elucidate the changes of the various compounds in PFL fermented by different probiotics at different fermentation stages, HPLC analysis was performed to present their chromatographic characterizations. According to the studies published previously by us and others, a total of 12 compounds were confirmed and quantified by comparing their retention time and UV spectrum to the standard, including gallic acid, (+)-catechin, chlorogenic acid, epicatechin, rutin, ferulic acid, rosmarinic acid, baicalin, luteolin, apigenin, hesperetin, and baicalein (12, 17, 39). These compounds are labeled in **Figures 4A,B** with Arabic numerals according to their elution order.

Firstly, samples fermented by different probiotics for 1 day were selected for comparative analysis, and their chromatograms

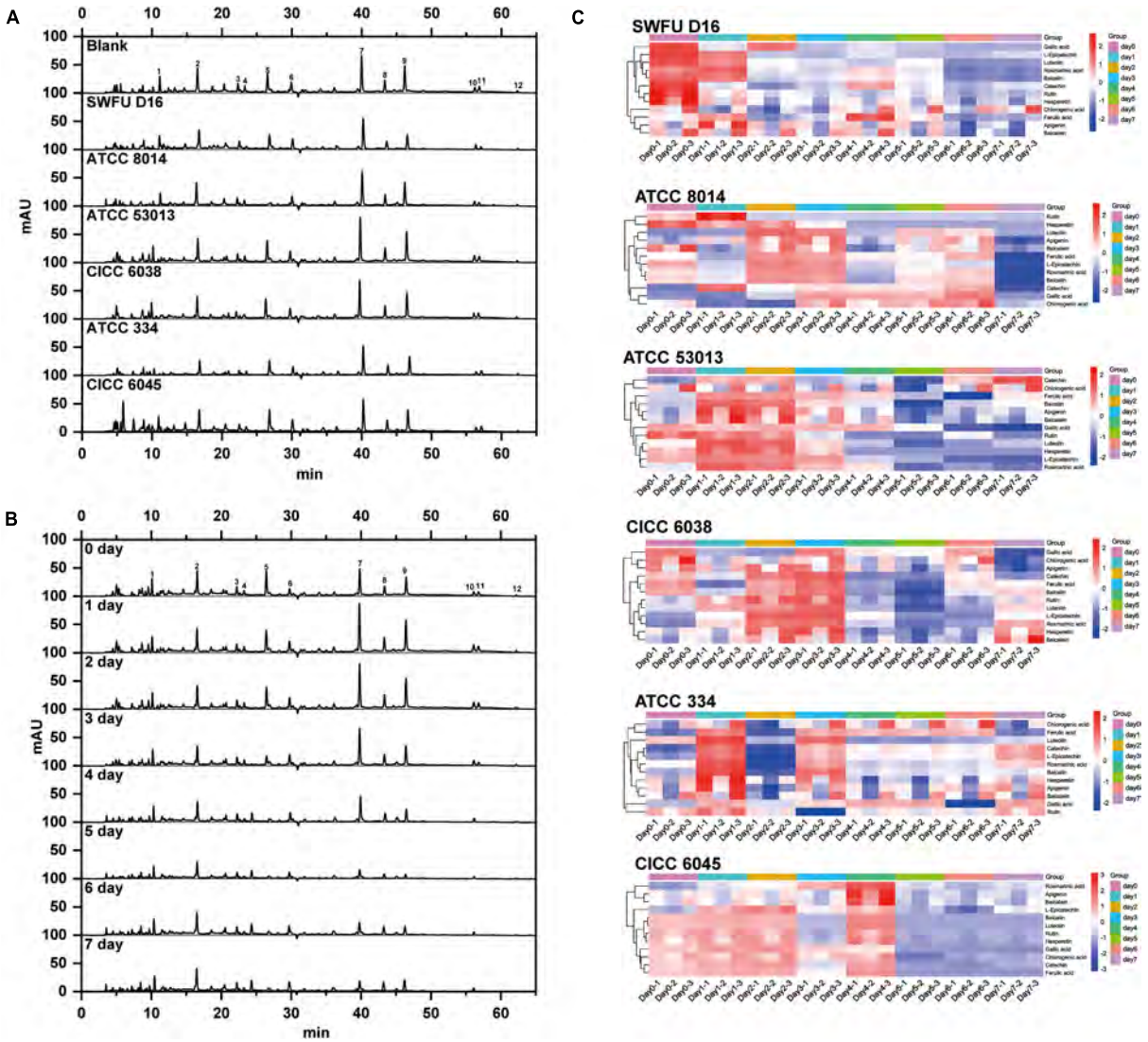

FIGURE 4 | HPLC chromatogram and heatmap of FPFL. **(A)** Chromatogram of FPFL for different probiotics at 280 nm on 1 day of fermentation. **(B)** Chromatogram of FPFL during different fermentation periods for ATCC 53013 at 280 nm. **(C)** Heatmap of compounds content of FPFL during different fermentation periods and different probiotics.

at 280 nm were shown in **Figure 4A**. For all probiotics, their chromatograms were essentially identical, while there was some difference in the height and area of some chromatographic peaks. Among them, the chromatographic peak of rosmarinic acid (peak 7) of ATCC 53013 was significantly higher than other probiotics. Similarly, the same phenomena can also be observed in other peaks for different probiotics. When compared to the blank sample (without probiotics), CICC 6045 had significantly higher and more chromatographic peaks in the first 10 min, which indicated that it could produce more high-polarity compounds.

Among all six probiotics, ATCC 53013 showed excellent promoting effects on nearly all the evaluation metrics of PFL, especially for α-glucosidase inhibition ability, thus it was a superior probiotic for the fermentation of PFL. In accordance with these experiment results, we choose FPFL fermented by ATCC 53013 to compare the changes of the various compounds each day. As shown in the chromatographs in **Figure 4B**, the peaks of rutin, hesperetin, and baicalein (peaks 5, 11, 12) decreased gradually and almost disappeared on day 4, while peaks of rosmarinic acid, baicalin, luteolin, and apigenin (peaks 7, 8, 9, 10) were increased first and decreased afterward, reaching the highest levels on the first day. For other peaks, there were no obvious changes. Interestingly, these compounds with large content changes were almost all flavonoids, except for rosmarinic acid, which means the biotransformation of flavonoids might be one of the major reactions during fermentation. Of which, luteolin (peak 9) has been previously reported to possess beneficial biological activities, such as anti-inflammatory, anti-allergic, and antibacterial activities, and could stably bind to α-glucosidase *via* hydrophobic force, which

in turn caused inactivation of α-glucosidase (40). Similarly, apigenin (peak 10) had potential therapeutic effects on a variety of neurodegenerative diseases such as Alzheimer's disease and Parkinson's disease (41). In addition, rosmarinic acid (peak 7) also had a lot of interesting pharmacological activities, including antiviral, antibacterial, anti-inflammatory, and antioxidant abilities, and was identified as a potential treatment for Alzheimer's disease (42, 43). The above results explained the improvement of antioxidant abilities, α-glucosidase inhibition ability, and acetylcholinesterase inhibition ability of PFL after fermentation.

To better present the changes of different probiotic groups at different stages of fermentation, the contents of these 12 compounds were visually exhibited as a heatmap in **Figure 4C**. Blue represented low content while red represented high content. It could be clearly seen that SWFU D16 and CICC 6045 showed an obvious trend from red to blue, which indicated the decreasing trend of the content of these compounds in these two probiotic groups. For ATCC 8014, ATCC 53013, CICC 6038, and ATCC 334 groups, their colors changed from blue to red and then to blue, showing that the levels of these compounds were first increased and then decreased. In addition, when compared with other probiotic groups, ATCC 53013, ATCC 8014, and CICC 6038 groups had significantly more red areas and darker color groups within 3 days of fermentation, which implied that the increase of these major compounds was more accentuated in these probiotic groups. Again, these results strongly supported the preceding results, especially for ATCC 53013 in **Figure 4B**. The significant difference between different strains could not only be found according to the heatmap but also between the different compounds from the same probiotic group. For the rutin, rosmarinic acid, and luteolin of these compounds, clear red color in the first 3 days and distinct changes were clearly observed. They have been reported to be the major compounds of PFL in our previous reports and exhibit excellent biological activity (12, 17).

Taken together, the above results suggested that probiotic fermentation had different effects on various compounds in PFL, and different probiotics exerted different effects, which might be due to the various mechanisms of action of probiotic fermentation, including formation, transformation, and degradation.

Metabolomic Analysis

To further elucidate the metabolite changes during fermentation, we analyzed the metabolites of FPFL (fermented by ATCC 53013 for 1 day) using a non-targeted metabolomics approach based on UHPLC–Triple–TOF–MS/MS. It is generally believed that ESI positive ion mode is more sensitive than the negative ion mode, while the negative ion mode is more suitable for acidic compounds (44). Positive and negative ion modes were complementary and they were both therefore used for analysis. The representative base peak chromatograms (BPC) of PFL (unfermented sample) and FPFL in both modes are shown in **Figures 5A–D**, respectively. According to the BPC plots, there were significant differences in the metabolites of the samples before and after fermentation. The spectral signal intensities of FPFL were weaker than PFL, which indicated that fermentation reduced the content of the primary metabolites and secondary metabolites in PFL.

The metabolites were identified by comparing accurate mass (error < 10 ppm), retention times, fragmentation patterns, and collision energies against standard compounds and the in-house database (Shanghai Applied Protein Technology Co., Ltd, Shanghai, China), and their confidence levels of compound annotations were at level 2 or higher (45). In this study, a total of 961 metabolites were identified, among which 574 and 387 were detected in positive mode and negative mode (**Supplementary Table 1**), respectively. To show the composition and classification of these metabolites more intuitively, the corresponding pie diagrams are plotted in **Figure 6**. The different colors in each pie chart represented different classifications, and the area represented the relative proportion of metabolites in the classification. As exhibited in **Figure 6**, the predominant superclass metabolites were lipids and lipid-like molecules, phenylpropanoids and polyketides, organoheterocyclic compounds, benzenoids, and organic oxygen compounds. At the class level, they were mainly prenol lipids, fatty acyls, flavonoids, organooxygen compounds, as well as benzene, and substituted derivatives. While at the subclass level, they were fatty acids and conjugates, flavonoid glycosides, carbohydrates and carbohydrate conjugates, o-methylated flavonoids, and terpene glycosides.

Next, we sought to quantify differences in metabolite compositions before and after fermentation with principal components analysis (PCA). In **Figures 7A,B**, highly significant discrimination between two groups, both in positive and negative ion modes, is shown, indicating significant variation in metabolites of PFL after fermentation. To display differentially metabolites, the volcano plots (**Figures 7C,D**) were constructed based on statistical value $p < 0.05$ and fold change ≥ 1.5. The results showed that 92 metabolites were significantly up-regulated and 33 were significantly down-regulated in positive ion mode, while 87 metabolites were significantly up-regulated and 25 were significantly down-regulated in negative ion mode. According to the variable importance in projection (VIP) value obtained by OPLS-DA and the results of *t*-tests, metabolites that had both VIP > 1 and $p < 0.05$ were selected to generate hierarchical cluster heatmaps (**Figures 7E,F**). The heatmaps in both positive and negative ion modes revealed significant changes in these compounds in different classes, including primary metabolites (fatty acids, lipids, and nucleosides) and secondary metabolites (alkaloids, flavonoids, phenols, and terpenoids). In brief, the upregulated metabolites were more numerous compared with the downregulated metabolites after fermentation, and the negative ion mode provided a higher ability to detect more significant metabolites.

To further explore the correlation between metabolites and functional activity, a series of Spearman's correlation analyses were conducted and illustrated with heatmaps and network diagrams in **Figure 8**. Interestingly, most of the metabolites that highly correlated with the previously described activity indicators belonged to the upregulated metabolites, no matter in both positive and negative ion modes. α-Glucosidase

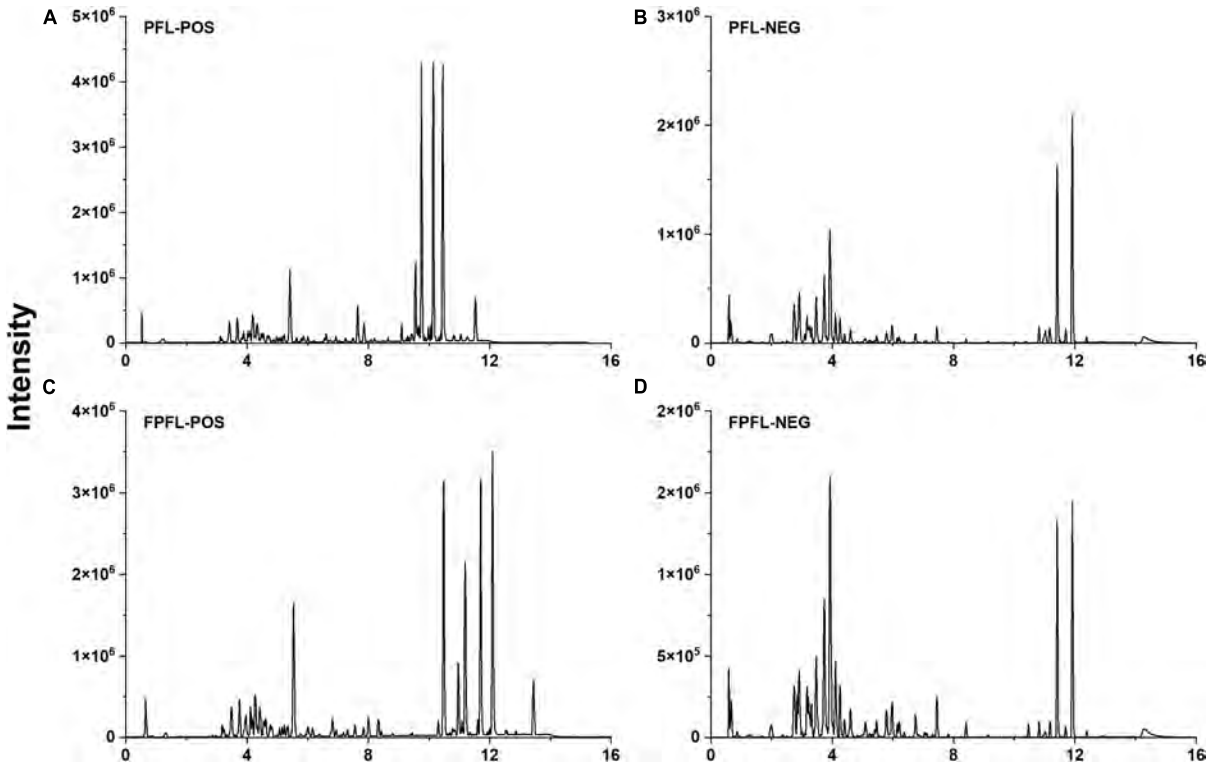

FIGURE 5 | Representative base peak chromatograms (BPC) of PFL and FPFL in the positive **(A,C)** and negative **(B,D)** ions mode.

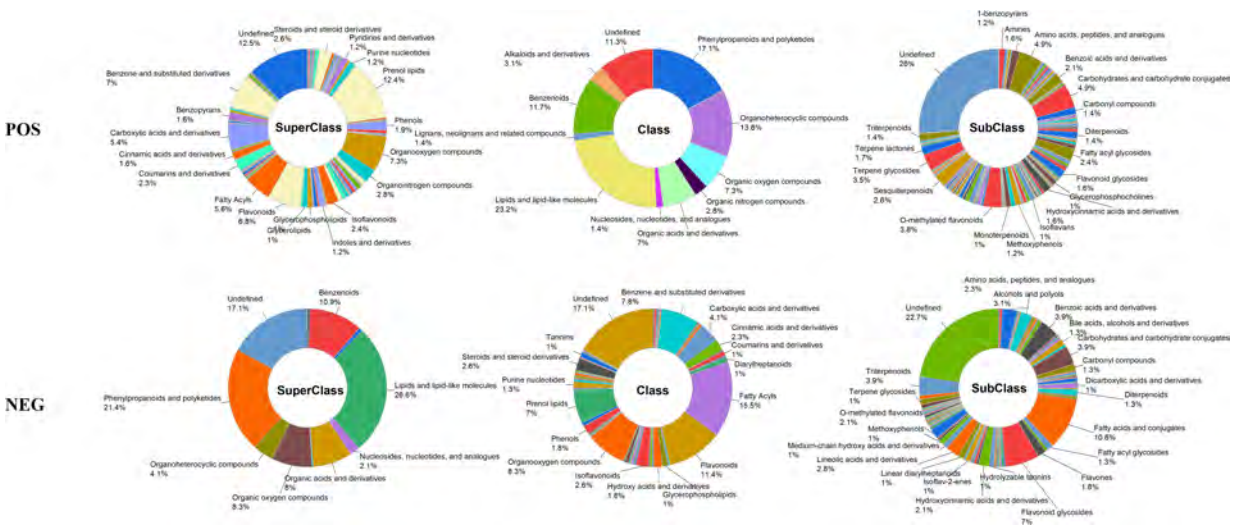

FIGURE 6 | The schematic diagram of the different classifications of the metabolites of FPFL.

inhibition ability and TFC were significantly associated with the greatest number of metabolites, followed by three antioxidant abilities, and acetylcholinesterase inhibition ability, which further explained the significant improvements of these metrics, especially the α-glucosidase inhibition ability. An unexpected observation was that no metabolites were significantly associated with TPC, which was also in agreement with the results in **Table 2**, that no significant changes were observed in TPC after 1 day of fermentation. The complex relationships between these indicators and key metabolites were further illustrated in **Figures 8B,D**. In addition, it was found that classifications at the class level of these key metabolites majorly belonged to flavonoids, isoflavonoids, prenol lipids, organooxygen compounds, hydroxy acids, and derivatives,

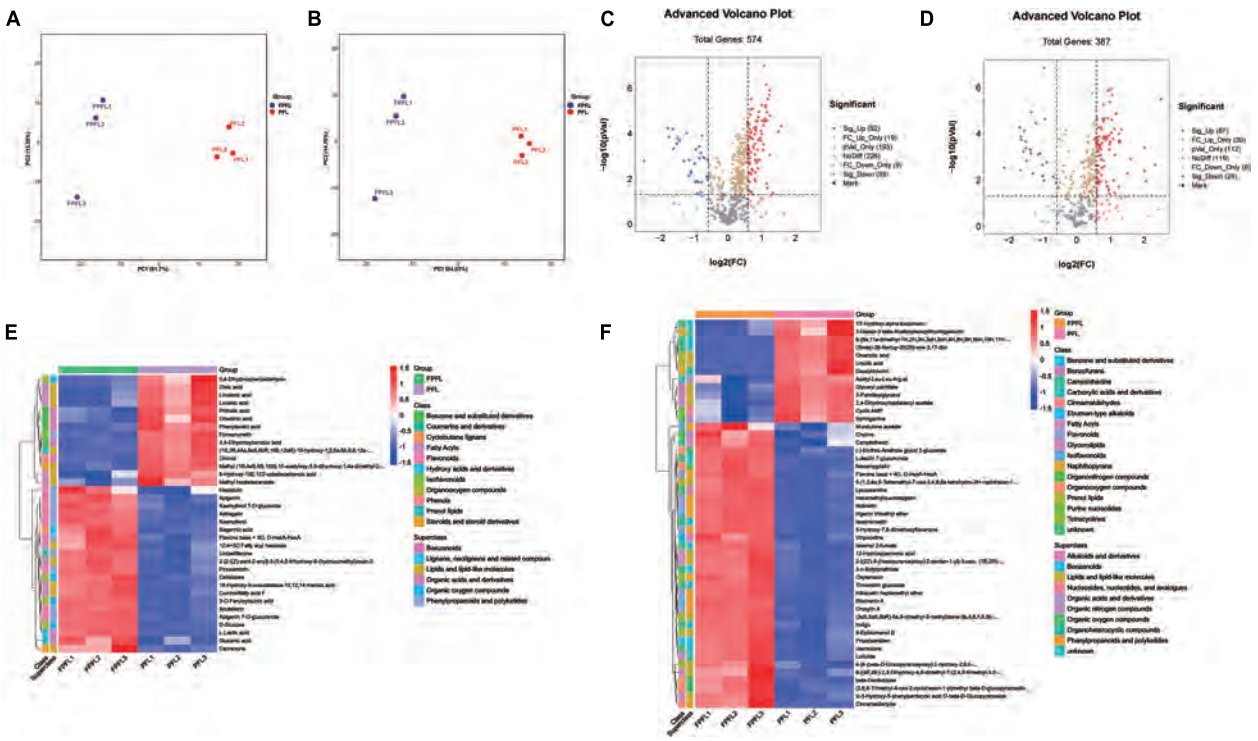

FIGURE 7 | PCA, volcano plots, and heat map show the changes of metabolites in PFL and FPFL. **(A)** Score plot in positive ions mode, **(B)** score plot in negative ions mode. Represent high cohesion within groups and good separation among before and after fermentation. **(C)** Volcano plot in positive ions mode. **(D)** Volcano plot in negative ions mode. The blue dots represent significantly downregulated differentially expressed metabolites, the red dots represent significantly upregulated differentially expressed metabolites. Significantly different metabolites between groups were determined by $p < 0.05$ and an absolute Log_2FC (fold change) ≥ 1. **(E)** Heat map in positive ions mode, **(F)** heat map in negative ions mode. Each sample is represented by one column, and each metabolite is visualized in one row. Red indicates high abundance; blue indicates relatively low metabolite abundance.

phenols, and fatty acyls. This illustrated the complicated chemical and biological changes that occurred during the fermentation process involving almost all the constituents of PFL.

It is well known that the secondary metabolites of plants are mainly regulated by their metabolic pathways, which in turn affect their functional activities. The KEGG pathway database[1] is a main public database of metabolic pathways, which could be used in studies of gene expression information and metabolite accumulation in a general network. In this study, all the differential metabolites were entered into the KEGG database for pathway analysis and obtained the pathway information of metabolite participation. Pathway enrichment analysis was performed using the KEGG ID of differential metabolites to derive the metabolic pathway enrichment results.

A total of 97 signaling pathways were significantly enriched through the KEGG pathway enrichment analysis, and these pathways are listed in **Supplementary Table 2**. As shown in **Figure 9A**, the bubble plot demonstrated the Top 20 most strongly enriched pathways, and flavonoid biosynthesis, biosynthesis of unsaturated fatty acids, and isoflavonoid biosynthesis were the most enriched pathways. This validated the results described in the previous paragraphs, with flavonoids and isoflavonoids being the most associated with their corresponding bioactivities. Flavonoids are dominant secondary metabolites in plants and play an important role in their biological functions. Notably, accumulation of antioxidants was often observed in the flavonoid biosynthesis pathway (46). **Figure 9B** presented the network plot of the relationships between these pathways and differential metabolites, and the metabolic differences of these metabolites were revealed by the corresponding heatmap. Among them, apigenin, kaempferol, and pinocembrin were the differential metabolites involved in the flavonoid biosynthesis pathway, and apigenin, biochanin A, and formononetin were involved in the isoflavonoid biosynthesis pathway, while for unsaturated fatty acid biosynthesis pathway, they were linoleic acid, linolenic acid, and oleic acid, respectively. In summary, the results of KEGG enrichment analyses further revealed the diversity of the metabolic pathways of PFL during the fermentation of probiotics and strongly supported the results previously mentioned.

DISCUSSION

As a traditional medicinal and edible plant, PFL has been shown to possess many bioactive compounds and health properties and has been widely cultivated as a major crop (47). Thus, both

[1] www.kegg.jp/kegg/pathway.html

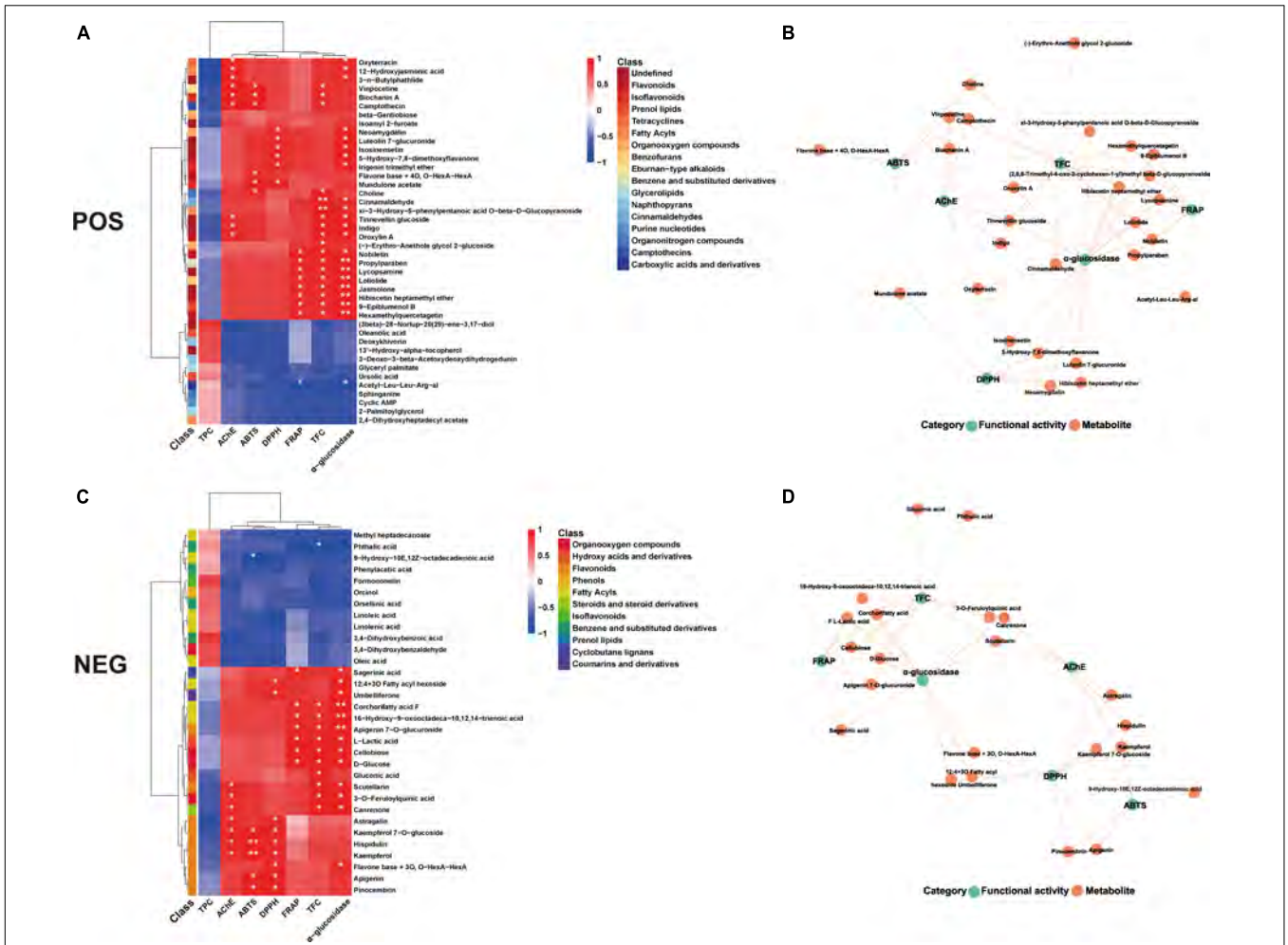

FIGURE 8 | Spearman's analysis and associated network diagram show the correlation between metabolites and 6 functional activities. **(A,C)** Spearman's analysis of FPFL in the positive and negative ions mode. **(B,D)** Associated network of FPFL in positive and negative ions mode. Asterisks represent $^{*}p < 0.05$, $^{**}p \leq 0.01$, respectively.

from the human nutrition and food bioprocessing perspective, various food processing techniques could be used to improve its sensory and dietary properties. Probiotic fermentation is one of the safe and effective means to improve the nutritional value, functional activity, and pharmacological efficacy of plants, and therefore, could be useful as an important processing technique for PFL. Our study offers several interesting findings. It illustrates the dynamic changes of the active components and functional activities of PFL during the fermentation process and also provides a superior probiotic (ATCC 53013) for the fermentation of PFL. It also deciphers its mechanism of action.

In this study, PFL was fermented by six different probiotics, and the dynamic changes of its active components and functional activities in the fermentation process were evaluated. The results showed that probiotic fermentation had obvious implications for the chemical components and functional activities of PFL, and it showed an overall trend of rising first and then falling. This might be attributed to the metabolism effect of microorganisms, and similar results were also reported in other studies (27, 48, 49). As is well known, for plants, fruits, or vegetables, their phytochemical concentrations and biological activities during the fermentation process are generally affected by the fermentation substrate, strains, and fermentation time (50). By comparing these samples of different times, different probiotics, and the addition of CN source or not, we found that the optimal fermentation time was 1–3 days, and ATCC 53013 was the best probiotic tool for the fermentation of PFL. After short-term fermentation, FPFL showed excellent biological activities, such as antioxidant abilities (ABTS, DPPH, FRAP), α-glucosidase, and Ache inhibition abilities, especially fermented for 1 day using ATCC 53013. Also, the addition of CN could improve the degree of fermentation.

It is known that microorganisms during the fermentation process could release various enzymes that could disrupt the major components of the plant cell wall, such as cellulose, hemicellulose, pectin, lignin, and protein, and promote the transformation of nutrients and hydrolysis of biological macromolecules, as well as increase the content of bioactive

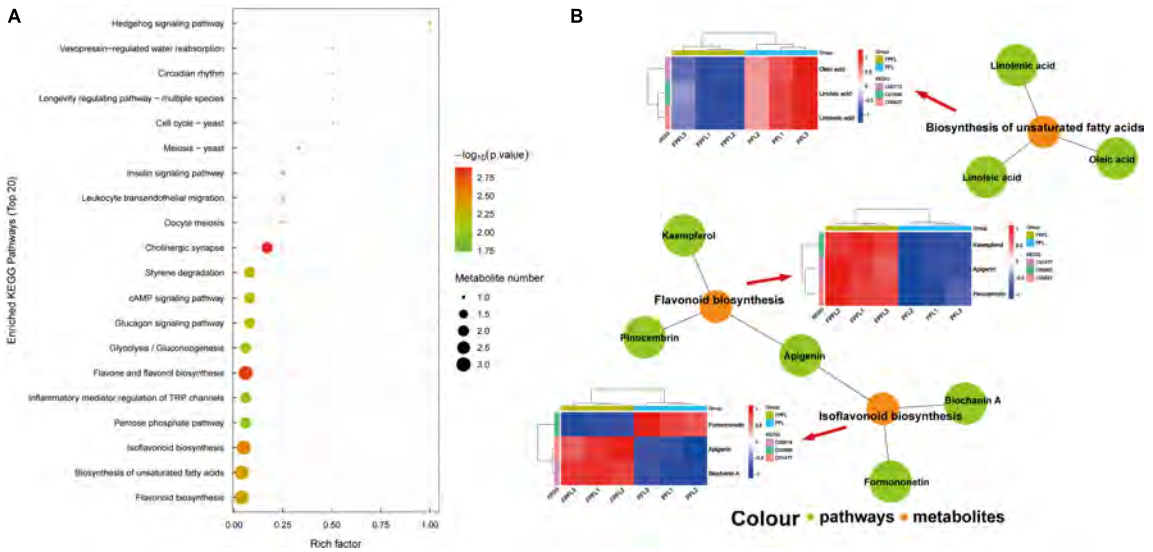

FIGURE 9 | Enriched KEGG pathways based on significantly different metabolites between PFL and FPFL. **(A)** Pathway enrichment analysis. Each bubble in the bubble graph represents a metabolic pathway, the bubble size being proportional to the enrichment. The top 20 items with the highest *p* values were selected. **(B)** Associated network diagram. The elliptical nodes represent pathways, and the rectangular nodes represent metabolites.

substances (49). On the other hand, organic matter and protein in PFL provide a partial CN source for microbial fermentation. Hence, short-term fermentation was found to increase the antioxidant activity of fermented food by the production of different active compounds (51, 52). As the fermentation process proceeded, the substrate was continuously consumed and the lignin degradation by ligninases generates inhibitory compounds, which inhibit cellulolytic enzymes and fermenting microorganisms, thus having a negative effect on fermentation (53, 54). Xiao et al. (48) also found that some active ingredients of tea such as degalloyl catechins and gallic acid increased in the initial stage of fermentation and decreased after long-term fermentation. This could be the reason why FPFL exhibited better biological activities following short-term fermentation. The above results were of importance for PFL fermentation and its application in food/drug engineering.

The HPLC assays further reveal the different effects between different probiotics by analysis of 12 standard compounds. Among them, rutin, rosmarinic acid, and luteolin were the major compounds with large variations. For different probiotics, ATCC 53013 and CICC 6038 showed better enhancement effects. A quantitative analysis further revealed the dynamic variation of these compounds at different fermentation times. The content of these compounds showed a trend of first decline and then rise, while some other compounds continued to rise or declined, or were relatively constant. In addition, some new peaks appeared for some probiotic groups when compared to the unfermented sample, which might imply that some new substances were produced. These changes suggested the different modes of action of probiotic fermentation, including formation, transformation, and degradation, which might be the reason for the variable change of the active components and functional activities of FPFL (55).

The metabolic products of plants were diverse, and many of them were biologically active molecules. Microbial fermentation could alter these metabolites and produce new metabolites, which in turn affect its functional activity. To analyze the metabolic profile changes of PFL before and after fermentation, the UPLC-MS/MS-based metabolomics method was applied. From the informative metabolic profiling data, we found significant differences in metabolites between PFL and FPFL, and they were mainly focused on some primary metabolites and secondary metabolites. Surprisingly, we observed significant upregulation of some flavonoids, phenols, and fatty acids, such as hispidulin, apigenin, kaempferol 7-O-glucoside, astragalin, kaempferol, sagerinic acid, mundulone acetate, choline, camptothecin, etc. Due to most of these compounds showing good functional activities, these could be the main reason for FPFL exhibiting good activity after short-term fermentation (56–58).

Further, KEGG pathway analysis of significantly differential metabolites found 97 metabolic signaling pathways, of which biosynthesis of unsaturated fatty acids, flavonoid biosynthesis, and isoflavonoid biosynthesis were the most enriched pathways. Among them, biosynthesis of unsaturated fatty acids was the significantly enriched lipid-related metabolic process, and it predominantly appeared in plants rich in proteins, oils, and carbohydrates (59). Moreover, flavonoid biosynthesis and isoflavonoid biosynthesis could be inducible by several abiotic and biotic stimuli (60). Studies have revealed that flavonoids and essential oils are the most abundant constituents in PFL, and we speculated that these three pathways were the main mechanisms of the action of probiotic fermentation on PFL (12, 37). These results further illustrated that in addition to strains and fermentation conditions, the fermentation substrate composition

played an important role in metabolic pathway; this might be considered for the biosynthesis of some bioactive metabolites by using probiotics.

CONCLUSION

In conclusion, this study employed six different probiotics to ferment PFL, and the dynamic change of the active components and functional activities of PFL during the fermentation process were evaluated. The results showed that short-term fermentation (1–3 days) could significantly improve its chemical components and functional activities. There were significant differences in fermentation performance for different strains, where ATCC 53013 was the best probiotic tool for fermentation PFL. HPLC analysis indicated that rutin, rosmarinic acid, and luteolin were the major compounds with large variations during fermentation. Metabolomics analysis further revealed the differential metabolites including flavonoids, phenols, and fatty acids. KEGG pathway analysis showed that biosynthesis of unsaturated fatty acids, flavonoid biosynthesis, and isoflavonoid biosynthesis were the most enriched metabolic signaling pathways. The results could provide a novel insight into the biotransformation of the active components in natural products, and represent a scientific basis for the further utilization of *Perilla frutescens*. More in-depth studies such as screening more probiotics and optimization of the fermentation process are needed in the following work.

DATA AVAILABILITY STATEMENT

The original contributions presented in this study are included in the article/**Supplementary Material**, further inquiries can be directed to the corresponding author/s.

AUTHOR CONTRIBUTIONS

ZW and XZ: methodology. ZW and XJ: validation, writing—review, and editing. XZ: formal analysis. ZW: data curation. XJ: writing—original draft preparation. XX: supervision. ZT and XH: project administration. XH: funding acquisition. All authors have read and agreed to the published version of the manuscript.

FUNDING

This work was supported by Yunnan Agricultural Joint Special General Project (202101BD070001-109 and 202101BD070001-089), China Agriculture Research System (CARS-21), Yunnan Special General Projects of Basic Research (202201AT070049), Major Science and Technology Project of Yunnan and Kunming (202102AE090042 and 2019ZG0901), Scientific Research Fund Project of Yunnan Provincial Department of Education (2022J0507), and Major Science and Technology Project of Kunming (2021JH002).

ACKNOWLEDGMENTS

We thank the support of National R&D Center for Freshwater Fish Processing and College of Health, Jiangxi Normal University, and also thank the support of Applied Protein Technology Co., Ltd. for mass spectrometry analysis.

SUPPLEMENTARY MATERIAL

The Supplementary Material for this article can be found online at: https://www.frontiersin.org/articles/10.3389/fnut.2022.933193/full#supplementary-material

REFERENCES

1. Mazzoli R, Bosco F, Mizrahi I, Bayer EA, Pessione E. Towards lactic acid bacteria-based biorefineries. *Biotechnol Adv.* (2014) 32:1216–36. doi: 10.1016/j.biotechadv.2014.07.005
2. Rangel-Huerta OD, Gil A. Nutrimetabolomics: an update on analytical approaches to investigate the role of plant-based foods and their bioactive compounds in non-communicable chronic diseases. *Int J Mol Sci.* (2016) 17:2072. doi: 10.3390/ijms17122072
3. Topfer N, Kleessen S, Nikoloski Z. Integration of metabolomics data into metabolic networks. *Front Plant Sci.* (2015) 6:49. doi: 10.3389/fpls.2015.00049
4. Demarque DP, Dusi RG, de Sousa FDM, Grossi SM, Silverio MRS, Lopes NP, et al. Mass spectrometry-based metabolomics approach in the isolation of bioactive natural products. *Sci Rep.* (2020) 10:1051. doi: 10.1038/s41598-020-58046-y
5. Anastasiou E, Lorentz KO, Stein GJ, Mitchell PD. Prehistoric schistosomiasis parasite found in the middle east. *Lancet Infect Dis.* (2014) 14:553–4. doi: 10.1016/s1473-3099(14)70794-7
6. Fujiwara Y, Kono M, Ito A, Ito M. Anthocyanins in *Perilla* plants and dried leaves. *Phytochemistry.* (2018) 147:158–66.
7. Ahmed HM, Tavaszi-Sarosi S. Identification and quantification of essential oil content and composition, total polyphenols and antioxidant capacity of *Perilla Frutescens* (L.) britt. *Food Chem.* (2019) 275:730–8. doi: 10.1016/j.foodchem.2018.09.155
8. Tipsuwan W, Chaiwangyen W. Preventive effects of polyphenol-rich *Perilla* leaves on oxidative stress and haemolysis. *ScienceAsia.* (2018) 44:162–9. doi: 10.2306/scienceasia1513-1874.2018.44.162
9. Cho E, Lee J, Sin JS, Kim SK, Kim CJ, Park MH, et al. Effects of *Perilla Frutescens* var. Acuta in amyloid beta toxicity and Alzheimer's disease-like pathology in 5xfad mice. *Food Chem Toxicol.* (2022) 161:112847. doi: 10.1016/j.fct.2022.112847
10. Zi Y, Yao M, Lu Z, Lu F, Bie X, Zhang C, et al. Glycoglycerolipids from the leaves of *Perilla Frutescens* (L.) britton (*Labiatae*) and their anti-inflammatory activities in lipopolysaccharide-stimulated raw264.7 cells. *Phytochemistry.* (2021) 184:112679. doi: 10.1016/j.phytochem.2021.112679
11. Chen AY, Chen YC. A review of the dietary flavonoid, kaempferol on human health and cancer chemoprevention. *Food Chem.* (2013) 138:2099–107. doi: 10.1016/j.foodchem.2012.11.139
12. Wang Z, Tu Z, Xie X, Cui H, Kong KW, Zhang L. *Perilla Frutescens* leaf extract and fractions: polyphenol composition, antioxidant, enzymes (alpha-glucosidase, acetylcholinesterase, and tyrosinase) inhibitory, anticancer, and antidiabetic activities. *Foods.* (2021) 10:315. doi: 10.3390/foods10020315
13. Hu Z, Lu C, Zhang Y, Tong W, Du L, Liu F. Proteomic analysis of *Aspergillus flavus* reveals the antifungal action of *Perilla frutescens* essential oil by interfering with energy metabolism and defense function. *LWT Food Sci Technol.* (2022) 154:112660. doi: 10.1016/j.lwt.2021.112660
14. Ghimire BK, Yoo JH, Yu CY, Kim S-H, Chung I-M. Profiling volatile and phenolic compound composition and characterization of the morphological

and biological activities of *Perilla frutescence* Britton Var. japonica accessions. *Acta Physiol Plant.* (2019) 41:1–16. doi: 10.1007/s11738-019-2890-1
15. Hong EY, Kim GH. Comparison of extraction conditions for phenolic, flavonoid content and determination of rosmarinic acid from *Perilla frutescens* var. Acuta. *Int J Food Sci Tech.* (2010) 45:1353–9. doi: 10.1111/j.1365-2621.2010.02250.x
16. Kawee-Ai A, Seesuriyachan P. Optimization of fermented *Perilla frutescens* seeds for enhancement of gamma-aminobutyric acid and bioactive compounds by *Lactobacillus casei* Tistr 1500. *Preparat Biochem Biotechnol.* (2019) 49:997–1009. doi: 10.1080/10826068.2019.1650377
17. Wang ZX, Lin QQ, Tu ZC, Zhang L. The influence of *in vitro* gastrointestinal digestion on the *Perilla frutescens* leaf extract: changes in the active compounds and bioactivities. *J Food Biochem.* (2020) 44:e13530. doi: 10.1111/jfbc.13530
18. Chen Y, Wang Y, Chen J, Tang H, Wang C, Li Z, et al. Bioprocessing of soybeans (*Glycine Max* L.) by solid-state fermentation with *Eurotium cristatum* Yl-1 improves total phenolic content, isoflavone aglycones, and antioxidant activity. *RSC Adv.* (2020) 10:16928–41. doi: 10.1039/C9RA10344A
19. Dong R, Yu Q, Liao W, Liu S, He Z, Hu X, et al. Composition of bound polyphenols from carrot dietary fiber and its in vivo and *in vitro* antioxidant activity. *Food Chem.* (2021) 339:127879. doi: 10.1016/j.foodchem.2020.127879
20. Ghane SG, Attar UA, Yadav PB, Lekhak MM. Antioxidant, anti-diabetic, acetylcholinesterase inhibitory potential and estimation of alkaloids (lycorine and galanthamine) from crinum species: an important source of anticancer and anti-Alzheimer drug. *Ind Crops Prod.* (2018) 125:168–77. doi: 10.1016/j.indcrop.2018.08.087
21. Xiao Y, Wu X, Yao X, Chen Y, Ho C-T, He C, et al. Metabolite profiling, antioxidant and α-glucosidase inhibitory activities of buckwheat processed by solid-state fermentation with *Eurotium cristatum* Yl-1. *Food Res Int.* (2021) 143:110262. doi: 10.1016/j.foodres.2021.110262
22. Moyo M, Aremu AO, Chukwujekwu JC, Gruz J, Skorepa J, Dolezal K, et al. Phytochemical characterization, antibacterial, acetylcholinesterase inhibitory and cytotoxic properties of *Cryptostephanus vansonii*, an endemic amaryllid. *Phytother Res.* (2017) 31:713–20. doi: 10.1002/ptr.5788
23. Pan T, Xiang H, Diao T, Ma W, Shi C, Xu Y, et al. Effects of probiotics and nutrients addition on the microbial community and fermentation quality of peanut hull. *Bioresour Technol.* (2019) 273:144–52. doi: 10.1016/j.biortech.2018.10.088
24. Dogan K, Akman PK, Tornuk F. Role of non-thermal treatments and fermentation with probiotic *Lactobacillus plantarum* on *in vitro* bioaccessibility of bioactives from vegetable juice. *J Sci Food Agric.* (2021) 101:4779–88. doi: 10.1002/jsfa.11124
25. Ng ZX, Than MJY, Yong PH. *Peperomia Pellucida* (L.) kunth herbal tea: effect of fermentation and drying methods on the consumer acceptance, antioxidant and anti-inflammatory activities. *Food Chem.* (2021) 344:128738. doi: 10.1016/j.foodchem.2020.128738
26. Liu N, Song M, Wang N, Wang Y, Wang R, An X, et al. The effects of solid-state fermentation on the content, composition and *in vitro* antioxidant activity of flavonoids from dandelion. *PLoS One.* (2020) 15:e0239076. doi: 10.1371/journal.pone.0239076
27. Wu H, Liu HN, Liu CQ, Zhou JZ, Liu XL, Zhang HZ. Hulless black barley as a carrier of probiotics and a supplement rich in phenolics targeting against h2o2-induced oxidative injuries in human hepatocarcinoma cells. *Front Nutr.* (2021) 8:790765. doi: 10.3389/fnut.2021.790765
28. Gullon B, Pintado ME, Fernández-López J, Pérez-Álvarez JA, Viuda-Martos M. *In Vitro* gastrointestinal digestion of pomegranate peel (*Punica granatum*) flour obtained from co-products: changes in the antioxidant potential and bioactive compounds stability. *J Funct Foods.* (2015) 19:617–28. doi: 10.1016/j.jff.2015.09.056
29. Lucas-Gonzalez R, Viuda-Martos M, Perez Alvarez JA, Fernandez-Lopez J. Changes in bioaccessibility, polyphenol profile and antioxidant potential of flours obtained from persimmon fruit (*Diospyros kaki*) co-products during *in vitro* gastrointestinal digestion. *Food Chem.* (2018) 256:252–8. doi: 10.1016/j.foodchem.2018.02.128
30. Ru YR, Wang ZX, Li YJ, Kan H, Kong KW, Zhang XC. The influence of probiotic fermentation on the active compounds and bioactivities of walnut flowers. *J Food Biochem.* (2022) 46:e13887. doi: 10.1111/jfbc.13887
31. Hunaefi D, Akumo DN, Smetanska I. Effect of fermentation on antioxidant properties of red cabbages. *Food Biotechnol.* (2013) 27:66–85. doi: 10.1080/08905436.2012.755694
32. Podsedek A, Majewska I, Redzynia M, Sosnowska D, Koziolkiewicz M. *In vitro* inhibitory effect on digestive enzymes and antioxidant potential of commonly consumed fruits. *J Agric Food Chem.* (2014) 62:4610–7. doi: 10.1021/jf5008264
33. Zhang C, Yang L, Ding Z, Yin B, Chen D, Guan C, et al. New selective media for isolation and enumeration of *Lactobacillus rhamnosus* and *Streptococcus thermophilus*. *J Food Meas Charact.* (2019) 13:1431. doi: 10.1007/s11694-019-00059-x
34. Rezvani F, Ardestani F, Najafpour G. Growth kinetic models of five species of *Lactobacilli* and lactose consumption in batch submerged culture. *Braz J Microbiol.* (2017) 48:251–8. doi: 10.1016/j.bjm.2016.12.007
35. Hassan SS, Bt Abd Malek R, Atim A, Jikan SS, Mohd Fuzi SFZ. effects of different carbon sources for high level lactic acid production by *Lactobacillus casei*. *Appl Mech Mater.* (2014) 695:220–3. doi: 10.4028/www.scientific.net/AMM.695.220
36. Gong JS, Li W, Zhang DD, Xie MF, Yang B, Zhang RX, et al. Biochemical characterization of an arginine-specific alkaline trypsin from *Bacillus licheniformis*. *Int J Mol Sci.* (2015) 16:30061–74. doi: 10.3390/ijms161226200
37. Lee Y, Lee J, Ju J. *Perilla frutescens* Britton Var. *Frutescens* leaves attenuate dextran sulfate sodium-induced acute colitis in mice and lipopolysaccharide-stimulated angiogenic processes in human umbilical vein endothelial cells. *Food Sci Biotechnol.* (2020) 29:131–40. doi: 10.1007/s10068-019-00711-8
38. Li XJ, Dong JW, Cai L, Mei RF, Ding ZT. Improving the acetylcholinesterase inhibitory effect of illigera henryi by solid-state fermentation with *Clonostachys rogersoniana*. *J Biosci Bioeng.* (2017) 124:493–7. doi: 10.1016/j.jbiosc.2017.05.012
39. Ha TJ, Lee JH, Lee M-H, Lee BW, Kwon HS, Park C-H, et al. Isolation and identification of phenolic compounds from the seeds of *Perilla frutescens* (L.) and their inhibitory activities against α-glucosidase and aldose reductase. *Food Chem.* (2012) 135:1397–403. doi: 10.1016/j.foodchem.2012.05.104
40. Wagle A, Seong SH, Shrestha S, Jung HA, Choi JS. Korean thistle (*Cirsium japonicum* Var. Maackii (Maxim.) matsum.): a potential dietary supplement against diabetes and Alzheimer's disease. *Molecules.* (2019) 24:649. doi: 10.3390/molecules24030649
41. George VC, Dellaire G, Rupasinghe HPV. Plant flavonoids in cancer chemoprevention: role in genome stability. *J Nutr Biochem.* (2017) 45:1–14. doi: 10.1016/j.jnutbio.2016.11.007
42. Choi SJ, Oh SS, Kim CR, Kwon YK, Suh SH, Kim JK, et al. *Perilla frutescens* extract ameliorates acetylcholinesterase and trimethyltin chloride-induced neurotoxicity. *J Med Food.* (2016) 19:281–9. doi: 10.1089/jmf.2015.3540
43. Ono K, Li L, Takamura Y, Yoshiike Y, Ikeda T, Takasaki J, et al. Phenolic compounds prevent beta-amyloid-protein oligomerization and synaptic dysfunction by site-specific binding. *Alzheimers Dement.* (2013) 9:361. doi: 10.1016/j.jalz.2013.05.690
44. Yang W, Yang X, Shi F, Liao Z, Liang Y, Yu L, et al. Qualitative and quantitative assessment of related substances in the compound ketoconazole and clobetasol propionate cream by HPLC-TOF-MS and HPLC. *J Pharm Anal.* (2019) 9:156–62. doi: 10.1016/j.jpha.2018.08.006
45. Blazenovic I, Kind T, Ji J, Fiehn O. Software tools and approaches for compound identification of LC-MS/MS Data in Metabolomics. *Metabolites.* (2018) 8:31. doi: 10.3390/metabo8020031
46. Zhang L, Zhang X, Li M, Wang N, Qu X, Fan S. Transcriptome analysis of ELM (*Ulmus pumila*) fruit to identify phytonutrients associated genes and pathways. *Forests.* (2019) 10:738. doi: 10.3390/f10090738
47. Zeng P, Wang XM, Ye CY, Su HF, Tian Q. The main alkaloids in *Uncaria Rhynchophylla* and their anti-Alzheimer's disease mechanism determined by a network pharmacology approach. *Int J Mol Sci.* (2021) 22:3612. doi: 10.3390/ijms22073612
48. Xiao Y, He C, Chen Y, Ho CT, Wu X, Huang Y, et al. UPLC-QQQ-MS/MS-based widely targeted metabolomic analysis reveals the effect of solid-state fermentation with *Eurotium cristatum* on the dynamic changes in the metabolite profile of dark tea. *Food Chem.* (2022) 378:131999. doi: 10.1016/j.foodchem.2021.131999
49. Hu JP, Zheng TT, Zeng BF, Wu ML, Shi R, Zhang Y, et al. Effects of *Lactobacillus plantarum* Fzu3013-fermented *Laminaria japonica* on lipid metabolism and gut microbiota in hyperlipidaemic rats. *Front Nutr.* (2021) 8:786571. doi: 10.3389/fnut.2021.786571
50. Liu L, Zhang C, Zhang H, Qu G, Li C, Liu L. Biotransformation of polyphenols in apple pomace fermented by beta-glucosidase-producing *Lactobacillus rhamnosus* L08. *Foods.* (2021) 10:1343. doi: 10.3390/foods10061343

51. Wang L, Bei Q, Wu Y, Liao W, Wu Z. Characterization of soluble and insoluble-bound polyphenols from *Psidium guajava* L. leaves co-fermented with *Monascus* anka and *Bacillus* Sp. and their bio-activities. *J Funct Foods.* (2017) 32:159. doi: 10.1016/j.jff.2017.02.029
52. Melini F, Melini V, Luziatelli F, Ficca AG, Ruzzi M. Health-promoting components in fermented foods: an up-to-date systematic review. *Nutrients.* (2019) 11:1189. doi: 10.3390/nu11051189
53. Teeravivattanakit T, Baramee S, Phitsuwan P, Sornyotha S, Waeonukul R, Pason P, et al. Chemical pretreatment-independent saccharifications of xylan and cellulose of rice straw by bacterial weak lignin-binding xylanolytic and cellulolytic enzymes. *Appl Environ Microbiol.* (2017) 83:e01522.
54. Li J, Zhang Y, Shi S, Tu M. Effect of residual extractable lignin on acetone-butanol-ethanol production in SHF and SSF processes. *Biotechnol Biofuels.* (2020) 13:67. doi: 10.1186/s13068-020-01710-2
55. Yin L, Zhang Y, Wang L, Wu H, Azi F, Tekliye M, et al. Neuroprotective potency of a soy whey fermented by *Cordyceps Militaris* SN-18 against hydrogen peroxide-induced oxidative injury in PC12 cells. *Eur J Nutr.* (2022) 61:792. doi: 10.1007/s00394-021-02679-w
56. Kim HA, Lee J. Hispidulin modulates epithelial-mesenchymal transition in breast cancer cells. *Oncol Lett.* (2021) 21:155. doi: 10.3892/ol.2020.12416
57. Subramanya SB, Venkataraman B, Meeran MFN, Goyal SN, Patil CR, Ojha S. Therapeutic potential of plants and plant derived phytochemicals against acetaminophen-induced liver injury. *Int J Mol Sci.* (2018) 19:3776. doi: 10.3390/ijms19123776
58. Griesser M, Vitzthum F, Fink B, Bellido ML, Raasch C, Munoz-Blanco J, et al. Multi-substrate flavonol o-glucosyltransferases from strawberry (*Fragaria* × *ananassa*) achene and receptacle. *J Exp Botany.* (2008) 59:2611–25. doi: 10.1093/jxb/ern117
59. Wu J, Peng L, Dong S, Xia X, Zhao L. Transcriptome analysis of *Chelidonium majus* elaiosomes and seeds provide insights into fatty acid biosynthesis. *Peer J.* (2019) 7:e6871. doi: 10.7717/peerj.6871
60. Dastmalchi M, Chapman P, Yu J, Austin RS, Dhaubhadel S. Transcriptomic evidence for the control of soybean root isoflavonoid content by regulation of overlapping phenylpropanoid pathways. *BMC Genom.* (2017) 18:15. doi: 10.1186/s12864-016-3463-y

Conflict of Interest: The authors declare that the research was conducted in the absence of any commercial or financial relationships that could be construed as a potential conflict of interest.

Publisher's Note: All claims expressed in this article are solely those of the authors and do not necessarily represent those of their affiliated organizations, or those of the publisher, the editors and the reviewers. Any product that may be evaluated in this article, or claim that may be made by its manufacturer, is not guaranteed or endorsed by the publisher.

Frontiers in Nutrition

Explores what and how we eat in the context of health, sustainability and 21st century food science

A multidisciplinary journal that integrates research on dietary behavior, agronomy and 21st century food science with a focus on human health.

Discover the latest Research Topics

See more →

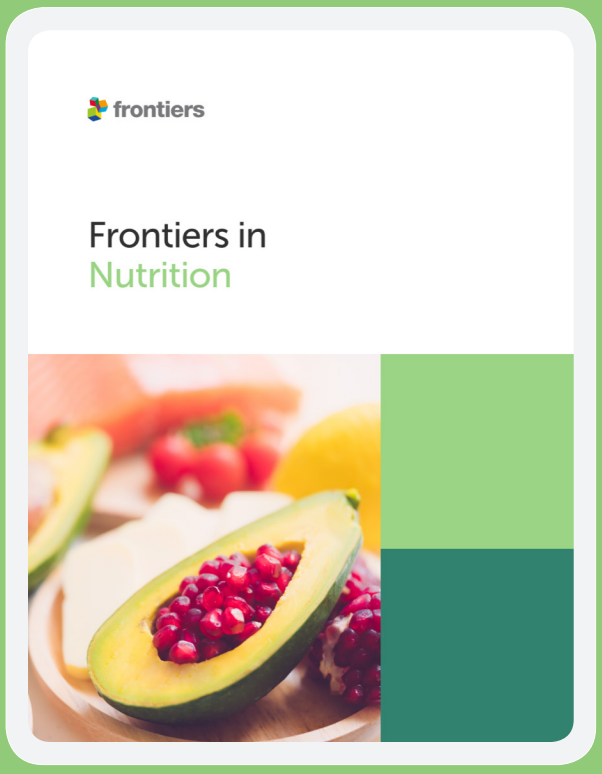

Frontiers

Avenue du Tribunal-Fédéral 34
1005 Lausanne, Switzerland
frontiersin.org

Contact us

+41 (0)21 510 17 00
frontiersin.org/about/contact